

Topics in Organometallic Chemistry 40

Gerard van Koten
David Milstein *Editors*

Organometallic Pincer Chemistry

 Springer

40

Topics in Organometallic Chemistry

Editorial Board:

M. Beller • J. M. Brown • P. H. Dixneuf

A. Fürstner • L. Goßen • L. S. Hegedus

P. Hofmann • T. Ikariya • L. A. Oro • Q.-L. Zhou

Topics in Organometallic Chemistry

Recently Published Volumes

Organometallics and Renewables

Volume Editors: Michael A. R. Meier,
Bert M. Weckhuysen, Pieter C. A. Bruijninx
Vol. 39, 2012

Transition Metal Catalyzed Enantioselective Allylic Substitution in Organic Synthesis

Volume Editor: Uli Kazmaier
Vol. 38, 2011

Bifunctional Molecular Catalysis

Volume Editors: T. Ikariya, M. Shibasaki
Vol. 37, 2011

Asymmetric Catalysis from a Chinese Perspective

Volume Editor: Shengming Ma
Vol. 36, 2011

Higher Oxidation State Organopalladium and Platinum Chemistry

Volume Editor: A. J. Canty
Vol. 35, 2011

Iridium Catalysis

Volume Editor: P. G. Andersson
Vol. 34, 2011

Iron Catalysis – Fundamentals and Applications

Volume Editor: B. Plietker
Vol. 33, 2011

Medicinal Organometallic Chemistry

Volume Editors: G. Jaouen, N. Metzler-Nolte
Vol. 32, 2010

C-X Bond Formation

Volume Editor: A. Vigalok
Vol. 31, 2010

Transition Metal Complexes of Neutral η^1 -Carbon Ligands

Volume Editors: R. Chauvin, Y. Canac
Vol. 30, 2010

Photophysics of Organometallics

Volume Editor: A. J. Lees
Vol. 29, 2010

Molecular Organometallic Materials for Optics

Volume Editors: H. Le Bozec, V. Guerschais
Vol. 28, 2010

Conducting and Magnetic Organometallic Molecular Materials

Volume Editors: M. Fourmigué, L. Ouahab
Vol. 27, 2009

Metal Catalysts in Olefin Polymerization

Volume Editor: Z. Guan
Vol. 26, 2009

Bio-inspired Catalysts

Volume Editor: T. R. Ward
Vol. 25, 2009

Directed Metallation

Volume Editor: N. Chatani
Vol. 24, 2007

Regulated Systems for Multiphase Catalysis

Volume Editors: W. Leitner, M. Hölscher
Vol. 23, 2008

Organometallic Oxidation Catalysis

Volume Editors: F. Meyer, C. Limberg
Vol. 22, 2007

N-Heterocyclic Carbenes in Transition Metal Catalysis

Volume Editor: F. Glorius
Vol. 21, 2006

Dendrimer Catalysis

Volume Editor: L. H. Gade
Vol. 20, 2006

Metal Catalyzed Cascade Reactions

Volume Editor: T. J. J. Müller
Vol. 19, 2006

Catalytic Carbonylation Reactions

Volume Editor: M. Beller
Vol. 18, 2006

Organometallic Pincer Chemistry

Volume Editors: Gerard van Koten · David Milstein

With Contributions by

A. Castonguay · S.L. Craig · L. Dostál · G.R. Freeman ·
J.A. Gareth Williams · D. Gelman · K.I. Goldberg ·
J.L. Hawk · D.M. Heinekey · J.-i. Ito · R. Jambor ·
D. Milstein · H. Nishiyama · E. Poverenov · D.M. Roddick ·
R. Romm · D.M. Spasyuk · A. St. John · K.J. Szabó ·
G. van Koten · D. Zargarian

 Springer

Editors

Gerard van Koten
Organic Chemistry & Catalysis
Debye Institute for Nanomaterials Science
Faculty of Science
Utrecht University
Utrecht
Netherlands

David Milstein
The Weizmann Institute of Science
The Kimmel Center for Molecular Design
Department of Organic Chemistry
Rehovot
Israel

ISBN 978-3-642-31080-5 ISBN 978-3-642-31081-2 (eBook)

DOI 10.1007/978-3-642-31081-2

Springer Heidelberg New York Dordrecht London

Library of Congress Control Number: 2012948954

© Springer-Verlag Berlin Heidelberg 2013

This work is subject to copyright. All rights are reserved by the Publisher, whether the whole or part of the material is concerned, specifically the rights of translation, reprinting, reuse of illustrations, recitation, broadcasting, reproduction on microfilms or in any other physical way, and transmission or information storage and retrieval, electronic adaptation, computer software, or by similar or dissimilar methodology now known or hereafter developed. Exempted from this legal reservation are brief excerpts in connection with reviews or scholarly analysis or material supplied specifically for the purpose of being entered and executed on a computer system, for exclusive use by the purchaser of the work. Duplication of this publication or parts thereof is permitted only under the provisions of the Copyright Law of the Publisher's location, in its current version, and permission for use must always be obtained from Springer. Permissions for use may be obtained through RightsLink at the Copyright Clearance Center. Violations are liable to prosecution under the respective Copyright Law.

The use of general descriptive names, registered names, trademarks, service marks, etc. in this publication does not imply, even in the absence of a specific statement, that such names are exempt from the relevant protective laws and regulations and therefore free for general use.

While the advice and information in this book are believed to be true and accurate at the date of publication, neither the authors nor the editors nor the publisher can accept any legal responsibility for any errors or omissions that may be made. The publisher makes no warranty, express or implied, with respect to the material contained herein.

Printed on acid-free paper

Springer is part of Springer Science+Business Media (www.springer.com)

Volume Editors

Gerard van Koten

Organic Chemistry & Catalysis
Debye Institute for Nanomaterials Science
Faculty of Science
Utrecht University
Utrecht
Netherlands
g.vankoten@uu.nl

David Milstein

The Weizmann Institute of Science
The Kimmel Center for Molecular Design
Department of Organic Chemistry
Rehovot
Israel
david.milstein@weizmann.ac.il

Editorial Board

Prof. Matthias Beller

Leibniz-Institut für Katalyse e.V.
an der Universität Rostock
Albert-Einstein-Str. 29a
18059 Rostock, Germany
matthias.beller@catalysis.de

Prof. John M. Brown

Chemistry Research Laboratory
Oxford University
Mansfield Rd.,
Oxford OX1 3TA, UK
john.brown@chem.ox.ac.uk

Prof. Pierre H. Dixneuf

Campus de Beaulieu
Université de Rennes 1
Av. du Gl Leclerc
35042 Rennes Cedex, France
pierre.dixneuf@univ-rennes1.fr

Prof. Alois Fürstner

Max-Planck-Institut für Kohlenforschung
Kaiser-Wilhelm-Platz 1
45470 Mülheim an der Ruhr, Germany
fuerstner@mpi-muelheim.mpg.de

Prof. Lukas J. Goossen

FB Chemie - Organische Chemie
TU Kaiserslautern
Erwin-Schrödinger-Str. Geb. 54
67663 Kaiserslautern, German
goossen@chemie.uni-kl.de

Prof. Louis S. Hegedus

Department of Chemistry
Colorado State University
Fort Collins, Colorado 80523-1872, USA
hegedus@lamar.colostate.edu

Prof. Peter Hofmann

Organisch-Chemisches Institut
Universität Heidelberg
Im Neuenheimer Feld 270
69120 Heidelberg, Germany
ph@uni-hd.de

Prof. Takao Ikariya

Department of Applied Chemistry
Graduate School of Science and Engineering
Tokyo Institute of Technology
2-12-1 Ookayama, Meguro-ku,
Tokyo 152-8552, Japan
tikariya@apc.titech.ac.jp

Prof. Luis A. Oro

Instituto Universitario de Catálisis Homogénea
Department of Inorganic Chemistry
I.C.M.A. - Faculty of Science
University of Zaragoza-CSIC
Zaragoza-50009, Spain
oro@unizar.es

Prof. Qi-Lin Zhou

State Key Laboratory of Elemento-organic
Chemistry
Nankai University
Weijin Rd. 94, Tianjin 300071 PR China
qlzhou@nankai.edu.cn

Topics in Organometallic Chemistry

Also Available Electronically

Topics in Organometallic Chemistry is included in Springer's eBook package *Chemistry and Materials Science*. If a library does not opt for the whole package the book series may be bought on a subscription basis. Also, all back volumes are available electronically.

For all customers who have a standing order to the print version of *Topics in Organometallic Chemistry*, we offer free access to the electronic volumes of the Series published in the current year via SpringerLink.

If you do not have access, you can still view the table of contents of each volume and the abstract of each article by going to the SpringerLink homepage, clicking on "Chemistry and Materials Science," under Subject Collection, then "Book Series," under Content Type and finally by selecting *Topics in Organometallic Chemistry*.

You will find information about the

- Editorial Board
- Aims and Scope
- Instructions for Authors
- Sample Contribution

at springer.com using the search function by typing in *Topics in Organometallic Chemistry*.

Color figures are published in full color in the electronic version on SpringerLink.

Aims and Scope

The series *Topics in Organometallic Chemistry* presents critical overviews of research results in organometallic chemistry. As our understanding of organometallic structures, properties and mechanisms grows, new paths are opened for the design of organometallic compounds and reactions tailored to the needs of such diverse areas as organic synthesis, medical research, biology and materials science. Thus the scope of coverage includes a broad range of topics of pure and applied organometallic chemistry, where new breakthroughs are being made that are of significance to a larger scientific audience.

The individual volumes of *Topics in Organometallic Chemistry* are thematic. Review articles are generally invited by the volume editors.

In references *Topics in Organometallic Chemistry* is abbreviated Top Organomet Chem and is cited as a journal. From volume 29 onwards this series is listed with ISI/Web of Knowledge and in coming years it will acquire an impact factor.

Preface

Privileged ligands play a key role in the development of organometallic chemistry, homogeneous catalysis and metal-mediated and -catalysed organic synthesis. Among the monoanionic, multidentate ligands, the Cyclopentadienyl (Cp) fragment is no doubt the most frequently used metal-binding platform. In fact, the hallmark isolation and structural elucidation of ferrocene represented a key benchmark moment in the development of organometallic chemistry [1].

In recent times, monoanionic Pincer [2] ligands have also become one of the privileged ligand platforms and are being used with increasing success; indeed sometimes astonishing results in all the three of the fields mentioned above can be realised with a single pincer framework. In a similar fashion to the Cp ligands, the Pincers bind to a metal centre as a multidentate ligand but, in addition, often engenders a number of unanticipated properties both in the way it interacts and also interplays with the metal fragment(s). In this book, we focus on pincer ligands of the type ECE' (Fig. 1). Initially, Pincer ligands had been designed simply as platforms intended to enforce *trans*-spanning bisphosphine (PCP [3]) or bis-sulphide donors (SCS [4]) or to act as a rigid *mer*-tridentate (NCN [5, 6]) ligand. However, in present times, now some 40 years later, the pincer-ligand platform has developed into a multifunctional building block that is used in a wide variety of metal complexes for a number of more diverse applications. These can include, for example, bond activation, organic synthesis, supramolecular chemistry, homogeneous catalysis, polymer chemistry, photochemistry and novel energy-related science [7–12].

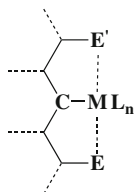


Fig. 1 Representation of the ECE' pincer–metal complexes with a central σ -M–C bond of a ML_n fragment to the monoanionic carbon centre (E and E' are neutral donor atom groupings) featuring in the chemistry covered in this volume. Note that in most compounds, the pincer ligand acts as a 6e ligand with both E and E' coordinating to M, see also Fig. 2 in ref. [13].

The aim of this volume of *Topics in Organometallic Chemistry* is to focus on the latest developments of pincer–metal chemistry based on complexes derived from monoanionic ligands as defined in Fig. 1.

This volume starts with a brief outline of both the scope of organometallic chemistry that makes use of the ECE' pincer platform and the applications of these compounds. In the following contributions, the main emphasis is on a discussion of the various synthetic aspects of new pincer–metal complexes (both transition and main group metals and metalloids), their structural features and details as to the interplay between the ligand's backbone and the metal centre (non-innocent behaviour, photochemical properties, etc.). Furthermore, this volume contains reports on both the synthesis and the applications of the pincer–metal complexes in metal-catalysed organic synthesis and materials science.

We hope that this volume not only informs the reader about the newest developments of the carbon-based pincer platform as a privileged ligand but also acts as an inspiration to the reader to use pincer–metal complexes in their own scientific endeavours.

Utrecht, Netherlands
Rehovot, Isreal

Gerard van Koten
David Milstein

References

1. Nobel Prize to Fischer EO, Wilkinson G (1973). http://www.nobelprize.org/nobel_prizes/chemistry/laureates/1973/
2. van Koten G (1989) Coining of the name “Pincer”. *Pure Appl Chem* 61:1681
3. Moulton CJ, Shaw BL (1976) *J Chem Soc Dalton Trans* 1020
4. Errington J, McDonald WS, Shaw (1980) *J Chem Soc Dalton Trans* 2312
5. van Koten G, Jastrzebski JTBH, Noltes JG (1978) *J Organometal Chem* 148:233
6. van Koten G, Timmer K, Noltes JG, Spek AL (1978) *J Chem Soc Chem Commun* 250
7. Albrecht M, van Koten G (2001) *Angew Chem Int Ed* 40:3750
8. van der Boom ME, Milstein D (2003) *Chem Rev* 103:1759
9. Rybtchinski B, Milstein D (2004) *ACS Symp Ser* 885:70
10. Morales-Morales D, Jensen CM (eds) (2007) Elsevier, Oxford
11. van Koten G, Klein Gebbink RJM (2011) *Dalton Trans* 40:8731
12. Gunanathan C, Milstein D (2011) Bond activation by metal–ligand cooperation: design of “Green” catalytic reactions based on aromatization–dearomatization of pincer complexes. In: Ikariya T, Shibasaki M (eds) *Bifunctional molecular catalysis. Topics in organometallic chemistry*, vol 37. Springer, Heidelberg, pp 55–84
13. van Koten G (2012) The mono-anionic ECE-pincer ligand—a versatile privileged ligand platform: general considerations. In: van Koten G, Milstein D (eds) *Organometallic pincer chemistry. Topics in organometallic chemistry*, vol. 40 Springer, Heidelberg

Contents

The Monoanionic ECE-Pincer Ligand: A Versatile Privileged Ligand Platform—General Considerations	1
Gerard van Koten	
Noninnocent Behavior of PCP and PCN Pincer Ligands of Late Metal Complexes	21
Elena Poverenov and David Milstein	
Tuning of PCP Pincer Ligand Electronic and Steric Properties	49
Dean M. Roddick	
Metal Complexes of Pincer Ligands: Excited States, Photochemistry, and Luminescence	89
Gemma R. Freeman and J.A. Gareth Williams	
ECE-Type Pincer Complexes of Nickel	131
Davit Zargarian, Annie Castonguay, and Denis M. Spasyuk	
The Chemistry of Pincer Complexes of 13–15 Main Group Elements ...	175
Roman Jambor and Libor Dostál	
Pincer Complexes as Catalysts in Organic Chemistry	203
Kálmán J. Szabó	
Optically Active Bis(oxazolinyl)phenyl Metal Complexes as Multipotent Catalysts	243
Jun-ichi Ito and Hisao Nishiyama	
Pincer Complexes as Catalysts for Amine Borane Dehydrogenation	271
Anthony St. John, Karen I. Goldberg, and D. Michael Heinekey	

PC(<i>sp</i>³)P Transition Metal Pincer Complexes: Properties and Catalytic Applications	289
Dmitri Gelman and Ronit Romm	
Physical and Materials Applications of Pincer Complexes	319
Jennifer L. Hawk and Stephen L. Craig	
Index	353

The Monoanionic ECE-Pincer Ligand: A Versatile Privileged Ligand Platform—General Considerations

Gerard van Koten

Abstract During the past 40 years, the monoanionic, tridentate ligand platform that has been named “Pincer” has established itself as a privileged ligand in a variety of research and application areas. Exciting discoveries with NCN and PCP-pincer metal complexes in the late 1970s created a firm basis for the tremendous development of the field. Some of the basic findings are summarized with emphasis on the organometallic aspects of the ECE-pincer metal system.

Keywords Coordination properties · Decomposition pathways · Pincer ligand · Preparation · Reactivity · Stability

Contents

1	Introduction	2
2	Coordination Modes	3
3	Preparation of Pincer-Metal Complexes	6
4	Stability and Decomposition Pathways of Pincer-Metal Complexes	10
5	Reactions with Electrophiles	12
6	Reactions with Small Molecules	14
7	Pincer Complexes with Unusual Formal Oxidation States	15
8	Conclusion	17
	References	18

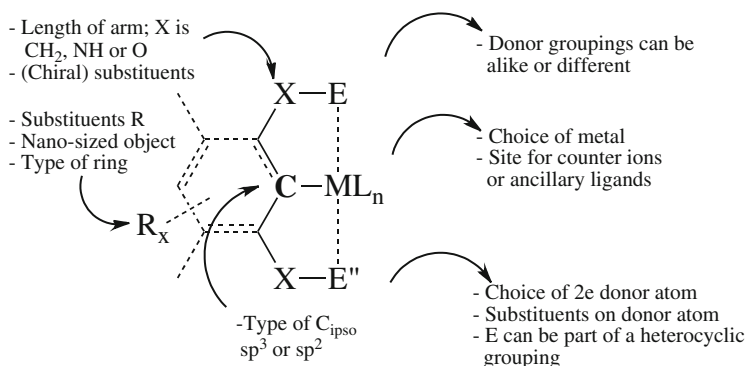


Fig. 1 The pincer-metal platform and the various possibilities to shape and modify it. The ECE'-pincer is potentially a six electron donor (similar to the Cp-anion)

1 Introduction

From the beginnings of “Pincer Chemistry” in 1976, the exploration of pincer-metal compounds mainly developed along the lines of the nature of the various donor atoms [1]. Whereas the pincer-transition metal chemistry primarily concentrated on the use of PCP- [2] and SCS-pincer ligands [3] (with the “soft” P- or S-donor sites), it was in the chemistry of copper, lithium, and the group 14 metals that researchers started to apply the NCN-pincer [4, 5] ligand (with the “hard” sp³ amine donor groupings). During the first 20 years, researchers mainly concentrated on ECE'-pincer ligands with a central phenyl (aryl) ring, bonded via its anionic C_{ippo} atom to a ML_n cationic unit and having two similar *ortho*-CH₂E substituents (E = PR₂, is PCP; E = SR, is SCS; E = NR₂, is NCN), coordinating to ML_n via its E-donors, see Fig. 1.

The present situation is an entirely different one; the monoanionic pincer ligand has emerged as a versatile “privileged” ligand platform indeed [1, 6–9]. All pincer-metal complexes have the central connection between the monoanionic site and the ML_n grouping as a common structural feature. The pincer ligands applied nowadays, however, show a striking variation of the nature of the ligand backbone. This includes changes in the formal hybridization of C_{ippo}, (either sp³ or sp²), the *ortho*-substituents (including the length and structure of the tether connecting C_{ippo} and the donor atom), the nature of the donor atom sites, as well as the substituents present in the backbone, etc. The available space (i.e., void space) [10] remaining around the metal center after coordination of the ECE'-pincer ligand is determined by both the actual coordination mode of the pincer and the steric requirements of the groupings present as the *ortho*-substituents. A further influence is exerted by the atomic radii of the donor atoms (cf. the atomic radius of N is much smaller than P or S), the form of its formal hybridization, the E–M bond length, and the nature of the X–E connector (e.g., amine or imine, part of a heterocyclic ring, phosphine or phosphite, P = S, etc.). The influence of the nature of the donor atom on the void

space has been studied in some detail for a series of bisamino-pincers [11] and more extensively for the corresponding bisphosphine-pincer ligand [10].

The ECE-pincer can act as a 2e (via C_{ipso}), 4e (via E and C_{ipso}), or as a 6e (via all three sites) donor ligand. A schematic representation of the pincer platform is shown in Fig. 1. A large series of reviews is available describing the various aspects of pincer chemistry from a variety of perspectives (e.g., [1, 6–9, 11–16]).

This chapter serves to illustrate some of the similarities and diversity of the various pincers used in the (now) vast field of pincer-metal chemistry. Various aspects such as the coordination properties, the synthetic routes available, the stability and reactivity properties of pincer-metal compounds in relation to applications as sensors and in catalysis will be touched upon with some illustrative examples. Many of these latter aspects are playing a role in the following chapters of this volume in which the current state of the pincer-metal chemistry in various directions is extensively outlined.

2 Coordination Modes

For square planar ECE-pincer transition metal complexes, a *mer*-E,C,E coordination mode for the terdentate, monoanionic aryl-pincer ligands was anticipated and initially indeed, that is what was also found. Inspection of the Cambridge Crystallographic Data Base [17] reveals about 350 hits for PCP-, 330 for NCN-pincers while SCS- and OCO-pincer metal complexes were represented by about 90 and 50 solid-state structures, respectively. In particular, the fixed, *trans*-orientation of the two phosphorous donor sites in the PCP-pincer metal complexes represented a new structural feature in transition metal chemistry, see Fig. 2. It is noteworthy that a few years after Shaw reported on the well-known *aryl* PCP-pincer metal-d⁸ complexes, he followed this up by publishing the synthesis of a series of complementary four- and five-coordinate *alkyl* PCP-pincer (Ir) complexes in which C_{ipso} is a monoanionic C_{sp3}-atom [18]. In five- and in six-coordinate complexes, the acute bonding angles cause a specific binding preference for the pincer. Specifically in five-coordinate complexes in a *tbp* configuration, an axial-equatorial-axial spanning is observed and for the square planar (*sp*) structures a binding to three basal sites is noted. In contrast, six-coordinate complexes contain all three binding sites situated in the same plane with the remaining three ligands in a plane perpendicular to it.

Whereas the terdentate bonding mode is the dominant one in the complexes with the PCP- and SCS-pincer ligands, in complexes with the NCN-pincer ligand a more diverse variety of binding modes was encountered even in early studies, see Fig. 2 [1, 6, 7]. For example, the monodentate *C*- and bidentate *C, N*-bonding mode was noted in complexes in which the amine ligands could not compete with, or were replaced by, stronger donor ligands. Moreover, when either one or both amine ligands could not bind to the metal, for example due to quaternarization by protonation, the resulting complexes contained a monodentate *C*-bonded NCN-pincer [19].

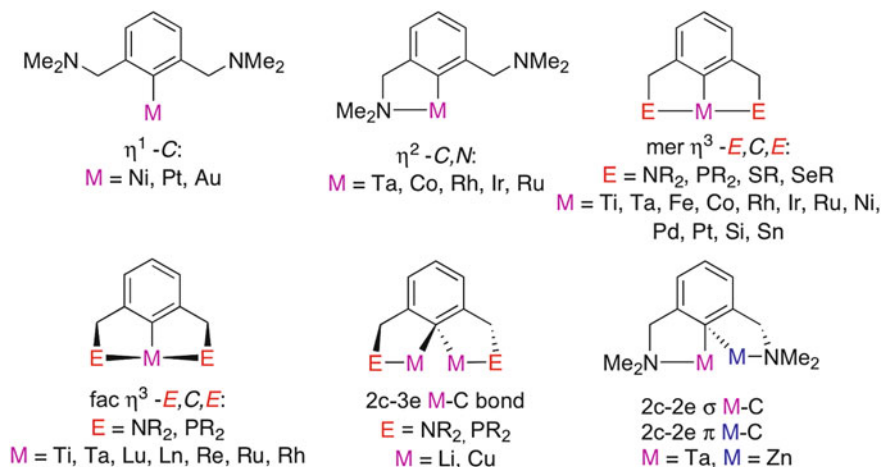


Fig. 2 The coordination modes found for ECE-pincer-metal complexes in the solid state [6]

It is noteworthy that free (noncoordinated) amine substituents can represent a steric constraint at the coordination site *cis* to the C_{ipso}-M bond. This aspect has been observed in NCN-pincer metal-d⁸ complexes that contain either a monodentate C- or bidentate C, N-bonded NCN-ligand. Often this steric interference may cause inter- or intramolecular rearrangements of the pincer-metal motif; a few examples of this are discussed below, cf. Fig. 9.

Many of the differences between the binding observed in the NCN- and OCO-pincers on one hand and the PCP- and SCS-ligands on the other hand are related to the differences in coordination properties of the various donor atoms: the respective N- and O-donor sites are σ -donors while the phosphine donor atoms have both σ -donor and π -accepting properties. Moreover, steric factors also affect the actual binding mode of the pincer ligand. In comparing the NCN- and PCP ligands, it is most likely the difference in atomic radii between N and P that make steric constraints in R₂N- vs. R₂P-groupings dominant, i.e., the M-P bond is longer than the M-N bond while increasing the size of the R groups in the R₂N grouping greatly affects the Lewis basicity of this grouping [11]. The difference in binding properties of the various donor groupings has recently been observed in hybrid ECE' complexes. For example, in NCP-pincer metal-d⁸ complexes the amino-phosphine pincer ligand is C, P-chelate bonded through its *ortho*-phosphine substituent whereas the *ortho*-amine substituent remains largely noncoordinating [20, 21].

Initially, the surprising observation was made in the fact that the NCN-pincer ligand can even display a *fac*-terdentate binding mode, see Figs. 2 and 3, a structural feature that on the basis of the presumed rigidity of the central benzene ring was not anticipated [1, 4, 5]. This *fac*-NCN-binding is characterized by a rather acute (amine)N-M-N(amine) bond angle (between 110° and 120°) and in some cases a characteristic bending of the arene C₆-ring [22]. This has been found for, e.g., NCN-pincer Ti [23], Ru [22], and La [24] complexes, see Fig. 3. An early example

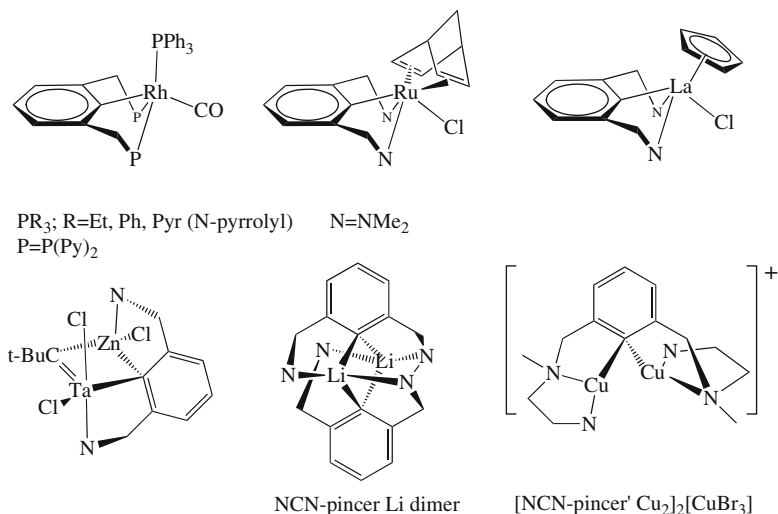


Fig. 3 Some of the bonding modes of the ECE'-pincer ligand

with PCP-pincer ligands is the *fac*-Rh(PCP)(PR₃)(CO) complexes containing (*N*-pyrrolyl)phosphinemethyl *ortho*-substituents as the phosphine donors of the pincer ligand [25]. More recently, several *fac*-PCP-pincer iridium complexes have been prepared and characterized with strongly electron withdrawing phosphine groupings containing organic fragments such as -CF₃ [10, 26]. These results indicate that the *fac* binding can be imposed upon the ECE-pincer ligand by selecting the right combination of steric and/or electronic properties (σ -donating or π -accepting or a combination) of the E donor atom groupings. Finally, it appears that this *fac*-binding leads to ECE-pincer metal complexes that have similar structural features to those of the corresponding Cp-metal compounds [6].

The three center-two electron bridge-bonding (via C_{ipso}) to two metals is another bonding mode that was established early on in both NCN-pincer lithium [27, 28] and copper [29] chemistries. In these complexes, C_{ipso} binds to two metal centers while the *ortho*-amine substituents are each coordinated to one of the bridged metal centers, see Figs. 2 and 3. For the corresponding PCP pincer lithium complex, selective bis *ortho*-lithiation of the corresponding (pincer)arene ligand could only be achieved for the ligand in which P represents the (dimethylphosphino)methyl group [30]. Apparently, this grouping has just the appropriate combination of "hard" σ -donating character and steric size to stabilize the final PCPLi compound and prevent alternate deprotonation reactions of, e.g., benzylic protons. Another type of bridge bonding is observed in TaCl₂(μ -*Ct*Bu)(NCN)(ZnCl) in which C_{ipso} is σ -bonded to the Ta(V) center and π -bonded to Zn, see Fig. 3 [31].

A special structural feature of the pincer platform is the fact that the aryl ring of the *mer*-bonded ECE-pincer ligand (in metal-d⁸ complexes) is nearly co-planar with the principal coordination plane of the bonded metal. This can allow for electronic communication between the metal and the aryl σ - and π -systems

[32, 33]. This type of interaction is clearly observable in the trend of the catalytic activity of $\text{NiX}(\text{C}_6\text{H}_2(\text{CH}_2\text{NMe}_2)_2\text{-2,6-R-4})$ catalysts observed in Kharasch reactions (i.e., the addition of halocarbons to alkenes) when the *para*-substituent R in the aryl group is varied from electron donating ($-\text{OMe}$) to electron withdrawing ($-\text{NO}_2$) [32, 34]. However, in a similar series of *para*-substituted $(\text{PCP})\text{Ir}(\text{CO})$ derivatives ($\text{P}=\text{CH}_2\text{P}(\text{t-Bu})_2$) only a small range of CO IR stretching frequencies is observed for a similar series of R groups [35].

In a number of studies, the *para*-R substituent can be used to bind ECE-pincer metal complex to either insoluble supports or to soluble, supramolecular systems. For example, this technique has been used to make nano-sized homogeneous (dendritic) catalysts [9, 36, 37], or to use the ECE-pincer metal units themselves as building blocks for the construction of supramolecular arrays [9, 38, 39].

3 Preparation of Pincer-Metal Complexes

The actual route for the synthesis of the various types of ECE'-pincer metal compounds depends largely on the nature of the E and E' donor atoms. In general, when at least one of the donor sites is a soft donor atom, direct and regioselective biscyclometallation (route a, $Z = \text{H}$ or Br and $M = \text{d}^8\text{-metal}$) of the corresponding arene ligand is observed. In particular, when $\text{E}=\text{E}' = -\text{PR}_2$ or $-\text{SR}$ and $M = \text{d}^8\text{-metal}$, the corresponding *mer*-ECE-pincer metal compound can be obtained in high yields. Also in the case of X-E being $\text{C}=\text{N}$ (e.g., imine [40], oxazoline [41]) regioselective biscyclometallation can be achieved (via C-H bond activation), but in a number of cases the oxidative addition route using C-Br bond cleavage is required or leads to superior product yields. For most of the NCN-diamino pincer ligands, the synthesis of the corresponding pincer metal complex requires a two-step process involving the prior, often in situ, synthesis of the corresponding pincer lithium reagent followed by transmetallation (route a, b in Fig. 4) [6, 42]. In order to avoid separation problems, the bis-*ortho*-lithiation must be quantitative. This can be achieved by the use of an *apolar* solvent and avoiding the presence of any polar or coordinating reagent/solvent(s) in the reaction mixture, cf. the solvent dependence of the yields of the two regioisomers in Fig. 4. As an alternative direct route, lithiation of a bromide-pincer can be used, again followed by transmetallation. For NCN-pincer complexes, C-SiMe_3 bond cleavage has likewise been employed for the regioselective introduction of various metal groupings to the NCN-ligand platform [43].

Synthesis of PCP-pincer metal- d^8 complexes by C-Z bond activation (e.g., $Z = \text{OR}$, OSiR_3 , or CR_3) has been demonstrated and its mechanistic details have been studied in detail ([8], Chapter 5 in [9]).

An alternate route for pincer compounds, that are not easily accessible by other routes, involves a transcyclometallation reaction which also affords for the selective interchange of a $\text{C}_{\text{ipso}}\text{-H}$ for a $\text{C}_{\text{ipso}}\text{-M}$ between *two different* ECE-pincer platforms, see Fig. 5 [44]. This transcyclometallation protocol proved its usefulness

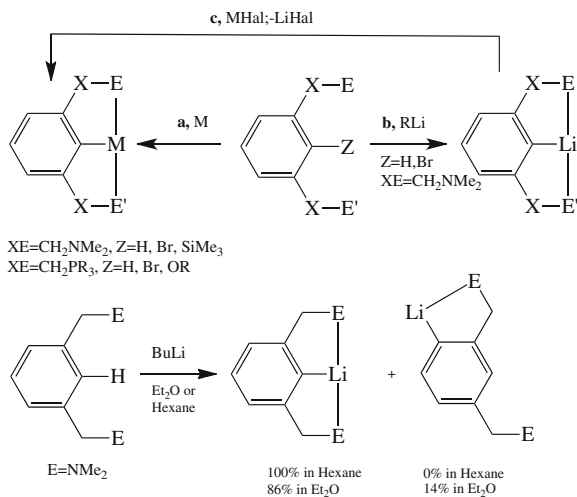


Fig. 4 Summary of some of the (cyclo)metallation routes and starting materials for the various types of ECE-pincer ligands (*top*). Example of the solvent dependence of the regioselective lithiation of NCN-pincers (*below*)

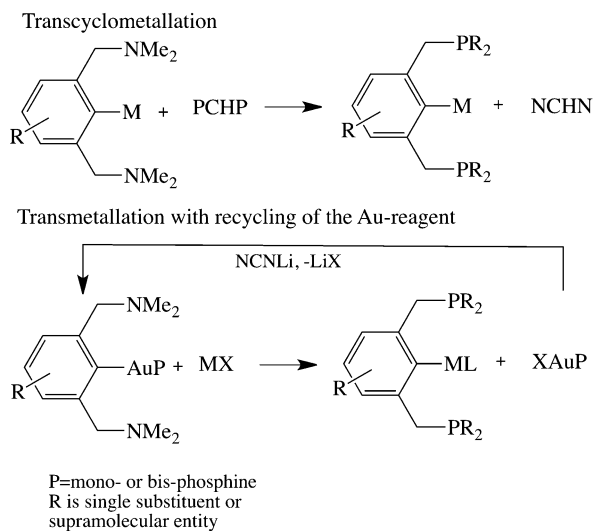


Fig. 5 Two alternate routes for the selective synthesis of pincer metal salts in which the difference in coordination strength of the various donor atoms is the driving force for reaction

in the clean synthesis of, for example, dendritic structures with multiple PCP-pincer ruthenium units [45].

Routes that make use of transmetalation via either tin or mercury intermediates are less advantageous for environmental reasons. However, the reaction of the

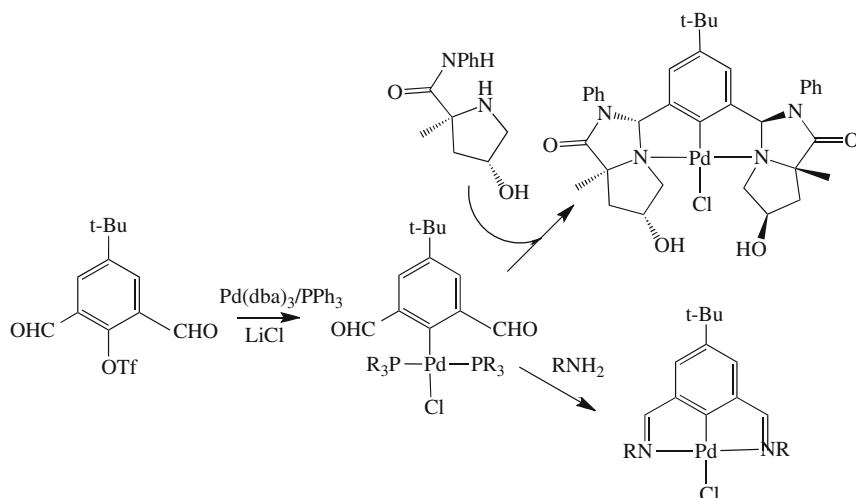


Fig. 6 Synthesis of a chiral NCN-pincer palladium complex by postderivatization

corresponding pincer gold(I) derivative with even highly electrophilic metal salts leads to the direct synthesis of the corresponding pincer metal derivative. It has been demonstrated that the gold(I) phosphine salt that is quantitatively formed can be recovered and recycled, see Fig. 5 [41, 46].

When more elaborate pincer metal platforms are needed, a choice can be made between either a route in which the organic pincer ligand is synthesized first which is then followed by the regioselective introduction of the metal grouping or an alternate protocol involving prior introduction of the metal center followed by functionalization of the resulting organometallic ECE-pincer metal compound. For example, the chiral pincer palladium compound shown in Fig. 6 has been synthesized by making first the bis-*ortho*-hydrocarbonylpincer palladium compound (which in itself is an interesting case with monodentate-*C*-coordination of the OCO-pincer ligand) followed by a condensation reaction that creates the final ligand framework [47].

In the next step, the aldehyde groupings have been selectively converted into the chiral *ortho*-scaffolds. The resulting enantiopure compound was one of the first chiral pincer-metal complexes to be successfully used in enantioselective catalysis [41, 47].

Further examples of postderivatization of pincer metal compounds are shown in Fig. 7 [48]. Starting from the iodo-bromo pincer compound, a chemoselective biscycloplatination has been carried out followed by a selective lithiation through a lithium-iodide exchange reaction (with *t*-BuLi) at low temperature. Subsequently, the lithium-platinum pincer intermediate is quenched in situ with an appropriate electrophile. This is the preferred route for the synthesis of materials carrying a large number of pincer metal entities, e.g., in the case of the synthesis of metallodendrimers for which purification procedures are cumbersome or

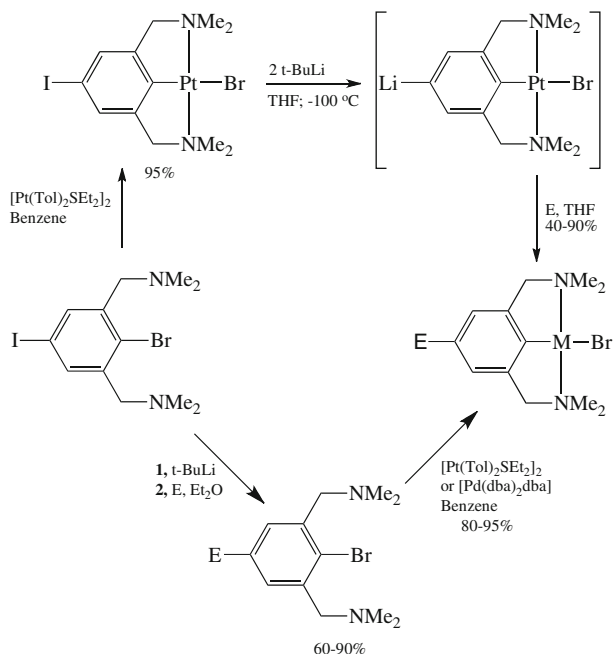


Fig. 7 Electrophile E is, e.g., CO₂, MeSSMe, ClP(OEt)₂, ClSiMe₃, M = Pd or Pt. Comparison of the synthesis of *para*-E-NCN-pincer palladium and platinum complexes by either prior metal introduction and then functionalization or synthesis of the complete pincer ligand and then metal introduction (postderivatization)

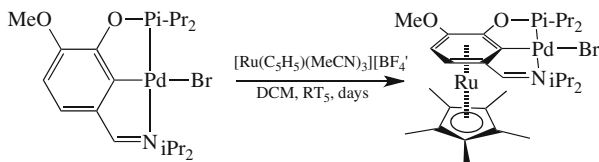


Fig. 8 Example of postderivatization resulting in the direct synthesis of a chiral η^5 -Cp^{*}- η^6 -(PCN-pincer Pd bromide)Ru complex

impossible. Moreover, starting from the in situ prepared lithium–platinum pincer intermediate (see Fig. 7), N-, O-, and α -C-pincer metal substituted α -aminoacids are accessible as well as polypeptides having distinctly positioned pincer metal moieties [48].

Another example of postderivatization, i.e., the direct synthesis of a chiral ruthenium–palladium–pincer derivative, as exemplified in Fig. 8, has recently been reported. Its synthesis involves an electrophilic attack of the arenophile [Cp^{*}RuL₃]³⁺ on the arene ring of a planar chiral imine-phosphite pincer palladium bromide compound [49].

4 Stability and Decomposition Pathways of Pincer-Metal Complexes

Many of the ECE-pincer metal compounds have a surprising thermal stability (decomposition on heating far above 100 °C) in comparison to similar compounds having the same set of E- and C-bonded groupings that are not, however, connected to one another as is the case in the ECE-pincer platform. Moreover, this stability is often accompanied with unmatched chemical stability of the central σ -M-C and the tridentate pincer motif, i.e., the pincer metal interaction is retained in reactions of pincer metal complexes with materials such as water, weak acids; small molecules such as CO, SO₂, isocyanides, dihydrogen, dihalides; oxidizing agents such as dioxygen, iodosobenzene, peroxides; and reducing agents such as organolithiums or even Na metal. However, these reagents can facilitate changes in the formal oxidation state of the metal or may lead to a modification of the pincer arene moiety, cf. Figs. 7 and 8. An interesting example is the reaction of PdCl(i-Pr-PCP) with Na in THF that leads to collapse of the mononuclear complex to an unprecedented bispincer bispalladium complex containing one nonplanar diamagnetic Pd(II) center P,C-bonded to two PCP ligands whereas the second palladium center is a 14e Pd(0) center that binds the remaining P ligands of each of the two PCP ligands (for an X-ray, see Fig. 7 in [21]). Regeneration into the original PdCl(i-Pr-PCP) complex occurs on oxidation of the (PCP)₂Pd(II)Pd(0) complex with either a silver salt or electrophile such as benzyl chloride [50].

A seminal discovery was the extremely high catalytic activity (5×10^5 t) of PCP-pincer palladium complexes such as 2,6-bis[(diiso-propylphosphino)methyl]phenylpalladium TFA in Heck coupling reactions (e.g., the reaction of iodobenzene with methyl acrylate in NMP) at temperatures around 140 °C during extended reaction times (>300 h) [51]. Extensive research followed this observation and clarified both the mechanistic aspects of this and led to the study of related C-C coupling reactions (e.g., Heck, Suzuki-Miyaura reactions, etc.). Hence, the search for the optimum structure reactivity relationship of the pincer palladium precursor in this catalysis area was undertaken. At first, a Pd(II)/Pd(IV) cycle, with retention of the pincer palladium platform, was proposed as a likely mechanism. However, consensus seems to have revised these hypotheses on consideration that the pincer metal compound acts simply as a precatalyst. The pincer-metal species decompose gradually thereby producing palladium nanoparticles (NPs) upon which the actual conversion of reagents to products occurs on the NP surface [52–54]. This view is supported by experiments with supported pincer-palladium catalysts, through experiments with poisoning reagents (e.g., Hg), the results of kinetic and spectroscopic studies as well as from the application of computational techniques. Ample evidence is now available that pincer palladium complexes function as sacrificial species that gradually produce Pd NPs. The rate at which this decomposition occurs is important for the size and constitution of the resulting Pd NPs. If the decomposition of the pincer palladium precursor is too fast, catalytically inactive Pd black is formed. Finally, it cannot be excluded that the pincer-arene species formed (next to

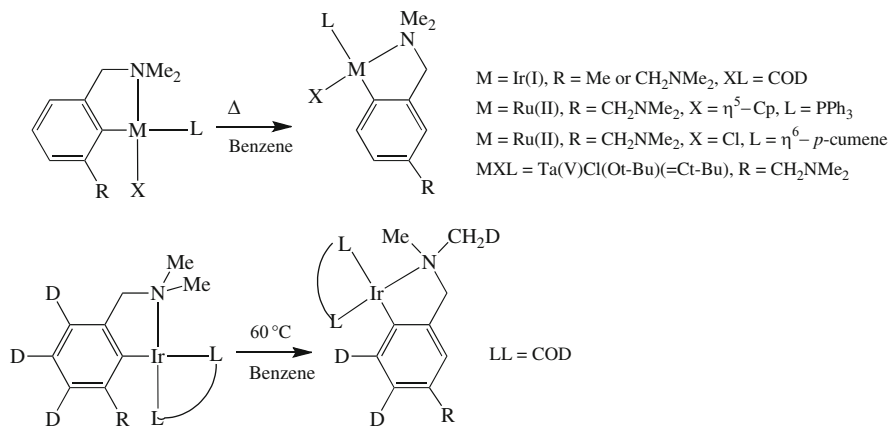


Fig. 9 Documented rearrangements of the NCN-pincer metal platform in NCN-pincer Ir(I), Ru(II), Ta(V) compounds

the Pd NPs) will ultimately also affect the size and constitution of the NPs by absorbing onto their surfaces. Consequently, this interaction can be expected to affect the aggregation rate of these particles as well as the activity of the Pd(0) species at the surface in subsequent catalytic cycles.

In the above-mentioned reactions, it is the cleavage of the $M\text{-C}_{\text{ipso}}$ bond that is the cause for the (controlled) decomposition of the ECE-pincer metal compound at higher temperatures. This (homolytic) bond cleavage leads to destruction of the pincer metal platform. However, loss of the unique stability and reactivity properties of the ECE-pincer metal motif can also occur as a result of selective rearrangement of the bis-*ortho*-E, C, E arrangement to an *ortho*-E, *para*-E, C one.

In addition to the decomposition by homolytic $C\text{-M}$ bond cleavage, occurrence of this selective rearrangement is of particular importance when ECE-pincer metal compounds are used as catalysts or, for example, in sensor devices. So far, these rearrangements have been observed for NCN-diamino pincers if the metal is Ir(I) [55], Ru(II) [56], or Ta(V) [57], again emphasizing the importance of the nature of the donor atoms E. In Fig. 9 a number of the observed rearrangements are summarized. The observed rearrangement of the pincer anion from the bis-*ortho*-N, C_{ipso} , N arrangement to an *ortho*-N, *para*-N, C_{ipso} could be extensively documented by model experiments and selective deuterium-labeling protocols. With all three metals, this rearrangement was kinetically driven by the fact that in the final *ortho*-N, *para*-N-isomer, the other *ortho*-position next to the C_{ipso} -metal bond is occupied by a C-H functionality rather than a free, sterically demanding CH_2NMe_2 -grouping, as would be the case in the bis-*ortho* chelated-isomer. This makes the C-H activation and subsequent oxidative addition processes irreversibly running towards the formation of a thermodynamically most stable isomer. It must be noted that these processes occur intramolecularly and provide almost quantitative yield of the rearranged product. For the NCN-pincer Ir COD compound, the result

of ^2H -labeling is shown. The process of apparent 1, 3-Ir migration involves four separate C–H bond activations in concert, see [55] for details of this rearrangement mechanism.

5 Reactions with Electrophiles

Organometallic complexes often undergo M–C bond cleavage in the presence of acids. In contrast to this common observation, a great variety of ECE-pincer metal complexes are stable in acidic media. However, in the case of NCN-pincers the *ortho*-amine substituent can become quaternarized (with retention of the M–C_{ipso} bond), see Fig. 10. As it is exclusively the free amine donor that undergoes quaternarization, this observation indicates that the M–N bond undergoes regular dissociation–association [19].

Reactions with electrophiles (e.g., H₂, X₂, alkyl halides) can lead to oxidative addition at the metal center of a pincer-metal complex with concomitant change of its formal oxidation state. Subsequent reductive elimination either involves the ancillary ligands or C_{ipso} of the pincer itself. Exchange of the ancillary halide ligands, as shown in Fig. 10, is observed in the reaction of Me–I with the neutral NCN-platinum halides [58]. However, the reaction of the cationic NCN-pincer platinum water complex with Me–I [58, 59] (and, e.g., benzyl iodide) [60, 61] takes an entirely different course (Fig. 10). This reaction results in quantitative formation of the arenium species via a 1, 2-shift of the methyl group along the Pt–C_{ipso} bond thus *making* a new C–C bond. In this process the formal Pt(II) oxidation state remains unchanged. During the entire process the *N, C, N*-terdentate bonding mode is retained. This is even the case when, in a subsequent reaction, the arenium cation is reacted with, for example, a strong but sterically large nucleophile. As shown in Fig. 10, the regioselective attack of the nucleophile at the 4-position converts the arenium ring into a 2, 5-cyclohexadien-1-yl. Smaller nucleophiles attack at the kinetically more favorable 2-position (not shown in the figure). These processes, including the C–C bond *cleavage*, are reversible [62]. However, once the C_{aryl}–C_{methyl} product has dissociated from the Pt center, the reaction becomes irreversible. That is, the free 1-Me-2,6-(Me₂NCH₂)₂C₆H₃ cannot re-coordinate to a suitable Pt salt in the proper coordination geometry to effect cleavage of the C_{aryl}–C_{methyl} bond and hence re-enter in the reaction scheme shown in Fig. 10. This observation underscores the great importance on activation processes that are governed by the coordination power of the *ortho*-donor atoms in pincer-metal complexes and pincer-type starting materials. This is nicely demonstrated in reactions of 1-alkyl-2, 6-(R₂PCH₂)₂benzene compounds with PtCl₂COD as studied extensively by Milstein et al., see Fig. 11 [21].

This reaction occurs via prior P, P-bidentate chelate bonding of the arene pincer and then proceeds to initiate alkyl–C bond cleavage which produces the corresponding PCP-pincer Pt(II)Cl compound [63]. This reaction is only one of the many examples documented in which cleavage of the C_{aryl}–C_{methyl} bond in

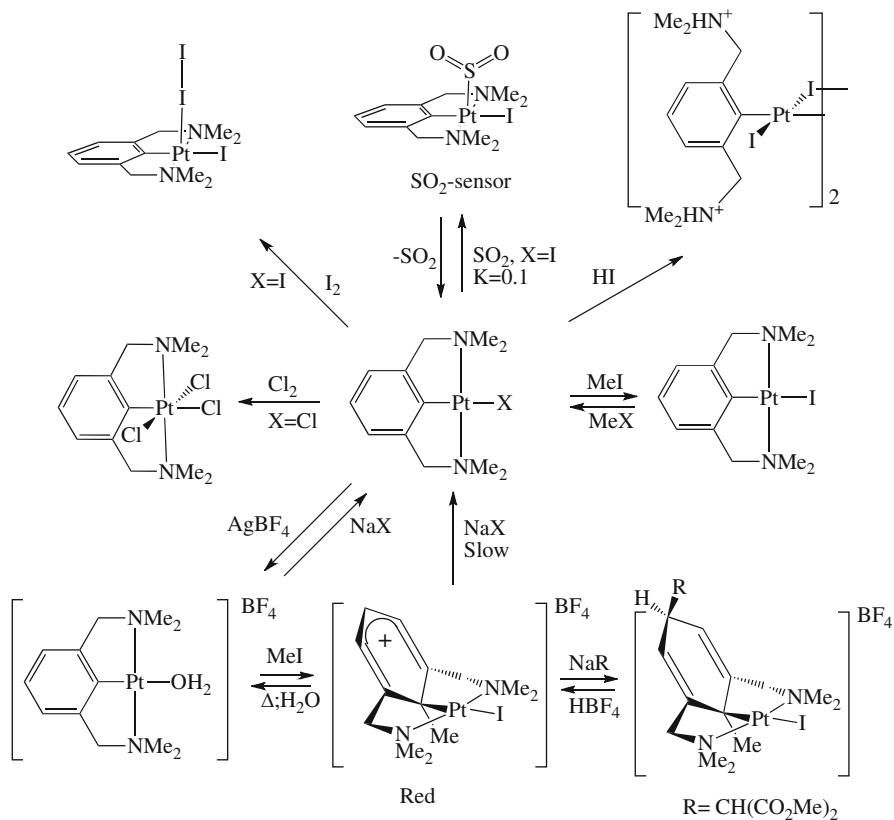


Fig. 10 Some reactions of NCN-pincer Pt(II) halide with electrophiles

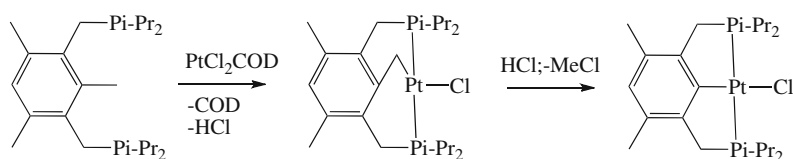


Fig. 11 C_{aryl}-C_{methyl} bond cleavage with a platinum salt

1-alkyl-2, 6-(R₂PCH₂)₂benzene compounds is demonstrated for a range of different metal salts (i.e., Ni, Rh, Ir, Ru, and Os). More importantly, detailed thermodynamic, kinetic, and computational studies of these processes led to vital mechanistic insights into the conditions facilitating such C-C bond cleavage processes [16]. Emerging from these studies are catalytic C-C bond activation chemistry of relevance to a number of areas of organic synthesis (see Fig. 12) [64].

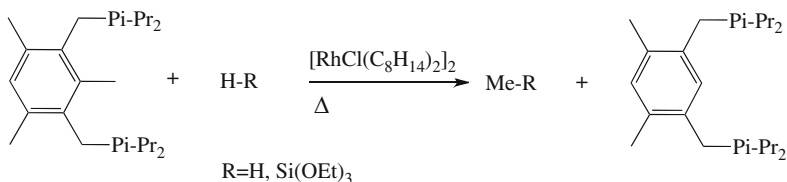


Fig. 12 Example of catalytic methyl transfer using C_{aryl}–C_{methyl} bond activation

6 Reactions with Small Molecules

During the past two decades, the pincer metal platform is increasingly used as a homogeneous (pre-)catalyst in organic synthesis and as a building block in supramolecular chemistry. This successful use of the pincer motif as a privileged ligand derives from the fact that the M–C_{ipso} bond of many ECE-pincer metal compounds appears to be relatively unreactive. In addition, because of its compact size and flexible and versatile bonding properties, the pincer ligand leaves a number of well-defined coordination sites and space available for other reactivity. Small molecules that are commonly used in homogeneous catalysis coordinate and react at the metal site of the pincer metal platform without interfering with the M–C_{ipso} bond. For example, reactions with CO yield CO complexes, whereas complexes with a similar binding set of monodentate ligands would readily undergo insertion chemistry to yield the corresponding acyl complexes. Similarly NCN-pincer platinum compounds bind *reversibly* SO₂ (in solution [65] and in the solid-state [66]) yielding the corresponding η¹-SO₂ coordination complexes (see Fig. 11) rather than yielding the otherwise expected SO₂-insertion products. Most interestingly, σ-coordination of CH₄ to the Rh center of PNP pincer Rh complexes has been recently documented [67].

Reactions with molecular hydrogen yield initially the H₂-coordination complexes and subsequently hydride derivatives. In many cases, the pincer-metal platform shows surprising stability toward reductive elimination of the hydride with C_{ipso} that would otherwise lead to formation of the arene pincer, i.e., would lead to destruction of the catalyst [cf. 21, 55]. An interesting example is the reaction of PCP (e.g., bis-phosphine [68] and bis-phosphinite [69]) pincer Ir complexes with alkanes that yield alkenes via dehydrogenation (cf. the σ-coordination of CH₄ mentioned earlier). Crucial in these reactions is the stability of the incipient ECE-pincer Ir manifold in the Ir-hydride intermediates towards decomposition (via C_{ipso}–H bond formation). A PCP-pincer Ir catalyst with considerable stability is shown in Fig. 13 that also visualizes the application of immobilization of homogeneous pincer catalysts on solid supports [70].

These heterogenized pincer catalysts combine the advantage of homogeneous (high reactivity and selectivity) catalysis with those of their immobilized analogues (easy separation of the catalyst from products) as was first demonstrated for dendritic NCN-pincer Ni catalysts [36].

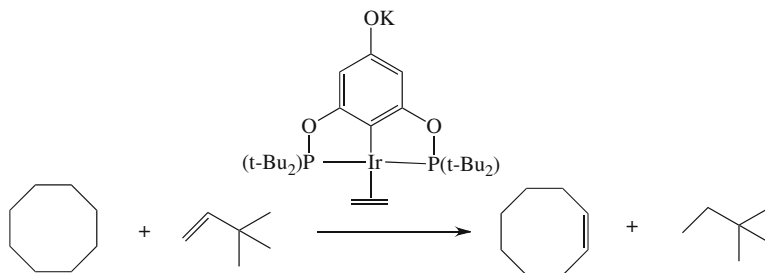


Fig. 13 Example of a highly active and recyclable (immobilized on γ -alumina) PCP-Ir catalyst for transfer dehydrogenation of alkanes

7 Pincer Complexes with Unusual Formal Oxidation States

The actual composition of the pincer platform affects both the reactivity and the thermodynamic stability of the pincer metal manifold particularly with respect to the formal oxidation state of the metal. An early observation represents the isolation of stable, paramagnetic NCN-pincer Ni(III)Br₂, see Fig. 14, from the reaction of NCN-Ni(II)X with X₂.

The facile and selective oxidation of the NCN Ni(II) to the corresponding Ni(III) complex pointed to the effect that the strong σ -donating NMe₂ groupings have on the NCN d⁸-metal manifold in facilitating oxidation of the metal and hence stabilization of the resulting higher oxidation state. NCN-Ni(III)X₂ is both water and air-stable whereas related NCN-Ni(II)X oxidizes readily under these conditions to the Ni(III) species [34, 36, 37, 71]. Likewise, the presence of stabilizing *ortho*-phosphine ligands allows for the synthesis of thermally stable low valent platinum species Na[PCP-Pt(0)] [21, 72]. Relatively rare NCN-pincer Rh(II) species (NCN is “benbox”) were isolated from the reaction of RhCl₃(H₂O)₃ with the corresponding benbox arene precursor via C–H bond activation. The complex is a paramagnetic species with a $S = 1/2$ ground state. These Rh(II) species are thermally unstable and disproportionate via a complex reaction scheme [73]. Following the early synthesis of NCN-pincerSn(II)R (R=Cl, *p*-tolyl) compounds [74], a whole series of pincer compounds were isolated and characterized having a variety of ECE'-pincer ligands [75]. Interestingly, reduction of the Sn(II) compounds with K [HBEt₃] afforded, instead of the desired NCNSn(II) hydride, the unusual distannyne NCNSn(I)Sn(I)NCN [76].

Until several years ago, all stable (isolated and characterized) organocopper compounds were copper(I) species [77], whereas organocopper(II) and (III) species were frequently postulated as reaction intermediates and/or transient species. This is also true for the few known pincer copper compounds, e.g., [N'NCNN/Cu(I)₂]₂[Cu(I)Br₃], see Fig. 3 [29]. This situation changed entirely when researchers started to use macrocyclic pincer type ligand platforms [78–80]. NCNCu(III)X₂ is a representative of new and exciting chemistry that afforded both stable and isolable

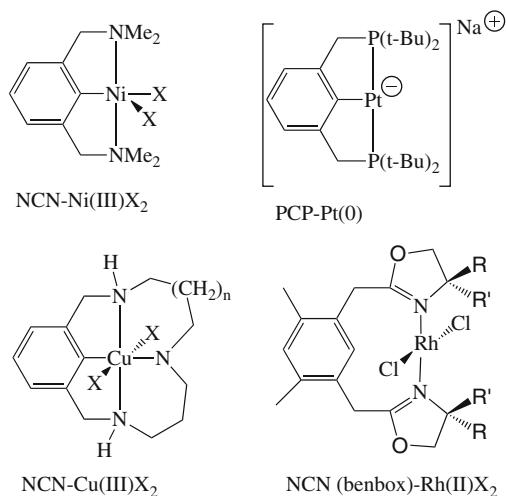


Fig. 14 Four complexes with the metal center in uncommon formal oxidation state

(paramagnetic) organocopper(II) and diamagnetic copper(III) compounds. Synthesis of these materials commonly involves C–H bond activation routes in which the $\text{C}_{\text{ipso}}\text{--Cu}$ bond is directly formed in a reaction of the arene derivative with a Cu(I) or Cu(II) salt. These compounds are frequently used as models in mechanistic studies directed towards the understanding of copper catalyzed C–X bond formation reactions, see for example ref [80].

Unprecedented oxidative coupling process occurred when 4-methylphenolbiphosphine was reacted with $[\text{RhCl}(\text{cyclooctene})_2]_2$ (alternately in the presence of an oxidant), see Fig. 15. This reaction afforded the PCP-pincer rhodium chloride complex, resulting from C–O bond cleavage chemistry and a bimetallic stilbenequinone.

This latter complex contains a rare η^2 -coordination of the two rhodium centers to the quinonoid C=O double bonds [21, 81]. In the case of NCNRu(II)terpy , oxidative coupling with two equivalents of Cu(II)Cl_2 yielded the diruthenium(III) 4, 4'-C–C coupled NCN-pincer compound, and *para*-chloroNCNRu(III)terpy [82]. The detailed mechanism of this reaction has been described. It involves prior one electron oxidation of NCNRu(II)terpy to the corresponding Ru(III) species. In this latter compound, the unpaired electron is partly localized on the *para*-position. In the second step, either dimerization (by oxidative C–C bond formation) or oxidative halogen transfer (from Cu(II)Cl_2 with formation of a C–Cl bond at the *para*-position) occurs [83].

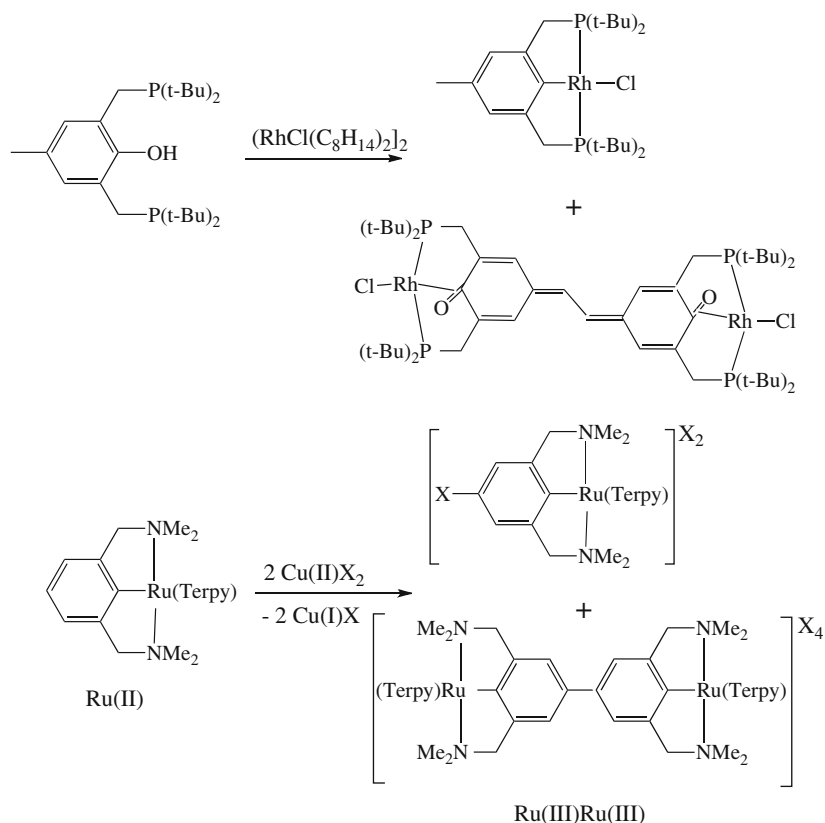


Fig. 15 Two reactions involving oxidative conversion of the pincer metal platform

8 Conclusion

Initially the pincer ligand motif, see Fig. 1, had been considered as an interesting monoanionic, terdentate ligand but with seemingly simple structural features. Since that time however (35 years later), its successful application in organometallic chemistry, materials and catalysis science has led to fascinating and novel chemistry and many unprecedented results. Many of these discoveries are a demonstration of the subtle interplay that occurs in these pincer-metal compounds between the monoanionic pincer ligand and metal center; it has given the pincer ligand motif the status of privileged ligand in organometallic chemistry that it features nowadays. Moreover, in many aspects the properties and structural features of the pincer ligand complement those of the unique cyclopentadienyl anion.

In recent years, novel pincer ligands have been developed, see Fig. 1, different connections X now representing, for example, $(\text{CH}_2)_n$ (n is e.g., 1 or 2), NH, or O and in which the anionic ligand site is not C but is a monoanionic N- or P-center

resulting in a central covalent M–N and M–P bond, respectively. Moreover, rather than having similar flanking ligands pincer platforms with two different ligand arms flanking the central covalent bond have been developed, cf. [84]. The understanding of the way these changes of the pincer platform affects both the structural features of the resulting pincer metal complexes and their reactivity is only at its beginning.

References

1. van Koten G (1989) Coining of the name “Pincer”. *Pure Appl Chem* 61:1681
2. Moulton CJ, Shaw BL (1976) *J Chem Soc Dalton Trans* 1020
3. Errington J, McDonald WS, Shaw BL (1980) *J Chem Soc Dalton Trans* 2312
4. van Koten G, Jastrzebski JTBH, Noltes JG (1978) *J Organomet Chem* 148:233
5. van Koten G, Timmer K, Noltes JG, Spek AL (1978) *J Chem Soc Chem Commun* 250
6. Albrecht M, van Koten G (2001) *Angew Chem Int Ed* 40:3750
7. Rietveld MHP, Grove DM, van Koten G (1997) *New J Chem* 21:751
8. van der Boom ME, Milstein D (2003) *Chem Rev* 103:1759
9. MoralesMorales D, Jensen CM (eds) (2007) *The chemistry of pincer compounds*. Elsevier, Oxford
10. Roddick DM (2012) Tuning of PCP pincer ligand electronic and steric properties. In: van Koten G, Milstein D (eds) *Organometallic pincer chemistry*. Topics in organometallic chemistry, Vol. 40. Springer, Heidelberg
11. van Beek JAM, van Koten G, Ramp MJ, Coeljaarts NC, Grove DM, Goubitz K, Zoutberg MC, Stam CH, Smeets WJJ, Spek AL (1991) *Inorg Chem* 30:3059
12. Rybtchinski B, Milstein D (2004) *ACS Symp Ser* 885:70
13. van Koten G, Klein Gebbink RJM (2011) *Dalton Trans* 40:8731
14. Albrecht M, Lindner MM (2011) *Dalton Trans* 40:8733
15. Niu J-L, Hao X-Q, Gong J-F, Song M-P (2011) *Dalton Trans* 40:5135
16. Rybtchinski B, Milstein D (1999) Review on C–C activation. *Angew Chem Int Ed* 38:870
17. Cambridge Crystallographic Data Base, www.ccdc.cam.ac.uk.
18. Crocker C, Errington RJ, McDonald WS, Odell KJ, Shaw BL (1979) *J Chem Soc Chem Commun* 498
19. Davidson MF, Grove DM, van Koten G, Spek AL (1989) *J Chem Soc Chem Commun* 1562
20. Gandelman M, Vigalok A, Shimon LJW, Milstein D (1997) *Organometallics* 16:3981
21. Poverenov E, Milstein D (2012) Non-innocent behavior of PCP and PCN pincer ligands of late metal complexes. In: van Koten G, Milstein D (eds) *Organometallic pincer chemistry*. Topics in organometallic chemistry, Vol. 40. Springer, Heidelberg
22. Sutter J-P, James SL, Steenwinkel P, Karlen T, Grove DM, Veldman N, Smeets WJJ, Spek AL, van Koten G (1996) *Organometallics* 15:941
23. Donkersvoort JG, Jastrzebski JTBH, Deelman B-J, Kooijman H, Veldman N, Spek AL, van Koten G (1997) *Organometallics* 16:4174
24. Hogerheide MP, Boersma J, Spek AL, van Koten G (1996) *Organometallics* 15:1505
25. Kossoy L, Iron M, Rybtchinski B, Ben-David Y, Konstantinovskii L, Martin JML, Milstein D (2005) *Chem Eur J* 11:2319
26. Adams JJ, Arulsamy N, Roddick DM (2011) *Organometallics* 30:697
27. Jastrzebski JTBH, van Koten G, Konijn M, Stam CH (1982) *J Am Chem Soc* 104:5490
28. Smeets WJJ, Spek AL, van der Zeijden AAH, van Koten G (1987) *Acta Crystallogr C* 43:3778
29. Wehman E, van Koten G, Erkamp CJM, Knotter DM, Jastrzebski JTBH, Stam CH (1989) *Organometallics* 8:94
30. Pape A, Lutz M, Muller G (1994) *Angew Chem Int Ed Engl* 33:2281

31. Abbenhuis HCL, Feiken N, Haarman HF, Grove DM, Horn E, Kooijman H, Spek AL, van Koten G (1991) *Angew Chem Int Ed* 30:996
32. van de Kuil LA, Grove DM, Gossage RA, Zwikker JW, Jenneskens LW, Drenth W, van Koten G (1997) *Organometallics* 16:1985
33. Freeman GR, Williams JAG (2012) Metal complexes of pincer ligands: excited states, photochemistry, and luminescence. In: van Koten G, Milstein D (eds) *Organometallic pincer chemistry. Topics in organometallic chemistry, Vol. 40*. Springer, Heidelberg
34. Zargarian D, Castonguay A, Spasyuk DM (2012) ECE-type pincer complexes of nickel. In: van Koten G, Milstein D (eds) *Organometallic pincer chemistry. Topics in organometallic chemistry, Vol. 40*. Springer, Heidelberg
35. Goettker-Schnetmann I, White PS, Brookhart M (2004) *Organometallics* 23:1766
36. Knapen JWJ, van der Made AW, de Wilde JC, van Leeuwen PWNM, Wijkens P, Grove DM, van Koten G (1994) *Nature* 372:659
37. Kleij AW, Gossage RA, Klein Gebbink RJM, Brinkmann N, Reijerse EJ, Kragl U, Lutz M, Spek AL, van Koten G (2000) *J Am Chem Soc* 122:12112
38. Yount WC, Juwarker H, Craig SL (2003) *J Am Chem Soc* 125:15303
39. Huck WTS, van Veggel FCJM, Reinhoudt DN (1996) *Angew Chem Int Ed Engl* 35:1213
40. Hoogervorst WJ, Goubitz K, Fraanje J, Lutz M, Spek AL, Ernsting JM, Elsevier CJ (2004) *Organometallics* 23:4550
41. Ito J-I, Nishiyama H (2012) *Synlett* 23:509
42. Gossage RA, Jastrzebski JTBH, van Koten G (2005) *Angew Chem Int Ed* 44:1448
43. Steenwinkel P, Gossage RA, Maunula T, Grove DM, van Koten G (1998) *Chem Eur J* 14:763
44. Dani P, Karlen T, Gossage RA, Smeets WJJ, Spek AL, van Koten G (1997) *J Am Chem Soc* 119:11317
45. Dijkstra HP, Albrecht M, Medici S, van Klink GPM, van Koten G (2002) *Adv Synth Catal* 344:1135
46. Churhuryukin AV, Huang R, van Faassen EE, van Klink GPM, Lutz M, Chadwick JC, Spek AL, van Koten G (2011) *Dalton Trans* 40:8887
47. Takenaka K, Minakawa M, Uozumi Y (2005) *J Am Chem Soc* 127:12273
48. Rodriguez G, Albrecht M, Schoenmaker J, Ford A, Lutz M, Spek AL, van Koten G (2002) *J Am Chem Soc* 124:5127
49. Bonnet S, Li J, Siegler MA, von Chrzanowski LS, Spek AL, van Koten G, Klein Gebbink RJM (2009) *Chem Eur J* 15:3340
50. Frech C, Shimon LJW, Milstein D (2005) *Angew Chem Int Ed* 44:1709
51. Ohff M, Ohff A, van der Boom ME, Milstein D (1997) *J Am Chem Soc* 119:11687
52. Sommer WJ, Yu K, Sears JS, Ji Y, Zheng X, Davis RJ, Sherrill CD, Jones CW, Weck M (2005) *Organometallics* 24:4351
53. Yu K, Sommer WJ, Richardson JM, Weck M, Jones CW (2005) *Adv Synth Catal* 347:161
54. Bergbreiter DE, Osburn PL, Freis JD (2005) *Adv Synth Catal* 347:172
55. van der Zeijden AAH, van Koten G, Luijk R, Nordemann RA (1988) *Organometallics* 7:1549
56. Steenwinkel P, James SL, Gossage RA, Grove DM, Kooijman H, Smeets WJJ, Spek AL, van Koten G (1998) *Organometallics* 17:4680
57. Rietveld MHP, Klumpers EG, Jastrzebski JTBH, Grove DM, Veldman N, Spek AL, van Koten G (1997) *Organometallics* 16:4260
58. Terheijden J, van Koten G, Vinke IC, Spek AL (1985) *J Am Chem Soc* 107:2891
59. Grove DM, van Koten G, Louwen JN, Noltes J, Spek AL, Ubbels HJC (1982) *J Am Chem Soc* 104:6609
60. Albrecht M, Spek AL, van Koten G (2001) *J Am Chem Soc* 123:7233
61. Albrecht M, Spek AL, van Koten G (1999) *J Am Chem Soc* 121:11898
62. Grove DM, van Koten G, Ubbels HJC (1982) *Organometallics* 1:1366
63. van der Boom ME, Kraatz HB, Hassner L, Ben-David Y, Milstein D (1999) *Organometallics* 18:3873
64. Liou SY, van der Boom ME, Milstein D (1998) *Chem Commun* 687

65. Albrecht M, Gossage RA, Frey U, Ehlers AW, Baerends EJ, Merbach AE, van Koten G (2001) *Inorg Chem* 40:850
66. Albrecht M, Gossage RA, Lutz M, Spek AL, van Koten G (2000) *Nature* 406:970
67. Bernskoetter WH, Schauer CK, Goldberg KI, Brookhart M (2009) *Science* 326:553
68. Xu W-W, Rosini, Gupta M, Jensen CM, Kaska WC, Krogh-Jespersen K, Goldman AS (1997) *Chem Commun* 2273
69. Göttker-Schnetmann I, White PS, Brookhart M (2004) *J Am Chem Soc* 126:1804
70. Huang Z, Brookhart M, Goldman AS, Kundu S, Ray A, Scott SL, Vicente BC (2009) *Adv Synth Catal* 351:188
71. Grove DM, van Koten G, Mul P, Zoet R, van der Linden JGM, Legters J, Schmitz JEJ, Murall NW, Welch AJ (1988) *Inorg Chem* 27:2466
72. Schwartsburd L, Cohen R, Konstantinovski L, Milstein D (2008) *Angew Chem Int Ed* 47:3606
73. Gerisch M, Krumper JR, Bergman RG, Tilley TD (2003) *Organometallics* 22:47
74. Jastrzebski JTBH, van der Schaaf PA, Boersma J, van Koten G, Zoutberg MC, Heijdenrijk D (1989) *Organometallics* 8:1373
75. Jambor R, Dostál L (2012) The chemistry of pincer complexes of 13–15 main group elements. In: van Koten G, Milstein D (eds) *Organometallic pincer chemistry. Topics in organometallic chemistry, Vol. 40*. Springer, Heidelberg
76. Jambor R, Kašná B, Kirschner KN, Schurmann M, Jurkschat K (2008) *Angew Chem Int Ed* 47:1650
77. van Koten G, Jastrzebski JTBH (2010) Structural organocopper chemistry. In: Rappoport Z, Marek I (eds) *The chemistry of organocopper compounds, vol 1*. Wiley, Chichester
78. Xifra R, Ribas X, Llobet A, Poater A, Duran M, Sola M, Stack TDP, Benet-Buchholz J, Donnadiou B, Mahia J, Parella T (2005) *Chem Eur J* 11:5146
79. Pawlicki M, Kahska I, Latos-Grazynski L (2007) *Inorg Chem* 46:6575
80. Huffman LM, Stahl SS (2011) *Dalton Trans* 40:8959
81. van der Boom ME, Zubkov T, Shukla A, Rybtchinski B, Shimon LJW, Rozenberg H, Ben-David Y, Milstein D (2004) *Angew Chem Int Ed* 43:5961
82. Steenwinkel P, Grove DM, Veldman N, Spek AL, van Koten G (1998) *Organometallics* 17:5647
83. Wadman SH, Havenith RWA, Lutz M, Spek AL, van der Klink GPM, van Koten G (2010) *J Am Chem Soc* 132:1914
84. Gossage RA (2011) *Dalton Trans* 40:8755

Noninnocent Behavior of PCP and PCN Pincer Ligands of Late Metal Complexes

Elena Poverenov and David Milstein

Abstract Pincer complexes are generally viewed as stable compounds in which the pincer ligand framework remains unchanged during stoichiometric and catalytic reactions. However, there are now several cases in which the pincer ligand itself undergoes transformations that result in extraordinary reactivity of the metal complex and formation of unusual species. In the current chapter, we review our work on “noninnocent” reactivity modes of various PCP and PCN-type pincer ligands of Rh, Ir, Ru, Os, Pd, and Pt. Participation of the arene ring in the reactivity of PCP type complexes has led to formation of unprecedented quinonoid complexes, including complexes in which the pincer ligand adopts structures of quinone methides, thioquinone methides, xylylenes, methylene arenium, and oxo-arenium compounds. In addition, pincer systems can collapse and be regenerated under redox conditions, and reduction can lead to a ring-localized radical anion complex. The generation of C–H agostic arene PCP complexes has led to new insights regarding the C–H bond activation process, and the effect of CO ligands on it.

Keywords Pincer ligands, xylylene complex, quinone methide complex, thioquinone methide complex, phenoxonium complex, methylene arenium complex, agnostic pincer complex, late transition metals, reactive intermediates

Contents

1	Introduction and Background	22
2	Arene System Perturbation	23
2.1	Quinone Methides and Quinonoid Compounds	23
2.2	Phenoxonium Cation Complex	25
2.3	Self-Oxidation of a Phenolate Complex to a Bimetallic Stilbene Quinone	27
2.4	σ -Coordinated Naphthyl Radical Anion	29

E. Poverenov • D. Milstein (✉)

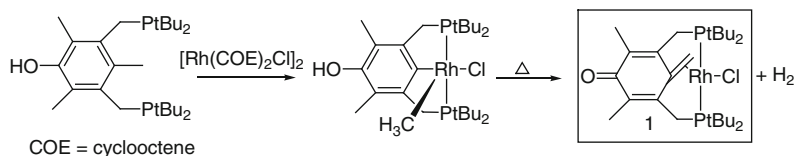
Department of Organic Chemistry, The Weizmann Institute of Science, 76100 Rehovot, Israel
e-mail: david.milstein@weizmann.ac.il

3	Agostic Systems	30
3.1	sp^3 C–H and sp^2 C–H Agostic Ruthenium Complexes	31
3.2	Unexpected Role of CO in C–H Oxidative Addition	33
4	Collapse and Regeneration	36
4.1	Redox Induced Collapse and Regeneration	36
4.2	A Pincer-Type Anionic Pt(0) Complex	38
5	Hemilabile Pincer-Type PCN Ligand	39
5.1	Anionic Complexes Based on a Hemilabile PCN Ligand	40
6	Conclusions	43
	References	44

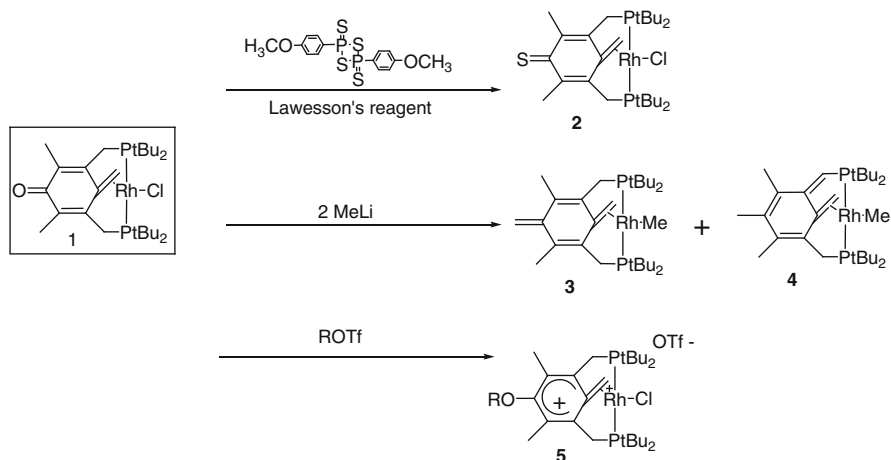
1 Introduction and Background

Pincer-type complexes constitute a large family of important compounds in organometallic chemistry [1–5]. Such complexes play key roles in chemical transformations relevant to organic synthesis, catalysis, bond activation, mechanistic studies, and the design of new materials [6, 7]. By systematic ligand modifications and/or by variation of the metal center it has been possible to readily control their reactivity and stability. The first pincer complexes, reported in the early 1970s, were PCP-type pincer complexes [8]. Since then, such pincer complexes have been utilized in various studies, including bond activation studies, such as carbon–carbon bond activation [9–11], formation of carbene species [12], trapping of elusive compounds [13], and in various catalytic applications [1, 2, 14]. For instance, PCP-type d^8 metal complexes have been utilized in alkane dehydrogenation [15–18] and C–C bond forming reactions such as Heck [19–22] and Suzuki [23–25] coupling.

While traditionally pincer complexes are viewed as stable compounds in which the pincer ligand framework remains unchanged during stoichiometric and catalytic reactions, in some cases the pincer ligand itself is capable of undergoing transformations that result in extraordinary reactivity of the metal complex and/or formation of unusual species. In the current chapter, we review the “noninnocent” reactivity modes of pincer-type complexes which were observed in our laboratory with PCP and PCN-type pincer ligands. Transformations of the aromatic part (to generate xylylene, methylene arenium, phenoxonium, radical anion type structures), C–H agostic coordination, N-arm hemilability, and collapse and regeneration of PCP and PCN pincer ligands are illustrated. Noninnocent behavior on PNP and PNN pyridine- and acridine-based complexes, which involve metal ligand cooperation by dearomatization of the pincer ligand [26, 27], and have led to the design of various catalytic reactions [28–32], are outside the scope of this chapter.



Scheme 1 Formation of the rhodium quinone methide complex **1** based on a PCP ligand



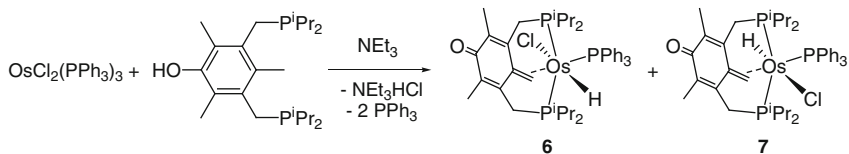
Scheme 2 Reactivity of the rhodium quinone methide complex **1**

2 Arene System Perturbation

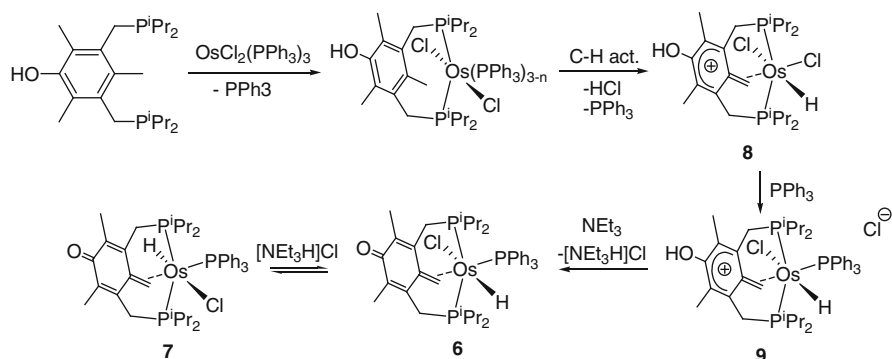
2.1 Quinone Methides and Quinonoid Compounds

Quinone methides (QMs) are quinones in which one oxygen atom has been replaced by an alkylidene group. They are highly reactive compounds which participate in many chemical and biological processes ([33–35] and references therein), such as formation of substituted phenols [36], Diels–Alder reactions [37], biosynthesis of the natural polymers [38–40], and radical scavenge [41, 42]. Quinone methides are also able to react with functional groups of biopolymers, such as DNA and proteins, and several drugs are believed to generate QM moieties as an active form [43, 44].

Quinone methides, especially the simple ones (those not having substituents at the exocyclic methylene group) are very unstable compounds and their isolation is seriously obstructed or requires extremely diluted solutions and low temperatures [45]. Being a highly polarized molecule, QMs rapidly react with both nucleophiles and electrophiles and easily convert to their bi-radical triplet form, opening up several additional reactivity patterns.



Scheme 3 Formation of osmium quinone methide complexes, **6** and **7**, based on a PCP ligand

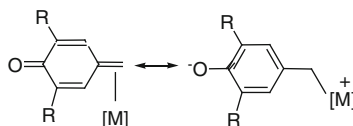


Scheme 4 Plausible mechanism leading to osmium quinone methide complexes

In the course of studies of the reactivity of pincer-type PCP complexes [9], we observed a dearomatization process to form the *para*-quinone methide complex (Scheme 1) [46]. In this process a phenolic pincer Rh(III) methyl complex, obtained by C–C activation [47] of the corresponding pincer ligand, was converted upon heating into the Rh(I) QM complex **1**.

The QM pincer complex is stable and allows selective modifications of the quinone methide moiety, still with no aromatization taking place, leading to rare species as part of the pincer framework (Scheme 2). Conversion of the QM carbonyl group to a thiocarbonyl group using Lawesson's reagent led to formation of the thioquinone methide complex **2** [46], while reaction with MeLi gave the *p*- and *o*-xylylene complexes, **3** and **4** [48]. Interestingly, even reaction with strong electrophiles, such as HOTf or Me₃SiOTf, did not lead to the expected rearomatization, but rather to the first stable methylene arenium complex **5** [48].

Utilizing a hydroxy substituted pincer ligand and a base, two isomeric quinone methide complexes of osmium, **6** and **7**, were prepared (Scheme 3) [49]. In the absence of base, the neutral and cationic methylene arenium intermediates, **8** and **9**, were isolated which, together with additional reactivity observations [49], allowed proposing a mechanistic pathway to formation of the quinone methides (Scheme 4). It was proposed that coordination of the pincer ligand to osmium followed by C–H activation and HCl elimination generates the zwitterionic complex **8** with a PCP ligand bearing a dearomatized methylene arenium form. Subsequent chloride



Scheme 5 Two resonance forms of a quinone methide coordinated to a metal center

substitution by a triphenylphosphine ligand affords the cationic methylene arenium complex **9**, which is deprotonated by the base to form the quinone methide complex **6**, while the generated triethylammonium chloride catalyzes the isomerization of **6** into a mixture of **6** and **7** (as observed in a separate experiment).

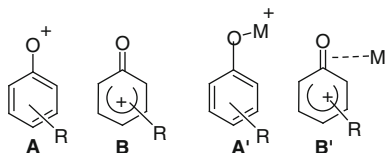
The dearomatization process toward quinonoidic structures observed with pincer ligand systems has led to the synthesis of nonpincer systems. Since quinone methides can be viewed as electron deficient conjugated olefins, their coordination to low valent metal complexes is expected to be very favorable [50], allowing the generation, trapping, and controlled release of these compounds, based on benzyloxy complexes (Scheme 5).

One-site coordinated quinonoid complexes (η^2 -coordinated quinone methide [51, 52] and methylene arenium [53] complexes), that can liberate the quinonoid moiety upon ligand substitution, were prepared. In addition, a platinum complex of a biologically compatible iminopyridine skeleton [54, 55] that can serve as an anchor for the generation and controlled release of quinone methides was developed [56].

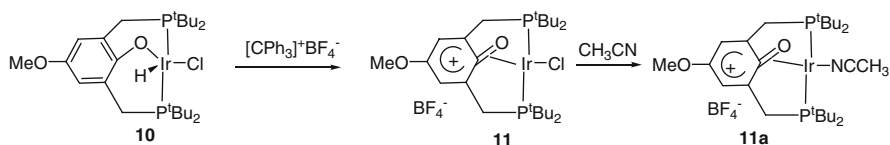
2.2 Phenoxonium Cation Complex

Phenoxonium cations, **A**, are reactive species involved as intermediates in many chemical and biological process, such as the oxidative coupling of phenols catalyzed by various metal complexes [57–60]. Too unstable to be isolated, phenoxonium cations have been generated as transients by various methods [61–63] and their trapping reactions have led to synthetic methodologies [64]. Mechanistic and theoretical studies of the oxidative coupling and polymerization of phenols have invoked a two-electron transfer process from a phenolate ligand to the metal [65, 66]. However, this process ($A' \rightarrow B'$) was never observed, and a phenoxonium cation (Scheme 6), complexed via the C–O group, or free, was never isolated, prior to the work described below.

Hydride abstraction from the iridium pincer complex **10** with $[Ph_3C]^+ BF_4^-$ led to dearomatization of the pincer part and formation of phenoxonium cation stabilized by metal coordination to the C=O bond, complex **11** (Scheme 7) [67]. The presence of positive charge at the phenoxonium ring causes dramatic downfield shifts of the aromatic carbon atoms in the $^{13}C\{^1H\}$ NMR spectrum. As most of the



Scheme 6 Free and complexed phenoxonium cations



Scheme 7 Formation of iridium phenoxonium complexes, **11** and **11a**, based on PCP ligand

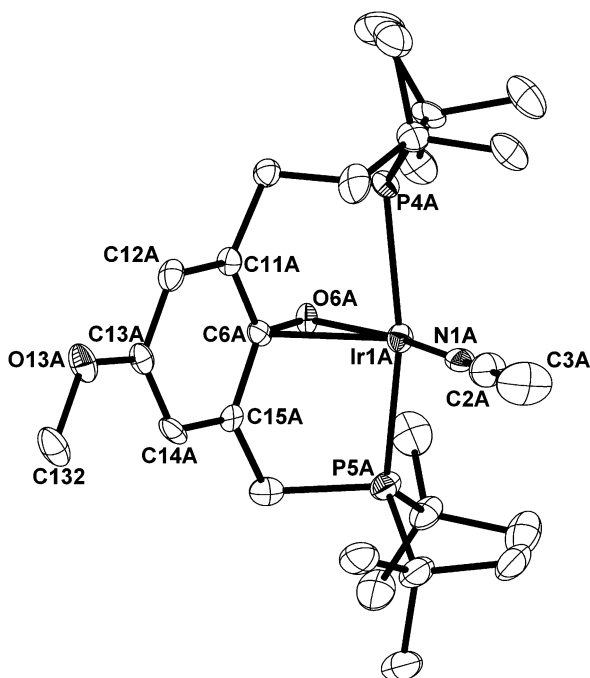


Fig. 1 ORTEP view of complex **11a** at 50 % probability. Hydrogen atoms are omitted for clarity. Bond lengths (Å): Ir1-O6 2.061, Ir1-C6 2.189, C6-O6 1.356, C6-C11 1.432

charge is localized at the ortho and para positions, the corresponding carbon atoms show a 20–40 ppm downfield shift compared with the neutral complex. Addition of acetonitrile to a solution of **11** resulted in a CH_3CN adduct **11a** (Scheme 7).

The X-ray structure of **11a** (Fig. 1) reveals a quinonoid compound in which the *exo*-cyclic double bond is η^2 -coordinated to the metal center. The long C–O bond (1.356 Å) indicates considerable back bonding from the metal center. The X-ray structure shows that all six carbon atoms are located in the same plane, with the coordinated oxygen atom pushed out of the plane by approximately 10° .

Isolation and characterization of complexes **11** and **11a** confirmed the postulated $A' \rightarrow B'$ process. While η^2 metal complexation to a C=C double bond is well known, no examples of such coordination to C=O bonds in quinonoid compounds have been reported. Complexes **11** and **11a** are, therefore, the first examples of metal-stabilized phenoxonium compounds.

2.3 Self-Oxidation of a Phenolate Complex to a Bimetallic Stilbene Quinone

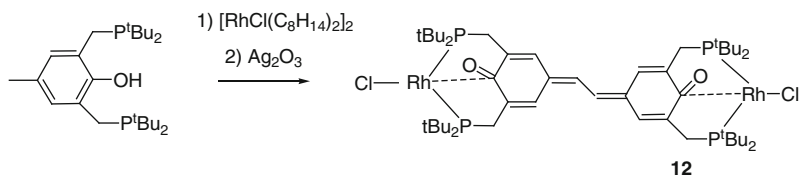
The oxidation chemistry of phenol derivatives is of much interest since it affords convenient routes to a variety of basic chemicals [68–70]. Selective oxidative C–C coupling of alkylated phenols to stilbenequinones is rare [71] and often requires strong oxidants [72, 73], while self-oxidation of phenols, in the absence of an external oxidant was not known. Such an unprecedented oxidative coupling process was observed in our group with a PCP ligand system [74]. Treatment of the 4-methylphenol bisphosphine ligand with $[\{\text{RhCl}(\text{cyclooctene})_2\}_2]$ followed by addition of Ag_2O resulted in the selective formation of the bimetallic complex with stilbenequinone derivate of PCP framework, **12** (Scheme 8).

Complex **12** was characterized by multinuclear NMR spectroscopy, UV/Vis spectroscopy, FAB mass spectrometry, and by single-crystal X-ray crystallography.

The X-ray structure of **12** reveals the formation of the bimetallic stilbenequinone structure and a rare η^2 -coordination mode of the metal centers to the quinonoid C=O double bonds (Fig. 2). The fourteen carbon atoms of the stilbenequinone backbone are located in the same plane with the 2 metal-coordinated oxygen atoms being out of the plane by about 0.3 Å.

The formation of a bimetallic product does not necessarily require an external oxidation reagent. NMR spectroscopy measurements indicate that the unstable Rh (III) hydride complex **13** is initially formed, while continuous stirring of the reaction mixture (still without Ag_2O) in a sealed vessel resulted in the disappearance of intermediate **13** with formation of the stilbenequinone **12** and complex **14** (Scheme 9). Formation of complex **14** by activation of the strong aryl C–O bond at room temperature is unexpected. Only a few cases of aryl–O bond cleavage of ethers or phenols under mild homogeneous reaction conditions were reported ([75–77] and references therein).

In sharp contrast to the reactivity of the rhodium complex, the analogous reaction with the $[\{\text{IrCl}(\text{cyclooctene})\}_2]$ precursor led to the Ir(III) phenoxy hydride complex **15** with no formation of bimetallic compounds even after 3 days of heating in a sealed pressure tube. Attempts to oxidize complex **15** with Ag_2O , O_2 ,



Scheme 8 Formation of the bimetallic stilbene quinone complex **12**

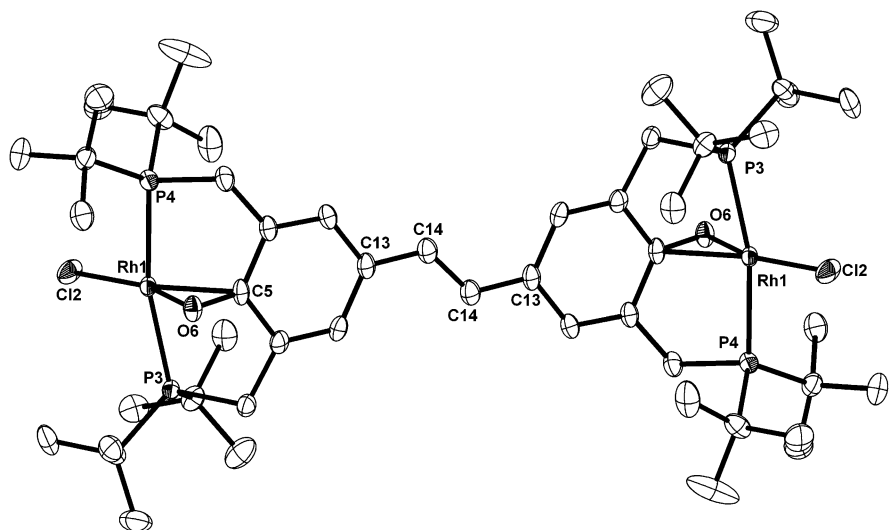
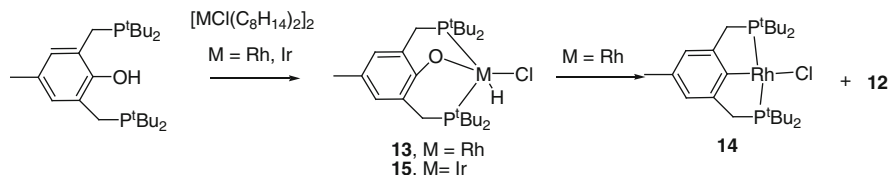
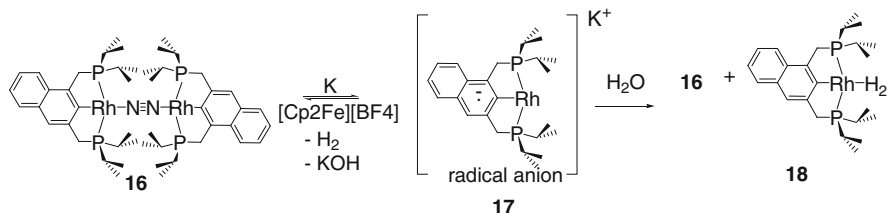


Fig. 2 An ORTEP diagram of complex **12** at 50 % of probability. Hydrogen atoms are omitted for clarity. Selected bond lengths (Å) and angles (°): Rh(1)-O(6) 2.056, Rh(1)-C(5) 2.186, Rh(1)-Cl(2) 2.316, Rh(1)-P(3) 2.329, Rh(1)-P(4) 2.346, C(5)-O(6) 1.325, C(13)-C(14) 1.395, C(14)-C(14A) 1.404; P(3)-Rh(1)-P(4) 167.84°



Scheme 9 Reactivity of rhodium and iridium precursors with a phenol-type pincer ligand, resulting in case of Rh(I) in C–O cleavage and oxidative coupling

ferrocenium hexafluorophosphate, or cyclic voltammetry resulted in mixtures of unidentifiable compounds. Apparently, the metal center plays an important role in the stilbenequinone complex formation. Although in both cases (**13**, **15**) a d^6 metal center was involved, the second-row metal hydride complex **13** is less stable and readily undergoes stilbenequinone formation, whereas the third-row metal hydride



Scheme 10 Formation of complex **17** by reduction of **16** with potassium metal and its reactivity towards water and ferrocene tetrafluoroborate

complex **15** is far more thermally robust but exhibits an unselective reactivity pattern upon oxidation.

2.4 σ -Coordinated Naphthyl Radical Anion

Aromatic radical anions have been extensively studied, involving structural, physical, theoretical, and reactivity aspects, and have found many applications [78–80]. They show interesting reactivity toward a variety of substrates such as alkanes, alkenes and alkynes, aliphatic and aromatic halides, silyl halides, aldehydes and ketones, sulfur dioxide, sulfonates and sulfonamides, carbon dioxide, dihydrogen, dinitrogen, as well as aliphatic and aromatic esters. An example for synthetic use is the reductive metalation of phenyl thioethers [81, 82], providing a useful route to the preparation of organo-alkali compounds difficult to prepare by other routes, such as tertiary organolithium compounds [83]. It occurred to us that it might be possible to generate a pincer-type radical anion complex.

The binuclear Rh pincer complex **16**, bearing an σ -bound naphthyl system, was utilized to generate an organometallic radical anion [84]. Formation of a stable radical anion by reduction of naphthalene is well known [78–80, 85]. Treatment of **16** with potassium metal in THF resulted in a new, NMR silent product, while EPR measurements gave rise to a strong, complex signal revealing formation of the paramagnetic anion radical complex **17** (Scheme 10).

The EPR signal of **17** has a g value of 2.0035, typical for aromatic hydrocarbon radicals (Fig. 3). The magnetic susceptibility of **17** was also measured by the Evans NMR method at 298 K in THF, giving a magnetic moment of 1.68 μ_B and confirming the presence of a single electron.

While the electron is localized in the naphthyl unit, reactivity of complex **17** is strikingly different from that of the naphthide radical anion (Scheme 10). Thus, when a THF solution of the reduced complex **17** was treated with water, immediate evolution of dihydrogen, with almost quantitative re-oxidation to the starting complex **16**, took place. A small amount (~10 %) of the dihydrogen complex ($\text{C}_{10}\text{H}_5(\text{CH}_2\text{P}^i\text{Pr}_2)_2\text{Rh}(\eta^2\text{-H}_2)$) (**18**) was also formed, as a result of the reaction of **16** with H_2 , as confirmed by the independent synthesis of **18**. No ligand protonation

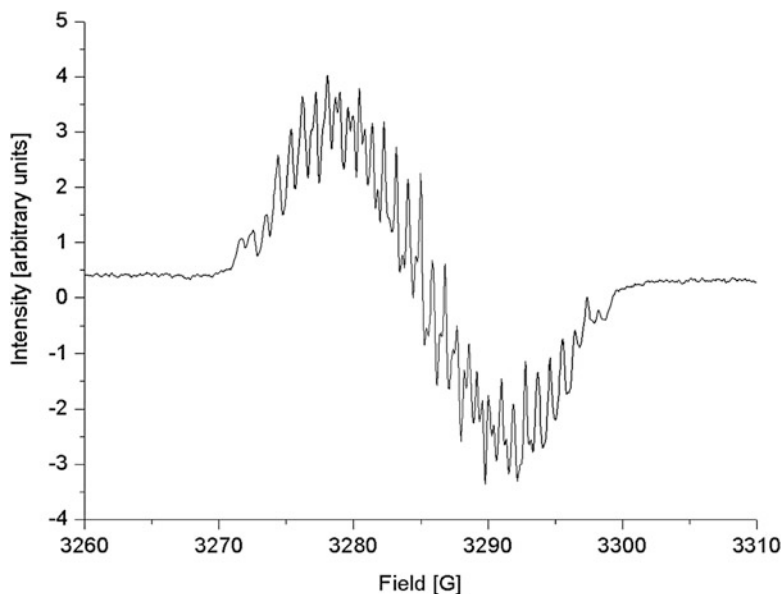
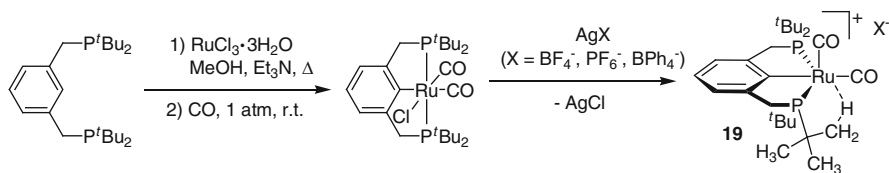


Fig. 3 EPR spectrum of **17** in THF at ambient temperature

of **17** was observed, in contrast to the known reactivity of the naphthalene radical anion, which undergoes protonation to yield 1,4-dihydronaphthalene and naphthalene in 1:1 ratio [86]. Apparently, the metal center dramatically influences the reactivity of the organic unit. This result is of interest regarding catalytic electron transfer reactions, with the possibility to store electrons in the aromatic ligand, with subsequent metal-centered reactions. The radical anion complex can be quantitatively oxidized to the diamagnetic complex, with no loss of structural integrity. Thus, upon treatment of **17** with $[\text{Fe}(\text{Cp})_2][\text{BF}_4]$, almost quantitative re-oxidation accompanied by formation of KBF_4 took place (Scheme 10).

3 Agostic Systems

Selective activation and functionalization of otherwise inert C–H bonds, such as those in alkanes or arenes, is a major challenge [87–89]. Despite intensive investigation of various artificial and natural systems there are not many examples of saturated C–H bond activation [90–92]. The C–H bond activation process may occur via several possible pathways that are generally dependant on the electron density on the metal center. Experimental and theoretical observations have shown that for electron-rich, low-valent transition metals C–H bond activation proceeds via $\eta^2(\text{C}-\text{H}\cdots\text{M})$ “agostic” intramolecular or σ C–H intermolecular intermediates [93–95]. Several metal complexes containing agostic $\eta^2(\text{C}-\text{H}\cdots\text{M})$ interactions



Scheme 11 Formation of sp^3 C–H agostic ruthenium complex **19**

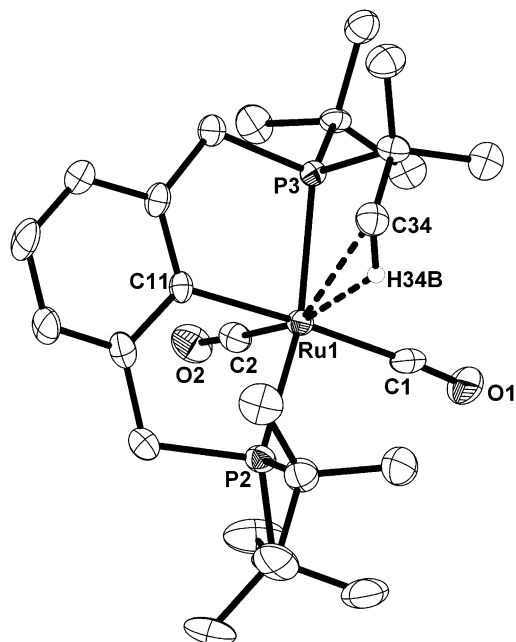
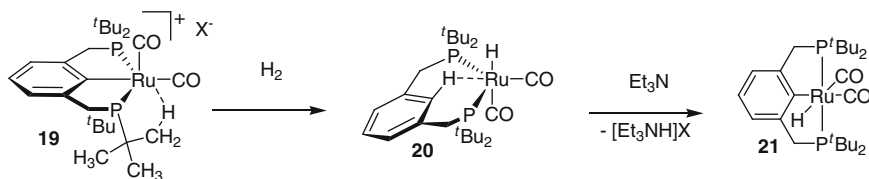


Fig. 4 ORTEP drawing of the molecular structure of **19** showing the agostic C–H...Ru(II) interaction. Thermal ellipsoids are drawn at 50 % probability

were isolated and fully characterized, including rhodium [96], iridium [97], and ruthenium [98–101] complexes based on cyclometallated bisphosphine ligands having *tert*-butyl or aryl substituents on both phosphorus donor atoms [2]. Herein, we present several examples of stable agostic complexes based on PCP pincer ligands.

3.1 sp^3 C–H and sp^2 C–H Agostic Ruthenium Complexes

As we observed, alkyl and aryl agostic interactions can occur in similar steric and electronic environments [102]. Halide abstraction from the 18 electron Ru(II)



Scheme 12 Transformation of **19** to an sp^2 C–H agostic complex **20** and formation of the neutral complex **21**

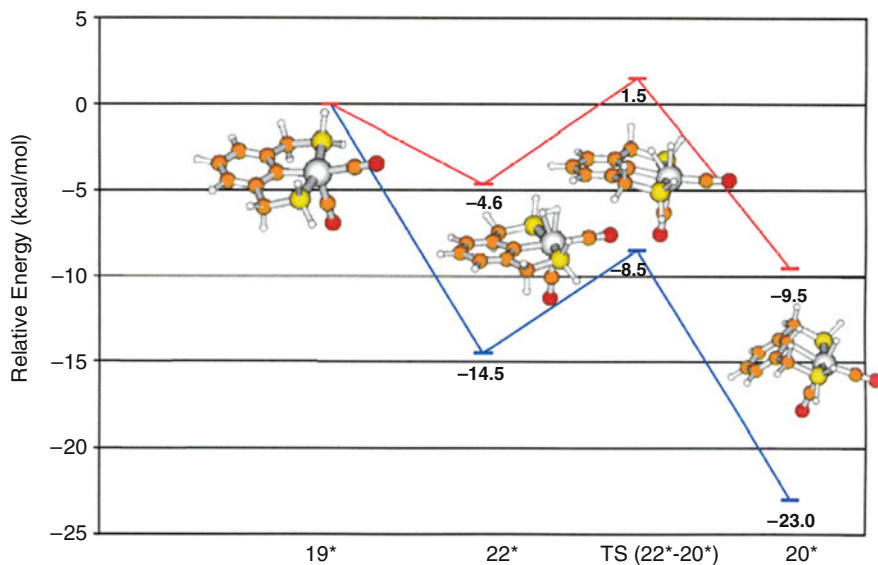


Fig. 5 Geometries of the calculated structures and the reaction profile. The energies are relative to **19*** + H_2 . The curve in blue is ΔE_c while the red curve is ΔG_{298} (atomic color schemes: C, brown; H, white; Ru, gray; O, red)

complex $RuCl(CO)_2[2,6-(CH_2P^tBu_2)_2C_6H_3]$ with $AgPF_6$ resulted in quantitative formation of the cationic complex **19** (Scheme 11). The NMR spectra of **19** are very different than those of the saturated precursor and indicate the presence of an unsaturated pincer complex.

The X-ray structure of **19** shows that the “vacant” coordination site is occupied by an alkyl $C-H \cdots M$ agostic interaction involving an sp^3 C–H bond of a *tert*-butyl substituent (Fig. 4). Density functional theory (DFT) gas phase calculations are in line with the solid state structure and show the necessity of two sterically demanding *tert*-butyl substituents on one P donor atom for the agostic interaction to occur.

Addition of dihydrogen to the sp^3 C–H agostic complex **19** resulted in a new complex **20** with an aryl $C-H \cdots M$ interaction, where the aromatic $C_{ipso}-H$ bond is η^2 -coordinated to the metal center. This agostic C–H bond becomes acidic to the

extent that complex **20** was deprotonated with Et_3N to form the neutral complex **21** (Scheme 12).

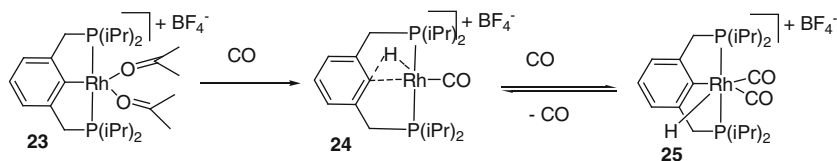
The **19** \rightarrow **20** transformation, involving both C–H bond formation and activation, has been mapped out in detail using DFT calculations (Fig. 5). The addition of H_2 to agostic **19*** leading to the $\sigma\text{-H}_2$ complex **22*** is exergonic ($\Delta G_{298} = -3.6$ kcal/mol). Complex **22*** is octahedral and has the “nonclassical” dihydrogen ligand aligned parallel to the Ru–C_{ipso} bond. The next step of H transfer from H_2 to the aromatic ring to give **20*** is also exergonic ($\Delta G_{298} = -5.9$ kcal/mol). In complex **20*** the aromatic ring is dramatically bent relative to the metal plane of coordination (Ru–C_{ipso}–C_{para} = 111.8°). The interaction with the ruthenium center is apparent from the elongated C–H bond (1.092 Å vs. 1.088 Å) and the bending of this H from the aromatic plane (H–C_{ipso}–C_{para} = 165.9°). The transition state **TS** (**22***–**20***) has a reaction barrier of $\Delta G_{298}^\ddagger = 5.1$ kcal/mol and a reverse reaction barrier of $\Delta G_{298}^\ddagger = 11.0$ kcal/mol. These values are consistent with the observed hydrogen addition and fluxional behavior of the system. It should be noted that a Ru(IV) dihydride intermediate is not observed. Thus, this H–H activation is better classified as an σ -bond metathesis rather than an oxidative addition reaction.

The formation and reactivity of complexes **19** and **20** demonstrate the ease by which cycloruthenated ligand systems undergo reversible two electron, three center C–H \cdots Ru interactions. It is also noteworthy that the cyclometalated Ru–C_{aryl} σ -bond can be formed and activated under very mild reaction conditions.

3.2 Unexpected Role of CO in C–H Oxidative Addition

According to the classic work of Saillard and Hoffmann [103], oxidative addition of a C–H bond to a transition metal center involves a two-way electron transfer (from the filled σ orbital of the C–H bond into an empty metal d orbital, and from a filled metal d orbital into the empty σ^* orbital of the C–H bond). Overall, this process produces net electron density transfer from the metal to the C–H bond (which splits into formally anionic hydrocarbyl and hydride ligands). Therefore, the presence of electron-withdrawing ligands, such as the strong π -acceptor ligand carbon monoxide, would be expected to hinder oxidative addition and to facilitate reductive elimination of C–H bonds by lowering the electron density at the metal center [104–106].

Our studies with a series of pincer-type bisphosphine cationic rhodium complexes yielded intriguing observations regarding the effect of CO on the activation of C–H bonds [107, 108]. When the Rh(III) aryl-hydride complex **23** was treated with one equivalent of CO, facile C–H reductive elimination took place, as expected, to yield the agostic Rh(I) complex **24** (Fig 6) [107]. Surprisingly, when a second equivalent of CO was added to this system, facile oxidative addition of the same C–H bond took place, yielding the Rh(III) aryl-hydride complex **25** (Scheme 13). Both experimental and theoretical evidence indicated that this



Scheme 13 CO promoted C–H bond activation via formation of agnostic complex

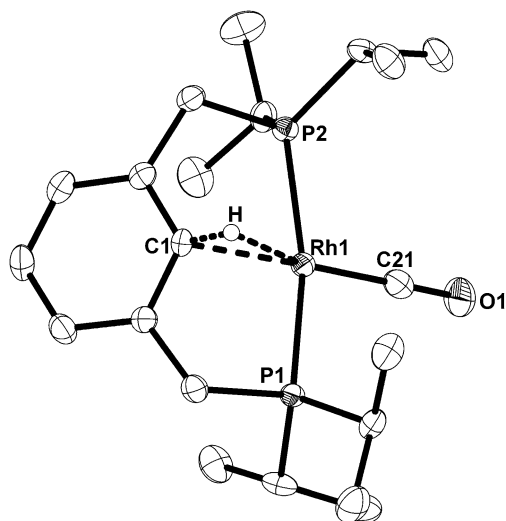
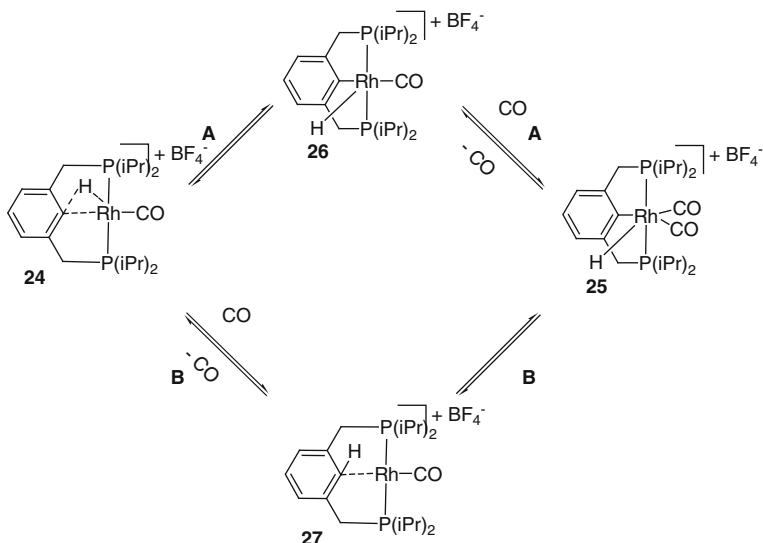


Fig. 6 Crystal structure of complex **24**. Selected bond distances (Å) and angles (°): Rh-C_{ipso} = 2.267, Rh-H = 1.97, Rh-P1 = 2.321, Rh-P2 = 2.327, Rh-CO = 1.816, C-O = 1.153, C_{ipso}-Rh-P1 = 83.491, C_{ipso}-Rh-P2 = 83.78, C_{ipso}-Rh-H = 23.90, C_{CO}-Rh-P1 = 96.09, C_{CO}-Rh-P2 = 96.61

oxidative addition reaction was actually *promoted* by CO, which did not merely act as a trapping agent.

Formation of complex **25** is unexpected. The agnostic complex **24** is by itself an electron-poor system, as judged by the low Rh-P coupling constant (99.3 Hz), and it is quite counter intuitive that the addition of a second equivalent of CO to **24** (which is expected to further diminish the electron density at the metal center), actually results in the oxidative addition of the same C–H bond. Nevertheless, this reaction was found to be highly reversible and CO dependent. The reversibility of the reaction was clearly evident by NMR measurements that demonstrated scrambling of labeled ¹³CO in complex **25** and a dynamic equilibrium of **24** ↔ **25** as indicated by spin saturation transfer (SST). In light of these observations it is reasonable to assume that the reaction leading from **24** to **25** involves two elementary steps: C–H cleavage and CO coordination. Consequently, two alternative mechanistic pathways were proposed, as shown in Scheme 14. Pathway **A** involves direct oxidative



Scheme 14 Two alternative mechanistic pathways for a C–H bond activation

addition of the agostic C–H bond to yield the square-pyramidal intermediate **26**, which then undergoes trapping by CO to afford complex **25**. Pathway **B** initially involves coordination of a CO ligand to complex **24**, yielding trigonal-bipyramidal (TBP) intermediate **27**, followed by cleavage of the arene C–H bond.

The unknown complexes **26** and **27** could not be detected. Therefore, DFT calculations were employed in order to investigate the systems described in Scheme 14. A priori, pathway **A** was assumed to be more probable than **B**, since the monocarbonyl complex **24** is expected to be more electron-rich than the dicarbonyl intermediate **27** and hence appears more likely to undergo oxidative addition of the C–H bond ($\mathbf{24} \rightarrow \mathbf{26}$). Moreover, the fact that **24** is an agostic complex made it a very reasonable candidate for C–H bond cleavage, since such complexes are widely accepted as precursors of C–H activation. Therefore, it was rather surprising to learn that the DFT calculations yielded very different results. Not only did they suggest that both pathways are possible, but the CO-promoted oxidative addition (pathway **B**) was found to be more favorable. Intermediate **27** was calculated to be 9.0 kcal/mol more stable than **26**, and even more stable than **24** by 1.2 kcal/mol. Strong experimental support for the involvement of intermediate **27** in the formation of complex **25** came from the observation that upon mixing the cationic Rh^I precursor $[\text{Rh}(\text{CO})_2(\text{acetone})_2]\text{BF}_4$ with the PCP ligand 1,3-bis((di-*iso*-propylphosphino)methyl)benzene in 1:1 ratio in acetone, complex **25** was obtained (as indicated by NMR at -55°C), with no significant amounts of complex **24** being observed. These results show that complex **25** can be produced by a direct reaction between the PCP ligand and a cationic Rh^I-dicarbonyl fragment.

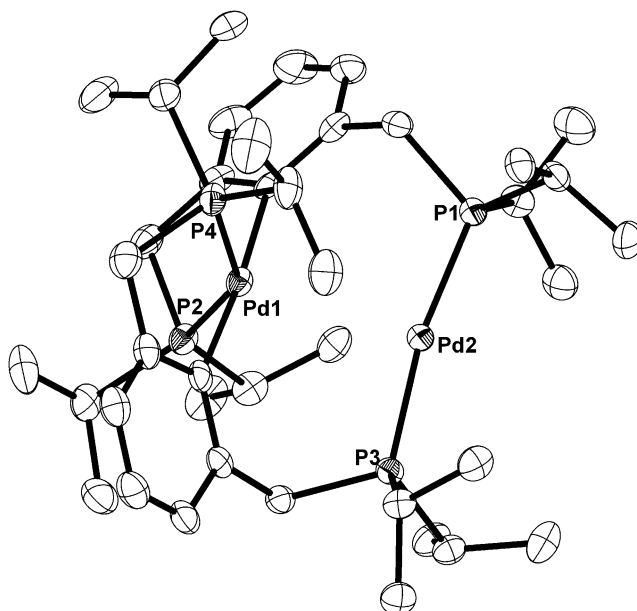


Fig. 7 ORTEP diagram of a molecule of **29**, showing the atom labeling scheme (50 % probability). Hydrogen atoms are omitted for clarity. Selected bond distances (Å) and angles (°): Pd1-P4 = 2.288, Pd1-P2 = 2.295, Pd1-Pd2 = 3.039, Pd2-P3 = 2.245, Pd2-P1 = 2.250; P4-Pd1-P2 = 144.82, P3-Pd2-P1 = 170.48

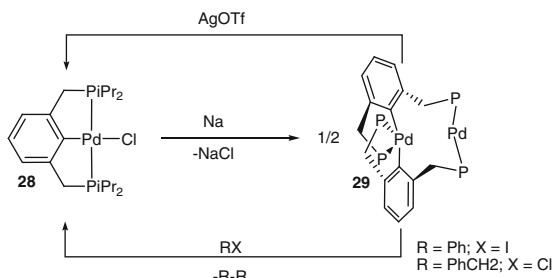
In addition, a rare agostic C–C complex of Rh based on the PCN ligand was demonstrated. In this system a remarkable degree of control over C–C vs. C–H bond activation was reached by choice of rhodium precursor [109].

4 Collapse and Regeneration

4.1 Redox Induced Collapse and Regeneration

The reduction of square planar d^8ML_4 complexes to d^{10} species is of relevance to a variety of catalytic reactions. For instance, Heck reactions catalyzed by PCP–Pd(II) complexes require reduction of the Pd(II) center to Pd(0) [19, 111]. Therefore, reduction of a Pd(II) PCP complex was examined.

¹We are aware of two examples of completely nonplanar (rather than distorted square planar) Pd(II) L_4 complexes, only one of them being diamagnetic [112, 113].



Scheme 15 Redox induced collapse and regeneration of a (PCP)Pd(II) complex

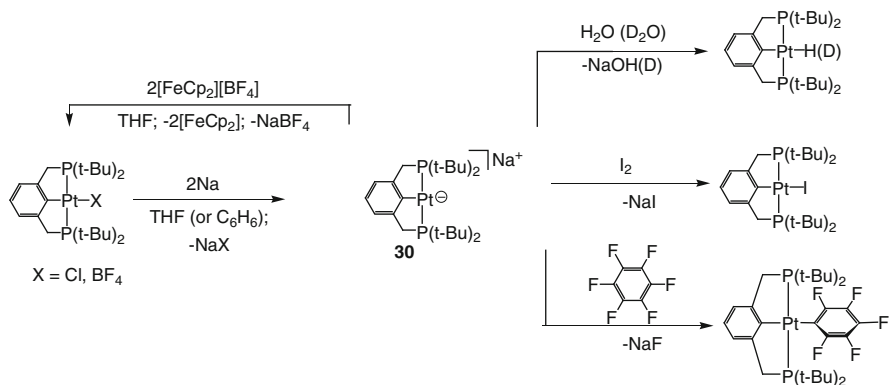
Upon reaction of the (PCP)Pd(II) complex **28** with sodium in THF, two new signals with the same intensity at δ 55.89 and 36.96 ppm were observed in the $^{31}\text{P}\{^1\text{H}\}$ NMR spectrum, suggesting formation of a binuclear complex. An X-ray diffraction study revealed that a new binuclear palladium complex **29** was formed, incorporating a very rare, *nonplanar* diamagnetic Pd(II)¹ center and a 14e Pd(0) center (Fig. 7). The solid state structure of **29** exhibits a 4-coordinate Pd(II) center with a distorted butterfly geometry and a Pd(0) center linearly complexed by two phosphine arms from different PCP ligands. The short Pd(II) \cdots Pd(0) distance (3.039 Å) suggests that the extremely rare butterfly arrangement of the Pd(II) center with almost linearly coordinated phosphine arms is probably a consequence of steric effects and the rigidity of the PCP ligands.

Remarkably, the original PCP Pd(II) mononuclear framework can be regenerated upon direct oxidation of the binuclear complex or upon its reaction with organic halides. Thus, when complex **29** was treated with an excess of benzyl chloride, immediate quantitative formation of the monomeric PCP–Pd–Cl complex was observed and dibenzyl was detected by GC. Similarly, addition of iodobenzene to a THF solution of complex **29** led to formation of the PCP–Pd–I complex and biphenyl but at a much slower reaction rate. These reactions likely indicate electron transfer from the Pd(0) center to the organic halide.² Supporting the electron transfer reaction, addition of two equivalents of AgOTf to a THF solution of **29** resulted in immediate and clean formation of the monomeric PCP–Pd–OTf complex as well as silver metal (Scheme 15).

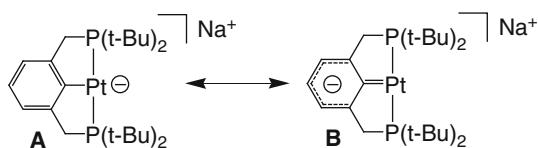
Although mechanistic studies were not performed, a possible scenario for formation of **29** might include a single electron transfer from Na to Pd(II) with precipitation of NaX and formation of a tri-coordinated Pd(I) intermediate which is

² A mechanism involving organic halide oxidative addition to generate dibenzyl or biphenyl is also possible. See, for example [114].

³ In analogy to nonchelating systems, where reduction of PtCl₂L₂ (L = bulky tert-phosphines) with Na/Hg in THF affords PtL₂ complexes, while reduction of PdCl₂L₂ (L = bulky tert-phosphines) with Na/Hg in THF resulted in formation of metallic palladium. The reduction was achieved only when excess phosphine was used. See [116] and references therein.



Scheme 16 Formation and reactivity of anionic Pt(0) complex, **30** based on PCP ligand



Scheme 17 Two resonance forms of anionic Pt(0) complex

likely to undergo dimerization, followed by disproportionation to Pd(0) and Pd(II). In this unprecedented process, the pincer system opened up and the aryl anchor was transferred from one Pd center to the other.

These results point out the possibility that reactions catalyzed by Pd(II) pincer complexes under reducing conditions can actually be catalyzed by Pd(0), even if the Pd(II) pincer complex is recovered at the end of the reaction.

4.2 A Pincer-Type Anionic Pt(0) Complex

Collapse of the pincer system upon reduction can be avoided by utilization of a (PCP)Pt(II) complex instead of (PCP)Pd(II), as a result of the more diffused nature of the Pt orbitals³ which might stabilize the reduced metal center. In addition, increasing the steric bulk of the pincer-phosphine ligand using tBu groups instead of iPr might hinder dimerization of Pt(I) centers. Indeed, a monometallic anionic Pt(0) complex **30** was formed by reduction of a PCP-type Pt(II) complex. This (PCP)Pt(0) complex **30** adopts a T-shaped structure and exhibits diverse reactivity.

⁴For nonisolated, anionic palladium(0) intermediates, and their involvement in oxidative addition reactions, see [119, 120].

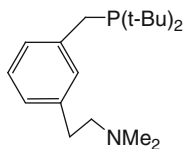


Fig. 8 “Long-arm” PCN ligand

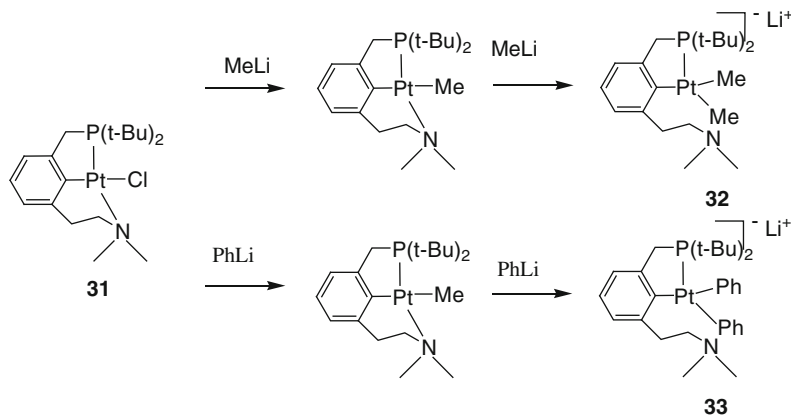
Complex **30** acts as a *Brønsted base* and endures protonation by water to give the Pt(II)-H complex, and as an efficient electron transfer reagent, being reoxidized quantitatively to Pt(II). It is capable of activation of the strong C–F bond of hexafluorobenzene even at $-35\text{ }^{\circ}\text{C}$ (Scheme 16).

The planar T-shaped geometry proposed for **30** based on NMR spectroscopy is supported by DFT calculations. The computational study also indicates that the negative charge is localized mostly at the metal center of the anionic complex **30** (Structure **A**), rather than delocalized between the metal center and the σ -bound aryl backbone (Structure **B**) (Scheme 17).

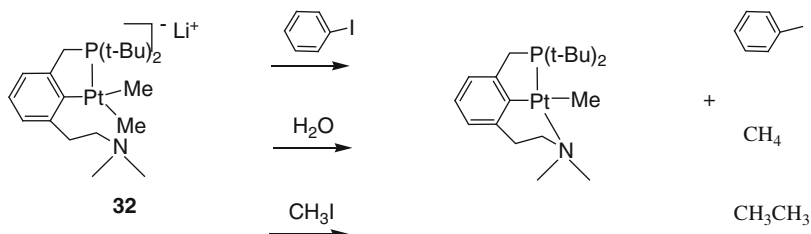
We are aware of only one monometallic anionic Pt(0) complex, $[\text{Pt}(\text{Me}_2\text{NCS}_2)(\text{PEt}_3)]^-$, which was generated in situ at $-78\text{ }^{\circ}\text{C}$, by proton abstraction from the Pt(II) hydride complex $[\text{PtH}(\text{Me}_2\text{NCS}_2)(\text{PEt}_3)]$ [117, 118]. This complex was not isolated but rather trapped with variety of electrophiles giving a range of Pt(II) complexes [117].⁴

5 Hemilabile Pincer-Type PCN Ligand

The hardness of the chelating N donor in NCN-type ligands vs. softness of P donor in the PCP system results in very different behavior of the corresponding NCN and PCP based complexes. While each of these systems has its own unique chemistry, the mixed PCN ligand benefits from advantages of both systems, demonstrating remarkable chemistry including exclusive C–C [47], C–H [47, 109], and catalytic C–N [121] bond activation. The different donor properties and more labile coordination of the amine “arm” in comparison to the phosphine [122] open up additional reactivity patterns. A more flexible complex with effective hemi-labile coordination could render the complex more adaptable to the different electronic, steric, and coordination requirements of different steps of a catalytic cycle, or to different stoichiometric reactions. In order to enhance the hemilability, a new PCN ligand with a longer amine “arm” was synthesized (Fig. 8), and utilized as described below.



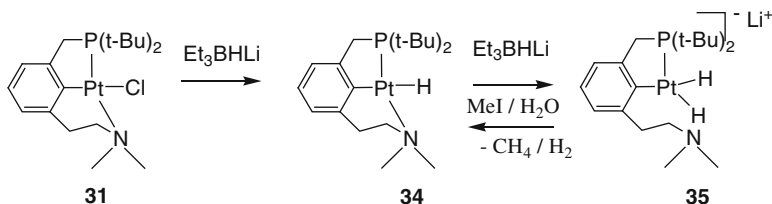
Scheme 18 Formation of the anionic “open arm” dimethyl and diphenyl Pt complexes **32** and **33**, based on “long arm” PCN ligand



Scheme 19 Reactivity of the anionic complex **32** with electrophiles, resulting in “arm closure”

5.1 Anionic Complexes Based on a Hemilabile PCN Ligand

Anionic transition metal complexes are of interest due to their nucleophilic reactivity toward organic molecules ([123] and references therein) and their utilization in the preparation of homo- and heteronuclear transition-metal clusters [124]. Usually, these complexes are stabilized by electron-acceptor ligands, which allow delocalizing of the electron density at the metal center. For instance, various anionic complexes containing carbonyl (for examples, see [125, 126]), olefin (for examples, see [127] and references therein) and PR₃ (R = F, OR, Me) [128–131] ligands were reported. However, since delocalization of charge density decreases the reactivity of such complexes toward electrophilic reagents, formation of relatively stable anionic complexes in the absence of strong electron accepting ligands is desirable, but relatively few examples of such compounds are known (for examples, see [107, 132]). Utilizing the hemilability of the “long arm” PCN ligand, a series of Pt(II) anionic complexes that bear no electron withdrawing ligands and exhibit relative stability and reactivity toward electrophiles were prepared.



Scheme 20 Formation of the anionic “open arm” dihydride complex **35**

5.1.1 Dialkyl and Diphenyl Anionic Complexes [133]

Upon reaction of the “long arm” pincer Pt complex **31** with two equivalents of methyllithium, the anionic dimethyl Pt(II) complex **32** was formed and was fully characterized by NMR spectroscopy and X-ray single crystal analysis (Scheme 15). According to the ^1H and $^{13}\text{C}\{^1\text{H}\}$ NMR data, the amine “arm” of the PCN ligand is not coordinated to the metal center, since the methyl groups of NMe_2 exhibit a single resonance without Pt satellites. It is likely that Li^+ is coordinated to the nitrogen of the dissociated amine “arm,” contributing to the stability of the anionic complex. The same mode of reactivity was observed with other organolithium compounds. Thus, reaction of **31** with a stoichiometric amount of phenyllithium led to formation of the mono-phenyl Pt(II) complex, while addition of two equivalents of PhLi to **31** gave the anionic diphenyl Pt(II) complex **33** (Scheme 18).

The anionic complexes are highly reactive with various electrophiles, thereby regenerating the pincer framework (Scheme 19). For example, reaction of **32** with MeI led to formation of the monomethyl neutral complex and ethane. Likewise, reaction of **32** with H_2O led to immediate formation of the monomethyl neutral complex and methane. Moreover, complex **32** is capable of reaction even with weak electrophiles such as iodobenzene or bromobenzene leading to monomethyl neutral complex and toluene. This reaction was slower than the reactions with MeI or water and quantitative formation of monomethyl neutral complex was observed only after 24 h.

5.1.2 Dihydride Anionic Complex [133]

The hemilability of the amine “arm” of the PCN ligand, enabled the preparation of the first anionic d^8 platinum dihydride complex, via direct nucleophilic attack on the metal center. Thus, upon reaction of complex **31** with one equivalent of Et_3BHLi , the expected monohydride complex **34** was formed, while using an

⁵ Very unstable, not isolated [144].

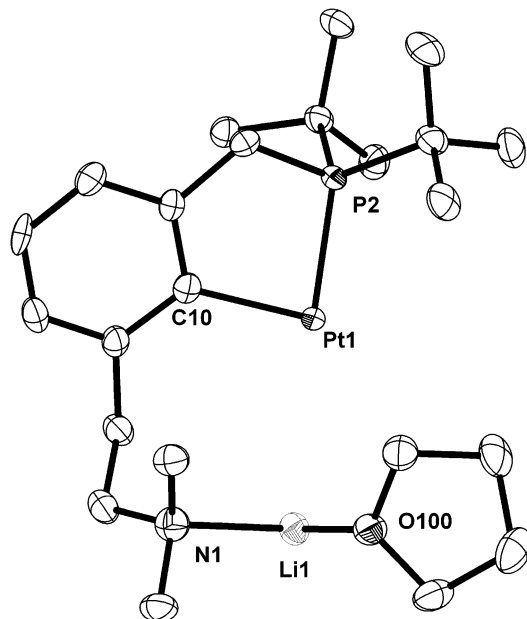
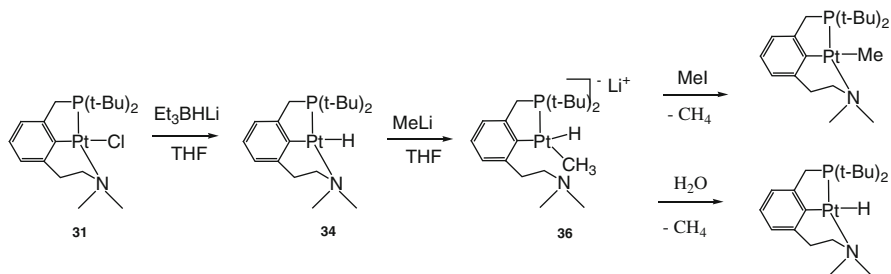
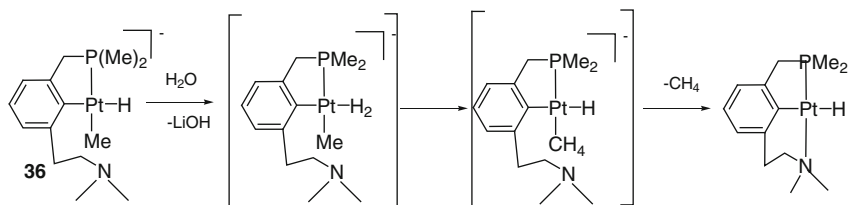


Fig. 9 ORTEP view of the X-ray structure of complex **35** at 50 % probability



Scheme 21 Formation and reactivity of the anionic methyl hydride complex **36**

excess of Et_3BHLi resulted in the novel anionic dihydride complex **35** (Scheme 20), which was fully characterized, including an X-ray structure (Fig. 9). Similarly to the anionic dialkyl and diaryl complexes, **35** is highly reactive with electrophiles. For example, it reacts readily with water and methyl iodide at room temperature, resulting in immediate formation of the monohydride complex and H_2 or methane, respectively.



Scheme 22 DFT-calculated mechanism of reaction of **36** with water

5.1.3 Alkyl Hydride Anionic Complex [134]

The selective functionalization of methane using platinum complexes has attracted much attention [135]. Although hydrido(alkyl)metal complexes are key intermediates in alkane functionalization, examples of such complexes of group 10 metals are not common, and limited mainly to the d₆ complexes [136–141], while stable Pt(II) alkyl hydride complexes are extremely rare [142, 143].⁵

We have utilized the “long arm” pincer complex **34** for the preparation of an unprecedented example of an anionic d⁸ alkyl hydride complex. Thus, upon addition of one equivalent of MeLi to a THF solution of complex **34**, the new anionic complex **36**, in which the hemilabile arm is not coordinated, was formed. Complex **36** readily reacts with electrophiles, like water and methyl iodide, to exclusively give methane and the corresponding pincer product (Scheme 21).

DFT calculations show that the reaction of **36** with water likely involves a η^2 -H₂ intermediate, in which the H₂ ligand’s axis is in plane with the PCN ligand, followed by the direct transfer of a hydrogen atom from it to the methyl group, forming a coordinated methane intermediate (Scheme 22).

6 Conclusions

In this chapter we aimed to demonstrate the unusual ligand-based behavior of pincer systems. Under the appropriate conditions, pincer systems can undergo rearrangement, giving rise to unusual and elusive structures. In addition, pincer systems can collapse and be regenerated, providing new possibilities for tuning the properties of the complexes, and allowing unique reactivity patterns. Participation of the arene ring in the reactivity of PCP type complexes has led to formation of a series of unprecedented quinonoid complexes, including complexes in which the pincer ligand adopts structures of quinone methides, thio-quinone methides, xylylenes, methylene arenium, and oxo-arenium compounds. Reduction of a naphthyl based pincer rhodium complex results in a unique radical anion complex, in which the radical is ring localized, but its reactivity is metal controlled. The generation of C–H agostic arene PCP complexes has led to new insights regarding the C–H bond activation process and the effect of CO ligands on it. Redox

chemistry of PCP Pd complexes has led to an interesting collapse and regeneration of the pincer system. In addition, a hemilabile PCN pincer system has enabled formation of a series of reactive anionic complexes that bear no stabilizing electron withdrawing ligands.

References

1. Milstein D (2003) *Pure Appl Chem* 75:445
2. van der Boom ME, Milstein D (2003) *Chem Rev* 103:1759
3. Albrecht M, van Koten G (2001) *Angew Chem Int Ed* 40:3750
4. Singleton JT (2003) *Tetrahedron* 59:1837
5. Rytchinski B, Milstein D (1999) *Angew Chem Int Ed* 28:870
6. Hartley FR, Patai S (eds) (1982) *The chemistry of the metal-carbon bond: the structure, preparation, thermochemistry and characterization of organometallic compounds*, vol 1. Wiley, New York
7. Dyke AM, Hester AJ, Lloyd-Jones GC (2006) *Synthesis* 24:4093
8. Moulton CJ, Shaw BLJ (1976) *J Chem Soc Dalton Trans* 1020–1024
9. Gozin M, Weisman A, Ben-David Y, Milstein D (1993) *Nature* 364:699
10. Liou S-Y, Gozin M, Milstein D (1995) *J Am Chem Soc* 117:9774
11. van der Boom ME, Kraatz H-B, Ben-David Y, Milstein D (1996) *J Chem Soc Chem Commun* 2167–2168
12. Crocker C, Empsall D, Errington RJ, Hyde EM, Mc-Donald WS, Markham R, Norton MC, Shaw BL (1982) *J Chem Soc Dalton Trans* 1829–1834
13. Vigalok A, Milstein D (2001) *Acc Chem Res* 34:798
14. Jensen CM (1999) *Chem Commun* 2443–2449
15. Renkema KB, Kissin YV, Goldman AS (2003) *J Am Chem Soc* 125:7770
16. Gottker-Schnetmann I, White PS, Brookhart M (2004) *J Am Chem Soc* 126:1804
17. Haenel MW, Oevers S, Angermund K, Kaska WC, Fan HJ, Hall MB (2001) *Angew Chem Int Ed* 40:3596
18. Morales-Morales D, Lee DW, Wang Z, Jensen CM (2001) *Organometallics* 20:1144
19. Sjövall S, Johansson MH, Anderson C (2001) *Eur J Inorg Chem* 2907–2912
20. Herrera-Alvarez C, Gomez-Bnitez V, Redon R, Garcia JJ, Hernandez-Ortega S, Toscano RA, Morales-Morales D (2004) *J Organomet Chem* 689:2464
21. Eberhard MR (2004) *Org Lett* 6:2125–2128
22. Ohff M, Ohff A, van der Boom ME, Milstein D (1997) *J Am Chem Soc* 119:11687
23. Olsson D, Wendt OF (2009) *J Organomet Chem* 694:3112
24. Serrano-Becerra JM, Morales-Morales D (2009) *Curr Org Synth* 6:169
25. Bedford RB, Draper SM, Noelle SP, Welch SL (2000) *New J Chem* 24:745
26. Feller M, Ben-Ari E, Iron MA, Diskin-Posner Y, Leitius G, Shimon LJW, Konstantinovski L, Milstein D (2010) *Inorg Chem* 49:1615
27. Ben-Ari E, Leitius G, Shimon LJW, Milstein D (2006) *J Am Chem Soc* 128:15390
28. Gnanaprakasam B, Milstein D (2011) *J Am Chem Soc* 133:1682
29. Gnanaprakasam B, Ben-David Y, Milstein D (2010) *Adv Synth Catal* 352:3169
30. Gunanathan C, Ben-David Y, Milstein D (2007) *Science* 317:790
31. Balaraman E, Gnanaprakasam B, Shimon LJW, Milstein D (2010) *J Am Chem Soc* 132:16756
32. Zhang J, Leitius G, Ben-David Y, Milstein D (2005) *J Am Chem Soc* 127:10840
33. Rokita SE (ed) (2009) *Quinone methides*. Wiley, Hoboken, NJ
34. Wagner HU, Gompper R (1974) In: Patai S (ed) *The chemistry of the quinonoid compounds*, vol 2. Wiley, New York, p 1145

35. Diao L, Yang C, Wan P (1995) *J Am Chem Soc* 117:5369
36. Amouri H, Le Bras A (2002) *J Acc Chem Res* 35:501
37. Ferreira SB, da Silva F, de Pinto AC, Gonzaga DTG, Ferreira VF (2009) *J Heterocycl Chem* 46:1080
38. Prota G (1995) *Progress in the chemistry of organic natural products*, vol 64. Springer, Wien-New York, pp 93–148
39. Bolon DA (1970) *J Org Chem* 35:3666
40. Marino JP, Dax SL (1984) *J Org Chem* 49:3671
41. Demeyer D, Raes K, Fievez V, de Smet S (2004) *Commun Agric Appl Biol Sci* 69:103–110
42. Ramalho VC, Jorge N (2006) *Quim Nova* 29:755
43. Moore HW, Czerniak R (1981) *Med Res Rev* 1:249
44. Thompson DC, Tompson JA, Sugumaran M, Moldeus P (1993) *Chem Biol Interact* 86:129
45. Dyall LK, Winstein S (1972) *J Am Chem Soc* 94:2196
46. Vigalok A, Milstein D (1997) *J Am Chem Soc* 119:7873
47. Gandelman M, Vigalok A, Shimon LJW, Milstein D (1997) *Organometallics* 16:3981
48. Vigalok A, Shimon LJW, Milstein D (1998) *J Am Chem Soc* 120:477
49. Gauvin RM, Rozenberg H, Shimon LJW, Ben-David Y, Milstein D (2007) *Chem Eur J* 13:1382
50. Silvestre J, Albright TA (1985) *J Am Chem Soc* 107:6829
51. Rabin O, Vigalok A, Milstein D (1998) *J Am Chem Soc* 120:7119
52. Rabin O, Vigalok A, Milstein D (2000) *Chem Eur J* 6:454
53. Poverenov E, Leitun G, Milstein D (2006) *J Am Chem Soc* 128:16450
54. Hall MD, Hambley TW (2002) *Coord Chem Rev* 232:49
55. Scolaro LM, Mazzaglia A, Romeo A, Romeo R (2002) *J Inorg Biochem* 91:237
56. Poverenov E, Shimon LJW, Milstein D (2007) *Organometallics* 26:2178
57. Kobayashi S, Higashimura H (2003) *Prog Polym Sci* 28:1015
58. Hay AS (1998) *J Polym Sci Polym Chem* 36:505
59. MacDonald PD, Hamilton GA (1973) In: Trahanovsky WS (ed) *Oxidation in organic chemistry*, part B, Chap. II. Academic, New York, pp 97–133
60. Taylor WI, Battersby AR (1967) *Oxidative coupling of phenols*. Marcel Dekker, New York
61. Abramovitch RA, Alvernhe G, Bartnik R, Dassanayake NL, Inbasekaran MN, Kato S (1981) *J Am Chem Soc* 103:4558
62. Shudo K, Orihara Y, Ohta T, Okamoto T (1981) *J Am Chem Soc* 103:943
63. Zagorevskii DV, Regimbal J-M, Holmes JL (1997) *Int J Mass Spectrom Ion Proc* 160:211
64. Swenton JS (1988) In: Patai S, Rappoport Z (eds) *The chemistry of quinonoid compounds*, vol 2. Wiley, New York, pp 899–962
65. Baesjou PJ, Driessen WL, Challa G, Reedijk J (1997) *J Am Chem Soc* 119:12590
66. Gao J, Reibenspies JH, Martell AE (2002) *Inorg Chim Acta* 338:157
67. Vigalok A, Rybtchinski B, Gozin Y, Koblenz TS, Ben-David Y, Rozenberg H, Milstein D (2003) *J Am Chem Soc* 125:15692
68. Feng Y, Liu L, Fang Y, Guo Q-X (2002) *J Phys Chem A* 106:11518
69. Davis CJ, Moody CJ (2002) *Synlett* 11:1874
70. Wright JS, Johnson ER, Dilabio GA (2001) *J Am Chem Soc* 123:1173
71. Oyaizu K, Saito K, Tsuchida E (2000) *Chem Lett* 29:1318–1319
72. Katsoulis DE, Pope MT (1989) *J Chem Soc Dalton Trans* 8:1483
73. Omura K (1984) *J Org Chem* 49:3046
74. van der Boom ME, Zubkov T, Shukla A, Rybtchinski B, Shimon LJW, Rozenberg H, Ben David Y, Milstein D (2004) *Angew Chem Int Ed* 43:5961
75. Shimasaki T, Tobisu M, Chatani N (2010) *Angew Chem Int Ed* 49:2929
76. Bonanno JB, Henry TP, Neithamer DR, Wolczanski PT, Lobkovsky EB (1996) *J Am Chem Soc* 118:5132
77. Kawaguchi H, Matsuo T (2003) *J Am Chem Soc* 125:14254
78. Harvey RG (1997) *Polycyclic aromatic hydrocarbons*. Wiley-VCH, New York

79. Hopf H (2000) *Classics in hydrocarbon chemistry: syntheses, concepts, perspectives*. Wiley-VCH, Weinheim
80. Benschafrit R, Shabtai E, Rabinovitz M, Scott LT (2000) *Eur J Org Chem* 1091–1106
81. Ireland T, Perea JJA, Knochel P (1999) *Angew Chem Int Ed Engl* 38:1457
82. Cohen T, Bhupathy M (1989) *Acc Chem Res* 22:152
83. Mudryk B, Cohen T (1993) *J Am Chem Soc* 115:3855
84. Frech CM, Weiner L, Milstein D (2006) *J Am Chem Soc* 128:7128
85. Clar E (1964) *Polycyclic hydrocarbons*. Academic, London
86. Mullen K (1984) *Chem Rev* 84:603
87. Jones WD, Vetter AJ, Wick DD, Northcutt TO (2004) In: Goldberg KI, Goldman AS (eds) *Activation and functionalization of C-H bonds*, ACS symposium series 885. American Chemical Society, Washington, DC, pp 56–69
88. Goldman AS, Goldberg KI (2004) In: Goldberg KI, Goldman AS (eds) *Activation and functionalization of C-H bonds*, ACS symposium series 885. American Chemical Society, Washington, DC, pp 1–43
89. Labinger JA, Bercaw JE (2002) *Nature* 417:507
90. Shilov AE, Shul'pin GB (1997) *Chem Rev* 97:2879
91. Lersch M, Tilset M (2005) *Chem Rev* 105:2471
92. Sakaki S (2005) *Top Organomet Chem* 12:31–78
93. Hall C, Perutz RN (1996) *Chem Rev* 96:3125–3146
94. Crabtree RH (1993) *Angew Chem Int Ed* 32:789
95. Brookhart M, Green MLH (1983) *J Organomet Chem* 250:395–408
96. Vigalok A, Uzan O, Shimon LJW, Ben-David Y, Martin JML, Milstein D (1998) *J Am Chem Soc* 120:12539
97. Mohammad HAY, Grimm JC, Eichele K, Mack H-G, Speiser B, Novak F, Quintanilla MG, Kaska WC, Mayer HA (2002) *Organometallics* 21:5775
98. Dani P, Karlen T, Gossage RA, Smeets WJJ, Spek AL, van Koten G (1997) *J Am Chem Soc* 119:11317
99. Albrecht M, Dani P, Lutz M, Spek AL, van Koten G (2000) *J Am Chem Soc* 122:11822
100. Gusev DG, Madott M, Dolgushin FM, Lyssenko KA, Antipin MY (2000) *Organometallics* 19:1734
101. Dani P, Toorneman MAM, van Klink GPM, van Koten G (2000) *Organometallics* 19:5287
102. van der Boom ME, Iron MA, Atasoylu O, Shimon LJW, Rozenberg H, Ben-David Y, Konstantinovski L, Martin JML, Milstein D (2004) *Inorg Chim Acta* 357:1854
103. Saillard J-Y, Hoffmann R (1984) *J Am Chem Soc* 106:2006–2026
104. Ozawa F (2003) In: Kurosaw H, Yamamoto A (eds) *Current methods in inorganic chemistry*, vol 3. Elsevier, Amsterdam, pp 479–512
105. Tatsumi K, Hoffmann R, Yamamoto A, Stille JK (1981) *Bull Chem Soc Jpn* 54:1857–1867
106. Su M-D, Chu S-Y (1998) *Inorg Chem* 37:3400–3406
107. Montag M, Schwartsburd L, Cohen R, Leitus G, Ben-David Y, Martin J-ML, Milstein D (2007) *Angew Chem Int Ed* 46:1901
108. Montag M, Efremenko I, Cohen R, Shimon LJW, Leitus G, Diskin-Posner Y, Ben-David Y, Salem H, Martin J-ML, Milstein D (2010) *Chem Eur J* 16:328
109. Gandelman M, Shimon LJW, Milstein D (2003) *Chem Eur J* 9:4295
110. Frech C, Shimon LJW, Milstein D (2005) *Angew Chem Int Ed* 44:1709
111. Kiewel K, Liu Y, Bergbreiter DE, Sulikowski GA (1999) *Tetrahedron Lett* 40:8945
112. Bröring M, Brandt CD (2002) *J Chem Soc Dalton Trans* 1391–1395
113. Yeo JSL, Vittal JJ, Hor TSA (1999) *Chem Commun* 1477–1478
114. Kraatz H-B, van der Boom ME, Ben-David Y, Milstein D (2001) *Isr J Chem* 41:163
115. Schwartsburd L, Cohen R, Konstantinovski L, Milstein D (2008) *Angew Chem Int Ed* 47:3603–3606
116. Otsuka S (1980) *J Organomet Chem* 200:191
117. Reger DL, Ding Y (1994) *Organometallics* 13:1047

118. Rendina LM, Hambley TW (2004) In: McCleverty JA, Meyer TJ (eds) *Comprehensive coordination chemistry II*, vol 6, 2nd edn. Elsevier, Oxford, pp 673–745
119. Amatore C, Jutand A (2000) *Acc Chem Res* 33:314
120. Amatore C, Jutand A, Lemaitre F, Ricard JL, Kozuch S, Shaik S (2004) *J Organomet Chem* 689:3728
121. Gandelman M, Milstein D (2000) *Chem Commun* 1603–1604
122. Togni A, Venanzi L (1994) *Angew Chem Int Ed Engl* 33:497
123. Kraus MJ, Bergman RG (1985) *J Am Chem Soc* 107:2972
124. Tachikawa M, Sievert AC, Muettterties EL, Day CS, Day VW (1980) *J Am Chem Soc* 102:1725
125. Ellis JE, Faltynek RA (1977) *J Am Chem Soc* 99:1801
126. Ellis JE, Parnell CP, Hagen GP (1978) *J Am Chem Soc* 100:3605
127. Jonas K, Schieferstein L, Kruger C, Tsay YH (1979) *Angew Chem Int Ed Engl* 18:550
128. Bennett MA, Patmore JD (1971) *Inorg Chem* 10:2387
129. Muettterties EL, Hirsekorn FJ (1974) *J Am Chem Soc* 96:7920
130. Watson PL, Muettterties EL (1978) *J Am Chem Soc* 100:6978
131. Klein HF, Schmidbaur H, Karsch HH (1975) *Angew Chem Int Ed Engl* 14:637
132. Del Paggio AA, Andersen RA, Muettterties EL (1987) *Organometallics* 6:1260
133. Poverenov E, Gandelman M, Shimon LJW, Rozenberg H, Ben-David Y, Milstein D (2004) *Eur J Org Chem* 10:4673–84
134. Poverenov E, Iron MA, Gandelman M, Ben-David Y, Milstein D (2010) *Eur J Inorg Chem* 13:1991–1999
135. Shilov AE, Shul'pin GB (2000) *Activation and catalytic reactions of saturated hydrocarbons in the presence of metal complexes*. Kluwer, Dordrecht
136. Batsanov AD, Howard JAK, Love JB, Spencer JL (1995) *Organometallics* 14:5657–5664
137. O'Reilly SA, White PS, Templeton JL (1996) *J Am Chem Soc* 118:5684–5689
138. Prokopchuk EM, Jenkins HA, Puddephatt RJ (1999) *Organometallics* 18:2861–2866
139. Vedernikov AN, Fettinger JC, Mohr F (2004) *J Am Chem Soc* 126:11160–11161
140. Iron MA, Lo HC, Martin JML, Keinan E (2002) *J Am Chem Soc* 124:7041–7054
141. Wick DD, Goldberg KI (1997) *J Am Chem Soc* 119:10235–10236
142. Stahl SS, Labinger JA, Bercaw JE (1995) *J Am Chem Soc* 117:9371–9372
143. Hackett M, Ibers JA, Whitesides GM (1988) *J Am Chem Soc* 110:1436–1448
144. Abis L, Sen A, Halpern J (1978) *J Am Chem Soc* 100:2915–2916

Tuning of PCP Pincer Ligand Electronic and Steric Properties

Dean M. Roddick

Abstract A survey of the electronic and steric characteristics of anionic (^RPCP, ^RPOCOP, ^RPNCNP) and neutral (^RPNP, ^RPONOP, ^RPNNNP) phosphine terdentate ligands is presented. A review of the scope of syntheses, particularly in regard to the variation of phosphine PR₂ substituents, is followed by a general discussion of pincer steric variation, terdentate ligand conformations, and coordination geometries. Buried volume parameters, %V_{bur}, provide a measure of overall steric influence, while the concepts of *cis* and *trans* ligand void space and PR₂ steric influence are used to more completely define asymmetric steric influence. Pincer arm conformations are categorized in terms of C₂ twist, C_s “gull wing,” and asymmetric bending, which accommodate a range of non-meridional P–M–P bending geometries. For 5-coordinate metal complexes, geometries can vary between two square pyramidal and two trigonal bipyramidal geometrical extremes and are distinguished using subtending angle parameters α, β, and γ. A key feature to note is that pincer ligands often assume non-meridional geometries with P–M–P angles as small as 107°. DFT studies on P–Ir–P bending energetics for (^RPCP)Ir(L) (L = CO, NH₃) with a wide range of R substituents show that destabilization from bending is primarily steric in origin and is particularly significant (+12 to 30 kcal mol⁻¹) for ^tBuPCP systems. Pincer electronic effects are surveyed using comparative IR, electrochemical, and binding affinity data. While R electronic effects are significant, particularly for our R = CF₃ systems, DFT calculations of ΔG_{dis}(Ir–CO) for (^RPCP)Ir(CO)₂ systems show that reduced Ir–CO binding correlates mostly with steric destabilization in non-meridional ^tBu-substituted pincer systems.

Keywords Coordination geometries · Electronic effects · Ligand conformation · Phosphine ligands · Pincer ligands · Polydentate ligands · Steric effects · Terdentate ligands

D.M. Roddick (✉)

Department of Chemistry, University of Wyoming, Box 3838, Laramie, WY 82071, USA
e-mail: dmr@uwyo.edu

Contents

1	Introduction	50
2	Phosphine Pincer Synthesis	51
2.1	Benzylic PCP Pincers	51
2.2	Resorcinol-Based POCOP Pincers	53
2.3	PENEP Pincers	56
3	Pincer Sterics, Conformation, and Coordination Geometries	57
3.1	Pincer C ₂ Twist Trends	68
3.2	P–M–P Angle Trends	69
3.3	5-Coordinate Pincer Systems	70
3.4	d ⁸ 5-Coordinate Pincer Systems	71
3.5	Nonmeridional Complexes and Reaction Intermediates	72
4	Phosphine Pincer Electronic Effects	76
4.1	$\nu(\text{CO})$ Trends	76
4.2	Electrochemical Studies	78
4.3	Reactivity and Coordination Affinity Trends	80
5	Summary	82
	References	83

1 Introduction

Terdentate “pincer” ligand coordination chemistry has undergone considerable development and enjoyed a variety of applications to metal-mediated organic synthesis and catalysis over the past 30 years [1–10]. While the tethering of pendant coordinating groups to a central ligand to achieve favorable 5- or 6-member chelate rings may be achieved with other linkage systems [11], much research effort has focused on more conformationally rigid central aromatic (aryl or pyridyl) ligating units with 2,6-benzylic or heteroatom (O, NR) links to the lateral coordination centers. This class of ligands is generally regarded as promoting a stable meridional coordination environment. The ability of such ligands to impart a remarkable degree of thermal and chemical stability is cited as a key to improvements in alkane dehydrogenation chemistry, ketone/alcohol transfer hydrogenation, and coupling chemistry (Heck, Suzuki-Miyaura, etc.). Stable pincer frameworks also provide the opportunity to stabilize unusual metal oxidation states [12], trap oxidative addition intermediates [13], and build supramolecular structures for sensor, materials, and catalytic applications [2, 14, 15].

The potential for modifying coordination properties by variation of pincer backbone, pendant arm, and lateral donor groups has been outlined in recent reviews [7, 10]. A considerable growing body of literature exists for ECE (E = N, O, S) ligand systems, particularly those with amine pendant arms. It is notable that, while development of ECE ligands continues, particularly by the van Koten research group, by far the most common NCN ligand employed in coordination chemistry is 1,3-C₆H₄(CH₂NR₂)₂, where R = Me. With some exceptions [16–19], relatively little work on modifying amine coordination properties by varying substituent steric and electronic influence has been reported. A key

difference between amine- and phosphine-based pincers is the lack of compensating π -acceptor ability in σ -only NR_2 coordination, a feature which is present in phosphine systems with electron-withdrawing substituents. As a result, most variation in NCN ligands has focused on backbone modification, either by incorporating σ ring substituents for tethering or electronic effects, or the addition of pincer η^6 -ligated metal units [20–22].

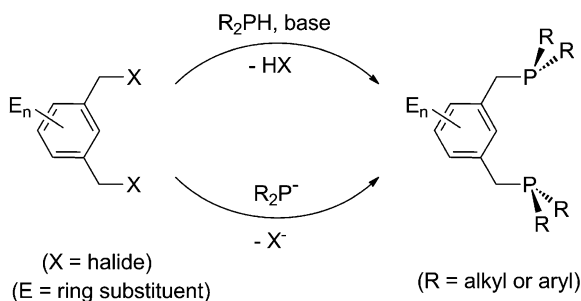
This chapter will focus primarily on anionic PCP and neutral PNP systems, with a particular emphasis on the effects of PR_2 substituent variation. We will follow the naming convention $^{\text{R}}\text{PCP}$ to denote simple symmetrically-substituted pincers with benzylic linking groups, 1,3- $\text{C}_6\text{H}_4(\text{CH}_2\text{PR}_2)_2$ (unmetallated) and 2,6- $\text{C}_6\text{H}_3(\text{CH}_2\text{PR}_2)_2$ (metallated, with the coordinated aryl carbon defined as the one position), and $^{\text{R}}\text{PNP}$ to denote neutral 2,6- $\text{C}_5\text{H}_3\text{N}(\text{CH}_2\text{PR}_2)_2$ ligands. Pincer ligands with oxygen or nitrogen (NH) linking groups $^{\text{R}}\text{POCOP}$, $^{\text{R}}\text{PONOP}$, and $^{\text{R}}\text{PNNNP}$ are abbreviated similarly. Heteroleptic or unsymmetrical phosphine substitution may be indicated by expanded superscripts such as $^{(\text{tBu},\text{Ph})_2}\text{PCP}$ or $^{\text{tBu}2\text{Ph}2}\text{PCP}$, and aryl backbone substitution may be denoted as 3,5- $^{\text{tBu}}\text{R}^{\text{PCP}}$, etc. As with all coordination chemistry, the range of ligands available for study hinges upon the availability of efficient ligand synthetic routes. Morales-Morales has recently summarized much of the pincer ligand synthesis literature [10]. In the following section, we shall summarize the current scope of PCP and PNP pincer synthesis, with a focus on the flexibility of these methods in introducing ligand steric and electronic variation at the phosphorus centers.

2 Phosphine Pincer Synthesis

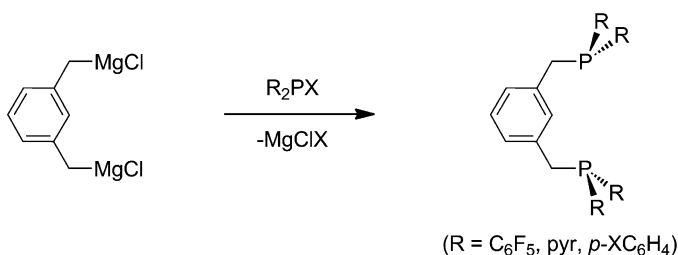
2.1 Benzylic PCP Pincers

The original $^{\text{tBu}}\text{PCPH}$ pincer synthesis, reported by Moulton and Shaw in 1976, relied on $\text{S}_{\text{N}}2$ halide displacement from 1,3- $\text{C}_6\text{H}_4(\text{CH}_2\text{Br})_2$ by $^{\text{tBu}}\text{Bu}_2\text{PH}$ followed by HBr elimination [23]. Together with direct substitution by R_2P^- ($\text{R} = \text{Me}, \text{Ph}$) [24, 25], with very few exceptions all dibenzylic phosphine pincer ligands with $\text{R} = ^{\text{tBu}}, \text{Et}$ [26], $^{\text{iPr}}$ [27, 28], Cy [29, 30], and Ad [31] and other hydrocarbyl-substituted PCP pincer ligands are prepared analogously. The preparation of unsymmetrical pincers 1,3- $\text{C}_6\text{H}_4(\text{CH}_2\text{PR}_2)(\text{CH}_2\text{PR}'_2)$ by sequential addition of secondary phosphines has been reported [32]. Chiral PCP ligands with substituted $\text{CH}(\text{R})$ benzyl arms or mixed PRR' groups are known which similarly rely on $\text{S}_{\text{N}}2$ substitution [33–38]. The synthetic scope of this route is limited to sufficiently nucleophilic electron-rich PR_2 groups, but any accessible 1,3- $\text{C}_6\text{E}_x\text{H}_{4-x}(\text{CH}_2\text{Br})_2$ ($\text{E} \neq \text{H}$) precursors may be used to prepare substituted aryl backbone pincer derivatives by this method (Scheme 1) [39–51].

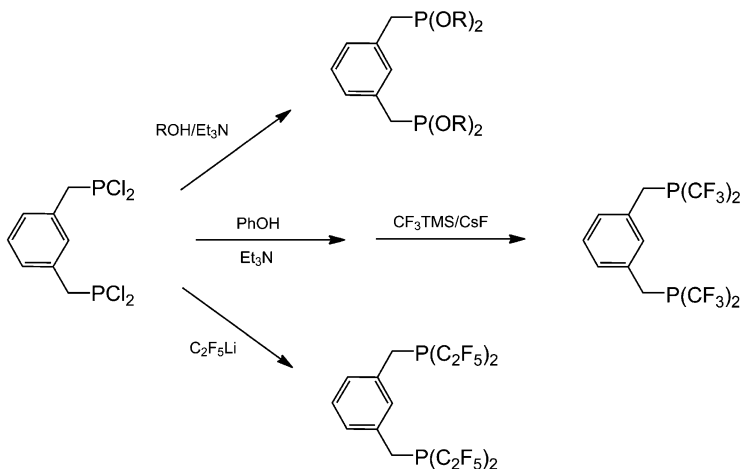
Most electron-withdrawing PCP systems have the general formula $^{\text{X}}\text{PCP}$ ($\text{X} =$ electron-withdrawing group). To access dibenzylic pincer ligands with insufficiently nucleophilic R_2PH or R_2P^- precursors, however, alternative synthetic approaches are required. In 2005, Milstein and van Koten introduced the use of the diGrignard 1,3- $\text{C}_6\text{H}_4(\text{CH}_2\text{MgCl})_2$ in the synthesis of the acceptor PCP ligands



Scheme 1 General PCP Ligand Synthesis

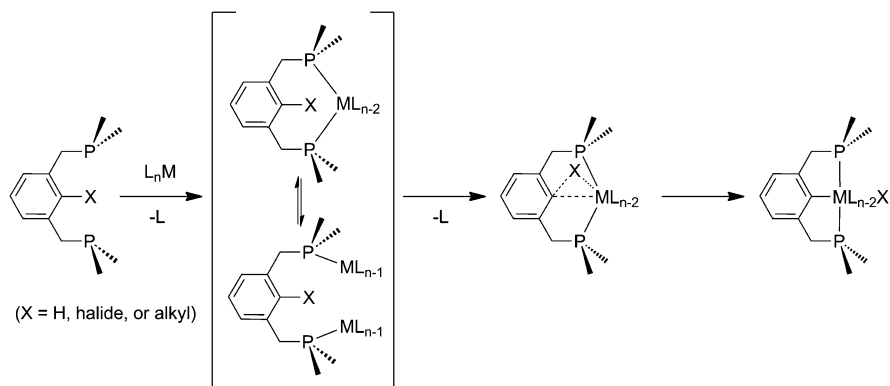


Scheme 2 Alternative PCP Synthesis for Non-nucleophilic Phosphorus Centers



Scheme 3 Perfluoroalkylphosphine PCP Ligand Synthesis

1,3-C₆H₄(CH₂P(pyr)₂)₂ and 1,3-C₆H₄(CH₂P(C₆F₅)₂)₂ (Schemes 2) [52, 53]. The diGrignard reagent has also been used by van Koten in the synthesis of *p*-aryl pincer systems 1,3-C₆H₄(CH₂P(*p*-C₆H₅X)₂)₂ [54]. In principle this approach should access a variety of PR₂ groups provided that the corresponding phosphinoyl halide R₂PX is



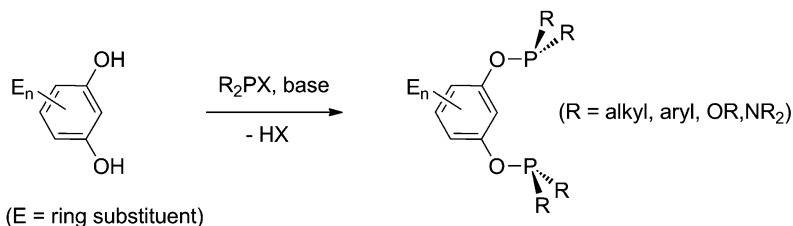
Scheme 4 General Mechanism of PCP Metallation

available. In 2007, our group reported the synthesis of $1,3\text{-C}_6\text{H}_4(\text{CH}_2\text{P}(\text{Cl})_2)_2$, a potentially versatile precursor which was used for the preparation of the strong π -acceptor pincers $1,3\text{-C}_6\text{H}_4(\text{CH}_2\text{P}(\text{R}_f)_2)_2$ ($\text{R} = \text{CF}_3, \text{C}_2\text{F}_5$), and also the pincer phosphite derivatives $1,3\text{-C}_6\text{H}_4(\text{CH}_2\text{P}(\text{OR})_2)_2$ ($\text{R} = \text{Me}, \text{CH}_2\text{CF}_3, \text{aryl}$) (Schemes 3) [55]. We note that benzylic fluorination of phosphonate esters $1,3\text{-C}_6\text{H}_4(\text{CH}_2\text{P}(\text{O})(\text{OR})_2)_2$ to form $1,3\text{-C}_6\text{H}_4(\text{CF}_2\text{P}(\text{O})(\text{OR})_2)_2$ has been reported [56–58], and in principle the synthesis of the most electron-withdrawing ligands $1,3\text{-C}_6\text{H}_4(\text{CF}_2\text{PR}_2)_2$ ($\text{R} = \text{Cl}, \text{OR}, \text{R}_f$) by a modification of our $1,3\text{-C}_6\text{H}_4(\text{CH}_2\text{P}(\text{Cl})_2)_2$ synthetic procedure should be possible.

Most pincer coordination chemistry relies upon aryl C–H bond metallation with a suitable metal complex precursor under thermal conditions (Scheme 4). Under mild conditions, unmetallated $(^{\text{R}}\text{PCPH})\text{ML}_n$ complexes presumably are formed initially, but most studies employ more vigorous thermal conditions and do not report unmetallated adducts. In our coordination studies with the fluorinated pincer $^{\text{CF}_3}\text{PCPH}$ we have structurally characterized several examples of $\mu\text{-}(^{\text{CF}_3}\text{PCPH})$ coordination [55, 59]. Several examples of PCPH ($\eta^2\text{-C}(\text{aryl})\text{-H}$)-M coordination, which model the key pincer metallation step, have been reported [46, 60, 61]. Alternative pincer complex syntheses by aryl C–X ($\text{X} = \text{I}$ or Br) metallation are known [28, 35, 62–66]. Since the initial report in 1993 [67], Milstein has extensively employed the special case of aryl–C bond addition to access a range of PCP pincer systems [4, 68–72].

2.2 Resorcinol-Based POCOP Pincers

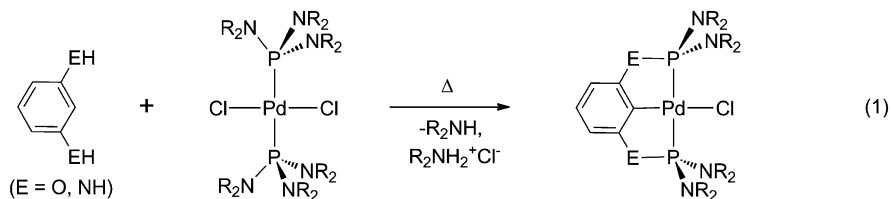
Pincer ligand systems based on a resorcinol backbone (abbreviated $^{\text{R}}\text{POCOP}$, where $\text{R} = \text{PR}_2$ substituent) have enjoyed extensive development owing to the simplicity and versatility of their synthesis from readily available resorcinol derivatives $1,3\text{-C}_6\text{H}_4\text{-}_x\text{R}_x(\text{OH})_2$ (Scheme 5). Following the earliest report in 1968

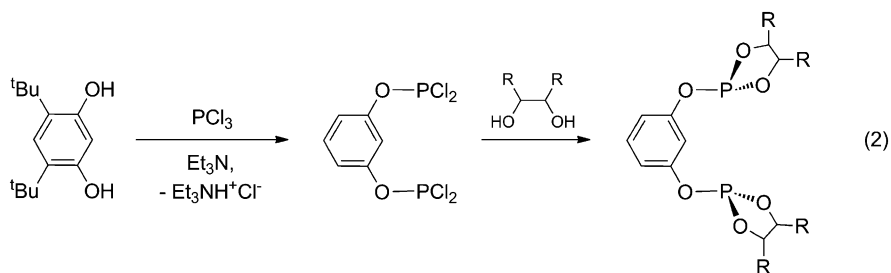


Scheme 5 General POCOP Ligand Synthesis

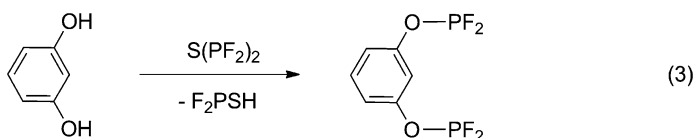
by Maier on the synthesis of $1,3\text{-C}_6\text{H}_4(\text{OP}(\text{tBu})_2)_2$ from resorcinol and ${}^t\text{Bu}_2\text{P}(\text{NEt}_2)$, more recent $1,3\text{-C}_6\text{H}_4(\text{OPR}_2)_2$ ligand syntheses with $\text{R} = {}^t\text{Bu}$ [73], ${}^i\text{Pr}$ [74], and Ph [75] directed toward metal coordination chemistry have appeared which are based on the reaction between resorcinol and $\text{R}_2\text{P}(\text{Cl})$ precursors. As with PCP pincers, the most common POCOP ligands with PR_2 ($\text{R} = \text{hydrocarbyl}$) employed in coordination chemistry studies are $1,3\text{-C}_6\text{H}_4(\text{OP}(\text{R})_2)_2$ ($\text{R} = {}^t\text{Bu}$, ${}^i\text{Pr}$). To our knowledge, $1,3\text{-C}_6\text{H}_4(\text{OPMe}_2)_2$ has been examined in theoretical studies but not synthesized. The parent arylphosphinite $1,3\text{-C}_6\text{H}_4(\text{OPPh}_2)_2$ has been prepared and employed in several studies [75–79]. The coordination chemistry of a bulky arylphosphinite with 2,4,6-trifluoromethyl substitution has recently been reported [80].

Since POCOP ligand syntheses usually rely on simple salt elimination with $\text{R}_2\text{P}(\text{Cl})$ precursors, convenient access to more electron-withdrawing heteroatom pincer systems ${}^{\text{RO}}\text{POCOP}$ and ${}^{\text{R}^2\text{N}}\text{POCOP}$ is possible with a wide range of available phosphoryl halide precursors. Biphenolic POCOP systems [64, 81–87], including chiral binol-type systems [64, 83, 84, 86, 88], have been most extensively studied, though other phenolate and alkoxy-substituted ${}^{\text{RO}}\text{POCOP}$ ligands have been reported [89–92]. The subclass of ${}^{\text{R}^2\text{N}}\text{POCOP}$ ligands includes Frech’s piperidiny-substituted phosphine, ${}^{\text{pip}}\text{POCOP}$, which is prepared “on-metal” by the sequential addition of $(\text{pip})_3\text{P}$ and resorcinol to $(\text{cod})\text{PdCl}_2$ (Eq. 1) [93]. An alternative approach to ${}^{\text{RO}}\text{POCOP}$ and ${}^{\text{R}^2\text{N}}\text{POCOP}$ pincers based on the chlorophosphite precursors ${}^{\text{Cl}}\text{POCOPH}$ is a promising and potentially versatile route to new POCOP ligands (Eq. 2) [88, 94].

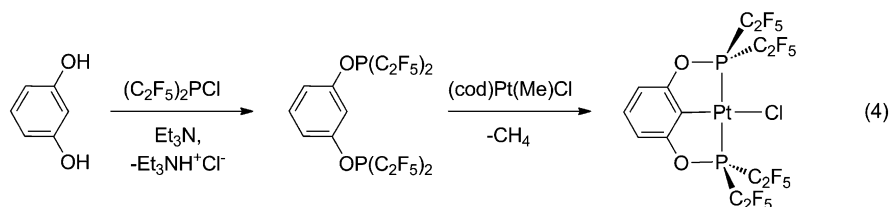




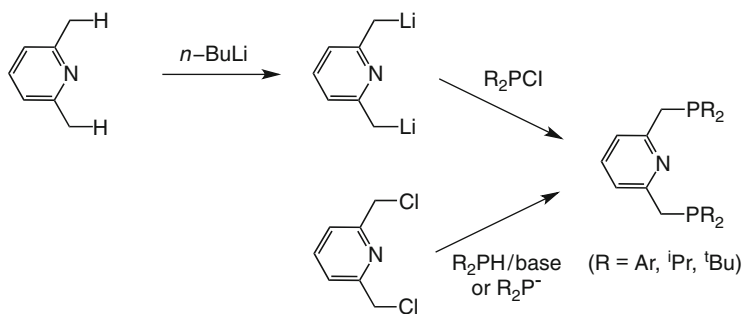
Strong electron-accepting ligands are of the general form $^X\text{POCOP}$ (X = electron-withdrawing group). POCOP analogues of the electron-accepting PCP pincers $1,3\text{-C}_6\text{H}_4(\text{CH}_2\text{P}(\text{pyr})_2)_2$ and $1,3\text{-C}_6\text{H}_4(\text{CH}_2\text{P}(\text{C}_6\text{F}_5)_2)_2$ should be obtainable from resorcinol and the appropriate phosphoryl halide, but have not been reported. Bedford's $^{\text{Cl}}\text{POCOPH}$ systems have not been examined as pincer ligands in their own right. In 1987, Rankin reported a novel synthesis of the fluorinated POCOP ligand $1,3\text{-C}_6\text{H}_4(\text{OPF}_2)_2$ from the reaction of resorcinol and $\text{S}(\text{PF}_2)_2$ (Eq. 3) [95]. While $^{\text{F}}\text{POCOP}$ is anticipated to be a powerful electron-accepting pincer ligand, only the unmetallated bimetallic bridged complexes $(\text{Mo}(\text{CO})_5)_2(\mu\text{-}^{\text{F}}\text{POCOPH})$ and $(\text{Mo}(\text{CO})_4)_2(\mu\text{-}^{\text{F}}\text{POCOPH})_2$ have been reported.



We have recently prepared $^{\text{C}_2\text{F}_5}\text{POCOPH}$ by the reaction of resorcinol with $(\text{C}_2\text{F}_5)_2\text{PCl}$ and Et_3N and formed the metallated complex $(^{\text{C}_2\text{F}_5}\text{POCOP})\text{PtCl}$ by reaction with $(\text{cod})\text{Pt}(\text{Me})\text{Cl}$ (Eq. 4) (Adams JJ, Thorn J, Roddick DM, unpublished results).



PNCNP pincer systems are thus far a relatively small subset in PCP coordination chemistry and are prepared analogously to POCOP pincers using *m*-phenylenediamine instead of a resorcinol derivative. Alkyl-substituted pincers $^{\text{R}}\text{PNCNP}$ ($\text{R} = \text{}^i\text{Pr}$, ^tBu , Ph) [63, 96] have been reported as well as $^{\text{RO}}\text{PNCNP}$ and $^{\text{R}_2\text{N}}\text{PNCNP}$ systems [63, 97, 98]. A single example of an asymmetrically substituted ligand, $^{\text{iPr}}\text{POCNP}$, has been prepared by the reaction of *m*-aminophenol with one equivalent. *n*-BuLi followed by the addition of two equivalents $^{\text{iPr}}\text{Pr}_2\text{PCl}$ [96].

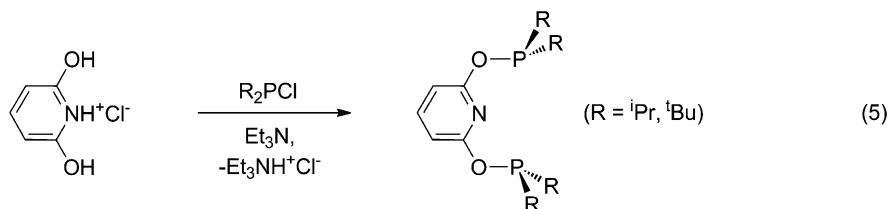


Scheme 6 General PNP Ligand Synthesis

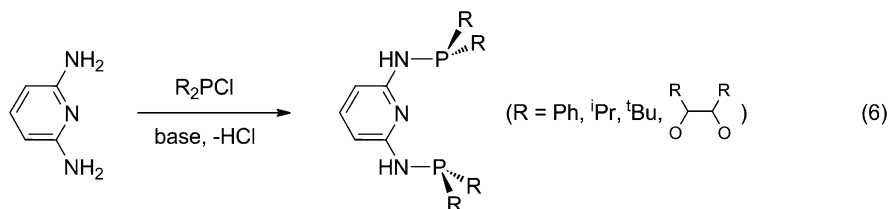
2.3 *PENEP Pincers*

The formal substitution of a neutral pyridyl central group for an anionic aryl affords the corresponding class of *PENEP* pincers (E = CH₂, NH, O) which may form isoelectronic (^RPENEP)ML_n⁺ analogues to (^RPECEP)ML_n. An advantage of pyridyl pincers is elimination of the aryl metallation step required in aryl pincer terdentate coordination. The original synthesis of ^{Ph}PNP, reported by Nelson in 1971 [99], involved the reaction of Ph₂P^{Na}⁺ with 2,6-bis(chloromethyl)pyridine; more recently, ^{Ar}PNP ligands have been similarly using the appropriate Ar₂PH with ^tBuO⁻K⁺ (Scheme 6) [100]. In light of the advances achieved in PCP chemistry using more electron-rich alkylphosphine pendant groups, the first alkylphosphine ^RPNP (R = ⁱPr, ^tBu) ligands were prepared more recently using the analogous reaction of 2,6-bis(chloromethyl)pyridine with ^tBu₂PH [101, 102] or ⁱPr₂PLi [103], or from lutidine dilithiation followed by reaction with ^tBu₂PCl [104]. The neopentyl-substituted ligand ^{Np}PNP has also been prepared recently by the lutidine dilithiation method [105]. ^{Me}PNP has not been prepared synthetically, but is widely used in metal complex calculations. As has been noted previously, the great majority of current coordination chemistry research has focused almost exclusively on the *tert*-butyl pincer ^tBuPNP.

Recognizing the susceptibility of PNP ligand systems to benzylic CH₂ proton loss to form dearomatized pincer complexes [106–108], and the enhanced reactivity of POCOP relative to PCP iridium pincer complexes toward hydrocarbon dehydrogenation [73], ^RPONOP (R = ⁱPr, ^tBu) pincer ligands have been prepared recently for study [109–111]. Reaction of 2,6-dihydropyridine hydrochloride with two equivalents of the appropriate dialkylphosphoryl chloride in the presence of base directly affords PONOP ligands in moderate yield (Eq. 5). This synthesis is analogous to POCOP syntheses and should readily generalize to any ^RPONOP ligands where R₂PCl precursors are available.



The ^{Ph}PNNNP ligand was originally reported by Haupt in 1987, prepared by reaction of 2,4-diaminopyridine with Ph₂PCl and Et₃N [112]. Kirchner has extended this synthesis to a broad range of achiral and chiral ^RPNNNP ligands for study (R = ⁱPr, ^tBu, 1,2-diolato) (Eq. 6) [113]. *N,N'*-dialkylated PNNNP ligands, 2,6-(NR'PPh₂)C₅H₃N (R' = hexyl, undecyl), were not obtainable from 2,6-(N(H)R')₂C₅H₃N and R₂PCl, but could be prepared by successive amine deprotonation/R₂PCl addition steps. A novel triazine pincer ligand was also prepared from 2,6-diamino-4-phenyl-1,3,5-triazine and Ph₂PCl.



3 Pincer Sterics, Conformation, and Coordination Geometries

Since Tolman's introduction of the simple cone angle model for assessing phosphine sterics [114], a number of subsequent steric models have appeared [115–119]. Except for a qualitative expectation of phosphine pincer sterics based on relative PR₂ correlations to R₃P steric size, the enveloping nature of pincer coordination imposes a special case of steric influence. The “horseshoe” of ligand meridional coordination blocks more than 180° of the equatorial volume about a metal, restricting approach to the metal center *trans* to the M–C(aryl) bond axis, while PR₂ steric bulk primarily controls access to the metal center *cis* to the M–C(aryl) bond axis, above and below the central aryl backbone plane (Fig. 1). Substitution of the central aryl backbone may block access to the metal center to a lesser extent. The pronounced asymmetrical steric influence of pincer ligands is similar in some respects to that of NHC ligands, which have been analyzed using the percent buried volume approach (%V_{bur}), a measure of the proportion of the first coordination sphere volume blocked by the ligand in question [120, 121]. In Table 1 we summarize %V_{bur} data for selected phosphine pincer systems. As noted previously, %V_{bur} values are sensitive to the nature of the metal and remaining coordination environment L_nM [121], but there is a substantial body of structural data for (pincer)PdX (X = Cl, Br, I) and other 4-coordinate 4d metal systems to allow many direct comparisons. Several trends are apparent: (1) %V_{bur} values for the different pincer frameworks with the same

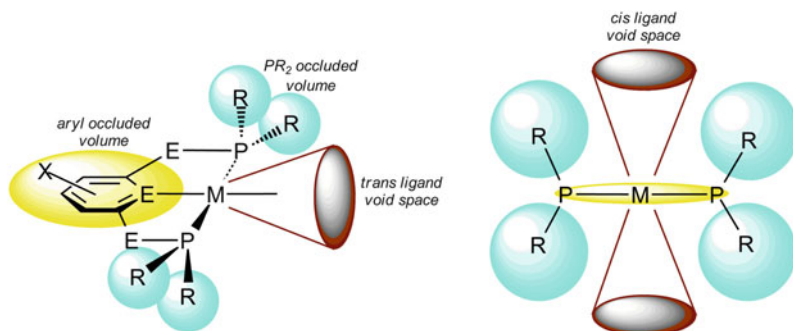


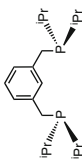
Fig. 1 Asymmetric steric influence of aryl-bridged pincer ligands

pendant phosphine groups are similar ($R = {}^t\text{Bu}$: 69.3–71.1; ${}^i\text{Pr}$: 64.6–66.3; Ph: 60.9–61.8). (2) With some exceptions, $\%V_{\text{bur}}$ data for 4-coordinate (pincer)M (L) systems follow expected steric influence and Tolman cone angle trends (when available) for the pendant PR_2 groups ($R = 2,4,6\text{-CF}_3\text{C}_6\text{H}_2$ (82.3) > adamantyl (79.8) > C_6F_5 (72.0) > ${}^t\text{Bu}$ (71.1) > Et_2N (68.2) > Cy (66.2) \sim ${}^i\text{Pr}$ (66.3) > pip (65.2) > pyr (62.1) \sim Ph (61.8) \sim CF_3 (61.8) > Et (60.7)). (3) $\%V_{\text{bur}}$ values for 6-coordinate complexes are significantly smaller (2–10 %) than comparable 4-coordinate systems, reflecting the ability of pincer systems to adjust and compress relative to the steric demand of other ancillary ligands.

There are some less predictable $\%V_{\text{bur}}$ values listed in Table 1. *o*-tolyl phosphine substituents are generally among the most sterically encumbering ($\theta(o\text{-tol})_3\text{Pp} = 194^\circ$), but $\%V_{\text{bur}}$ for $({}^{o\text{-tol}}\text{POCOP})\text{PdI}$ is only 65.4, comparable to that of $({}^i\text{Pr}\text{POCOP})\text{PdCl}$ (64.6). This reflects the adoption of a more efficient conformation of the aryl methyl groups in the pincer system, which avoids ortho aryl steric congestion about a metal imposed by the C_3 symmetry of the $(o\text{-tol})_3\text{P}$ ligand. Another significant trend is the unusual compactness of biarylphosphite systems, $({}^{\text{biaryl-O}}\text{PECEP})\text{PdX}$ ($E = \text{O}$ or NH ; $X = \text{Cl}$, I), where $\%V_{\text{bur}}$ is only ~ 54 . Incorporation of ortho and para ${}^t\text{Butyl}$ groups on biphenolate substituents only results in an increase of $\%V_{\text{bur}}$ to 66.2 for the rhodium carbonyl derivative. Conformational ambiguities for $(\text{RO})_3\text{P}$ ligands are well recognized [116], but biarylphosphite pincer systems appear to uniformly adopt a “curled-over” geometry where one C_2 -related set of P-OAr groups is bent forward along the C(aryl)-M-X pincer axis. This results in a pronounced C_2 pincer twist, with an associated minimization of $\%V_{\text{bur}}$, which has been exploited in asymmetric synthesis [64, 81–83, 86, 88]. In contrast, the nonchelating aryloxide phosphite pincer $p\text{-MeO-C}_6\text{H}_4\text{OPOCOP}$ adopts an aryloxide conformation where all phosphine substituents are directed away and essentially perpendicular to the pincer aryl backbone plane, resulting in an unusually large $\%V_{\text{bur}}$ value of 67.8 for the palladium iodide complex.

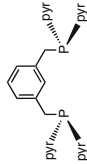
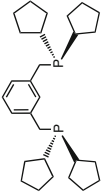
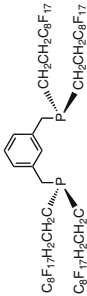
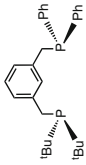
$\%V_{\text{bur}}$ data give only an aggregate estimate of pincer steric influence. In contrast to the *cis* ligand void space (Fig. 1), which is largely controlled by the sterics of

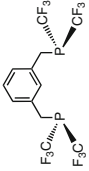
Table 1 Pincer steric and conformational properties

Pincer	ML _n	Coord. #	%buried V	Pincer C ₂ twist, θ	P–M–P angle	References
PCCCP ligands		4	66.3	7.7, 9.5	167.4	[122]
	RhCl ₂ (C ₄ H ₈ O ₂) _{1/2}	6	59.6	19.0	163.5	[123]
PCCCP ligands	PdCl	4	71.1	10.8	165.8	[124]
	Ir(NH ₃)	4	70.4	7.6, 12.0	164.5	[125]
	Ru(CO) ₂ Cl	6	62.1	22.6	157.9	[126]
	Ir(CO)Ph ₂	6	61.4	22.7	157.8	[127]
PCCCP ligands	PdCl	4	61.8	9.6	165.7	[37]
	Pd(PEt ₃) ⁺	4	61.7	20.6	158.0	[128]
	Ru(terpy) ⁺	6	58.3	15.2	157.4	[129]
PdCl	4	65.7	11.8	163.6	[34]	
PCCCP ligands	PdCl	4	66.2	3.6	165.5	[130]
	NiBr	4	75.0	4.0	167.6	[30]
	RhCl ₂ (H ₂ O)	6	59.2	14.4	165.8	[131]

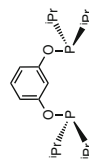
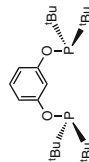
(continued)

Table 1 (continued)

Pincer	ML_n	Coord. #	%buried V	Pincer C_2 twist, θ	P–M–P angle	References
	Rh(PPh ₃)	4	64.7	15.9	154.1	[132]
	Rh(CO)	4	62.1	16.4	156.8	[133]
	Rh(PEt ₃)MeI	6	56.9	17.9	157.5	[133]
	Pd(O ₂ CF ₃)	4	67.7	8.4	163.0	[134]
	Pd(O ₂ CCF ₃)	4	63.9	1.2	167.0	[135]
	Pd(MeCN) ⁺	4	71.2	15.9	161.2	[53]
	PdCl	4	72.0	20.7	160.8	[53]
	PdCl	4	67.2	11.8	165.6	[136]

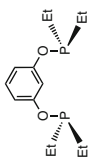
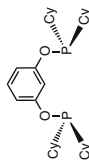
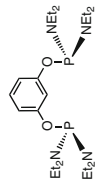
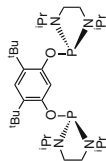
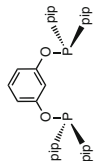
	PtCl	4	61.8	14.3	161.6	[55]
	Ir(CO)	4	61.2	13.4, 12.4	159.3	[137]
	Ir(CO)MeI	6	59.8	16.6	157.7	[137]
	Ir(X)H	5	79.8	11.1	165.2	[31]
	Rh(PEt ₃)MeCl	6	54.3	22.1	157.7	[138]
	Ir(CO)	4	69.3	0.6	157.6	[139]
	Ir(PPh ₃)	4	65.1	1.3	155.3	[140]
	PdCl	4	64.6	1.3, 2.1	160.4	[74]
	RhCl ₂ (dmap)	6	58.6	2.9	159.9	[141]

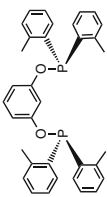
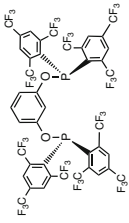
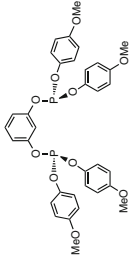
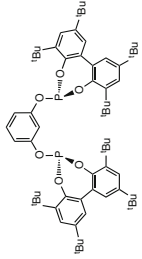
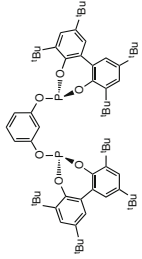
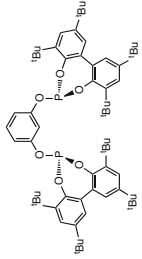
POCOP ligands



(continued)

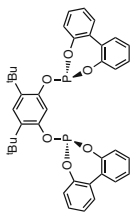
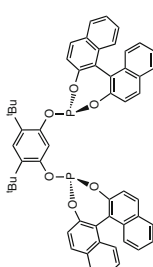
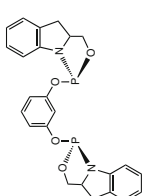
Table 1 (continued)

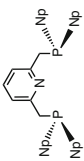
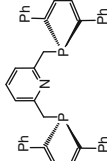
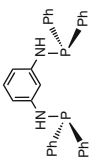
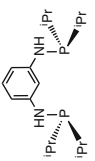
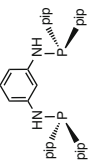
Pincer	ML _n	Coord. #	%buried V	Pincer C ₂ twist, θ	P–M–P angle	References
	PdI	4	60.7	2.1, 3.6	160.2	[142]
	PdI	4	63.1	0.3	160.8	[142]
	PdI	4	68.2	3.8	160.8	[142]
	PdCl	4	66.8	0.6, 3.0	163.4	[94]
	PdCl	4	65.2	1.9, 0.6	160.8	[93]

	PdI	4	65.4	4.2	159.9	[142]
	Ir(N ₂)	4	82.3	4.7	157.9	[80]
	PdI	4	67.8	0.4	159.8	[91]
	Rh(CO)	4	66.2	1.3	156.4	[143]
	Rh(PPh ₃) ₃	4	62.2	3.0	155.0	[143]
	Rh(PPh ₃)(H)Cl	6	56.0	7.3	154.5	[143]

(continued)

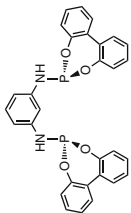
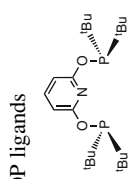
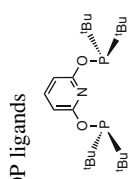
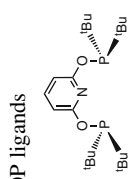
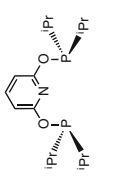
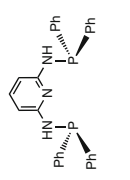
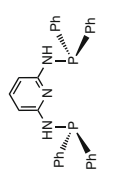
Table 1 (continued)

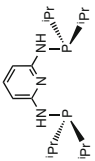
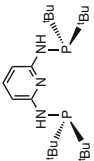
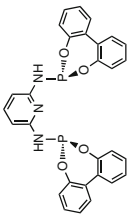
Pincer	ML_n	Coord. #	%buried V	Pincer C_2 twist, θ	P–M–P angle	References
	PdCl	4	54.0	2.4, 3.8	159.6	[81]
	PdCl	4	54.6	3.9	158.1	[88]
	PdI	4	60.8	1.0, 2.9	161.1	[65]
PCNCP ligands	PdX	4	67.0	11.5, 7.7	169.4	[144]
	RuCl ₂ (CC(TMS)Ph)	4	58.8	13.7	162.1	[145]
	ReCl ₃	6	58.0	12.2	162.0	[144]

	Ir(C ₂ H ₄) ⁺	4	72.8	9.9	164.3	[105]
	NiBr ⁺	4	70.9	0.6	176.4	[146]
PNCNP ligands						
	PdCl	4	61.1	3.5	163.5	[63]
	PdCl	4	66.1	2.1	163.9	[96]
	PdCl	4	64.9	5.6	163.1	[93]

(continued)

Table 1 (continued)

Pincer		ML _n	Coord. #	%buried V	Pincer C ₂ twist, θ	P–M–P angle	References
		Pd(O ₂ CCF ₃)	4	54.1	8.9	159.2	[63]
		Ir(Ph)	4	69.3	0.8	160.1	[109]
		Ru(CO)H ₂	6	66.5	1.2	159.8	[111]
		Ru(CO)(H)Cl	6	59.6	2.4	159.4	[111]
		PdCl ⁺	4	60.9	1.3	166.4	[147]
		Mo(CO) ₃	6	55.2	1.4	155.0	[112]

	Mo(CO) ₃	6	57.5	2.9	155.6	[148]
	PdCl ⁺ Mo(CO) ₃	4 6	70.4 62.3	4.7 5.7	166.5 151.7	[148]
	PdCl ⁺	4	54.4	3.1	164.4	[148]

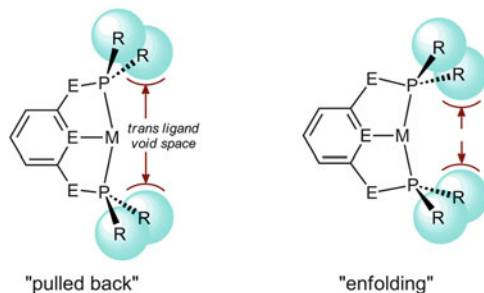


Fig. 2 Effect of “pulled back” and “enfolded” geometries on *trans* void space

pendant phosphine groups, the factors which control the *trans* ligand void space are more complex. In addition to phosphine group steric influence, the *trans* pocket is dependent on the degree of pincer “pull-back,” which is controlled by both metal bonding radii and subtending pincer arm metrics (Fig. 2). For a given pincer ligand smaller metals with shorter M–C(aryl) and M–P bond lengths are enfolded more, as illustrated by the significantly greater % V_{bur} value for $(^{Cy}PCP)NiBr$ (75.0) compared to $(^{Cy}PCP)PdCl$ (66.2) [30, 130]. The smaller C(aryl)–O and O–P bond lengths inherent in POCOP systems result in pincer pull-back and afford greater steric access to the metal center. The more open *trans* void space of $(^{tBu}POCOP)Ir$ relative to $(^{tBu}PCP)Ir$ has recently been quantified by comparing the contact distances between opposing tBu_2P groups in DFT-optimized geometries (4.14 Å versus 2.92 Å) [1]. This difference in steric access to the 3-coordinate catalyst intermediate correlates with the increased alkane dehydrogenation activity of iridium POCOP catalysts relative to PCP analogues.

3.1 Pincer C_2 Twist Trends

In meridional pincer coordination, the coplanarity of the ligating atoms is often accompanied by a C_2 twist of the aryl backbone and the arms attaching the PR_2 groups (Fig. 3). This is summarized in Table 1. Several clear trends are observed. First, for 4-coordinate systems, CH_2 -bridged pincers exhibit the most C_2 twisting (10.1° average), followed by NH -bridged pincers (4.2° average) and finally O-bridged pincers, which with few exceptions possess a virtually planar P–O–Ar–O–P–M array (2.4° average) [143]. 6-coordinate CH_2 -bridged pincer complexes are significantly more twisted (19° average). The twist distortion is energetically soft, as evidenced by a variation of up to 4° (2° average) in twist values between crystallographically independent molecules. This C_2 twist trend follows the corresponding decrease in covalent bond radii for the bridging atom and the resulting effect on the subtending pincer phosphine groups. The average values for C(Ar)– CH_2 (1.51 Å) and CH_2 –P (1.83 Å) bonds in PCP pincer systems total 0.33 Å longer than the corresponding C(Ar)–O (1.37 Å) and O–P (1.64 Å)

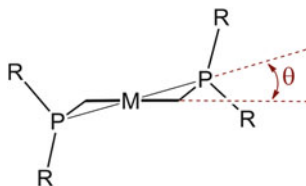


Fig. 3 C_2 pincer twist parameter, θ

bond lengths in POCOP pincers systems.¹ Thus, the pendant PR_2 groups for POCOP systems have significantly smaller chelate bite angles and form essentially planar 5-member chelate rings.

3.2 $P-M-P$ Angle Trends

$P-M-P$ angles subtended by pincer ligands are restricted by the metrics of the $P-E-Ar-E-P$ framework ($E = CH_2, NH, O$) to values less than 180° and readily reflect steric influences about the metal coordination environment. For all 4-coordinate systems, a survey of the Cambridge Crystallographic Database gives an average of 163° (range $152-173^\circ$); for the subset of PCP pincers, the average is higher (164.6°) than for POCOP systems (160.6°). For 6-coordinate systems the overall $P-M-P$ angle is 159.9° . The smaller average angle for POCOP systems is consistent with the smaller covalent radius of oxygen. Two clear trends are evident: (1) The smallest $P-M-P$ angles are generally associated with a sterically demanding ligand such as PPh_3 *trans* to the pincer central aryl group. (2) In pincer systems where steric demand is undifferentiated above and below the planes (i.e., in 4-coordinate compounds and 6-coordinate compounds with *trans* ligands of comparable size), decreases in $P-M-P$ angles are due to bending *toward the pincer aryl unit*. In less symmetrical complexes (such as 5-coordinate pincer complexes, discussed later), the overall $P-M-P$ angle is usually a combination of bending both parallel and perpendicular to the $C(Ar)-M$ bond axis. (3) The largest $P-M-P$ pincer angles are associated with smaller transition metals such as nickel in $(^{C^4H_2Ph_2}PNP)NiBr^+ Ni(H)$ (176.4°), where the $N(Ar)-Ni$ bond length is 1.91 \AA and the PNP ring can more effectively enfold the metal center; for comparison, typical $C(Ar)-M$ and $N(Ar)-M$ bond distances for 4d and 5d metals are $\sim 0.1 \text{ \AA}$ longer.

An examination of PCP ligand C_2 twist and $P-M-P$ angles in Table 1 reveals a rough inverse correlation between high C_2 twist and small $P-M-P$ angles: most reported structures with C_2 twists greater than 15° have $P-M-P$ values below 160° . For a given PCP pincer ligand system, these higher distortions accompany a

¹Pincer metrical parameters are obtained from the Cambridge Crystallographic Database, CSD version 5.32, using data up till May 2011.

decrease in $\%V_{\text{bur}}$ values and reflect a more compact pincer conformation. In general, for all phosphine pincer classes under consideration here, *P–M–P angles below approximately 158° may be taken to reflect some degree of pincer chelate strain and steric constriction.*

3.3 5-Coordinate Pincer Systems

The pincer complexes tabulated in Table 1 are, with one exception, restricted to square planar and octahedral coordination complexes in order to simplify ligand steric comparisons. However, a large number of 5-coordinate pincer systems are known with coordination geometries that vary between the classical extremes of trigonal pyramidal and square pyramidal ligand environments. Most structures can be classified as one of four geometries, defined by angles α , β , γ (Fig. 4). Many d^6 metal complexes (Ru(II), Os(II), Rh(III), Ir(III)) adopt a relatively undistorted square pyramidal geometry where $\alpha \sim 180^\circ$, $\gamma \sim 90^\circ$, and $\beta \sim 160^\circ$ (a typical “unstrained” pincer P–M–P angle, rather than 180° ; see earlier discussion). Ru(II) examples with little distortion include $(^t\text{BuPCP})\text{Ru}(\text{CO})_2^+$ and $(^t\text{BuPCP})\text{Ru}(\text{H})(\text{CO})$ [61, 126]. For Rh(III) and Ir(III), there are many examples with $\alpha \sim 180^\circ$: $(^t\text{BuPCP})\text{Rh}(\text{NO})(\text{CO})^+$ and $(^t\text{BuPNP})\text{Rh}(\text{NO})(\text{MeCN})^{2+}$ [149], $(^t\text{BuPNP})\text{Rh}(\text{NO})(\text{Cl})^+$ [150], $(^t\text{BuPNP})\text{Rh}(\text{Me})(\text{Y})^+$ (Y = I, CN) [151], $(^t\text{BuPOCOP})\text{Rh}(\text{X})(\text{Y})$ (X = H, Me, CH_2Ph ; Y = Cl or BF_4) [152], $(^R\text{PCP})\text{Ir}(\text{H})(\text{Cl})$ (R = ^tBu , Ad) [31], $(^t\text{BuPOCOP})\text{Ir}(\text{H})(\text{Y})$ (Y = NHC_5F_5 , $\text{NHC}(\text{O})\text{C}_6\text{F}_5$) [153], and $(^t\text{BuPNP})\text{Ir}(\text{H})(\text{Ar})^+$ [154, 155]. A common feature of these structures is an apical X ligand with small steric demand (H, Me, NO^- , CO), though undistorted complexes with flat or linear apical ligands which fit well within the cleft above the pincer plane are known: $(^t\text{BuPCP})\text{Ir}(\text{X})(\text{Y})$ (X = Ph, alkenyl, alkynyl; Y = halide) [127, 156]. The complexes $(^t\text{BuPCP})\text{M}(\text{CO})(\text{Cl})$ (M = Fe ($\alpha = 164.3^\circ$), Os ($\alpha = 161.1^\circ$)) with apical CO ligands are significantly distorted and are an exception to this trend [61, 157].

A series of PCP complexes $(^R\text{PCP})\text{M}(\text{PPh}_3)\text{Cl}$ (M = Ru, Os; R = Ph, ^iPr , Cy, C_6F_5) with an apical PPh_3 ligand have been reported with a reduced α value [33, 70, 158–160]. The P–M–P (β) values are less than those found in unstrained pincer systems ($151\text{--}159^\circ$) and reflect a distortion of the pendant PR_2 arms away from the apical PPh_3 ligand. α values do not simply correlate with R steric influence: R = Ph (153.4) > Cy (151.4) > ^iPr (146.6), but appear to track the ability of R groups to flatten away from the Ph_3P phenyl rings and influence the steric pocket about the Y ligand (chloride). The least distorted structural example from this series is $(^t\text{Bu,PhPCP})\text{Ru}(\text{PPh}_3)\text{Cl}$ ($\alpha = 169.4$) [33], where the PPh_3 ligand meshes well with the pincer Ph and ^tBu groups and the PPh_3 rings are staggered with respect to the Ru–Cl bond. The most distorted example from this series, $(^{\text{C}_6\text{F}_5}\text{PCP})\text{Ru}(\text{PPh}_3)\text{Cl}$, ($\alpha = 96.5^\circ$) was reported by van Koten [159]. In this complex the pincer aryl binding site assumes the apical position of a square pyramidal coordination and C_6F_5 rings are engaged in π -stacking with the PPh_3 rings. The Cl ligand is bent drastically away to avoid steric interaction with the C_6F_5 ortho fluorines, but it is not

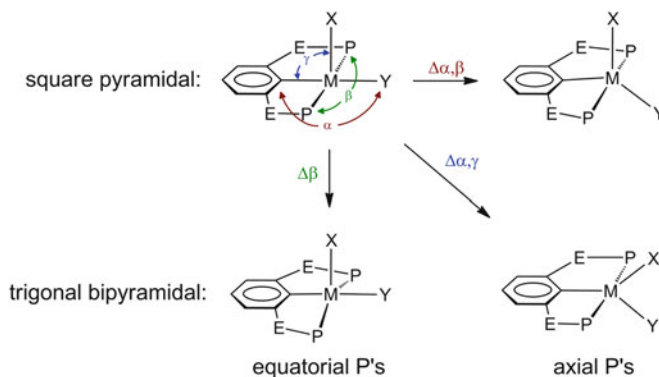


Fig. 4 5-Coordinate pincer complex geometric parameters

clear whether this unique coordination geometry is solely due to steric factors or the electronic influence of the strongly π -accepting C^{6F5} PCP ligand.

A series of 5-coordinate iron d^6 PNP pincer complexes (R PNP)FeCl₂ have been structurally characterized which are significantly distorted from a square pyramidal geometry ($160^\circ > \alpha > 145^\circ$; $149^\circ > \beta > 140^\circ$) [102, 113, 161, 162]. In these systems the primary distortion is an elevation of the iron center above the pincer backbone plane by 0.29–0.59 Å in order to accommodate unusually long N–Fe and P–Fe bond distances to the high-spin iron center [102]. Cobalt(II) d^7 5-coordinate (A rPNP)CoCl₂ complexes have also been reported [100]. The structures of these compounds are best described as distorted trigonal bipyramidal, with axial PR₂ pincer groups ($\beta = 155^\circ$) and equatorial Cls (Ar = *o*-tol: $\alpha = 130.4^\circ$, $\gamma = 111.9^\circ$; Ar = Mes: $\alpha = \gamma = 120.6^\circ$). A very large pincer C₂ twist of 27° is present in these compounds and is probably induced by very long (2.62 Å) Co–P bonds to the high-spin cobalt center.

3.4 d^8 5-Coordinate Pincer Systems

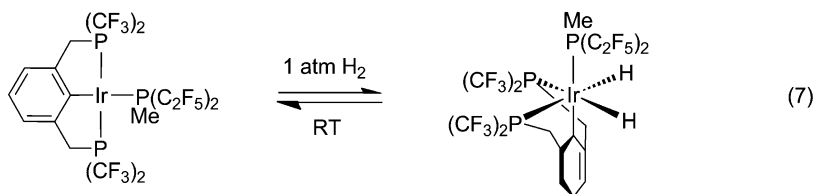
5-Coordinate d^8 pincer systems are much rarer. There are several examples of zerovalent group 8 systems: (R PNP)Fe(CO)₂ (R = ^tBu, ⁱPr) [102, 163] and (^tBuPONOP)Ru(CO)₂ [111]. While (^tBuPNP)Fe(CO)₂ exhibits a $\Delta\alpha, \beta$ square pyramidal distortion ($\alpha = 152.5^\circ$, $\beta = 152.9^\circ$), (ⁱPrPONOP)Ru(CO)₂ is more accurately described by a $\Delta\alpha, \gamma$ TBP distortion ($\alpha = 136.6^\circ$, $\gamma = 111.5^\circ$). In contrast, (ⁱPrPNP)Fe(CO)₂ adopts a nearly ideal TBP geometry with axial phosphorus ligation ($\alpha = \gamma = 120.0^\circ$, $\beta = 166.0^\circ$). Thus, relatively modest changes in pincer ligand sterics can favor either SP or TBP geometries and the energetic difference is probably not large.

In 2005, Milstein reported the first examples of d^8 M(I) 5-coordinate pincer complexes, ($^{PY^T}$ PCP)Rh(PR₃)(CO) (R = Ph, Et, pyr), formed from the reaction of ($^{PY^T}$ PCP)Rh(PR₃) with CO [132]. Crystallographic data for ($^{PY^T}$ PCP)Rh(PEt₃)(CO)

confirmed a relatively undistorted $\Delta\beta$ rather than a $\Delta\alpha$, γ TBP geometry, with axial CO and equatorial P(pyr)₂ pincer and PEt₃ groups ($\alpha = 178.9$, $\beta = 128.3^\circ$, $\gamma = 87.9^\circ$). More recently, an example of a d⁸ Co(I) pincer complex, (^{Ph}POCOP)Co(PMe₃)₂, has been reported [164]. As was the case for (^{Pyr}PCP)Rh(PR₃)(CO), (^{Ph}POCOP)Co(PMe₃)₂ adopts a $\Delta\beta$ distortion which places the pincer phosphorus groups and one PMe₃ in the TBP equatorial plane ($\alpha = 172.0$, $\beta = 131.5^\circ$).

Milstein has argued on the basis of DFT calculations that coordination of a fifth ligand to square planar (^{Pyr}PCP)Rh(PR₃) systems is favored by stabilization of a bent “see-saw” geometry by the electron-withdrawing pyrrolyl phosphine substituents, which lower the energy of the frontier d orbitals [132]. The 5-coordinate dicarbonyl complex (^{Pyr}PCP)Rh(CO)₂ was predicted to be marginally stable ($\Delta H(\text{CO dissociation}) \sim 3 \text{ kcal mol}^{-1}$) but was not prepared. As part of our research program exploring the chemistry of perfluoroylalkylated phosphine complexes, we recently reported the synthesis of Ir(I) pincer complexes incorporating the strong acceptor ligand ^{CF3}PCP [137]. In agreement with Milstein’s prediction, a series of stable 5-coordinate Ir(I) complexes (^{CF3}PCP)Ir(L)(L′) (L = L′ = CO, MeP(C₂F₅)₂; L = C₂H₄, L′ = PhCN; L, L′ = cod, nbd, (C₂F₅)₂PCH₂CH₂P(C₂F₅)₂) were isolated and structurally characterized. All nonchelating systems were found to adopt TBP geometries with a $\Delta\beta$ distortion and equatorial pincer P(CF₃)₂ groups ((^{CF3}PCP)Ir(CO)₂: $\alpha = 171.6$, $\beta = 130.3^\circ$; (^{CF3}PCP)Ir(MeP(C₂F₅)₂)₂: $\alpha = 173.6$, $\beta = 124.2^\circ$; (^{CF3}PCP)Ir(C₂H₄)(PhCN): $\alpha = 177.9$, $\beta = 123.8^\circ$).

In general, unequal steric influence above and below the nominal pincer chelate plane in 5-coordinate systems leads to a decrease in P–M–P angles. Besides the d⁸ and d⁶ systems discussed above, several examples of pincer complexes with small P–M–P angles which can be more accurately described as “cisoidal” have been reported. The most exceptional examples are Jia’s osmium 3-legged ($\eta^5\text{-C}_5\text{H}_x\text{R}_{5-x}$)Os(^{Ph}PCP) and 4-legged ($\eta^5\text{-C}_5\text{H}_x\text{R}_{5-x}$)Os(^{Ph}PCP)(X) piano-stool compounds with P–Os–P angles as small as 107–108° [165]. As part of our studies of (^{CF3}PCP)Ir(L) (L = CO, MeP(C₂F₅)₂) chemistry, we have reported the reaction of (^{CF3}PCP)Ir(MeP(C₂F₅)₂) with H₂ to form what can be best classified as a 6-coordinate complex with a facial pincer, *fac.cis*-(^{CF3}PCP)Ir(MeP(C₂F₅)₂)(H)₂ with a P–Ir–P angle of 118° (Eq. 7) [137]. VT NMR confirmed that the reaction of (^{CF3}PCP)Ir(CO) with H₂ similarly proceeds via the intermediacy of *fac.cis*-(^{CF3}PCP)Ir(CO)(H)₂.



3.5 Nonmeridional Complexes and Reaction Intermediates

For ^{CF3}PCP systems we have structurally characterized examples of meridional (“flat”) 4-coordinate, TBP 5-coordinate, and facial octahedral 6-coordinate pincer coordination modes which demonstrate a flexible range of pincer flexibility (Fig. 5).

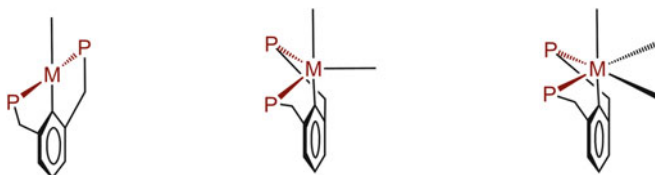


Fig. 5 Meridional, *eq,ax,eq*, and facial pincer coordination

For 4-coordinate pincers such as $(\text{CF}_3\text{PCP})\text{Ir}(\text{CO})$, the facile addition of H_2 is likely to proceed via the formation of a 5-coordinate dihydrogen complex $(\text{CF}_3\text{PCP})\text{Ir}(\text{CO})(\eta^2\text{-H}_2)$. More generally, any associative or oxidative addition reaction of a substrate (A–B) to 4-coordinate (pincer)M(L) systems should similarly involve 5-coordinate (pincer)M(L)(AB) intermediates. H_2 addition to $(\text{R}^i\text{PCP})\text{M}(\text{CO})$ ($\text{M} = \text{Rh}, \text{Ir}$) has a remarkable dependence on the nature of R: When $\text{R} = \text{CF}_3$ or ^iPr , H_2 addition occurs readily to form dihydride products, but when $\text{R} = ^t\text{Bu}$ no reaction is reported [166]. In light of the minimal steric demand of H_2 , the dramatic difference between $\text{R} = ^i\text{Pr}$ and ^tBu reactivity is quite surprising. As discussed earlier, Milstein has invoked electronic effects to explain the energetically favorable formation of $(\text{P}^{\text{yr}}\text{PCP})\text{Rh}(\text{R}_3\text{P})(\text{CO})$ adducts [132]. van Koten, in contrast, has rationalized differences in $(\text{R}^i\text{NCN})\text{Pt}(\text{X})$ binding of Lewis acids in terms of steric interference of pendant R groups in the bent pincer product geometry [2, 16–19]. The restriction of pincer coordination cavity by R group sizes and contact distances has been discussed by other researchers [143, 167].

Expanding upon Milstein's earlier work, we have carried out a systematic DFT study of PCP bending energetics for $(\text{R}^i\text{PCP})\text{Ir}(\text{CO})$ complexes for pincer phosphine substituents with a wide range of steric influence and donating ability (Fig. 6). Very little divergence in total complex energy is observed when the pincer P–Ir–P angle is reduced 10° from the optimized complex geometries. This is due to the ability of pincer ligands to readily distort in one of several ways (Fig. 7). Except for $(^t\text{BuPOCOP})\text{Ir}(\text{CO})$ (which like virtually all POCOP systems is essentially flat, with the oxygen arms in the plane of the pincer aryl ring), and $(\text{C}^6\text{F}_5\text{PCP})\text{Ir}(\text{CO})$, whose ground-state geometry adopts a slight C_s distortion to enhance C_6F_5 ring π -stacking, all $(\text{R}^i\text{PCP})\text{Ir}(\text{CO})$ systems adopt a twisted C_2 ground-state geometry. Three derivatives ($\text{R} = \text{H}, \text{Me}, \text{pyr}$) accommodate the enforced 10° P–Ir–P angle decrease by increasing the C_2 distortion ($\text{R} = \text{H}: 7.9 \rightarrow 18.6^\circ$; $\text{Me}: 15.1 \rightarrow 23.1^\circ$; $\text{pyr}: 12.6 \rightarrow 21.5^\circ$) without undergoing a P–Ir–P bend orthogonal to the C(aryl)–Ir bond axis. This type of symmetrical distortion was noted for 6- relative to 4-coordinate pincer systems (Table 1). In contrast, three pincer derivatives ($\text{R} = ^t\text{Bu}, ^i\text{Pr}, \text{F}$) undergo an asymmetrical distortion where one pincer CH_2PR_2 arm twists further above the aryl pincer plane, but the other arm twists back toward the aryl plane. $(^t\text{BuPOCOP})\text{Ir}(\text{CO})$ similarly accommodates the decreased P–Ir–P angle by asymmetrically twisting one OP^tBu_2 pincer arm out of the aryl pincer plane. $(\text{CF}_3\text{PCP})\text{Ir}(\text{CO})$ is unique in that both pincer arms swing upward directly into the “gull wing” conformation observed for non-meridional pincer systems.

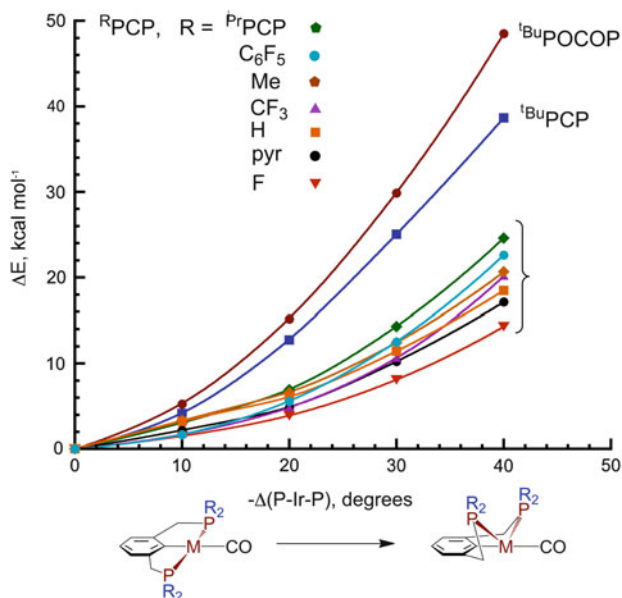


Fig. 6 Calculated (^RPCP)Ir(CO) P–Ir–P bending energetics. DFT tpssh meta-GGA functional (Gaussian 09 Rev A.02) using Dunning cc-pVDZ basis sets with augmented diffuse P, F, and N. Figen pseudopotentials and a correlation-consistent diffuse basis set for iridium were used [168]

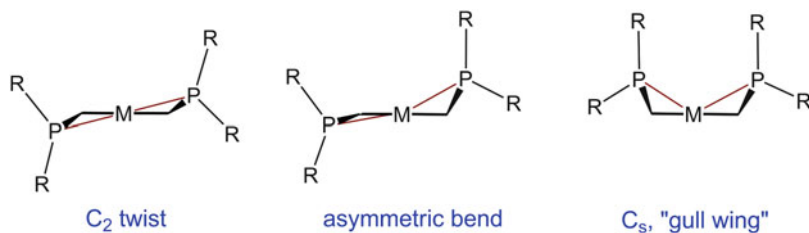


Fig. 7 Types of pincer bending conformations

Further decreases in the P–Ir–P pincer angle result in a significant destabilization of the bulkiest pincer systems, (^tBuPOCOP)Ir(CO) and (^tBuPCP)Ir(CO), relative to all the other ^RPCP complexes. For decreases in the P–Ir–P angle beyond 10°, all smaller pincer ligand systems adopt a symmetrical gull wing pincer arm conformation. (^tBuPCP)Ir(CO) undergoes an increasing asymmetric distortion of one pincer arm out of the aryl plane while maintaining the other arm essentially coplanar to the aryl ring, while (^tBuPOCOP)Ir(CO) adopts progressively distorted gull wing conformations. To test whether the strong π -acceptor CO ligand *trans* to the pincer aryl group has an influence on pincer bending energetics, an analogous series of DFT calculations were performed for the ammonia adducts, (^RPCP)Ir(NH₃) (Fig. 8). Apart from a slightly greater spread of distortion energies at 10° (the energy cost

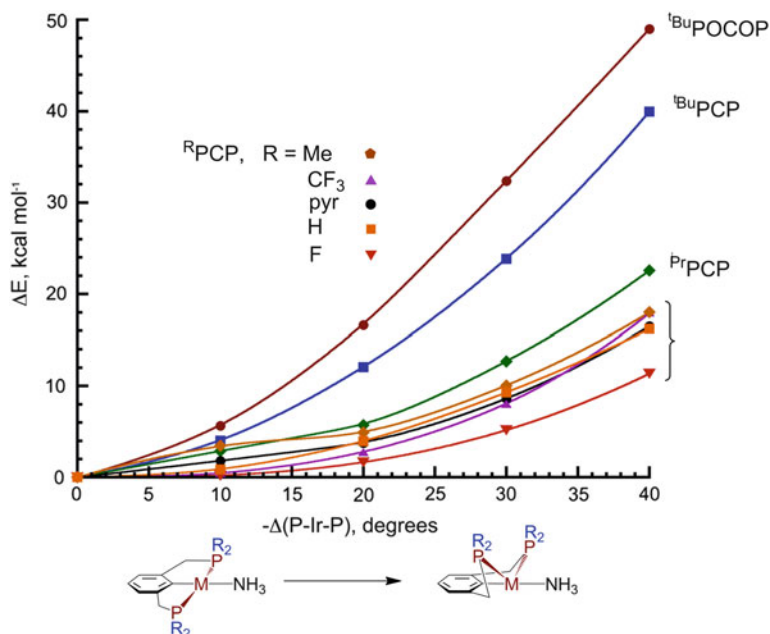


Fig. 8 Calculated (^RPCP)Ir(NH₃) P–Ir–P bending energetics. DFT calculations carried out as described for Fig. 5

for $R = F$ and CF_3 pincer distortion is very small, $<0.5 \text{ kcal mol}^{-1}$), the same basic trend is observed. At the maximum distortion angle calculated, 40° , the difference in energy between the strongest pincer acceptor, $R = F$, and the donor $R = Me$ is only $6.3 \text{ kcal mol}^{-1}$. As noted by Milstein, the strongest acceptor pincers have the least energetic cost for bending into a “see-saw” configuration. Methyl fluorination has *virtually no net effect* on bending energetics: at $-\Delta(P-Ir-P) = 40^\circ$, the difference in ΔE for both Ir–CO and Ir–NH₃ derivatives is less than 1 kcal mol^{-1} . The similarity between $R = CF_3$ and CH_3 pincer systems is likely due to a compensating steric destabilization for the larger CF_3 groups. At 40° the larger (^{iPr}PCP)Ir(CO) complex is destabilized relative to (^{Me}PCP)Ir(CO) by only $\sim 3.5 \text{ kcal mol}^{-1}$.

It is clear from Figs. 6 and 8 that the dominant factor in bending energetics is the steric influence of the phosphine substituents. ^tBu pincer systems pay the highest price: while relatively flat $R = ^iPr$ and pyr substituents adopt rotamer conformations that minimize PR_2 axial–axial repulsions, the rigid nature of aryl-bridged terdentate ligands enforces a highly unfavorable ^tBu–^tBu interaction. The highest destabilization is found for the POCOP system ($\sim 10 \text{ kcal mol}^{-1}$ relative to ^tBuPCP), which has shorter pendant arm bond lengths and the least conformational flexibility. The chemical and structural consequences for 5- and 6-coordinate complexes with non-meridional pincer ancillary ligands ($\Delta\beta$ distortions) are very significant. Taking ^{Me}PCP as a baseline, we can estimate the steric cost for the most commonly used pincer types, ^tBuPECEP and ^tBuPENEP as being $12 < \Delta E < 20 \text{ kcal mol}^{-1}$ for

non-meridional pincers with $130^\circ > \beta > 120^\circ$ and $E = \text{CH}_2$, to as much as $18 < \Delta E < 30 \text{ kcal mol}^{-1}$ for POCOP and PONOP systems. PNCNP and PNNNP systems should have an intermediate pincer distortion behavior. In our discussion of non-meridional reaction intermediates (see earlier), we noted the surprising failure of $(^t\text{BuPCP})\text{Ir}(\text{CO})$ to react with H_2 [166]. Assuming $\beta = 130^\circ$ for an initial H_2 adduct $(^t\text{BuPCP})\text{Ir}(\text{CO})(\text{H}_2)$, we can estimate a steric destabilization of $\sim 10 \text{ kcal mol}^{-1}$ relative to $(^i\text{PrPCP})\text{Ir}(\text{CO})(\text{H}_2)$, which may be sufficient to account for the observed substituent effect. This t-Butyl substituent steric effect is illustrated very nicely by Krogh-Jespersen and Goldman's combined theoretical and experimental study of alkane dehydrogenation by $(^R\text{PCP})\text{IrH}_4$ ($R = ^t\text{Bu}$ or Me) systems [32]. Substitution of only one ^tBu group by Me results in a calculated 10 kcal mol^{-1} decrease in the β -H elimination transition state and a corresponding increase in catalytic activity. Further methyl substitutions result in less dramatic effects and complex oligomerization becomes favored. These observations are consistent with the idea that removing even a single ^tBu group greatly facilitates non-meridional pincer bending.

4 Phosphine Pincer Electronic Effects

4.1 $\nu(\text{CO})$ Trends

Despite the variety of ligand variation in phosphine and arene ring substituents as well as pincer linkages (CH(R), NH, O), relatively little in the way of direct systematic experimental comparisons of pincer electronic influence has been reported. Most available comparative $\nu(\text{CO})$ data concern isostructural ^RPCP and $^R\text{POCOP}$ complexes and variations in phosphine R groups. Very little information exists for analogous PNCNP carbonyl compounds. Table 2 summarizes $\nu(\text{CO})$ data for isostructural classes of pincer carbonyl complexes where a suitable range of systematic data has been reported. Only a single direct comparison of PNCNP versus POCOP has been reported, $(^{\text{pip}}\text{PNCNP})\text{Pd}(\text{CO})^+$ ($\nu(\text{CO}) = 2,106 \text{ cm}^{-1}$) and $(^{\text{pip}}\text{POCOP})\text{Pd}(\text{CO})^+$ ($\nu(\text{CO}) = 2,133 \text{ cm}^{-1}$), which clearly shows the expected greater electron donating influence of $^R\text{PNCNP}$ relative to $^R\text{POCOP}$ [93]. Some direct $^R\text{POCOP}$ comparisons to corresponding ^RPCP carbonyl compounds are available: $(^R\text{PCP})\text{M}(\text{CO})$ and $(^R\text{POCOP})\text{M}(\text{CO})$ ($M = \text{Rh, Ir}$; $R = ^t\text{Bu, } ^i\text{Pr}$) systems have $\Delta\nu(\text{CO})$'s of $21\text{--}26 \text{ cm}^{-1}$. This increase in $\nu(\text{CO})$ going from ^RPCP to $^R\text{POCOP}$ is similar to the 27 cm^{-1} difference between $^{\text{pip}}\text{PNCNP}$ and $^{\text{pip}}\text{POCOP}$ and suggests that the baseline donating abilities of ^RPCP and $^R\text{PNCNP}$ ligands are comparable. This similarity most likely reflects a balancing of electron-withdrawing NH pincer arms on phosphine donor ability and NH π -donation into the central aryl backbone.

Trends in phosphine substituent influence on $\nu(\text{CO})$ follow the expected order of R donor ability, as judged by Hammett σ_m parameters: [174, 175] $\text{Ad}(-0.12) > ^t\text{Bu}$

Table 2 Pincer carbonyl complex data

Complex	$\nu(\text{CO}), \text{cm}^{-1}$	$\Delta\nu$ range, cm^{-1}	References
Pd(CO) ⁺ systems			
(^t BuPCP)Pd(CO) ⁺	2,078	↓	[169]
(^{pi} PNCNP)Pd(CO) ⁺	2,106		[93]
(^{pi} POCOP)Pd(CO) ⁺	2,133		[93]
(ⁱ PrPOCOP)Pd(CO) ⁺	2,141		[170]
		63	
Pt(CO) ⁺ systems			
(^t BuPCP)Pt(CO) ⁺	2,074	↓	[171]
(ⁱ PrPCP)Pt(CO) ⁺	2,080		[171]
(^{CF} ₃ PCP)Pt(CO) ⁺	2,143		[55]
		69	
Ir(CO) systems			
(^{Ad} PCP)Ir(CO)	1,916	↓	[31]
(Me ₂ N- ^t BuPCP)Ir(CO)	1,918		[42]
(MeO- ^t BuPCP)Ir(CO)	1,923		[42]
(H- ^t BuPCP)Ir(CO)	1,925		[42]
(MeO ₂ C- ^t BuPCP)Ir(CO)	1,931		[42]
(^t Bu ₂ PO- ^t BuPOCOP)Ir(CO)	1,934		[42]
(MeO- ^t BuPOCOP)Ir(CO)	1,947		[172]
(Me- ^t BuPOCOP)Ir(CO)	1,947		[172]
(H- ^t BuPOCOP)Ir(CO)	1,949		[172]
(F- ^t BuPOCOP)Ir(CO)	1,953		[172]
(C ₆ F ₅ - ^t BuPOCOP)Ir(CO)	1,955		[172]
(Ar ^F - ^t BuPOCOP)Ir(CO) ^a	1,955		[172]
(^t BuPNP)Ir(CO) ⁺	1,962		[173]
(^{CF} ₃ PCP)Ir(CO)	2,018		[137]
		102	

^aAr^F = 3,5-(CF₃)₂C₆H₃

(-0.10) > Me(-0.07), Cy(-0.05), ⁱPr(-0.04) > Ph(0.06) > PhO(0.25) > CF₃(0.43). Brookhart has reported a range of (R-^tBuPOCOP)Ir(CO) derivatives which provide a measure of the para ring substituent effect on pincer electronics, ranging from electron-donating R = MeO ($\nu(\text{CO}) = 1,947 \text{ cm}^{-1}$) to electron-withdrawing R = C₆F₅ ($\nu(\text{CO}) = 1,955 \text{ cm}^{-1}$) [172]. The small $\Delta\nu(\text{CO})$ of 8 cm^{-1} range indicates that para effects are quite minor. An identical $\Delta\nu(\text{CO}) = 8 \text{ cm}^{-1}$ for R = MeO to C₆F₅ is seen for (R-^tBuPCP)Ir(CO) systems [42].

Goldman and Krogh-Jespersen have carried out a DFT analysis of the contrasting effects of O → C(aryl) π -donation for (R-^tBuPCP)Ir and (R-^tBuPOCOP)Ir (R = H or MeO) and have concluded that the induced net charge effects on iridium for PCP and POCOP pincer frameworks are actually quite comparable [176]. The ~20 cm^{-1} increase in $\nu(\text{CO})$ for POCOP carbonyl systems relative to PCP analogues was

Table 3 Calculated (^RPCP)Ir(CO) properties

Complex	$\nu(\text{CO})$ (exp), cm^{-1}	Ir charge	P charge	C(aryl) charge	Dipole, D^{a}
(^t BuPOCOP)Ir(CO)	1,974 (1,949)	-0.401	+0.241	+0.089	-0.55
(^t BuPCP)Ir(CO)	1,952 (1,925)	-0.637	-0.039	+0.071	0.91
(ⁱ PrPCP)Ir(CO)	1,962	-0.601	-0.026	+0.066	0.97
(^{Me} PCP)Ir(CO)	1,980	-0.423	-0.196	+0.052	1.39
(^H PCP)Ir(CO)	2,007	-0.115	-0.076	+0.039	2.47
(^{C6F5} PCP)Ir(CO)	2,021	-0.364	+0.494	+0.066	3.87
(^{pyr} PCP)Ir(CO)	2,023	-0.325	+0.324	+0.071	3.06
(^{CF3} PCP)Ir(CO)	2,040 (2,018)	-0.396	+0.134	+0.058	4.77
(^F PCP)Ir(CO)	2,052	-0.151	+0.959	+0.032	4.67

Geometry optimization and frequency DFT calculations as described for Fig. 6

^aPositive D values denote dipoles directed along the Ir–C(aryl) bond axis, negative D values are directed along the Ir–CO bond axis

attributed to an electrostatic effect on coordinated CO due to a greater POCOP dipole directed opposite the Ir–CO bond axis.

As part of our (^RPCP)Ir(CO) DFT bending energetic studies described earlier, we have examined (^RPCP)Ir(CO) compounds with both electron-donating and -withdrawing R groups (Table 3). Calculated $\nu(\text{CO})$ values (unscaled) for the very electron-poor (^{CF3}PCP)Ir(CO) complex as well as the ^tBu derivatives (^tBuPCP)Ir(CO) and (^tBuPOCOP)Ir(CO) are consistently shifted $25 \pm 2 \text{ cm}^{-1}$ to higher energy; thus, we anticipate that the remaining calculated values should track $\nu(\text{CO})$ to a similar level of accuracy. The variation of net atomic charges on iridium, phosphorus, and C(aryl) does not follow any obvious correlation with pincer donating/withdrawing ability. However, the increase of molecular dipole magnitude tracks the electron withdrawing ability of phosphorus substituents and correlates well with $\nu(\text{CO})$.

4.2 Electrochemical Studies

A number of pincer systems have been analyzed by cyclic voltammetry, which can provide more direct comparisons of relative metal electron density (all $E_{1/2}$ values cited are versus Fc/Fc^+). Early work by DuBois with PCP and PNP palladium pincer systems reported irreversible reductions for (^{Ph}PCP)Pd(L)⁺ (L = MeCN (-1.99 V), Et₃P (-2.20 V)) and a 2-electron reversible reduction for (^{Ph}PNP)Pd(Et₃P)²⁺ (-1.22 V) [128]. Mayer and Speiser have examined the electrochemistry of (R-^tBuPCP)Ir(H)Cl (R = H, MeO). While oxidation to Ir(IV) is complicated by subsequent metallation of the pincer pendant ^tBu groups, CV simulations afforded oxidation potentials of +0.56 V (R = H) parent system and +0.283 V for the more electron-rich *p*-MeO derivative [44, 177].

Van Koten has reported a series of pincer electrochemical studies which provide important information on pincer electronic effects. Increasing Ru(II)/Ru(III) oxidation potentials for (^{Me}NCN)Ru(tpy)⁺ (-0.178 V), (ⁱPrPCP)Ru(tpy)⁺ (+0.056 V),

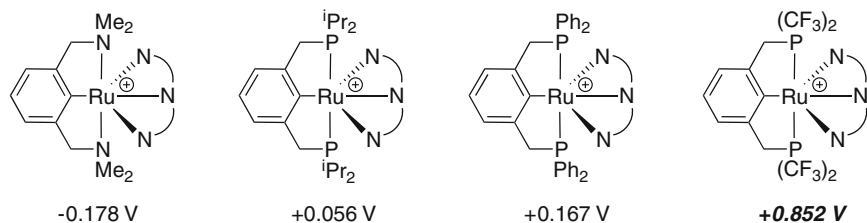


Fig. 9 Comparison of ruthenium pincer redox potentials

(^{Ph}PCP)Ru(tpy)⁺ (+0.167 V), and Ru(tpy)₂⁺ (+1.32 V) give the ligand donor strength ordering ^{Me}NCN > ^{iPr}PCP⁻ > ^{Ph}PCP⁻ ≫ tpy (Fig. 9) [129]. While the 111 mV difference between the PCP systems can be readily attributed to the more electron-releasing nature of ^{iPr} relative to Ph, the stronger donating ability of ^{Me}NCN is not as readily explained. The presumed greater affinity of Ru³⁺ for harder NCN Lewis base provides a tentative qualitative rationale.

We have recently prepared the analogous ruthenium terpyridine complex (^{CF3}PCP)Ru(tpy)⁺ and examined its electrochemistry (Adams JJ, Roddick DM, unpublished results). In acetonitrile (0.1 M TBAP) a fully reversible Ru(II)/Ru(III) oxidation couple is observed at a remarkably high potential of +0.852 V. The increase of 0.7–0.8 V in oxidation potential relative to ruthenium supported by ^{iPr}PCP and ^{Ph}PCP pincer ligands (Fig. 9) is slightly less than the effect on oxidation potentials previously reported by us for the replacement of aryl or alkyl groups with perfluoroethyl groups in chelating phosphine systems: $\Delta E_{\text{ox}} = +1.3$ V (CpMn(dfepe)(CO) (dfepe = (C₂F₅)₂PCH₂CH₂P(C₂F₅)₂) versus CpMn(PPh₃)₂(CO)) [178], $\Delta E_{\text{ox}} = +1.3$ V (Cp^{*}Ru(dfepe)Cl versus Cp^{*}Ru(depe)Cl) [179], and +0.9 V ((η^6 -arene)Mo(dfepe)(CO) versus (η^6 -arene)Mo(dppe)(CO)) [180]. The very large electron-withdrawing inductive effect of perfluoroalkyl groups on phosphine ligands is broadly established by electrochemical data across a range of metal systems.

Zargarian has recently presented $E_{1/2}$ (Ni(II)/Ni(III)) data for analogous PCP and POCOP complexes, as well as a related hydrocarbyl-bridged pincer compound: [(^tBu₂PCH₂CH₂)CH]NiBr (−0.01 V), (^{iPr}PCP)NiBr (+0.34 V), (^{iPr}POCOP)NiBr (+0.64 V), and (3,5-Cl₂-^{iPr}POCOP)NiBr (+0.75 V) (Fig. 10) [181, 182]. The increase of 330 mV in oxidation potential between the hydrocarbyl- and aryl-bridged pincer complexes is consistent with the greater electron-donating ability of the C(sp³) relative to C(sp²). The 300 mV difference between corresponding PCP and POCOP complexes is the only literature example thus far of the greater electron-withdrawing effect of the POCOP ligand. Interestingly, the addition of two meta Cl substituents to (^{iPr}POCOP)NiBr results in only a 110 mV increase in oxidation potential, significantly less than the 280 mV reduction in oxidation potential induced by the presence of a single MeO para group in (MeO-^tBuPCP)Ir(H)Cl (see above).

Van Koten's 2005 comparison of (^RPCP)Ru(Ph₃P)Cl (R = C₆H₅, C₆F₅) complexes confirmed both structural and electronic effects imparted by aryl

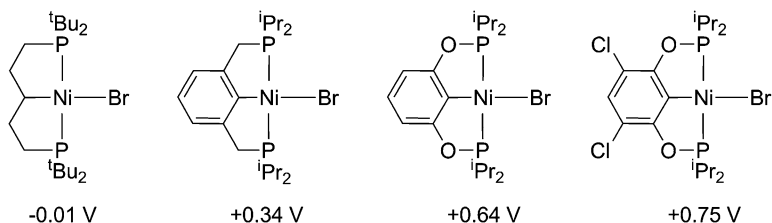


Fig. 10 Comparison of nickel pincer redox potentials

fluorination [159]. Both of these systems exhibit reversible Ru(II)/Ru(III) redox couples ($R = C_6H_5$ (-0.01 V), C_6F_5 ($+0.39$ V)). The coordination geometries of these 5-coordinate, roughly square pyramidal, systems differ significantly (see earlier), with a large α distortion for $(C_6F_5PCP)Ru(Ph_3P)Cl$ that results in apical C (aryl) coordination rather than apical Ph_3P coordination. Owing to structural and frontier orbital changes [183], it is not obvious how much of the 400 mV increase in oxidation potential upon fluorination is simply due to the significantly lower donating ability of C_6F_5PCP relative to $PhPCP$.

A single electrochemical study for a PNP pincer system has been reported by Milstein: $(tBuPNP)RhCl$ and $(tBuPNP)Rh(acetone)^+$ exhibit reversible Rh(I)/Rh(II) couples at -0.30 V and -0.28 V, respectively [150]. Van Koten has recently examined the oxidation potentials of $(iPr^tECE)PdCl$ ($E = S, P$) and their bimetallic $\eta^6-(C_5R_5)Ru^+$ adducts $[\eta^6-(C_5R_5)Ru^+ - iPr^tECE]PdCl$, and observed irreversible anodic waves which are ~ 400 mV ($E = S$) and ~ 600 mV ($E = P$) higher for the ruthenium-modified pincer systems, indicating a significant electronic effect for this mode of pincer ligand modification [20].

4.3 Reactivity and Coordination Affinity Trends

Considerable caution must be exercised when attributing differences in complex reactivity and/or structure specifically to ligand electronic influence. Nevertheless, there are a number of studies comparing the coordination behavior of different pincer complex types that are informative. Enhanced substrate binding to more electrophilic pincer metal centers is invoked in several studies. In catalytic alkane dehydrogenation chemistry, DFT calculations on the effect of *p*-MeO ring substitution (increased aryl π -donor ability) and POCOP versus PCP (increased ring π -donation as well as decreased PR_2 donor ability) predict lower kinetic barriers to C–H bond addition, in accord with higher observed catalytic activities [176]. The preference for (POCOP)Ir(I) adducts relative to (PCP)Ir(III) OA products has been noted [184]. NH_3 coordination to $(tBuPCP)Ir(I)$ is favored versus oxidative addition to more electron-rich aliphatic-bridged phosphine iridium pincers [185, 186]. Ligand competition between $(R^tPCP)Pd(L)^+$ ($R = Ph, C_6F_5$; $L = MeCN$ or py)

Table 4 Calculated CO bond dissociation free energies for (^RPCP)Ir(CO)₂

Pincer ligand	$\nu(\text{CO})$ (exp), cm^{-1}	P–Ir–P, deg	C (Ar)–Ir–CO _{ax}	OC–Ir–CO, deg	$\Delta G_{\text{diss}}(\text{Ir–CO})$, kcal mol^{-1}
^t BuPOCOP	1,938, 1,982	143.0	162.0	105.9	–6.2
^t BuPCP	1,906, 1,943	147.5	158.7	106.1	–1.2
ⁱ PrPCP	1,920, 1,971	134.2	165.7	102.5	7.6
^{C6F5} PCP	1,976, 2,038	125.9	170.5	99.5	8.6
^{Me} PCP	1,925, 1,986	126.2	167.9	100.8	9.1
^H PCP	1,950, 2,015	121.5	171.7	98.4	9.7
^{pyr} PCP	1,978, 2,036	128.2	169.5	99.7	11.6
^{CF3} PCP	2,005, 2,062 (2,020, 2,068)	128.5	173.0	97.4	13.2
^F PCP	2,016, 2,072	129.7	171.0	98.6	15.1

Geometry optimization and frequency DFT calculations as described for Fig. 6. ΔG_{diss} values were calculated from ΔG_{calc}^0 for (^RPCP)Ir(CO)₂, (^RPCP)Ir(CO), and free CO using the Gaussian 09 IEFPCM solvation model with CH₂Cl₂ as solvent

revealed a modest preference of the more electrophilic complex (^{C6F5}PCP)Pd(L)⁺ for the stronger base pyridine [53].

We have noted in our studies of Ir(III) and Ru(II) ^{CF3}PCP coordination chemistry a general preference for metal coordinative saturation: 18-electron (^{CF3}PCP)Ir(H)(L)X and (^{CF3}PCP)Ru(L)₂X compounds are isolated rather than 16-electron (^RPCP)Ir(H)X and (^RPCP)Ru(L)X compounds that are typical for donor PCP systems [59, 137, 187]. More significant are the 5-coordinate d⁸ 18-electron compounds (^RPCP)M(L)₂ (R = pyr or CF₃). DFT calculations by Milstein for (^{pyr}PCP)Rh(CO)₂ gave a CO dissociation energy of 3.3 kcal mol^{–1} complexes; the dicarbonyl adduct was not directly observed [132]. The favorable binding of a second CO ligand to the square planar (^{pyr}PCP)Rh(CO) center was rationalized by DFT calculations, which show a lowering of d orbital energies (increased electrophilicity) and stabilization of the bent “see-saw” 4-coordinate rhodium moiety induced by the phosphine pyrrolyl groups. On the basis of dynamic NMR data, we have estimated a CO dissociation energy for (^{CF3}PCP)Ir(CO)₂ of 9.7 kcal mol^{–1} [137].

We have carried out DFT calculations on the energetics of CO dissociation for a range of (^RPCP)Ir(CO)₂ systems, the results of which are summarized in Table 4. The negative $\Delta G_{\text{diss}}(\text{Ir–CO})$ values for (^tBuPOCOP)Ir(CO)₂ (–6.2 kcal mol^{–1}) and (^tBuPCP)Ir(CO)₂ (–1.2 kcal mol^{–1}) predict that association of CO to the corresponding monocarbonyls will not occur. Optimized geometries for these systems have larger P–Ir–P bond angles (>140°) as well as larger OC–Ir–CO and smaller C(Ar)–Ir–CO angles than other pincer analogues without *tert*-butyl phosphine groups. These distortions produce less stable structures and avoid unfavorable *tert*-butyl close contacts. $\Delta G_{\text{diss}}(\text{Ir–CO})$ for (^{Me}PCP)Ir(CO)₂, +9.1 kcal mol^{–1}, is 10–15 kcal mol^{–1} more favorable and reflects the energy cost of bending *tert*-butyl substituted pincers an additional 20° to achieve a more optimal 5-coordinate geometry. $\Delta G_{\text{diss}}(\text{Ir–CO})$ values for (^RPCP)Ir(CO)₂ (R = H, Me, ⁱPr, C₆F₅) are similar, 8–10 kcal mol^{–1}, and the more electrophilic pincers with R = pyr, CF₃, F have higher dissociation energies which track increasing $\nu(\text{CO})$ values. The calculated

dissociation value for (CF_3 PCP)Ir(CO) $_2$, 13.2 kcal mol $^{-1}$, is consistent with the 9.7 kcal mol $^{-1}$ experimental value obtained from dynamic NMR data. $\Delta G_{\text{diss}}(\text{Ir-CO})$ for (C_6F_5 PCP)Ir(CO) $_2$ is slightly less than predicted and probably reflects some steric destabilization. Once again, the general picture is that pincer electronic effects are significant, but any process which involves non-meridional pincer bending is dominated by steric destabilization in tBu-substituted pincer systems.

5 Summary

The development of terdentate phosphine pincer ligands has accelerated greatly over the past decade. Much of the expansion of this ligand class (variations in aryl backbone substitution and PR $_2$ substituents) has been motivated by catalytic applications, particularly in the area of palladium-mediated coupling reactions. Unfortunately any correlation of catalytic activity with ligand parameters is complicated by the complexities inherent in multistep catalyst pathways, so in most cases the information gained is largely empirical and does not address basic questions of pincer ligand coordination chemistry. Nevertheless, we now have a large “arsenal” of formally anionic (PECEP) and neutral (PENEP) phosphine pincers at our disposal with CH $_2$, NR, and O-tethered PR $_2$ groups. Donor alkyl R phosphine substituents range in size from R = Me to R = admantyl, but it is notable that, in contrast to the rich chemistry of ^{Me}NCN , very little experimental research has focused on methyl-substituted phosphine pincers [25]. Aryl-substituted pincers with varying ring substitution (Me, CF $_3$, etc.) are available. OR and NR $_2$ -substituted phosphine pincers, including chiral derivatives, are likewise easily prepared. In recent years, POCOP pincer applications have overtaken PCP systems owing to their ease of synthesis and ligand variation. The class of strong acceptor phosphines remains quite small; only van Koten’s C_6F_5 PCP, Milstein’s pyr PCP, and our own R_f PCP (R $_f$ = CF $_3$, C $_2$ F $_5$) pincer systems have been examined to any extent. These acceptor pincer systems are intriguing due to the enforced *trans* disposition of acceptor groups, a coordination geometry that is relatively uncommon (Fig. 11).

A common paradigm driving much pincer research has been the stabilization and enforcement of meridional coordination preferences. As noted previously, the great majority of pincer coordination chemistry has focused on $^t\text{Bu}_2\text{P}$ systems. It is evident from some prior studies and the plots in Figs. 6 and 8 that there is a significant energy cost to access non-meridional ^tBu PEEEP products or intermediates. In cases where associative reactions with 4-coordinate pincer complexes are desirable, we conclude that the incorporation of at least one smaller phosphine pincer group is an essential requirement.



Fig. 11 Acceptor versus donor pincer ligands

References

1. Choi J, MacArthur AHR, Brookhart M, Goldman AS (2011) *Chem Rev* 111:1761
2. Albrecht M, van Koten G (2001) *Angew Chem Int Ed* 40:3750
3. Singleton JT (2003) *Tetrahedron* 59:1837
4. van der Boom ME, Milstein D (2003) *Chem Rev* 103:1759
5. Morales-Morales DJ, Craig M (2007) *The Chemistry of Pincer Compounds*. Elsevier, Amsterdam
6. Benito-Garagorri D, Kirchner K (2008) *Acc Chem Res* 41:201
7. Morales-Morales D (2008) *Mini-Rev Org Chem* 5:141
8. Albrecht M, Morales-Morales D, in (2009) *Iridium Complexes in Organic Synthesis*. Chp. 12, Wiley-VCH, p 299
9. Morales-Morales D, in (2009) *Iridium Complexes in Organic Synthesis*. Chp. 13, Wiley-VCH, p 325
10. Serrano-Becerra JM, Morales-Morales D (2009) *Curr Org Synth* 6:169
11. Leis W, Mayer HA, Kaska WC (2008) *Coord Chem Rev* 252:1787
12. Gerisch M, Krumper JR, Bergman RG, Tilley TD (2001) *J Am Chem Soc* 123:5818
13. van Koten G, Grove DM, Van der Zeijden AAH (1989) *NATO ASI Ser Ser C* 257:477
14. Suijkerbuijk BMJM, Schamhart DJ, Kooijman H, Spek AL, van Koten G, Klein GRJM (2010) *Dalton Trans* 39:6198
15. Suijkerbuijk BMJM, Tooke DM, Lutz M, Spek AL, Jenneskens LW, van Koten G, Klein GRJM (2010) *J Org Chem* 75:1534
16. Grove DM, Verschuuren AHM, van Koten G, van Beek JAMJ (1989) *J Organomet Chem* 372:C1
17. Schimmelpfennig U, Zimmering R, Schleinitz KD, Stößer R, Wenschuh E, Baumeister U, Hartung H (1993) *Zeitschrift für Anorganische und Allgemeine Chemie* 619:1931
18. van Beek JAM, van Koten G, Ramp MJ, Coenjaarts NC, Grove DM, Goubitz K, Zoutberg MC, Stam CH, Smeets WJJ, Spek AL (1991) *Inorg Chem* 30:3059
19. van de Kuil LA, Grove DM, Gossage RA, Zwickler JW, Jenneskens LW, Drenth W, van Koten G (1997) *Organometallics* 16:4985
20. Bonnet S, Lutz M, Spek AL, van Koten G, Klein GRJM (2010) *Organometallics* 29:1157
21. Mehendale NC, Bezemer C, van Walree CA, Klein GRJM, van Koten GJ (2006) *Mol Catal A Chem* 257:167
22. Mehendale NC, Sietsma JRA, de Jong KP, van Walree CA, Gebbink RJMK, van Koten G (2007) *Adv Synth Catal* 349:2619
23. Moulton CJ, Shaw BL (1976) *J Chem Soc Dalton Trans* 1020
24. Bennett MA, Jin H, Willis AC (1993) *J Organomet Chem* 451:249
25. Creaser CS, Kaska WC (1978) *Inorg Chim Acta* 30:L325
26. Lu Q, Chen M, Chaloupka S, Venanzi LM (1998) *Wuji Huaxue Xuebao* 14:449
27. Frech Christian M, Ben-David Y, Weiner L, Milstein D (2006) *J Am Chem Soc* 128:7128
28. Rybtchinski B, Ben-David Y, Milstein D (1997) *Organometallics* 16:3786
29. Hollink E, Stewart JC, Wei P, Stephan DW (2003) *Dalton Trans* 3968
30. Kennedy AR, Cross RJ, Muir KW (1995) *Inorg Chim Acta* 231:195
31. Punji B, Emge TJ, Goldman AS (2010) *Organometallics* 29:2702

32. Kundu S, Choliy Y, Zhuo G, Ahuja R, Emge TJ, Warmuth R, Brookhart M, Krogh-Jespersen K, Goldman AS (2009) *Organometallics* 28:5432
33. Medici S, Gagliardo M, Williams SB, Chase PA, Gladiali S, Lutz M, Spek AL, van Klink GPM, van Koten G (2005) *Helv Chim Acta* 88:694
34. Morales-Morales D, Cramer RE, Jensen CM (2002) *J Organomet Chem* 654:44
35. Williams BS, Dani P, Lutz M, Spek AL, van Koten G (2001) *Helv Chim Acta* 84:3519
36. Longmire JM, Zhang X, Shang M (1998) *Organometallics* 17:4374
37. Gorla F, Venanzi LM, Albinati A (1994) *Organometallics* 13:43
38. Gorla F, Togni A, Venanzi LM, Albinati A, Lianza F (1994) *Organometallics* 13:1607
39. Kozhanov KA, Bubnov MP, Cherkasov VK, Vavilina NN, Efremova LY, Artyushin OI, Odinets IL, Abakumov GA (2008) *Dalton Trans* 2849
40. Watson WH, Poola B, Liu J, Richmond MG (2007) *J Chem Crystallogr* 37:349
41. Krogh-Jespersen K, Czerw M, Zhu K, Singh B, Kanzelberger M, Darji N, Achord PD, Renkema KB, Goldman ASJ (2002) *Am Chem Soc* 124:10797
42. Huang Z, Brookhart M, Goldman AS, Kundu S, Ray A, Scott SL, Vicente BC (2009) *Adv Synth Catal* 351:188
43. Grimm JC, Nachtigal C, Mack HG, Kaska WC, Mayer HA (2000) *Inorg Chem Commun* 3:511
44. Mohammad HAY, Grimm JC, Eichele K, Mack H-G, Speiser B, Novak F, Quintanilla MG, Kaska WC, Mayer HA (2002) *Organometallics* 21:5775
45. Karlen T, Dani P, Grove DM, Steenwinkel P, van Koten G (1996) *Organometallics* 15:5687
46. Dani P, Karlen T, Gossage RA, Smeets WJJ, Spek AL, van Koten G (1997) *J Am Chem Soc* 119:11317
47. Beletskaya IP, Chuchurjukin AV, Dijkstra HP, van Klink GPM, van Koten G (2000) *Tetrahedron Lett* 41:1081
48. Beletskaya IP, Chuchurjukin AV, Dijkstra HP, van Klink GPM, van Koten G (2000) *Tetrahedron Lett* 41:1075
49. Dani P, Richter B, van Klink GPM, van Koten G (2001) *Eur J Inorg Chem* 125
50. Sommer WJ, Yu K, Sears JS, Ji Y, Zheng X, Davis RJ, Sherrill CD, Jones CW, Weck M (2005) *Organometallics* 24:4351
51. Ashkenazi N, Vigalok A, Parthiban S, Ben-David Y, Shimon LJW, Martin JML, Milstein D (2000) *J Am Chem Soc* 122:8797
52. Kossoy E, Iron Mark A, Rytchinski B, Ben-David Y, Shimon Linda JW, Konstantinovsk L, Martin Jan ML, Milstein D (2005) *Chem Eur J* 11:2319
53. Chase PA, Gagliardo M, Lutz M, Spek AL, van Klink GPM, van Koten G (2005) *Organometallics* 24:2016
54. Gagliardo M, Chase PA, Brouwer S, van Klink GPM, van Koten G (2007) *Organometallics* 26:2219
55. Adams JJ, Lau A, Arulsamy N, Roddick DM (2007) *Inorg Chem* 46:11328
56. Taylor SD, Dinaut AN, Thadani AN, Huang Z (1996) *Tetrahedron Lett* 37:8089
57. Taylor SD, Kotoris CC, Dinaut AN, Chen M-J (1998) *Tetrahedron* 54:1691
58. Caplan NA, Pogson CI, Hayes DJ, Blackburn GM (2000) *Perkin* 1:421
59. Adams JJ, Lau A, Arulsamy N, Roddick DM (2011) *Organometallics* 30:689
60. Vigalok A, Uzan O, Shimon LJW, Ben-David Y, Martin JML, Milstein D (1998) *J Am Chem Soc* 120:12539
61. Gusev DG, Madott M, Dolgushin FM, Lyssenko KA, Antipin MY (2000) *Organometallics* 19:1734
62. Kozhanov KA, Bubnov MP, Cherkasov VK, Fukin GK, Abakumov GA (2004) *Dalton Trans* 2957
63. Benito-Garagorri D, Bococik V, Mereiter K, Kirchner K (2006) *Organometallics* 25:3817
64. Wallner OA, Olsson VJ, Eriksson L, Szabo KJ (2006) *Inorg Chim Acta* 359:1767
65. Li J, Lutz M, Spek AL, van Klink GPM, van Koten G, Klein GRJM (2010) *Organometallics* 29:1379

66. Niu J-L, Chen Q-T, Hao X-Q, Zhao Q-X, Gong J-F, Song M-P (2010) *Organometallics* 29:2148
67. Gozin M, Weisman A, Ben-David Y, Milstein D (1993) *Nature* 364:699
68. van der Boom ME, Kraatz H-B, Ben-David Y, Milstein D (1996) *Chem Commun* 2167
69. van der Boom ME, Kraatz H-B, Hassner L, Ben-David Y, Milstein D (1999) *Organometallics* 18:3873
70. Gauvin RM, Rozenberg H, Shimon LJW, Milstein D (2001) *Organometallics* 20:1719
71. van der Boom ME, Liou S-Y, Shimon LJW, Ben-David Y, Milstein D (2004) *Inorg Chim Acta* 357:4015
72. Salem H, Ben-David Y, Shimon LJW, Milstein D (2006) *Organometallics* 25:2292
73. Goettker-Schnetmann I, White P, Brookhart M (2004) *J Am Chem Soc* 126:1804
74. Morales-Morales D, Grause C, Kasaoka K, Redon R, Cramer RE, Jensen CM (2000) *Inorg Chim Acta* 300–302:958
75. Bedford RB, Draper SM, Noelle SP, Welch SL (2000) *New J Chem* 24:745
76. Gomez-Benitez V, Baldovino-Pantaleon O, Herrera-Alvarez C, Toscano RA, Morales-Morales D (2006) *Tetrahedron Lett* 47:5059
77. Ceron-Camacho R, Gomez-Benitez V, Le LR, Morales-Morales D, Toscano RAJ (2006) *Mol Catal A Chem* 247:124
78. Wallner OA, Szabo KJ (2004) *Org Lett* 6:1829
79. Hunks WJ, Jennings MC, Puddephatt RJ (2000) *Inorg Chem* 39:2699
80. Huang Z, White PS, Brookhart M (2010) *Nature* 465:598
81. Li J, Lutz M, Spek AL, van Klink GPM, van Koten G, Klein GRJM (2010) *J Organomet Chem* 695:2618
82. Feng J-J, Chen X-F, Shi M, Duan W-L (2010) *J Am Chem Soc* 132:5562
83. Aydin J, Ryden A, Szabo KJ (2008) *Tetrahedron-Asymmetry* 19:1867
84. Aydin J, Conrad CS, Szabo KJ (2008) *Org Lett* 10:5175
85. Rubio M, Suarez A, del RD, Galindo A, Alvarez E, Pizzano A (2007) *Dalton Trans* 407
86. Aydin J, Kumar KS, Sayah MJ, Wallner OA, Szabo KJ (2007) *J Org Chem* 72:4689
87. Ini S, Oliver AG, Tilley TD, Bergman RG (2001) *Organometallics* 20:3839
88. Baber RA, Bedford RB, Betham M, Blake ME, Coles SJ, Haddow MF, Hursthouse MB, Orpen AG, Pilarski LT, Pringle PG, Wingard RL (2006) *Chem Commun* 3880
89. Balakrishna MS, Kumar P, Punji B, Mague JTJ (2010) *Organomet Chem* 695:981
90. Sokolov VI, Bulygina LA (2004) *Russ Chem Bull* 53:2355
91. Miyazaki F, Yamaguchi K, Shibasaki M (1999) *Tetrahedron Lett* 40:7379
92. Nifanteyev EE, Rasadkina EN, Vasyanina LK, Belsky VK, Stash AIJ (1997) *Organomet Chem* 529:171
93. Bolliger JL, Blacque O, Frech CM (2007) *Angew Chem Int Ed* 46:6514
94. Bedford RB, Betham M, Charmant JPH, Haddow MF, Orpen AG, Pilarski LT, Coles SJ, Hursthouse MB (2007) *Organometallics* 26:6346
95. Bell GA, Rankin DWH, Reinisch PFJ (1987) *Chem Soc Dalton Trans* 3023
96. Ozerov OV, Guo C, Foxman BMJ (2006) *Organomet Chem* 691:4802
97. Frech CM, Shimon LJW, Milstein D (2005) *Angew Chem Int Ed* 44:1709
98. Bolliger JL, Frech CM (2009) *Adv Synth Catal* 351:891
99. Nelson SM, Dahlhoff WV (1971) *J Chem Soc A* 2184
100. Muller G, Klinga M, Leskela M, Rieger BZ (2002) *Anorg Allg Chem* 628:2839
101. Hermann D, Gandelman M, Rozenberg H, Shimon LJW, Milstein D (2002) *Organometallics* 21:812
102. Pelczar EM, Emge TJ, Krogh-Jespersen K, Goldman AS (2008) *Organometallics* 27:5759
103. Jansen A, Pitter S (1999) *Monatsh Chem* 130:783
104. Kawatsura M, Hartwig JF (2001) *Organometallics* 20:1960
105. Yano T, Moroe Y, Yamashita M, Nozaki K (2008) *Chem Lett* 37:1300
106. Zhang J, Leitus G, Ben-David Y, Milstein D (2005) *J Am Chem Soc* 127:10840
107. Ben-Ari E, Leitus G, Shimon LJW, Milstein D (2006) *J Am Chem Soc* 128:15390

108. Zhang J, Leitus G, Ben-David Y, Milstein D (2006) *Angew Chem Int Ed* 45:1113
109. Bernskoetter WH, Hanson SK, Buzak SK, Davis Z, White PS, Swartz R, Goldberg KI, Brookhart M (2009) *J Am Chem Soc* 131:8603
110. Bernskoetter WH, Schauer CK, Goldberg KI, Brookhart M (2009) *Science* 326:553
111. Salem H, Shimon LJW, Diskin-Posner Y, Leitus G, Ben-David Y, Milstein D (2009) *Organometallics* 28:4791
112. Schirmer W, Floerke U, Haupt HJZ (1987) *Anorg Allg Chem* 545:83
113. Benito-Garagorri D, Wiedermann J, Pollak M, Mereiter K, Kirchner K (2007) *Organometallics* 26:217
114. Tolman CA (1977) *Chem Rev* 77:313
115. Brown TL, Lee KJ (1993) *Coord Chem Rev* 128:89
116. Bunten KA, Chen L, Fernandez AL, Poe AJ (2002) *Coord Chem Rev* 233–234:41
117. Dunne BJ, Morris RB, Orpen AG (1991) *J Chem Soc Dalton Trans* 653
118. Brown TL (1992) *Inorg Chem* 31:1286
119. White D, Coville NJ (1994) *Adv Organomet Chem* 36:95
120. Albert P, Biagio C, Andrea C, Simona G, Francesco R, Vittorio S, Luigi C (2009) *Eur J Inorg Chem* 2009:1759
121. Clavier H, Nolan SP (2010) *Chem Commun* 46:841
122. Poverenov E, Leitus G, Shimon LJW, Milstein D (2005) *Organometallics* 24:5937
123. Frech CM, Shimon LJW, Milstein D (2009) *Organometallics* 28:1900
124. Kimmich BFM, Marshall WJ, Fagan PJ, Hauptman E, Bullock RM (2002) *Inorg Chim Acta* 330:52
125. Kanzelberger M, Zhang X, Emge TJ, Goldman AS, Zhao J, Incarvito C, Hartwig JF (2003) *J Am Chem Soc* 125:13644
126. van der Boom ME, Iron MA, Atasoylu O, Shimon LJW, Rozenberg H, Ben-David Y, Konstantinovskii L, Martin JML, Milstein D (2004) *Inorg Chim Acta* 357:1854
127. Ghosh R, Emge TJ, Krogh-Jespersen K, Goldman AS (2008) *J Am Chem Soc* 130:11317
128. Steffey BD, Miedaner A, Maciejewski-Farmer ML, Bernatis PR, Herring AM, Allured VS, Carperos V, DuBois DL (1994) *Organometallics* 13:4844
129. Gagliardo M, Dijkstra HP, Coppo P, De CL, Lutz M, Spek AL, van Klink GPM, van Koten G (2004) *Organometallics* 23:5833
130. Cross RJ, Kennedy AR, Muir KWJ (1995) *J Organomet Chem* 487:227
131. Kennedy AR, Cross RJ, Muir KW (1995) *Inorg Chim Acta* 231:207
132. Kossoy E, Iron MA, Rybtchinski B, Ben-David Y, Shimon LJW, Konstantinovskii L, Martin JML, Milstein D (2005) *Chem Eur J* 11:2319
133. Kossoy E, Rybtchinski B, Diskin-Posner Y, Shimon LJW, Leitus G, Milstein D (2009) *Organometallics* 28:523
134. Bergbreiter DE, Frels JD, Rawson J, Li J, Reibenspies JH (2006) *Inorg Chim Acta* 359:1912
135. Tuba RT, Verona, Dinh Long V, Hampel Frank, Gladysz John A (2005) *J Chem Soc Dalton Trans* 2275
136. Naghipour A, Sabounchei SJ, Morales-Morales D, Hernandez-Ortega S, Jensen CM (2004) *J Organomet Chem* 689:2494
137. Adams JJ, Arulsamy N, Roddick DM (2011) *Organometallics* 30:697
138. Liou S-Y, Gozin M, Milstein D (1995) *J Am Chem Soc* 117:9774
139. Kuklin SA, Sheloumov AM, Dolgushin FM, Ezernitskaya MG, Peregudov AS, Petrovskii PV, Koridze AA (2006) *Organometallics* 25:5466
140. Cartwright SA, White P, Brookhart M (2006) *Organometallics* 25:1664
141. Polezhaev AV, Kuklin SA, Ivanov DM, Petrovskii PV, Dolgushin FM, Ezernitskaya MG, Koridze AA (2009) *Russ Chem Bull* 58:1847
142. Kimura T, Uozumi Y (2006) *Organometallics* 25:4883
143. Rubio M, Suarez A, Del RD, Galindo A, Alvarez E, Pizzano A (2009) *Organometallics* 28:547
144. Lang H-F, Fanwick PE, Walton RA (2002) *Inorg Chim Acta* 329:1

145. Katayama H, Wada C, Taniguchi K, Ozawa F (2002) *Organometallics* 21:3285
146. Melaimi M, Thouzamet C, Ricard L, Floch PLJ (2004) *Organomet Chem* 689:2988
147. Wiedermann J, Benito-Garagorri D, Kirchner K, Mereiter K (2006) *Acta Crystallogr Sect E Struct Rep Online* E62:m1106
148. Benito-Garagorri D, Becker E, Wiedermann J, Lackner W, Pollak M, Mereiter K, Kisala J, Kirchner K (2006) *Organometallics* 25:1900
149. Gaviglio C, Ben-David Y, Shimon LJW, Doctorovich F, Milstein D (2009) *Organometallics* 28:1917
150. Feller M, Ben-Ari E, Gupta T, Shimon LJW, Leitus G, Diskin-Posner Y, Weiner L, Milstein D (2007) *Inorg Chem* 46:10479
151. Feller M, Iron MA, Shimon LJW, Diskin-Posner Y, Leitus G, Milstein D (2008) *J Am Chem Soc* 130:14374
152. Salem H, Shimon LJW, Leitus G, Weiner L, Milstein D (2008) *Organometallics* 27:2293
153. Sykes AC, White P, Brookhart M (2006) *Organometallics* 25:1664
154. Ben-Ari E, Gandelman M, Rozenberg H, Shimon LJW, Milstein D (2003) *J Am Chem Soc* 125:4714
155. Ben-Ari E, Cohen R, Gandelman M, Shimon LJW, Martin JML, Milstein D (2006) *Organometallics* 25:3190
156. Ghosh R, Zhang X, Achord P, Emge TJ, Krogh-Jespersen K, Goldman AS (2007) *J Am Chem Soc* 129:853
157. Gusev DG, Dolgushin FM, Antipin MY (2001) *Organometallics* 20:1001
158. Amoroso D, Jabri A, Yap GPA, Gusev DG, dos Santos EN, Fogg DE (2004) *Organometallics* 23:4047
159. Gagliardo M, Chase PA, Lutz M, Spek AL, Hartl F, Havenith RWA, van Klink GPM, van Koten G (2005) *Organometallics* 24:4553
160. Wen TB, Cheung YK, Yao J, Wong W-T, Zhou ZY, Jia G (2000) *Organometallics* 19:3803
161. Zhang J, Gandelman M, Herrman D, Leitus G, Shimon LJW, Ben-David Y, Milstein D (2006) *Inorg Chim Acta* 359:1955
162. Benito-Garagorri D, Puchberger M, Mereiter K, Kirchner K (2008) *Angew Chem Int Ed* 47:9142
163. Trovitch RJ, Lobkovsky E, Chirik PJ (2006) *Inorg Chem* 45:7252
164. Lian Zhe, Xu G, Li Xiaoyan (2010) *Acta Crystallogr Sect E Struct Rep Online* 66:m636
165. Wen TB, Zhou ZY, Jia G (2006) *Angew Chem Int Ed* 45:5842
166. Liu F, Goldman AS (1999) *Chem Commun* 655
167. Huang K-W, Grills DC, Han JH, Szalda DJ, Fujita E (2008) *Inorg Chim Acta* 361:3327
168. Figgien D, Peterson KA, Dolg M, Stoll H (2009) *J Chem Phys* 130:164108/1
169. Gerber R, Fox T, Frech CM (2010) *Chem Eur J* 16:6771
170. Bolliger JL, Blacque O, Frech CM (2008) *Chem Eur J* 14:7969
171. Vuzman D, Poverenov E, Diskin-Posner Y, Leitus G, Shimon LJW, Milstein D (2007) *Dalton Trans* 5692
172. Goettker-Schnetmann I, White PS, Brookhart M (2004) *Organometallics* 23:1766
173. Kloek SM, Heinekey DM, Goldberg KI (2006) *Organometallics* 25:3007
174. Hansch C, Leo A, Taft RW (1991) *Chem Rev* 91:165
175. Perrin L, Clot E, Eisenstein O, Loch J, Crabtree RH (2001) *Inorg Chem* 40:5806
176. Zhu K, Achord PD, Zhang X, Krogh-Jespersen K, Goldman AS (2004) *J Am Chem Soc* 126:13044
177. Novak F, Speiser B, Mohammad HAY, Mayer HA (2004) *Electrochim Acta* 49:3841
178. Merwin RK, Ontko AC, Houllis JF, Roddick DM (2004) *Polyhedron* 23:2873
179. Ontko AC, Houllis JF, Schnabel RC, Roddick DM, Fong TP, Lough AJ, Morris RH (1998) *Organometallics* 17:5467
180. Ernst MF, Roddick DM (1990) *Organometallics* 9:1586
181. Castonguay A, Beauchamp AL, Zargarian D (2008) *Organometallics* 27:5723

182. Castonguay A, Spasyuk DM, Madern N, Beauchamp AL, Zargarian D (2009) *Organometallics* 28:2134
183. Gagliardo M, Havenith RWA, van Klink G, van Koten GJ (2006) *Organomet Chem* 691:4411
184. Goettker-Schnetmann I, Brookhart M (2004) *J Am Chem Soc* 126:9330
185. Zhao J, Goldman AS, Hartwig JF (2005) *Science* 307:1080
186. Bursten BE, Chen S, Chisholm MH (2008) *J Organomet Chem* 693:1547
187. Gruver BC, Adams JJ, Warner SJ, Arulsamy N, Roddick DM (2011) *Organometallics* 30:5133

Metal Complexes of Pincer Ligands: Excited States, Photochemistry, and Luminescence

Gemma R. Freeman and J.A. Gareth Williams

Abstract Pincer ligands of the form ECE that incorporate *N*-heterocyclic lateral units, E, are terdentate analogues of NC-cyclometallating ligands such as 2-phenylpyridine. They are able to form a variety of highly luminescent complexes with platinum(II) and iridium(III). They can also be thought of as cyclometallating analogues of the NNN-coordinating ligand terpyridine. The introduction of the carbon atom can impart significant changes on the nature and energy of the electronic excited states, as is evident for complexes of ruthenium(II), where a shift in the absorption to low energy in the metallated systems has sparked interest in applications for dye-sensitised solar cells. Investigations in these areas over the past decade are reviewed. We also consider related complexes in which the lateral coordinating units are aliphatic N donors, phosphines, or sulphur ligands. The lack of good π -accepting units in such compounds tends to lead to weaker ligand fields and hence to low-energy metal-centred states. These states dictate much of the excited-state chemistry and compromise the efficiency of luminescence at room temperature.

Keywords Cyclometallated complex · Electroluminescence · Imaging · Iridium · OLED · Phosphorescence · Platinum · Ruthenium · Sensing

Contents

1	Introduction	90
2	Complexes of SCS Ligands	92
3	Complexes of PCP Ligands	97

4	Complexes of NCN Ligands with Non-aromatic Amines	100
5	Complexes of NCN Ligands with Aromatic Amines	107
5.1	Ruthenium(II) and Osmium(II) Complexes	108
5.2	Iridium(III) Complexes	111
5.3	Platinum(II) Complexes	117
	References	126

1 Introduction

Whilst most research on pincer ligand complexes is concerned with molecules in their ground electronic state, there is increasing interest in the excited electronic states of such molecules, formed through either absorption of light or application of an electric field. Much of this interest stems from the light-emitting properties of certain types of cyclometallated complexes of the second and third row transition elements. Research in the 1980s and 1990s on compounds incorporating NC-coordinated 2-phenylpyridine (ppy) (Fig. 1) and related ligands, with metals such as ruthenium(II), iridium(III), and platinum(II), revealed that the synergistic combination of a strongly σ -donating metallated carbon atom and a π -accepting pyridine ring can lead to low-energy metal-to-ligand charge-transfer (MLCT) states [1–3]. Following absorption of light to singlet MLCT states, the strong spin-orbit coupling (SOC) associated with the heavy metal ion typically promotes very fast intersystem crossing (ISC) to the corresponding triplet state [4]. The subsequent emission of light—formally a spin-forbidden $T_1 \rightarrow S_0$ process known as phosphorescence—is facilitated by the SOC effect [5]. As a result, phosphorescence can sometimes be observed from such complexes under ambient conditions in solution. This contrasts with purely organic molecules, where the rate of the $T_1 \rightarrow S_0$ process is so slow that it cannot compete with non-radiative decay processes in which the electronic excited state is transferred into vibrational modes and finally dissipated into the solvent. Phosphorescence of conjugated organic molecules is rarely visible at room temperature!

The ability of such complexes to emit from triplet states, sometimes with very high efficiency, has led to vast interest over the past decade as “triplet-harvesting phosphors” in organic light-emitting devices (OLEDs) [6]. In an OLED, the application of electric fields to a thin layer of a conjugated material leads to the formation of both singlet and triplet states. Spin statistics lead to an excess of triplet states over singlets, but the triplet states for a purely organic material do not emit at room temperature, compromising device efficiency. By incorporating triplet harvesting agents, emission from the triplet states can be induced and device efficiency increased [7].

Another area in which the luminescence of metal complexes is attracting interest is that of sensing and bioimaging [8, 9]. Fluorescence is widely used in analytical science and in the biosciences, owing to the exquisite sensitivity with which light can be detected, coupled with the high spatial resolution that is possible using optical microscopes, especially confocal systems. The use of phosphorescent metal

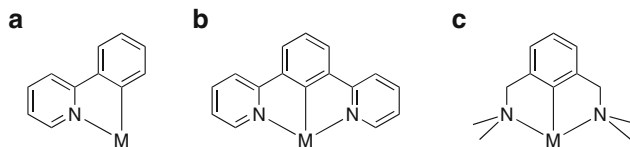


Fig. 1 Generic structure of an NC-cyclometallating ligand (exemplified by 2-phenylpyridine) coordinated to a metal ion (a); the corresponding NCN pincer coordination offered by a ligand such as dipyridylbenzene (b); NCN coordination to a ligand with saturated aliphatic amine donors (c)

complexes in place of fluorescent organic molecules in such applications is driven in part by the possibility of time-gating as a means of eliminating background emission [10]. The luminescence lifetimes of metal complexes are on a much longer timescale than the fluorescence of organic molecules (typically around 1 μ s compared to around 1 ns).

Pincer ligands form two cyclometallated rings when they coordinate to a metal ion (Fig. 1b, c). Those which incorporate aromatic lateral ligating units, such as 1,3-di(2-pyridyl)benzene (dpyb), are terdentate analogues of ppy, and may therefore be expected to form a range of emissive complexes having features in common with those of ppy [11]. Indeed, the pincer system may even offer advantages: since the metal ion in such a complex is coordinated to a conformationally constrained terdentate ligand system, the resulting complex should be more rigid compared to one that incorporates bidentate ligands. Take the case of a square-planar complex with two bidentate ligands. The planes of the two ligands can rotate relative to one another leading to a change in the local symmetry from D_{4h} to D_{2d} . If such distortion accompanies the formation of the excited state from the ground state, it can provide a pathway of non-radiative decay, at the expense of luminescence [12]. On the other hand, no such change is open to a tridentate complex of a pincer ligand.

Section 5 of this chapter provides an overview of some of the complexes that have been studied incorporating such pincer ligands with *N*-heterocyclic lateral units. Some of the most highly luminescent metal complexes known have been designed using these ligands [11]. Corresponding ligands of saturated N donors, e.g. ligands based on 1,3-bis(*N,N*-dialkylaminomethyl)benzenes, lack the good π -accepting units of the *N*-heterocyclic systems. The same is true of phosphine PCP and sulphur SCS ligands. As a result, MLCT states may be expected to be of higher energy, and metal-centred states to be of lower energy, in complexes of such ligands, due to weaker ligand fields. This latter point, in particular, tends to militate against obtaining highly emissive systems. Metal-centred excited states involve the promotion of electrons from filled to empty d orbitals; for example, from the d_{xy} to the $d_{x^2-y^2}$ orbital in the case of square-planar d^8 complexes [e.g. Pt(II)], and similarly from the $d_{xy/yz/xz}$ to d_{z^2} or $d_{x^2-y^2}$ orbitals in octahedral complexes [e.g. Ru(II), Ir(III)]. Clearly, these orbitals to which the electrons are promoted are strongly antibonding with respect to the metal–ligand binding, and so the molecule will undergo severe distortion in the excited state. Distortion promotes

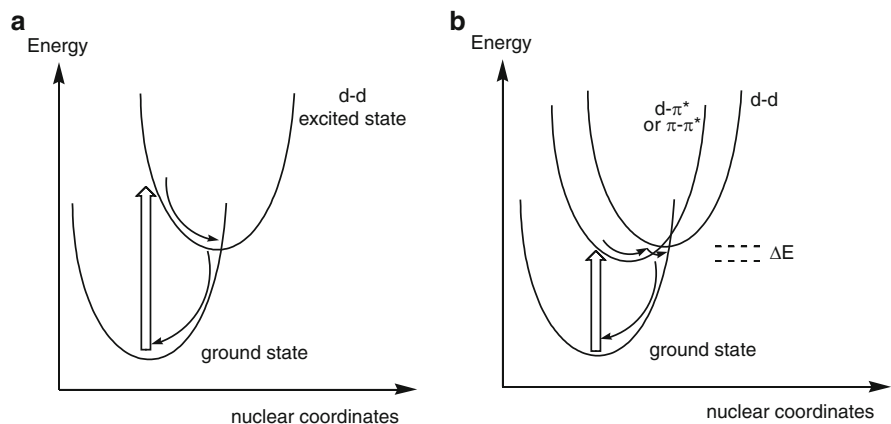


Fig. 2 (a) Metal-centred d–d excited states involve population of strongly antibonding orbitals, such that the potential energy surface of the excited state is severely displaced relative to that of the ground state. (b) At a given temperature T , the d–d state can provide a thermally activated pathway for other, lower-lying excited states if ΔE is comparable to kT . *Thick arrows* represent absorption of light; *thin* ones indicate vibrational relaxation and non-radiative decay [13]

non-radiative decay to the ground state, owing to the presence of a low-energy crossing of the potential energy surfaces, as illustrated simply in Fig. 2a. Even if MLCT or ligand-centred (LC) states lie lower in energy than these d–d states, the latter can still exert a deleterious influence on emission if they are thermally accessible, i.e. if ΔE is comparable to kT (Fig. 2b) [13].

Nevertheless, even though complexes with such pincer ligands are less likely to be good emitters, yet interesting chemistry and applications are still possible, for example, involving absorption rather than emission of light. The chemistry of such compounds is discussed in Sects. 2–4, which deal with SCS, PCP, and non-aromatic NCN complexes, respectively

2 Complexes of SCS Ligands

Kanbara, Yamamoto, and co-workers have prepared the platinum(II) complexes of a number of SCS-binding pincer ligands, and have investigated their luminescence properties. The phosphine sulphide ligand in Fig. 3, which was prepared by palladium-catalysed phosphination of 3,5-dibromotoluene followed by oxidation with elemental sulphur, was found to undergo regioselective cyclometallation at position C⁴ upon treatment with K_2MCl_4 ($M = Pd$ or Pt) [14]. Both complexes (**1**, $M = Pd$ and **2**, $M = Pt$) emit in a frozen glass at 77 K, displaying a broad unstructured emission band in each case, $\lambda_{max} = 580$ and 540 nm, respectively. The emission was attributed to a ³MLCT state. The very large Stokes shift implies significant distortion in the excited state compared to the ground state, which may

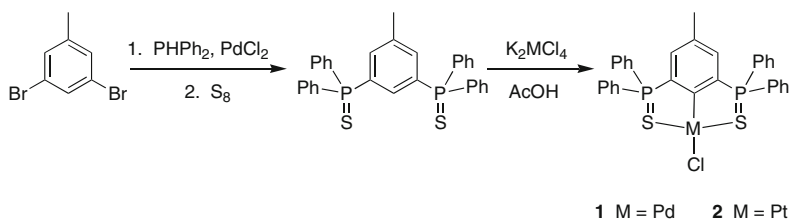


Fig. 3 The synthesis of SCS-coordinated Pt(II) and Pd(II) complexes incorporating phosphine sulphide ligands [14]

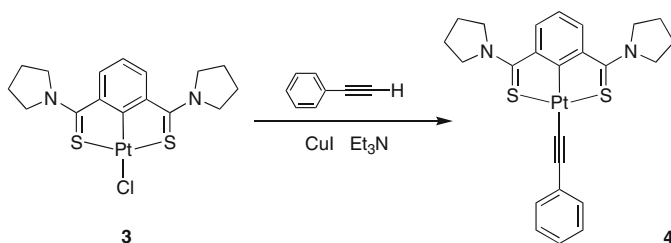


Fig. 4 Thioamide-based SCS-coordinated platinum complexes [15]

account for the absence of emission in fluid solution at room temperature, as outlined in the Introduction. The Pt(II) complex, however, does emit in the solid state at room temperature, displaying a similar spectrum to that in the glass at 77 K, indicating that no aggregation effects are occurring in the solid. This observation is supported by the long Pt . . . Pt distance of 8.79 Å found between neighbouring molecules of **2** in the crystal structure and likewise the large separation between the ligand planes (>5 Å), prohibiting the overlap of π orbitals.

Platinum(II) complexes of related thioamide ligands have been studied. 1,3-Bis(pyrrolidinothiocarbonyl)benzene undergoes platination to give complex **3** upon treatment with bis(benzonitrile)platinum(II) dichloride (Fig. 4); the metallation proceeds under remarkably mild conditions—acetonitrile solution at 65 °C [15]. Metathesis of the chloride co-ligand with an acetylide to give complex **4** could be accomplished upon treatment with phenylacetylene under Sonogashira-type conditions (CuI catalyst and Et₃N as the base). Though neither complex emits in solution at room temperature, both display red luminescence in the solid state, $\lambda_{\text{max}} = 630$ and 640 nm for **3** and **4**, respectively. As in the case of **2**, the spectra are very similar to those obtained in frozen glasses at 77 K, and indeed the crystal structure of **3** reveals that the interligand and intermetallic separations are again too large for aggregation effects to occur.

The two complexes were tested as phosphors in multilayer OLEDs having the architecture shown in Fig. 5, where the electroluminescence from the devices is also shown. Although the reported EL efficiency was low (422 cd m⁻² or 0.2 % ph/e at 100 mA cm⁻²), this study probably represents the first example of the use of platinum(II) complexes with terdentate ligands in OLEDs. Further work on devices incorporating a wider range of such complexes has since been carried out [16].

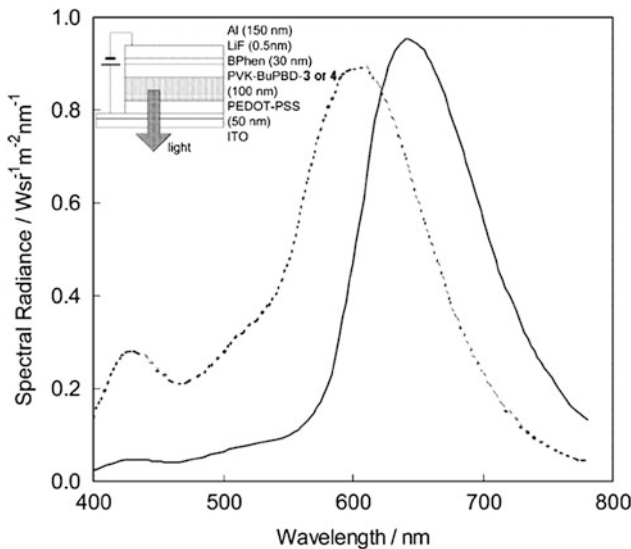


Fig. 5 Electroluminescence spectra of OLEDs prepared using **3** and **4** as emitters in the multilayer device structure shown in the inset. *BPhen* bathophenanthroline, *PVK* poly(9-vinylcarbazole), *BuPBD* 2-(4-biphenyl)-5-(4-tert-butylphenyl)-1,3,4-oxa-diazole, *PEDOT-PSS* poly [3,4-(ethylenedioxy)thiophene]-poly(styrenesulfonic acid)} (reprinted with permission from [15] © 2004 Elsevier)

Related secondary thioamide pincer ligands form similar complexes but those of *N*-arythioamides offer additional scope due to the possibility of subjecting them to oxidative cyclisation reactions. Thus, proligand **5** can be cyclised to give **6** upon treatment with $K_3[Fe(CN)_6]$ (Fig. 6) [17]. Both complexes react with K_2PtCl_4 to form complexes in which the ligand is bound in a terdentate pincer fashion (**7** and **8** respectively) but, whereas the ligand is SCS-coordinating in **7**, it binds as an NCN-coordinating ligand in **8**, owing to the very poor ligating properties of the sulphur atoms in benzothiazoles.

Both complexes emit in the solid state at room temperature and in a frozen glass at 77 K, but only the NCN-coordinated complex **8** is luminescent in fluid solution at room temperature. Though the authors did not comment on the likely origin of this difference, we speculate that the weaker ligand field strength offered by SCS-coordinating ligands compared to aromatic NCN ligands may lead to metal-centred excited states being thermally accessible at room temperature, thus introducing an additional deactivation pathway, as mentioned in the Introduction. It is also likely that the SCS complex will be less rigid, favouring intramolecular electronic-to-vibrational energy transfer and subsequent energy loss to the solvent. Indeed, such characteristics would apply equally to complexes **2–4** discussed above.

The emission spectra of **7** and **8** at 77 K are shown in Fig. 7. The SCS complex **7** displays a broad structureless spectrum in the red region, which is assigned to a 3MLCT state. In contrast, the spectrum of the NCN-coordinated complex appears at

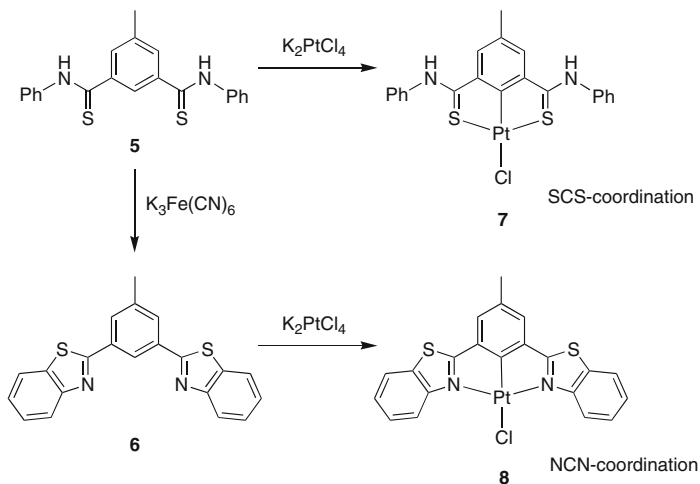


Fig. 6 SCS and NCN coordinated pincer Pt(II) complexes derived from the thioamide proligand **5** [17]

higher energy and reveals well-resolved vibrational structure, a feature more typical of excited states of predominantly ligand-centred (${}^3\pi-\pi^*$) character. Indeed the profile of the spectrum is similar to that of the Pt(II) complex of 1,3-dipyridylbenzene (see Sect. 5.3.1), where a ligand-centred assignment is generally accepted, but with an emission energy somewhat lower, consistent with the expected decrease in excited-state energy on going from pyridine to benzothiazole units. In the solid state at room temperature, the emission is red-shifted in both cases compared to that in solution, suggesting the formation of aggregates or excimer-like species, an observation in line with the rather short interplanar distances of 3.56 and 3.40 Å in the crystal structures of **7** and **8**, respectively.

More recent work from the same group has focused on the reactivity of the thioamide N–H in such secondary thioamide complexes: it can be deprotonated by strong bases and can also act as a hydrogen bond donor, with the potential to lead to modulation of the ground-state absorption and excited-state emission properties [18]. Investigations were carried out on the dibenzylaminothiocarbonyl complex **9** (Fig. 8). In contrast to its anilinothiocarbonyl analogue **7**, complex **9** is luminescent in solution at room temperature ($\Phi_{lum} = 0.06$ in THF). Upon addition of increasing amounts of a strong base such as DBU (1,8-diazabicyclo[5.4.0]undec-7-ene), the absorption spectrum changes, as shown in Fig. 9a, with two well-defined isosbestic points, until the point at which two equivalents of base have been added relative to **9**. The changes in absorption are accompanied by a decrease in the emission intensity (Fig. 9b). The original spectra are restored upon addition of methanesulfonic acid, and hence the effect is interpreted in terms of the reversible equilibria shown in Fig. 8. The excited-state pK_a of **9** was estimated to be 17.7.

In contrast to the effect of base, the addition of tetra-*n*-butylammonium chloride to a solution of **9** leads to a blue-shift in the lowest-energy absorption band and of the emission (Fig. 9c, d). The emission intensity is enhanced, and the lifetime is

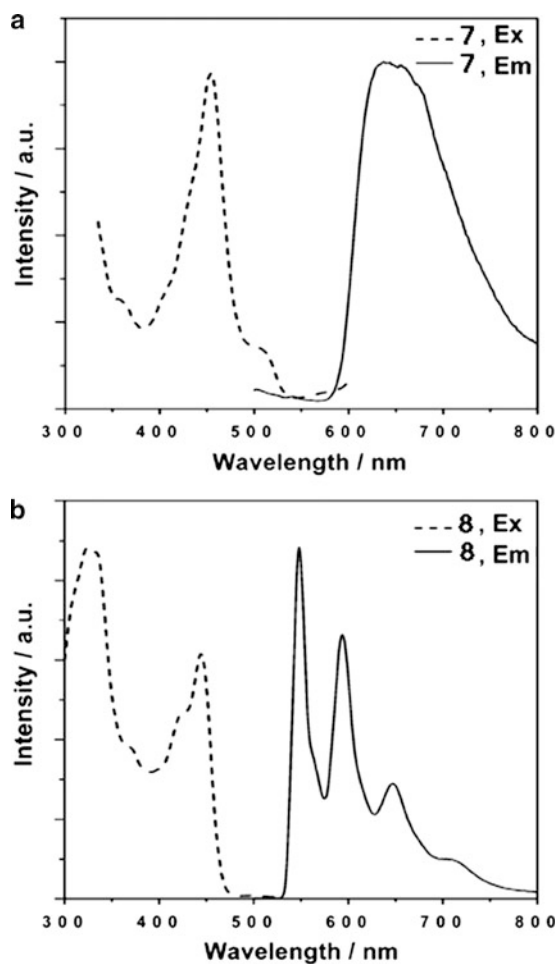


Fig. 7 Emission spectra of the Pt(SCS) complex **7** and Pt(NCN) complex **8** at 77 K in a frozen glass of $\text{CH}_2\text{Cl}_2/\text{THF}$ (3:2 v/v) (reprinted with permission from [17] © 2006 American Chemical Society)

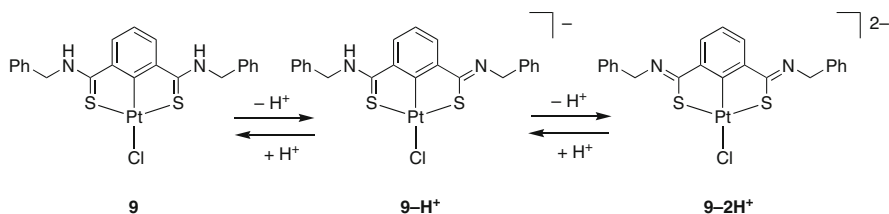


Fig. 8 Pt(II) SCS pincer complex **9** and the reversible double-deprotonation reaction it undergoes upon treatment with strong base

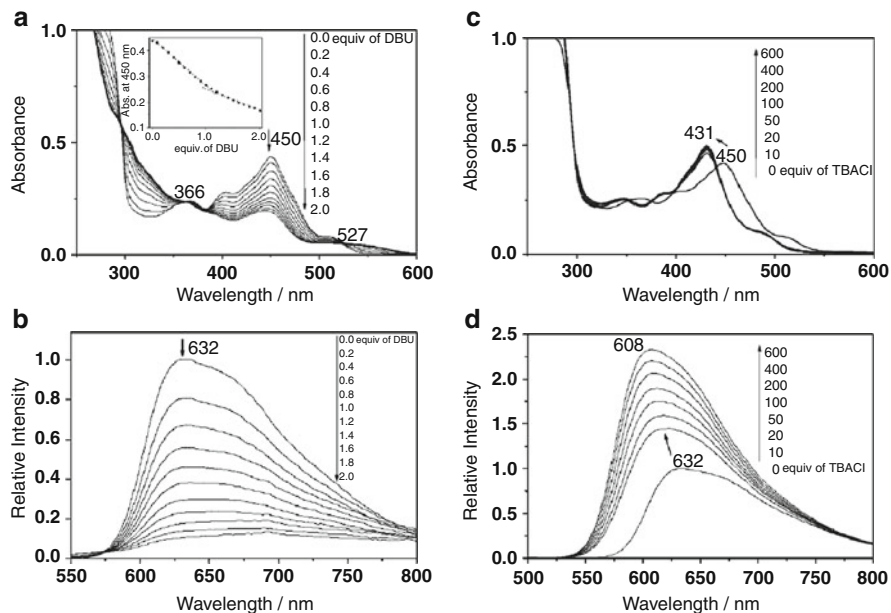


Fig. 9 Left: Changes in the (a) absorption (*inset*: absorbance change at 450 nm) and (b) emission spectra of **9** (5×10^{-5} M in THF at room temperature) upon addition of DBU. Right: Changes in the absorption (c) and emission (d) spectra of **9**, under the same conditions, upon addition of $[\text{Bu}_4\text{N}]^+\text{Cl}^-$ (reprinted with permission from [18] © 2009 American Chemical Society)

increased. These effects have been interpreted in terms of hydrogen bonding of the N–H of the thioamide group to the added chloride ions. It is suggested that this interaction may either inhibit the quenching of the $^3\text{MLCT}$ state by the solvent or help to rigidify the molecules in solution, making non-radiative decay pathways less efficient. In line with this notion is the magnitude of the effect with other anions, being in the order $\text{Cl}^- > \text{Br}^- > \text{BF}_4^- > \text{PF}_6^-$, which mirrors their hydrogen bond acceptor ability. The lack of any changes in the absorption spectrum of a related dimethylaminothiocarbonyl complex (a tertiary thioamide) upon addition of either base or chloride ions also confirms the requirement for the N–H unit, supporting the proposed hypotheses.

Finally in this section, we note that asymmetric SCS ligands incorporating one thioamide and one phosphine sulphide unit have recently been reported, and the palladium complex of one such ligand displays weak emission in the deep-red/NIR region ($\lambda_{\text{max}} = 740$ nm) in the crystalline state at room temperature [19].

3 Complexes of PCP Ligands

An intriguing study of platinum(II) complexes of an anthracene-based PCP ligand has been described recently by Yip and co-workers [20]. The ligand is 1,8-bis(diphenylphosphino)anthracene (DPA), which metallates at C⁹ whilst coordinating

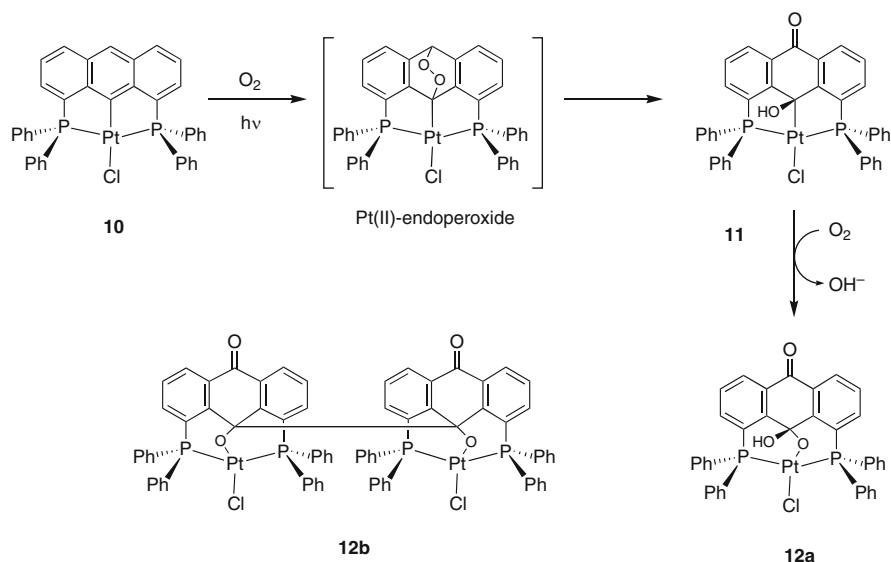


Fig. 10 Photo-oxidation of the PCP coordinated Pt(II) complex **10**

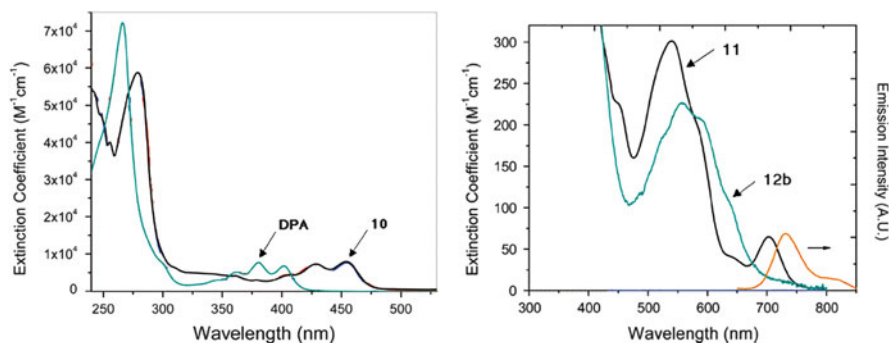


Fig. 11 *Left*: Absorption spectra of 1,8-bis(diphenylphosphino)anthracene (DPA) and its PCP-coordinated Pt(II) complex **10** in CH_2Cl_2 at 298 K. *Right*: Absorption spectra of the photo-oxidised species **11** and **12b** and the emission spectrum of **11** in degassed CH_2Cl_2 at room temperature (reprinted with permission from [20] © 2009 American Chemical Society)

to the Pt(II) ion through the two phosphorus atoms to give complex **10** (Fig. 10). The corresponding compounds with bromide or iodide in place of chloride as the co-ligand could be prepared from **10** by halide metathesis. The low-energy, vibronically resolved ${}^1\pi\text{-}\pi^*$ bands typical of anthracene (in which they appear at 380 nm) are modestly red-shifted on going to DPA and shifted substantially further in **10** (Fig. 11). Transitions of MLCT and LLCT character are also anticipated on the basis of symmetry, but these are presumably masked by the ligand-centred transitions. Complex **10** is strongly photoluminescent in deoxygenated

dichloromethane solution at room temperature ($\lambda_{\text{max}} = 474 \text{ nm}$, $\Phi_{\text{lum}} = 0.22$). The small Stokes shift of 900 cm^{-1} relative to the lowest-energy absorption band has been interpreted as indicative of emission from the $\pi\text{-}\pi^*$ state, although whether this has singlet or triplet character is not clear from the report. No luminescence lifetime is available, but the emission is modestly quenched by O_2 (intensity in air-equilibrated solution is 70 % of that of a degassed solution), suggesting that the lifetime is likely to be at least tens of nanoseconds.

Upon irradiation of an air-saturated “wet chloroform” solution of **10**, the complex undergoes photo-oxidation to generate a deep-red Pt(II)–hydroxyanthrone complex (**11**), which has been unequivocally identified by X-ray crystallography. The consequent disruption of the conjugated system of the anthracene unit is reflected in the bleaching of the $\pi\text{-}\pi^*$ transitions, but this is accompanied by the appearance of much weaker bands centred at 538 and 706 nm. On the basis of the known spectroscopy of anthrones [21], these bands are attributed to formally forbidden $^1\text{n} \rightarrow \pi^*$ and $^3\text{n} \rightarrow \pi^*$ transitions, respectively. Complex **11** is weakly emissive in the NIR region ($\lambda_{\text{max}} = 732 \text{ nm}$, $\Phi_{\text{lum}} = 3 \times 10^{-3}$ in CH_2Cl_2 , Fig. 11). The conversion of **10** to **11** is thought to proceed via the 9,10-endoperoxide, formed by reaction with $^1\text{O}_2$. The complex itself is likely to be able to sensitise dissolved oxygen to the singlet state. The role of $^1\text{O}_2$ is supported by the observation that the rate of reaction is faster in CDCl_3 than in CHCl_3 , consistent with the longer lifetime of $^1\text{O}_2$ in the former solvent (300 μs compared to 30 μs respectively).

Upon prolonged further irradiation in the presence of O_2 , **11** is oxidised to **12a** (identified in solution), which undergoes acid-catalysed ketalisation to generate **12b** (crystallographically characterised). The formation of these products from **11**, and their interconversion, is thought to proceed via a Pt(II)–anthraquinone intermediate. The oxidation of **11** to **12a** also proceeds in darkness, but at a much slower rate, which is interpreted in terms of sensitisation of $^1\text{O}_2$ (more oxidising than ground state $^3\text{O}_2$) by **11** in the presence of light.

Overall, the study shows that the platinum(II) ion has a profound influence on the photo-oxidation of the anthracene unit. It contrasts with the behaviour of anthracene itself which, following the formation of the endoperoxide, gives rise to a range of photoproducts and thermal products.

A ruthenium(II) complex incorporating a PCP-binding ligand has been investigated as a sensitiser of lanthanide(III) excited states [22]. The lanthanide (III) ions suffer from low molar absorptivities (for the f–f excited states), and the strategy of using d-block complexes as “antennae” is one which has been widely explored over recent years [23]. The excited state of the sensitiser moiety should be higher in energy than the lanthanide excited state, in order for efficient energy transfer to occur. The ruthenium complex **13** (Fig. 12), related to the widely studied complex $[\text{Ru}(\text{tpy})_2]^{2+}$ and its cyclometallated analogues (see Sect. 5.1), shows no detectable emission, even at 77 K, possibly owing to quenching by the anilino nitrogen atom. However, upon binding of the pendant azacarboxylate to Gd^{3+} (**13-Gd**), weak emission bands are observed at 560 and 650 nm, attributed to ^3LC and Ru-based $^3\text{MLCT}$ states, respectively. Apparently, the binding of the lanthanide ion attenuates the quenching effect of the amine. The ^3LC excited state of the system is

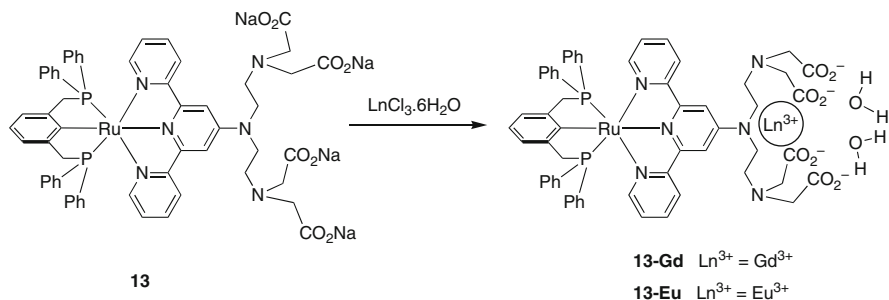


Fig. 12 A d-f hybrid incorporating a Ru(PCP) moiety [22]

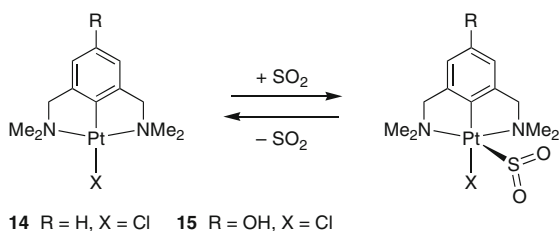


Fig. 13 NCN-coordinated Pt(II) complexes with saturated amine donors can bind SO_2 reversibly

sufficiently high to be able to populate the $^5\text{D}_0$ state of Eu^{3+} and, indeed, in the corresponding Eu^{3+} complex (**13-Eu**), a weak band is observed, attributable to the $^5\text{D}_0 \rightarrow ^7\text{F}_2$ transition, together with the lower-energy $^3\text{MLCT}$ state band. Energy transfer from the Ru-based $^1\text{MLCT}$ and from the ^3LC states to the Eu^{3+} ion is inferred. The origin of another sharp band at 545 nm in the Eu^{3+} complex is, however, unclear.

4 Complexes of NCN Ligands with Non-aromatic Amines

Van Koten and co-workers have made extensive studies of NCN-coordinated platinum and palladium complexes based on 1,3-bis(*N,N*-dialkylaminomethyl)-benzene ligands. It was noted in a study from 1986 that the complex $\text{PtX}\{\text{C}_6\text{H}_3(\text{CH}_2\text{NMe}_2)_2\}$ is able to bind sulphur dioxide, both in solution and in the solid state ($\text{X} = \text{Cl}, \text{Br}$ or I) (**14**, Fig. 13) [24]. The reaction is accompanied by a change from colourless to orange and, unusually for a transition metal- SO_2 adduct, the process was found to be reversible. For the $\text{X} = \text{Br}$ complex, an SO_2 adduct was crystallographically characterised, which showed η^1 -binding of the SO_2 molecule to the platinum(II) ion through the sulphur atom, with a square-pyramidal geometry at the metal [24].

A larger range of complexes were subsequently investigated, with differing alkyl groups on the nitrogen atoms and substituents at the 4-position of the benzene ring [25]. The response of the system to SO₂ was found to be tunable according to such modifications in the structure of the ligand. Dendrimeric systems were synthesised, comprising a core and branches of 1,3,5-benzene tricarboxylic esters, on the periphery of which were substituted NCN complexes of this type through an ester bond (i.e. using the phenolic derivative **15**). Systems incorporating six adsorption-active metal sites within a single well-defined molecule could thus be prepared. With this system, where the platinum centres work in concert, in conjunction with UV-visible absorption spectroscopy, it was found to be possible to detect SO₂ concentrations in solution as low as 100 μM [26].

An interesting further development in this area was the study of the mononuclear complex **15** in the solid state. Crystal structures of both **15** and its SO₂ adduct were obtained [27]. Unusually for a solid-state chemical transformation, there is no loss of crystallinity during the uptake or loss of SO₂ from the solid. A network of hydrogen bonding in **15** is retained in the structure of the SO₂ adduct. The fixation of SO₂ in the latter involves Pt...S(O)₂...Cl bond formation perpendicular to the hydrogen bond network. Exposure of crystalline **15** to SO₂ gas for around 1 min is sufficient to convert it quantitatively to the SO₂ adduct. Shorter times of a few seconds give a mixture of the two crystalline compounds **15** and **15**-SO₂, based on comparison of the recorded powder diffraction pattern with that simulated from the diffraction patterns of the two compounds.

A theoretical study of the nature of the bonding of SO₂ in such complexes has been undertaken by Zhang and co-workers, who used a combination of Møller-Plesset (MP2) and density functional theory (DFT) [28]. They are of the view that geometries in such weakly bound adducts can be optimised more reliably using the former, ab initio methods, owing to the dependence of the latter on the choice of functional. Of three possible geometries of η¹-binding of SO₂ at the apical position of the square pyramid, that referred to as *trans* pyramidal—in which the oxygen atoms are tilted backwards over the NCN unit *trans* to the Pt-Cl bond—was found to be the most stable. The Pt-S interaction occurs between the HOMO and LUMO of SO₂ and the filled d_{xz} orbital, whilst Pt-S σ* (d_{z²-p_z}) bonding character in the LUMO is proposed to facilitate the reversibility of the reaction. The difference between the absorption spectra of **14** and its SO₂ adduct was accurately reproduced using time-dependent DFT (TDDFT). The low-energy absorption of the latter, which accounts for the appearance of the orange colour upon SO₂ binding, is attributed to a transition of predominant Pt(d_{xz})/phenyl/Cl (p_z) → SO₂ charge transfer character.

Connick and co-workers have explored the emission properties of a number of NCN-coordinated platinum(II) complexes with saturated amine units [29–31]. In place of the dimethylamino groups of **14** and **15**, their ligand is based on lateral piperidyl groups, viz. 1,3-bis(piperidylmethyl)benzene. In an initial study, they prepared the complexes **17–20** (Fig. 14), via lithiation of the bromo-substituted starting material **16** [29]. The monodentate imine co-ligand in **20** was formed in situ from the reaction of methylamine with acetone. All four complexes are colourless, but absorb strongly in

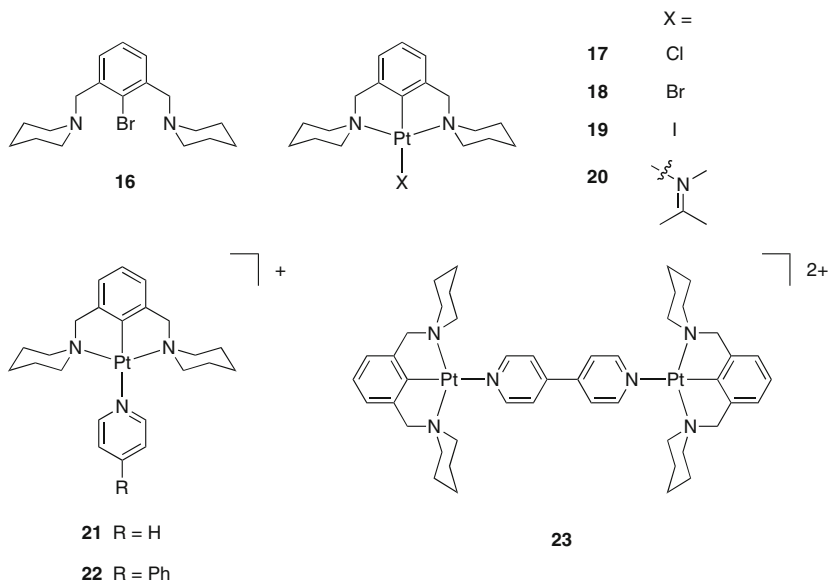


Fig. 14 A selection of NCN-coordinated pincer Pt(II) complexes prepared by Connick and co-workers from proligand **16**

the UV, displaying intense bands in the 250–300 nm region ($\epsilon > 7,000 \text{ M}^{-1} \text{ cm}^{-1}$) which have no counterparts in the uncomplexed proligand (Fig. 15a). These bands are attributed to MLCT transitions; metal-centred d–d states would be expected at higher energies and, being formally forbidden, would have smaller extinction coefficients. The MLCT assignment is supported by the observed trend in energies: **20** > **17** > **18** > **19**; i.e. the transition shifts to lower energy with increasing electron density on the metal centre. A weaker shoulder around 300 nm is visible for all but the iodo complex, which is attributed to the formally spin-forbidden transition to the corresponding $^3\text{MLCT}$ state: the singlet-triplet splitting of around $2,500 \text{ cm}^{-1}$ is of an order of magnitude typical for MLCT states of Pt(II) diimine complexes [32].

No luminescence could be detected from the complexes in solution at room temperature but, at 77 K in a frozen glass, all four display orange to red emission, with broad, Gaussian-shaped bands (Fig. 15b). The luminescence is attributed to ^3MC excited states, i.e. of $d\pi(xy,xz,yz) \rightarrow d\sigma^*(x^2-y^2)$ character. The order of emission energies is **20** > **17** > **18** > **19**, consistent with the positions of the monodentate co-ligands in the spectrochemical series. The weak band around 370 nm observed in the excitation spectra (Fig. 15b), and whose position displays the same trend in energy, is likely to be due to direct excitation to the ^3MC state. The large Stokes shifts and broadness of the emission bands are consistent with a relaxed excited-state geometry that is very different from that of the ground state, as expected for an excited state that involves population of an antibonding (i.e. $d_{x^2-y^2}$) orbital.

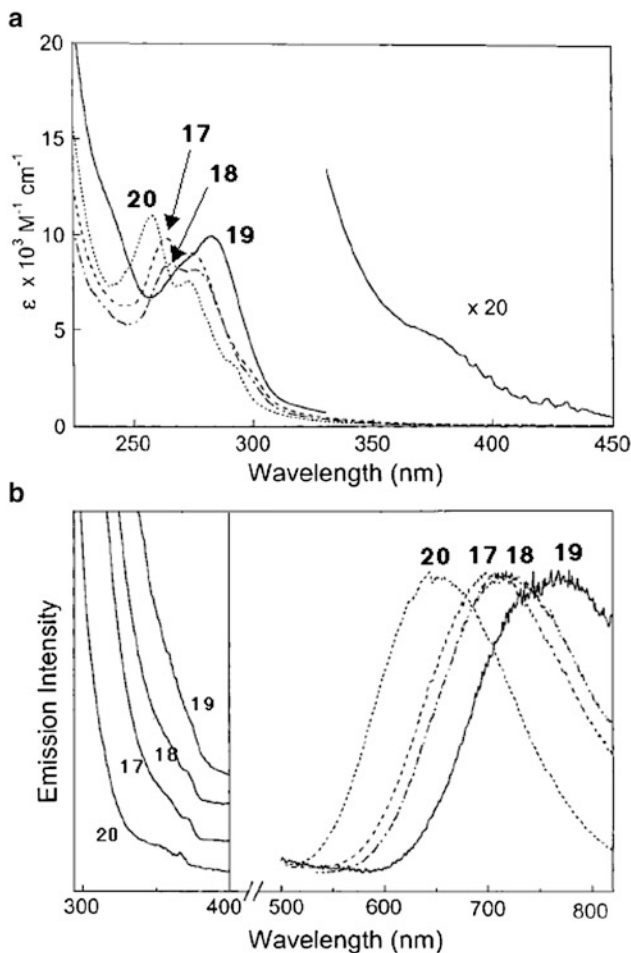


Fig. 15 (a) Room temperature absorption spectra of **17–20** in MeOH. (b) Normalised emission spectra of **17–20** at 77 K in a glass of EtOH/MeOH (3:1 v/v) with corresponding excitation spectra shown in the left panel (reprinted with permission from [29] © 2002 American Chemical Society)

The authors noted that the emission of the imine and chloro complexes, **20** and **17**, appears at lower energies than that observed from $\text{Pt}(\text{NH}_3)_2\text{Cl}_2$, despite the generally accepted view that the phenyl anion should be a stronger field ligand than imine or chloride. They note the importance of the orientation of the ring with respect to the orbitals of the metal ion. In the NCN complexes, it is not optimised for π -back-bonding with the d_{xy} level, and therefore the $d_{xy} \rightarrow d\sigma^*$ energy gap is low. On the other hand, the orientation of the phenyl ring favours relatively low-energy $\text{Pt} \rightarrow \text{phenyl MLCT}$ excited states. These occur at 270–285 nm for the present set of complexes, compared to shorter wavelengths (<260 nm) for the corresponding transitions in $\text{Pt}(\text{PEt}_3)_2\text{PhCl}$, where the phenyl rings are tilted relative to the coordination plane.

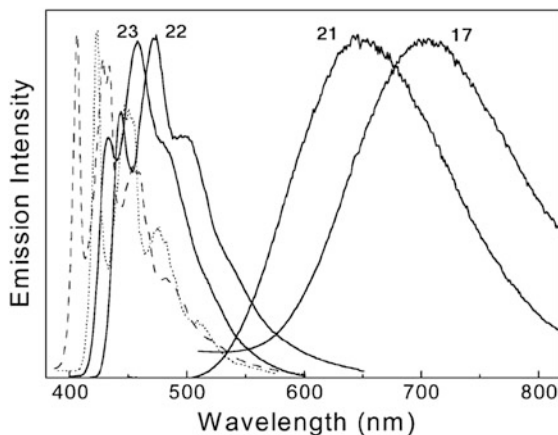


Fig. 16 Emission spectra of **21–23** at 77 K in a glass of EtOH/MeOH (4:1 v/v) together with that of **17** and of 4-phenylpyridine (dotted line) and 4,4'-bipyridine (dashed line) under the same conditions for comparison (reprinted with permission from [30] © 2004 American Chemical Society)

Subsequent work examined pyridine, 4-phenylpyridine (4-ppy), and 4,4'-bipyridine (4,4'-bpy) as the co-ligand (**21–23**) [30]. The crystal structures of these complexes reveal that the plane of the aromatic co-ligand is approximately orthogonal to that of the NCNpt unit, a geometry that *does* favour interaction with the high-lying d_{xy} orbital, in contrast to the phenyl of the NCN ligand as mentioned above. The weak emission spectrum of **21** at 77 K is similar to that of the previous series **17–20**, indicative of a 3MC emitting state. In contrast, **22** and **23** are much more intensely luminescent, emitting at substantially higher energy around 450–500 nm, with long lifetimes ($>100 \mu\text{s}$), and displaying clear vibrational structure in their spectra (Fig. 16). This striking difference is interpreted in terms of emission from $^3\pi-\pi^*$ states localised on the 4-ppy and 4,4'-bpy ligands, which lie at much lower energy than the 3MC state. Whilst this may at first sight seem counter-intuitive, given that the 3MC bands appeared at much lower energies in the other complexes, it should be noted that MC states are likely to have much larger Stokes shifts than LC states. Thus, there may be insignificant contribution of the 0–0 transition to the spectrum in the former case, and the position of the emission band is likely to be a poor indicator of the energy of the MC state. Indeed, from the excitation spectra of **17–20**, the transition thought to correspond to excitation to the 3MC state appeared at around 380 nm.

Three other dimeric systems, analogous to **23** but with pyrazine (**24**), 1,2-bis(4-pyridyl)ethane (**25**), and *trans*-1,2-bis(4-pyridyl)ethene (**26**) as the bridging ligands, were subsequently reported [31]. Not surprisingly, given the insulating and conjugating nature of the $\text{CH}_2\text{--CH}_2$ and $\text{CH}=\text{CH}$ linkers, respectively, the emission from **25** and **26** resembles that of **21** (3MC) and **23** ($^3\pi-\pi^*$), respectively. On the other hand, the pyrazine-bridged system is unique amongst these systems in displaying emission assigned to a 3MLCT excited state, although the analysis is complicated by a tendency for the dimer to dissociate in solution.

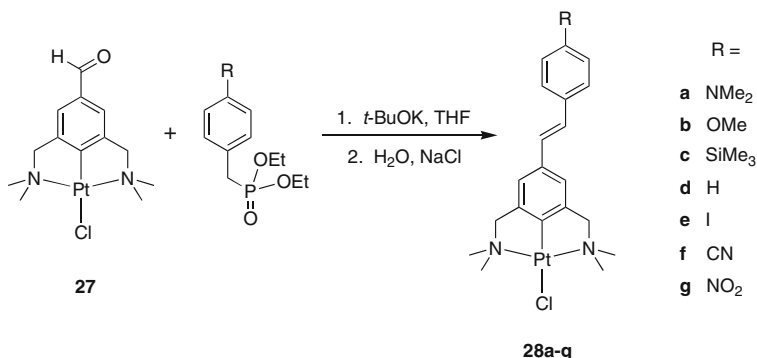


Fig. 17 NCN-coordinated Pt(II) complexes incorporating styryl pendants [33, 34]

A series of NCN-coordinated platinum(II) complexes based on **14**, incorporating styryl substituents $p\text{-R-C}_6\text{H}_4\text{-CH=CH-}$ at the 4-position of the cyclometallated benzene ring, **28a–g**, have been investigated in detail by van Koten and collaborators [33, 34]. They were prepared by a chemistry-on-the-complex approach, in which the pre-formed formyl-substituted complex **27** was reacted with the appropriate phosphonate ester under Horner–Wadsworth–Emmons conditions (Fig. 17). The pure *trans* isomers precipitated from solution. They do not undergo photochemical *trans*–*cis* isomerisation in the solid state, but do so in solution. These compounds can be regarded as organometallic analogues of 4,4'-donor–acceptor-substituted stilbenes such as 4-dimethylamino-4'-nitrostilbene (DANS), an important class of molecules in the field of non-linear optics (NLO), owing to the large changes in dipole moment that accompany the formation of their intramolecular charge-transfer (ICT) excited states [35]. In the present set of platinum compounds, the metallated PtCl moiety acts as one of the *para* substituents. On the basis of the correlation of the ^{195}Pt and ^{13}C (for the metallated carbon) chemical shifts with the Hammett σ_p parameter for the substituents R, the PtCl unit is assessed to be a π -donor; for PtI it is of comparable strength to a dimethylamino group.

The absorption spectra of these complexes in solution are shown in Fig. 18, with that of DANS for comparison. The spectra are dominated by an ICT band. Amongst the four complexes with R = H, I, CN, NO₂ (**28d–g**), the band moves to lower energy as the R group becomes more electron-accepting, supporting the notion that the NCNPtCl unit behaves as a donor group. Such a trend is not apparent for **28a–d**, but subsequent TD-DFT studies were able to account for this on the basis of the effects of R on both the HOMO and LUMO orbitals [34].

Three of the complexes within this series are fluorescent at room temperature, namely **28a**, **f**, and **g**; ($\lambda_{\text{max}} = 432, 466, \text{ and } 677 \text{ nm}$, respectively, in CH₂Cl₂ solution). The emission is quite strongly solvatochromic, shifting to the red with increasing solvent polarity, indicative of the dipolar nature of the ICT state from which the fluorescence emanates. The emission is short-lived in each case, with a

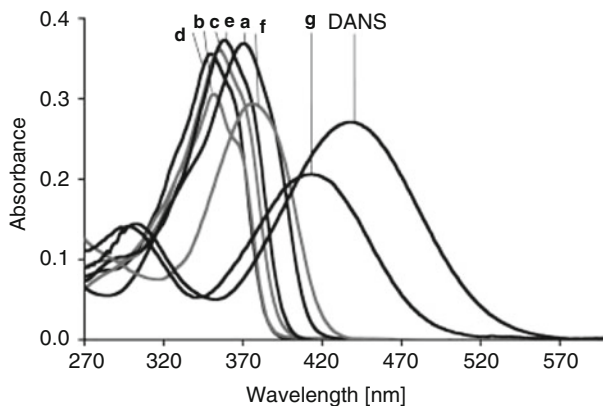


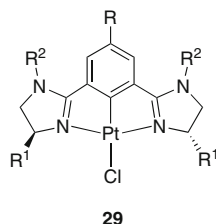
Fig. 18 Absorption spectra of **28a–g** in CH_2Cl_2 , together with that of DANS for comparison (reprinted with permission from [33] © 2007 Wiley-VCH)

lifetime of the order of 200 ps in CH_2Cl_2 , suggestive of a singlet rather than triplet origin, despite the presence of the heavy metal ion. One possible explanation is that the rate of fluorescence is too fast—and the SOC effect of the platinum(II) in the excited state is too small in such extended conjugated systems—for efficient ISC to the triplet state to compete with fluorescence. However, the quantum yields of fluorescence are much lower than those of organic stilbenes. Thus, it is quite possible that ISC is highly competitive with fluorescence but that the triplet state, once formed, does not lead to observable phosphorescence under ambient conditions, due to efficient non-radiative decay pathways. Support for the latter explanation comes from recent studies of the electroluminescence of an OLED fabricated using a spin-coated layer of **28f** as the emitting layer [34]. It was noted that the EL spectrum of the device was dominated by an emission band around 470 nm, consistent with the behaviour of this complex in solution. However, an additional longer wavelength band was also observed, at around 650 nm. This observation prompted a study of the emission of **28f** in the solid state. At low temperatures, a new band appears at 660 nm, accompanied by the second component of a vibrational progression visible at 730 nm. These bands are attributed to phosphorescence from the triplet state, which is quenched by non-radiative decay processes at ambient temperature. A similar situation has been observed in cyclometallated platinum(II) complexes with phenylpyridine ligands incorporating styryl substituents [36].

Finally, we note that the NLO properties of these complexes have been explored. The incorporation of metal fragments into conjugated organic systems is one which is opening up new possibilities in the field of NLO [37, 38]. The β_{zzz} component of the hyperpolarisability tensor (where z is the charge transfer axis) has been determined for **28a–g** by hyper-Rayleigh scattering, from which the static quadratic hyperpolarisability, β_0 , is calculated. The complexes show values of β_0 (up to 211×10^{-30} esu for $R = \text{I}$) that are similar to or higher than those of purely

organic stilbenes such as DANS ($\beta_0 = 56 \times 10^{-30}$ esu), probably reflecting potential for polarisation along the C–Pt bond. There is, however, no clear-cut correlation between the donor or acceptor properties of the R group and the magnitude of β_0 , probably because of the dependence of the latter not only on the energy of the first excited state, but also on the absorption coefficient, and possibly also on contributions of other excited states.

1,3-Bis(2'-imidazolyl)benzene ligands are under investigation as analogues of the well-known chiral pincer ligands based on 1,3-bis(2'-oxazolyl)benzene (phebox) [39, 40]. Ligands of this type form chiral C_2 -symmetric complexes upon NCN-cyclometallation with metal ions such as palladium(II) and platinum(II). The luminescence properties of the complexes **29a–d** have been investigated by Hao et al. [41]. These complexes are all luminescent in solution at room temperature. Although the quantum yields are quite low, 0.13–0.18 %, the behaviour contrasts with that of related complexes discussed earlier in this section with saturated nitrogen donors (e.g. **17–20**), for which luminescence is only observed at low temperature. The emission maxima in CH_2Cl_2 solution are around 575 nm in each case: the substituents have no significant effects. A further difference is that the complexes are yellow rather than colourless. These differences that arise upon changing from amine- to imine-based ligands can be understood in terms of two effects of the introduction of the C=N bonds. Firstly, the π -acceptor nature of the C=N bond should serve to stabilise the $^{1,3}\text{MLCT}$ states. Secondly, the ligand-field strength of an imino-NCN ligand should be greater than for an amino-NCN analogue, such that $^{1,3}\text{MC}$ (d–d) states will be destabilised. Thus, one might anticipate that the lowest energy excited states in **29a–d** will be $^3\text{MLCT}$ in character, less subject to distortion compared to the MC states of **17–20**, and thus less prone to non-radiative deactivation. Indeed, one might regard these complexes as being intermediate in nature between the fully saturated and the aromatic NCN systems discussed in Sect. 5.3, where substantially higher quantum yields are encountered.



- a** $\text{R}^1 = i\text{-Pr}$ $\text{R}^2 = p\text{-Tol}$
- b** $\text{R}^1 = i\text{-Pr}$ $\text{R}^2 = p\text{-Anisyl}$
- c** $\text{R}^1 = \text{CH}_2\text{Ph}$ $\text{R}^2 = p\text{-Anisyl}$
- d** $\text{R}^1 = \text{CH}_2\text{Ph}$ $\text{R}^2 = p\text{-Anisyl}$

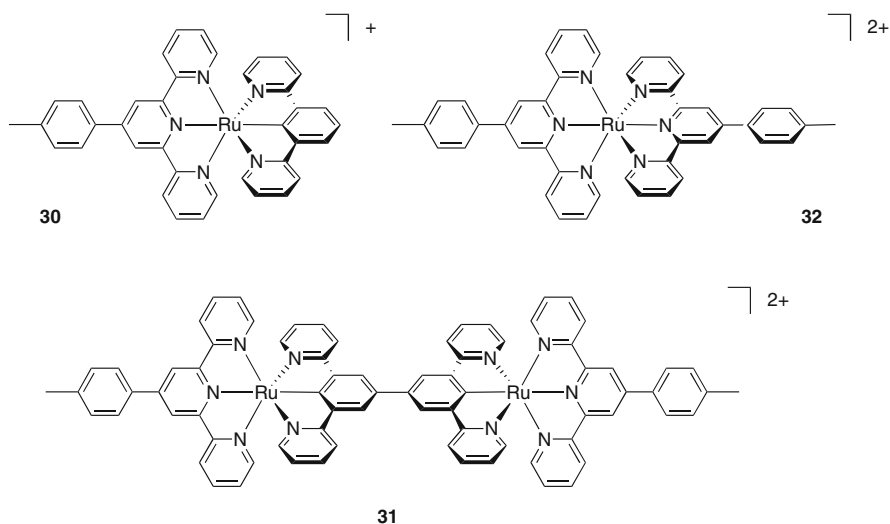
5 Complexes of NCN Ligands with Aromatic Amines

This section deals principally with ligands based on 1,3-di(2-pyridyl)benzene (Fig. 1b) and analogues comprising other *N*-heterocycles such as pyrazoles, benzimidazoles, and quinolines. Again the bulk of our discussion will focus on

square-planar platinum(II) complexes with such ligands of the general formula $\text{Pt}(\text{NCN})\text{Cl}$, but we shall first provide an overview of some background as well as recent developments on ruthenium(II), osmium(II), and iridium(III) complexes containing such ligands.

5.1 Ruthenium(II) and Osmium(II) Complexes

The first example of a cyclometallated, NCN-coordinated metal complex of 1,3-di(2-pyridyl)benzene (dpyb) was reported in 1991 by Sauvage and co-workers [42]. They prepared $[\text{Ru}(\text{ttpy})(\text{dpyb})]^+$, **30**, by treatment of $\text{Ru}(\text{ttpy})\text{Cl}_3$ with silver triflate in acetone, followed by reaction with dpybH. The role of the Ag^+ ions was to facilitate the removal of the chloride ligands from the ruthenium ion. In fact, Ag^+ was found to have an additional effect owing to its oxidising power, namely to promote oxidative coupling of two molecules of **30** to generate the dimeric side-product **31**. Related dimers with one, two, or three interposed phenyl rings were synthesised using Suzuki cross-couplings [43, 44]. The osmium(II) analogue of **30**, $[\text{Os}(\text{ttpy})(\text{dpyb})]^+$, was prepared by reduction of the Os(VI) compound $[\text{Os}(\text{ttpy})(\text{O})_2(\text{OH})]^+$ in the presence of dpybH [45]. A variety of mixed-metal Ru–Os dimers related to **31** with two, one, or no interposed phenyl rings were also synthesised. Mixed valency in the homometallic Ru_2 dimers and $\text{Ru} \rightarrow \text{Os}$ energy transfer in the heterometallic dimers were investigated in a number of studies in the 1990s [46–48]. The reader is directed to a recent review of the coordination chemistry of dpyb for a more detailed overview of this early work [11].



Comparison of the photophysical and electrochemical properties of $[\text{Ru}(\text{ttpy})(\text{dpyb})]^+$ **30** with those of its non-cyclometallated analogue $[\text{Ru}(\text{ttpy})_2]^{2+}$, **32**, is particularly instructive for an appreciation of the chemistry described in this and

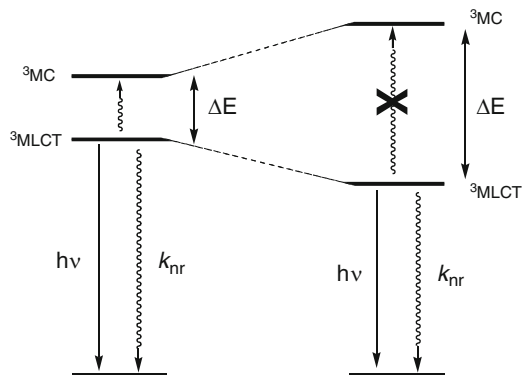


Fig. 19 Schematic illustration of the influence of cyclometallation on the energies of MLCT and MC states

subsequent sections. The metal-centred oxidation process in the cyclometallated complex **30** is shifted cathodically by 0.76 V compared to **32** ($E_{1/2}^{\text{ox}} = 0.49$ and 1.25 V, respectively), an effect that can be readily understood in terms of the lower charge on the former and the strong σ -donor character of the metallated carbon. The terpyridyl-based reduction process is, in contrast, destabilised by almost 0.4 V (-1.61 and -1.24 V for **30** and **32**, respectively). A similar trend emerges for the osmium(II) complexes, albeit more readily oxidised than their Ru(II) counterparts.

A substantial red-shift of the lowest-energy absorption bands accompanies the metallation: $\lambda_{\text{max}} = 490$ and 550 nm in acetonitrile solution for **32** and **30**, respectively. Corresponding values for $[\text{Os}(\text{tpy})_2]^{2+}$ and $[\text{Os}(\text{tpy})(\text{dpyb})]^+$ are 667 and 765 nm, respectively. Given that the lowest-energy transition in ruthenium(II) and osmium(II) polypyridyl complexes is normally formulated as an $^1\text{MLCT}$ state, such a shift is to be expected in the light of the electrochemical data, showing that the highest-occupied metal-centred orbitals are destabilised more than the unoccupied orbitals on the terpyridine.

The same trend is also observed in emission. The $^3\text{MLCT}$ luminescence emission maximum shifts from 640 to 784 nm on going from **32** to **30**, with values for the corresponding Os(II) complexes of 734 and 824 nm, respectively. An important feature to note for the pair of ruthenium(II) complexes is that the luminescence lifetime in solution at room temperature is increased upon metallation, contrary to what might be anticipated on the basis of the energy gap law, whereby non-radiative decay processes for a given type of excited state tend to increase with decreasing excited-state energy. The values are 0.95 and 4.5 ns in CH_3CN for **32** and **30**, respectively. This effect can be interpreted in terms of an increased separation, ΔE , between the emitting $^3\text{MLCT}$ state and higher-lying metal-centred states. As briefly explained in Sect. 1, metal-centred d–d excited states can provide a deactivation pathway for $^3\text{MLCT}$ excited states if they are thermally accessible, i.e. if $\Delta E \approx kT$ (Fig. 19). Since cyclometallation has the effect of both lowering the MLCT state *and* raising the MC states, ΔE is increased and non-radiative decay by this pathway is reduced. It should be noted that no such effect is observed for the Os(II) complexes, since the MLCT states are already significantly lower-lying in this case.

The red-shift induced by cyclometallation in such complexes has potential in the field of dye-sensitised solar cells (DSSCs). That the photosensitisation of a wide-band-gap semiconductor could be achieved using a ruthenium(II) polypyridyl complex was first demonstrated by O'Regan and Grätzel in 1991 [49]. The concept, which exploits the MLCT nature of the excited states of such complexes as the prelude to photo-induced charge injection, offers an alternative to bulk heterojunction solar cells as a means of converting sunlight into electrical energy with viable efficiencies [50]. In both types of technology, however, a major problem facing the scientific community is the question of how to harvest the red and NIR end of the solar spectrum. The bench-mark Ru(II) complex in DSSCs has been $[\text{Bu}_4\text{N}]_2[\text{Ru}(\text{dcbpyH}_2)_2(\text{NCS})_2]$ {"N719", where $\text{dcbpy} = 4,4'$ -dicarboxy-2,2'-bipyridine}. A challenge that has attracted many researchers is the development of alternatives to such dyes that do not contain NCS^- ligands (which, in practice, are labile, compromising device performance and longevity) and that absorb efficiently at long wavelengths.

The possibility of using anionic cyclometallating ligands in place of the combination of neutral bipyridines and monodentate anionic ligands such as NCS^- was put forward by van Koten and co-workers in 2007 [51]. They examined complexes of the form $[\text{Ru}(\text{tpy})(\text{NNC})]^+$, where NNC represents a tridentate, cyclometallated 6-phenylbipyridine derivative incorporating one or two CO_2H pendant groups for anchoring to the TiO_2 semiconductor. Spectral coverage and photocurrent action spectra were obtained that are comparable to that with N719 under the same conditions. A natural question that then arises is how would the corresponding complexes incorporating dipyritylbenzene ligands, $[\text{Ru}(\text{tppy})(\text{NCN})]^+$, compare? The same researchers and, independently, Berlinguette and co-workers, have been addressing this question recently [52, 53]. It transpires that the NCN systems are inferior to the NNC analogues. For example, Fig. 20 shows the photocurrent action spectra of DSSCs using the set of four complexes 33–36. Whilst the performance of the NNC systems is superior to the bis-terpyridyl complex, that of the NCN complex is poorer. The difference can be rationalised in terms of the different localisation of the LUMO [54]. Thus, in the case of NNC complexes 35 and 36, the LUMO is localised on the NNC ligand: the charge transfer occurs in the direction of the TiO_2 , to which the NNC ligand is anchored. On the other hand, in the NCN complex 34, the LUMO is localised on the terpyridine. Electron density thus moves in the direction of this ligand in the excited MLCT state, remote from the TiO_2 , and from where electron injection has low efficiency. Berlinguette's study considered, in addition, the alternative scenario in which an NCN ligand is used in conjunction with an ester-substituted terpyridine, where the CT should occur in the desired direction. However, the long-wavelength absorption tail in such complexes was found to extend less far into the red—and to be less intense—than for the corresponding NNC analogues, and so the conclusion is again that the NNC systems are preferable.

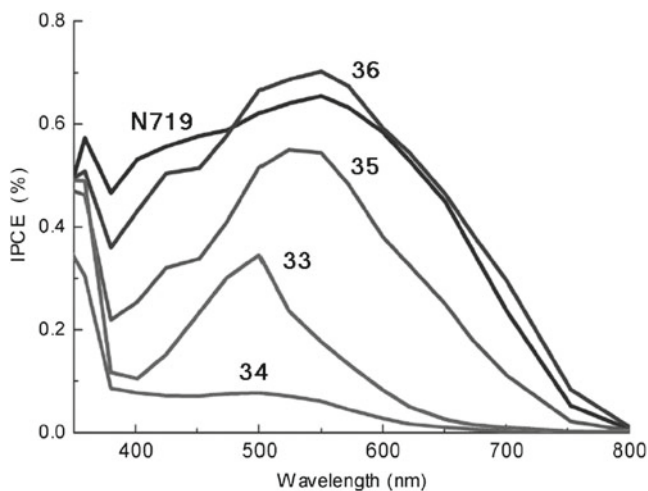
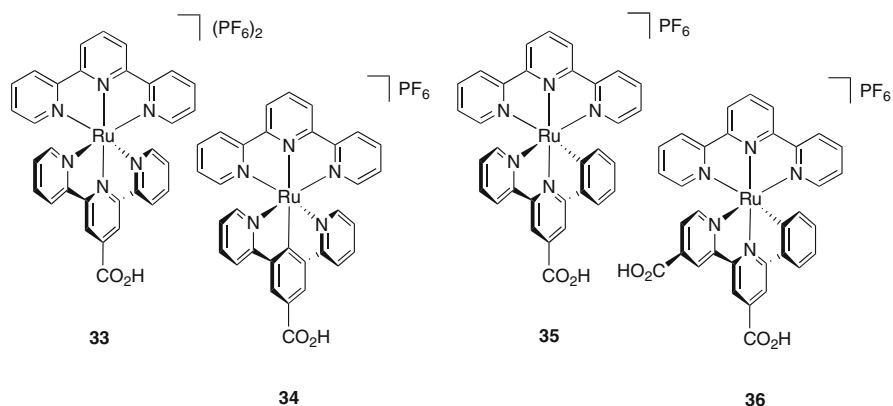


Fig. 20 Photocurrent action spectra of 33–36 in a TiO_2 solar cell using 0.5 M LiI and 0.05 M I_2 in γ -butyrolactone as electrolyte, with the performance of N719 shown for comparison (reprinted with permission from [52] © 2010 American Chemical Society)

5.2 Iridium(III) Complexes

As seen above, dpyb binds as an NCN-coordinating ligand to Ru(II) and Os(II) ions, cyclometallating at position 2 of the benzene ring. In contrast, reaction of dpybH with hydrated iridium(III) chloride gives products in which the ligand metallates at position 4 of the central ring: the ligand is thus bound in a bidentate fashion, with one pendant, uncoordinated pyridine ring ($N^{\wedge}C$ binding mode, Fig. 21) [55]. It seems that metallation at C^4 is kinetically favoured over C^2 . A similar pattern of reactivity has been observed for palladium(II), at least when $Pd(OAc)_2$ is used as the metal source [56].

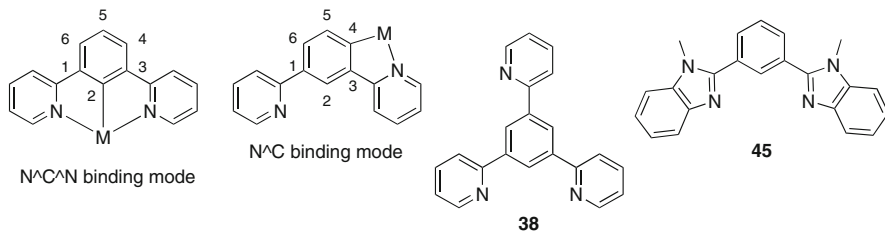


Fig. 21 NCN and NC binding modes of 1,3-di(2-pyridyl)benzene; the structure of 1,3,5-tris(2-pyridyl)benzene, **38**, in which all three C–H bonds of the benzene ring are equivalent; and the ligand 1,3-bis(*N*-methyl-benzimidazol-2-yl)benzene, **45**, which favours the NCN over the NC binding mode, even with Ir(III)

Blocking of the C^4 and C^6 position of dypbH with substituents such as CH_3 , CF_3 or F successfully directs the metallation to position C_2 , allowing NCN-coordinated Ir(III) complexes to be obtained. The initial products formed upon reaction with $\text{IrCl}_3 \cdot 3\text{H}_2\text{O}$ are chloro-bridged dimers of the form $[\text{Ir}(\text{NCN})\text{Cl}(\mu\text{-Cl})_2]$ (e.g. **37**, Fig. 22), which can be cleaved by a variety of ligands to generate mononuclear complexes [57].

Another way to induce the NCN binding mode is to use the C_3 symmetric proligand 1,3,5-tris(2-pyridyl)benzene (**38**, Fig. 21): all three C–H bonds in this compound are equivalent, so the question of regiochemistry does not arise.

A representative selection of the NCN-coordinated mononuclear complexes of varying charge that can be obtained via the intermediacy of the chloro-bridged dimer, **37**, obtained from 1,3-bis(2-pyridyl)-4,6-dimethylbenzene (dpyxH), is illustrated in Fig. 22. Reaction with terpyridines leads to dicationic complexes such as $[\text{Ir}(\text{dpyx})(\text{tpty})]^{2+}$, **39**, the Ir(III) analogue of the Ru(II) complex **30** discussed in Sect. 5.1. Dimetallic complexes of the type $[\{\text{Ir}(\text{dpyx})\}_2(\mu\text{-tpty}-\phi_n\text{-tpty})]^{4+}$ ($n = 0-2$), **40**, comparable to the Ru dimer **31**, can be isolated upon reaction of **37** with back-to-back bridged terpyridines [58]. If a bipyridine is used rather than a terpyridine, only two of the three chloride ligands around the metal are displaced, leading to monocationic complexes of the type $[\text{Ir}(\text{dpyx})(\text{bpy})\text{Cl}]^+$, **41**.

Iridium(III) has a higher propensity to undergo cyclometallation than ruthenium(II): Ir(III) complexes incorporating two or three metallated carbon atoms in the coordination sphere are common [2], whereas Ru(II) is typically limited to mono-cyclometallation. In the present instance, further cyclometallating ligands can readily be introduced. For example, reaction of **37** with 6-phenyl-2,2'-bipyridine (phbpyH) leads to $[\text{Ir}(\text{dpyx})(\text{phbpy})]^+$, **42**, a doubly cyclometallated bis-terdentate complex featuring *cis*- C_2N_4 coordination [59]. Such complexes are terdentate analogues of the well-known class of cationic tris-bidentate iridium complexes of which $[\text{Ir}(\text{N}^C\text{-ppy})_2(\text{N}^W\text{-bpy})]^+$ is the archetypal example [60]. They display electrochemical properties quite similar to those of $[\text{Ru}(\text{bpy})_3]^{2+}$, viz. reversible first oxidation and reduction waves at accessible potentials (Fig. 23), rendering them of interest for a variety of applications such as light-emitting electrochemical cells and photosensitisers for “water splitting” [61].

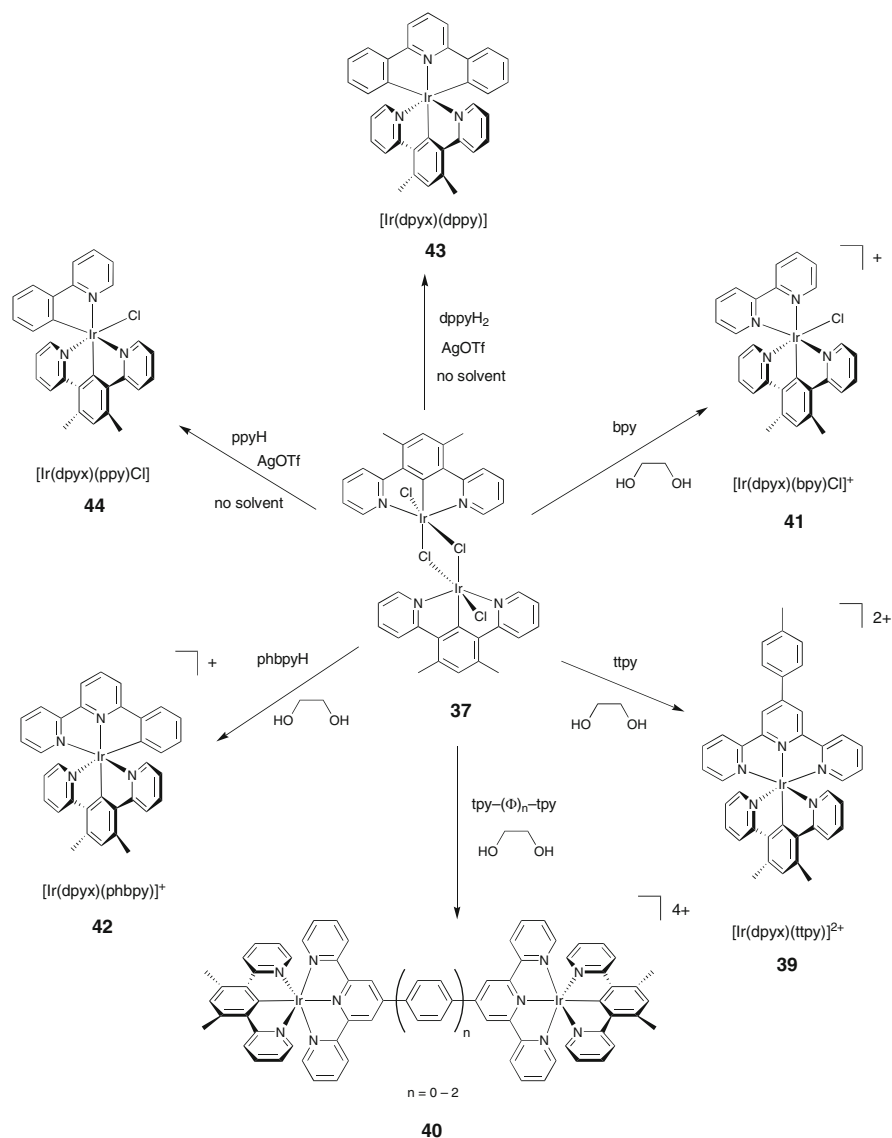


Fig. 22 Structures of a range of Ir(III) complexes containing the NCN-bound dpyx ligand, obtained through the intermediacy of the chloro-bridged dimer **37**

Alternatively, 2,6-diphenylpyridine (dppyH_2) can be introduced as a bis-cyclometallating CNC-binding ligand to generate charge-neutral complexes such as $[\text{Ir}(\text{dpyx})(\text{dppy})]$, **43**, terdentate analogues of the much-studied $[\text{Ir}(\text{ppy})_3]$ class of compound. Note, however, that whereas $[\text{Ir}(\text{ppy})_3]$ can exist as either *fac* or *mer* isomers [62], a *mer*-like configuration of donor atoms is enforced in $[\text{Ir}(\text{dpyx})(\text{dppy})]$. The two metallated carbon atoms of dppy are forced to adopt positions

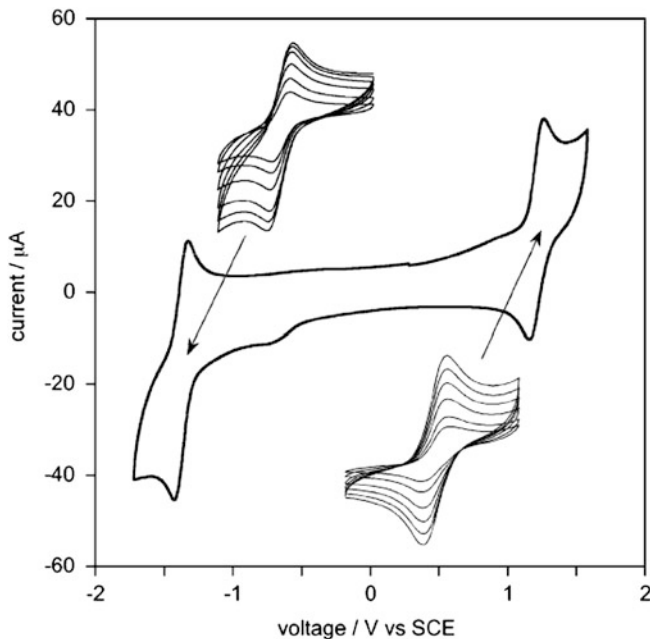


Fig. 23 Cyclic voltammogram of **42** in CH_3CN at 298 K, at a scan rate of 300 mV s^{-1} . The insets show the redox processes at a series of scan rates ($50, 100, 200, 300, 400,$ and 500 mV s^{-1}); the reversibility of each process is confirmed by the linear dependence of the current on the square root of the scan rate

trans to one another, and are therefore labilised, due to the high *trans* influence of cyclometallated carbon atoms. The result is that $[\text{Ir}(\text{dpyx})(\text{dppy})]$ has poor stability in solution, particularly in the presence of light, under which conditions one of the two *trans*-disposed Ir–C bonds is cleaved, and the sixth coordination site probably occupied by a weakly bound solvent molecule. It is interesting to note that no such instability is observed for complexes of the type $[\text{Ir}(\text{dppy})(\text{NNN})]^+$, despite their having the same arrangement of *trans* Ir–C bonds [63]. Evidently, the ligand field states through which Ir–C dissociation occurs in $[\text{Ir}(\text{dpyx})(\text{dppy})]$ are destabilised by the presence of the third cyclometallated carbon. 2,6-Bis(2-benzimidazolyl)pyridine has similarly been used recently as a “pseudo-biscyclometallating” analogue of dppy, involving deprotonation of the benzimidazole rings to give a dianionic ligand [64].

If a bidentate cyclometallating ligand, such as ppy, is used in place of dppy, then a chloride ligand remains in the sixth site, e.g. $[\text{Ir}(\text{dpyx})(\text{ppy})\text{Cl}]$, **44**. Being *trans* to the Ir–C bond, the Ir–Cl does show some lability, but the rate of dissociation is much slower than that observed for $[\text{Ir}(\text{dpyx})(\text{dppy})]$. Moreover, the chloride can be replaced by stronger field, acceptor ligands such as CN^- , which increase the stability.

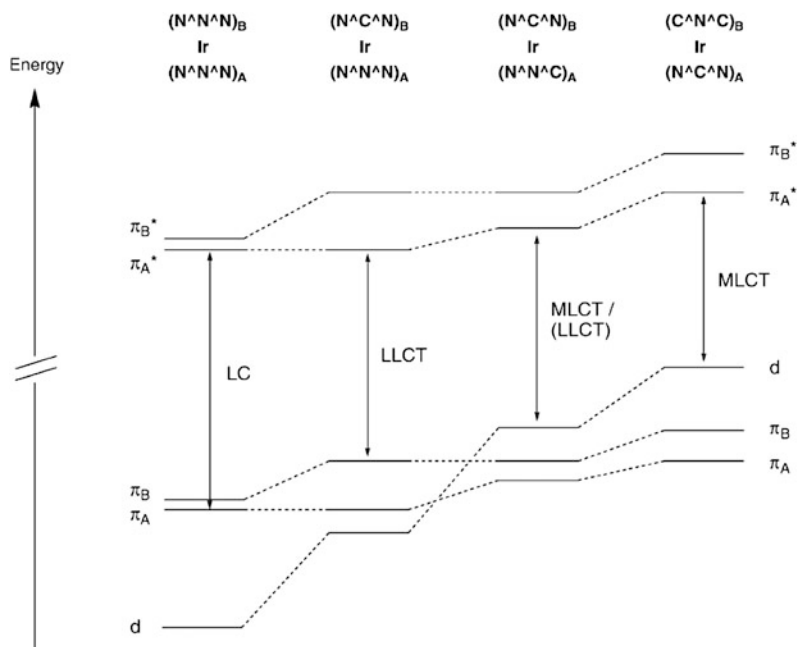


Fig. 24 Simplified schematic energy level diagram showing the influence of cyclometallation on the frontier orbitals in bis-terdentate Ir(III) complexes containing NCN-coordinated dipyriddybenzene ligands, leading to excited states of different character. A and B represent the two different ligands [11]

The different classes of complexes that can be generated, as summarised in Fig. 22, differ greatly from one another in terms of their luminescence properties, particularly with regard to the quantum yields. The underlying factors for the trends have been elucidated with the aid of TDDFT calculations, revealing the influence of the number of cyclometallated carbon atoms on the energies of ligand and metal orbitals (Fig. 24). Here we present a brief summary of the main points; the reader is directed to a more comprehensive recent review for further details [65].

The $[\text{Ir}(\text{NCN})(\text{NNN})]^{2+}$ class of complex shows no luminescence at room temperature, and even at 77 K, emission is barely detectable. $[\text{Ir}(\text{NNN})_2]^{3+}$ complexes, in contrast, are modestly luminescent in solution at 298 K (Φ typically around 1–3 %) [66, 67]. TDDFT calculations on $[\text{Ir}(\text{dpyx})(\text{tpy})]^{2+}$ reveal that the lowest-energy excited state has a large degree of NCN \rightarrow NNN ligand-to-ligand charge-transfer (LLCT) character, with the HOMO predominantly localised on the former and the LUMO on the latter, and with little contribution from the metal orbitals. Thus, there is a low degree of orbital overlap and, probably, inefficient SOC, leading to a low radiative rate constant. The situation contrasts with the case of ruthenium(II), where cyclometallation had a beneficial effect, since the Ru 4d orbitals are higher in energy, ensuring MLCT character.

The introduction of a second cyclometallating carbon atom into the other ligand, as in **42**, raises the energy of metal-centred orbitals, and reduces the LLCT character, both of which lead to an augmentation in the radiative rate constant. Filled metal and ligand orbitals probably become quite comparable in energy in this case, with the LUMO being localised on the NN part of the NNC ligand, leading to higher MLCT character to the excited state. Indeed, these complexes emit quite efficiently in the orange-red region of the spectrum, with quantum yields of around 2–6 % according to the substituents, comparable to $[\text{Ru}(\text{bpy})_3]^{2+}$ and $[\text{Ir}(\text{ppy})_2(\text{bpy})]^+$ derivatives [59]. Finally, the introduction of a third cyclometallating carbon atom, as in **43**, or an anionic chloride as in **44**, raises the energy of the metal orbitals further, leading to unequivocal MLCT character. Indeed, complex **44** is very highly emissive in degassed solution at room temperature: $\Phi_{\text{lum}} = 76\%$, $\tau = 1.6 \mu\text{s}$, $\lambda_{\text{max}} = 508 \text{ nm}$ in CH_3CN . OLEDs employing **44** or its derivatives as triplet-harvesting dopants show high efficiencies, competitive with many of the best iridium emitters reported to date. Haga and co-workers have also obtained similar, highly efficient emitters in their work using 1,3-bis(*N*-methyl-benzimidazol-2-yl)benzene (**45**, Fig. 21) as an NCN ligand [68]. Interestingly, in that case, no $\text{C}^{4/6}$ blocking groups are required in the central ring: NCN rather than NC coordination is observed with the parent ligand.

An interesting feature of cyclometallation is that it is accompanied by an increase in the electron density within the metallated aryl ring, particularly at the position *para* to the site of metallation. The propensity of the ring to undergo electrophilic aromatic substitution reactions is thus enhanced selectively at this position [69]. This feature can be put to use for introducing functionality into a ligand post-complexation, rather than into the ligand prior to complexation. For example, $[\text{Ir}(\text{dpyx})(\text{tpty})]^{2+}$, **39**, undergoes bromination under mild conditions (NBS in MeCN at room temperature) specifically at the *para* position of the central ring of dpyx. Naturally, in the case of the bis-cyclometallated complex $[\text{Ir}(\text{dpyx})(\text{phbpy})]^+$, **42**, the lateral phenyl ring of the NNC ligand undergoes a comparable reaction. The modified system $[\text{Ir}(\text{dpyx})(\text{mtbpy}-\phi-\text{Br})]^+$ (**46**, Fig. 25) has been developed as a core for linear stepwise expansion along the $\text{C}^{\text{dpyx}}-\text{Ir}-\text{N}^{\text{phbpy}}$ axis, through an iterative sequence of cross-coupling with a boronic acid-substituted substrate (a purely organic compound or a metal complex), in situ bromination, and a second cross-coupling [59, 70]. The bromination step occurs specifically at the dpyx ligand, because the corresponding reaction at the phenyl ring of the NNC ligand is blocked by the presence of the methyl group. Using this strategy, a variety of linearly elaborated mononuclear complexes and heterotrimetallic systems have been created in a controlled regiospecific manner. With regard to such multimetallic systems, it should be noted that bis-terdentate complexes offer structural advantages over those with bidentate ligands, because the latter, normally having D_3 or C_2 symmetry, are chiral, whereas the former (normally D_{2d} symmetry) are not. When two or more chiral complexes are linked together, mixtures of diastereoisomers are formed unless the starting mononuclear complexes are resolved first.

It is, however, possible to prepare chiral complexes with terdentate ligands, if the ligand is desymmetrised, i.e. comprising different lateral groups on either side of the central ring. An elegant example comes from the group of Haga, who were able to

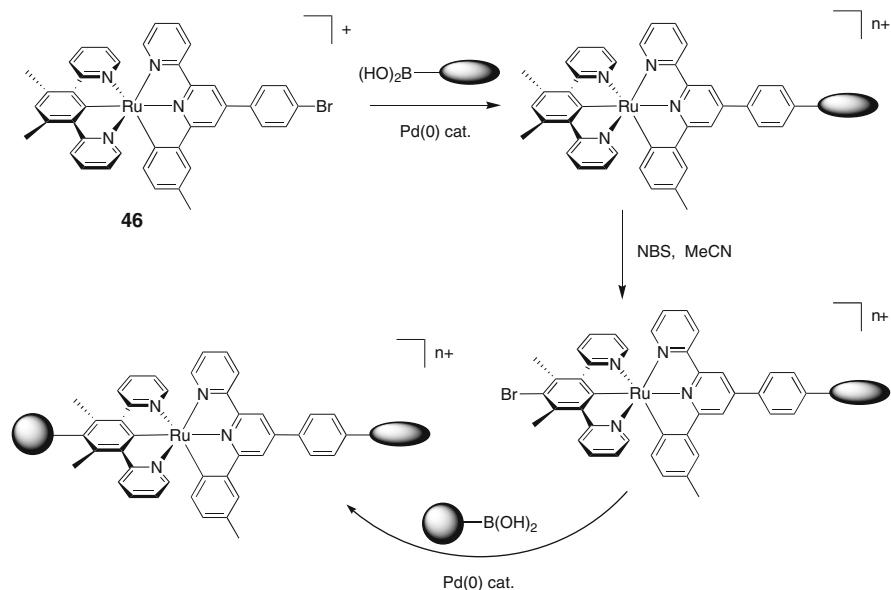


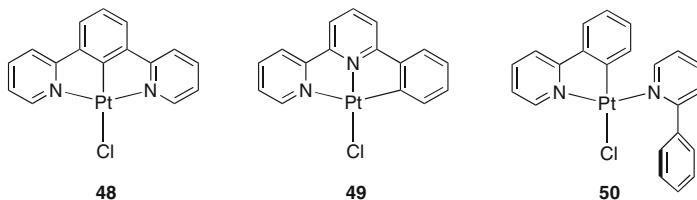
Fig. 25 Sequential cross-coupling—bromination—cross-coupling applied to complex **46** for the elaboration of bis-terdentate iridium(III) complexes, relying on the activation of the 4'-position of the dpyx ligand to electrophilic substitution reactions. The shaped spheres represent either charge-neutral organic units (hence $n = 1$) or metal complexes, in which case, n depends on the charge of the complexes introduced

resolve complex **47** into its two enantiomers, as confirmed by their equal but opposite circular dichroism spectra (Fig. 26, top) [71]. More unusually for transition metal complexes, circularly polarised luminescence spectra could also be recorded (Fig. 26, bottom).

5.3 Platinum(II) Complexes

5.3.1 Pt(dpyb)Cl and Derivatives

Reaction of dpybH with K_2PtCl_4 gives the NCN-coordinated complex Pt(dpyb)Cl, **48** [56]. In contrast to the reaction with $\text{Pd}(\text{OAc})_2$ or IrCl_3 , there is no evidence of competitive metallation at $\text{C}^{4/6}$ in the case of platinum(II).



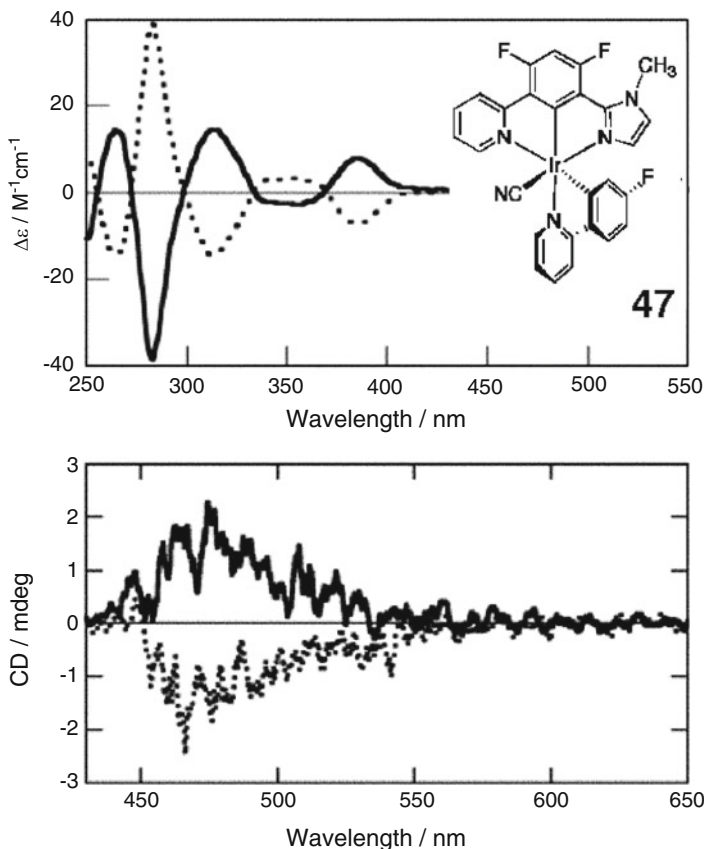


Fig. 26 Circular dichroism spectra (*top*) and circularly polarised luminescence spectra (*bottom*) of the two enantiomers of complex **47** resolved by HPLC on a chiral column. Solvent = CH_2Cl_2 (reprinted with permission from [71] © 2009 Royal Society of Chemistry)

$\text{Pt}(\text{dpyb})\text{Cl}$ displays intense green luminescence in solution at room temperature, $\Phi_{\text{lum}} = 0.60$ and $\tau = 7.2 \mu\text{s}$ in deoxygenated dichloromethane [72]. The superiority compared to the equivalent non-metallated complex $[\text{Pt}(\text{tpy})\text{Cl}]^+$, which is essentially non-emissive under these conditions, is extraordinary. This can be attributed, at least in part, to the stronger ligand field of the metallated system ensuring that deactivating d–d excited states are shifted to higher energy, similar to the beneficial effect discussed earlier for ruthenium(II) [73]. However, the quantum yield and lifetime of this complex are also an order of magnitude superior to those of the isomeric complex $\text{Pt}(\text{phbpy})\text{Cl}$, **49**, containing an NNC rather than a NCN ligand [74], and of the related bidentate complex $\text{Pt}(\text{ppy})(\text{ppyH})\text{Cl}$, **50**, which has the same local coordination sphere comprised of two pyridine rings: one cyclometallated carbon atom and one chloride ligand [75]. The greater rigidity associated with binding of a metal to a terdentate ligand compared to a bidentate one could explain the latter point: the instability of square planar complexes with

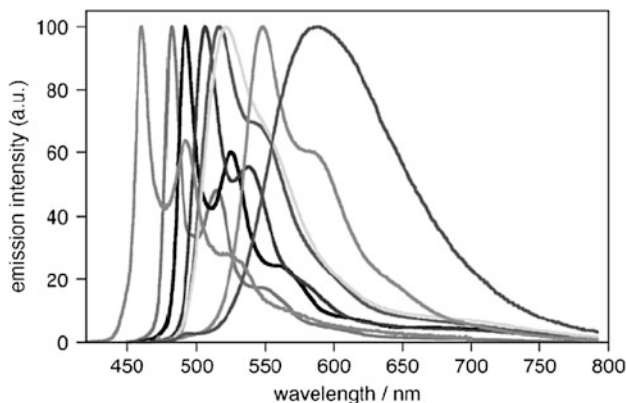


Fig. 27 Showing how the emission spectra of the Pt(dpyb)Cl class of complex can be tuned from that of the parent **48** (third from *left*), either to longer wavelengths through the introduction of electron-donating substituents at the 4-position, or to shorter wavelengths using electron-withdrawing groups at this position/substituents in the pyridyl rings. Spectra are recorded in CH_2Cl_2 at 298 K; $\lambda_{\text{ex}} = 400$ nm; intensities have been normalised

bidentate ligands with respect to distortion from D_{4h} to D_{2d} symmetry in the excited state has long been recognised as a potential sink for the excited-state energy [3, 12]. As far as the pair of terdentately bound complexes are concerned, it has been noted that the Pt–C bond is significantly shorter (ca. 1.90 Å vs. 2.05 Å) in the NCN complex than in the NNC analogue, which may ensure a stronger ligand field and hence displacement of the deactivating d–d states to higher energy [72]. However, a recent comparison of these systems by TDDFT suggests that the key point is the greater rigidity of the former, with a lower degree of reorganisation in the excited state compared to the ground state [76].

The emission energy of complexes of this type can be tuned over a wide range, without significantly compromising the quantum yields, by introducing substituents into the cyclometallated aryl ring or into the pyridine rings. Electron-releasing substituents in the central 4-position of the benzene ring lead to increasingly red-shifted emission according to their electron-donating ability, e.g. λ_{max} increases in the order $\text{R} = \text{CO}_2\text{Me} < \text{H} < \text{mesityl} < \text{Me} < 2\text{-pyridyl} < 4\text{-tolyl} < 4\text{-biphenyl} < 3,4\text{-dimethoxyphenyl} < 2\text{-thienyl}$ (Fig. 27) [77]. There is a good correlation between the emission energy and the oxidation potentials E_{p}^{ox} of the complexes, with a slope of $4,900 \text{ cm}^{-1}\text{V}^{-1}$, whereas the reduction potentials vary little with the 4-substituent. The obvious inference is that the substituent influences primarily the HOMO, such that the observed red shift with increasing electron-donating ability reflects an increase in the HOMO level and a LUMO that remains essentially unchanged. TDDFT calculations support this picture, revealing a major contribution to the HOMO but not to the LUMO (Fig. 28a) [78]. The LUMO, in contrast, is localised predominantly on the pyridyl rings, and it may be noted that the 4'-position makes no contribution to the HOMO. Thus electron-donating substituents in this position are expected to increase the LUMO level without significantly

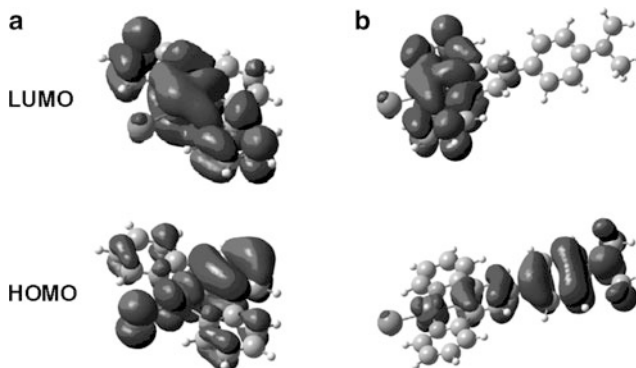


Fig. 28 Frontier orbital diagrams for Pt(dpyb)Cl **48** (a) and the derivative **51** incorporating a 4-(*N,N*-dimethylamino)phenyl group at the 4-position (b), calculated by TDDFT including CH₂Cl₂ as the solvent

affecting the HOMO and, indeed, substituents such as methoxy groups in these positions have been found to blue-shift the emission [79, 80].

For the complex with the strongly electron-donating pendant R = -C₆H₄NMe₂, **51** (Fig. 28b), the emission energy is substantially lower than what is predicted on the basis of the E^{em} vs. E_{p}^{ox} correlation. Moreover, the emission band for this complex in CH₂Cl₂ is broad and structureless, and displays a high degree of positive solvatochromism, in contrast to the other systems whose spectra are structured and whose energies are insensitive to the solvent. This behaviour is thought to be due to a switch in the nature of the lowest-energy excited state from π - π^* to one of primarily intraligand charge transfer (ILCT), akin to the behaviour of donor-acceptor molecules such as 4-(dimethylamino)benzonitrile. TDDFT calculations support this notion (Fig. 28b), showing the HOMO to be largely localised on the pendant group, with the LUMO on the NCN moiety. Reversible switching from the ILCT to the π - π^* state can be induced by protonation of the amine, both forms being highly luminescent ($\Phi = 0.46$ and 0.40 , respectively), but with significantly different spectra (Fig. 29) [77, 78]. The effect has been extended to azacrown-ether-appended complexes, in which a similar switching is observed upon complexation of divalent metal ions such as Ca²⁺ to the macrocycle, which bind to the N lone pair in a comparable way to H⁺ [78].

5.3.2 Pt(NCN)Cl Complexes with other *N*-Heterocycles

Pyrazole is a more electron-rich heterocycle than pyridine. Thus on the basis of the HOMO-LUMO description above, one might anticipate that a pyrazolyl-based Pt(NCN)Cl complex should display blue-shifted emission compared to Pt(dpyb)Cl. However, the bite angle offered by the NCN system will change on going from dpyb to dpyzb {dpyzbH = 1,3-bis(1-pyrazolyl)benzene}, and may be less well suited for

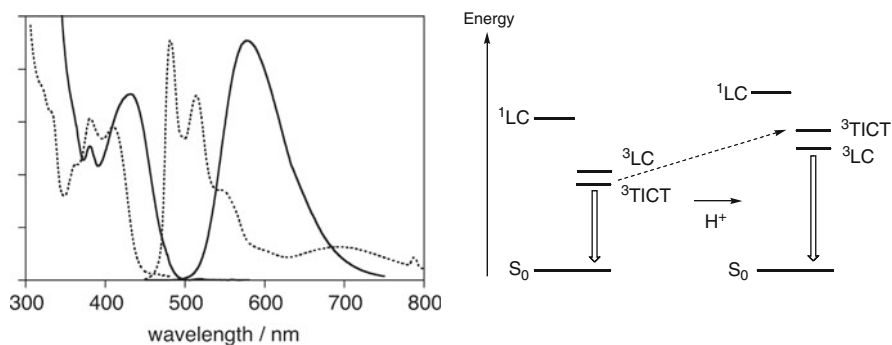


Fig. 29 *Left*: Emission and excitation spectra of **51** in CH_2Cl_2 (6×10^{-5} M) at 298 K (solid lines) and the corresponding blue-shifted spectra after addition of trifluoroacetic acid (10^{-2} M) (dotted lines). *Right*: A schematic illustration of the effect of protonation of the amine on the relative energies of the intraligand charge transfer (TICT) and NCN-centred (LC) excited states

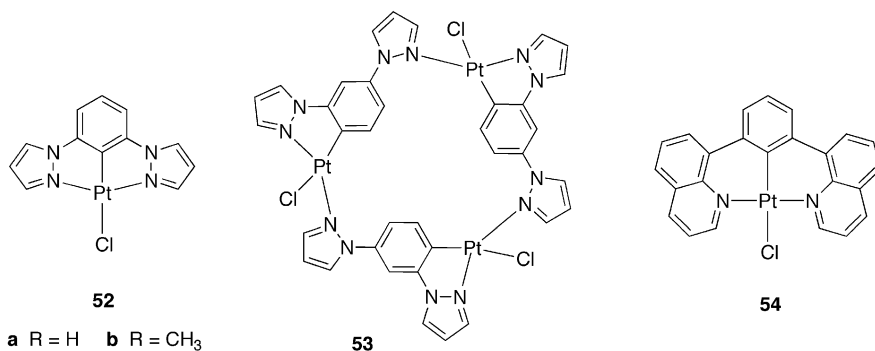


Fig. 30 Mononuclear (**52**) and trinuclear (**53**) complexes of platinum with 1,3-bis(1-pyrazolyl)benzene, and a complex of 1,3-bis(8-quinolyl)benzene featuring 6-membered chelate rings, **54**. The structure of **53** is reprinted with permission from [81] © 2008 American Chemical Society

binding. Indeed, Connick and co-workers observed that reaction of dpyzbH with K_2PtCl_4 can give either the terdentately bound $\text{Pt}(\text{bpyzb})\text{Cl}$, **52a** {the analogue of $\text{Pt}(\text{dpyb})\text{Cl}$, **48**} or a trimer $[\text{Pt}(\mu\text{-dpyzb})\text{Cl}]_3$, **53** (Fig. 30), in which each ligand is bound N^{AC}-bidentate with one metal, with the second pyrazole ring bridging to a second platinum centre [81]. In an independent study, Williams and co-workers found that the former binding mode is promoted over the latter by substituents as small as a methyl group at the 4-position of the benzene ring [82]. They investigated the emission characteristics of complexes such as **52b**. The emission of **52b** was indeed found to be substantially blue-shifted compared to that of $\text{Pt}(\text{dpyb})\text{Cl}$, as had been predicted. However, the quantum yield drops by a factor of 30, and this again seems to be associated with the inferiority of dpyzb as a ligand. From the large shift in the emission spectrum of **52b** on cooling to 77 K, it is evident that the excited state of this complex suffers from more distortion than that of $\text{Pt}(\text{dpyb})\text{Cl}$.

Along a different vein, the introduction of 8-substituted quinolines in place of pyridines leads to NCN-coordinated pincer complexes (e.g. **54**) which—unusually—involve 6-membered chelate rings rather than the 5-membered chelates common to all the systems discussed up to this point [83]. The larger chelate ring size leads to a more optimal *trans*-N–M–N angle (ca. 180°) than in Pt(dpyb)Cl (ca. 160°), an effect which has proved advantageous in related NNN-coordinated ruthenium(II) complexes [84]. However, in the case of the cyclometallated Pt(II) complexes, the quantum yield is adversely affected, apparently due to a lower contribution of metal character in the excited state and to poor orbital overlap, both of which factors lead to a very low radiative rate constant and to weak emission.

5.3.3 Excimers and Aggregates in Pt(NCN)Cl Complexes

The square-planar geometry of platinum(II) complexes offers the possibility of face-to-face intermolecular interactions, which may involve overlap of metal orbitals, ligand orbitals, or a combination of both [85]. For many sterically unhindered Pt(II) complexes, such interactions lead to concentration quenching phenomena: as the concentration increases, the lifetimes and quantum yields decrease. Molecules may interact in the ground state to give dimers or higher aggregates, or the interaction may become attractive only when one of the two molecules involved is in the excited state, in which case the resulting species is an excimer. Originally observed for planar aromatic molecules like pyrene [86], true excimers exist only in the excited state since the potential energy surface is repulsive in the ground state, and no vibrational structure is observed. Since the excimer is stabilised relative to the isolated excited-state monomer, the excimer emission is always red-shifted relative to that of the monomer.

Pt(dpyb)Cl and many of its derivatives investigated to date form unusually strongly emissive excimers in solution, with quantum yields of excimer emission of around 0.35 [72]. Whilst the excimer band is centred around 700 nm for Pt(dpyb)Cl itself, as well as for 4-aryl-substituted derivatives, considerable scope is emerging for the tuning of the excimer energy. For example, replacing one of the pyridyl rings with a pyrazole ring destabilises the excimer without affecting the monomer [82]. Moreover, substituents in the 4-position of the pyridyl rings are found to have a remarkably large effect on the excimer (Fig. 31) [87].

In the solid state, it might be anticipated that molecules can interact with one another in the ground state, leading to dimeric or aggregate species with distinct, lower-energy emission compared to the isolated molecules. Effects of this type are observed, for example, in the red form of Pt(bpy)Cl₂. Such species can sometimes be distinguished from excimers on the basis that the former may display low-energy absorption bands that are not present in the spectra of the isolated molecules in solution. Also, aggregate bands are likely to shift to lower energy as the temperature is decreased or the pressure raised, as the interaction between the molecules becomes stronger. For Pt(dpyb)Cl and its derivatives in the solid state, the emission profile depends subtly on the packing of the molecules. For example, three

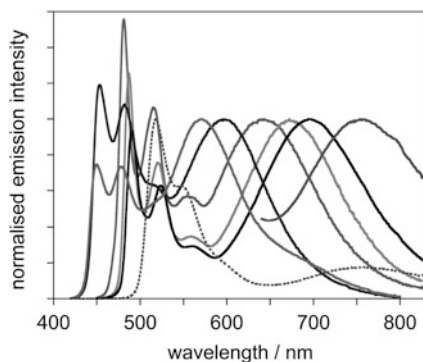


Fig. 31 Illustrating the control over the excimer energy that can be achieved in the Pt(dpyb)Cl class of complex through the introduction of substituents into the pyridyl rings

distinctly different polymorphs of Pt(dpyb–Br)Cl have been isolated, two of which exhibit green monomer-like bands and the third displaying red, excimer-like emission [88]. For others, there is often a mixture of monomer and excimer-like bands. However, no additional bands are observed in absorption, and the proportion of monomer emission increases rather than decreases with temperature [89], suggestive of thermally activated formation of excimer-like species.

The appendage of long alkyl chains onto such complexes leads to interesting liquid crystalline (LC) effects that influence whether monomer or excimer emission is observed. For example, an LC state of a derivative of Pt(dpyb)Cl, incorporating 3,4,5-tris(hexyloxy)benzene groups at the 5-positions of the pyridine rings, can be obtained by slowly cooling an isotropic melt to 170 °C and then rapidly cooling to room temperature [90]. Structural analysis reveals that this LC phase is composed of a columnar arrangement of anti-parallel complexes which are independent of one another. Emission is green and purely monomeric in character (Fig. 32). In contrast, a non-crystalline phase formed by rapid cooling of the isotropic melt consists of a high degree of isotropic grain boundaries, with molecules in close contact and, indeed, the emission from this phase is red and excimer-like. In some cases, thermally induced switching of one form to the other has proved possible in thin films.

5.3.4 Applications in OLEDs, Biosensors, and Bioimaging

Being charge-neutral, low-molecular-weight, sublimable materials that emit efficiently from triplet excited states, the family of Pt(dpyb)Cl emitters are attractive as triplet-harvesting phosphors for OLEDs [91]. High-efficiency devices have been fabricated by doping them into organic hosts (e.g. 4,4'-*N,N'*-dicarbazole-biphenyl, CBP) within a multilayer structure (Fig. 33a). The colour tunability with

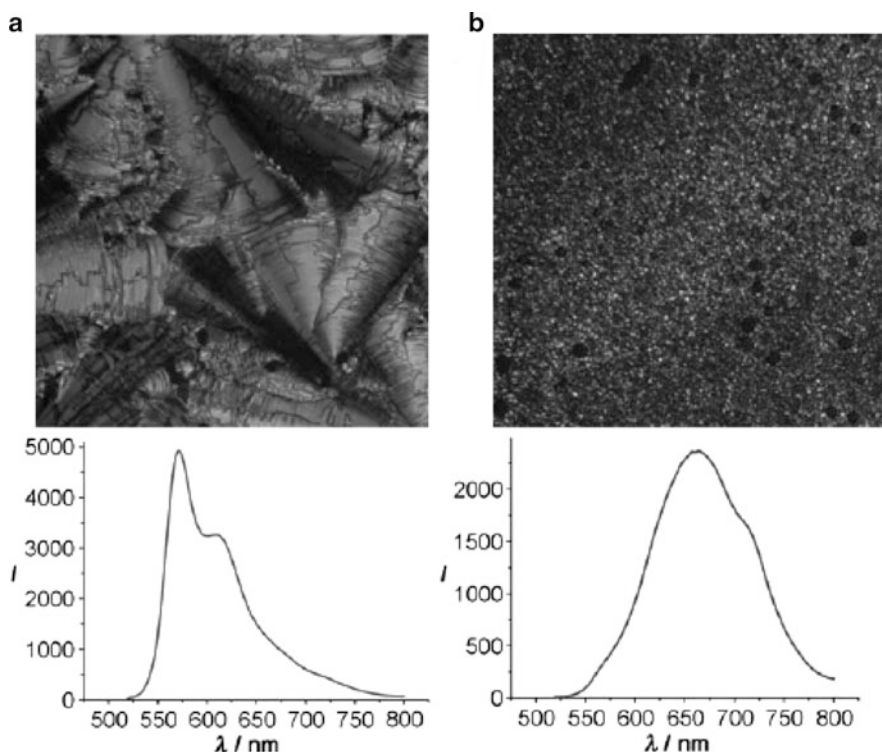


Fig. 32 Photomicrographs taken between cross polarisers (*top*) and emission spectra (*bottom*) of the chloroplatinum complex of 1,3-[5-(3,4,5-trihexyloxyphenyl)pyridin-2-yl]benzene (**a**) fast cooled from the LC phase after the texture is developed, and (**b**) fast cooled from the isotropic phase (reprinted with permission from [90] © 2008 Wiley-VCH)

substituents at the 4-position is illustrated by the spectra and corresponding CIE coordinates (Fig. 33b). External electroluminescence quantum efficiencies of 4–16 % photons/electron and luminous efficiencies of 15–40 cd A⁻¹ have been achieved using this device structure [92]. The use of a neat film of the complex as the EML leads to exclusively excimer-like emission and to NIR-emitting devices with unusually high efficiencies of 10.7 % photons/electron and light output of 15 mW cm⁻² [93, 94].

The combination of monomer and excimer emission offers a strategy for obtaining single-dopant white-light-emitting devices (WOLEDs), as originally demonstrated by Thompson and Forrest [95]. The high emission efficiencies of both monomer and excimer for the Pt(dpyb)Cl family of compounds render them particularly successful in the generation of WOLEDs [96–98]. In fact, the camel-shaped profile nicely matches the photosynthetic action spectrum of green plants, and the systems have been proposed as efficient growth lights for horticultural applications [99]. Nevertheless, for WOLEDs for ambient lighting purposes, a camel shape is less desirable, as it means that there is a trough of low emission

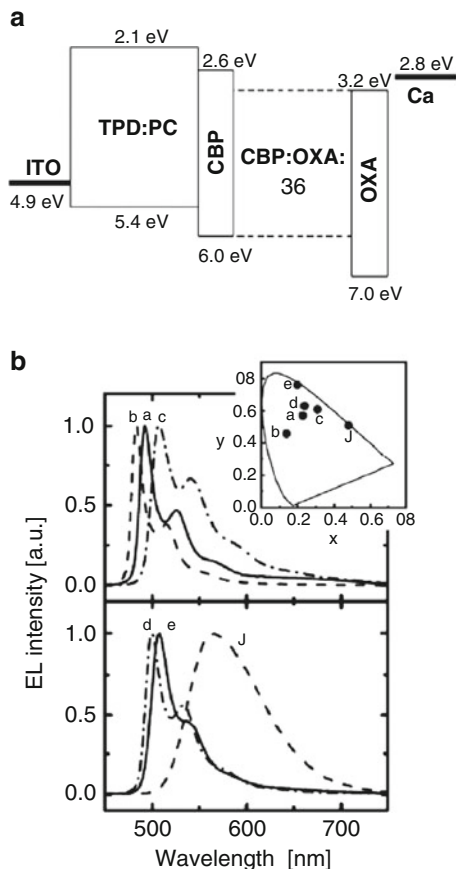


Fig. 33 Devices of the structure shown in (a) prepared using the Pt(dpyb)Cl class of complex within the emitting layer (6 % by mass) display the emission spectra shown in (b). The corresponding CIE coordinates are shown in the *inset*. Compounds are Pt(dpyb)Cl (a), and derivatives with 4-substituent = $-\text{CO}_2\text{Me}$ (b), $-\text{Me}$ (c), mesityl (d), pyridyl-2-yl (e), and $\text{C}_6\text{H}_4\text{NMe}_2$ (f) (reprinted with permission from [92] © 2007 Wiley-VCH)

intensity between the monomer and excimer regions. Kalinowski and co-workers have shown that the problem can be overcome by ‘filling in’ this region with emission from an exciplex. A WOLED with a colour rendering index of 90 and an external quantum efficiency of 6.5 % has been produced in this way [100]. The use of derivatives with blue-shifted excimers offers another strategy for achieving this goal. The reader is directed to a recent comprehensive review on the subject for a more detailed description of this work [101].

Finally, we note that complexes of this type are attracting interest in the fields of biosensing and imaging. Luminescent oxygen sensors [102] and probes of protein binding [103, 104] have been developed. Pt(dpyb)Cl has also been used to

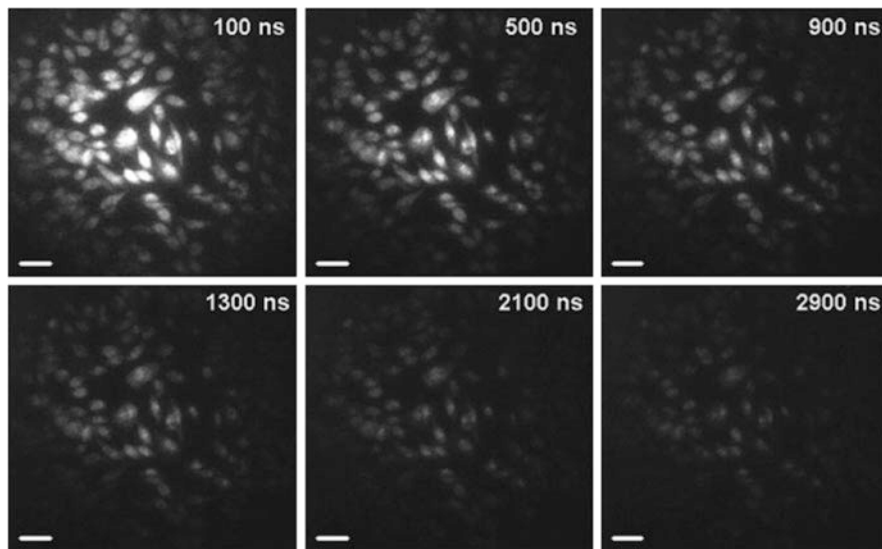


Fig. 34 Time-resolved gated emission images of CHO cells incubated with Pt(dpyb)Cl, **48**. The images were recorded after 355 nm laser excitation at the time delays shown between 100 and 2,900 ns after the laser flash. The time gate used was 100 ns, exposure time 20 ms, five accumulations per time delay. Scale bar: 50 μm [105]

demonstrate the technique of time-resolved emission imaging microscopy (TREM) in live cells on the microsecond timescale [105]. The compound is highly cell-permeable, entering cells under essentially diffusion control, and localising to the nucleoli. A long lifetime of around 700 ns is retained even inside the cell (Fig. 34).

References

1. Campagna S, Puntoriero F, Nastasi F, Bergamini G, Balzani V (2007) *Top Curr Chem* 280:117
2. Flamigni L, Barbieri A, Sabatini C, Ventura B, Barigelletti F (2007) *Top Curr Chem* 281:143
3. Williams JAG (2007) *Top Curr Chem* 281:205
4. Danilov EO, Pomestchenko IE, Kinayyigit S, Gentili PL, Hissler M, Ziessel R, Castellano FN (2005) *J Phys Chem A* 109:2465
5. Yersin H, Rausch AF, Czerwieniec R, Hofbeck T, Fisher T (2011) *Coord Chem Rev.* 255:2622
6. Yersin H (ed) (2007) *Highly efficient OLEDs with phosphorescent materials*. Wiley-VCH, Berlin
7. Adachi C, Baldo MA, Thompson ME, Forrest SR (2001) *J Appl Phys* 90:5048
8. Zhao Q, Li F, Huang C (2010) *Chem Soc Rev* 39:3007
9. Fernandez-Moreira V, Thorp-Greenwood FL, Coogan MP (2010) *Chem Commun* 46:186
10. Murphy L, Congreve A, Pålsson LO, Williams JAG (2010) *Chem Commun* 46:8743
11. Williams JAG (2009) *Chem Soc Rev* 38:1783

12. Andrews LJ (1979) *J Phys Chem* 83:3203
13. Murphy L, Williams JAG (2010) *Top Organomet Chem* 28:75
14. Kanbara T, Yamamoto T (2003) *J Organomet Chem* 688:15–19
15. Kanbara T, Okada K, Yamamoto T, Ogawa H, Inoue T (2004) *J Organomet Chem* 689:1860–1864
16. Kuwabara J, Kanbara T (2008) *J Photopolym Sci Technol* 21:349
17. Okamoto K, Kanbara T, Yamamoto T, Wada A (2006) *Organometallics* 25:4026–4029
18. Okamoto K, Yamamoto T, Akita M, Wada A, Kanbara T (2009) *Organometallics* 28:3307–3310
19. Kozlov VA, Aleksanyan DV, Nelyubina YV, Lyssenko KA, Gutsul EI, Puntus LN, Vasil'ev AA, Petrovskii PV, Odinets IL (2008) *Organometallics* 27:4062
20. Hu J, Xu H, Nguyen M-H, Yip JHK (2009) *Inorg Chem* 48:9684
21. Lipson M, McGarry PF, Koptyug IV, Staab HA, Turro NJ, Doetschman DC (1994) *J Phys Chem* 98:7504
22. Gagliardo M, Rizzo F, Lutz M, Spek AL, van Klink GPM, Merbach AE, De Cola L, van Koten G (2007) *Eur J Inorg Chem* 2853
23. Bünzli JCG, Piguet C (2005) *Chem Soc Rev* 34:1048
24. Terheijden J, van Koten G, Mul WP, Stufkens DJ, Muller F, Stam CH (1986) *Organometallics* 5:519
25. Albrecht M, Gossage RA, Lutz M, Spek AL, van Koten G (2000) *Chem Eur J* 6:1431
26. Albrecht M, van Koten G (1999) *Adv Mater* 11:171
27. Albrecht M, Lutz M, Spek AL, van Koten G (2000) *Nature* 406:970
28. Zhou X, Pan QJ, Li MX, Xia BH, Zhang HX (2007) *J Mol Struct Theochem* 822:65
29. Jude H, Krause Bauer JA, Connick WB (2002) *Inorg Chem* 41:2275
30. Jude H, Krause Bauer JA, Connick WB (2004) *Inorg Chem* 43:725
31. Jude H, Krause Bauer JA, Connick WB (2005) *Inorg Chem* 44:1211
32. Connick WB, Miskowski VM, Houlding VH, Gray HB (2000) *Inorg Chem* 39:2585
33. Batema GD, van de Westelaken KTL, Guerra J, Lutz M, Spek AL, van Walree CA, de Mello Donegá C, Meijerink A, van Klink GPM, van Koten G (2007) *Eur J Inorg Chem* 1422
34. Batema GD, Lutz M, Spek AL, van Walree CA, de Mello Donegá C, Meijerink A, Havenith RWA, Pérez-Moreno J, Clays K, Büchel M, van Dijken A, Bryce DL, van Klink GPM, van Koten G (2008) *Organometallics* 27:1690
35. Meier H (1992) *Angew Chem Int Ed* 31:1399
36. Yin B, Niemeyer F, Williams JAG, Jiang J, Boucekkine A, Toupet L, Le Bozec H, Guerchais V (2006) *Inorg Chem* 45:8584
37. Cariati E, Pizzotti M, Roberto D, Tessore F, Ugo R (2006) *Coord Chem Rev* 250:1210
38. Di Bella S, Dragonetti C, Pizzotti M, Roberto D, Tessore F, Ugo R (2010) *Top Organomet Chem* 28:1
39. Nishiyama H, Shiomi T, Tsuchiya Y, Matsuda I (2005) *J Am Chem Soc* 127:6972
40. Stark MA, Jones G, Richards CJ (2000) *Organometallics* 19:1282
41. Hao XQ, Gong JF, Du CX, Wu LY, Wu TJ, Song MP (2006) *Tetrahedron Lett* 47:5033
42. Beley M, Collin JP, Louis R, Metz B, Sauvage JP (1991) *J Am Chem Soc* 113:8521
43. Beley M, Chodorowski S, Collin JP, Sauvage JP (1993) *Tetrahedron Lett* 34:2933
44. Chodorowski-Kimmes S, Beley M, Collin JP, Sauvage JP (1996) *Tetrahedron Lett* 37:2963
45. Beley M, Collin JP, Sauvage JP (1993) *Inorg Chem* 32:4539
46. Patoux C, Launay JP, Beley M, Chodorowski-Kimmes S, Collin JP, James S, Sauvage JP (1998) *J Am Chem Soc* 120:3717
47. Barigelletti F, Flamigni L, Guardigli M, Juris A, Beley M, Chodorowski-Kimmes S, Collin JP, Sauvage JP (1996) *Inorg Chem* 35:136
48. Barigelletti F, Flamigni L, Collin JP, Sauvage JP (1997) *Chem Commun* 333
49. O'Regan B, Grätzel M (1991) *Nature* 353:737
50. Hagfeldt A, Boschloo G, Sun L, Kloo L, Pettersson H (2010) *Chem Rev* 110:6595

51. Wadman SH, Kroon JM, Bakker K, Lutz M, Spek AL, van Klink GPM, van Koten G (2007) *Chem Commun* 1907
52. Wadman SH, Kroon JM, Bakker K, Havenith RWA, van Link GPM, van Koten G (2010) *Organometallics* 29:1569
53. Robson KCD, Koivisto BD, Yella A, Sporinova B, Nazeeruddin MK, Baumgartner T, Grätzel M, Berlinguette CP (2011) *Inorg Chem* 50:5494
54. Wadman SH, Lutz M, Tooke DM, Spek AL, Hartl F, Havenith RWA, van Klink GPM, van Koten G (2009) *Inorg Chem* 48:1887
55. Wilkinson AJ, Goeta AE, Foster CE, Williams JAG (2004) *Inorg Chem* 43:6513
56. Cárdenas DJ, Echavarren AM, Ramírez de Arellano MC (1999) *Organometallics* 18:3337
57. Wilkinson AJ, Puschmann H, Howard JAK, Foster CE, Williams JAG (2006) *Inorg Chem* 45:8685
58. Auffrant A, Barbieri A, Barigelletti F, Collin JP, Flamigni L, Sabatini C, Sauvage JP (2006) *Inorg Chem* 45:10990
59. Whittle VL, Williams JAG (2008) *Inorg Chem* 47:6596
60. King KA, Watts RJ (1987) *J Am Chem Soc* 109:1589
61. Lowry MS, Bernhard S (2006) *Chem Eur J* 12:7970
62. Tamayo AB, Alleyne BD, Djurovich PI, Lamansky S, Tsyba I, Ho NH, Bau R, Thompson ME (2003) *J Am Chem Soc* 125:7377
63. Polsson M, Ravaglia M, Fracasso S, Garavelli M, Scandola F (2005) *Inorg Chem* 44:1282
64. Choi D, Kim T, Reddy SM, Kang J (2009) *Inorg Chem Commun* 12:41
65. Williams JAG, Wilkinson AJ, Whittle VL (2008) *Dalton Trans* 2081
66. Collin JP, Dixon IM, Sauvage JP, Williams JAG, Barigelletti F, Flamigni L (1999) *J Am Chem Soc* 121:5009
67. Arm KJ, Leslie W, Williams JAG (2006) *Inorg Chim Acta* 359:1222
68. Obara S, Itabashi M, Okuda F, Tamaki S, Tanabe Y, Ishii Y, Nozaki K, Haga M (2006) *Inorg Chem* 45:8907
69. Arm KJ, Williams JAG (2005) *Chem Commun* 230
70. Whittle VL, Williams JAG (2009) *Dalton Trans* 3929
71. Ashizawa M, Yang L, Kobayashi K, Sato H, Yamagishi A, Okuda F, Harada T, Kuroda R, Haga M (2009) *Dalton Trans* 1700
72. Williams JAG, Beeby A, Davies ES, Weinstein JA, Wilson C (2003) *Inorg Chem* 42:8609
73. Collin JP, Beley M, Sauvage JP, Barigelletti F (1991) *Inorg Chim Acta* 196:91
74. Lai SW, Chan MCW, Cheung TC, Peng SM, Che CM (1999) *Inorg Chem* 38:4046
75. Mdleleni M, Bridgewater JS, Watts RJ, Ford PC (1995) *Inorg Chem* 34:2334
76. Tong GSM, Che CM (2009) *Chem Eur J* 15:7225
77. Farley SJ, Rochester DL, Thompson AL, Howard JAK, Williams JAG (2005) *Inorg Chem* 44:9690
78. Rochester DL, Develay S, Zálaiš Williams JAG (2009) *Dalton Trans* 1728
79. Cocchi M, Kalinowski J, Murphy L, Williams JAG, Fattori V (2010) *Org Electron* 11:388
80. Kalinowski J, Cocchi M, Fattori V, Murphy L, Williams JAG (2010) *Org Electron* 11:724
81. Willison SA, Krause JA, Connick WB (2008) *Inorg Chem* 47:1258
82. Develay DL, Blackburn O, Thompson AL, Williams JAG (2008) *Inorg Chem* 47:11129
83. Garner KL, Parkes LF, Piper JD, Williams JAG (2010) *Inorg Chem* 49:476
84. Abrahamsson M, Jäger M, Österman T, Eriksson L, Persson P, Becker HC, Johansson O, Hammarström L (2006) *J Am Chem Soc* 128:12616
85. Pettijohn CN, Jochowitz EB, Chuong B, Nagle JK, Vogler A (1998) *Coord Chem Rev* 171:85
86. Förster T (1962) *Pure Appl Chem* 4:121
87. Murphy L, Brulatti P, Fattori V, Cocchi M, Williams JAG (2012) *Chem Commun* 48:5817
88. Kalinowski J, Cocchi M, Murphy L, Williams JAG, Fattori V (2010) *Chem Phys* 378:47
89. Develay S, Williams JAG (2008) *Dalton Trans* 4562
90. Kozhevnikov VN, Donnio B, Bruce DW (2008) *Angew Chem Int Ed* 47:6286

91. Williams JAG, Develay S, Rochester DL, Murphy L (2008) *Coord Chem Rev* 252:2596
92. Cocchi M, Virgili D, Fattori V, Rochester DL, Williams JAG (2007) *Adv Funct Mater* 17:285
93. Cocchi M, Virgili D, Fattori V, Williams JAG, Kalinowski J (2007) *Appl Phys Lett* 90:023506
94. Cocchi M, Kalinowski J, Virgili D, Williams JAG (2008) *Appl Phys Lett* 92:113302
95. Adamovich V, Brooks J, Tamayo A, Alexander AM, Djurovich PI, D'Andrade BW, Adachi C, Forrest SR, Thompson ME (2002) *New J Chem* 26:1171
96. Cocchi M, Kalinowski J, Virgili D, Fattori V, Develay S, Williams JAG (2007) *Appl Phys Lett* 90:163508
97. Mróz W, Botta C, Giovannella U, Rossi E, Colombo A, Dragonetti C, Roberto D, Ugo R, Valore A, Williams JAG (2011) *J Mater Chem* 21:8653
98. Cocchi M, Kalinowski J, Fattori V, Williams JAG, Murphy L (2009) *Appl Phys Lett* 94:073309
99. Fattori V, Williams JAG, Murphy L, Cocchi M, Kalinowski J (2008) *Photon Nanostruct Fundam Appl* 6:225
100. Kalinowski J, Cocchi M, Virgili D, Fattori V, Williams JAG (2007) *Adv Mater* 19:4000
101. Kalinowski J, Fattori V, Cocchi M, Williams JAG (2011) *Coord Chem Rev.* doi:[10.1016/j.ccr.2011.01.049](https://doi.org/10.1016/j.ccr.2011.01.049)
102. Evans RC, Douglas P, Williams JAG, Rochester DL (2006) *J Fluoresc* 16:201
103. Chen Y, Li K, Lu W, Chui SSY, Ma CW, Che CM (2009) *Angew Chem Int Ed* 48:9909
104. Wieczorek B, Lemcke B, Dijkstra HP, Egmond MR, Klein Gebbink RJM, van Koten G (2010) *Eur J Inorg Chem* 1929
105. Botchway SW, Charnley M, Haycock JW, Parker AW, Rochester DL, Weinstein JA, Williams JAG (2008) *Proc Natl Acad Sci USA* 105:16071

ECE-Type Pincer Complexes of Nickel

Davit Zargarian, Annie Castonguay, and Denis M. Spasyuk

Abstract Pincer complexes of transition metals have demonstrated valuable catalytic reactivities and desirable properties as functional materials. Much more is known about pincer complexes of noble metals, but the pincer chemistry of nonprecious, 3d metals is poised for rapid growth over the next decade. This chapter presents a literature survey of nickel complexes based on tridentate ECE-type pincer ligands featuring a meridional coordination of the central metal atom through two dative E → Ni interactions and a covalent C–Ni linkage. The discussion is focused on the synthesis, characterization, and reactivities of complexes featuring both symmetrical and unsymmetrical ligands, ECE and ECE'. The material is organized into various sections according to the type of donor moiety E and E' (phosphine, amine, phosphinite, phosphinimine, thioether, and *N*-heterocyclic carbene) and the hydrocarbyl linker (aromatic or aliphatic). Where possible, the presentation reflects the chronological order of the developments in this field of study. The review concludes with an overview of the current state of the chemistry of (ECE)Ni complexes and offers some predictions on the future prospects of this field.

Keywords NCN · PCP · Pincer complexes of nickel · PNCN · PNCNP · POCN · POCOP · SCS

Contents

1	Introduction	132
2	PCP Complexes	134
2.1	Complexes Based on the Archetypal 1,3-(CH ₂ PR ₂) ₂ -C ₆ H ₃ Ligand Backbone	134
2.2	Reactivities of (PCP)Ni Complexes	138
2.3	PC _{sp} ³ P Complexes	141

D. Zargarian (✉) • A. Castonguay • D.M. Spasyuk
Département de chimie (PRG-A-618), Université de Montréal, C. P. 6128, succursale
centre-ville Montréal, Québec, Canada
e-mail: zargarian.davit@umontreal.ca

2.4	Reactivities of (PC _{sp³} P)Ni Complexes	143
3	NCN Complexes	145
3.1	The Early (NCN)Ni(II) Complexes	146
3.2	(NCN)Ni(III) Complexes	148
3.3	Catalytic Activities of (NCN)Ni Complexes: Atom Transfer Radical Additions ..	149
3.4	More Recently Introduced (NCN)Ni Complexes	151
4	POCOP and PNCNP Complexes	155
4.1	(POCOP)Ni Complexes	155
4.2	Reactivities of (POCOP)Ni Complexes	156
4.3	(POC _{sp³} OP)Ni Complexes	161
4.4	PNC _{sp³} NP Complexes	162
5	POCN and PNCN Complexes	163
6	SCS and ĆĆĆ Complexes	166
7	Conclusions and Perspectives	167
	References	169

1 Introduction

It is a long-established fact that chelating ligands greatly influence the stability and reactivities of transition metal complexes. Among the numerous types of chelating ligands used to control the reactivities of organometallic complexes, terdentate pincer ligands stand out for their ability to bestow high stability and enhanced reactivities to many transition metals. Since their initial introduction in the late 1970s by the groups of Shaw [1] and van Koten [2, 3], pincer complexes have evolved into a diverse class of compounds possessing highly desirable practical applications in addition to displaying rare or unprecedented structural/bonding features that have challenged our fundamental notions of metal–ligand interactions.

A survey of the pincer literature indicates that bulk of the reports appearing to date concern complexes of noble metals, whereas complexes based on their 3d analogues—Fe, Co, and Ni—have received much less attention. Of the latter metals, pincer complexes of nickel were among the first pincer complexes reported by Shaw [1] and their chemistry is more developed. This is especially true for complexes based on the 1,3-bis(aminomethyl)phenyl ligands introduced and developed by van Koten's group. The chemistry of these so-called NCN-type complexes (Fig. 1) has been studied extensively over the past 3 decades, whereas the organonickel chemistry of complexes based on the original PCP-type ligands introduced by Shaw's group has developed over the last decade.

This chapter will review the chemistry of nickel complexes featuring ECE-type pincer ligands possessing the common feature of a covalent C–Ni linkage at the central position of the pincer ligand. The discussion will focus on the synthesis, characterization, and reactivities of nickel complexes based on both symmetrical and unsymmetrical ligands, ECE and ECE', composed of an anionic hydrocarbyl moiety flanked by two neutral donor moieties such as phosphine, amine, phosphinite, thioether, and *N*-heterocyclic carbene. Pincer-type nickel complexes based on a nonhydrocarbyl linker moiety (e.g., ENE, ESiE, etc.) do not fall within the scope of this review; readers interested in the chemistry of these systems are

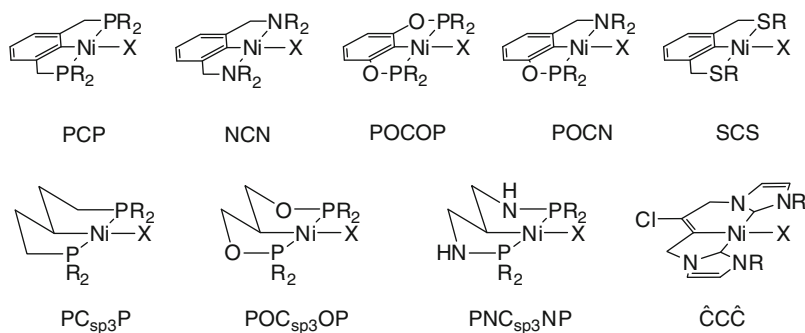


Fig. 1 Various pincer complexes discussed in this chapter

encouraged to consult the primary literature and other reviews of pincer complexes [4–11]. We have strived to cite all pertinent literature on (ECE)Ni complexes reported over the period 1976–2011; any omission is unintentional. To our knowledge, this is the first review covering solely the chemistry of pincer complexes of nickel.

The discussion is organized into five main sections representing the various families of (ECE)Ni complexes based on the type of pincer ligand featured in them. Presentation of the different sections reflects the chronological order in which the target complexes appeared in the literature. Thus, the bis(phosphine)- and bis(amine)-type complexes that were introduced in the 1970s and 1980s, respectively, will be presented first, followed by the recently introduced complexes featuring phosphinite, phosphinimine, thioether, and *N*-heterocyclic carbene donor moieties. The following rules of nomenclature have been applied to designate the various types of pincer ligands discussed here: bis(phosphine)- and bis(amine)-based pincer ligands are referred to as PCP and NCN ligands, respectively; the symmetrical ligands based on bis(phosphinite), bis(phosphinimine), bis(thioether), and bis(*N*-heterocyclic carbene) moieties are referred to, respectively, as POCOP, PNCNP, SCS, and $\hat{C}\hat{C}\hat{C}$; the POCN and PNCN designations will be used to refer to the unsymmetrical phosphinite/amine or phosphinimine/amine ligands. Where appropriate, the unmetallated state of the ligand will be denoted by inserting an “H” or a halide next to the “C” in the ligand designation, for example, PCHP or NCB_rN. Moreover, hybridization of the carbon atom will always be indicated for ligands featuring an sp^3 hydrocarbyl moiety, for example PC_{sp³}P or POC_{sp³}OP, but not for ligands based on an aryl or vinyl moiety; the latter constitute a majority among the pincer ligands used to date and so the hybridization of the nickellated carbon in these compounds will only be specified when emphasis of this feature is called for in the context of the discussion. Finally, where necessary, the *N*- or *P*-substituents will be denoted as a superscript next to the donor atom, for example (NCN^{Me}). Some of the main types of complexes discussed in this review are illustrated in Fig. 1.

2 PCP Complexes

2.1 Complexes Based on the Archetypal 1,3-(CH₂PR₂)₂-C₆H₃ Ligand Backbone

The PCP ligand 1,3-(*t*-Bu₂PCH₂)₂-C₆H₄ and the first pincer-type complexes derived from it were introduced in a seminal report by Moulton and Shaw that appeared in 1976 [1]. It is of historical significance to note that this ligand and its complexes were not referred to as “pincer” in this original report; indeed, the “pincer” designation for this family of ligands/complexes was coined much later by van Koten [12].

The preparation of PCHP^{*t*-Bu} was carried out in ca. 97 % yield via a very simple procedure involving the quaternization of 1,3-(BrCH₂)₂-C₆H₄ with *t*-Bu₂PH in refluxing acetone (<1 h), followed by dehydrobromination by sodium acetate in deoxygenated water at r.t. Over the past 3 decades, a number of alternative synthetic routes to this family of ligands have been reported, including reacting the dihalide precursors with Li metal in the presence of XPR₂ (X = Cl, Br) [13] or with NaPR₂ in liquid ammonia [14]. The efficacy of Shaw’s original procedure has been reaffirmed in a very recent report by Johnson and Wendt: reaction of HPCy₂ with 1,3-(BrCH₂)₂-C₆H₄ in MeOH at ambient temperature over 3 h followed by neutralization of the in-situ generated HBr with NaOMe furnishes PCHP^{Cy} in 92 % yield (gram scale) [15].

The first pincer-type complex of nickel, (PCP^{*t*-Bu})NiCl, was prepared in 57 % yield by stirring PCHP^{*t*-Bu} and NiCl₂·6H₂O in EtOH; remarkably, the nickellation takes place at room temperature in just a few minutes [1]. The authors pointed out the enhanced binding/metallating properties of this family of bisphosphine ligands by noting that similarly bulky monophosphines such as *t*-Bu₂EtP display much lower reactivities. The presence of sterically demanding *P*-substituents was thus thought to be crucial for the preparation of pincer complexes. Shortly after the publication of Shaw’s report, Venanzi’s group reported that the much less bulky ligand 1,3-(Ph₂PCH)₂-C₆H₄ also undergoes metallation to give (PCP^{Ph})NiCl, but the nickellation step of this synthesis required much more forcing conditions (EtOH, 60 °C for 3 h, followed by refluxing for 10 min in the presence of base) [14, 16]. These authors pointed out that the main problem in the synthesis of PCP complexes was the formation of a *cis*-MX₂(PCHP) intermediate that precludes metallation; the nature of metal precursor and reaction conditions were, thus, seen as important for the initial formation of the putative *trans* isomer that proceeds to the metallation step. These observations were confirmed more than 2 decades later by detection and/or isolation of nonnickellated species during the synthesis of PC_{sp3}P- and POC_{sp3}OP-type pincer complexes (*vide infra*). Very recently, Johnson and Wendt reported that reaction of PCHP^{Cy} with anhydrous NiCl₂ in THF at 50 °C and over 50 min leads to an orange-yellow compound that is postulated to be the nonnickellated 1:1 adduct *cis*-(κ^P,κ^{P'}-PCHP^{Cy})NiCl₂; standing overnight converts

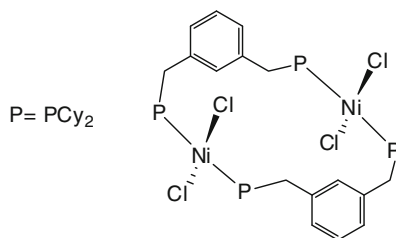


Fig. 2 $\{trans-(\mu - \kappa^P, \kappa^{P'}\text{-PCHP}^{\text{Cy}})_2\text{Ni}_2\text{Cl}_4\}$

this orange–yellow complex into a sparingly soluble purple solid that was identified as the nonnickellated, 2:2 adduct $\{trans-(\mu - \kappa^P, \kappa^{P'}\text{-PCHP}^{\text{Cy}})_2\text{Ni}_2\text{Cl}_4\}$ (Fig. 2) [15]. These observations are in stark contrast to the facile nickellation of PCHP^{Cy} when reacted with $[\text{Ni}(\text{H}_2\text{O})_6]\text{X}_2$ in refluxing EtOH ($\text{X} = \text{Cl}, \text{Br}$; *vide infra*). Interestingly, the non-metallated 2:2 adduct could not be made to undergo nickellation, raising the question of whether such nonmetallated species are intermediates en route to metallation, or mere side-products.

Shaw's first report also described the preparation of a few derivatives of $(\text{PCP}^{t\text{-Bu}})\text{Ni}$, including the cyano and phenylalkynyl derivatives and the cationic CO adduct; the latter was reportedly prepared by reacting $(\text{PCP}^{t\text{-Bu}})\text{NiCl}$ with NaBPh_4 and CO in EtOH. It should be noted that this report provides the characteristic IR band for the phenylalkynyl derivative ($\nu(\text{C}\equiv\text{C}) \sim 2,075 \text{ cm}^{-1}$), but the corresponding data for the cyano or carbonyl species, $\nu(\text{C}\equiv\text{N})$ and $\nu(\text{C}\equiv\text{O})$, respectively, were not reported. The preparation of $(\text{PCP}^{t\text{-Bu}})\text{NiH}$ was also attempted by reacting the corresponding chloride complex with NaBH_4 in refluxing EtOH. The anticipated high-field signal for the Ni–H moiety was not observed in the ^1H NMR spectrum of the product, but its IR spectrum showed a metal-hydride-like stretching frequency at $\sim 1,757 \text{ cm}^{-1}$. As will be described below, the reaction of $(\text{PCP}^{t\text{-Bu}})\text{NiCl}$ with NaBH_4 has been revisited recently and shown to lead to the initial formation of $(\text{PCP}^{t\text{-Bu}})\text{Ni}(\text{BH}_4)$, which might explain why Moulton and Shaw could not detect the signals due to a terminal hydride in the NMR and IR spectra.

Other interesting observations noted in Shaw's original report touch on the generally high thermal stability of PCP complexes and the fact that PCHP ligands appear to be metallated more readily with nickel compared to Pd and Pt. For instance, the synthesis of $(\text{PCP}^{t\text{-Bu}})\text{PtCl}$ yielded a nonmetallated side-product that was formulated as $[(\text{PCHP})\text{PtCl}_2]_n$ ($n > 2$); prolonged heating of this species did not give the desired metallated product.

Although $(\text{PCP})\text{Ni}$ complexes were among the first pincer complexes of nickel to be introduced, the chemistry of these complexes remained essentially dormant over the 2 preceding decades. Indeed, the pincer chemistry of nickel during the 1980s and most of the 1990s was dominated by the $(\text{NCN})\text{Ni}$ chemistry developed by van Koten's group (*vide infra*). The only reports of PCP-type nickel complexes appearing in the 1990s concerned the structural characterization of $(\text{PCP})\text{Ni}(\text{halide})$ complexes (*vide infra*) [17] and their use in preparation of metallodendrimeric

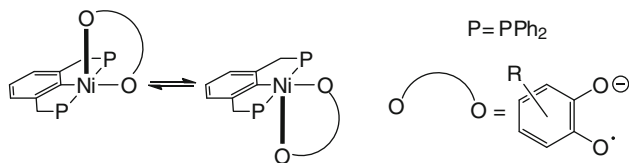


Fig. 3 Structural fluctuations in $[(\text{PCP}^{\text{Ph}})\text{Ni}(\text{II})(o\text{-semiquinone})]^\cdot$

materials inspired by van Koten's reports on analogous NCN-based dendrimers (*vide infra*) [18]. The main advantage of working with metallodendrimers based on $(\text{PCP}^{\text{Ph}})\text{NiCl}$ and $[(\text{PCP}^{\text{Ph}})\text{NiL}]\text{BF}_4$ units ($\text{L} = \text{H}_2\text{O}, \text{CH}_3\text{CN}$) is their facile characterization by the distinct ^{31}P chemical shifts of these units [18].

Kennedy et al. reported for the first time in 1995 structural analyses for $(\text{PCP}^{\text{R}})\text{NiX}$ ($\text{R} = i\text{-Pr}, t\text{-Bu}, \text{Ph}, \text{Cym Me}$; $\text{X} = \text{Br}, \text{OCHO}$) [17]. These authors also reported the synthesis of $(\text{PCP}^{\text{Cy}})\text{NiBr}$ in about 30 % yield by refluxing the mixture of PCHP^{Cy} and $[\text{Ni}(\text{H}_2\text{O})_6]\text{Br}_2$ in EtOH/water ; a higher-yielding synthesis of this compound was reported later by Goldberg and Kemp (*vide infra*). A careful analysis of the solid state structure of $(\text{PCP}^{\text{Ph}})\text{NiBr}$ was also reported by Bachechi in 2003 [19]. The main feature of the latter compound is a puckering of the fused 5-membered rings, which creates a chair-like conformation for the two metallacycles and makes them approximately related by a twofold axis of symmetry. Moreover, the two P atoms come to occupy positions on opposite sides of the cyclometallated ring, while the $P\text{-Ph}$ substituents assume pseudo-equatorial and pseudo-axial positions, thereby blocking the axial positions above and below the Ni atom. Also as a result of the ring puckering, the central aromatic ring and the coordination plane are twisted by ca. 20° with respect to each other, which creates in the solid state structure a C_2 -chirality. Similar observations were made for the Pd and Pt analogues.

The chemistry of $(\text{PCP})\text{Ni}$ complexes has experienced a veritable resurgence over the past decade as new derivatives have been prepared and their spectroscopic properties and chemical reactivities explored. For instance, Kozhanov et al. have reported a series of investigations on $(\text{PCP})\text{Ni}$ complexes bearing a radical anion ligand [20–25]. These authors have prepared spin-labeled complexes by combining a diamagnetic $(\text{PCP})\text{Ni}$ moiety and a radical anionic o -semiquinone ligand. Interestingly, the $(\text{PCP}^{\text{Ph}})\text{NiBr}$ precursor used in the synthesis of these spin-labeled complexes was prepared by reaction of $\text{Ni}(\text{CO})_4$ with 1-Br-2,6- $(\text{CH}_2\text{PPh}_2)_2\text{-C}_6\text{H}_3$ as opposed to using the parent ArH with NiX_2 [21]. Displacement of the bromide in these diamagnetic Ni(II) precursors by the thallium salt of o -semiquinone furnished pentacoordinate, 17-electron, diamagnetic-at-Ni complexes; these compounds stand in nice contrast to their analogous trivalent, paramagnetic-at-Ni complexes $(\text{ECE})\text{NiX}_2$ that will be described below. The solid state structure of one such complex, $(\text{PCP}^{\text{Ph}})\text{Ni}(\text{II})(o\text{-semiquinone})$, shows a square pyramidal coordination geometry with the expected *mer*-arrangement of the pincer ligand ($\text{P-Ni-P} = 146^\circ$; $\text{C-Ni-O} = 176^\circ$; *cis* angles range from 81 to 116°). Variable temperature EPR spectra have revealed a dynamic process that exchanges the apical and basal positions of the two O moieties (Fig. 3).

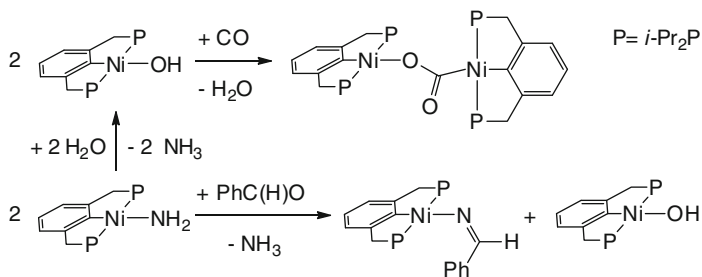


Fig. 4 Reactivities of (PCP^{*i*-Pr})Ni–OH and (PCP^{*i*-Pr})Ni–NH₂ complexes

In spite of this solution fluxionality, the solid state structure shows that the *o*-semiquinone ligand binds the Ni center in an unsymmetrical fashion: the basal O atom bearing the negative charge makes a shorter Ni–O distance, while the apical O atom bearing the single electron forms a longer Ni–O distance. These observations can be justified by invoking the repulsive interactions between the d_z^2 and p_z hybrid orbitals with the ligand orbital bearing the single electron.

Cámpora's group has introduced a number of interesting (PCP^{*i*-Pr})NiX complexes that show how this ligand frame allows the isolation of rare and reactive derivatives [26, 27]. The precursor (PCP^{*i*-Pr})NiBr was prepared by reacting Ni(COD)₂ with 1-Br-2,6-(*i*-Pr₂PCH₂)₂-C₆H₃ (–80 °C) and reacted with NaOH or NaNH₂ (in THF and under sonication) to give (PCP^{*i*-Pr})Ni(OH) and (PCP^{*i*-Pr})Ni(NH₂), respectively. It is interesting to note that the analogous Pd–NH₂ complex is much less stable and could not be isolated. (PCP^{*i*-Pr})Ni(OH) reacts with CO to give the unusual CO₂-bridged species {[(PCP^{*i*-Pr})Ni]₂(μ,κ^C,κ^O-CO₂)} (Fig. 4); this compound displays a very characteristic ¹³C NMR signal for the μ-CO₂ (tt, 206 ppm, ³J_{P-C} ~ 21 and 6 Hz). (PCP^{*i*-Pr})Ni(NH₂) reacts readily with water or MeOH to generate ammonia and the analogous Ni–OH and Ni–OMe derivatives; the latter was characterized by crystallography. The nucleophilicity of the amido moiety is apparent from the facile reaction with benzaldehyde that generates the corresponding aldimido and hydroxy complexes (PCP^{*i*-Pr})Ni(N = CHPh) and (PCP^{*i*-Pr})Ni(OH), in addition to ammonia (Fig. 4).

The above species have been characterized convincingly by ¹H NMR (e.g., a triplet at –2.59 ppm, ³J_{P-H} ~ 6 Hz, for the Ni–OH proton; a triplet at –1.00 ppm, ³J_{P-H} ~ 8 Hz, for the Ni–NH protons), IR (e.g., ν(O–H) ~ 3,600 cm^{–1}; (ν(N–H) ~ 3,355 and 3,295 cm^{–1}), and X-ray diffraction studies. The hydroxo complex is a monomer in solution, as established by cryoscopic measurements, but in the solid state two discrete molecules are paired up through O···H–CMe₂ interactions to produce a suprastructure. The Ni–NH₂ derivative is a monomer in the solid state showing a fairly short Ni–N bond distance (ca. 1.87 Å). A comparison of the fairly similar Ni–C bond distances in (PCP^{*i*-Pr})NiX (ca. 1.92 Å for X = Br [28], OH, OMe, and NH₂) implies fairly similar trans influences for these X ligands.

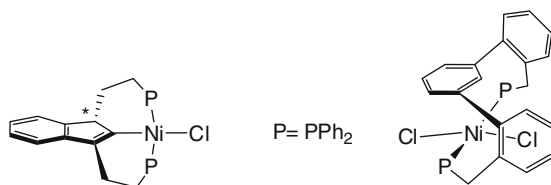


Fig. 5 New PCP-type pincer and “pincer-like” complexes

The first fully characterized hydrido derivative of (PCP)Ni was reported by Goldberg, Kemp and colleagues. $(\text{PCP}^{t\text{-Bu}})\text{NiH}$ was prepared by reacting the chloro precursor with NaBH_4 in EtOH/benzene at r.t. [29]. Interestingly, this compound is more difficult to prepare from super hydride, whereas the opposite was the case for the $\text{PCP}^{c\text{-Hex}}$ and $\text{PCP}^{i\text{-Pr}}$ analogues; on the other hand, none of the reagents tested allowed the formation of $(\text{PCP}^{\text{Ph}})\text{NiH}$, underlining the importance of *P*-substituents for stabilizing the hydride moiety. The ^1H NMR signal for the Ni–H in these complexes appears at ca. -10 ppm (t, $J_{\text{P-H}} \sim 53\text{--}56$ Hz) and the $\nu(\text{Ni-H})$ was observed at $1,726\text{--}1,754\text{ cm}^{-1}$ in the IR spectra. X-ray diffraction studies of $(\text{PCP}^{t\text{-Bu}})\text{NiX}$ ($\text{X} = \text{Cl}, \text{ONO}_2$) have also been reported by this group [30, 31].

A unique PCP-type nickel complex based on a 1,3-disubstituted indenyl backbone has been reported by Groux et al. [32]. The most notable features of this complex are the rare η^1 -coordination of a 2-indenyl moiety and the presence of an optically active carbon at the C-1 position of the indenyl ligand (Fig. 5). The localized nature of the bonding inside the 5-membered ring of the indenyl moiety renders the two PPh_2 moieties inequivalent, as evident from the observation of AB doublets in the $^{31}\text{P}\{^1\text{H}\}$ NMR spectrum ($^2J_{\text{P-P}} = 330$ Hz). The presence of two 6-membered metallacycles results in the out-of-plane tilting of the indenyl moiety with respect to the coordination plane.

Protasiewicz's group has introduced a new family of “trans-spanning” diphosphine ligands based on a *m*-terphenyl scaffold that has the potential to serve as pincer-type ligands [33]. In contrast to the planar *m*-xylyl-based ligands introduced by Shaw, these *m*-terphenyl-based ligands provide pincer-type structures featuring nonplanar backbones that might adopt a C_2 -symmetric geometry. Initial attempts to prepare pincer-type complexes of nickel have failed, however, because the metallation step does not proceed, giving instead unusual *trans*-diphosphino complexes (Fig. 5). Metallated Pd complexes featuring phosphine, phosphinite, and amine donor moieties were prepared eventually by oxidative addition of the brominated ligands to Pd(0) precursors [34–36].

2.2 Reactivities of (PCP)Ni Complexes

The reactivities of $(\text{PCP}^{t\text{-Bu}})\text{NiR}$ have not been explored extensively, but recent reports have identified reactions of potential promise. For example, Hazari's group

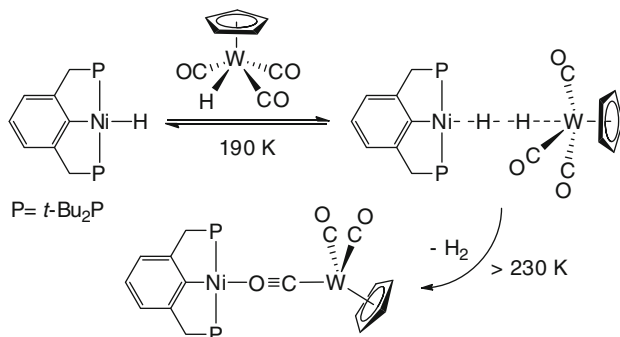


Fig. 6 Interaction of (PCP^{*t*-Bu})NiH with CpW(CO)₃H

has reported the insertion of CO₂ into Ni–R bonds in (PCP^{*t*-Bu})Ni–R (R = H, Me, η¹ – allyl) [37]. This study has shown that the rate of CO₂ insertion varies as a function of the R moiety, proceeding at r.t. over minutes for Ni–H or hours for Ni–allyl, but requiring extensive heating at 150 °C for Ni–Me. DFT studies have shown that the formate derivative resulting from CO₂ insertion into Ni–H is much less stable than the corresponding products with the Ni–Me and Ni–allyl precursors, which explains why only the insertion into the Ni–hydride complex is reversible. Reversible insertion of CO₂ has also been observed with (POCOP^{*t*-Bu})NiH; in this system, CO₂ can be reduced to methanol in the presence of catecholborane (*vide infra*). DFT studies of the PCP^{*t*-Bu} system also suggest that the insertion reaction involves a concerted, 4-centered mechanism involving the Ni–H and one of the C=O moieties, whereas in the case of the methyl and allyl derivatives the insertion follows a path involving interaction between the CO₂ and the R moieties only, with Ni playing a spectator role.

A recent report by Peruzzini's group describes the reactivities of (PCP)NiH complexes and underlines the general ability of pincer complexes to stabilize unstable species and highly unusual bonding arrangements [38]. This report has shown that the “hydridic” Ni–H moiety in (PCP^{*t*-Bu})NiH reacts with protic acids to generate H₂. Protonation with the strong acid HBF₄ was rapid, whereas the reaction with CF₃CH₂OH was found to go through an observable intermediate featuring Ni–H···H–OCH₂CF₃ type interactions (Δ*H*[°] = –2.5 kcal/mol) as evidenced by the following observations: IR spectrum of the mixture showed a lowering of ν(O–H) frequency, whereas the ¹H NMR spectrum showed the downfield displacement of the NiH signal from –9.77 ppm to ca. –0.25 ppm. The reaction with the “acidic” tungsten hydride species CpW(CO)₃H allowed observation of unusual intermediates featuring a μ,η^{1:1}–H₂ moiety and isolation of the very rare species [CpW(CO)₂(μ, κ^C, κ^O–CO···Ni(PCP^{*t*-Bu}))] (Fig. 6).

Relative to terminal CO ligands, the “isocarbonylic” ligand bridging Ni and W centers displays a somewhat longer C–O bond (ca. 1.20 vs. 1.15 Å) and a somewhat shorter W–C bond (ca. 1.91 vs. 1.92 and 1.96 Å), implying significant π-backbonding from both metal centers. The W–C–O–Ni arrangement is fairly

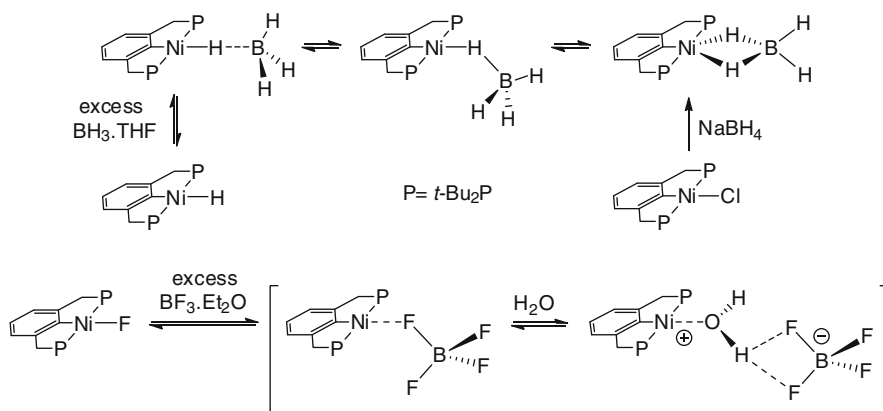


Fig. 7 Interaction of $(PCP^{t-Bu})NiX$ with BX_3 ($X = H, F$)

linear and the Ni–O distance is ca. 1.97 Å. Interestingly, while three distinct signals are observed in the solid state ^{13}C CPMAS NMR spectrum for the three different CO ligands (δ 224, 229, and 240), the solution spectrum shows only one signal at δ 224, implying a dynamic exchange process.

Another recent report from Peruzzini's group describes new examples of unusual "cation-like" species being stabilized by the PCP^{t-Bu} ligand [39]. This report explores the reactivities of the Lewis acids BH_3 and BF_3 with the isolobal Lewis bases H^- and F^- coordinated to $[(PCP^{t-Bu})Ni]^+$. Monitoring the reaction of $(PCP^{t-Bu})NiH$ with $BH_3 \cdot THF$ at 190 K showed the formation, over 8 h, of $(PCP^{t-Bu})Ni(BH_4)$ (^{11}B NMR: -33 ppm, t, $^1J_{B-H} \sim 82$ Hz), but this species was not stable to isolation, yielding instead the starting hydride species (Fig. 7). The same BH_4 species could be obtained by reaction of $(PCP^{t-Bu})NiCl$ with $NaBH_4$, a reaction reported more than 3 decades earlier by Shaw in the attempt to prepare the hydride species (*vide supra*). Combined DFT and $^1H\{^{11}B\}$ NMR studies of D-labeled $(PCP^{t-Bu})Ni(BH_4)$ have revealed that an isotopomeric mixture forms as a result of facile H/D exchange via intermediates of the type $(PCP^{t-Bu})Ni(\eta^2-\kappa^H:\kappa^D-BH_xD_{4-x})$.

The analogous reaction between $BF_3 \cdot THF$ and $(PCP^{t-Bu})NiF$, prepared from the corresponding chloride and five equivalents of thallium fluoride, led to facile formation of $(PCP^{t-Bu})Ni(BF_4)$, which was characterized unambiguously from the broad quintet in the ^{31}P NMR spectrum ($J_{P-F} \sim 8$ Hz) and the characteristic broad ^{19}F NMR signal for coordinating BF_4 anion (ca. -178 ppm). The same product was also obtained by reacting the corresponding chloro precursor with $AgBF_4$. Both synthetic routes also gave the cationic aquo adduct $[(PCP^{t-Bu})Ni(OH_2)][BF_4]$ as a minor side-product (^{19}F NMR: -157 ppm); the latter was also the only species that could be isolated from both reaction mixtures (Fig. 7). Solid state structures of the fluoro and aquo derivatives showed "normal" bond distances for Ni–F (1.87 Å) and Ni–O (1.96 Å); two fluorine atoms of the BF_4 anion were found to interact with one H atom of the aquo ligand. The crossover experiments (Ni–F + BH_3 and Ni–H + BF_3) gave the same mixture of products arising from H/F scrambling

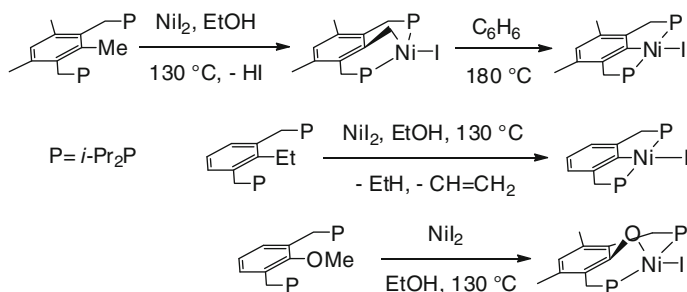


Fig. 8 (PCP^{*i*-Pr})NiI complexes via C–H, C–C, and O–H activation

(Ni–H...BF₃, Ni(BH₄), and Ni(BF₄)). It is worth adding here that a very similar “cation-like” Ni–BF₄ species as well as cationic Ni–OH₂ species have been prepared with the PC_{sp³}P ligand; moreover, the cation [(PCP^{*i*-Pr})Ni(NCMe)]⁺ has been prepared and shown to be a good promoter for Michael-type hydroamination of acrylonitrile. These results are described in the PC_{sp³}P section below.

2.3 PC_{sp³}P Complexes

In an interesting report by Milstein, it was demonstrated that PCP-type ligands possessing an alkyl or alkoxy substituent at the 1-position on the central benzene ring (the metallation site) can display very unusual C–H, C–C, and C–O bond activation reactions [40]. For example, heating an ethanol solution of NiI₂ and 1,3,5-Me₃-2,6-(CH₂PR₂)₂-C₆H (R = *i*-Pr) resulted in the initial activation of the C_{sp³}-H bond of the Me substituent at the 1-position, giving the unusual complex with a benzyl, as opposed to an aryl, moiety in the central position of the pincer ligand (Fig. 8). Although this new species, the first PC_{sp³}P derivative of nickel, showed remarkable thermal stability (up to 130 °C), heating it in a closed system to 180 °C resulted in the net elimination of “CH₂” and generating the PCP complex that might be anticipated from the reaction of 1,3-(CH₂PR₂)₂-4,6-Me₂-C₆H₂. In contrast to the above, using the pre-ligand 1-Et-2,6-(CH₂PR₂)₂-C₆H₃ under analogous conditions gave the (PCP^{*i*-Pr})NiI complex that can also be obtained from the unsubstituted PCHP^{*i*-Pr} ligand. This net dealkylation reaction presumably proceeds through the activation of the Ar-Et bond and generates ethylene and ethane as side-products. Finally, the analogous reaction with 1-MeO-2,6-(CH₂PR₂)₂-C₆H₃ proceeded by C_{sp³}-O bond activation to give the pincer-type product featuring a phenoxy moiety in the pincer ligand (Fig. 8).

The first PC_{sp³}P-type pincer complexes of nickel featuring a 1,5-bis(phosphino)pentane backbone were reported by Castonguay et al. in 2006 [41]. These authors showed that the nickellation of the aliphatic C_{sp³}-H bond requires high temperatures, and that the *P*-substituents affect the course of this reaction. For instance, reacting *t*-Bu₂P(CH₂)₅P(*t*-Bu)₂ with NiX₂ (X = Cl, Br, I) in refluxing

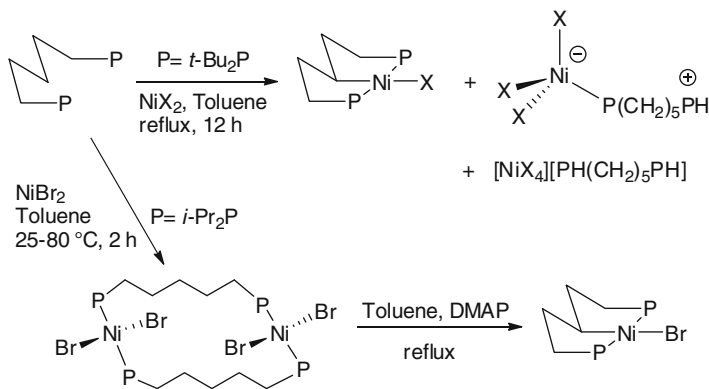


Fig. 9 Reactions of $\text{PC}_{\text{sp}^3}\text{HP}$ with NiX_2

toluene furnishes 37–47 % yields of the desired pincer complexes $(\text{PC}_{\text{sp}^3}\text{P}^{t\text{-Bu}})\text{NiX}$ along with variable amounts of nonmetallated tetrahedral species featuring protonated ligands (Fig. 9). Interestingly, these side-products form even if external bases such as NEt_3 or DMAP are present in the reaction mixture. In contrast, the main side-product in the synthesis of $(\text{PC}_{\text{sp}^3}\text{P}^{i\text{-Pr}})\text{NiBr}$ is the nonmetallated macrocyclic species shown in Fig. 9. Preliminary computational studies indicate that dimeric complexes of this type are the thermodynamically preferred species arising from the interaction of the nickel precursor and the ligand; dissociation of the dimer into a monomer precedes the C–H nickellation step [42].

The complexes $(\text{PC}_{\text{sp}^3}\text{P}^{\text{R}})\text{NiX}$ ($\text{R} = t\text{-Bu}, i\text{-Pr}; \text{X} = \text{Cl}, \text{Br}, \text{I}$) are thermally stable and can be handled in air, both in the solid state and in solution, without noticeable decomposition over extended periods. These complexes display quasi reversible redox waves at ca. $E^{1/2} \sim 0.1\text{--}0.2$ V (with respect to ferrocene), indicating that they are more electron-rich than their aromatic counterparts (for instance, $E^{1/2}$ for $(\text{PC}_{\text{sp}^2}\text{P}^{i\text{-Pr}})\text{NiBr}$ is ca. 0.4 V [28]). The availability of structural data for LNiBr ($\text{L} = \text{PC}_{\text{sp}^2}\text{P}^{\text{R}}$ and $\text{PC}_{\text{sp}^3}\text{P}^{\text{R}}$) allows instructive comparisons of overall structures and pertinent parameters as a function of the hybridization of the metallated carbon atom and *P*-substituents [28, 41, 43]. As mentioned earlier, the aromatic and benzylic carbons in $(\text{PCP}^{\text{R}})\text{NiBr}$ ($\text{R} = t\text{-Bu}, i\text{-Pr}, c\text{-Hex}, \text{and Ph}$) are in the coordination plane; since the two *P* atoms are on opposite sides of this plane the complex possesses a C_2 axis, but not a mirror plane (C_2 symmetry in the solid state). In $(\text{PC}_{\text{sp}^3}\text{P}^{\text{R}})\text{Ni}$ ($\text{R} = t\text{-Bu}$ and $i\text{-Pr}$), the two *P* atoms are in the coordination plane, but two of the nonmetallated CH_2 units ($\text{R}_2\text{PCH}_2\text{CH}_2$) are out-of-plane, leaving no C_2 axis and only one mirror plane (C_s symmetry in the solid state). The average Ni–*P* distances vary in the order $\text{PC}_{\text{sp}^2}\text{P}^{i\text{-Pr}} < \text{PC}_{\text{sp}^3}\text{P}^{t\text{-Bu}} < \text{PC}_{\text{sp}^3}\text{P}^{i\text{-Pr}}$, the shortest Ni–C distance is also found in $\text{PC}_{\text{sp}^2}\text{P}^{i\text{-Pr}}$, whereas the $\text{PC}_{\text{sp}^3}\text{P}^{i\text{-Pr}}$ and $\text{PC}_{\text{sp}^3}\text{P}^{t\text{-Bu}}$ complexes showed very similar Ni–C distances.

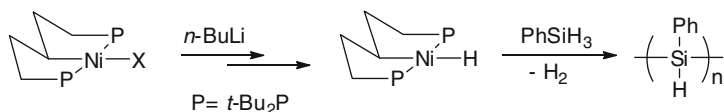


Fig. 10 Reactivity of $(PC_{sp^3}P^{t\text{-Bu}})NiH$

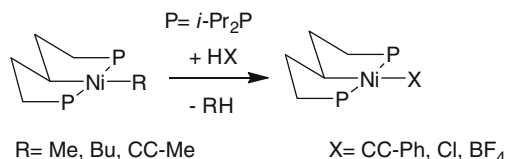


Fig. 11 Protonolysis of $(PC_{sp^3}P^{i\text{-Pr}})NiR$

2.4 Reactivities of $(PC_{sp^3}P)Ni$ Complexes

Charge neutral alkyl, phenyl, and alkynyl derivatives $(PC_{sp^3}P^{i\text{-Pr}})NiR$ are more accessible than their analogous $PC_{sp^3}P^{t\text{-Bu}}$ counterparts [28]. For instance, $(PC_{sp^3}P^{t\text{-Bu}})Ni(n\text{-Bu})$ is much less stable than its $PC_{sp^3}P^{i\text{-Pr}}$ analogue, undergoing facile β -H elimination to generate $(PC_{sp^3}P^{t\text{-Bu}})NiH$. This hydride species could not be isolated, because it is thermally unstable toward reductive elimination, but it was identified by the characteristic upfield triplet in 1H NMR (-10 ppm; $^2J_{P-H} = 53$ Hz) [41]. $(PC_{sp^3}P^{t\text{-Bu}})NiH$ is inert toward olefins and alkynes, but can promote the oligomerization of phenylsilane (Fig. 10).

As anticipated, Ni–C bond distances in $(PC_{sp^3}P^{i\text{-Pr}})NiR$ vary according to the hybridization of the carbon atom ($Ni-C_{sp} < Ni-C_{sp^2} < Ni-C_{sp^3}$) [28]. Moreover, all of these distances are longer than the mean values reported in the literature for the corresponding Ni–C distances in comparable complexes, reflecting the strong trans influence of the metallated central carbon of pincer ligands. The observed thermodynamic trend partially mirrors the kinetic stabilities of Ni–R moieties in the protonolysis reaction with phenylacetylene to generate RH and $(PCP^{i\text{-Pr}})Ni$ ($C\equiv CPh$). Thus, the Ni–Me and Ni–Bu derivatives reacted with phenylacetylene at room temperature, whereas the Ni– $C\equiv CMe$ derivative required heating to undergo protonolysis and the Ni–Ph derivatives did not react even at higher temperatures. Similar protonolysis reactivities were observed when HCl or HBF_4 was used instead of PhCCH (relative rates: $Ph < C\equiv CMe < Me$; Fig. 11) [44]. It is not known whether these protonolysis reactions proceed via a concerted, constant-oxidation-state process or in a step-wise fashion, beginning with oxidative addition of the alkynyl C–H bond followed by reductive elimination of the R–H.

The alkyl derivatives $(PC_{sp^3}P^{i\text{-Pr}})NiR$ ($R = \text{Me, } n\text{-Bu}$) also react with PhX ($X = \text{Cl, Br, I}$) to give Ph–R and $(PC_{sp^3}P^{i\text{-Pr}})NiX$ [28]. This reaction can be carried out under catalytic conditions to give the anticipated products of Corriu-Kumada coupling with up to 80 catalytic turnovers; the homocoupling product Ph–Ph is also

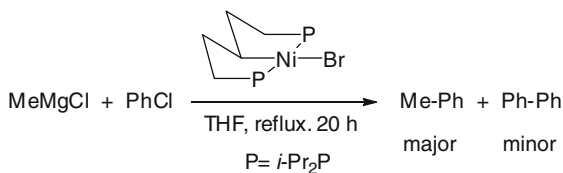


Fig. 12 Corriu-Kumada coupling catalyzed by $(PC_{sp^3}P^{i-Pr})NiBr$

generated in minor quantities (Fig. 12). A number of mechanistic clues have been obtained from the following experimental observations. First, NMR monitoring of the catalytic runs has indicated that the alkyl derivative is the resting state in the catalytic cycle, which implies that the coupling reaction catalyzed by this family of pincer complexes does not involve Ni(0) species according to the conventionally accepted Corriu-Kumada reaction mechanism. Second, the coupling efficacy diminishes as *i*-Pr₂P groups are replaced by *t*-Bu₂P, underlining the importance of steric factors, whereas the analogous $PC_{sp^2}P^{i-Pr}$ system is virtually inactive, highlighting the importance of electron density on the Ni center (*vide infra*). Moreover, the observation that the homocoupling product Ph–Ph does not form when $(PCP^{i-Pr})NiPh$ is allowed to react with PhCl implies that the side reaction leading to homocoupling likely proceeds via an outer-sphere (electron-transfer) mechanism.

The charge neutral $(PC_{sp^3}P^R)NiBr$ complexes can be converted into different cationic adducts. Thus, reacting the bromo precursors with $MBPh_4$ ($M = Na, Ag$) in the presence of nitriles generates $[(PC_{sp^3}P^R)Ni(N\equiv CR')][BPh_4]$ ($R' = Me, CH=CH_2$) [41, 45]. Comparison of the $\nu(C\equiv N)$ values in free acetonitrile and $[(PC_{sp^3}P^{i-Bu})Ni(N\equiv CMe)][BPh_4]$ (2,254 vs. 2,270 cm^{-1}) indicates some degree of activation arising from the effective $N \rightarrow Ni$ σ -donation, whereas the corresponding values for free and coordinated acrylonitrile (2,232 and 2,231 cm^{-1} , respectively) imply much less activation of acrylonitrile. The $\nu(C\equiv N)$ values in the acetonitrile adducts featuring $PC_{sp^3}P^{i-Pr}$ (2,274 cm^{-1}) and $PC_{sp^2}P^{i-Pr}$ (2,282 cm^{-1}) indicate that the latter ligand is a weaker donor in comparison to its $PC_{sp^3}P^R$ analogues, thus corroborating the redox data (*vide supra*). This conclusion is also consistent with the observation that the $[(PC_{sp^2}P^{i-Pr})Ni]^+$ moiety better activates acrylonitrile toward Michael-type hydroamination in comparison to its $PC_{sp^3}P^R$ counterparts [45]. Available experimental evidence indicates that the Ni center in these cationic pincer complexes acts like a Lewis acid to activate the $C=C$ double bond of κ^N -acrylonitrile toward nucleophiles. Consistent with this postulate, reacting aniline with $[(PC_{sp^3}P^{i-Bu})Ni(N\equiv CMe)]^+$ produced $[(PC_{sp^3}P^{i-Bu})Ni(N\equiv CCH_2CH_2N(Ph)H)]^+$, which was isolated and fully characterized [45].

An interesting complex was obtained from the reaction of $(PC_{sp^3}P^{i-Pr})NiBr$ with $AgBF_4$. Even though the solid state structure of the product could not be determined, comparison of its spectral data to those for similar M-F-BF₃ compounds has allowed a fairly confident identification as $(PC_{sp^3}P^{i-Pr})Ni(BF_4)$ [44]; the analogous $PC_{sp^2}P$ complex was reported by Peruzzini's group very recently (*vide supra*). Facile displacement of BF_4 from $(PC_{sp^3}P^{i-Pr})Ni(BF_4)$ has allowed the preparation

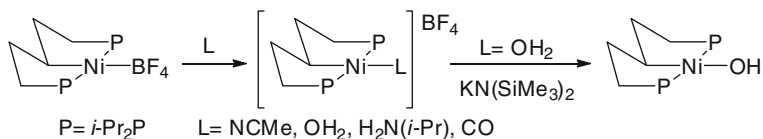


Fig. 13 Reactivities of $(\text{PCP}^{i\text{-Pr}})\text{Ni}(\text{BF}_4)$

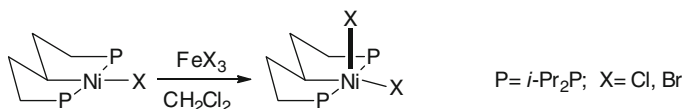


Fig. 14 Preparation of $(\text{PC}_{\text{sp}^3}\text{P}^{i\text{-Pr}})\text{NiX}_2$

of cationic adducts with acetonitrile, water, $\text{H}_2\text{N}(i\text{-Pr})$, and CO (Fig. 13). Deprotonation of the aquo adduct led to formation of a charge-neutral hydroxy derivative that displays a characteristic ^1H NMR signal for the $\text{Ni}-\text{OH}$ proton at -3 ppm ($t, {}^3J_{\text{P}-\text{H}} = 6$ Hz). The solid state structure of this species was analogous to that of its PCP counterpart reported earlier by Cámpora (*vide supra*), showing H-bonding interactions between the hydroxyl oxygen and the methyne proton of the $i\text{-Pr}_2\text{P}$ moiety in the second molecule of the unit cell [44]. The CO adduct shows evidence of π -backdonation from the cationic Ni center ($\nu(\text{CO}) = 2,040$ cm^{-1}).

An important characteristic of the ligand $\text{PC}_{\text{sp}^3}\text{P}^{i\text{-Pr}}$ is its ability to stabilize trivalent nickel species. Thus, $(\text{PC}_{\text{sp}^3}\text{P}^{i\text{-Pr}})\text{NiX}_2$ ($\text{X} = \text{Cl}, \text{Br}$) were prepared by reacting their divalent precursors with FeX_3 (Fig. 14). Similarly to their NCN-based predecessors reported much earlier by van Koten's group (*vide infra*), these paramagnetic 17-electron compounds adopt a distorted square-pyramidal geometry wherein the Ni center is displaced out of the basal plane in the direction of the apical halogen by ca. 0.35 Å [28]. All Ni-ligand distances are somewhat longer, but the $\text{Ni}-\text{X}_{\text{apical}}$ is significantly longer than the $\text{Ni}-\text{X}_{\text{basal}}$, in agreement with the partial population of the antibonding d_z^2 orbital (SOMO). It is interesting to note that even though the oxidation potential of $(\text{PC}_{\text{sp}^3}\text{P}^{i\text{-Bu}})\text{NiBr}$ is only slightly higher than that of $(\text{PC}_{\text{sp}^3}\text{P}^{i\text{-Pr}})\text{NiX}$, no trivalent species could be isolated by chemical oxidation of the $t\text{-Bu}$ precursors, underlining the importance of steric bulk for stabilization of these trivalent species. Electronic factors are also crucial for stabilization of such species since no $\text{PC}_{\text{sp}^2}\text{P}$ analogue of these trivalent species has been isolated to date.

3 NCN Complexes

As mentioned earlier, the NCN complexes of nickel were introduced shortly after the first (PCP)Ni complexes, but the chemistry of NCN complexes experienced a much faster growth owing, primarily, to their outstanding properties as catalysts,

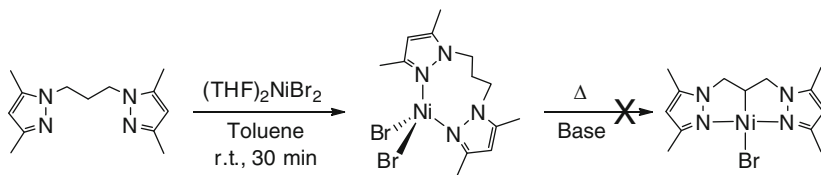


Fig. 15 Attempted nickellation of an NCN ligand

sensors, functional materials, bioactive agents, etc. [46]. In the context of organonickel chemistry, the most important feature of NCN systems is the presence of the “hard” *N*-based donor moieties that bestow to these ligands a very coveted property, namely: the potential to stabilize high oxidation state complexes of nickel. Investigating the chemistry of uncommon trivalent (and monovalent) nickel species is important not only to further our knowledge in fundamental inorganic chemistry, but also to elucidate the biochemical pathways favored by nickel-containing enzymes [47]. Such knowledge is also of tremendous importance for the development of novel “green” catalysts that can promote desirable but difficult transformations at low temperatures and pressures.

This section summarizes the preparation of different NCN complexes of Ni(II) and Ni(III), and describes some of their catalytic reactivities. The initial developments in the chemistry of (NCN)Ni and (PCP)Ni complexes have inspired the introduction of new “hybrid” ligand systems soft donor moieties; the emerging chemistry/soft donor moieties; the emerging chemistry of these hybrid systems will be described in Sect. 5.

3.1 The Early (NCN)Ni(II) Complexes

van Koten and his coworkers have played a pioneering role in the development of (NCN)Ni complexes. This group reported in the early 1980s the synthesis of (NCN)Ni(II) compounds and demonstrated their oxidation to Ni(III) species using mild oxidants [48, 49]. Unlike their PCP counterparts that can feature either sp^2 or sp^3 carbon centers at the central position of the ligand, all known NCN complexes of nickel feature sp^2 carbon centers only, most being of the type 1,3-(CH_2NR_2) $C_6R'_3$. Another important difference between PCP and NCN ligands is that the latter do not undergo nickellation readily and must, therefore, be introduced via different routes. Moreover, when NCN ligands do undergo C–H metallation, with Pd precursors for instance, the orthometallation often occurs at sites other than the central carbon (C-2) of the ligand. van Koten et al. have proposed that the resistance of NCN ligands to C–H nickellation is due to weak Ni–N bonds that hinder the prior chelation of the metal center by the amine moieties [50]. On the other hand, it has been shown at least in one case that C–H nickellation does not ensue even when the nickel center is chelated (Fig. 15) [51]. One possible reason why C–H nickellation does not occur in

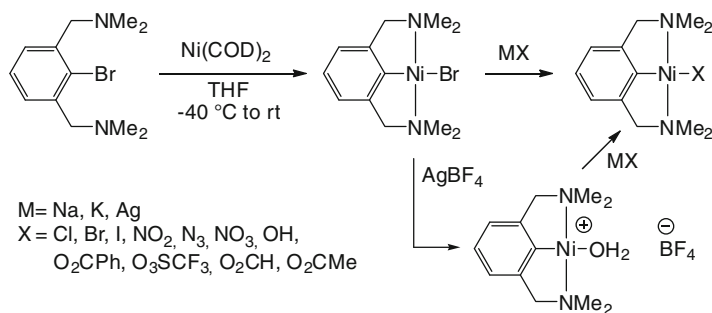


Fig. 16 Synthesis of the first (NCN)Ni complexes

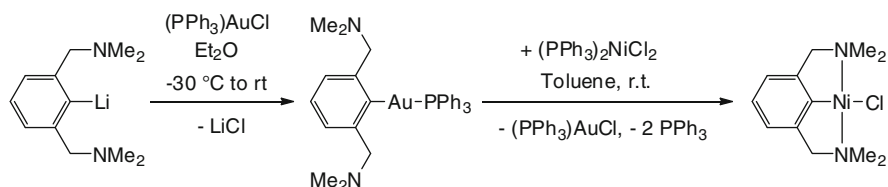


Fig. 17 Transmetalation strategy for preparation of (NCN)NiCl

this system is the weak ligand field of amine donors that leads to a tetrahedral coordination as opposed to a square planar intermediate required for metallation.

Preparation of the very first (NCN)Ni complex was achieved via the oxidative addition of 1,3-(CH₂NMe₂)C₆H₃Br to Ni(COD)₂ (Fig. 16) [48, 49]. Subsequent metathetic reactions using different salts (AgX, NaX or KX, where X = Cl [43], I, BF₄, NO₂, N₃, NO₃, OH, O₂CH, O₂CMe, O₂CPh, O₃SCF₃) led to charge-neutral derivatives (NCN^{Me})NiX. The acetate and formate derivatives were more easily prepared with the cationic aquo adduct [(NCN^{Me})Ni(OH₂)]⁺[BF₄]⁻. Interestingly, the normally labile formate ligand was found to bind strongly to Ni in (NCN^{Me})Ni(OCHO), which was characterized by X-ray diffraction studies. Indeed, this compound proved more stable than its platinum analogue, remaining unaltered in refluxing benzene. (NCN)Ni complexes, in general, are thermally stable and can be sublimed. Curiously, given the superior electron donating ability of NCN ligands, generation of pure samples of cationic species was reported to be somewhat difficult as these compounds were found to be air-sensitive. Later reports confirmed the difficulty in isolating cationic (NCN)Ni adducts, but it was shown that the problem can be resolved in some cases by altering reaction conditions and/or using appropriate counter anions [52, 53].

An alternative to the oxidative addition route for preparing (NCN)Ni complexes is the metathesis of a lithiated ligand with a Ni(II) precursor. This approach has been used for the synthesis of many derivatives, including those used in the manufacture of carbosilane-based dendrimers (*vide infra*). A third method, introduced in 2002 by van Koten's group, consisted of an elegant strategy based

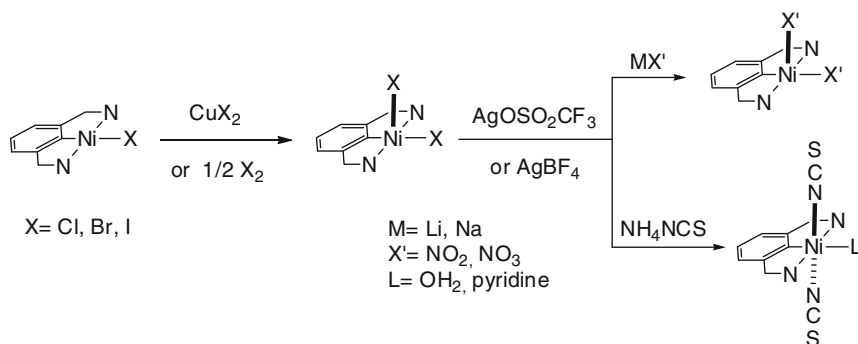


Fig. 18 Synthesis of the first (NCN)Ni(III) species

on transmetallation reaction between $\text{NiCl}_2(\text{PPh}_3)_2$ and $(\text{NCN})\text{Au}(\text{PPh}_3)$ (Fig. 17) [54]. This synthetic method has the following advantages over the traditional metathesis routes using organolithium or Grignard reagents: (1) the new transmetallating agent is not sensitive to air, moisture, or light, which means that it does not need to be used in excess, (2) the Au(I) co-product can easily be recovered, which makes the reaction atom-efficient, and (3) it avoids the use of toxic metals such as Hg or Tl.

Before ending this section, it is worth noting that a new family of imidazole-based (NCN)Ni species has been prepared recently via direct C–H nickellation; this exciting development will be discussed in Sect. 3.4.

3.2 (NCN)Ni(III) Complexes

An exciting characteristic of most (NCN)Ni complexes is their aptitude to undergo facile oxidation and form stable trivalent species. The preliminary report of a $(\text{NCN})\text{NiX}_2$ complex was communicated in 1983 [48], followed by a complete report in 1988 [55]. These paramagnetic, square pyramidal, d^7 complexes were prepared by reacting $(\text{NCN}^{\text{Me}})\text{NiX}$ with CuX_2 , Br_2 , or I_2 ($X = \text{Cl, Br, and I}$; Fig. 18). Consistent with the ready oxidation of the divalent precursors, cyclic voltammetry experiments revealed remarkably low oxidation potentials for Ni $(\text{NCN})\text{X}$ (+0.24 to +0.57 V vs. Ag/AgCl).

An X-ray diffraction analysis of the diiodide complex showed a square pyramidal geometry distorted toward a trigonal bipyramid. The Ni–I bond lengths in this structure were noticeably unequal, with the one in the basal position being 0.014 Å longer (2.627(1) vs. 2.613(1) Å) [55]. ESR studies and EHMO calculations indicated that the unpaired electron resides in an out-of-plane antibonding MO arising from the combination of the nickel d_z^2 orbital and the p_z orbital of the apical iodide ligand.

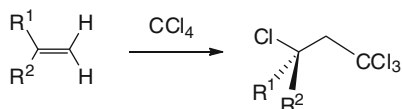


Fig. 19 Atom-transfer radical-addition (ATRA, Kharasch addition)

van Koten et al. also showed that the dihalo Ni(III) complexes discussed above can be converted into various pseudo-halogen derivatives [56]. Interestingly, while Ni(III) species bearing NO_2 and NO_3 gave the expected pentacoordinate complexes, the SCN derivative turned out to be the 19 electron, hexacoordinated Ni(III) species shown in Fig. 18. The solid state structure of this unusual complex showed longer than expected Ni–N_{NCN} bond distances. Taken together with ESR data, it was proposed that the unpaired electron in this paramagnetic octahedral species resides in the $d_{x^2-y^2}$ orbital due to a rare tetragonal contraction along the z-axis.

Kozhanov et al. have studied the structures and EPR spectra of $(\text{NCN}^R)\text{Ni(III)}$ systems ($R = \text{Me}$ or piperidinyl) featuring a bidentate *o*-semiquinone spin-label ligand [57]. Interestingly, they showed that the nature of the *N*-substituent determines whether the unpaired electron will reside on the metal, which results in a Ni(III) species, or on the semiquinone ligand, which gives a Ni(II) species. This group has also investigated a mixed-halogen version of the first $(\text{NCN})\text{NiX}_2$ complexes reported by van Koten et al. Solution EPR studies of $(\text{NCN})\text{Ni(Br)Cl}$ indicated that it exists as two isomers differing in the positions of Br and Cl (apical or basal); this was confirmed by comparison to the spectra of independently prepared homohalogen species $(\text{NCN})\text{NiCl}_2$ and $(\text{NCN})\text{NiBr}_2$ [58]. Interestingly, X-ray diffraction analysis of $(\text{NCN})\text{Ni(Br)Cl}$ showed that the only isomer in the solid state was the one with apical Br.

3.3 Catalytic Activities of $(\text{NCN})\text{Ni}$ Complexes: Atom Transfer Radical Additions

$(\text{NCN})\text{Ni}$ complexes have been shown to be active catalysts for the addition of polyhalogenoalkanes to olefins, commonly referred to as the Kharasch addition reaction or atom-transfer radical-addition (ATRA, Fig. 19). This reaction is of great importance since it is atom efficient, creates a new C–C bond and introduces halogen substituents which are useful for further chemical transformations. van Koten et al. [59, 60] have demonstrated that the catalytic activities of $(\text{NCN})\text{Ni}$ complexes are comparable to those of the best catalysts known for this transformation, such as $\text{RuCl}_2(\text{PPh}_3)_3$ [61] and $\text{Pd}(\text{OAc})_2/\text{PPh}_3$ [62]. For instance, $(\text{NCN})\text{NiCl}$ (0.05 mol %) promotes the regioselective addition of CCl_4 to methylmethacrylate, at 25 °C and after 72 h, with TON $\sim 1,700$ (CCl_4 :alkene, ~ 5.6 :1). With a higher catalyst loading (~ 0.8 %), $(\text{NCN})\text{NiCl}$ is active even at 0 °C, whereas $\text{RuCl}_2(\text{PPh}_3)_3$ is inactive below 40 °C [61]. The favorable electronic and steric properties of NCN

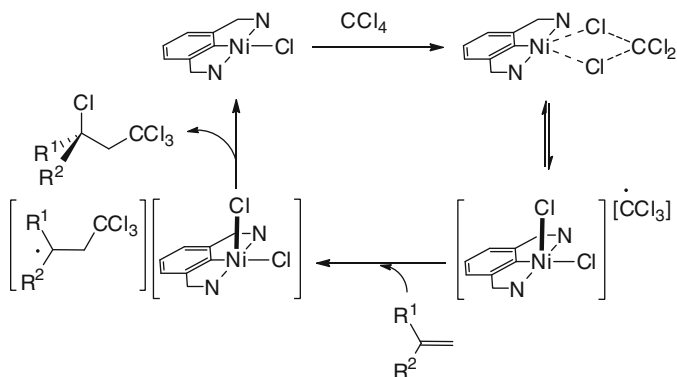


Fig. 20 Proposed catalytic cycle for (NCN)Ni(II)-promoted Kharasch addition

ligands are highlighted by the fact that $\text{NiX}_2(\text{PPh}_3)_2$ has a very limited activity for promoting this reaction.

Detailed mechanistic studies have been performed and the main features of the catalytic cycle have been identified (Fig. 20) [59, 60, 63]. The mechanism follows a radical pathway involving the persistent radical pair species $[(\text{NCN})\text{NiCl}_2][\text{CCl}_3]$. Consistent with the proposed mechanism, no induction of chirality is noted in the Kharasch addition product when precursor complexes bearing chiral ligands are used [64]. One deactivation pathway appears to involve the slow but irreversible consumption of $[\text{CCl}_3]$, which leads to the formation of inactive $(\text{NCN})\text{NiCl}_2$; such trivalent species are commonly found at the end of a catalytic reaction.

An important factor to consider for the Kharasch addition reactions catalyzed by $(\text{NCN})\text{NiX}$ is that the haloalkane (e.g., CCl_4) and the olefin substrate (e.g., MMA) must be used in approximately equimolar ratios in order to avoid an atom-transfer radical polymerization (ATRP); this is the predominant reaction observed when a large MMA: CCl_4 ratio is used. Thus, it has been shown that $(\text{NCN})\text{NiBr}$ can promote the ATRP of MMA and *n*-butyl methacrylate (*n*-BuMA) at temperatures lower than 100 °C [65]. The final polymers were found to have very high molecular weights ($\sim 10^5$ g/mol) and very narrow polydispersities ($M_w/M_n < 1.3$). Block copolymerization was also successfully achieved between MMA and *n*-butyl methacrylate. It is worth noting that since these NCN complexes are stable to water, they can be used for aqueous suspension polymerization reactions. Preliminary results show that monodisperse PMMA can be obtained when the polymerization reaction is performed in aqueous media: $M_n/M_w = 1.7$, $M_n = 60,000$ g/mol compared to $M_n/M_w = 6.5$, $M_n > 290,000$ g/mol without catalyst.

van Koten et al. have also demonstrated that active catalysts for the Kharasch addition can be prepared by anchoring NCN pincer complexes at the periphery of monodisperse, tree-like macromolecules commonly referred to as dendrimers [66]. A great advantage of using dendrimer-based catalysts is that they can be retained

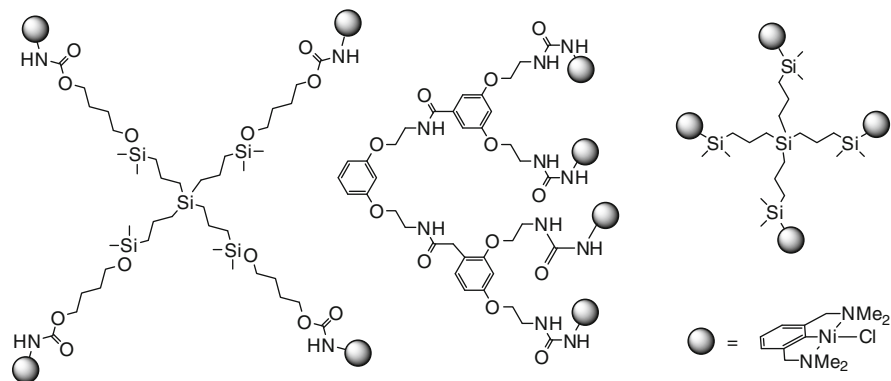


Fig. 21 Metallodendrimers based on $(\text{NCN}^{\text{Me}})\text{NiCl}$

inside a membrane reactor during the catalytic reaction, allowing ready separation of the catalysts from the reaction mixtures and their recycling. The feasibility of this concept was first demonstrated with carbosilane dendrimers linked to $\text{NC}(\text{Br})\text{N}$ ligand moieties via carbamate units (Fig. 21).

Dendrimers bearing four and twelve catalyst end-groups were prepared in one step via the oxidative addition of C-Br bonds to $\text{Ni}(\text{PPh}_3)_4$. Other dendrimer-based materials have since appeared, including an amino acid-based dendrimer featuring four $(\text{NCN})\text{NiBr}$ end-groups linked via urea units [67], and carbosilane dendrimers bearing 4, 12, and 36 $(\text{NCN})\text{NiBr}$ end units (Fig. 21) [68]. The latter dendrimers were assembled via the lithiation of the $\text{NC}(\text{Br})\text{N}$ end-groups and transmetalation with $\text{NiCl}_2(\text{PEt}_3)_2$ (*vide supra*). Other systems based on silica particles or polysiloxane polymers have also been introduced [69, 70]. These metallodendrimers have been shown to be active catalysts for the Kharasch addition reaction of CCl_4 to MMA, but comparison of reactivities has shown that dendrimers decorated with four $(\text{NCN})\text{NiBr}$ units display lower turnover frequencies per nickel site compared to the corresponding monometallic species; moreover, these macromolecular catalysts deactivate more rapidly. van Koten et al. propose that this deactivation is due to the close proximity of the $\text{Ni}(\text{II})$ units at the dendrimer periphery that accelerates the irreversible formation of inactive $\text{Ni}(\text{III})$ species [68].

3.4 More Recently Introduced $(\text{NCN})\text{Ni}$ Complexes

New families of $(\text{NCN})\text{Ni}$ complexes have been introduced over the past few years and shown to promote catalytic reactions other than radical additions. For instance, Richards et al. have reported the first bisoxazoline-based pincer complexes (known as *phebox*, Fig. 22) and shown that they can act like Lewis acid catalysts [52]. Iodide abstraction using $\text{Ag}(\text{OSO}_2\text{CF}_3)$ (in acetone over 27 h) led to a poorly characterized product that could, nonetheless, promote the Michael addition of

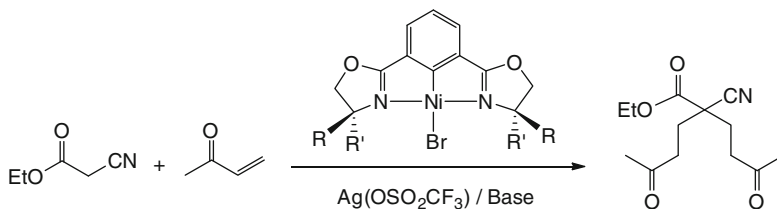


Fig. 22 Michael addition promoted by the first *phebox* pincer complex of nickel

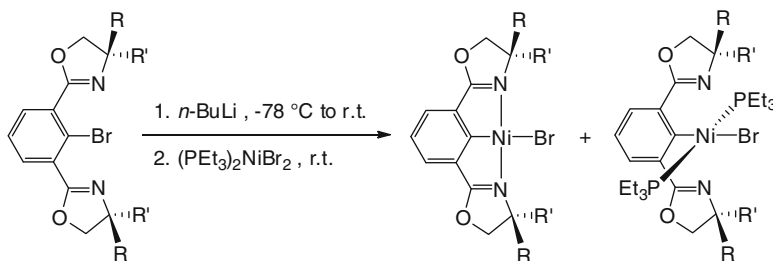


Fig. 23 Synthesis of pincer-type nickel complexes of *phebox*

ethyl cyanoacetate to methyl vinyl ketone (5 mol% pre-catalyst based on the charge-neutral precursor, 10 mol% Hunig's base). This reaction gave only 55 % yield of 5-cyano-5-ethoxycarbonyl-2,8-nonadione, however, due to fairly rapid catalyst deactivation.

A series of complexes based on the above *phebox* ligands were reported by van Koten et al. in 2007 [71]. Interestingly, this study showed that reaction of Ni(PEt₃)₂Br₂ with the (NCN)Li salt leads to the desired pincer complex in addition to a species featuring a monohapto *phebox* ligand linked to Ni(PEt₃)₂Br via its central *ipso* carbon only (Fig. 23). The monohapto species formed exclusively when a sterically hindered *phebox* ligand was used, but its formation could be avoided altogether by using the oxidative addition route. These (*phebox*)NiBr complexes cannot promote the Kharasch addition of CCl₄ to MMA or its ATRP. Consistent with these observations, cyclic voltammetry measurements have established that these complexes show no oxidation wave between -1.00 and +1.50 V (vs. Ag/AgCl), and theoretical calculations have confirmed that oxidation of (NCN)NiBr is considerably more facile.

In 2008, Mitsudo and Tanaka reported that reacting AgBF₄ with the same iodo precursor used by Richards et al. in a mixture of acetonitrile and dichloromethane (r.t., 1 h) gave the air stable, cationic bisoxazoline pincer complex [53]. This cationic acetonitrile adduct was found to be two to three times more efficient than its precursor for promoting Michael additions, which often require electron-deficient (Lewis acidic) catalysts. Interestingly, the same adduct also catalyzes the Heck coupling (Fig. 24), a reaction known to require electron-rich catalysts capable of promoting oxidative addition of aryl halides. The observation of an

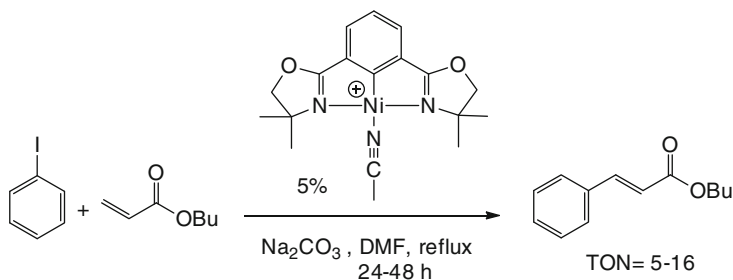


Fig. 24 Heck coupling catalyzed by a cationic *phebox* complexes

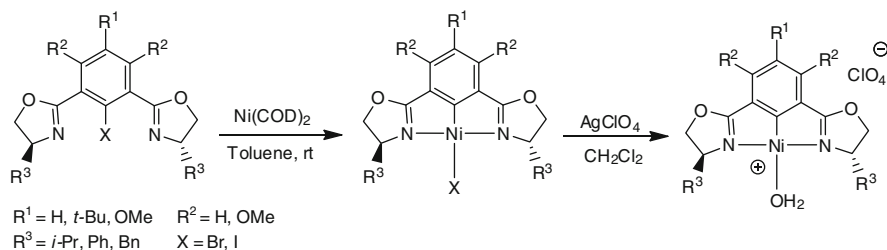


Fig. 25 Synthesis of optically active *phebox* complexes

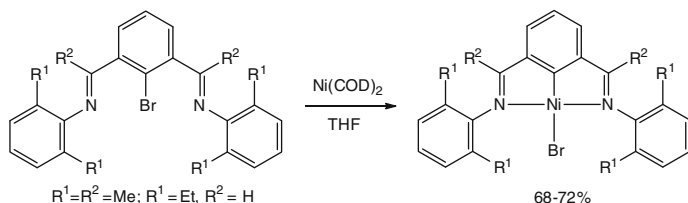


Fig. 26 Synthesis of (NCN)Ni complexes based on imine donor moieties

induction period in the Heck coupling reaction prompted these authors to suggest that the cationic adduct is only a pre-catalyst for this reaction.

Bugarin and Connell have reported the preparation of numerous neutral and cationic pincer complexes bearing chiral *phebox* ligands (Fig. 25) [72]. These complexes should be ideal candidates for establishing structure/activity relationships, but no study has been reported yet on their catalytic activities. Structural analyses carried out on four of these complexes showed that the presence of an electron-donating group such as *t*-Bu on the ligand resulted in elongation of the Ni–X bond, presumably because the more electron-rich aryl ring exerts a greater trans influence. The relative Lewis acidity of the cationic aquo adducts was evaluated by studying their ligand exchange reactions in the presence of a sub-stoichiometric quantity of acetonitrile (0.9 equiv.). Measuring the downfield shift of the $\text{CH}_3\text{CN-Ni}$ signal compared to free acetonitrile, and assuming that this shift would be proportional to

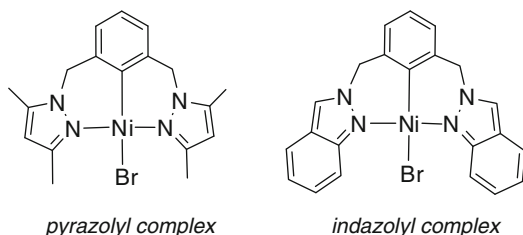


Fig. 27 (NCN)NiBr complexes based on bis(azolylmethyl)phenyl ligands

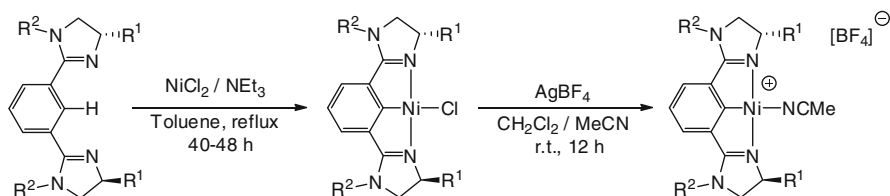


Fig. 28 New (NCNim)NiCl complexes via direct C–H nickellation

the Lewis acidity of the (*phebox*)Ni⁺ fragment, a decrease in Lewis acidity was noted as more electron-donating substituents were introduced on the *phebox* ligand.

New (NCN)Ni complexes featuring imine donor moieties have been prepared by the groups of van Koten [71] and Park [73] (Fig. 26). As was the case for the above-discussed *phebox* systems, theoretical calculations have suggested that, unlike their bis(amine) analogues, these bis(imine)phenyl ligands are not suitable for stabilizing trivalent species. The bis(ketimine)phenyl complex prepared by Park et al. was found to be inactive for the polymerization of ethylene, giving only small amounts of oligomers even with a high pressure of ethylene gas (200 psi) and in the presence of large excess of methylaluminoxane (MAO, 1,000 equiv.; 3 h, 60 °C).

A very recent report by Valderrama et al. describes new NCN pincer complexes based on bis(azolylmethyl)phenyl ligands (Fig. 27) [74]. The charge-neutral bromides were prepared via the oxidative addition of the brominated ligands to Ni(COD)₂, but attempts at isolating cationic adducts failed. Even though it was found to be less active than its Pd counterpart for polymerization of ethylene, the Ni-based bis(indazolyl) complex can produce under fairly mild conditions (60 °C, 3.5 bar) high molecular weight polyethylene of relatively narrow polydispersities ($M_w \sim 119,000\text{--}200,000$ g/mol; $M_w/M_n \sim 2.3\text{--}2.8$). According to the mechanism proposed for this reaction, the catalytically active species is generated by dissociation of one of the Ni–N bonds; the lower activities of the Ni complex is attributed to the short and less labile Ni–N bonds relative to the Pd complexes.

Finally, it was demonstrated very recently that (NCN)Ni species can be prepared via C–H nickellation: C₂-symmetrical 1,3-bis(2'-imidazolyl)benzenes react with anhydrous NiCl₂ in refluxing toluene to give a variety of (NCN^{im})NiCl in 40–87 %

yields (Fig. 28) [75]. Preliminary studies have shown that these optically active complexes fail to promote stereoselective transformations, but their facile synthesis via direct C–H nickellation bodes well for further development of the chemistry of this family of (NCN^{imm})Ni complexes.

4 POCOP and PNCNP Complexes

Pincer-type Pd complexes based on bis(phosphinite) donor moieties were introduced in 2000 by the groups of Jensen and Bedford who showed that these compounds were highly effective for promoting Heck and Suzuki coupling reactions [76, 77]. Since then, POCOP complexes of other metals have also appeared and many have shown enhanced reactivities relative to their PCP-type analogues. By comparison, the chemistry of analogous complexes featuring the PNCNP ligand remains much less developed. The synthesis of POCOP and PNCNP ligands is very convenient and operationally simple, while their aptitude for undergoing C–H metallation is fairly similar to PCP ligands, making this family of ligands and complexes very attractive for reactivity studies. This section summarizes the development of (POCOP)Ni and (PNC_{sp3}NP)Ni complexes.

4.1 (POCOP)Ni Complexes

The first POCOP complex of nickel, (POCOP^{Ph})NiCl, was introduced in 2006 by the group of Morales-Morales [78]. Shortly thereafter, Pandarus et al. reported the halo complexes (POCOP^{i-Pr})NiX (X = Cl, Br, I) [79, 80]. The latter reports emphasized the importance of the nickel precursor for the synthesis of POCOP complexes. Thus, simple derivatives such as NiBr₂L_n (L = THF or MeCN; n = 1.5 or higher, depending on the conditions of preparation) proved to be superior to NiBr₂, whereas the bromo precursors gave cleaner reactions and higher yields than their corresponding chloro and iodo counterparts. Other precursors such as Ni(OAc)₂, Ni(NO₃)₂, Ni(acac)₂, etc. were also less effective although little effort has been expended on optimizing the metallation reaction with these precursors [51, 79].

The presence of a base such as DMAP or NEt₃ was also found to be beneficial for the yield. The (POCOP)NiBr can thus be obtained in 80–95 % yields from the ambient temperature reaction of NiBr₂(NCMe)₂ with POCHOP in the presence of NEt₃; more recent work has shown that 90% or better yields are possible routinely and on multi-gram scale [81]. It should be emphasized, however, that bases affect only the yields of the final complexes and are not essential for the C–H metallation reaction. Indeed, Morales-Morales reports that (POCOP)NiCl can be prepared in 80 % yield without any added base [78]; it is not clear how the HCl generated in-situ is neutralized or removed from the reaction medium. This latter point is important for our understanding of the mechanism of the nickellation step (*vide infra*).

Finally, the ease of formation of (POCOP)NiX is also influenced by *P*-substituents, (POCOP^{Ph})NiBr forming more sluggishly than (POCOP^{*i*-Pr})-NiBr (12 h at r.t. vs. minutes) [82].

Other halo complexes of POCOP reported recently include (POCOP^{Ph})NiBr by Salah et al. [82] and (POCOP^R)NiCl (R = *t*-Bu, Me, *c*-Pen) by Guan's group [83–85]. The POCOP^{Me} system reported recently by Guan's group is of particular interest because very few POCOP complexes are known with nonbulky OPR₂ moieties. Most of these halo complexes show high thermal stabilities. For instance, DMF solutions of (POCOP^{*i*-Pr})NiX can be heated up to 200 °C. The halo complexes are also generally stable to ambient air in the solid state, but exposing their solutions to humid air leads to gradual decomposition. As anticipated on the basis of the greater π -acidity of the phosphinite moieties relative to phosphines, the redox potentials of POCOP systems indicate that these complexes are more difficult to oxidize [45, 79, 80], and structural studies indicate that they possess shorter Ni–C and Ni–P bond distances in comparison to their PCP counterparts [45, 78–80, 82–85].

The preparation and characterization of the following charge-neutral derivatives and cationic adducts have been reported recently: (POCOP^{*i*-Pr})NiX (X = OSO₂CF₃, Me, Et) and [(POCOP^{*i*-Pr})Ni(N≡CR)]⁺ (R = Me, CH=CH₂); [80] (POCOP^{*i*-Pr})NiX (X = C≡N, N=C=O) and [(POCOP^{*i*-Pr})NiL]⁺ (L = *t*-BuN≡C, OH₂); [86] (POCOP^{Ph})NiX (X = C≡N, ONO₂, OAc, C≡CPh) and [(POCOP^{Ph})Ni(N≡CR)]⁺ (R = Me, CH=H₂, C(Me)=CH₂, CH=C(Me)CH, CH₂CH₂N(H)Ph); [82, 87] (POCOP^R)NiH and (POCOP^R)Ni(OC(O)H) (R = *t*-Bu, *i*-Pr, *c*-Pen), (POCOP^{Ph})Ni(SAr) [83, 84, 88], and (POCOP^{*i*-Pr})Ni(OAr) [89]. The interesting reactivities promoted by these compounds will be discussed below. It is noteworthy that cyclic voltammetry studies have shown that some of these derivatives undergo quasi-reversible oxidation, but high valent species featuring POCOP ligands have not been isolated, whereas trivalent species have been isolated with POC_{sp3}OP systems (*vide infra*) [79, 80, 82].

4.2 Reactivities of (POCOP)Ni Complexes

Cationic acrylonitrile adducts featuring POCOP ligands, pre-formed or generated in-situ, have shown good reactivities as Lewis acid-like promoters of Michael-type hydroaminations leading to C–N bond formations (Fig. 29). As discussed earlier, the IR data for [LNi(NCR)]⁺ are particularly useful for assessing the electrophilicity of the cationic fragment [LNi]⁺ and, by extension, the donor strength of the pincer ligand. Comparison of the $\nu(\text{CN})$ values in POCOP and PCP complexes indicates that the POCOP-based cations are more electrophilic than their PCP analogues, which is consistent with the much greater reactivities of POCOP complexes in promotion of Michael-type hydroamination reactions [45]. The catalytic reactivities of POCOP^R precursors vary as a function of *P*-substituents: the *i*-Pr analogue is a more active catalyst for the hydroamination of acrylonitrile, especially in the presence of NEt₃ as a H⁺-transfer agent, because the amine substrates

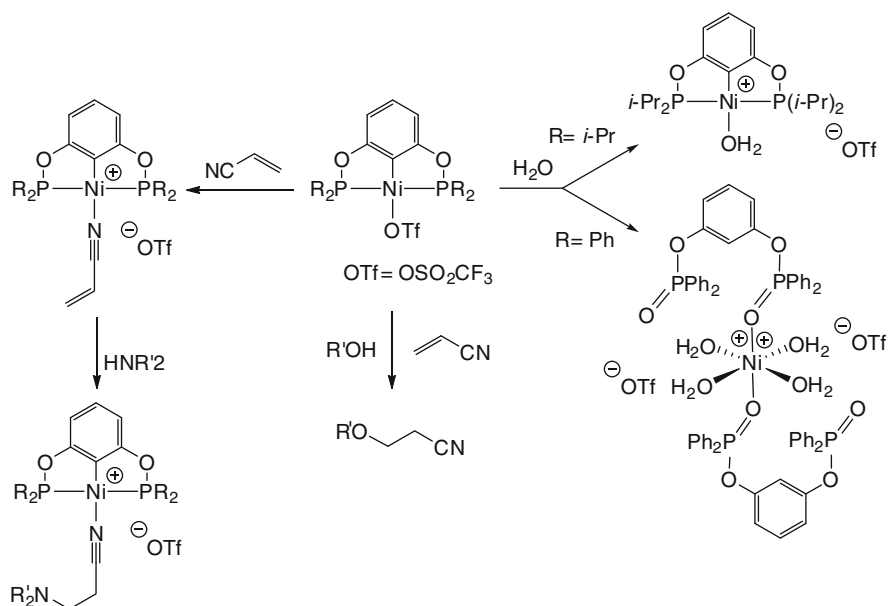


Fig. 29 Reactivities of (POCOP)Ni(OTf)

appear to compete with acrylonitrile for coordination to the Ni center in the Ph analogue. On the other hand, the latter promotes the C–N bond-forming reaction in the presence of small quantities of water as H⁺-transfer agent [87]. (POCOP^{Ph})Ni(OSO₂CF₃) is also a better catalyst for the alcoholysis of acrylonitrile compared to the *i*-Pr analogue (Fig. 29). It is interesting to note that while the Michael-type aminations proceed most readily with nucleophilic amines, the O–C bond formation (alcoholysis) works best with the least nucleophilic alcohols. Experimental observations indicate that the alcoholysis reactions proceed via charge-neutral Ni–OR species.

The nature of *P*-substituents also influences other reactivities of (POCOP)Ni complexes. For instance, the two triflate complexes (POCOP^R)Ni(OSO₂CF₃) react differently with water depending on the nature of R: the triflate moiety in the *i*-Pr analogue is displaced readily upon contact with humid air to give the corresponding aquo adduct [(POCOP^{*i*-Pr})Ni(OH₂)](OSO₂CF₃) [86], whereas the Ph analogue undergoes an oxidative hydrolysis in the presence of a large excess of water, giving an unusual octahedral dication featuring four water ligands and two P = O moieties (Fig. 29) [87]. In addition, (POCOP^{*i*-Pr})NiR (R = Me and Et) can be prepared and characterized fully [80], whereas the corresponding POCOP^{Ph} derivatives are inaccessible [82]. Interestingly, (POCOP^{*i*-Pr})NiMe proved very ineffective for promoting the coupling of PhCl and MeMgCl, in contrast to its POC_{sp³}OP counterpart (*vide infra*) [45]. On the other hand, intermediates generated in-situ from (POC_{sp²}OP^{Ph})NiBr and MeMgBr reacted with a mixture of aryl bromides ArBr and Ar'⁺Br to give 50 % yields of the heterocoupling products Ar–Ar' [82]. These observations implicate reaction pathways involving electron transfer processes [90].

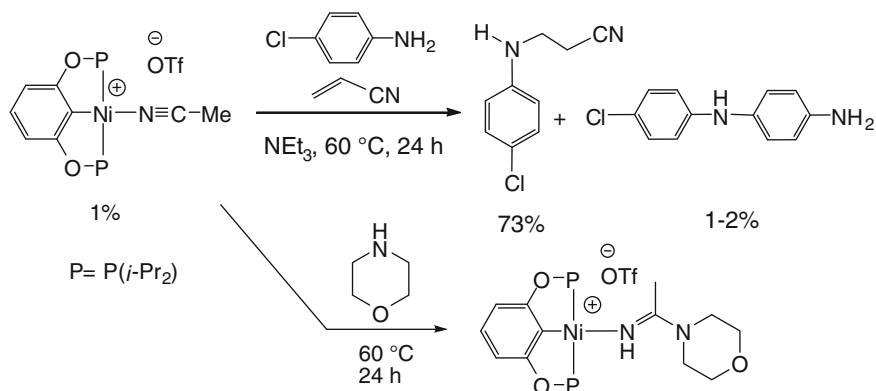


Fig. 30 C–N bond formations promoted by $[(\text{POCOP}^{i\text{-Pr}})\text{Ni}(\text{NCMe})][\text{OTf}]$

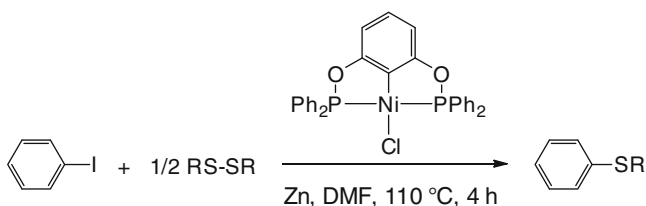


Fig. 31 C–S bond formation catalyzed by $(\text{POCOP}^{\text{Ph}})\text{NiCl}/\text{Zn}$

A number of interesting observations have been made during the study of Michael-type hydroaminations promoted by $(\text{POCOP})\text{Ni}$ systems. First, the reaction of *p*-chloroaniline with acrylonitrile catalyzed by $[(\text{POCOP}^{i\text{-Pr}})\text{Ni}(\text{NCR})]^+$ gave the anticipated product of N–C_{acrylonitrile} bond formation in addition to trace amounts of another product arising from an unexpected N–C_{aryl} bond formation reaction (Fig. 30) [91]. The mechanism of this homocoupling reaction has not been studied, but by analogy to the Kumada-type coupling reactions discussed earlier, it is possible to envisage the formation of an anilido intermediate that could react with the Ar–Cl moiety of the aniline to furnish the observed side-product. Another interesting observation was the formation of Ni-bound amidines through nucleophilic amination of coordinated nitriles lacking a reactive C=C double bond (acetonitrile, cinnamionitrile, *p*-cyanostyrene; Fig. 30) [91].

A recent report by Sun et al. has shown that $(\text{POCOP}^{\text{Ph}})\text{NiCl}$ complexes can catalyze C–C bond formation reactions involving the coupling of $\text{RC}\equiv\text{CLi}$ and $\text{R}'\text{X}$ ($\text{R} = \text{Ph}, \text{SiMe}_3$; $\text{R}' = \text{alkyl}$; $\text{X} = \text{Cl}, \text{Br}, \text{I}$) at r.t. [92]. The reaction proceeds best with primary halides ($\text{I} > \text{Br} > \text{Cl}$) and $\text{PhC}\equiv\text{CLi}$; secondary alkyl halides and $\text{Me}_3\text{SiC}\equiv\text{CLi}$ give much lower yields. The type of solvent used seems to be a crucial factor for the success of this reaction, NMP or DMF being the most suitable choices. Indeed, the C_{sp}–C_{sp3} coupling appears to proceed in NMP with 50 % yield even in the absence of Ni. The authors propose the involvement of Ni(IV)

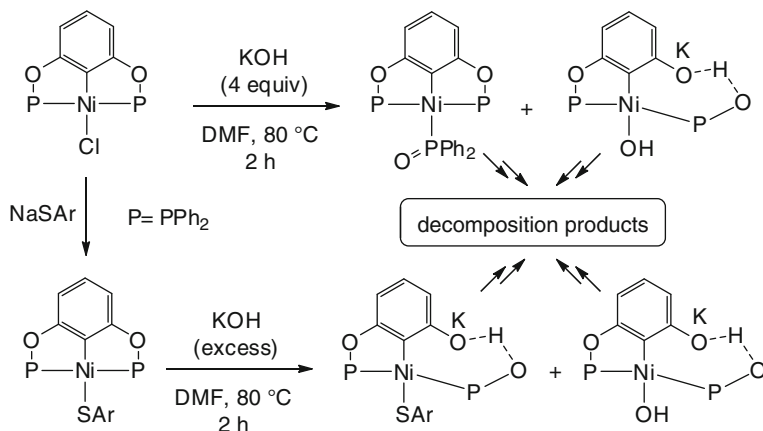


Fig. 32 Decomposition of (POCOP^{Ph})NiX (X = Cl, SAr) in basic media

intermediates arising from oxidative addition of R'X to (POCOP^{Ph})NiC≡CR, but no mechanistic studies have been performed to support this contention.

Morales-Morales' group has shown that (POCOP^{Ph})NiCl can promote the coupling of RS-SR and PhI, giving Ph-SR (Fig. 31) [78]. Best results (500–860 catalytic turnovers) were obtained by conducting the reactions in the presence of one equivalent of Zn in DMF at 110 °C for 4 h. Reactions using (*t*-BuS)₂ and (PhS)₂ as substrates also generated 35 % and 8 % yields, respectively, of biphenyl. The authors have proposed a catalytic cycle involving Ni(I) species generated by the reduction of the divalent precatalyst by zinc dust; the main side-product is thought to form in a secondary reaction involving Ni(III) intermediates.

Guan's group has reported that (POCOP^R)NiCl precursors, and in particular (POCOP^{Ph})NiCl, can catalyze the coupling of PhI and ArSH (typical conditions: 1 % Ni, one equivalent of PhI and ArSH, two equivalents KOH, DMF, 80 °C, 2–3 h; up to 99 % yield) [84]. Mechanistic probes of this C–S bond-forming reaction have shown that the preformed Ni–SAr species react only very sluggishly with PhI, implying that the catalysis is unlikely to proceed through a direct reaction between the Ni–SAr precursor and PhI. This led the authors to re-examine the mechanism and they discovered that KOH leads to the decomposition of (POCOP)NiCl, generating various species bearing oxidized P-containing moieties, as shown in Fig. 32. These observations underline the limitations of POCOP ligands wherein the P–O linkage is unstable in basic conditions.

Guan's group has also reported very interesting reactivities with the hydrido complexes (POCOP^R)NiH (R = *i*-Pr, *t*-Bu, *c*-Pen). For instance, (POCOP^{*i*-Pr})NiH reacts with benzaldehyde to give (POCOP^{*i*-Pr})NiOCH₂Ph (Fig. 33), the first directly observed insertion of a carbonyl group into a Ni-hydride [83]. The analogous insertion reaction with ketones was found to be more sluggish, and no insertion took place with alkenes and alkynes. Significantly, some hydrosilanes reacted with the benzyloxide derivative to give silyl ethers and regenerate the initial hydride

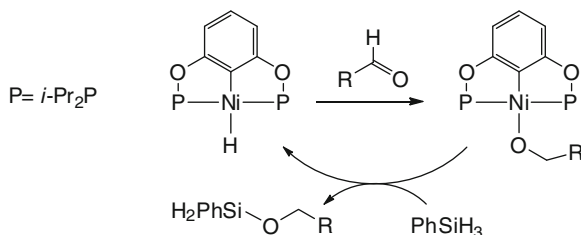


Fig. 33 Aldehyde hydrosilylation catalyzed by $(\text{POCOP}^{i\text{-Bu}})\text{NiH}$

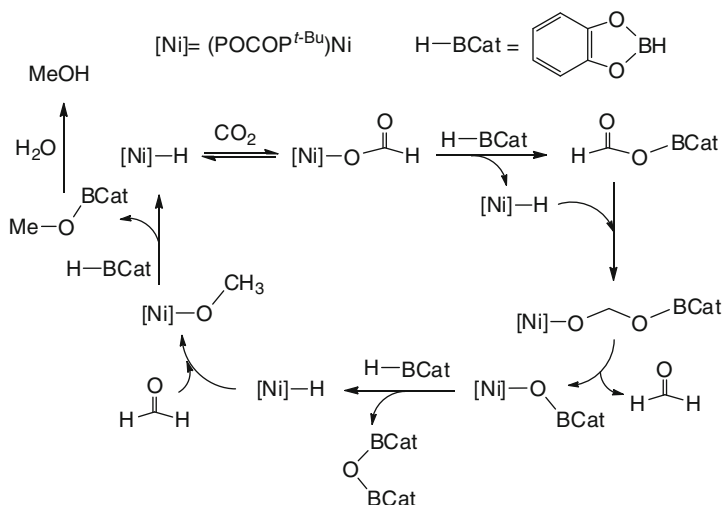


Fig. 34 Reduction of CO_2 catalyzed by $(\text{POCOP}^{i\text{-Bu}})\text{NiH}$

($\text{PhSiH}_3 \sim \text{Ph}_2\text{SiH}_2 > \text{Et}_3\text{SiH}$, $(\text{OSi}(\text{Me})\text{H})_n \gg \text{HSi}(\text{OEt})_3$), thus making possible a catalytic cycle for hydrosilylation of aldehydes (Fig. 33). Screening studies showed that $(\text{POCOP}^{i\text{-Pr}})\text{NiH}$ catalyzes hydrosilylation of a variety of aromatic and aliphatic aldehydes with 300–450 catalytic turnovers; α,β -unsaturated aldehydes gave products of 1,2-addition and isolated $\text{C}=\text{C}$ was not hydrosilylated. Hydrosilylation of ketones gave generally lower yields, and the $\text{POCOP}^{i\text{-Bu}}$ analogue was much less active. The inertness of $(\text{POCOP}^{i\text{-Pr}})\text{NiH}$ toward PhSiH_3 even at elevated temperatures indicated that the hydrosilylation mechanism in this system involves initial insertion of the carbonyl group.

The complexes $(\text{POCOP}^{\text{R}})\text{NiH}$ also react with CO_2 to generate a labile formate derivative, which is in equilibrium with the starting hydride (Fig. 34) [85, 88]. Interestingly, excess catecholborane drives this equilibrium toward formaldehyde and, eventually, methanol. This process is favored by bulky phosphinite moieties ($t\text{-Bu} > c\text{-Pen}$ and $i\text{-Pr}$). Experimental observations and computational studies have helped uncover a complex catalytic cycle based on metathesis-type reactions of the type $\text{LNi}(\text{R}) + \text{A-X} \rightarrow \text{LNi-X} + \text{R-A}$ [93].

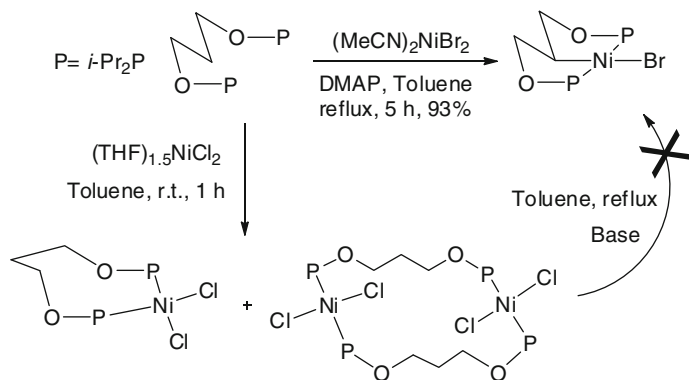


Fig. 35 Reaction of $\text{POC}_{\text{sp}^3}\text{HOP}^{i\text{-Pr}}$ with L_nNiX_2

4.3 $(\text{POC}_{\text{sp}^3}\text{OP})\text{Ni}$ Complexes

All $(\text{POC}_{\text{sp}^3}\text{OP})\text{Ni}$ complexes reported to date were introduced by Pandarus et al. [51, 79, 80]. In contrast to the straight forward and facile syntheses of $(\text{POCOP})\text{Ni}$ (halo) complexes discussed above, the preparation of analogous aliphatic complexes $(\text{POC}_{\text{sp}^3}\text{OP})\text{NiX}$ ($\text{X} = \text{Cl}, \text{Br}, \text{I}$) requires extended heating and goes through detectable, nonmetallated intermediates (Fig. 35). Some of these species form in the ambient temperature reaction of $\text{POC}_{\text{sp}^3}\text{HOP}$ with Ni precursors; they have been formulated as the dimeric species featuring large macrocycles reminiscent of the *trans*-2:2-adducts observed in the preparation of Pd, Pt, and Rh complexes reported by Shaw's group [94–96] and the corresponding Ni complexes reported by Castonguay et al. [28]. These side-products usually undergo metallation upon heating and in the presence of bases or acids to give the desired pincer-type products. On the other hand, the reaction of $\text{POC}_{\text{sp}^3}\text{HOP}$ with NiCl_2 gave the unusual *cis*- $(\kappa^P, \kappa^{P'})\text{-POC}_{\text{sp}^3}\text{HOP}^{i\text{-Pr}}\text{NiCl}_2$, which does not proceed to metallation even upon extended heating (Fig. 35) [51]. The ease of nickellation of pincer ligands was discussed briefly in the NCN section; a detailed study on the mechanism and energetics of this reaction is in progress [42].

Like their aromatic counterparts, $(\text{POC}_{\text{sp}^3}\text{OP}^{i\text{-Pr}})\text{Ni}(\text{halo})$ complexes are fairly stable in air and show good thermal stabilities, but cyclic voltammetry measurements have indicated that $\text{POC}_{\text{sp}^3}\text{OP}$ systems are easier to oxidize ($E^{1/2} \sim 0.4$ vs. 0.7 V vs. Ag/AgCl) [80]. Solid state structures of these halo complexes are very similar to those of their $\text{PC}_{\text{sp}^3}\text{P}$ analogues, but somewhat shorter Ni–C and Ni–P distances were found in $\text{POC}_{\text{sp}^3}\text{OP}^{i\text{-Pr}}$ systems, as discussed above. Similarly to the POCOP systems, triflate derivatives of $\text{POC}_{\text{sp}^3}\text{OP}^{i\text{-Pr}}$ can be used as precursors for preparation of cationic acetonitrile and acrylonitrile adducts. The IR data for these cationic complexes have confirmed that the aliphatic ligands are stronger donors [80]. Alkyl derivatives of $\text{POC}_{\text{sp}^3}\text{OP}^{i\text{-Pr}}$ could not be isolated due to their limited thermal stabilities, but in-situ generated $(\text{POC}_{\text{sp}^3}\text{OP}^{i\text{-Pr}})\text{NiMe}$

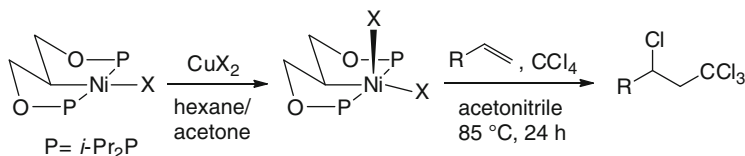


Fig. 36 Preparation and reactivities of $(\text{POC}_{\text{sp}^3}\text{OP}^{i\text{-Pr}})\text{NiX}_2$

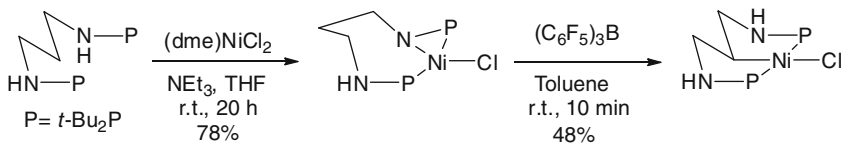


Fig. 37 Preparation of $(\text{PNC}_{\text{sp}^3}\text{NP}^{t\text{-Bu}})\text{NiCl}$

was shown to have comparable reactivities to $(\text{PCP}^{i\text{-Pr}})\text{NiMe}$ in Kumada-Corriu type C–C coupling reactions.

As with their $\text{PC}_{\text{sp}^3}\text{P}$ counterparts, an important feature of the $\text{POC}_{\text{sp}^3}\text{OP}^{i\text{-Pr}}$ ligand is its propensity to allow the preparation and isolation of fairly stable trivalent species. $(\text{POC}_{\text{sp}^3}\text{OP}^{i\text{-Pr}})\text{NiX}_2$ have thus been synthesized by mild oxidants such as CuBr_2 and CX_4 ($\text{X} = \text{Cl}, \text{Br}$; Fig. 36). Structures of these trivalent compounds are quite similar to those of their $\text{PC}_{\text{sp}^3}\text{P}^{i\text{-Pr}}$ analogues (*vide supra*), but $\text{POC}_{\text{sp}^3}\text{OP}^{i\text{-Pr}}$ species possess a greater thermal stability. $(\text{POC}_{\text{sp}^3}\text{OP}^{i\text{-Pr}})\text{NiCl}_2$, preformed or generated in-situ, can also promote the Kharasch addition of CCl_4 to alkenes such as styrene, 4-methylstyrene, methyl methacrylate, acrolein, methylacrylate, and acrylonitrile with 650–970 catalytic turnovers [79, 80]. Two important differences have been noted between the activities of trivalent complexes based on $\text{POC}_{\text{sp}^3}\text{OP}^{i\text{-Pr}}$ and NCN ligands. First, Kharasch addition reactions promoted by $\text{POC}_{\text{sp}^3}\text{OP}^{i\text{-Pr}}$ systems require refluxing in acetonitrile for 24 h, whereas van Koten's NCN systems are active at room temperature (*vide supra*). On the other hand, radical addition reactions proceed with preformed $(\text{POC}_{\text{sp}^3}\text{OP}^{i\text{-Pr}})\text{NiCl}_2$ but not with the analogous NCN -based trivalent species. The latter difference likely originates from the higher temperatures at which the trivalent $\text{POC}_{\text{sp}^3}\text{OP}^{i\text{-Pr}}$ complexes operate, since these species are prone to unimolecular decomposition to divalent species at high temperatures.

4.4 $\text{PNC}_{\text{sp}^3}\text{NP}$ Complexes

The first, and so far only, authentic $(\text{PNCNP})\text{Ni}$ complexes featuring an anionic, terdentate ligand is the complex $[\text{CH}\{(\text{CH}_2)_2\text{NHP}(t\text{-Bu})_2\}_2]\text{NiCl}$ reported very recently by Gwynne and Stephan [97]. These authors showed that metallation of $\text{PNC}_{\text{sp}^3}\text{HNP}^{t\text{-Bu}}$ is more facile with Pd than Ni: whereas this ligand undergoes

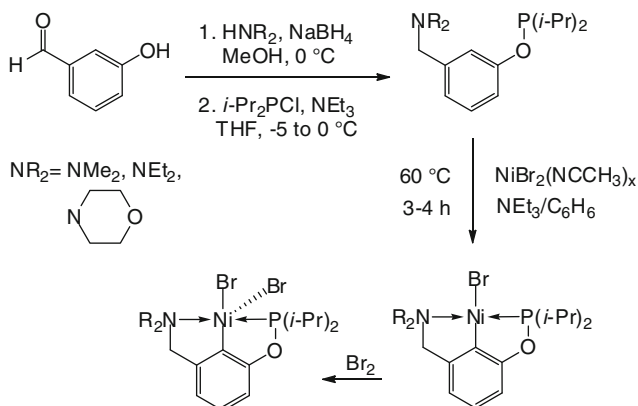


Fig. 38 Preparation of (POCN)NiBr and (POCN)NiBr₂

metallation with PdI₂ at r.t., the reaction with (dme)NiCl₂ at r.t. and in the presence of NEt₃ gave a purple solid arising from the activation of the N–H bond instead (Fig. 37). Subsequent reaction of this unusual species featuring a strained three-membered P–Ni–N metallacycle (Ni–P–N angle $\sim 58^\circ$) with the strong Lewis acid (C₆F₅)₃B furnished the desired (PNC_{sp3}NP^{*t*-Bu})NiCl in 48 % yield via a net transfer of proton from the central CH₂ moiety to the metallated N atom. The mechanistic details of this transformation remain obscure, but DFT studies seem to suggest that the C-metallated compound is more stable than the N-metallated analogue by ca. 10 kcal/mol. Structural characterization of (PNC_{sp3}NP^{*t*-Bu})NiCl has revealed a fairly large bite angle (P–Ni–P $\sim 168^\circ$); interestingly, the Ni–C and Ni–P distances are longer than those observed in the analogous (POC_{sp3}OP^{*i*-Pr})NiCl [80]. The reactivities or redox properties of this new pincer compound have not been reported.

5 POCN and PNCN Complexes

The recently developed PXCN (X = O, N) pincer-type ligands provide an unsymmetrical ligand framework combining the complementary properties of amines and phosphinites/phosphinimines such as hard/soft donor atoms and different σ -donor/ π -acceptor bonding tendencies. Thus, in comparison to PCP and POCOP systems, the amine moiety in PXCN complexes offers enhanced air-stability and greater choice of optically active precursors, while the presence of a P-moiety in these ligands preserves the important advantage of using ³¹P NMR to follow reactions and characterize complexes. Significantly, PXCN ligands also maintain the important advantage inherent to PCP and POCOP ligands of undergoing C–H nickellation, which greatly facilitates the synthesis of this family of complexes.

The first (POCN)Ni complexes were introduced by Spasyuk et al. in 2009. These ligands are accessible via a relatively simple two-step synthetic route and their nickellation proceeds at 60 °C over 3–4 h (Fig. 38) [98]. As was observed for the preparation of PCP and POCOP complexes, the judicious choice of nickel precursor and base is important for maximizing the yield of the desired pincer species. Most examples of (*i*-PrPOCN^R)NiBr examined to date are stable to ambient air, both in the solid state and in solution. Moreover, solid samples of these compounds are thermally stable above their melting points and can be sublimed under vacuum. Solid state characterization shows a fairly planar structure, consistent with the presence in the solution of a plane of symmetry incorporating the coordination plane and the aromatic ring. Consistent with the weaker trans influence of an amine moiety relative to a phosphinite donor, the Ni–P distances are shorter in POCN systems relative to their POCOP analogues (2.11 vs. 2.15–2.16 Å), whereas the Ni–N distances are longer in POCN complexes relative to their NCN analogues (ca. 2.05–2.07 vs. 1.97–1.99 Å). The Ni–C distances are similar in POCN and POCOP complexes (ca. 1.88–1.90 Å), but much shorter in their NCN analogues (ca. 1.81–1.83 Å), presumably reflecting the tighter binding of the NCN ligand.

Another major difference between (POCOP)NiBr and (POCN)NiBr is that the latter are easier to oxidize electrochemically and give access to isolable trivalent species (Fig. 38), making these the only pincer-type *aromatic* ligands other than NCN to allow isolation of trivalent species. Single-crystal X-ray diffraction studies have revealed that (POCN)NiBr₂ adopt structures similar to the above-discussed (POC_{sp3}OP^{*i*-Pr})NiBr₂ and (PC_{sp3}P^{*i*-Pr})NiBr₂ with elongated Ni–Br_{apical} distances (2.43–2.46 vs. 2.37 Å) [98]. That the unpaired electron resides in primarily Ni-based molecular orbitals (a hybrid of d_z² and p_z orbitals) was confirmed by EPR spectra, which displayed a nearly axial *g*-tensor with strong hyperfine coupling to the Br nucleus on the *g*_{zz} component. In addition, a number of small, partially resolved hyperfine splittings were observed due to coupling by the phosphorus (spin 1/2), nitrogen (spin 1), and/or in-plane Br nuclei (spin 3/2).

It is noteworthy that (POCN)NiBr₂ are fairly robust both in the solid state and in solution, and that thermal stability of these complexes appears to be greater in systems bearing less bulky amine moieties. Thus, solid state samples of the morpholinyl and NMe₂ analogues can be heated up to 160 °C without significant decomposition, whereas the NEt₂ derivative decomposes above 60–70 °C; similarly, the solutions of the latter display a *t*_{1/2} of ~20 min at 30 °C, whereas the morpholinyl and NMe₂ analogues showed half-lives of 3–4 h at 70 °C. The less bulky complexes are also more active in the Kharasch addition of CCl₄ to styrene [98].

Spasyuk et al. have also introduced a (POCN)NiBr complex featuring a secondary amine moiety that allows the preparation of new derivatives, including a rare dimeric system that has shown interesting reactivities [99]. Deprotonation of the N–H moiety of (*i*-PrPOCN^H)NiBr results in formation of a dimeric species that adopts an overall butterfly-like structure consisting of two T-shaped (POCN)Ni halves that are rotated with respect to each other by about 70 °C (Fig. 39). These two halves are connected to each other by two Ni–N linkages and form a central Ni₂N₂ core. The cyclobutane-like conformation of this Ni₂N₂ core places the

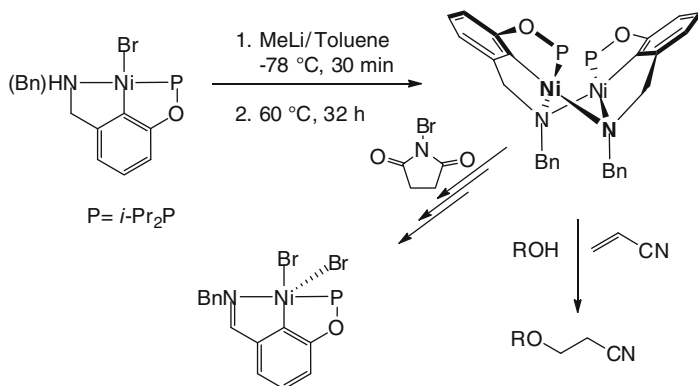


Fig. 39 Preparation and reactivities of $\{(\mu^N\text{-POCN})\text{Ni}\}_2$

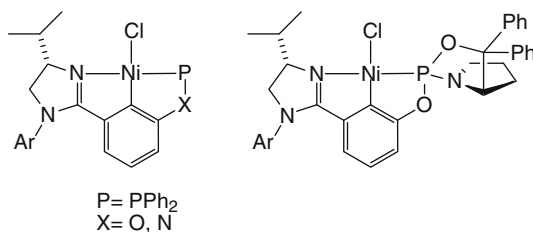


Fig. 40 Preparation of optically active $(\text{POCN})\text{NiCl}$ and $(\text{PNCN})\text{NiCl}$

N-substituents *syn* to each other and the Ni centers within covalent bonding distance. This dimeric species has proven to be an efficient catalyst for the alcoholysis of acrylonitrile, giving the anti-Markovnikov (linear) product with up to 2,000 catalytic turnovers; nonbulky alcohols possessing an acidic O–H moiety showed the highest activities.

The dimeric species also displays interesting redox properties [100]. Cyclic voltammetry measurements have shown that the dimer undergoes a reversible one-electron oxidation, and DFT analyses have concluded that most of the spin density in the putative radical cation is localized on one of the two Ni centers, creating a mixed-valent species. Chemical oxidation of the dimer using NBS led to the formation of divalent and trivalent monomeric complexes featuring a new imine-type POCN ligand; the direct preparation and characterization of these new species was undertaken as part of a study to investigate the mechanism of the oxidation process. The solid state structures of these new POCN–imine complexes are quite similar to those of their POCN–amine homologues, but the sp^2 -hybridized nitrogen atom of the imine moiety forms somewhat shorter Ni–N bonds [100].

The first optically active POCN-type pincer complexes of nickel were reported by Song, Gong, and coworkers in 2010 (Fig. 40) [101]. One ligand precursor featuring an imidazolinyli moiety was prepared in four steps and subjected to a

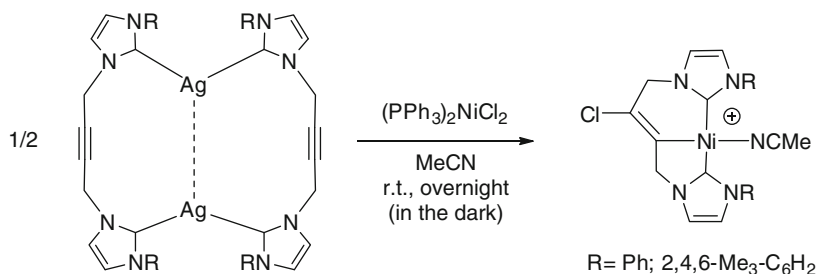


Fig. 41 Preparation of a $(\hat{\text{C}}\hat{\text{C}}\hat{\text{C}})\text{Ni}$ complex

one-pot phosphorylation/nickellation step to give the target (POCN)NiCl as air- and moisture-stable yellow solids in 41 % yield. The PNCN analogue of this complex was prepared in 30 % yield from 3-(2'-imidazolyl)aniline (Fig. 40) [102]. Unfortunately, the POCN complex showed no activity in the promotion of Suzuki coupling, whereas the PNCN complex promoted the hydrophosphination of chalcone with about nine catalytic turnover but no chiral induction.

A different POCN ligand precursor has also been prepared by reacting the optically active amino alcohol (S)-diphenyl(pyrrolidin-2-yl)-methanol with PCl_3 , followed by the one-pot reaction of this chiral-at-P intermediate with an imidazolyl-containing *m*-phenol derivative and NiCl_2 to give 20 % yield of the first POCN-type nickel complex featuring a P-stereogenic center (Fig. 40) [103]. Single crystal X-ray diffraction studies of this complex established the absolute configuration of the N and P centers. This complex promotes the allylation of a sulfonimine in low yields and with no chiral induction.

6 SCS and $\hat{\text{C}}\hat{\text{C}}\hat{\text{C}}$ Complexes

The first, and so far only, nickel complex featuring an anionic terdentate SCS-type pincer ligand was reported by Gebink, van Koten, and coworkers [104]. The complex $(\text{SCS}^{\text{Me}})\text{NiBr}$ was prepared in 72 % yield as an air-stable yellow solid by oxidative addition of SCBrS^{Me} to $\text{Ni}(\text{COD})_2$ at -80 °C. Interestingly, this complex does not undergo reversible oxidation as do its NCN and PCP analogues, presumably because the sulfur moieties are prone to oxidative decomposition. The solid state structure of $(\text{SCS}^{\text{Me}})\text{NiBr}$ has revealed that it adopts a *rac* conformation with the two *S*-Me groups positioned on opposite sides of the coordination plane. The Ni–C distance is similar to the corresponding distance in PCP systems (ca. 1.90 Å) and somewhat longer than that in NCN complexes (1.81–1.83 Å). Variable temperature solution NMR studies have revealed a fluxional process involving ring puckering inversion. The chemistry of $(\text{SCS}^{\text{Me}})\text{Ni}$ complexes remains unexplored.

The first, and so far only, nickel complexes featuring an anionic terdentate ECE-type pincer ligand based on NHC carbene donor moieties were reported by Chen's

group in 2009 [105]. The cationic complexes $[(\hat{C}CC^R)Ni(NCMe)]^+$ (\hat{C} represents an NHC carbene moiety) were prepared by reacting $(PPh_3)_2NiCl_2$ with the Ag adduct of the precursor ligand, a bidentate ligand featuring two NHC carbene moieties bridged by a 2-butyndiyl linker (Fig. 41). The unprecedented chloronickellation of the alkyne moiety generates the $(\hat{C}CC^R)Ni$ product, the first example of a pincer-type Ni obtained via a route other than salt metathesis or C–X metallation ($X = H$, halogen). $\hat{C}CC$ -type complexes of other metals have also been reported recently [106–108].

The main NMR features of these complexes include the characteristic ^{13}C NMR signals for the carbene carbon nuclei (ca. 170 ppm) and the two nonaromatic sp^2 carbons CCl (ca. 140 ppm) and CNi (ca. 115 ppm). The solid state structures of these complexes show that the three carbon atoms of the $\hat{C}CC$ ligand lie in the coordination plane, while the acetonitrile moiety is pushed out of this plane by the bulky carbene substituents. The 5-membered metallacycle is fairly planar while the 6-membered ring (which contains the $C=C$ moiety) adopts a boat conformation; the three Ni–C distances are about 1.90 Å and the C–Ni–C trans angle is about 164–170°. These new pincer complexes are excellent catalysts for coupling Ar–Cl and Ar'MgBr (0.5 % loading of Ni, room temperature reactions).

7 Conclusions and Perspectives

The literature survey presented in this chapter reveals that the chemistry of pincer-type (ECE)Ni complexes is experiencing a resurgence that should lead to exciting developments over the next decade. As was pointed out throughout the discussion above, the family of NCN complexes has been at the forefront of this area of organonickel chemistry for the past 3 decades. The relative maturity of the chemistry of (NCN)Ni complexes is undoubtedly owing to the pioneering studies and sustained efforts of van Koten's group, but the past few years have witnessed the emergence on the scene of a number of new research groups that promise to expand the frontiers of this area in new directions. A similar scenario is at play in other families of (ECE)Ni complexes. For example, after being fairly dormant for nearly 2 decades, the chemistry of PCP complexes is being pursued by a growing number of research groups that are re-examining the chemistry of complexes pioneered by Shaw's group, introducing new complexes based on new ligand frameworks and exploring their reactivities. The related family of POCOP complexes has grown even more rapidly since its introduction barely 5–6 years ago, and new catalytic transformations are being developed based on these complexes. The chemistry of recently introduced PNCNP, POCN, PNCN, SCS, and $\hat{C}CC$ complexes is less-developed, but these compounds are poised to make major contributions to the chemistry of pincer-type nickel complexes.

While it is generally true that predicting future developments in scientific research is an exercise of questionable value, it is nevertheless interesting to try to identify the likely direction of future developments in the area of pincer-type nickel chemistry.

Regarding NCN complexes, for example, the reactivities of trivalent complexes will likely be a fertile area of growth, as it has been over the past. An important development would be the expansion of the radical chemistry promoted by open-shell (NCN)Ni(III) species to different types of C–C coupling reactions, including olefin oligomerization/polymerization chemistry and cyclization reactions. It is also tempting to speculate that any development in this area should spill into the chemistry of trivalent compounds featuring POCN, PC_{sp3}P, and POC_{sp3}OP ligands. Related developments are also anticipated in the family of diamagnetic-at-Ni complexes featuring unpaired electrons residing on an auxiliary ligand.

The very recently reported reactivities of (PCP)NiH and (POCOP)NiH complexes augur well for significant future developments. Initial observations indicate that insertion chemistry with unsaturated substrates such as CO₂, aldehydes, ketones, imines, nitriles, etc. should lead to interesting discoveries and applications, whereas new reactivities in the area of C–H activation cannot be ruled out. The related hydrocarbyl derivatives (PCP)NiR and (POCOP)NiR have shown interesting C–C coupling reactivities with aryl and alkyl halides; studies aimed at elucidating the mechanistic details of these reactions (e.g., establishing whether these coupling reactions follow a constant-oxidation-state path or proceed via fleeting Ni(IV) intermediates) should open the way for more efficient and sophisticated applications. Similarly, developments in delineating the mechanistic features of Michael addition reactions promoted by cationic complexes (e.g., [(NCN)NiL]⁺ or [(POCOP)NiL]⁺) and alcoholysis of olefins catalyzed by (POCOP)Ni(OR) or {(μ^N-POCN)Ni}₂ should lead to new reaction pathways and useful applications.

The above developments are fairly easy to anticipate on the basis of recent observations, but it is harder to envisage new developments in areas that have seen little or no activity. For instance, the above-discussed proposal by the Morales-Morales group regarding the involvement of monovalent species generated in-situ from (POCOP)NiX/Zn has the potential to open up a new horizon in the reactivities of pincer-type nickel complexes. It remains to be seen, however, whether well-defined monovalent species will be isolable and amenable to reactivity studies. An even more intriguing possibility is the development of synthetic routes to tetravalent species, which would promise exciting developments paralleling the more developed chemistry of high oxidation state Pt and Pd complexes. Based on their respective oxidation potentials, the best candidates for tetravalent species should be complexes of NCN or PC_{sp3}P pincer ligands.

The potential developments outlined above should make the chemistry of (ECE)Ni pincer complexes an exciting field of research over the next decade.

Acknowledgments The authors wish to thank the Natural Sciences and Engineering Research Council of Canada for financial support of our studies on pincer complexes of nickel. We recognize gratefully all those collaborators who have helped us in our studies, including those whose unpublished results are cited in this review, as well as those pioneers of pincer chemistry whose discoveries have inspired our own work.

References

1. Moutlon CJ, Shaw BL (1976) Transition metal–carbon bonds. Part XLII. Complexes of nickel, palladium, platinum, rhodium and iridium with the tridentate ligand 2,6-bis[(di-*t*-butylphosphino)methyl]phenyl. *Dalton Trans* 1020–1024
2. van Koten G, Jastrzebski JTBH, Noltes JG, Spek AL, Schoone JC (1978) Triorganotin cations stabilized by intramolecular Sn–N coordination; synthesis and characterization of {C, N, N′-2,6-bis[(dimethylamino)methyl]phenyl}diorganotin bromides. *J Organomet Chem* 148:233–245
3. van Koten G, Timmer K, Noltes JG, Spek AL (1978) A novel type of Pt–C interaction and a model for the final stage in reductive elimination processes involving C–C coupling at Pt; synthesis and molecular geometry of [1, N, N′-q-2,6-bis((dimethylamino)methyl)-toluene]iodoplatinum(II)Tetrafluoroborate. *J Chem Soc Chem Commun* 250–252
4. Fryzuk MD, Montgomery CD (1989) Amides of the platinum group metal. *Coord Chem Rev* 95:1–40
5. Adhikari D, Huffman JC, Mindiola DJ (2007) Structural elucidation of a nickel boryl complex. A recyclable borylation Ni(II) reagent of bromobenzene. *Chem Commun* 4489–4491
6. Ozerov OV, Guo C, Fan L, Foxman BM (2004) Oxidative addition of N–C and N–H bonds to zerovalent nickel, palladium, and platinum. *Organometallics* 23:5573–5580
7. Csok Z, Vechorkin O, Harkins SB, Scopelliti R, Hu X (2008) Nickel complexes of a pincer NN₂ ligand: multiple carbon–chloride activation of CH₂Cl₂ and CHCl₃ leads to selective carbon–carbon bond formation. *J Am Chem Soc* 130:8156–8157
8. Ingleson MJ, Fullmer BC, Buschhorn DT, Fan H, Pink M, Huffman JC, Caulton KG (2008) Influence of the d-electron count on CO binding by three-coordinate [(^tBu₂PCH₂SiMe₂)₂N]Fe, -Co, and -Ni. *Inorg Chem* 47:407–409
9. Liang L-C, Chien P-S, Huang Y-L (2006) Intermolecular arene C–H activation by nickel(II). *J Am Chem Soc* 128:15562–15563
10. Mitton SJ, McDonald R, Turculet L (2009) Nickel and palladium silyl pincer complexes: unusual structural rearrangements that involve reversible Si–C(sp³) and Si–C(sp²) bond activation. *Angew Chem* 121:8720–8723
11. Rozenel S, Kerr JB, Arnold J (2011) Metal complexes of Co, Ni and Cu with the pincer ligand HN(CH₂CH₂PⁱPr₂)₂: preparation, characterization and electrochemistry. *Dalton Trans* 40:10397–10405
12. van Koten G (1989) Tuning the reactivity of metals held in a rigid ligand environment. *Pure Appl Chem* 61:1681–1694
13. Gusev DG, Lough AJ (2002) Experimental and computational study of pincer complexes of ruthenium with Py, CO, and N₂ ligands. *Organometallics* 21:5091–5099
14. Rimml H, Venanzi LM (1983) The facile cyclometallation reaction of 1,3-bis[(diphenylphosphino)methyl]benzene. *J Organomet Chem* 259:C6–C7
15. Johnson MT, Wendt OF (2011) Synthesis, characterisation and crystal structure of a novel nickel(II) phosphine complex, trans-[Ni₂Cl₄{cis-(Cy₂PCH₂)₂C₆H₄}]₂. *Inorganica Chim Acta* 367:222–224
16. Rimml H, Venanzi LM (1984) A stable binuclear complex containing Pd–H–Pd bonds. *J Organomet Chem* 260:C52–C54
17. Kennedy AR, Cross RJ, Muir KW (1995) Preparation and crystal structure of *trans*-[NiBr{C₆H₃-2,6-(CH₂PCy₂)₂}]₂. *Inorganica Chim Acta* 231:195–200
18. Huck WTS, Snellink-Ruël B, van Veggel FCJM, Reinhoudt DN (1997) New building blocks for the noncovalent assembly of *homo*- and *hetero*-multinuclear metallodendrimers. *Organometallics* 16:4287–4291
19. Bachechi F (2003) X-ray structural analysis of Ni^{II}, Pd^{II}, and Pt^{II} complexes with the potentially tridentate ligand 1,3-bis(diphenylphosphinomethyl)-benzene, 1,3-C₆H₄(CH₂PPh₂)₂. *Struct Chem* 14:263–269

20. Kozhanov KA, Bubnov MP, Cherkasov VK, Abakumov GA (2006) EPR study of spin-labeled nickel NCN-pincer complexes. *Dokl Chem* 407:35–38
21. Kozhanov KA, Bubnov MP, Cherkasov VK, Fukin GK, Abakumov GA (2004) *Dalton Trans* 2957–2962
22. Kozhanov KA, Bubnov MP, Vavilina NN, Efremova LY, Fukin GK, Cherkasov VK, Abakumov GA (2009) *Polyhedron* 28:2555–2558
23. Starikov AG, Minyaev RM, Kozhanov KA, Bubnov MP, Cherkasov VK, Abakumov GA (2010) *Russ Chem Bull Int Ed* 59:1110–1115
24. Kozhanov KA, Bubnov MP, Cherkasov VK, Vavilina NN, Efremova LY, Artyushin OI, Odinet IL, Abakumov GA (2008) *Dalton Trans* 2849–2853
25. Kozhanov KA, Bubnov MP, Cherkasov VK, Fukin GK, Abakumov GA (2003) *Chem Commun* 2610–2611
26. Cámpora J, Palma P, del Río D, Álvarez E (2004) *Organometallics* 23:1652–1655
27. Cámpora J, Palma P, del Río D, Conejo MM, Álvarez E (2004) *Organometallics* 23:5653–5655
28. Castonguay A, Beauchamp AL, Zargarian D (2008) *Organometallics* 27:5723–5732
29. Boro BJ, Duesler EN, Goldberg KI, Kemp RA (2009) *Inorg Chem* 48:5081–5087
30. Boro BJ, Dickie DA, Goldberg KI, Kemp RA (2008) *Acta Cryst E* E64:m1304
31. Boro BJ, Dickie DA, Duesler EN, Goldberg KI, Kemp RA (2008) *Acta Cryst E* E64:m1402
32. Groux LF, Bélanger-Gariépy F, Zargarian D (2005) *Can J Chem* 83:634–639
33. Smith RC, Protasiewicz JD (2004) *Organometallics* 23:4215–4222
34. Ma L, Wobser SD, Protasiewicz JD (2007) *J Organomet Chem* 692:5331–5338
35. Ma L, Imbesi PM, Updegraff JB III, Hunter AD, Protasiewicz JD (2007) *Inorg Chem* 46:5220–5228
36. Lipke MC, Woloszynek RA, Ma L, Protasiewicz JD (2009) *Organometallics* 28:188–196
37. Schmeier TJ, Hazari N, Incarvitoa CD, Raskatovb JA (2011) *Chem Commun* 47:1824–1826
38. Levina VA, Rossin A, Belkova NV, Chierotti MR, Epstein LM, Filippov OA, Gobetto R, Gonsalvi L, Lledós A, Shubina ES, Zanobini F, Peruzzini M (2011) *Angew Chem Int Ed* 50:1367–1370
39. Rossin A, Peruzzini M, Zanobini F (2011) *Dalton Trans* 40:4447–4452
40. van der Boom ME, Liou S-Y, Shimon LJW, Ben-David Y, Milstein D (2004) *Inorganica Chim Acta* 357:4015–4023
41. Castonguay A, Sui-Seng C, Zargarian D, Beauchamp AL (2006) *Organometallics* 25:602–608
42. Ess DH, Brigham Young University, Unpublished results communicated privately
43. Castonguay A, Charbonneau F, Beauchamp AL, Zargarian D (2005) {2,6-Bis [(dimethylamino)methyl]phenyl-κ2-N, C1, N'}-chloronickel(II). *Acta Cryst E* E61: m2240–m2241
44. Castonguay A, Beauchamp AL, Zargarian D (2009) *Inorg Chem* 48:3177–3184
45. Castonguay A, Spasyuk DM, Madern N, Beauchamp AL, Zargarian D (2009) *Organometallics* 28:2134–2141
46. Albrecht M, van Koten G (2001) Platinum group organometallics based on pincer complexes: sensors, switches, and catalysts. *Angew Chem Int Ed* 40:3750–3781
47. Frey M (2002) Hydrogenases: hydrogen-activating enzymes. *ChemBioChem* 3:153–160
48. Grove DM, van Koten G, Zoet R (1983) Unique stable organometallic nickel(III) complexes: syntheses and the molecular structure of Ni[C6H3(CH2NMe2)-o, o']12. *J Am Chem Soc* 105:1379–1380
49. Grove DM, van Koten G, Ubbels HJC, Zoet R (1984) Organonickel(II) complexes of the terdentate monoanionic ligand o, o'-bis[(dimethylamino)methyl]phenyl(N-C-N). Syntheses and the X-ray crystal structure of the stable nickel(II) formate [Ni(N-C-N)O2CH]. *Organometallics* 3:1003–1009

50. Steenwinkel P, Gossage RA, van Koten G (1998) Recent findings in cyclometallation of *meta*-substituted aryl ligands by platinum group metal complexes by C_{Ar}Yl-R bond activation (R=H, CR₃, SiR₃). *Chem Eur J* 4:759–762
51. Pandarus V, Castonguay A, Zargarian D (2008) Ni(II) complexes featuring non-metallated pincer-type ligands. *Dalton Trans* 4756–4761
52. Fossey JS, Richards CJ (2004) Synthesis and X-ray crystal structure analysis of the first nickel bisoxazoline pincer complex. *J Organomet Chem* 689:3056–3059
53. Mitsudo K, Imura T, Yamaguchi T, Tanaka H (2008) Preparation of a cationic bisoxazolinic nickel pincer catalyst and its applications to Michael addition and Mizoroki-Heck reaction. *Tetrahedron Lett* 49:7287–7289
54. Contel M, Stol M, Casado MA, van Klink GPM, Ellis DD, Spek AL, van Koten G (2002) A bis(*ortho*-amine)aryl-gold(I) compound as an efficient, nontoxic, arylating reagent. *Organometallics* 21:4556–4559
55. Grove DM, van Koten G, Mul P, Zoet R, van der Linden JGM, Legters J, Schmitz JEJ, Murrall NW, Welch AJ (1988) Syntheses and characterization of unique organometallic nickel(III) aryl species. ESR and electrochemical studies and the X-ray molecular study of square-pyramidal [Ni{C₆H₃(CH₂NMe₂)₂-o, o'}I₂]. *Inorg Chem* 27:2466–2473
56. Grove DM, van Koten G, Mul WP, van der Zeijden AH, Terheijden J (1986) Arylnickel(III) species containing NO₃, NO₂, and NCS ligands. ESR data and the X-ray crystal structure of hexacoordinate (pyridine)bis(isothiocyanato)-[o, o'-bis{(dimethylamino)methyl}phenyl]nickel(III). *Organometallics* 5:322–326
57. Kozhanov KA, Bubnov MP (2006) EPR study of spin-labeled nickel NCN-pincer complexes. *Dokl Akad Nauk* 407:49–52
58. Kozhanov KA, Bubnov MP, Cherkasov VK, Fukin GK, Vavilina NN, Efremova LY, Abakumov GA (2009) First structurally characterized mixed-halogen nickel(III) NCN-pincer complex. *J Magn Res* 197:36–39
59. Grove DM, van Koten G, Verschuuren AHM (1988) New homogeneous catalysts in the addition of polyhalogenoalkanes to olefins; organonickel(II) complexes [Ni{C₆H₃(CH₂NMe₂)₂-o, o'}X] (X=Cl, Br, I). *J Mol Catal* 45:169–174
60. Grove DM, Verschuuren AHM, van Koten G (1989) The homogeneously catalysed addition reaction of polyhalogenoalkanes to olefins by divalent arylnickel complexes: comparative reactivity and some important mechanistic leads. *J Organomet Chem* 372:C1–C6
61. Sasson Y, Rempel GL (1975) Selective transfer hydrogenolysis of 1,1,1,3-tetrachloro to 1,1,3-trichloro compounds. *Synthesis* 448–450
62. Tsujii J, Sato K, Nagashima H (1981) Activation of polyhaloalkanes by palladium catalyst. Facile addition of polyhaloalkanes to olefins. *Chem Lett* 1169–1170
63. van de Kuil LA, Grove DM, Gossage RA, Zwikker JW, Jenneskens LW, Drenth W, van Koten G (1997) Mechanistic aspects of the Kharasch addition reaction catalyzed by organonickel(II) complexes containing the monoanionic terdentate arylidiamine ligand system [C₆H₂(CH₂NMe₂)₂-2,6-R-4]. *Organometallics* 16:4985–4994
64. van de Kuil LA, Veldhuizen YSJ, Grove DM, Zwikker JW, Jenneskens LW, Drenth W, Smeets WJJ, Spek AL, van Koten G (1994) Organonickel(II) complexes containing aryl ligands with chiral pyrrolidinyl ring systems; syntheses and use as homogeneous catalysts for the Kharasch addition reaction. *Recl Trav Chim Pays-Bas* 113:267–277
65. Granel C, Dubois Ph, Jérôme R, Teyssié Ph (1996) Controlled radical polymerization of methacrylic monomers in the presence of a bis(*ortho*-chelated) arylnickel(II) complex and different activated alkyl halides. *Macromolecules* 29:8576–8582
66. Knapen JWJ, van der Made AW, de Wilde JC, van Leeuwen PWNM, Wijkens P, Grove DM, van Koten G (1994) Homogeneous catalysts based on silane dendrimers functionalized with arylnickel(II) complexes. *Nature* 372:659–663
67. Gossage RA, Jastrzebski TBH, van Ameijde J, Mulders SJE, Brouwer AJ, Liskamp RMJ, van Koten G (1999) Synthesis and catalytic application of amino acid based dendritic macromolecules. *Tetrahedron Lett* 40:1413–1416

68. Kleij AW, Gossage RA, Klein Gebbink RJM, Brinkmann N, Reijerse EJ, Kragl U, Lutz M, Spek AL, van Koten G (2000) A “dendritic effect” in homogeneous catalysis with carbosilane-supported arylnickel(II) catalysts: observation of active-site proximity effects in atom-transfer radical addition. *J Am Chem Soc* 122:12112–12124
69. Pathmamanoharan C, Wijkens P, Grove DM, Philipse AP (1996) Paramagnetic silica particles: synthesis and grafting of a silane coupling agent containing nickel ions onto colloidal silica particles. *Langmuir* 12:4372–4377
70. van de Kuil LA, Grove DM, Zwikker JW, Jenneskens LW, Drenth W, van Koten G (1994) New soluble polysiloxane polymers containing a pendant terdentate aryldiamine ligand substituent holding a highly catalytically active organometallic nickel(II) center. *Chem Mater* 6:1675–1683
71. Stol M, Snelders DJM, Godbole MD, Havenith RWA, Haddleton D, Clarkson G, Lutz M, Spek AL, van Klink GPM, van Koten G (2007) 2,6-Bis(oxazolonyl)phenylnickel(II) bromide and 2,6-bis(ketimine)phenylnickel(II) bromide: synthesis, structural features, and redox properties. *Organometallics* 26:3985–3994
72. Bugarin A, Connell BT (2008) Chiral nickel(II) and palladium(II) NCN-pincer complexes based on substituted benzene: synthesis, structure, and lewis acidity. *Organometallics* 27:4357–4369
73. Lee DH, Sungwon JH, Park S (2008) Bis(imino)aryl complex of nickel(II): N, C, N-pincer type complex, (2,6-(2,6-Et₂PhN=CH)2C₆H₃)NiBr. *Bull Korean Chem Soc* 29:187–190
74. Hurtado J, Ibanez A, Rojas R, Valderrama M, Fröhlich R (2011) Organonickel(II) complexes with anionic tridentate 1,3-bis(azolylmethyl)phenyl ligands. synthesis, structural characterization and catalytic behavior. *J Braz Chem Soc* 22:1750–1757
75. Shao D-D, Niu J-L, Hao X-Q, Gong J-F, Song M-P (2011) Neutral and cationic chiral NCN pincer nickel(II) complexes with 1,3-bis(2'-imidazolonyl)benzenes: synthesis and characterization. *Dalton Trans* 40:9012–9013
76. Morales-Morales D, Grause C, Kasaoka K, Redón R, Cramer RE, Jensen CM (2000) *Inorg Chim Acta* 300–302:958–963
77. Bedford RB, Draper SM, Scully PN, Welch SL (2000) *New J Chem* 24:745–747
78. Gómez-Benítez V, Baldovino-Pantaleón O, Herrera-Álvarez C, Toscano RA, Morales-Morales D (2006) *Tetrahedron Lett* 47:5059–5062
79. Pandarus V, Zargarian D (2007) *Chem Commun* 978–980
80. Pandarus V, Zargarian D (2007) *Organometallics* 26:4321–4334
81. Spasyuk D M, Sakhi HG, Zargarian D, unpublished results
82. Salah A, Zargarian D (2011) *Dalton Trans* 40:8977–8985
83. Chakraborty S, Krause JA, Guan H (2009) *Organometallics* 28:582–586
84. Zhang J, Medley CM, Krause JA, Guan H (2010) *Organometallics* 29:6393–6401
85. Chakraborty S, Patel YJ, Krause JA, Guan H (2011) *Polyhedron* doi:10.1016/j.poly.2011.04.030
86. Lefèvre X, Spasyuk DM, Zargarian D (2011) *J Organomet Chem* 696:864–870
87. Salah A, Offenstein C, Zargarian D (2011) *Organometallics* 30:5352–5364
88. Chakraborty S, Zhang J, Krause JA, Guan H (2010) *J Am Chem Soc* 132:8872–8873
89. Spasyuk DM, Salhi N-L, Zargarian D (unpublished results)
90. Tsou TT, Kochi JK (1979) *J Am Chem Soc* 101:7547–7560
91. Lefèvre X, Durieux G, Lesturgez S, Zargarian D (2011) *J Mol Catal A Chem* 335:1–7
92. Xu G, Li X, Sun H (2011) *J Organomet Chem* 696:3011–3014
93. Huang F, Zhang C, Jiang J, Wang Z-X, Guan H (2011) *Inorg Chem* 50:3816–3825
94. Al-Salem NA, Empsall HD, Markham R, Shaw BL, Weeks B (1979) *J Chem Soc Dalton Trans* 1972–1982
95. Al-Salem NA, McDonald WS, Markham R, Norton MC, Shaw BL (1980) *J Chem Soc Dalton Trans* 59–63
96. Crocker C, Errington JR, Markham R, Moulton CJ, Odel KJ, Shaw BL (1980) *J Am Chem Soc* 102:4373–4379

97. Gwynne EA, Stephan DW (2011) Nickel(II) and palladium(II) bis-aminophosphine pincer complexes. *Organometallics* 30:4128–4135
98. Spasyuk DM, Zargarian D, van der Est A (2009) *Organometallics* 28:6531–6540
99. Spasyuk DM, Zargarian D (2010) *Inorg Chem* 49:6203–6213
100. Spasyuk DM, Gorelsky SI, van der Est A, Zargarian D (2011) *Inorg Chem* 50:2661–2674
101. Zhang B-S, Wang W, Shao D-D, Hao X-Q, Gong J-F, Song M-P (2010) *Organometallics* 29:2579–2587
102. Yang M-J, Liu Y-J, Gong J-F, Song M-P (2011) *Organometallics* 30:3793–3803
103. Niu J-L, Chen Q-T, Hao X-Q, Zhao Q-X, Gong J-F, Song M-P (2010) *Organometallics* 29:2148–2156
104. Kruihof CA, Dijkstra HP, Lutz M, Spek AL, Gebbink RJMK, van Koten G (2008) *Organometallics* 27:4928–4937
105. Liu A, Zhang X, Chen W (2009) *Organometallics* 28:4868–4871
106. Ebeling G, Meneghetti MR, Rominger F, Dupont J (2002) *Organometallics* 21:3221–3227
107. Consorti CS, Ebeling G, Flores FR, Rominger F, Dupont J (2004) *Adv Synth Catal* 346:617–624
108. Chianese AR, Mo A, Lampland NL, Swartz RL, Bremer PT (2010) *Organometallics* 29:3019–3026

The Chemistry of Pincer Complexes of 13–15 Main Group Elements

Roman Jambor and Libor Dostál

Abstract Recent achievements in the chemistry of selected group 13–15 elements containing pincer type coordinating ligands are summarized. This chapter covers chemistry of heavier elements Ga, In, Tl from the group 13; Ge, Sn, Pb—especially low valent compounds with formal oxidation state +II or +I and their reactivity from the group 14; and As, Sb, Bi from the group 15. Only the classical pincer type ligands containing nitrogen or oxygen atoms as in-built donor functionalities are considered, i.e., 2,6-(R₂NCH₂)₂C₆H₃ (**L**^{N1}), 2,6-(ArN=C(CH₃))₂C₆H₃ (**L**^{N2}), 2,6-(ROCH₂)C₆H₃ (**L**^{O1, 2}, R = Me, *t*-Bu), 2-(Me₂NCH₂)-6-(ROCH₂)C₆H₃ (**L**^{NO1,2}, R = Me, *t*-Bu), 2,6-((RO)₂P(O))₂-4-(*t*-Bu)C₆H₃ (**L**^{PO}). The influence of the present pincer ligands on the structures of the compounds as well as their key role in the stabilization of these compounds is discussed.

Keywords Main group metals · Pincer ligands · Reactivity · Structure

Contents

1	Introduction	176
2	Result and Discussion	176
2.1	Group 13: Ga, In, Tl	176
2.2	Group 14: Ge, Sn, Pb	178
2.3	Group 15: As, Sb, Bi	188
3	Conclusions and Outlook	196
	References	196

R. Jambor (✉) · L. Dostál (✉)

Faculty of Chemical Technology, Department of General and Inorganic Chemistry, University of Pardubice, Studentská 573, Pardubice 532 10, Czech Republic
e-mail: roman.jambor@upce.cz; libor.dostal@upce.cz

1 Introduction

The chemistry of pincer ligands and their organometallic derivatives belongs for more than 30 years to the most exciting and interesting areas of the chemical research in the field of organometallic chemistry. Since the first utilization of these ligands in late 1970s [1–3], the pincer chemistry has been developing to very rich branch of chemistry and the topic results have been often reviewed [4–6]. The main afford in the field has been devoted to the chemistry of transition metals and prepared compounds were found wide utilization in catalysis, material sciences, and various types of physical applications as well demonstrated by other chapter of this thematic issue of Topics on Organometallic Chemistry. On the contrary, related chemistry of main groups stood a bit in the background, although, for example, organotin(IV) compounds were studied directly at beginning of the pincer story in 1978 [7]. The situation has recently changed, when Cowley and others have started to prepare wide range of main group metal compounds and later on Jurkschat et al. reported syntheses of the first OCO pincer type ligand and its utilization in organotin and organosilicon chemistry. Since that time it seems that pincer chemistry of main group elements starts to retrieve and several noteworthy achievements were obtained.

This chapter is focused on recent progress in the pincer chemistry of heavier group 13–15 elements, i.e., Ga, In Tl from the group 13, Ge, Sn, Pb—especially low valent compound with formal oxidation state +II or +I from the group 14, and As, Sb, Bi from the group 15. Only the classical pincer ligands, which constitute from disubstituted phenyl rings, containing nitrogen or oxygen donor atoms are considered (Fig. 1). Related ligands containing other donor atoms such as P, S, etc. and ligands, which are called pincer ligands, but differ significantly from the former classical ligands by their structures are not covered and are beyond the scope of this chapter.

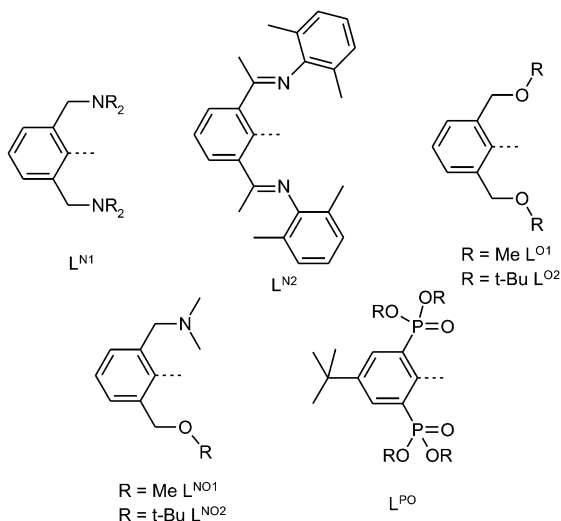
2 Result and Discussion

The result and discussion section is organized in such a way that the chemistry is discussed according to the central atom used and the authors try to encompass all results till spring 2011 with one exception of compounds containing tetravalent group 14 elements. This pincer chemistry is rather rich and has been already reviewed [8]. Thus, the part dealing with group 14 elements is devoted mainly to low valent compounds and their reactivity.

2.1 Group 13: Ga, In, Tl

Regarding the chemistry of the group 13 elements, it is strictly limited to the chemistry of NCN pincer ligand L^{N1} . Noteworthy, some organoaluminum(III)

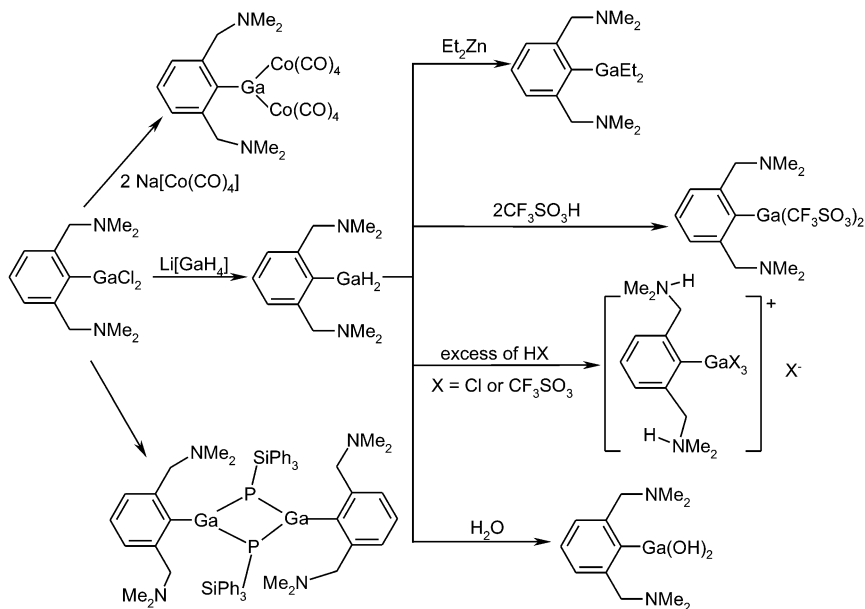
Fig. 1 Structures of pincer ligands considered in this chapter



compounds derivatives of $\text{L}^{\text{O}1,2}$ were prepared and characterized, but these are beyond scope of this text [9, 10].

The starting chloro-complexes of gallium and indium $\text{L}^{\text{N}1}\text{GaCl}_2$ a $\text{L}^{\text{N}1}\text{InCl}_2$ are easily prepared by conversion of starting lithium compound with gallium(III) and indium(III) chloride, respectively. The mixed chloro-alkyl-compounds may be obtained *via* the same reaction pathway with respective alkyl derivatives [11]. The chemistry of $\text{L}^{\text{N}1}\text{GaCl}_2$ a $\text{L}^{\text{N}1}\text{InCl}_2$ has been further studied. Thus, the reaction of $\text{L}^{\text{N}1}\text{GaCl}_2$ with $\text{Li}[\text{GaH}_4]$ produces expected gallane $\text{L}^{\text{N}1}\text{GaH}_2$, which display significant stability thanks to presence of the pincer ligand $\text{L}^{\text{N}1}$. Using of $\text{Li}[\text{GaH}_4]$ as a reagent is not casual, because using of aluminum analogue $\text{Li}[\text{AlH}_4]$ led to transmetalation under formation of $\text{L}^{\text{N}1}\text{AlH}_2$. Analogously, treatment of $\text{L}^{\text{N}1}\text{InCl}_2$ with $\text{Li}[\text{GaH}_4]$ gave only compound $\text{L}^{\text{N}1}\text{GaH}_2$. Reactivity of the gallane $\text{L}^{\text{N}1}\text{GaH}_2$ with various reagents including Et_2Zn and acids was further investigated according to the Scheme 1 [12]. Furthermore reaction of $\text{L}^{\text{N}1}\text{GaCl}_2$ with sodium azide yielded $\text{L}^{\text{N}1}\text{Ga}(\text{N}_3)_2$, which was studied as a potential precursor of production of GaN [13].

Reaction of $\text{L}^{\text{N}1}\text{GaCl}_2$ and $\text{L}^{\text{N}1}\text{InCl}_2$ with $\text{Na}[\text{Co}(\text{CO})_4]$ led to formation of interesting bimetallic compounds with two Ga–Co and In–Co bonds [14]. Similarly interesting is preparation of four membered Ga_2P_2 ring system, in which the gallium atoms are stabilized by the pincer ligand $\text{L}^{\text{N}1}$ [15]. Regarding the indium chemistry, compound 9,10-dihydro-9,10-bis[2,6-bis-((dimethylamino)methyl)phenyl]-9,10-diindaanthracene with the first six-membered diindacycle In_2C_4 was prepared by the reaction of $\text{L}^{\text{N}1}\text{InCl}_2$ with *o*-phenylmagnesium, characterized in the solid state and indium atoms are again supported by the ligand $\text{L}^{\text{N}1}$ [16]. Finally, partial reduction of $\text{L}^{\text{N}1}\text{InCl}_2$ allowed isolation of the compound $\text{L}^{\text{N}1}\text{In}(\text{Cl})\text{-In}(\text{Cl})\text{L}^{\text{N}1}$, which contains In–In bond and indium atoms have unusual oxidation state II^+ [17].



Scheme 1 Reactivity of NCN chelated gallium(III) compounds

Compound $L^{N^1}TiBrCl$ represents the only example of pincer thallium compound with the pincer ligand L^{N^1} , which was prepared and characterized to this moment [18].

2.2 Group 14: Ge, Sn, Pb

As mentioned earlier, the chemistry of 14 group elements in the oxidation state +IV is intensively studied and behind several articles, there are also reviews dealing with this topic [8, 19–22]. The organotin(IV) compounds containing NCN-chelating ligand L^{N^1} were most probably the first main group metal complexes bearing pincer type ligand and they are investigated so far. While group of Corriu used the same ligand in the organosilicon(IV) chemistry [23–30], examples of NCN-ligand containing organogermanium(IV) complexes are practically unknown [31]. Furthermore, the influence of Y,C,Y-pincer ligands on the reactivity and coordination arrangement of central tin atom in organotin(IV) compounds has been shown. For these reasons, the following paragraphs will be mainly focused on low valent compounds of 14 group heavier elements containing YCY-ligands.

There are several methods used for the preparation of low valent compounds of 14 group elements providing hundreds of compounds. Most of these compounds are, however, so-called homoleptic metallylenes of type R_2M with different

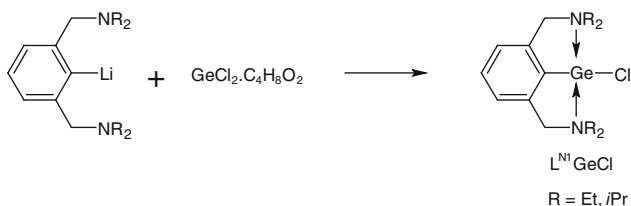
sterically demanding organic substituents and polar groups R (R = alkyl, aryl, alkoxide, amide) [32–42]. Even the introduction of the so-called *built-in* ligands containing one side chain substituent with nitrogen [43–47] or oxygen [48–50] donor atom provides similar homoleptic metallylenes R_2M . From this point of view, the stabilization of halometallylenes as precursors for the synthesis of many functionalized metallylenes is of particular utility. Their preparation can be, however, rather problematic in itself. The utilization of M(II) center by sterically demanding terphenyl ligands or Cp-based ligands allowed the synthesis of halometallylenes and stabilized metal–halogen bond [51–57]. In 1989, the report by Prof. van Koten on the synthesis of organostannylene $L^{N1}SnCl$ [58, 59] suggested the potential of pincer type ligands to stabilize halometallylenes. Interestingly, despite the relatively long history of organostannylene $L^{N1}SnCl$ [58, 59], the investigation of its reactivity was limited to several reactions, in particular to oxidative additions [58, 59] and there were no other reports on pincer type ligand containing metallylenes. Recent works, however, showed the general ability of YCY-ligands to stabilize halometallylenes and in the meantime they are used for the synthesis of variety metallylenes. The presence of two intramolecular $Y \rightarrow M$ bonds in the prepared complexes suggests that YCY-ligands behave like six electron donors similarly to Cp-based ligands.

2.2.1 Chemistry of Germanium

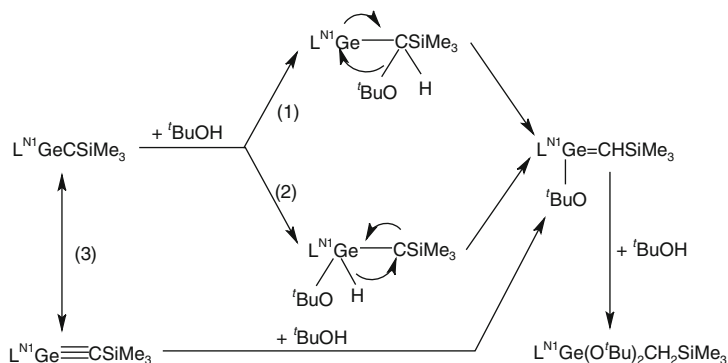
The heteroleptic germylenes $L^{N1}GeCl$ were prepared by treatment of 2,6-bis(dialkylaminomethyl)phenyl lithium with $GeCl_2 \cdot$ dioxane and used for further reactions (Scheme 2) [60]. While the chlorine atom could be substituted by other polar groups, a presence of the lone electron pair located in *s* orbital of Ge(II) was used for the interaction of germylenes with transition metals.

The molecular structures of heteroleptic germylenes $L^{N1}GeCl$ showed the elongation of Ge–Cl bond due to the $N \rightarrow Ge$ interactions [60], making thus both complexes useful starting materials for nucleophilic substitutions. New germylene amides $L^{N1}GeNR_2$ [61] and substituted diazomethanes $L^{N1}GeC(N_2)SiMe_3$ were successfully prepared and structurally characterized [62]. It was also found out that the irradiation of $L^{N1}GeC(N_2)SiMe_3$ in toluene at $-50^\circ C$ gave polymeric material of formula $(ArGeCSiMe_3)_n$ together with N_2 . The same reaction, in the presence of *tert*-butanol, yielded $L^{N1}Ge(O^tBu)_2CH_2SiMe_3$ and three possible mechanisms were suggested (Scheme 3) [62]. Further studies showed that the reaction proceeded via mechanism 3, where germyne is attacked by two equivalents of alcohol [62]. The reaction of germylene amide $L^{N1}GeNR_2$ with alcohols provided corresponding alkoxide $L^{N1}GeOR$ (R is mesityl) [61].

The treatment of germylene amides $L^{N1}GeNR_2$ with $W(CO)_5 \cdot THF$ produced germylene complex $[L^{N1}GeNR_2]W(CO)_5$ [61]. The hydrolysis of the later compound yielded the first stable hydroxo-germylene complex $[L^{N1}Ge(OH)]W(CO)_5$. The hydrolytic reaction also produced siloxy-germylene complex $[L^{N1}Ge(OSiMe_3)]W(CO)_5$ [61]. The explanation for formation of the later product goes



Scheme 2 Preparation of NCN chelated germylenes



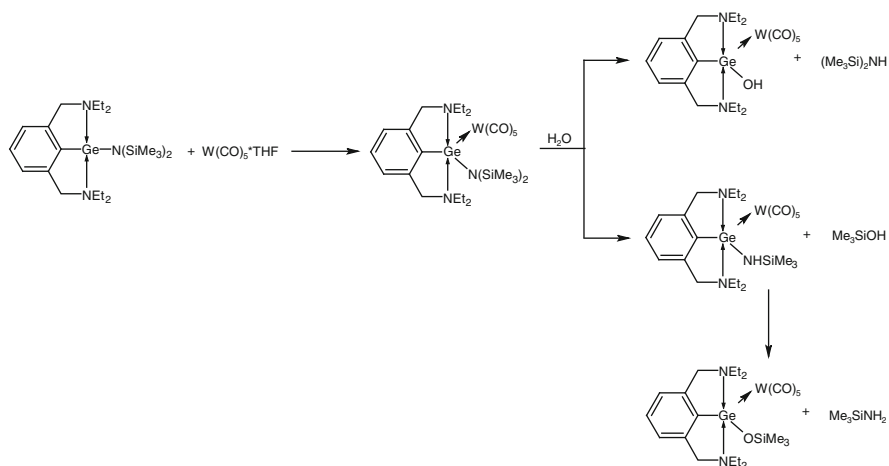
Scheme 3 Hydrolysis of NCN chelated germyne

from hydrolytic cleavage of Si–N bond along the formation of Me_3SiOH leaving thus Ge–N bond unaffected. In the second step, acidic silanol can attack the Ge–N bond producing $[\text{L}^{\text{N}1}\text{Ge}(\text{OSiMe}_3)]\text{W}(\text{CO})_5$ (Scheme 4).

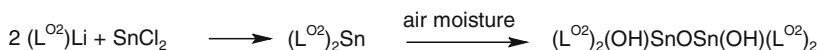
2.2.2 Chemistry of Tin

As was mentioned earlier, the organostannylene $\text{L}^{\text{N}1}\text{SnCl}$ was synthesized in 1989 by simple treatment of appropriate lithium salt with SnCl_2 in Et_2O . The synthetic method was successfully applied for the synthesis of further heteroleptic stannylenes $\text{L}^{\text{O}1,2}\text{SnCl}$, and $\text{L}^{\text{PO}}\text{SnX}$ (where X is Cl, Br, I) [63, 64]. The stannylenes $\text{L}^{\text{N}1}\text{SnCl}$ and $\text{L}^{\text{PO}}\text{SnX}$ are stable compounds that were structurally characterized. Molecular structures showed the presence of strong $\text{Y} \rightarrow \text{Sn}$ interaction that is the key reason of their stability. In contrast, stannylenes $\text{L}^{\text{O}1,2}\text{SnCl}$, which are supposed to have weaker $\text{O} \rightarrow \text{Sn}$ interaction, are unstable in solution. Interestingly, this weakness of $\text{O} \rightarrow \text{Sn}$ interaction in $\text{L}^{\text{O}2}\text{SnCl}$ allowed the synthesis of $(\text{L}^{\text{O}2})_2\text{Sn}$ as the only example of homoleptic stannylene bearing the pincer type ligands [65]. It has been further shown that the $(\text{L}^{\text{O}2})_2\text{Sn}$ is easily oxidized to form stannoxane $[(\text{L}^{\text{O}2})_2\text{Sn}(\text{OH})_2(\mu\text{-O})]$ (Scheme 5).

As all heteroleptic stannylenes contain halide as the functional group, further studies dealt with substitution reactions.



Scheme 4 Mechanism of hydrolysis of germylene amide



Scheme 5 Hydrolysis of homoleptic OCO chelated stannylene

The heteroleptic stannylene $\text{L}^{\text{N}1}\text{SnCl}$ reacts with 4-tolylolithium to afford stannylene $\text{L}^{\text{N}1}\text{Sn}(4\text{-tolyl})$. This compound readily undergoes oxidative addition reactions and the treatment with MeI or I_2 yielded corresponding organotin(IV) compounds $\text{L}^{\text{N}1}(4\text{-tolyl})(\text{Me})\text{SnI}$ and $\text{L}^{\text{N}1}(4\text{-tolyl})\text{SnI}_2$ [58, 59]. The oxidation product $[\text{L}^{\text{N}1}(\text{OSiMe}_3)\text{Sn}(\mu\text{-O})]_2$ was also isolated from the reaction of $\text{L}^{\text{N}1}\text{SnCl}$ with $\text{Me}_3\text{SiC}(\text{Li})\text{N}_2$ instead of expected stannylene diazomethane $\text{L}^{\text{N}1}\text{SnC}(\text{N}_2)\text{SiMe}_3$ (Jambor R, unpublished results) (Fig. 2).

The treatment of $\text{L}^{\text{N}1}\text{SnCl}$ with sodium salt of 2-mercaptopyridine (SPy) yielded organotin(II) derivative $\text{L}^{\text{N}1}\text{Sn}(\text{SPy})$ [66]. Similarly, thiophenol derivative $\text{L}^{\text{PO}}\text{Sn}$ (SPh) was prepared when $\text{L}^{\text{PO}}\text{SnCl}$ reacted with Na(SPh) [64]. Interestingly, when $\text{L}^{\text{N}1}\text{SnCl}$ was treated with $\text{K}[\text{BHET}_3]$ with the aim of preparation of organotin(II) hydride, deep red solution was obtained from which $\text{L}^{\text{N}1}\text{SnSnL}^{\text{N}1}$ was isolated. This compound represent example of single bonded heavy carbene analogue [67] (Scheme 6).

Experimentally determined bond distance Sn–Sn (2.9712 Å) together with DFT calculations supports the presence of single bond between both tin atoms [67]. Oxidation state of tin atoms is formally +I and this was further corroborated experimentally. The oxidation of $\text{L}^{\text{N}1}\text{SnSnL}^{\text{N}1}$ by S_8 or Se gave corresponding organotin(II) chalcogenides $(\text{L}^{\text{N}1}\text{Sn})_2\text{E}$ (E = S, Se) in the first step of oxidation. Further oxidations yielded compounds containing the central tin atom in oxidation state +IV ($(\text{L}^{\text{N}1})_2\text{Sn}_2\text{S}_7$ and $(\text{L}^{\text{N}1})_2\text{Sn}_2\text{Se}_3$ (Scheme 7) [68, 69].

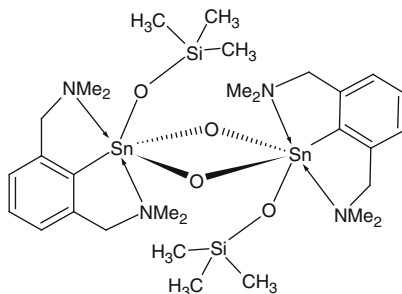
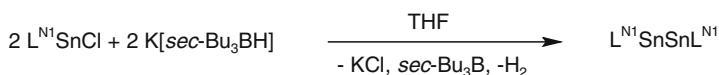
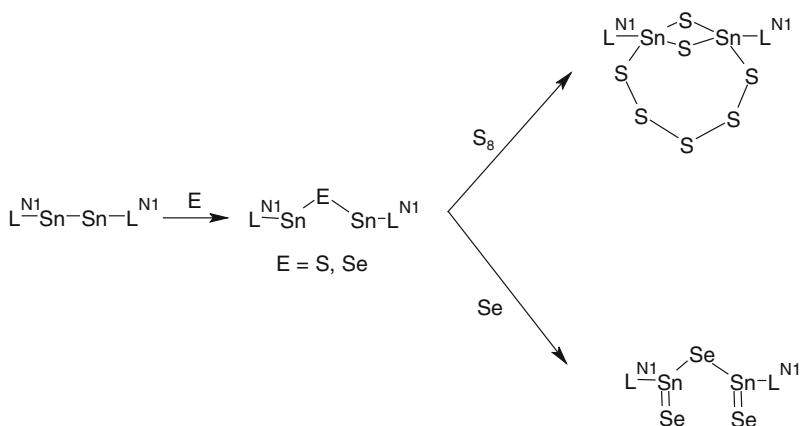


Fig. 2 Schematic drawing of $[L^{N1}(\text{OSiMe}_3)\text{Sn}(\mu\text{-O})]_2$



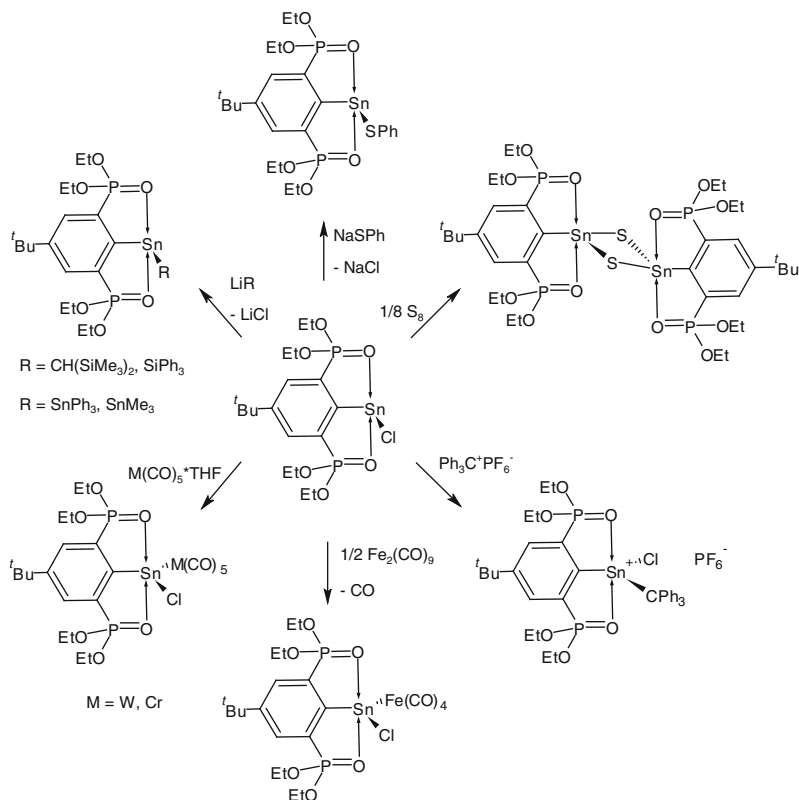
Scheme 6 Preparation of distannyne $L^{N1}\text{SnSn}L^{N1}$



Scheme 7 Oxidation of distannyne $(L^{N1}\text{Sn})_2$ with sulfur and selenium

The heteroleptic stannylenes $L^{\text{PO}}\text{SnX}$ ($X = \text{Cl}, \text{Br}$) were used as precursors for preparation of the heteroleptic stannylenes $L^{\text{PO}}\text{SnX}$ ($X = \text{CH}(\text{SiMe}_3)_2, \text{SiPh}_3, \text{SnPh}_3, \text{and SnMe}_3$) as a result of the substitution reactions. The oxidation of the former stannylenes provided the tetravalent monorganotin derivatives $\{L^{\text{PO}}\text{SnCl}(\mu\text{-S})\}_2$ and $L^{\text{PO}}\text{SnBr}_3$ and the diorganotin cation $\{L^{\text{PO}}(\text{Ph}_3\text{C})(\text{Cl})\text{Sn}\}^+[\text{PF}_6]^-$ (Scheme 8) [70].

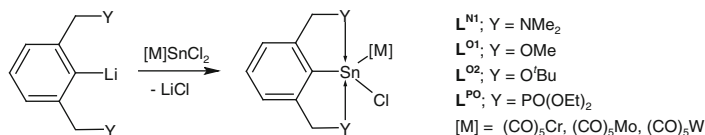
As the oxidation state of the tin atom is +II and there are only two covalent bonds presented in the stannylenes, these compounds can be an alternative to the carbene. In these functional substituted organostannylenes, the Lewis base character of the



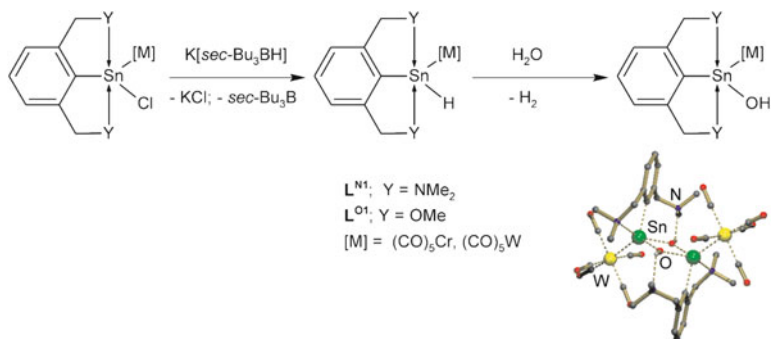
Scheme 8 Reactivity of OCO chelated heteroleptic stannylene $\text{L}^{\text{PO}}\text{SnCl}$

Sn(II) atom is increased as a result of the intramolecular donor $Y \rightarrow \text{Sn}$ coordination. This, in turn, should increase the ability to form complexes with Lewis acids such as transition metals. These predictions were fulfilled and it was shown that heteroleptic stannylenes are able to complex variety of transition metals. The carbonyl complexes of the 6th group elements seem to be the most frequent and popular. Stable chromium, molybdenum, or tungstenpentacarbonyl complexes of stannylenes $\text{L}^{\text{N}^1}\text{SnCl}$, $\text{L}^{\text{O}^1,2}\text{SnCl}$, and $\text{L}^{\text{PO}}\text{SnCl}$ were prepared [63, 64, 70]. These complexes were readily obtained by reaction of the corresponding organolithium compounds with in situ-generated precursor $(\text{CO})_5\text{M}\cdot\text{SnCl}_2$, (Scheme 9). Alternatively, the complexes $[\text{L}^{\text{PO}}\text{SnCl}]\text{M}(\text{CO})_n$ ($n = 5$ for $M = \text{Cr}, \text{W}$ and $n = 4$ for $M = \text{Fe}$) were obtained when $\text{L}^{\text{PO}}\text{SnCl}$ was reacted with $\text{M}(\text{CO})_5\cdot\text{THF}$ ($M = \text{W}, \text{Cr}$) or with $\text{Fe}_2(\text{CO})_9$ [70].

Molecular structures revealed the five coordinated tin atoms with $Y \rightarrow \text{Sn}$ interactions and the NMR studies showed that structures are retained in solution. As the consequence of presence of Sn–Cl bond, these complexes are suitable precursors for the substitution reaction. Treatment of complexes $[\text{L}^{\text{N}^1}\text{SnCl}]\text{M}(\text{CO})_5$ and $[\text{L}^{\text{O}^1}\text{SnCl}]\text{M}(\text{CO})_5$ with $\text{K}[\text{BHEt}_3]$ yielded corresponding organotin(II)



Scheme 9 Preparation of complexes of group 6 metals with chelated stannylenes



Scheme 10 Hydrolysis of complexes of heteroleptic stannylenes with transition metals of 6 group

hydrides $[\text{L}^{\text{N}1}\text{Sn}(\text{H})]\text{M}(\text{CO})_5$ and $[\text{L}^{\text{O}1}\text{Sn}(\text{H})]\text{M}(\text{CO})_5$ [63, 64, 71]. These compounds are not stable in solution and hydrolyze via hydrogen elimination to give organotin(II) hydroxides $[\text{L}^{\text{N}1}\text{Sn}(\text{OH})]\text{M}(\text{CO})_5$ and $[\text{L}^{\text{O}1}\text{Sn}(\text{OH})]\text{M}(\text{CO})_5$ (Scheme 10) [71]. The molecular structure of $[\text{L}^{\text{N}1}\text{Sn}(\text{OH})]\text{W}(\text{CO})_5$ was determined by X-ray diffraction technique and revealed that the complex is dimeric with hydroxide group in bridging position.

Substitution reaction also proceeded via the abstraction of chloride by silver salts of various polar groups. These reactions provided complexes $[\text{L}^{\text{N}1}\text{SnX}]\text{M}(\text{CO})_5$ and $[\text{L}^{\text{O}1}\text{SnX}]\text{M}(\text{CO})_5$ containing different polar groups X (X = OAc, O₂CCH=CH₂) [72]. This research was, however, focused on the stabilization of organotin(II) cations and ligands $\text{L}^{\text{N}1}$ and $\text{L}^{\text{O}1}$ were shown as suitable systems for this purpose. The introduction of low coordinating anions $[\text{OTf}]^-$ or $[\text{CB}_{11}\text{H}_{12}]^-$ yielded organotin(II) cations $[(\text{L}^{\text{N}1}\text{Sn})\text{W}(\text{CO})_5]^+ [\text{CB}_{11}\text{H}_{12}]^-$, $[(\text{L}^{\text{O}1}\text{Sn})\text{Cr}(\text{CO})_5]^+ [\text{OTf}]^-$, and $[(\text{L}^{\text{O}1}\text{Sn})\text{Cr}(\text{CO})_5]^+ [\text{CB}_{11}\text{H}_{12}]^-$ (Fig. 3) [73, 74]. The molecular structures proved their ionic character. The compounds $[(\text{L}^{\text{N}1}\text{Sn})\text{W}(\text{CO})_5]^+ [\text{CB}_{11}\text{H}_{12}]^-$ and $[(\text{L}^{\text{O}1}\text{Sn})\text{Cr}(\text{CO})_5]^+ [\text{OTf}]^-$ crystallized as the aqua complexes $[\{\text{L}^{\text{N}1}\text{Sn}(\text{H}_2\text{O})\}\text{W}(\text{CO})_5]^+ [\text{CB}_{11}\text{H}_{12}]^-$ and $[\{\text{L}^{\text{O}1}\text{Sn}(\text{H}_2\text{O})\}\text{Cr}(\text{CO})_5]^+ [\text{OTf}]^-$, with five coordinated tin atoms. While in the complex $[\{\text{L}^{\text{N}1}\text{Sn}(\text{H}_2\text{O})\}\text{W}(\text{CO})_5]^+ [\text{CB}_{11}\text{H}_{12}]^-$ molecule of water further coordinates the nitrogen atom of $\text{L}^{\text{N}1}$ ligand, in the case of $[\{\text{L}^{\text{O}1}\text{Sn}(\text{H}_2\text{O})\}\text{Cr}(\text{CO})_5]^+ [\text{OTf}]^-$, the $[\text{OTf}]^-$ group is coordinated by O–H(w) hydrogen bond. The $[(\text{L}^{\text{O}1}\text{Sn})\text{Cr}(\text{CO})_5]^+ [\text{CB}_{11}\text{H}_{12}]^-$ crystallized as the adduct of two THF molecules providing six coordinated tin(II) atoms in $[\{\text{L}^{\text{O}1}\text{Sn}(\text{THF})_2\}\text{Cr}(\text{CO})_5]^+ [\text{CB}_{11}\text{H}_{12}]^-$.

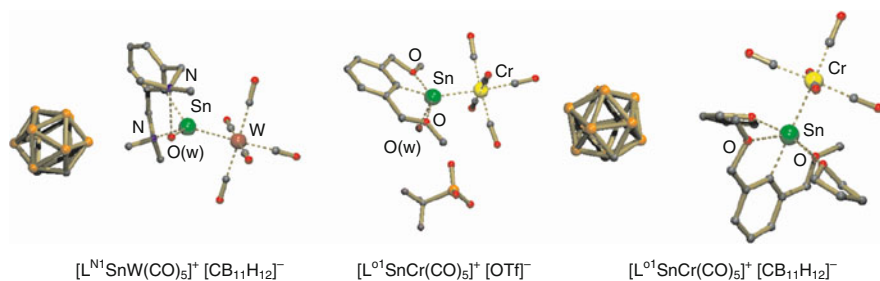
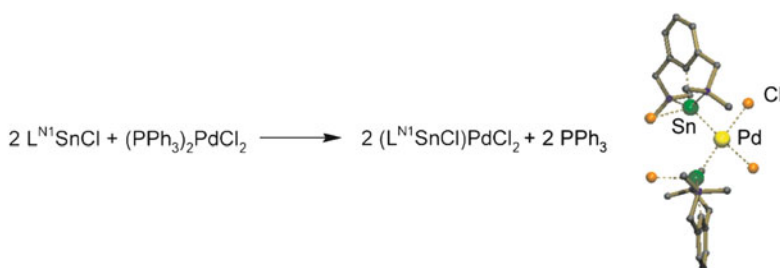


Fig. 3 Molecular structures of organotin(II) cations



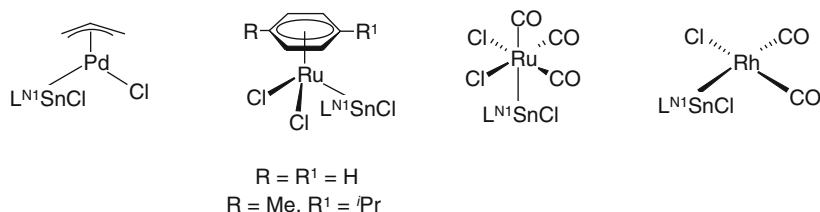
Scheme 11 Preparation of palladium(II) complex with NCN chelated stannylene

The heteroleptic stannylene $L^{N^1}SnCl$ was able to substitute PPh_3 groups in the complex $(PPh_3)_2PdCl_2$ to provide palladium–stannylene complex *cis*- $[L^{N^1}SnCl]_2PdCl_2$ that was structurally characterized and showed Pd–Sn bond being in the range of Pd=Sn double bonds (Scheme 11) [75].

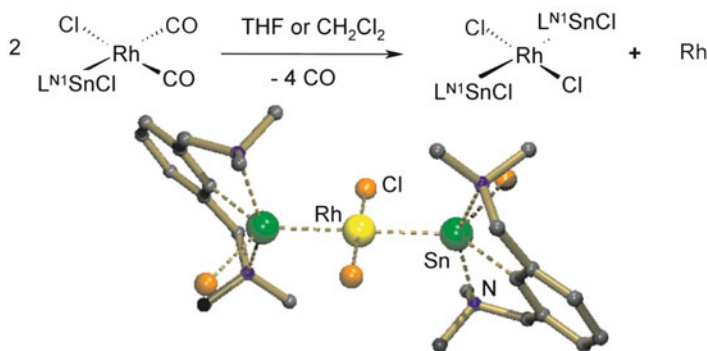
This observation indicates that stannylene $L^{N^1}SnCl$ can behave as a true heavy carbene analogue. Further studies revealed that simple treatment of $L^{N^1}SnCl$ with $PdCl_2$, PdI_2 , or $PtCl_2$ yielded corresponding *cis*- $[L^{N^1}SnCl]_2MX_2$ complexes with short Sn–M bond lengths (M = Pd, Pt; X = Cl, I) [76]. The ^{119}Sn NMR spectra of prepared complexes revealed signals shifted downfield compared to the starting compound. The ability of stannylene $L^{N^1}SnCl$ to complex transition metals was shown when treated with variety of dimeric transition metal complexes. The reactions proceeded via the chloride bridge scission yielding the corresponding complexes of Pd(II), Ru(II), and Rh(I) (Scheme 12) [77].

While the Pd(II) and Ru(II) complexes are stable, the complex $[L^{N^1}SnCl]Rh(CO)_2Cl$ was characterized in solution only. The ^{119}Sn showed a doublet at 60.8 ppm with the $^1J(^{119}Sn, ^{103}Rh) = 880$ Hz and clearly proved the formation of a Rh(I)–Sn(II) bond. This complex decomposes to paramagnetic complex *trans*- $[L^{N^1}SnCl]_2RhCl_2$ that was unambiguously determined by X-ray structure analysis (Scheme 13).

When stannylene $L^{N^1}SnCl$ reacted with $[Mo(CO)_2Cp(CH_3CN)_2]^+BF_4^-$, complex $[L^{N^1}SnCl]Mo(CO)_2CpCl$ as crystalline material and some rather poorly soluble amorphous white precipitate was received [78]. The former complex is the



Scheme 12 Schematic drawing of prepared tin-transition metal complexes



Scheme 13 Decomposition pathway of the complex $[L^{N^1}SnCl]Rh(CO)_2Cl$

result of the simultaneous replacement of CH_3CN by the $L^{N^1}SnCl$ and chloride ion transfer from another molar equivalent of stannylene. As all prepared complexes of $L^{N^1}SnCl$ contain both Sn–Cl and M–Cl bonds, the question concerning the reactivity of these functionalities towards nucleophiles came into mind. The organostannylene palladium-based complexes were studied in this field unsuccessfully and the only positive result was obtained when the organostannylene complex $[L^{N^1}SnCl][2-(Me_2NCH_2)C_6H_4]PdCl$ that contains both a NCN- and a CN-coordinating ligand was treated with silver acetate ($AgOAc$). This reaction gave, under exclusive Sn–Cl substitution, the monoacetate-substituted complex $[L^{N^1}SnOAc][2-(Me_2NCH_2)C_6H_4]PdCl$ [78].

For further reactivity studies, kinetically more stable complex *cis*- $[L^{N^1}SnCl]_2PtCl_2$ was chosen. Treatment of *cis*- $[L^{N^1}SnCl]_2PtCl_2$ with four equivalents of NaI provided *trans*- $[L^{N^1}SnI]_2PtI_2$ [76]. Both platinum complexes undergo reaction with three equivalents of NaSPy providing interesting complexes $[L^{N^1}Sn]^+[PtX(SP_y)_2]^-$ ($X = Cl, I$), where stannylidenium ($L^{N^1}Sn$)⁺ coordinates Pt center (Fig. 4) [66].

From the structural point of view, the Sn–Pt interaction could be interpreted as a $Sn \rightarrow Pt$ or $Sn \leftarrow Pt$ interaction or a covalent bond in these complexes. DFT calculations of $[L^{N^1}Sn]^+[PtX(SP_y)_2]^-$ ($X = Cl, I$) were performed and the NBO analysis revealed no lone pair at the tin atom and the natural charge of Sn atom is

Fig. 4 Molecular structure of stannylidenium ($L^N Sn$)⁺ coordinating Pt center

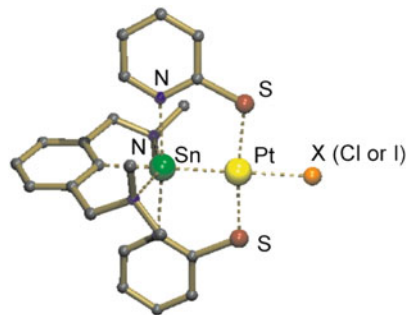
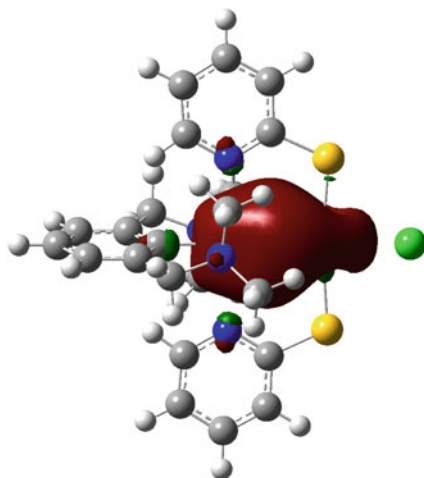


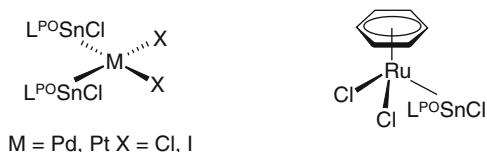
Fig. 5 MO orbital describing Sn–Pt bond in compounds $[L^N Sn]^+ [PtX(SP_y)_2]^-$ ($X = Cl, I$)



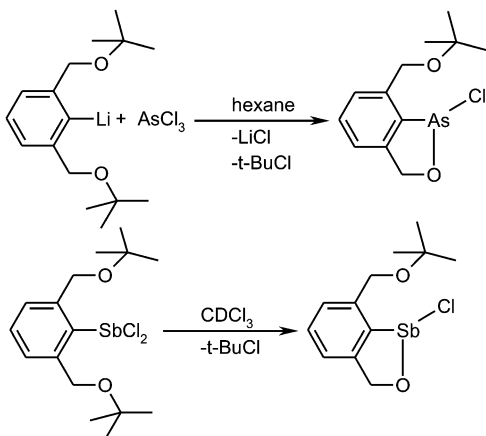
+1.709, while at the Pt atom is -0.486 . These observations were rationalized with the lone electron pair of Sn(II) atom being shared by both atoms and consumed for the formation of tin–platinum bond. The NBO analysis showed that the nature of the Sn–Pt bond is mediated by sp -hybridized orbitals on the tin atom (Fig. 5). The bonding situation was also described within a Sn(IV) \leftarrow Pt(0) formalism [66].

The ability of the heteroleptic stannylenes containing YCY-chelating ligands to complex late transition metals is probably the function of the strength of $Y \rightarrow Sn$ interaction. When stannylenes $L^{O1,2}SnCl$ were treated with late transition metal complexes, only the decomposition reactions were observed. However, when another oxygen atom containing stannylene $L^{PO}SnCl$ having stronger $O \rightarrow Sn$ coordinations was applied for binding of transition metals, stable Sn–TM complexes were prepared. Treatment of $L^{PO}SnCl$ with $PdCl_2$, PdI_2 , and $PtCl_2$ yielded *cis*- $[L^{PO}SnCl]_2MX_2$ complexes, similarly to $L^N SnCl$ [76]. After reaction of $L^{PO}SnCl$ with dimeric Ru(II) complex, stable complex $[L^{PO}SnCl]Ru(C_6H_6)Cl_2$ was isolated (Scheme 14) [79].

Scheme 14 Complexes of heteroleptic stannylene $L^{PO}SnCl$



Scheme 15 Cyclization of organoarsenic(III) and organoantimony(III) OCO chelated compounds



Comprehensive study of both $L^{N1}SnCl$ and $L^{PO}SnCl$ stannylenes towards Pd(0) complex was also investigated. The reaction of $L^{N1}SnCl$ with $Pd(PPh_3)_4$ gave, regardless of the stoichiometry (1:1 to 1:6), a yellow solid $cis-[L^{N1}SnCl]_2PdCl_2$, while similar reaction of $L^{PO}SnCl$ produced only trace of $trans-(Ph_3P)_2PdCl_2$. The reactions are the redox-type reactions and heavy acetylene analogues $L^{N1}SnSnL^{N1}$ and $L^{PO}SnSnL^{PO}$ were proposed as side products [78].

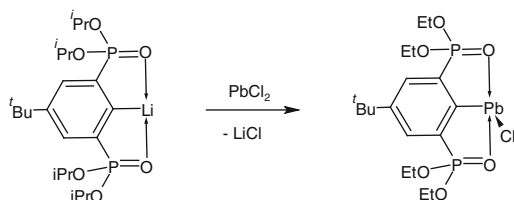
2.2.3 Chemistry of Lead

The chemistry of organoplumblylenes is rather rare. The compound $L^{PO}PbCl$ that was prepared by the reaction of $L^{PO}Li$ with $PbCl_2$ in Et_2O is the only example. The molecular structure was determined by X-ray diffraction analysis (Scheme 15) [64].

2.3 Group 15: As, Sb, Bi

The chemistry of the group 15 elements was not studied so often in the past, but during the last few years this field has been opened again by our group and groups of Prof. Breunig, Prof. Silvestru, and more recently by Prof. Evans.

Organoarsenic(III) compounds were prepared by simple reaction of organolithium compounds with $AsCl_3$ of pincer ligands L^{N1} and L^{NO2} and targeted



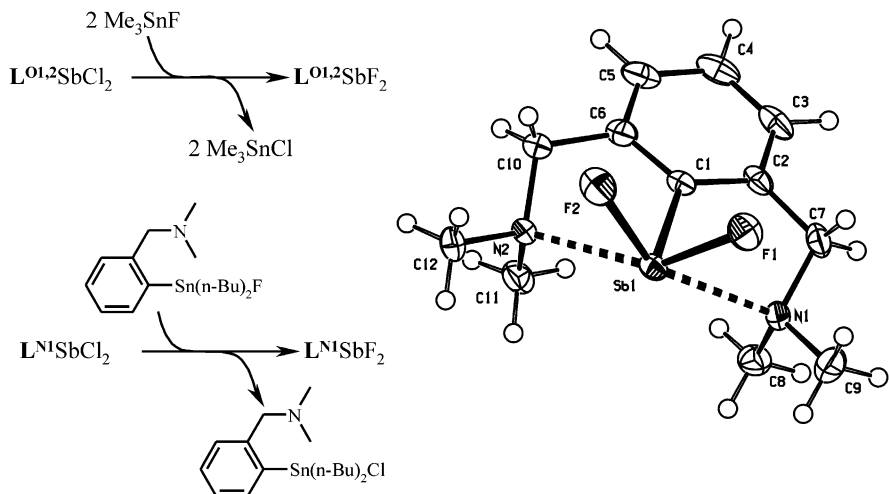
Scheme 16 Synthesis of heteroleptic plumbylene $L^{PO}PbCl$

compounds $L^{N1}AsCl_2$ and $L^{NO2}AsCl_2$ could be isolated. On the contrary, analogous reaction using OCO pincer ligand L^{O2} produced a cyclized product, in which one of the ligand's arm is broken under elimination of *t*-BuCl and a new As–O covalent bond formation (Scheme 16) [80, 81]. Compound $L^{N1}AsCl_2$ may be easily transformed into corresponding hydrido-complex $L^{N1}AsH_2$ by treatment with Li $[AlH_4]$ [80]. Subsequently, this compound can be deprotonized with formation of $L^{N1}AsLi_2$ and used for reaction with $[t\text{-BuGaCl}_2]_2$ giving product $[L^{N1}AsGa(t\text{-Bu})_2]_2$ with central four-membered Ga_2As_2 ring [82].

Although the pincer chemistry of arsenic is still quite limited, the corresponding organotimony and organobismuth chemistry was developed significantly during last few years. Ligands $L^{N1,2}$, $L^{O1,2}$, $L^{NO1,2}$ were used in this research and only compounds with ligand L^{PO} were not reported to this moment.

All starting compounds are prepared by treatment of organolithium precursor of respective pincer ligand with $SbCl_3$ or $BiCl_3$ [80, 81, 83, 84]. The exceptions of this fact are reactions with lithium compounds of OCO pincer ligands $L^{O1,2}$. The intermediate $\{[(L^{O1})_2Sb]^+\}_4[Sb_6Cl_{22}]^{4-}$ was isolated from the reaction of corresponding organolithium compound and antimony chloride; this compound decomposes slowly to chloride $L^{O1}SbCl_2$ and $SbCl_3$ upon standing in solution of chlorinated solvents [85]. The congener $L^{O2}SbCl_2$ undergoes a cyclization in solution similarly to arsenic analogue Scheme 16 [81]. The antimony and bismuth chloro-complexes of ligands L^{N1} and $L^{O1,2}$ can be converted to corresponding bromides or iodides by treatment with an excess of KBr or KI. Recently, the organoantimony chlorides were utilized for preparation of fluorides using tin reagents Me_3SnF and $[2-(Me_2NCH_2)C_6H_4]Sn(n\text{-Bu})_2F$ as well, but this reaction does not work for bismuth compounds and analogous bismuth fluorides remain still elusive (Scheme 17) [86].

The resulting compounds are in most cases air stable solids and molecular structures of majority of compounds were established by X-ray diffraction technique. Detailed description of all structures is beyond the scope of the chapter. The molecular structures range for trigonal pyramidal array around the central atoms (Sb or Bi), which is *cis* attacked by two donor atoms of the pincer ligand (usually weak intramolecular interaction), to distorted tetragonal pyramidal environment, where the donor atoms are strongly coordinated mutually in *trans* positions. There are numerous additional metal to halide intermolecular contacts in majority of



Scheme 17 Preparation of antimony fluorides containing pincer type ligands and an example of molecular structure

derivatives, especially in organobismuth compounds, which further distort the coordination geometry around the central metals.

Pincer type ligands are very well suited for stabilization of highly Lewis acidic species as the central metal atom may benefit from two dative interactions with heteroatoms of the ligands as Lewis bases. This fact has been recently reflected among antimony and bismuth chlorides $LMCl_2$ containing ligands L^{N1} , $L^{O1,2}$, L^{NO2} by preparation of ionic complexes containing positively charged central atoms, which are stabilized by the help of pincer ligands. Similar species are easily accessible by conversion of starting chlorides with silver salts of various polar groups AgX ($X = RCO_2$, OTf , $CB_{11}H_{12}$). In such a way, several sets of carboxylates [87] and triflates [88] were prepared and characterized, but in these compounds contacts between the central antimony or bismuth atoms and polar groups were detected in the solid state. Thus, these compounds could not be designated as ionic. Only using of low nucleophilic anions such as $[CB_{11}H_{12}]^-$ or aryl borate $[BPh_4]^-$ allowed isolation of well-separated ionic pairs $[LMCl]^+[X]^-$ [88–90]. The central atom is in all cases strongly coordinated by donor atoms of the pincer ligand, which results in major cases in vacant trigonal bipyramidal array around the central metals. The high Lewis acidity of the central metals is in some cases documented by coordination of a THF molecule or forming dinuclear ionic compounds (Fig. 6) [89].

Reactions of $L^{N1}SbCl_2$ a $L^{N1}BiCl_2$ with appropriate hydrolytic agent (KOH for antimony and t -BuOK/ H_2O for bismuth) produce corresponding dimeric oxides $[L^{N1}SbO]_2$ a $[L^{N1}BiO]_2$ in good yield as stable solids [91, 92]. Both oxides are soluble in range of solvents including hexane, which means that these compounds are promising precursors for further reactivity studies. $[L^{N1}SbO]_2$ is able to bind

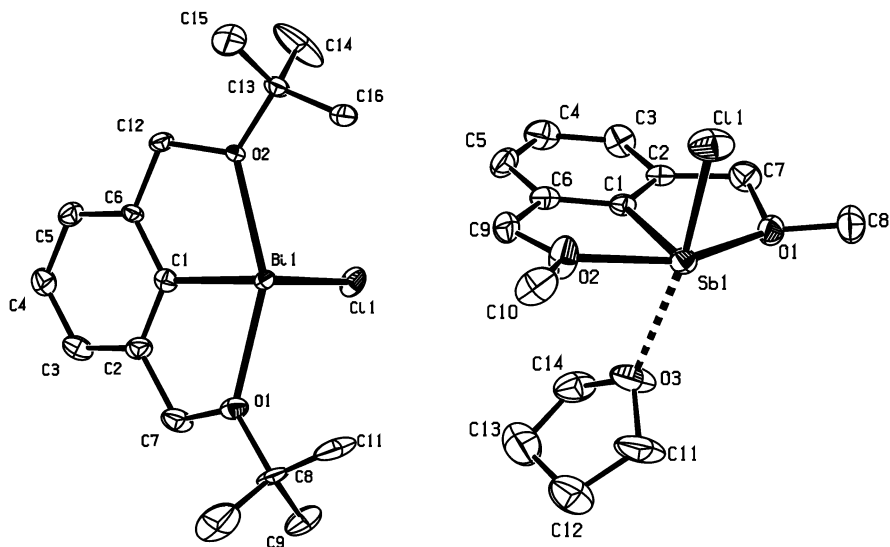
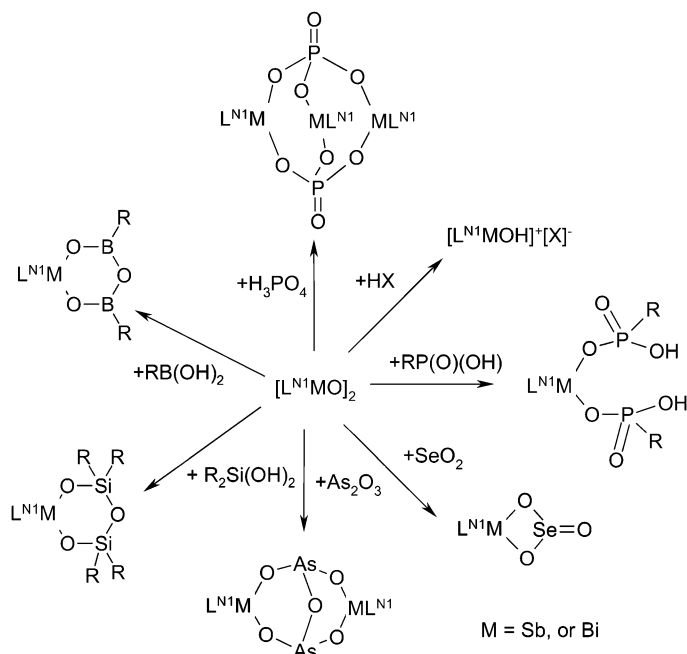


Fig. 6 Molecular structures of bismuth and antimony cations stabilized by pincer ligands, the structures of counter-anions $[\text{CB}_{11}\text{H}_{12}]^-$ are omitted for clarity and each central atom carries +1 charge

carbon dioxide reversibly under mild reaction conditions forming carbonate $\text{L}^{\text{N}1}\text{SbCO}_3$. The smooth reversibility of this reaction may be ascribed to the interesting coordination mode of the carbonate group, which is bonded as a terminal ligand to the antimony atom. This bonding situation is rather unusual in the chemistry of main groups and most probably makes the carbon dioxide fixation reversible [91]. Furthermore, both oxides can be protonated at the oxygen atom forming unprecedented monomeric hydroxo compounds $[\text{L}^{\text{N}1}\text{SbOH}]^+[\text{X}]^-$ ($\text{M} = \text{Sb}$ or Bi , $\text{X} = \text{OTf}$). These unique structures are stabilized mainly by pincer ligand $\text{L}^{\text{N}1}$, which stabilizes significant positive charge on the central atoms in these ionic pairs [92]. The oxides $[\text{L}^{\text{N}1}\text{SbO}]_2$ and $[\text{L}^{\text{N}1}\text{BiO}]_2$ were also proved to be extremely useful materials for preparation of mixed oxido-compounds, where two main group elements are bridged by single oxygen atom. The reactions are simple just mixing starting oxides with an acid or main group oxide and proceed in majority of cases smoothly with high yields (Scheme 18).

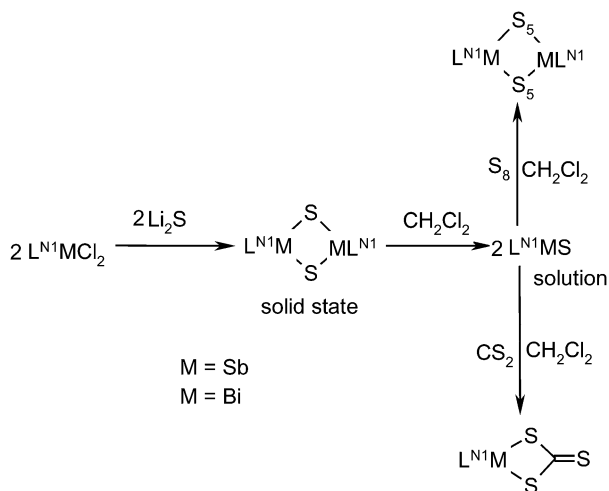
Antimony and bismuth phosphates, phosphites, and phosphonates were obtained using this reaction pathway. All these compounds retain good solubility in organic solvents, which is not very usual for these polymeric compounds. This fact is a result of the presence of the pincer ligand, which coordinates the central atoms and renders oligomerization or polymerization of these compounds by forming intermolecular contacts [93–95]. The mentioned synthetic strategy allowed also isolation of unprecedented ring systems and small clusters (Scheme 18) (Dostál L et al., unpublished results). Breunig et al. have recently reported on preparation of other organobismuth oxido-compounds, i.e., $\text{L}^{\text{N}1}\text{BiX}$ ($\text{X} = \text{SO}_4, \text{CO}_3$) and $\text{L}^{\text{N}1}\text{Bi}(\text{NO}_3)_2$;



Scheme 18 Reactivity of intramolecularly oxides $[\text{L}^{\text{N}1}\text{SbO}]_2$ a $[\text{L}^{\text{N}1}\text{BiO}]_2$

these compounds form infinite chains in the solid state via bridging by oxo-anions or dimeric structure in the case of the nitrate $\text{L}^{\text{N}1}\text{Bi}(\text{NO}_3)_2$ [96]. Evans et al. enriched this class of compounds by preparation of bismuth bulky phenolates containing ligand $\text{L}^{\text{N}1}$, which undergo an extremely interesting CH activation, and formation of NCN chelated organobismuth compound with a monodentate carbon-bound oxyaryl dianion $(\text{C}_6\text{H}_2-t\text{-Bu}_2-3,5\text{-O-4})^{2-}$ [97].

Not only oxides are stabilized by pincer type ligands, but also heavier chalcogenides are accessible. Thus, the reactions of chlorides $\text{L}^{\text{O}1,2}\text{MCl}_2$ ($\text{M} = \text{Sb}$ or Bi) with an excess of sodium sulfide gave corresponding sulfides $[\text{L}^{\text{O}1,2}\text{MS}]_2$, which are dimeric both in the solid state and in solution with central M_2S_2 four-membered central ring. The pincer ligands may be placed on this ring in a *cis* or *trans* fashion and both isomers were detected in solution and in the solid state; the central M_2S_2 ring is planar in the *trans* isomer but strongly puckered in the *cis* one [98]. Analogous NCN chelated compounds $[\text{L}^{\text{N}1}\text{MS}]_2$ ($\text{M} = \text{Sb}$ or Bi) are also dimers in the solid state according to X-ray crystallography studies, but more importantly they dissociate in solution into monomeric compounds with terminal M–S bonds. Presence of these unprecedented monomeric derivatives was established by trapping experiments with sulfur and carbon disulfide (Scheme 19) [99, 100]. Especially isolation of dinuclear bispentasulfides is noteworthy, because they represent new structural type among organometallic polysulfides in general. Reaction of low valent organoantimony(I) compound $[\text{L}^{\text{N}1}\text{Sb}]_4$ (see next



Scheme 19 Reactivity of NCN chelated organobismuth and organoantimony sulfides

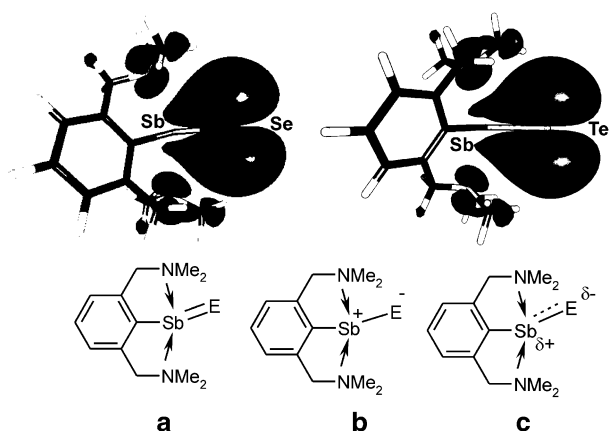
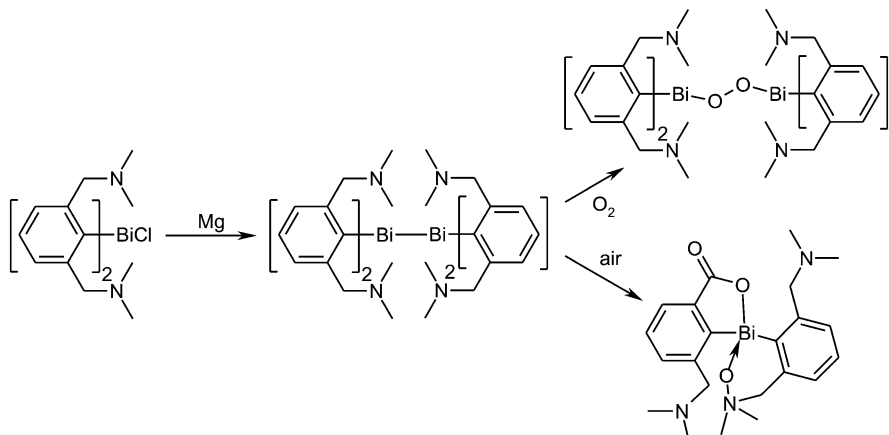


Fig. 7 Description of terminal Sb–E (E = Se, Te) bonds based on theoretical considerations

discussion) with elemental selenium and tellurium gave unprecedented compounds $L^{N1}SbE$ (E = Se or Te), which are monomeric not only in solution but also in the solid state as shown by X-ray diffraction technique. The terminal Sb–E bond should be in principle double bond, but as shown by theoretical studies these bonds are strongly polarized with significant partial charges on the corresponding atoms Sb (δ^+)-E(δ^-). The presence of the pincer ligand is crucial for stabilization of these highly polarized systems as demonstrated by theory as well (Fig. 7) [101]. The reactions of Li_2S or Li_2Se with antimony precursor containing bulky NCN pincer



Scheme 20 Preparation and reactivity of low valent NCN chelated organobismuth compound

ligand $L^{N2}SbCl_2$ gave besides expected monomeric selenide $L^{N2}SbSe$ also unprecedented monomeric sulfide $L^{N2}SbS$ with the first terminal Sb–S bond (Dostál L et al., unpublished results). Heavier chalcogenides (Se, Te) of organobismuth pincer compounds remain still elusive and represent synthetic challenge for future research.

Besides wide utilization of pincer ligands in the field of organoantimony(III) and organobismuth(III) compounds, it has been recently demonstrated that these ligands are able to stabilize low valent organoantimony and organobismuth compounds, which display interesting reactivity.

The reduction of $(L^{N1})_2BiCl$ with magnesium in THF produced compound $(L^{N1})_2BiBi(L^{N1})_2$ with single bond between two bismuth atoms. This compound reacts with oxygen under formation of compound $(L^{N1})_2Bi(O_2)Bi(L^{N1})_2$, where the bond distance O–O approach classical value for peroxides and thus the $(L^{N1})_2Bi(O_2)Bi(L^{N1})_2$ represents the first example of organobismuth peroxide reported. The further oxidation to $(L^{N1})_2BiBi(L^{N1})_2$ in air led not only to oxidation of the central bismuth atoms, but even the backbone of the ligand is oxidized (Scheme 20) [102].

Alternative approach was used for reduction of analogous antimony compound $L^{N1}SbCl_2$. The compound was reacted with two equivalents of K-selectride $K[B(s-Bu)H]$, which produced highly unstable hydrido compound $L^{N1}SbH_2$, which smoothly eliminates hydrogen gas and the central antimony atom is reduced to formal oxidation state +I. According to the reaction time two compounds were obtained, i.e., tetrameric compound $[L^{N1}Sb]_4$ with central puckered Sb_4 ring and unprecedented cluster compound $(L^{N1})_3Sb_5$. This compound has a propellane-like structure (five antimony atoms occupy apexes of a trigonal bipyramid) with three ligands bonded to the atoms in the formal equatorial plane and the antimony atoms in an axial position remain naked [103]. Using the more bulky NCN pincer ligand

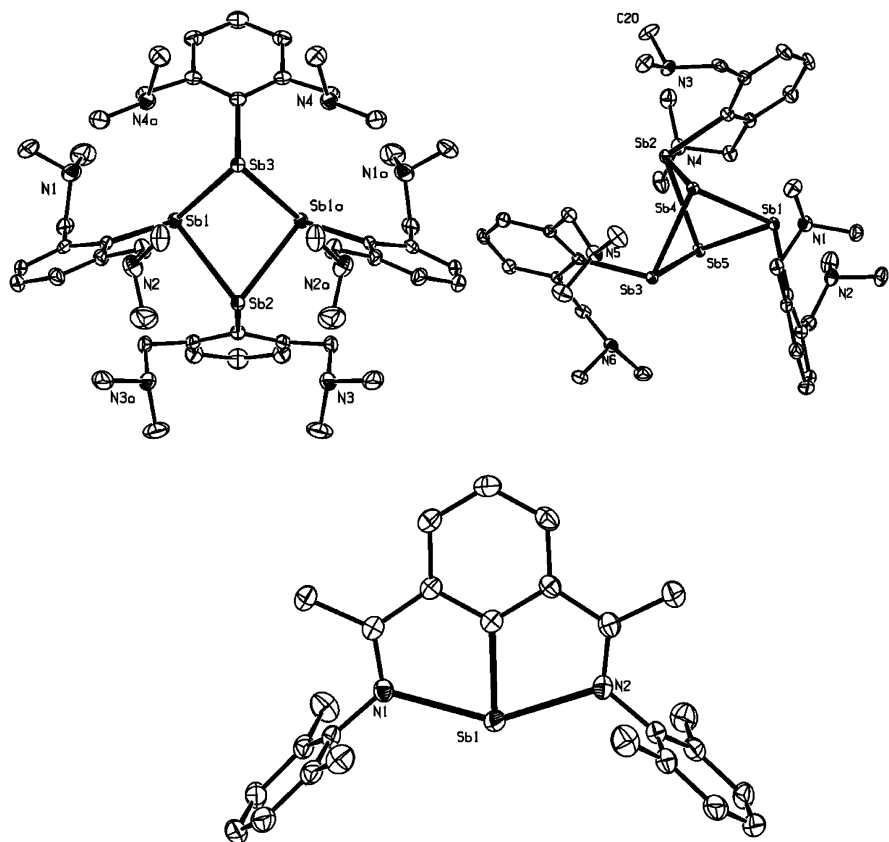


Fig. 8 Molecular structures of selected organoantimony(I) compounds stabilized by the ligands L^{N1} and L^{N2}

L^{N2} and the same synthetic protocol, i.e., reduction of starting chlorides with K-selectride allowed isolation of unique deep blue compounds $L^{N2}M$ ($M = Sb$ or Bi) [104]. These compounds contain the central atoms in formal oxidation state +I and there are no additional intermolecular contacts between the central atoms, which makes them exclusively monomeric, which is unprecedented in the group 15 chemistry. This is again result of excellent properties of the NCN pincer ligand, which blocks empty p-type orbital of the central atom by interaction with nitrogen donor atoms and at once shields the full p-type orbital of the central atoms by its sterical demanding flanking aryls on the ligand's arms. As shown by theoretical calculations presence of the pincer type ligand is crucial for stabilization of these compounds $L^{N2}M$ ($M = Sb$ or Bi). This fact was further supported by experiment, which showed that using only NC single-armed chelating ligand allowed isolation of low valent antimony compounds, which are tetrameric [105] (Fig. 8).

3 Conclusions and Outlook

The pincer chemistry of main group elements has recently been enriched significantly and several very interesting results were discovered; nevertheless, it is felt that this chemistry in comparison to the transition metals analogues is still in its infancy. The pincer type ligands are able to stabilize not only routine compounds but also rather unstable and reactive species even with low valent metal atoms. In such a way they may form an attractive alternative to sterically demanding ligands used by Power and others for stabilization of such organometallic species. As it is known, compounds with low valent metal centers and(or) with metal–metal bonds display an extremely interesting reactivity [106], similar reaction pattern may be expected for the pincer type compounds. From this point of view, the pincer chemistry of main groups may be very interesting for further research in the field of organometallic chemistry. This investigation will be based on using of new pincer type ligands known from transition metals chemistry in the field of main groups. Combination of intramolecular dative interaction mediated by one arm of the pincer ligand with sterical shielding by the second one and thus building new class of hybrid pincer ligands would be to our opinion also challenging for future research. Using of these ligand systems will combine the best properties of sterically demanding ligands and donating ability of pincer type ligands in one pot.

Main group metal compounds containing neutral pincer type ligands, which are nearly unknown in this moment, seem to be next rational target in the field. Especially recent excellent achievements by Prof. Milstein (e.g., see [107]) in the field on transition metal derivatives of NNP or NPN systems are highly inspirational for main group chemists and accommodation of low valent main group metals within the cavity of such systems may lead to interesting and unprecedented results.

Acknowledgments Support of the grant of the Grant Agency of the Czech Republic no. P207/10/0130 is kindly acknowledged.

References

1. Moulton CJ, Shaw BL (1976) Transition metal–carbon bonds. 42. Complexes of nickel, palladium, platinum, rhodium and iridium with tridentate ligand 2,6-bis((di-*t*-butylphosphino)methyl)phenyl. *J Chem Soc Dalton Trans* 1020–1024
2. Creaser CS, Kaska WC (1978) Complexes of 1,3-bis(dimethylphosphinomethyl)-benzene with nickel(II), palladium(II) and iron(II) halides. *Inorg Chim Acta* 30:L325–L326
3. van Koten G, Timmer K, Noltes JG, Spek AL (1978) Novel type of Pt–C interaction and a model for final stage in reductive elimination processes involving C–C coupling at Pt - synthesis and molecular-geometry of [1,N,N'- η -2,6-bis((dimethylamino)methyl)-toluene]iodoplatinum(II) tetrafluoroborate. *J Chem Soc Chem Commun* 250–252
4. Albrecht M, van Koten G (2001) Platinum group organometallics based on “Pincer” complexes: sensors, switches, and catalysts. *Angew Chem Int Ed* 40:3750–3781

5. van der Boom ME, Milstein D (2003) Cyclometalated phosphine-based pincer complexes: mechanistic insight in catalysis, coordination, and bond activation. *Chem Rev* 103:1759–1792
6. Morales-Morales D, Jensen CM (2007) *The chemistry of pincer compounds*. Elsevier, Amsterdam
7. van Koten G, Jastrzebski JTBH, Noltes JG, Spek AL, Schoone JC (1978) Triorganotin cations stabilized by intra-molecular Sn-N coordination - synthesis and characterization of (C, N, N'-2,6-bis[(dimethylamino)methyl]phenyl)diorganotin. *J Organomet Chem* 148:233–245
8. Jambor R, Dostál L (2007) Hypervalent organotin, aluminium, antimony and bismuth Y,C,Y chelate complexes. In: Morales-Morales D, Jensen CM (eds) *The chemistry of pincer compounds*. Elsevier, Amsterdam
9. Dostál L, Jambor R, Růžička A, Jirásko R, Císařová I, Holeček J (2006) Reactivity of intramolecularly coordinated aluminum compounds to R₃EOH (E = Sn, Si) remarkable migration of N, C, N and O, C, O pincer ligands. *J Organomet Chem* 691:35–44
10. Dostál L, Jambor R, Růžička A, Císařová I, Holeček J (2005) Aluminium alkyls with intramolecularly coordinated oxygen. *Appl Organomet Chem* 19:797–802
11. Schumann H, Hartmann U, Wassermann W (1991) Synthesis and characterization of organogallium and organoindium compounds with tridentate 2,6-bis[(dialkylamino)methyl]phenyl ligands. *Chem Ber* 124:1567–1569
12. Cowley AH, Gabbäi FP, Atwood DA (1994) An intramolecularly base-stabilized gallium dihydride - a link between organometallic and aqueous gallium chemistry. *J Am Chem Soc* 116:1559–1560
13. Cowley AH, Gabbäi FP, Olbrich F, Corbelin S, Lagow RJ (1995) Surprising stability of a monomeric bis azide of gallium(III). *J Organomet Chem* 487:C5–C7
14. Olazábal CA, Gabbäi FP, Cowley AH (1994) Intramolecular base stabilization of cobalt-gallium and cobalt-indium compounds. *Organometallics* 13:421–423
15. Cowley AH, Jones RA, Mardones MA, Ruiz J, Atwood JL, Bott SG (1990) Synthesis and structure of a diphosphadigallate - a novel base-stabilized Ga₂P₂ ring-system. *Angew Chem Int Ed* 102:1150–1151
16. Dam MA, Nijbacker T, de Pater BC, de Kanter FJJ, Akkermann OS, Bickelhaupt F, Smeets WJJ, Spek AL (1997) Synthesis, structure, and properties of an intramolecularly coordinated diindacycle: 9,10-dihydro-9,10-bis[2,6-bis((dimethylamino)methyl)phenyl]-9,10-diindaanthracene. *Organometallics* 16:511–512
17. Lomeli V, McBurnett BG, Cowley AH (1998) An indium(II)-indium(II) compound with intramolecular donor-acceptor bonds. *J Organomet Chem* 562:123–125
18. van der Ploeg AFMJ, van Koten G, Vrieze K (1981) Aspects of transmetallation reactions of 2-Me₂NCH₂C₆H₄⁻ and 2,6-(Me₂NCH₂)C₆H₃⁻ metal (Pd, Pt, Hg, Tl) complexes with metal carboxylates and low-valent metal (Pd, Pt) complexes. *J Organomet Chem* 222:155–174
19. Manju KD, Kumar D (2011) Cadmium and tin complexes of Schiff-base ligands. *J Coord Chem* 64:2130–2156
20. Hadjikakou SK, Hadjiliadis N (2009) Antiproliferative and anti-tumor activity of organotin compounds. *Coord Chem Rev* 253:235–249
21. Chandrasekhar V, Gopal K, Thilagar P (2007) Nanodimensional organostannoxane molecular assemblies. *Acc Chem Res* 40:420–434
22. Rivard E, Power PP (2008) Recent developments in the chemistry of low valent Group 14 hydrides. *Dalton Trans* 4336–4343
23. Corriu RJP, Mix A, Lanneau FG (1998) Intramolecular nitrogen ligand stabilization of phenyl-imidazolidine derived silicon species. *J Organomet Chem* 570:183–193
24. Carre FH, Corriu RJP, Lanneau GF, Merle P, Soulaïrol F, Yao JC (1997) Synthesis and structural characterization of functional bicyclic intramolecularly coordinated aminoarylsilanes in a series of dibenzyl(1,5) azasilocenes. *Organometallics* 16:3878–3888

25. Carre F, Chauhan M, Chuit C, Corriu RJP, Reye C (1997) Influence of the solvent and of the counteranion on the structure of silyl cations stabilized by a terdentate aryldiamine ligand. *J Organomet Chem* 540:175–183
26. Chauhan M, Chuit C, Corriu RJP, Mehdi A, Reye C (1996) Study of silyl cations bearing an aryldiamine pincer ligand. *Organometallics* 15:4326–4333
27. Chuit C, Corriu RJP, Mehdi A, Reye C (1996) Unexpected basicity of a hexacoordinate silicon compound, {2,6-bis[(dimethylamino)methyl]phenyl}bis(1,2-benzenediolato)silicate. *Chem Eur J* 2:342–347
28. Corriu RJP, Chauhan BPS, Lanneau GF (1995) Unexpected reactivity of functionalized lewisbase stabilised silanediyl transition-metal complexes toward organolithium nucleophiles. *Organometallics* 14:4014–4017
29. Carre F, Chuit C, Corriu RJP, Mehdi A, Reye C (1995) Synthesis, structure and fluxional behavior of a dihydrosilane bearing an aryldiamine pincer ligand. *Organometallics* 14:2754–2759
30. Corriu RJP, Chauhan BPS, Lanneau G (1995) Base stabilization of functionalized silylene transition metal complexes. *Organometallics* 14:1646–1656
31. Benin VA, Martin JC, Willcott MR (1997) Solution and solid state studies of some new silicon and germanium compounds stabilized by tridentate ligands. *Tetrahedron* 53:10133–10154
32. Lappert MF, Power PP (1985) Subvalent group-4B metal alkyls and amides. Transition-metal chemistry of metal(II) bis(trimethylsilyl)amides $\text{Ge}'[\text{N}(\text{SiMe}_3)_2]_2$, $\text{Sn}'[\text{N}(\text{SiMe}_3)_2]_2$, $\text{Pb}'[\text{N}(\text{SiMe}_3)_2]_2$. *J Chem Soc Dalton Trans* 51
33. Campbell GK, Hitchcock PB, Lappert MF (1985) Heterobimetalllic (Pd/Pt-Ge/Sn) trinuclear clusters containing a planar $\text{M}_3(\text{CO})_3(\text{m}^2\text{-M}')_3$ core. *J Organomet Chem* 289:C1–C4
34. Hitchcock PB, Lappert MF, Misra CM (1985) Homoleptic, three-co-ordinate group 8c noble metal(0) complexes having Ge' or Sn' ligands, $[\text{M}\{\text{M}'(\text{NR}_2)_2\}_3]$ ($\text{M} = \text{Pd}$ or Pt , $\text{M}' = \text{Ge}$ or Sn , $\text{R} = \text{SiMe}_3$), and the X-ray structure of one of them ($\text{M} = \text{Pd}$, $\text{M}' = \text{Sn}$). *J Chem Soc Chem Commun* 13:863–864
35. Hawkins SM, Hitchcock PB, Lappert MF (1985) Neutral η -arene complexes of rhodium(I); X-ray structure of η -toluene(η -cyclooctene) [bis{bis(trimethylsilyl)amido} chlorostannate (II)]rhodium(I). *J Chem Soc Chem Commun* 1592–1593
36. Schager F, Seevogel K, Pörschke KR, Kessler M, Krüger C (1996) Reversible water and methanol activation at the $\text{Pd}=\text{Sn}$ bond. *J Am Chem Soc* 118:13075–13076
37. Krause J, Haack KJ, Pörschke KR, Gabor B, Goddard R, Pluta C, Seevogel K (1996) A Palladium-catalyzed stannole synthesis. *J Am Chem Soc* 118:804–821
38. Knorr M, Hallauer E, Huch V, Veith M, Braunstein P (1996) Reactions of heterodinuclear Fe-Pt and Fe-Pd complexes with cyclic bis(amino)germylenes and stannylenes: a bridging metal (II) amide unit between two different transition metal centers and donor stabilization of terminal germylene and stannylene ligands by $\text{Si}(\text{OMe})_3$. *Organometallics* 15:3868–3875
39. Veith M, Müller A, Stahl L, Nötzel M, Jarczyk M, Huch V (1996) Formation of metal clusters or nitrogen-bridged adducts by reaction of a bis(amino) stannylene with halides of two-valent transition metals. *Inorg Chem* 35:3848–3855
40. Zabula AV, Pape T, Hepp A, Hahn FE (2008) Coordination chemistry of bisstannylenes with platinum(0). *Dalton Trans* 43:5886–5890
41. Zabula AV, Pape T, Hepp A, Hahn FE (2008) Homoleptic complexes of bisstannylenes with nickel(0): synthesis, X-ray diffraction studies, and ^{119}Sn NMR investigations. *Organometallics* 27:2756–2760
42. Nickl C, Eichele K, Joosten D, Langer T, Schappacher FM, Pöttgen R, Englert U, Wesemann L (2011) 1,1,1-tris(distanna-closo-dodecaborate)stannate: a tripodal tin ligand. *Angew Chem Int Ed* 50:5766–5769
43. Angermund K, Jonas K, Krüger C, Latten JL, Tsay YH (1988) The synthesis and crystal structure of $\text{Sn}(\text{C}_6\text{H}_4\text{CH}_2\text{NMe}_2\text{-o})_2$, and reaction with $\text{Co}(\eta^5\text{-C}_5\text{H}_5)(\eta^2\text{-C}_2\text{H}_2)_2$. *J Organomet Chem* 353:17–25

44. Drost C, Hitchcock PB, Lappert MF (1998) Stable intramolecularly base-stabilized germylene- and Stannylene-Borane adducts: $M[C_6H_3(NMe_2)_2-2,6]_2BH_3$ ($M = Ge, Sn$). *Organometallics* 17:3838–3840
45. Drost C, Hitchcock PB, Lappert MF (1999) Thermally stable heterobinuclear bivalent Group 14 metal complexes $Ar_2MSn[1,8-(NR)_2C_{10}H_6]$ ($M=Ge, Sn$; $Ar=2,6-(Me_2N)_2C_6H_3$; $R=CH_2^tBu$). *Angew Chem Int Ed* 38:1113–1116
46. Drost C, Hitchcock PB, Lappert MF, Pierssens LJM (1997) The novel, chelating C, N-bidentate 2,6-bis(dimethylamino)phenyl ligand (R2), showing ambidentate N, N'-character in $M(R)_2$ ($M = Ge, Sn, Pb$) and $Sn(R)X$ [$X = N(SiMe_3)_2, CH(SiMe_3)_2, Cl$]. *Chem Commun* 12:1141–1142
47. Schmidt H, Keitemeyer S, Neumann B, Stammler HG, Schoeller WW, Jutzi P (1998) Germylenes and germyl cations with the 2,4-di-tert-butyl-6-(N,N-dimethylaminomethyl) phenyl ligand. *Organometallics* 17:2149–2151
48. Henn M, Schürmann M, Mahieu B, Zanella P, Cinquantini A, Jurkschat K (2006) A ferrocenyl-bridged intramolecularly coordinated bis(diorganostannylene): synthesis, molecular structure and reactivity of $[4-t-Bu-2,6-\{P(O)(O-i-Pr)_2C_6H_2Sn\}C_5H_4]_2Fe$. *J Organomet Chem* 691:1560–1572
49. Driess M, Dona N, Merz K (2004) Novel hypervalent complexes of main-group metals by intramolecular ligand. Metal electron transfer. *Chem Eur J* 10:5971–5976
50. Jutzi P, Keitemeyer S, Neumann B, Stammler A, Stammler HG (2001) Synthesis and structure of the first oxygen-donor-stabilized organogermanium(II) compounds. *Organometallics* 20:42–46
51. Fischer RC, Power PP (2010) π -Bonding and the lone pair effect in multiple bonds involving heavier main group elements: developments in the new millennium. *Chem Rev* 110:3877–3923
52. Power PP (2003) Silicon, germanium, tin and lead analogues of acetylenes. *Chem Commun* 2091–2101
53. Peng Y, Wang X, Fettinger JC, Power PP. Reversible complexation of isocyanides by the distannyne $ArSnSnAr$ ($Ar = C_6H_3-2,6(C_6H_3-2,6-i-Pr_2)_2$). *Chem Commun* 46 943–945
54. Eichler BE, Philip PP (2000) $[2,6-Trip_2H_3C_6Sn(\mu-H)]_2$ ($Trip = C_6H_2-2,4,6-i-Pr_3$): synthesis and structure of a divalent group 14 element hydride. *J Am Chem Soc* 122:8785–8786
55. Olmstead MM, Simons RS, Power PP (1997) Synthesis and characterization of $[Sn_2\{C_6H_3-2,6(2,4,6-i-Pr_3C_6H_2)_2\}]^+$: a singly reduced valence isomer of a "Distannyne. *J Am Chem Soc* 119:11705–11706
56. Jones JN, Cowley AH (2005) π -Indenyl tin(II) and lead(II) compounds. *Chem Commun* 1300–1302
57. Constantine SP, De Lima GM, Hitchcock PB, Keates JM, Lawless GA, Marziano I (1997) Synthesis and characterization of $Sn(\eta^5-C_5Me_5)Cl$ and $Sn\{\eta^5-C_5Me_4(SiMe_2But)\}Cl$. *Organometallics* 16:793–795
58. Jastrzebski JTBH, van der Schaaf PA, Boersma J, van Koten G, Zoutberg MC, Heijdenrijk D (1989) Synthesis and characterization of (2,6-bis[(dimethylamino)methyl]phenyl)tin(II) chloride and (2,6-bis[(dimethylamino)methyl]phenyl)4-tolyltin(II), the first example of a mixed diaryltin(II) compound. *Organometallics* 8:1373–1375
59. Jastrzebski JTBH, van der Schaaf PA, Boersma J, van Koten G, de Wit M, Wang Y, Heijdenrijk D, Stam CH (1991) Oxidative-addition reactions of molecular diiodine and dibromine to divalent organotin compounds. Crystal structures of bis[8-(dimethylamino)-1-naphthyl]tin(IV) dibromide and $\{2,6-[bis(dimethylamino)methyl]phenyl\}(4-tolyl)$ tin(IV) diiodide. *J Organomet Chem* 407:301–311
60. Bibal C, Mazieres S, Gornitzka H, Couret C (2002) New arylchlorogermynes stabilized by two ortho side-chain donor ligands. *Polyhedron* 21:2827–2834
61. Bibal C, Mazieres S, Gornitzka H, Couret C (2002) From chlorogermynes to stable hydroxy- and siloxy-germylene-tungsten complexes. *Organometallics* 21:2940–2943

62. Bibal C, Mazieres S, Gornitzka H, Couret C (2001) A route to a germanium - carbon triple bond: first chemical evidence for a germyne. *Angew Chem Int Ed Engl* 40:952–954
63. Kašná B, Jambor R, Schürmann M, Jurkschat K (2008) Synthesis and characterization of novel intramolecularly O, C, O-coordinated heteroleptic organostannylenes and their tungstenpentacarbonyl complexes. *J Organomet Chem* 693:3446–3450
64. Henn M, Deáky V, Krabbe S, Schürmann M, Prosenc MH, Herres-Pawlis S, Mahieu B, Jurkschat K (2011) Heteroleptic organostannylenes and an organoplumbylene bearing phosphorus-containing pincer-type ligands – structural variations and insights into the configurational stability. *Z Anorg Allg Chem* 637:211–223
65. Kašná B, Jambor R, Schürmann M, Jurkschat K (2007) [2,6-(*t*-BuOCH₂)₂C₆H₃Sn(OH)]₂O: A rare example of a monomeric tetraorganodistannoxane stabilized by intramolecular hydrogen bridges. *J Organomet Chem* 692:3555–3558
66. Martinová J, Dostál L, Herres-Pawlis S, Růžička A, Jambor R (2011) Intramolecularly coordinated [2,6-(Me₂NCH₂)₂C₆H₃]Sn^{II}]+: a strong σ donor for Pt(II). *Chem Eur J* 17:7423–7427
67. Jambor R, Kašná B, Kirschner KN, Schürmann M, Jurkschat K (2008) [2,6-(Me₂NCH₂)₂C₆H₃]Sn]₂: an intramolecularly coordinated diorganodistannylene. *Angew Chem Int Ed* 47:1650–1653
68. Bouška M, Dostál L, Růžička A, Beneš L, Jambor R (2011) Oxidation of intramolecularly coordinated distannylene by S₈: from tin(I) to tin(IV) polysulfide via tin(II) sulfide. *Chem Eur J* 17:450–454
69. Bouška M, Dostál L, de Proft F, Růžička A, Lyčka A, Jambor R (2011) Intramolecularly coordinated Tin(II) selenide and triselenoxostannonic acid anhydride. *Chem Eur J* 17:455–459
70. Mehring M, Low C, Schürmann M, Uhlig F, Jurkschat K, Mahieu B (2000) Novel heteroleptic stannylenes with intramolecular O, C, O-donor stabilization. *Organometallics* 19:4613–4623
71. Jambor R, Herres-Pawlis S, Schürmann M, Jurkschat K (2011) [2,6-(Me₂NCH₂)₂C₆H₃]Sn(μ -OH)W(CO)₅]₂: a transition-metal-coordinated organotin(II) hydroxide. *Eur J Inorg Chem* 3:344–348
72. Dostalova R (2009) Complexes of transition metals with (YCY)SnCl stannylene: synthesis and reactivity, Thesis of University Pardubice
73. Jambor R, Kašná B, Koller SG, Strohmann C, Schürmann M, Jurkschat K (2010) [2,6-(Me₂NCH₂)₂C₆H₃(H₂O)Sn]W(CO)₅]+CB₁₁H₁₂⁻: aqua complex of a transition-metal-bound organotin(II) cation versus an ammonium-type structure. *Eur J Inorg Chem* 6:902–908
74. Dostálova R, Dostál L, Růžička A, Jambor R (2011) Chromiumpentacarbonyl-coordinated organotin(II) cation. *Organometallics* 30:2405–2410
75. Martinová J, Dostál L, Růžička A, Taraba J, Jambor R (2007) Palladium(II) complexes of the (N, C, N)SnCl stannylene. *Organometallics* 26:4102–4104
76. Deaky V, Schürmann M, Jurkschat K, Martinová J, Jambor R, Herres-Pawlis S (2011) Syntheses and molecular structures of transition metal complexes (R₂SnCl)₂MX₂ (R = 4-*t*-Bu-2,6-[P(O)(*O*-*i*-Pr)₂]₂C₆H₂, 2,6-(Me₂NCH₂)₂C₆H₃; X = Cl, Br, I; M = Pd, Pt) bearing heteroleptic intramolecularly coordinated organostannylenes. *Chem Eur J*
77. Martinová J, Dostálova R, Dostál L, Růžička A, Jambor R (2009) The stannylene {2,6-(Me₂NCH₂)₂C₆H₃}SnCl as a ligand in transition metal complexes of palladium, ruthenium, and rhodium. *Organometallics* 28:4823–4828
78. Martinová J, Jambor R, Schürmann M, Jurkschat K, Honzický J, Almeida Paz FA (2009) Palladium and molybdenum complexes of the heteroleptic organostannylene [2,6-(Me₂NCH₂)₂C₆H₃]SnCl. *Organometallics* 28:4778–4782
79. Deaky V, Schürmann M, Jurkschat K (2009) The first ruthenium complex of a heteroleptic organostannylene: [4-*t*-Bu-2,6-[P(O)(*O*-*i*-Pr)₂]₂C₆H₂]Sn(Cl)Ru(C₆H₆)Cl₂. *Z Anorg Allg Chem* 635:1380–1383

80. Atwood DA, Cowley AH, Ruiz J (1992) Use of the 2,6-bis[(dimethylamino)methyl]phenyl ligand to form some pentacoordinate derivatives of P(III), As(III), Sb(III) and Bi(III). *Inorg Chim Acta* 198:271–274
81. Dostál L, Jambor R, Růžička A, Jirásko R, Holeček J, De Proft F (2011) OCO and NCO chelated derivatives of heavier group 15 elements. Study on possibility of cyclization reaction via intramolecular ether bond cleavage. *Dalton Trans* 40:8922–8934
82. Atwood DA, Cowley AH, Jones RA, Mardones MA (1992) Synthesis of the 1st diarsadigallatane. *J Organomet Chem* 439:C33–C35
83. Soran AP, Silvestru C, Breunig HJ, Balázs G, Green JC (2007) Organobismuth(III) dihalides with T-shaped geometry stabilized by intramolecular N → Bi interactions and related diorganobismuth(III) halides. *Organometallics* 26:1196–1203
84. Dostál L, Císařová I, Jambor R, Růžička A, Jirásko R, Holeček J (2006) Structural diversity of organoantimony(III) and organobismuth(III) halides containing O, C, O chelating ligands. *Organometallics* 25:4366–4373
85. Dostál L, Jambor R, Císařová I, Beneš L, Růžička A, Jirásko R, Holeček J (2007) Unexpected product formed by the reaction of [2,6 - (MeOCH₂)₂C₆H₃]Li with SbCl₃. Structure of Sb - O intramolecularly coordinated organoantimony cation. *J Organomet Chem* 692:2350–2353
86. Dostál L, Jambor R, Růžička A, Jirásko R, Císařová I, Holeček J (2008) The synthesis of organoantimony(III) difluorides containing Y, C, Y pincer type ligands using organotin(IV) fluorinating agents. *J Fluorine Chem* 129:167–172
87. Machuča L, Dostál L, Jambor R, Handlřík K, Jirásko R, Růžička A, Císařová I, Holeček J (2007) Intramolecularly coordinated organoantimony(III) carboxylates. *J Organomet Chem* 692:3969–3975
88. Dostál L, Novák P, Jambor R, Růžička A, Císařová I, Jirásko R, Holeček J (2007) Synthesis and structural study of organoantimony(III) and organobismuth(III) triflates and cations containing O, C, O pincer type ligands. *Organometallics* 26:2911–2917
89. Dostál L, Jambor R, Jirásko R, Padělková Z, Růžička A, Holeček J (2010) Structural study on the organoantimony(III) NCN - chelated compounds [2,6 - (Me₂NCH₂)₂C₆H₃]SbX₂ - influence of the polar group X. *J Organomet Chem* 695:392–397
90. Casely IJ, Ziller JW, Mincher BJ, Evans WJ (2011) Bismuth coordination chemistry with allyl, alkoxide, aryloxy, and tetraphenylborate ligands and the {[2,6-(Me₂NCH₂)₂C₆H₃]₂Bi}(⁺) cation. *Inorg Chem* 50:1513–1520
91. Dostál L, Jambor R, Růžička A, Erben M, Jirásko R, Černošková Z, Holeček J (2009) Efficient and reversible fixation of carbon dioxide by NCN chelated organoantimony(III) oxide. *Organometallics* 28:2633–2636
92. Fridrichová A, Svoboda T, Jambor R, Padělková Z, Růžička A, Erben M, Jirásko R, Dostál L (2009) Synthesis and structural study on organoantimony(III) and organobismuth(III) hydroxides containing an NCN pincer type ligand. *Organometallics* 28:5522–5528
93. Svoboda T, Jambor R, Růžička A, Padělková Z, Erben M, Jirásko R, Dostál L (2010) NCN chelated organoantimony and organobismuth phosphonates: syntheses and structures. *Eur J Inorg Chem* 2010:1663–1669
94. Svoboda T, Jambor R, Růžička A, Padělková Z, Erben M, Dostál L (2010) NCN chelated organoantimony(III) and organobismuth(III) phosphinates and phosphites: synthesis, structure and reactivity. *Eur J Inorg Chem* 2010:5222–5230
95. Svoboda T, Dostál L, Jambor R, Růžička A, Jirásko R, Lyčka A (2011) NCN chelated organoantimony(III) and organobismuth(III) phosphates: synthesis, solid state and solution structure. *Inorg Chem* 50:6411–6413
96. Breunig HJ, Nema MG, Silvestru C, Soran AP, Varga RA (2010) Organobismuth compounds with the pincer ligand 2,6-(Me₂NCH₂)₂C₆H₃: monoorganobismuth(III) carbonate, sulfate, nitrate, and a diorganobismuthenium(III) salt. *Dalton Trans* 39:11277–11284
97. Casely IJ, Ziller JW, Fang M, Furche F, Evans WJ (2011) Facile bismuth-oxygen bond cleavage, C-H activation, and formation of a monodentate carbon-bound oxyaryl dianion, ((C₆H₂Bu₂)-Bu-*t*-3,5-O-4)(2-). *J Am Chem Soc* 133:5244–5247

98. Chovancová M, Jambor R, Růžička A, Jirásko R, Císařová I, Dostál L (2009) Synthesis, structure and reactivity of intramolecularly coordinated organoantimony and organobismuth sulfides. *Organometallics* 28:1934–1941
99. Dostál L, Jambor R, Růžička A, Jirásko R, Lochař V, Beneš L, De Proft F (2009) Non-conventional behavior of NCN chelated organoantimony(III) sulfide and isolation of cyclic organoantimony(III) bis-pentasulfide. *Inorg Chem* 28:10495–10497
100. Dostál L, Jambor R, Růžička A, Jirásko R, Černošková Z, Beneš L, De Proft F (2010) [2+2] cycloaddition of carbon disulfide to NCN-chelated organoantimony(III) and organobismuth (III) sulfides – an evidence for terminal Sb-S and Bi-S bonds in solution. *Organometallics* 29:4486–4490
101. Dostál L, Jambor R, Růžička A, Lyčka A, Brus J, De Proft F (2008) Synthesis and structure of organoantimony(III) compounds containing antimony – selenium and -tellurium terminal bonds. *Organometallics* 27:6059–6062
102. Balázs L, Breunig HJ, Lork E, Soran AP, Silvestru C (2006) Isomers of a dibismuthane, $R_2Bi-BiR_2$ [$R=2,6-(Me_2NCH_2)_2C_6H_3$], and unusual reactions with oxygen: formation of $[R_2Bi]_2(O-2)$ and $R' R'' Bi$ [$R'=2-(Me_2NCH_2)-6-(Me_2N(O)CH_2)C_6H_3$; $R''=2-(Me_2NCH_2)-6-(O(O)C)C_6H_3$]. *Inorg Chem* 45:2341–2346
103. Dostál L, Jambor R, Růžička A, Holeček J (2008) Syntheses and structures of Ar_3Sb_5 and Ar_4Sb_4 compounds ($Ar = C_6H_3-2,6-(CH_2NMe_2)_2$). *Organometallics* 27:2169–2171
104. Šimon P, De Proft F, Jambor R, Růžička A, Dostál L (2010) Monomeric organoantimony(I) and organobismuth(I) compounds stabilized by NCN chelating ligand: syntheses and structures. *Angew Chem Int Ed* 49:5468–5471
105. Dostál L, Jambor R, Růžička A, Šimon P (2011) On the reduction of NC chelated organoantimony(III) chlorides. *Eur J Inorg Chem* 2011:2380–2386
106. Power PP (2010) Main-group elements as transition metals. *Nature* 463:171–177
107. Gunanathan C, Milstein D (2011) Metal–ligand cooperation by aromatization–dearomatization: a new paradigm in bond activation and green catalysis. *Acc Chem Res* 44:588–602

Pincer Complexes as Catalysts in Organic Chemistry

Kálmán J. Szabó

Abstract Application of pincer complexes in catalytic applications is a rapidly expanding field in organic synthesis. This chapter is mainly focused on selective formation of carbon–carbon, carbon–nitrogen, and carbon–metal (C–B, C–Si, and S–Sn) bonds, as well as transfer hydrogenation reactions. The described pincer-complex catalyzed processes are more efficient and more selective than the corresponding transformations catalyzed by metal salts and added ligands. Some of the described pincer-complex catalyzed reactions are not amenable by traditional metal catalysts at all. It has been demonstrated that the superiority of pincer-complex catalysts over the traditional ones is based on the high stability and well-defined structure and stoichiometry of these species. These properties of pincer complexes allow a rational design of active and highly selective catalysts.

Keywords Aldol reaction · Allylation · Hydrogenation · Michael addition · Palladium · Pincer complexes · Rhodium · Ruthenium

Contents

1	General Considerations	204
2	Aldol Reactions	205
2.1	Aldol Reaction of Aldehydes and Isocyanides	205
2.2	Reductive Aldol Coupling	209
3	Michael Additions	209
4	Allylation of Aldehydes and Imines	211
4.1	Pincer Complexes as Lewis-Acid Catalysts	212
4.2	Allylated Pincer Complexes as Reactive Intermediates	212

K.J. Szabó (✉)

Department of Organic Chemistry, Stockholm University, SE-106 91 Stockholm, Sweden
e-mail: kalman@organ.su.se

5	Pincer-Complex Catalyzed Synthesis of Unsaturated Organo-Boron, -Silicon and -Tin Species	217
5.1	Pincer-Complex Catalyzed Synthesis of Functionalized Allylboronic Acids	218
5.2	Formation of Allyl Stannanes Using Hexaalkylditin Reagents	220
5.3	Stannylation of Propargylic Substrates	221
5.4	Preparation of Allenyl Silanes	223
5.5	Mechanistic Aspects of the Pincer-Complex Catalyzed Metal Substitution Reactions	223
6	Pincer-Complex Catalyzed Kharasch Addition	225
6.1	Nickel Pincer-Complex Catalyzed Kharasch Reaction	225
6.2	Mechanism of the Pincer-Complex Catalyzed Kharasch Reaction	226
7	Metallopincer Catalyzed Heck and Suzuki Reactions	226
7.1	Application of Palladium Pincer-Complex Catalysts for Heck and Suzuki Couplings	227
7.2	Mechanistic Aspects of the Pincer-Complex Catalyzed Coupling Reactions	230
8	Hydroamination Reactions Catalyzed by Palladium Pincer-Complex Catalysts	234
9	Ruthenium Pincer-Complex Catalyzed Transfer Hydrogenation Reactions	235
10	Conclusions and Outlook	237
	References	238

1 General Considerations

Transition metal catalyzed transformations represent an important synthetic tool in modern organic chemistry, because of their high efficiency, selectivity, and an economical use of the reactants [1–4]. The metal complexes are reused in many catalytic cycles, and therefore a metal catalyst is able to selectively convert a large number of substrate molecules to products. Therefore, the predictability and stability of the catalytic species in a certain organic transformation are properties of critical importance. In this respect pincer-complex catalysts have some attractive features [5–9]. Several metal pincer complexes are remarkably stable species, because of their terdentate chelating structure and amazingly stable carbon–metal σ -bond(s). Therefore, the air- and thermostability of certain nickel, palladium, and platinum containing pincer complexes remind more to the ordinary organic substances than to organometallic species. The high stability of the complexes and the tight metal ligand interaction make pincer complexes particularly suitable for immobilization to solid or dendrimeric support creating robust recyclable catalysts [5, 6].

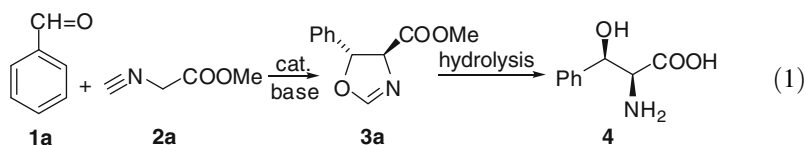
Another important consequence of the terdentate coordination is that the number of free coordination sites on the metal is reduced by three. The relatively low number of accessible coordination sites on the metal atom often represents an important factor to increase the regio- and stereoselectivity of the organic transformations or to alter the reactivity of the metal atom. The third important factor is the well-defined stoichiometry and bonding structure of the pincer complexes, which facilitates the rational design of the catalytic transformations, as well as an efficient tuning of the catalytic properties. Considering the above, the high current interest for application of pincer complexes as catalysts in organic transformations is clearly justified. In the last half-decade several excellent reviews were published focusing fully or partially on the catalytic application of pincer

complexes [5–16] and also a comprehensive monography appeared on the chemistry of pincer compounds [17]. These publications have clearly shown that existing transition metal catalyzed reactions can be considerably improved and fine-tuned by using pincer-complex catalysts; and even new synthetic routes not amenable with commonly used catalysts can be opened by the application of these species. The present review is focused on application of pincer-complex catalysts in important organic transformations, such as selective formation of carbon–carbon, carbon–nitrogen, and carbon–metal (C–B, C–Si, and S–Sn) bonds, as well as transfer hydrogenation reactions. Some other, very important pincer-complex catalyzed synthetic applications are given in other reviews in this special issue of Topics in Organometallic Chemistry or were reviewed very recently. Thus concerning dehydrogenation reactions [18] as well as aromatization–dearomatization processes [19] based on pincer-complex catalysts we refer the reader to the corresponding specialized reviews.

2 Aldol Reactions

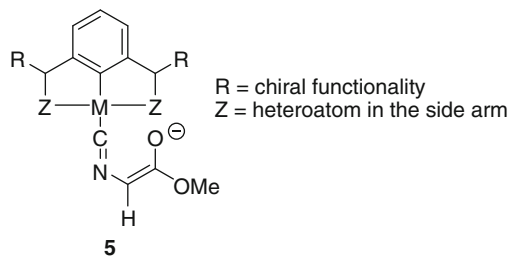
2.1 Aldol Reaction of Aldehydes and Isocyanides

Pincer-complex catalysts have been extensively applied (Eq. 1) in aldol reactions of aldehydes (e.g., **1a**) or ketones with isocyanides (e.g., **2a**). This reaction results in oxazoline derivatives (**3a**), which can be hydrolyzed to amino acids (**4**). Thus, the asymmetric version of the reaction is suitable for synthesis of enantiomerically pure amino acids, which is an obvious driving force for developing of new chiral catalysts (Eq. 1). The first studies of these reactions were performed by Hayashi and coworkers [20] using ferrocenylphosphine–gold complexes. Subsequently, a large number of studies were published based on application of pincer-complex catalysts [21–28].

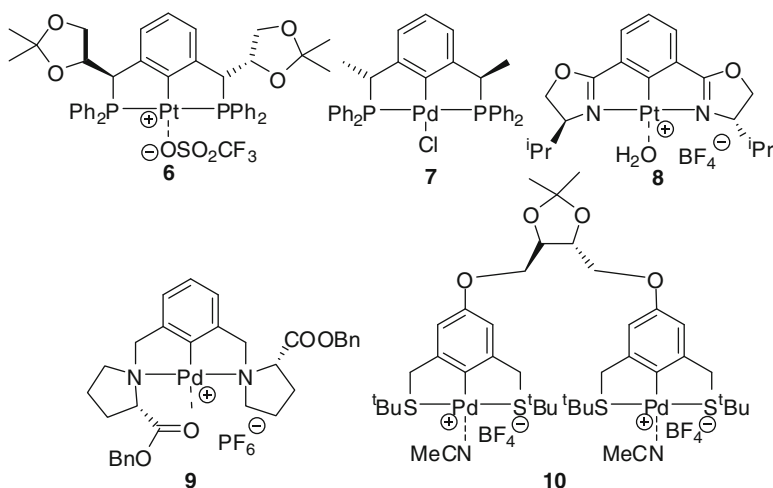


The pincer-complex catalyzed version of the aldol reaction is performed in the presence of base [such as $\text{NEt}(\text{}^i\text{Pr})_2$], which is necessary for the enolization of the isocyanide component. In the active catalysts (**5**) the enolized isocyanide (**2a**) is directly coordinated to the metal atom of the pincer complex (Scheme 1) [21] and the rate-determining step of the reaction is the electrophilic attack of the aldehyde on the coordinated isocyanide.

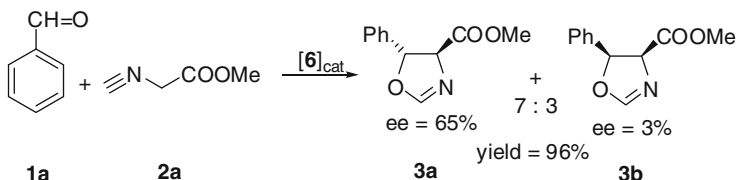
In particular, platinum and palladium containing complexes, such as **6–10**, proved to be efficient catalysts for synthesis oxazolidines derivatives (Scheme 2). Venanzi and coworkers [21] reported the first enantioselective aldol reaction using



Scheme 1 Reaction intermediate of the pincer complex catalyzed synthesis of oxazolidines **3a–b**

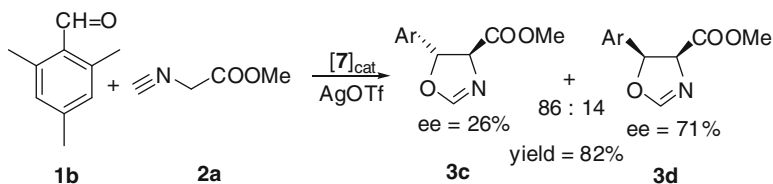


Scheme 2 Example for pincer complex catalyzed aldol reaction of aldehydes and isocyanides

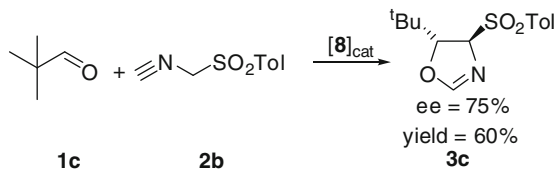


Scheme 3 Aldol reaction published by Venanzi and coworkers [21]

platinum pincer complex **6** (Scheme 3). The reaction resulted in a mixture of two diastereomers **3a** and **3b** up to 65 % ee. The major diastereomer, the *trans* form (**3a**), could be obtained with a higher enantioselectivity than the *syn* diastereomer **3b**. *Ortho* substitution of the aromatic ring of aldehyde **1a** led to the improvement of the diastereoselectivity; however the enantioselectivity was decreased.



Scheme 4 Enantioselective formation *cis* oxazolidine **3d** catalyzed by complex **7** [22]



Scheme 5 Employment of tosylmethyl isocyanide **2b** increase the diastereoselectivity of the aldol reaction [23]

Zhang and coworkers [22] replaced the metal atom of **6** with palladium and implemented methyl groups in the side arms presenting complex **7**. The catalyst activated by silver triflate afforded *cis* and *trans* diastereomeric mixtures (Scheme 4).

Interestingly, this catalyst gave the *cis* product in higher enantioselectivity than the *trans* product. The best results (up to 71 % ee) were obtained using mesitaldehyde **1b** (Scheme 4). Van Koten and coworkers employed chiral NCN palladium pincer complexes to achieve promising levels (up to 42 % ee) of enantioselectivity [29]. Subsequent studies have shown that the diastereoselectivity of the pincer-complex catalyzed reactions can be substantially improved by variation of the employed isocyanide. Thus Motoyama and coworkers [23] reacted tosylmethyl isocyanide **2b** with various aldehydes in the presence of phebox-derived palladium and platinum (**8**) complexes (Scheme 5) to obtain exclusively *trans* oxazolidine derivatives (**3c**). Similar to the above studies [21, 22] the degree of the enantioselection was dependent on the structure of the aldehyde component. The best result (75 % ee) was presented for the coupling of **2b** with pivalaldehyde **1c**. Interestingly, the same catalyst (**8**) provided low levels of diastereo- and enantioselectivity, when isocyanide **2a** was employed in place of **2b** [23]. Furthermore, the platinum-based complexes seem to provide higher enantioselectivity than the palladium analogs [24].

Van Koten and coworkers [25–27] have developed a new generation of easily tunable chiral NCN-pincer-complex catalysts (such as **9**) for aldol reaction of aldehydes and isocyanides. These complexes are often easily accessible because of the modern metallorganic techniques developed for their preparation. Although the preliminary results for coupling of **1a** and **2a** display lower enantioselectivities than the above-described complexes (**6–8**), further optimization of the reaction

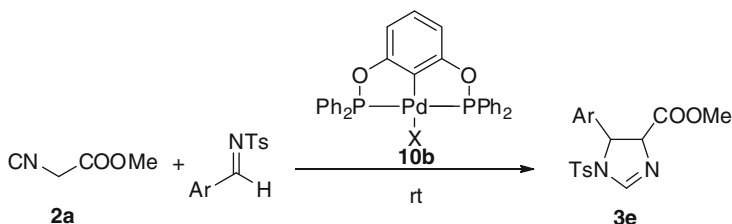


Fig. 1 Synthesis of imidazolines by pincer-complex catalyzed condensation of isocyanates with imines

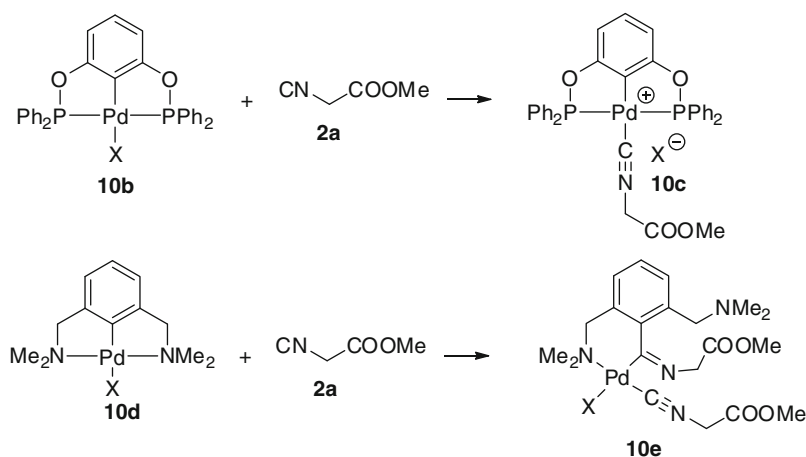
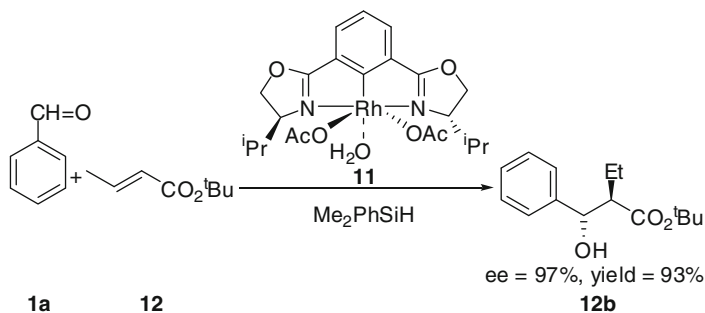


Fig. 2 PCP-type complexes activate **2a** by coordination to palladium [30], while NCN complexes undergo insertion with **2a** [29, 32]

conditions and substrates is expected to considerably increase the selectivity of these catalysts.

Swager and Giménez [28] described the synthesis of the isopropylidene bridged dimetallic SCS complex **10** (Scheme 2). Although this complex readily catalyzed the aldol reaction of aldehydes with **2a**, the resulted oxazolidine products were racemic, probably because the chiral centers are remote from the palladium atoms. On the other hand, catalyst **10** could easily be immobilized to silica gel via hydrolysis of the ketal functionality. Interestingly, the silica gel immobilized catalyst performed some moderate enantioselectivity (up to 3 % ee).

Szabó and coworkers [30] have shown that the reagent scope of the above cyclization reactions can be extended to sulfonimines (Fig. 1). The imidazoline derivatives could easily be hydrolyzed to α,β -aminoacids. The reaction proceeds with high stereoselectivity with simple PCP pincer complexes. The same group has developed an asymmetric version of the reaction using chiral pincer-complex catalysts [31]. Enantioselectivities up to 86 % ee were reported for this process.



Scheme 6 Highly selective asymmetric reductive aldol condensation [33]

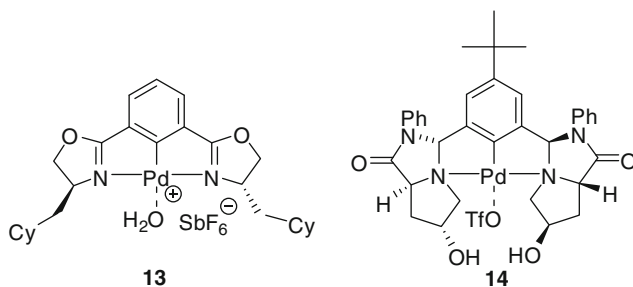
Mechanistic studies by the van Koten [29, 32] and the Szabó [30] groups have shown that the mechanism of the pincer-complex catalyzed aldol reactions is strongly influenced by the electronic properties of the side arms (Fig. 2). In case of π -acceptor side arms, such as in PCP complexes **10b**, the isocyanato group tightly coordinates to palladium (**10c**) without affecting the integrity of the pincer-complex structure. However, in case of σ -donor side arms, such as in NCN (**10d**) or SCS complexes, the isocyanatoacetate is inserted to the Pd–C bond, such as in complex **10e**. Accordingly, PCP complexes are direct catalysts to the aldol reactions with isocyanates, while NCN (and related σ -donor) pincer complexes are precursors of the palladacyclic catalysts.

2.2 Reductive Aldol Coupling

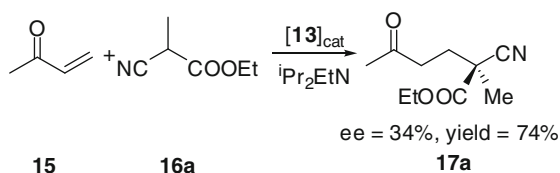
Nishiyama and coworkers [33] described a new type of asymmetric aldol reaction catalyzed by phebox-derived pincer complex **11**. In the so-called reductive aldol reaction α,β -unsaturated esters are activated with hydrosilanes followed by metal catalyzed condensation with aldehydes. Using benzaldehyde (**1a**) and tertiary-butyl acrylate or crotylate (**12**) the reductive aldol condensation proceeds with remarkably high stereo- and enantioselectivity (Scheme 6). The main product (such as **12b**) formed in excellent *trans* diastereoselectivity and the enantiomeric excess of the reactions was typically over 90 %. In some of the greatest applications the condensation product was obtained with 97 % ee and 93 % yield (Scheme 6) [33].

3 Michael Additions

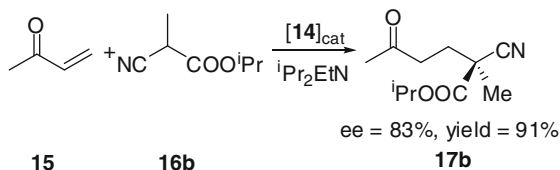
Similar to the aldol condensations the Michael additions are also fundamentally important reactions for carbon–carbon bond formation. Development and application of pincer complexes (such as **13** and **14**, Scheme 7) in Michael additions are mainly concentrated to the area of asymmetric catalysis. In the usual form of the



Scheme 7 Pincer complexes efficiently catalyzing Michael additions



Scheme 8 Michael addition catalyzed by oxazolidine complex **13** [24]



Scheme 9 Asymmetric Michael addition by Uozumi and coworkers [34, 35]

pincer-complex catalyzed process vinyl ketones (**15**) are reacted with α -cyanopropionates (**16a–b**) to obtain the corresponding Michael adducts, such as **17a** and **17b** (Schemes 8 and 9). The reaction is base catalyzed and the cyano group of **16** is believed to coordinate the metal atom in the activated catalyst [24, 26, 34, 35].

The first asymmetric Michael addition was published by Richards and Stark (Scheme 8) [24]. These authors employed oxazolinyl-based palladium pincer complexes (**13**) as catalysts. These complexes catalyzed the Michael reaction of **15** and **16a** with good yield, but with a moderate ee. The best enantioselectivity (34 % ee) could be achieved using the cyclohexyl substituted complex **13** (Scheme 8). Considerable further efforts were taken [36, 37] for synthesis of efficient oxazolinyl-based catalysts for Michael additions.

Ouzumi and coworkers [34, 35] have developed a new synthetic technique to obtain sterically hindered chiral NCN complexes (such as **14**), which proved to be an excellent catalysts for Michael additions. This method is based on site controlled metallation of the aromatic ring followed by introduction of the chiral ligand

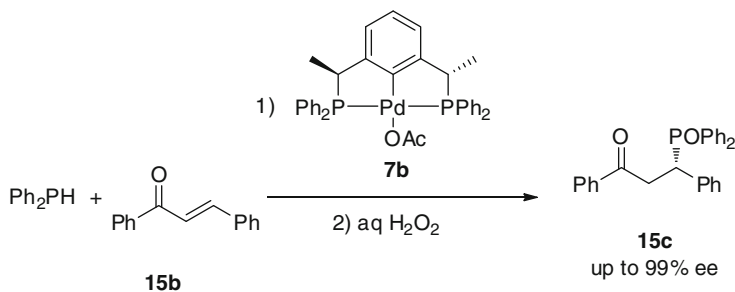


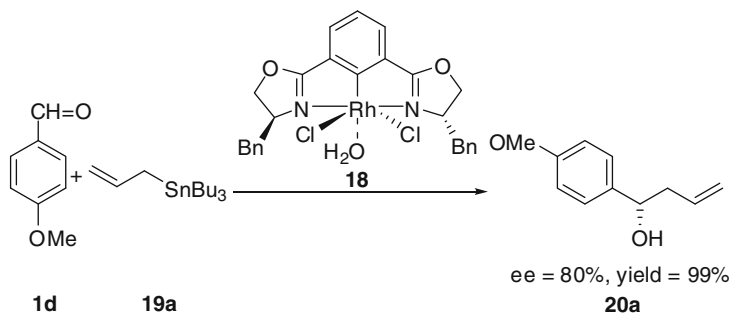
Fig. 3 Asymmetric addition of diphenyl phosphine to chalcone [38]

affording the desired pincer complex. Using this method several pyrroloimidazolone derived pincer complexes (**14**) were synthesized [34, 35]. The enantioselectivity of the Michael addition critically depended on the substituents of the pyrroloimidazolone ring system. It was shown that the high enantioselectivity requires the presence of hydroxy groups in the vicinity of palladium. It is suggested that the hydroxy functionalities are directly involved in the enantioselection process via hydrogen bonding. Employing catalyst **14** and isopropyl ester **16b** the enantioselectivity of the reaction could be increased to 83 % ee with excellent yield (Scheme 9).

A nice example for asymmetric aldol addition was reported by Duan and coworkers [38]. In this process diphenyl phosphine was reacted with chalcone in the presence of the chiral PCP complex **7b** (Fig. 3). This complex reported by Zhang and coworkers [22] proved to be an efficient catalyst in asymmetric aldol reaction (Sect. 2.1) as well. However, in the Michael addition excellent enantioselectivity, up to 99 % ee, could be achieved. In subsequent studies **15b** was replaced by unsaturated *N*-acylpyrrole derivatives to broaden the synthetic scope of the reaction [39].

4 Allylation of Aldehydes and Imines

Allylic alkylation is one of the most important metal catalyzed transformations for selective synthesis of unsaturated organic species [1–3]. Several transition metal species such as palladium, ruthenium, iridium, and rhodium catalyze allylation reactions; however, in the most established processes nucleophilic reagents, such as malonates and congeners, are allylated [40, 41]. Recently, however transition metal catalyzed allylation of electrophiles, such as aldehydes and imines, received much attention [42]. Pincer-complex catalysis proved to be a particularly useful tool for rhodium- and palladium-catalyzed allylation reactions. From mechanistic point of view the catalysts can be divided into two categories: Lewis-acid type catalysts and allyl transfer catalysts. In Lewis-acid type catalysts the metal atom activates the carbonyl group of the electrophile, while in allyl transfer catalysts the allyl moiety is transferred from the metal atom of the pincer complex to the electrophile.



Scheme 10 Application of pincer complex **18** as chiral Lewis-acid catalyst [43, 44]

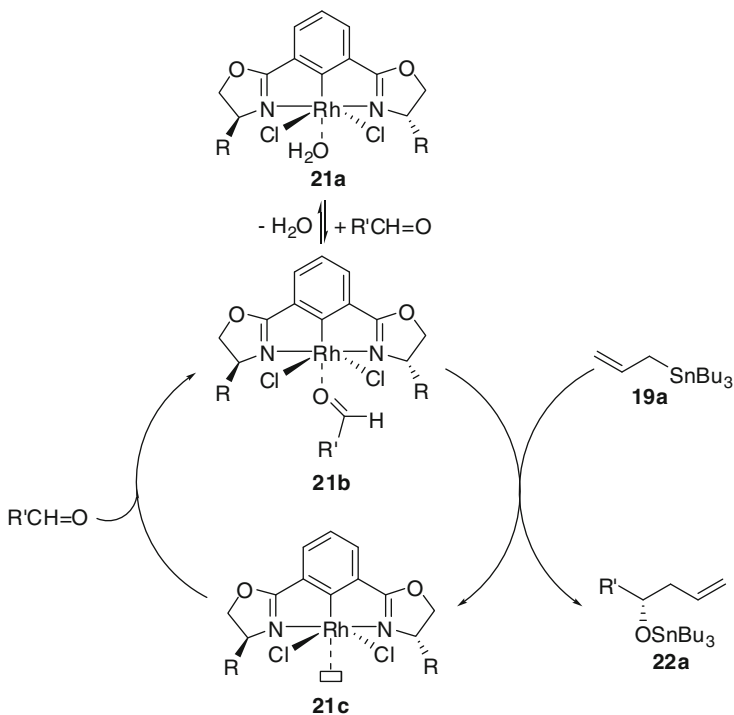
4.1 Pincer Complexes as Lewis-Acid Catalysts

Nishiyama and coworkers [43, 44] have shown that phebox-based rhodium pincer complexes (e.g., **18**) readily catalyze the allylation of various aldehydes (**1a** and **1d**) using tributyl allyl stannane (**19a**) as allyl source (Scheme 10). The reaction proceeds with high yields and good levels of enantioselectivity (up to 80 %). Based on detailed X-ray studies and NMR experiments the authors concluded that the reaction proceeds by Lewis-acid mechanism.

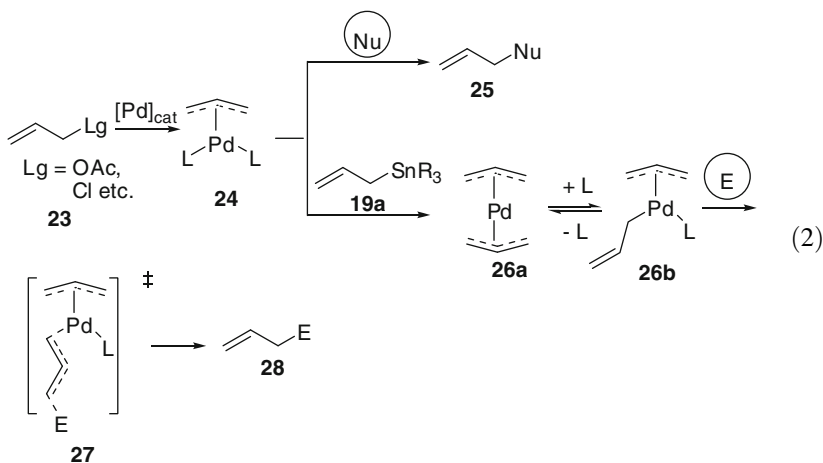
The key intermediate (**21b**) of the reaction [44] is generated by replacement of the water ligand of **21a** with the carbonyl group of the aldehyde substrate (Scheme 11). Thus, the electron-deficient rhodium(III) center activates the aldehyde molecule for electrophilic attack of allyl stannane **19a** affording **22a**, which is then hydrolyzed to the homoallylic alcohol product. This step also recovers the catalyst **21c**, which enters to the next catalytic cycle. Based on NMR studies [44], transmetalation of **19a** to **21a** generating a new allylrhodium species could be ruled out.

4.2 Allylated Pincer Complexes as Reactive Intermediates

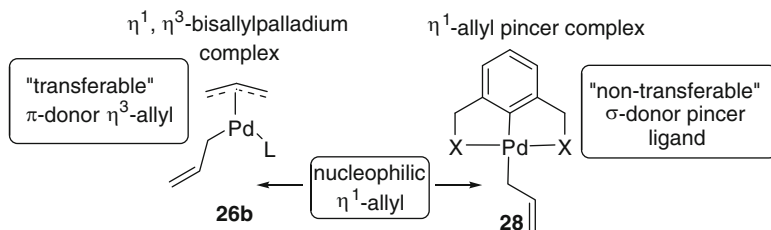
Palladium catalysis offers a versatile tool for allylic alkylation reactions [40, 41]. A vast majority of these reactions (Eq. 2) proceed via nucleophilic attack on (η^3 -allyl)palladium complexes (such as **24**) generated from allyl acetates, chlorides or related reagents (**23**) [2, 45–48]. The electrophilic character of the η^3 -coordinated allyl moiety is a prerequisite of the high reactivity toward nucleophiles leading to allylated nucleophiles (**25**) as products. Electrophiles (such as aldehydes and imines) can also be allylated using palladium catalysis by generating bis-allylpalladium complexes (**26**) under catalytic conditions [42, 49]. This can be realized by using allyl chlorides and allyl stannanes in the presence of catalytic amounts of palladium (Eq. 2). The (η^3, η^3 -bis)allylpalladium complexes (**26a**) readily isomerize to the corresponding η^1, η^3 -forms (**26b**), in which the η^1 -allyl moiety is nucleophilic, and therefore it can easily react with electrophiles (**27**) affording allylated electrophile as product (**28**) [50].



Scheme 11 Mechanism of the rhodium pincer complex catalyzed allylation of aldehydes [44]

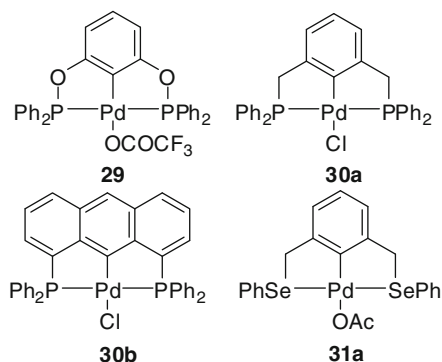


The palladium-catalyzed electrophilic allylation via bis-allylpalladium complexes is a useful reaction with many important synthetic applications [42, 49, 51–56]. However, the diverse reactivity of the bis-allylpalladium intermediates (**26**) imposes certain synthetic limitations as well. For example, bis-allylpalladium complexes readily undergo allyl–allyl coupling instead of reaction with



Scheme 12 Comparison of the η^1 -allyl coordinated bis-allylpalladium and allyl pincer architectures

Scheme 13 Examples for pincer complexes for allylation of aldehydes and imines

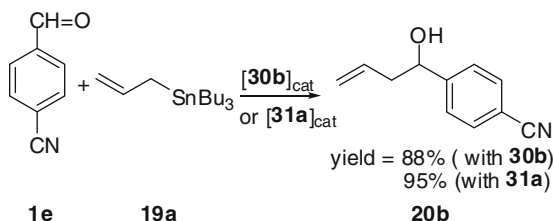


electrophiles [57, 58], and the regioselectivity of the allylation is difficult to control in the presence of allylic terminal substituents [55, 56]. Szabó and coworkers [9, 59–63] employed pincer-complex catalysis to avoid the drawbacks caused by formation of bis-allylpalladium complexes in palladium-catalyzed allylic substitution reactions. The basic idea (Scheme 12) was the replacement of the electron-supplying η^3 -allyl ligand of the η^1, η^3 -bis-allylpalladium intermediates (26b) with an electron-supplying pincer ligand (28). As in palladium pincer complexes only one coordination site is accessible, the allyl moiety will coordinate in an η^1 -fashion, which is required to the nucleophilic reactivity [50].

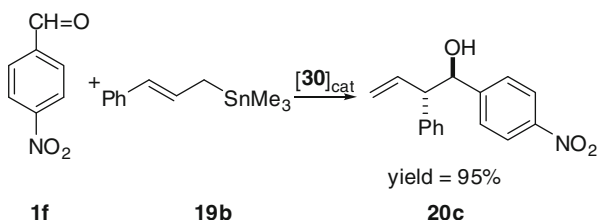
A clear advantage of the η^1 -allyl pincer complexes (28) over bis-allylpalladium intermediates (26b) is that the spectator pincer ligand cannot be transferred from 28, while the spectator η^3 -allyl ligand of 26b can be removed by allyl–allyl coupling or via isomerization to η^1 -coordinated ligand followed by electrophilic attack.

Several pincer complexes [64–66] (such as 29–31) proved to be active catalysts in electrophilic allylation reactions (Scheme 13) [59–63, 67]. In these reactions aldehydes (Scheme 14) (such as 1e and 1f) are readily allylated (Schemes 14 and 15) with allyl and cinnamyl stannanes (19a–b). Wendt and coworkers [68, 69] have shown that pincer-complex catalysis can be employed for allylation of carbon dioxide. In these reactions also η^1 -allyl pincer complexes (such as 28) were suggested as key-intermediates. Allylation of sulfonimines (e.g. 32a) could also be carried out smoothly (Scheme 16) with both allyl stannanes (19a–b) and allyl trifluoroborates (33a). The reactions display

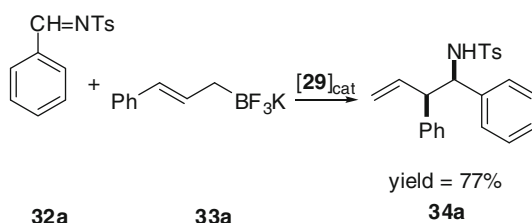
Scheme 14 Palladium pincer-complex catalyzed allylation of aldehydes [60, 61, 67]



Scheme 15 Stereo- and regioselective allylation of aldehyde **1f** [60–62]



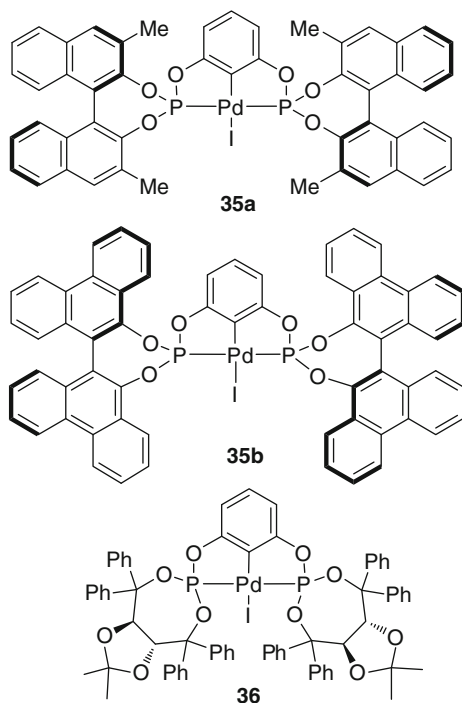
Scheme 16 Allylation of imine **32a** with trifluoroborate **33a** as allyl source [61, 70]



a high level of functional group tolerance as keto, nitro, cyano, and carbethoxy functionalities remained unchanged in the allylation reactions.

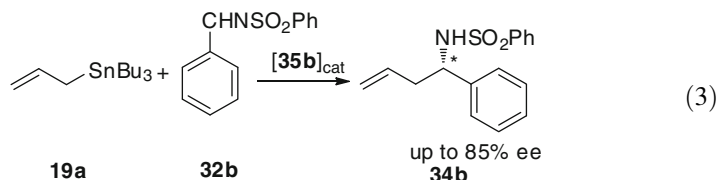
Using cinnamyl substrates (e.g., **19b** and **33a**) the reaction proceeded with a high level of regio- and stereoselectivity (Schemes 15 and 16). Interestingly, allylation of the aldehydes proceeds with anti-selectivity, while the allylation of imines gives syn diastereoselectivity. The different stereoselectivities could be explained by the structure of the TS geometries of the reaction, which were modeled by DFT calculations [70]. It was found that the catalytic activity was also dependent on the structure of the pincer-complex catalysts. Complexes with PCP ligands displayed higher activity than NCN complexes [59]. Complex **29** proved to be very stable under the catalytic conditions and showed higher activity than **30** and **31** [59, 60].

The asymmetric version of the allylation of imines has also been developed [63, 71] using chiral pincer-complex catalysts such as **35** and **36** (Scheme 17). This reaction affords enantioenriched homoallylic sulfonamides, which can easily be converted to the corresponding amine product. It was shown that γ -substitution of the BINOL ligand leads to increase of the enantioselectivity of the reaction. Unfortunately, the TADDOL-based complex **36** gives very low levels of enantioselectivity. The best results (up to 85 % ee) were reported using bis-phenantroline complex **35b** (Eq. 3) The van Koten group [72] obtained promising levels of enantioselectivity by asymmetric

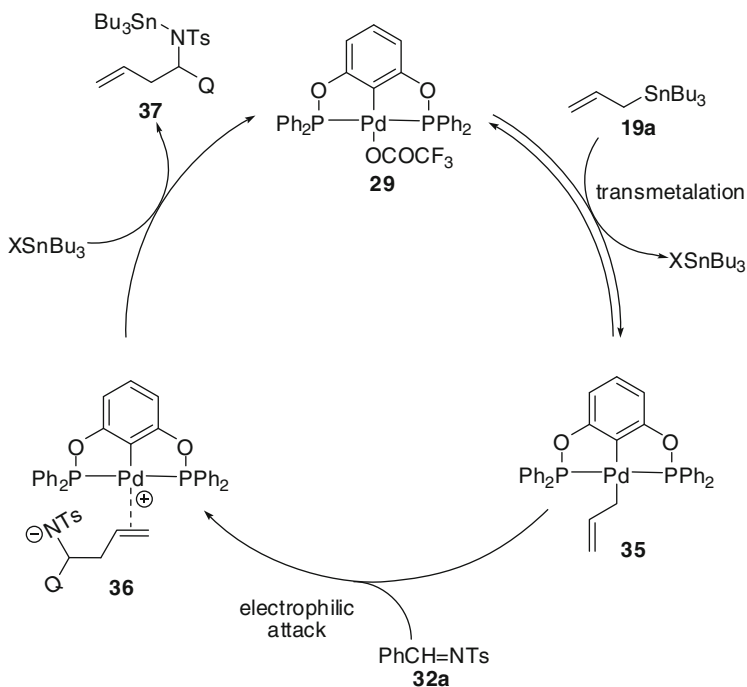


Scheme 17 Chiral pincer complexes employed in asymmetric allylation of sulfonimines [63]

allylation of sulfamoyl imines, while the Bedford group [73] presented asymmetric allylation of aldehydes using pincer-complex catalysis with good ee.



The mechanistic aspects of the allylation reactions (Scheme 18) were investigated by NMR and DFT modeling studies [60, 61, 70]. The NMR studies clearly showed that the introducing step of the catalytic reaction is transmetalation of the allyl stannane (**19a**) or allyl trifluoroborate substrate (**33a**) with the pincer-complex catalyst (**29**) generating (η^1 -allyl)palladium pincer-complex intermediate **35**. DFT modeling studies indicate that the η^1 -allyl moiety of this complex undergoes electrophilic attack with the imine (**32a**) or aldehyde (**1**) electrophiles with a remarkably low activation barrier [60, 70]. This step determines the regio- and stereoselectivity of the process, which could be rationalized on the basis of DFT calculations [60, 70]. The transmetalation and electrophilic attack has an opposite electron demand, which requires a careful optimization of the electronic properties of the employed pincer-



Scheme 18 Catalytic cycle for allylation of imines via (η^1 -allyl)palladium pincer complex intermediate [60, 70]

complex catalysts. It was found that relatively electron-deficient PCP complexes (**29–31**) have a higher catalytic activity than electron-rich NCN complexes. Application of weakly coordinating counterions such as in acetate [67] and trifluoroacetate [60] also reacts faster than halogenide complexes, such as **30a** and **30b**. It was reasoned that the transmetalation step is faster, when the electron-rich allyl moiety coordinates to an electron poor palladium atom (PCP) than to an electron-rich one (NCN) [60]. Obviously, a weakly coordinating ligand (acetate or trifluoroacetate) can be more easily replaced by an allyl ligand than a halogenide.

5 Pincer-Complex Catalyzed Synthesis of Unsaturated Organo-Boron, -Silicon and -Tin Species

Transition metal catalysis offers an attractive synthetic approach for preparation of unsaturated organometallic compounds from dimetallic and other reagents [74–76]. In particular, palladium catalysts are employed in these processes because of the high selectivity and functional group tolerance of the reactions [74–78]. One of the most important issues in these processes arises from the fact that palladium

complexes are usually able to both create and cleave carbon–metal bonds [74–78]. Therefore, when synthesis of organometallic species is desired, the electronic properties of the catalyst have to be carefully tuned to avoid carbon–metal bond cleavage of the products. As it was pointed out in Sect. 1, the tight metal–ligand bonding allows an efficient tuning of the pincer reactivity of pincer complexes; and thus some of these species are excellent catalysts for selective synthesis of allylboranes, allyl stannanes, allenyl and propargyl stannanes, and silanes.

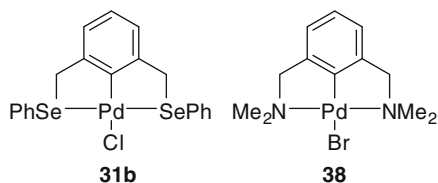
5.1 Pincer-Complex Catalyzed Synthesis of Functionalized Allylboronic Acids

Allyl acetates are known to undergo Pd₂(dba)₃ catalyzed transformation to allyl pinacolboronates using bis(pinacolato)diboron as boron source [79]. However, the synthetic value of this transformation is limited by the allyl–allyl coupling side-reaction of the pinacolboronate products [79]. The allyl–allyl coupling probably takes place via formation of bis-allylpalladium complexes, such as **26** (Eq. 2). Szabó and coworkers [80–87] have shown that efficient synthesis of functionalized boronic acids can be achieved by using pincer complex **31b** [88] (Scheme 19) and diboronic acid [89] as boron source. Allyl–allyl coupling product did not form in these reactions as bis-allylpalladium complexes (**26**) cannot be formed from pincer complexes.

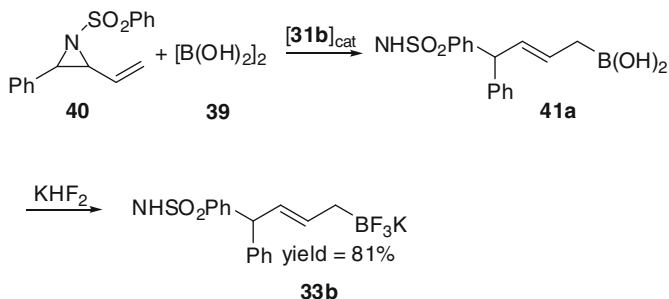
The pincer-complex catalyzed boronation reactions have a very broad substrate scope as vinyl cyclopropanes, vinyl aziridines (Scheme 20), allyl acetates, and even allyl alcohols can be borinated [80, 81]. The reactions have a very high level of functional group tolerance as silyl, acetate, amide, and aromatic halogenide functionalities remained unchanged under the catalytic reactions. Allylboronic acids (such as **41a**) are not sufficiently stable under conventional purification conditions, and therefore the boronic acid functionality was converted to trifluoroborate yielding stable easy to handle allyl trifluoroborates [90] (such as **32b**).

Allyl alcohols are readily available substrates, which smoothly undergo direct boronation reactions (Scheme 21) [82, 84–87]. These reactions can be carried out under remarkably mild reaction conditions (typically 20–40 °C) in the presence of methanol as co-solvent. The boronation reactions are accelerated by employment of catalytic amounts of strong acids, such as toluenesulfonic acid; however this acid catalysis is not necessary in most of the presented reactions [82]. The regio- and stereoselectivity of the reaction is excellent, and therefore it can be employed for selective synthesis of densely functionalized allyl boronates, such as **41b** and **33c** from inexpensive starting materials (such as **42**) (Scheme 21).

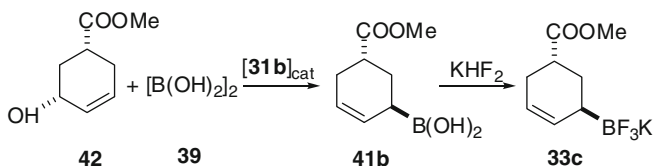
Remarkably, the rate of boronation for cinnamyl alcohol was faster than for cinnamyl acetate (Eq. 4) [82]. Moreover, certain substrates did not react at all in the boronation reaction, when their hydroxy functionality was converted to acetate.



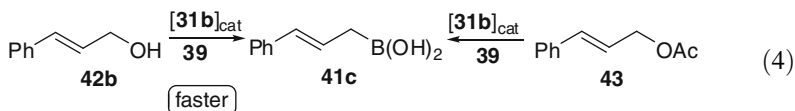
Scheme 19 Pincer complexes employed for preparation of unsaturated allyl, allenyl and propargyl metal species



Scheme 20 Boronation of vinyl aziridine to obtain organoboronic acids and trifluoroborates [80]

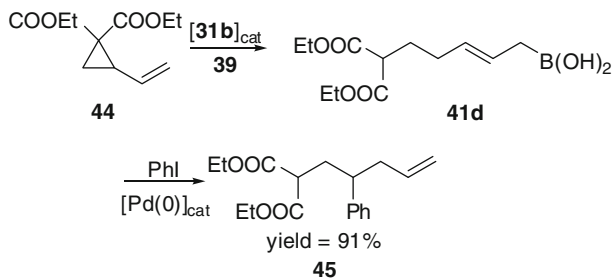


Scheme 21 Allyl alcohols as substrates in pincer complex catalyzed boronation [82]

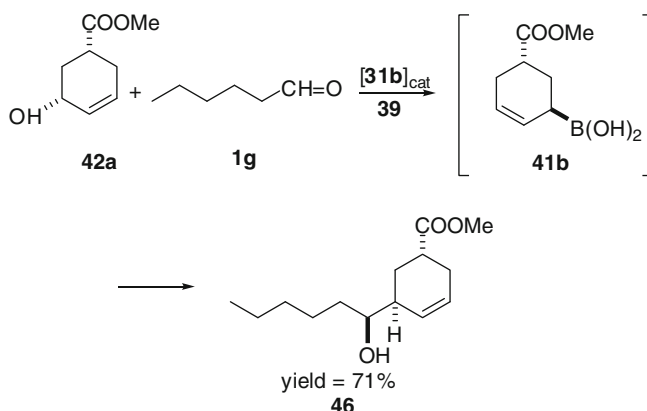


The boronation reactions could also be coupled with other transformations employing boronic acids as substrates. For example, boronic acids, such as **41d**, readily undergo palladium(0)-catalyzed coupling with aryl iodides under standard Suzuki-Miyaura [91–93] conditions (Scheme 22) [81]. Interestingly, this allylation reaction results in the branched allylic product **45** exclusively, while the allylation reaction via (η^3 -allyl)palladium intermediate (c.f. **24**) is expected to give the corresponding linear product.

Szabó and coworkers [83] developed an efficient one-pot reaction for allylation of aldehydes (**1g**) with allyl alcohols in the presence of diboronic acid and catalytic amounts of **31b** (Scheme 23). By this reaction stereo- and regiodefined homo allyl



Scheme 22 Employment of boronic acids in palladium(0) coupling with aryl iodides [81]

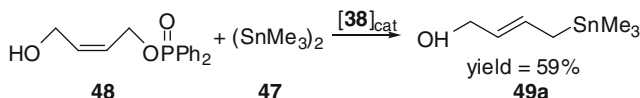


Scheme 23 One-pot reaction for highly diastereoselective allylation of aldehydes with allyl alcohols [83]

alcohols (**41b**) can be prepared starting from easily accessible reactants (**42a**). Subsequent studies have shown that the Petasis [94, 95] borono-Mannich reaction can also be combined with the catalytic borylation [84]. It was shown that α -aminoacids can be prepared from allyl alcohols by pincer-complex catalyzed borylation followed by the Petasis reaction in a one-pot sequence. Furthermore, ring-closing metathesis and pincer-complex catalyzed borylation–allylation can also be performed as a one-pot reaction resulting in stereodefined carbocyclic products [86].

5.2 Formation of Allyl Stannanes Using Hexaalkylditin Reagents

Pincer-complex catalyzed substitution reactions were also successfully employed for preparation of allyl stannanes using hexamethyl- (**47**) or hexabutylditin as stannane precursors [62]. In these processes NCN complex **38** (Scheme 19) proved to be a very active catalyst (Scheme 24). Similar to the borylation reactions



Scheme 24 Example for pincer complex catalyzed stannylation reaction [62]

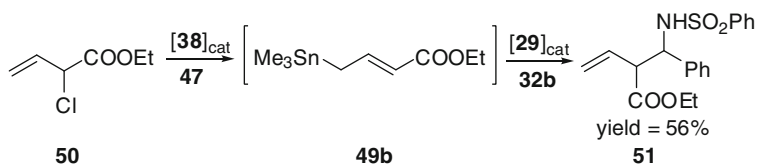
(Sect. 5.1), formation of the allyl–allyl coupling by-products could be avoided by application of pincer-complex catalysis.

The stannylation reactions have a broad substrate scope as many different precursors, such as allyl chloride, phosphonate (**48**), and epoxide substrates, could be employed. Because of the high level of functional group tolerance this procedure is suitable for preparation of functionalized allyl stannanes, such as **49a**. Van Koten and coworkers [96] have shown that stannylation of cinnamyl chloride can be performed with immobilized pincer-complex catalyst, which was reusable in several runs. Isolation of functionalized allyl stannanes is usually a cumbersome process because of the instability of these species. In particular, allyl stannanes with electron-withdrawing substituents (such as **49b**) very easily undergo decomposition and polymerization reactions under the isolation procedure. Therefore, a one-pot reaction was designed using transient allyl stannanes produced by the NCN complex (**38**) catalyzed process. The one-pot conditions involved that aldehyde or imine substrates (**32b**) were added together with catalytic amounts of PCP complex **29** to the reaction mixture of the stannylation. Thus, **49b** and **32b** could undergo allylation reaction (Sect. 4.2) affording stable homoallyl amine products, such as **51** (Scheme 25). Addition of PCP complex **29** was also required since NCN complex **38** is very sluggish in the allylation reactions [59]. On the other hand, **32b** alone is not able to catalyze the stannylation reactions.

A joint study of the van Koten and the Szabó groups [97] has shown that the above type of one-pot reactions can also be performed using a single pincer-complex catalyst, such as **38b**. In this reaction **38b** acts as tandem catalyst performing a stannylation and a subsequent allylation reaction affording homoallyl alcohol from cinnamyl chloride and aldehydes in the presence of **47** (Fig. 4).

5.3 Stannylation of Propargylic Substrates

Palladium-catalyzed addition of hexaalkylditin to alkynes is a widely applied attractive synthetic route for preparation of distannylated olefins [75, 98]. The initial step of this process is oxidative addition of the palladium(0) catalyst to the Sn–Sn bond generating a bis-stannyl palladium(II) species, which subsequently undergoes addition to the triple bond of the alkyne substrate [99]. As there is only a single coordination site available in palladium pincer complexes, formation of distannylated palladium species is unlikely; and therefore these complexes are not expected to catalyze addition of stannanes to triple bonds. Indeed, it was



Scheme 25 One-pot reaction for allylation of sulfonimines with allyl chlorides using NCN complex **38** and PCP complex **29** to catalyze the consecutive steps [62]

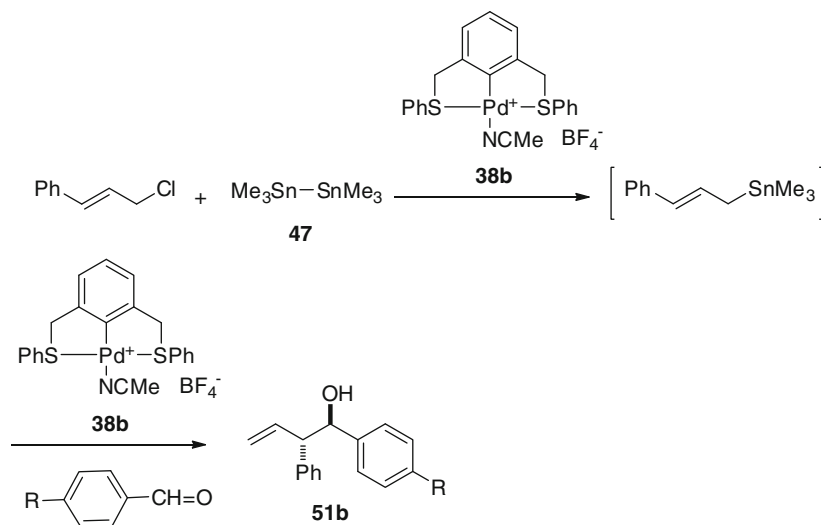
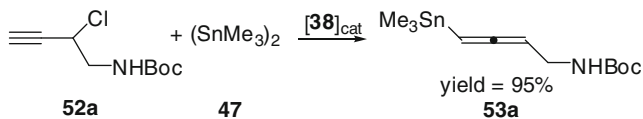


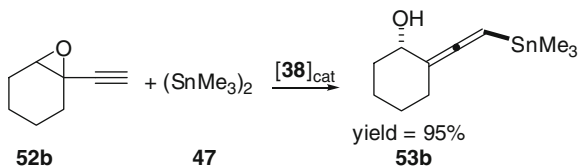
Fig. 4 One-pot reaction for allylation of aldehydes with allyl chlorides using a single pincer-complex catalyst **38b** [97]

shown [100, 101] that using NCN complex **38** as catalyst hexamethylditin (**47**) undergoes substitution of propargylic substrates instead of addition of the distannanes to the triple bonds (Scheme 26).

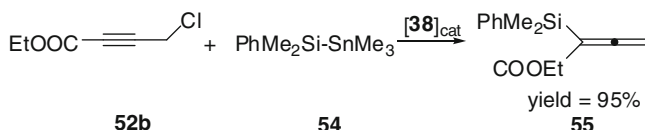
The reactions are highly selective and stannylation of secondary propargyl chlorides (**52a**) results in exclusively allenyl stannane products (such as **53a**) [101]. In case of primary propargyl chlorides the regioselectivity is determined by the substituents directly attached to the triple bonds [100, 101]. Propargyl epoxides can also be employed as substrates in the substitution reactions [101]. Thus, stannylation of cyclic epoxide **52b** proceeded with excellent allenyl selectivity and high anti-stereoselectivity affording **53b** as product (Scheme 27). In the stannylation reactions SeCSe pincer complex **31b** also proved to be a highly active catalyst; however, in some reactions it gave lower propargyl to allenyl regioselectivity than NCN complex **38**.



Scheme 26 Pincer complex catalyzed stannylation of propargyl chlorides [100, 101]



Scheme 27 Regio- and stereoselective stannylation of propargyl epoxides [101]



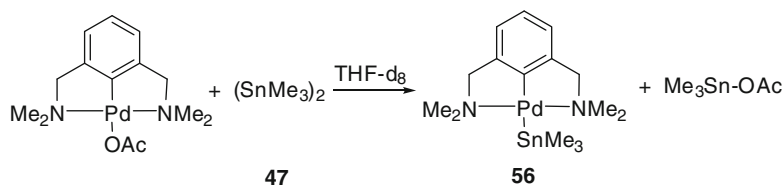
Scheme 28 Catalytic silylation of propargyl chlorides [101]

5.4 Preparation of Allenyl Silanes

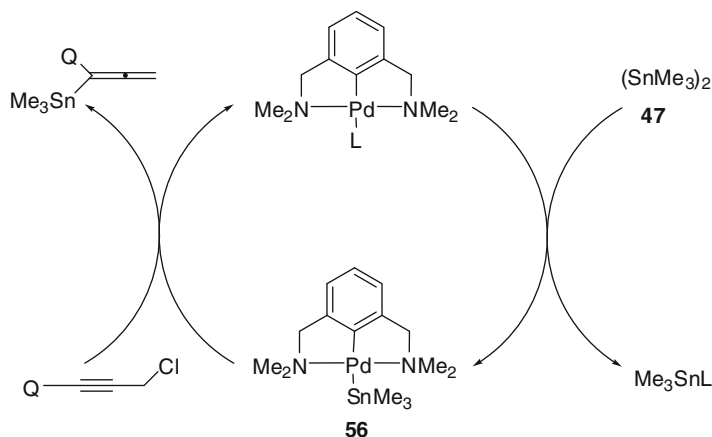
Unsymmetrical dimetallic reagents such as silyl-stannane **54** were also applied in the pincer-complex catalyzed substitution of propargyl reagents [101]. In these reactions exclusively the silyl functionality was transferred from **54** to the organic substrate (such as **52b**) (Scheme 28). The silylation reaction proceeded with even higher regioselectivity than the stannylation by **47** (Sect. 5.3), as exclusively the allenyl silane products were obtained with both electron-supplying and electron-withdrawing substituents on the triple bond.

5.5 Mechanistic Aspects of the Pincer-Complex Catalyzed Metal Substitution Reactions

Although a detailed mechanistic exploration of the recently published borylation (Sect. 5.1), stannylation (Sects. 5.2 and 5.3), and silylation reactions (Sect. 5.4) is an ongoing effort, NMR and DFT studies have already been reported on the mechanism of the organotin transfer process [100, 101]. It was shown that propargyl or allyl chlorides do not react with NCN complex **38** in the absence of dimetallic reagents. On the other hand, hexamethylditin (**47**) was readily reacted with the



Scheme 29 Stoichiometric reaction indicating the transfer of trimethylstannyl group to palladium [101]

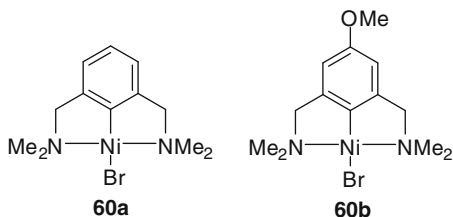


Scheme 30 Proposed catalytic cycle of the stannane transfer process [101]

NCN pincer-complex catalyst affording complex **56**, which could be detected by ^{119}Sn NMR spectroscopy [101] (Scheme 29).

Based on the above stoichiometric results and DFT modeling studies a catalytic cycle was constructed for the stannylation process (Scheme 30) [101]. Accordingly, the catalytic reaction is initialized by transmetalation of hexamethylditin **47** to the NCN complex catalyst. Subsequently, the trimethyltin functionality is transferred from palladium to the propargylic or allyl substrate. The DFT calculations revealed that the transfer of the metallorganic group proceeds with relatively low activation energy in a process similar to nucleophilic substitution of organohalogenides. Formation of the allenyl regioisomer required lower activation energy than the formation of the propargyl isomer. In the stannylation and boronation reactions the electron-rich SeCSe (**31b**) and NCN (**38**) complexes (Scheme 19) display a higher activity than PCP complexes (**29** and **30**). A possible explanation is that the nucleophilic substitution of propargyl and allyl substrates requires a high energy metal–palladium (Pd–B, Pd–Sn) bond in the key intermediate (such as in **56**) requiring electron-rich palladium atom, which is present in NCN and SeCSe complexes, but not in PCP catalysts. It has also been hypothesized that the transmetalation of the pincer-complex catalyst with dimetallic reagents (such as

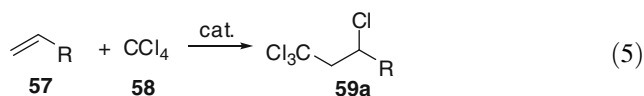
Scheme 31 Pincer complexes employed as catalysts in the Kharasch reaction [104]



47 and **39**) may require opening of the side arm of the catalyst, which is easier in NCN and SeCSe complexes than in PCP ones.

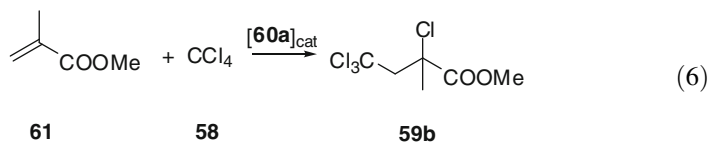
6 Pincer-Complex Catalyzed Kharasch Addition

Kharasch and coworkers [102, 103] extensively studied (Eq. 5) the addition of organohalides to terminal alkenes (**57**). In case of chlorinated substrates (such as **58**) the addition requires peroxide catalysis affording the anti-Markovnikov product such as **59a** (Eq. 5). The reaction proceeds via radical mechanism, which is classified as “atom transfer radical addition” (ATRA). A limitation of the peroxide catalyzed process is the difficult control of the product distribution, as formation of **59a** is usually accompanied by telomerization and polymerization reactions occurring via common radical intermediates.



6.1 Nickel Pincer-Complex Catalyzed Kharasch Reaction

Van Koten and coworkers [104–108] have found that the product distribution of the Kharasch reaction can be controlled by using nickel pincer-complex catalyst **60** (Eq. 6, Scheme 31). Employing this catalyst the addition reaction leads exclusively to the 1:1 adduct (such as **59b**) without formation telomerization and polymerization products (Eq. 6).



The reaction is very robust and the high selectivity is maintained employing a wide variety of substrates [106]. The reactivity of the catalyst could be efficiently tuned [109] by substitution of the *para* position of **60a** (such as **60b**) and by changing the steric bulk of the substituents in the side arms [104]. It was found that electron-donating groups, such as methoxy (**60b**) and dimethyl-amino groups, increase the reactivity of the complex, while electron-withdrawing substituents

decreased the catalytic activity. Replacement of the methyl groups in the side arms with isopropyl groups led to reduced catalytic activity probably because of steric interactions [104].

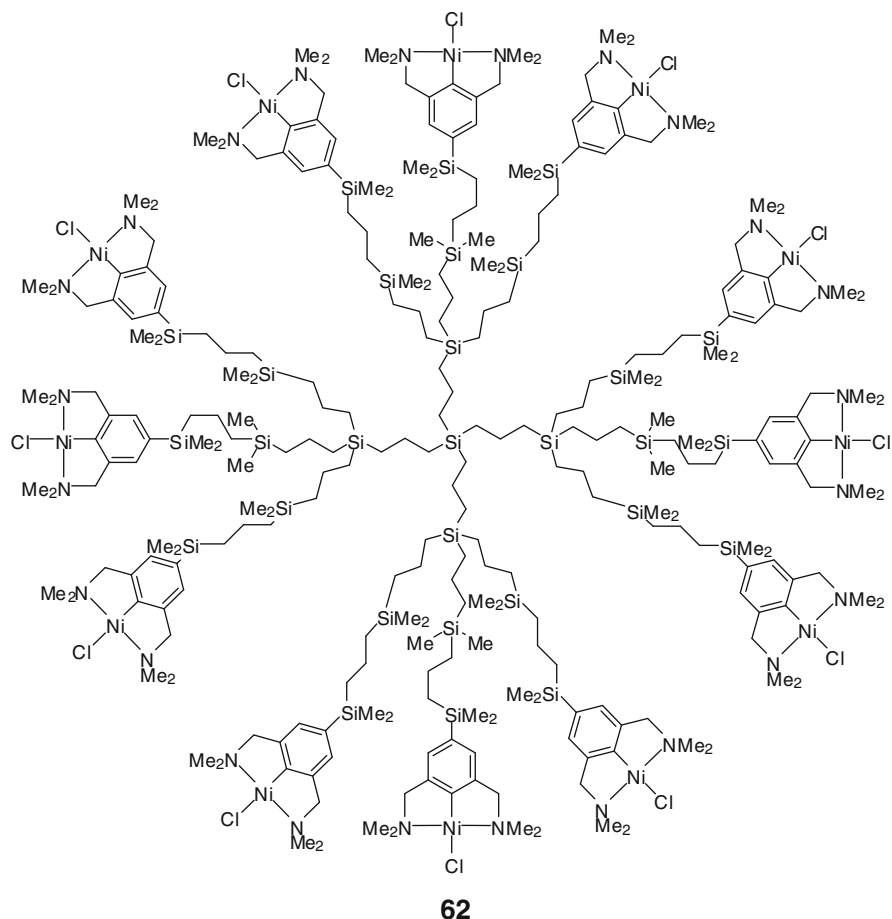
The high catalytic stability and tunability of **60a** makes it particularly suitable for binding to various supports to obtain recyclable catalysts. Van Koten and coworkers [105, 110] have shown that nickel palladium complexes can be attached to carbosilane dendrimers such as **62**. Application of these dendrimer catalysts in membrane reactors allows, in principle, a continuous catalytic process [110]. Dendrimer **62** proved to be an active catalyst in the Kharasch reaction of **61** with carbon tetrachloride **58** for selective formation of adduct **59b** and the catalyst could be recovered by filtration (Scheme 32).

6.2 Mechanism of the Pincer-Complex Catalyzed Kharasch Reaction

Based on kinetic measurements and spectroscopic studies van Koten and coworkers [106] proposed a catalytic cycle for the pincer-complex catalyzed Kharasch reaction (Scheme 33). Accordingly, the catalytic cycle is initiated by a single electron transfer (SET) from the nickel atom of **60c** to carbon tetrachloride **58**. This step proceeds via activated complex **63a**, which undergoes oxidative addition to nickel (IV) complex **63c** followed by fragmentation to give nickel(III) complex **63d** and a trichloromethyl radical. An interesting feature of this process is that it takes place in the absence of a free coordination site on the nickel atom of **63c**. The three species **63a–c** involved in this process are in a fast equilibrium. It was suggested that electron-donating *para* substituents (such as in **60b**) are able to stabilize Ni(III) complexes (such as **63d**), and therefore these substituents increase the catalytic activity of the complex. The next step is the addition of the trichloromethyl radical to the terminal alkene leading to complex **63e**. According to kinetic measurements this is the rate-determining step of the catalytic process. In the next step complex **63** undergoes reversible SET from the radical carbon center to nickel producing adduct **64** and recycling the catalyst **60c**.

7 Metallopincer Catalyzed Heck and Suzuki Reactions

Palladium-catalyzed vinylation of aryl halides using the so-called Heck reaction is one of the most fundamental areas of organic synthesis. In this process aryl halides (such as **65**) undergo catalytic coupling reaction with alkenes (such as **66**) activated with electron-withdrawing substituents affording functionalized styrene derivatives (Scheme 34) [2, 41, 111].

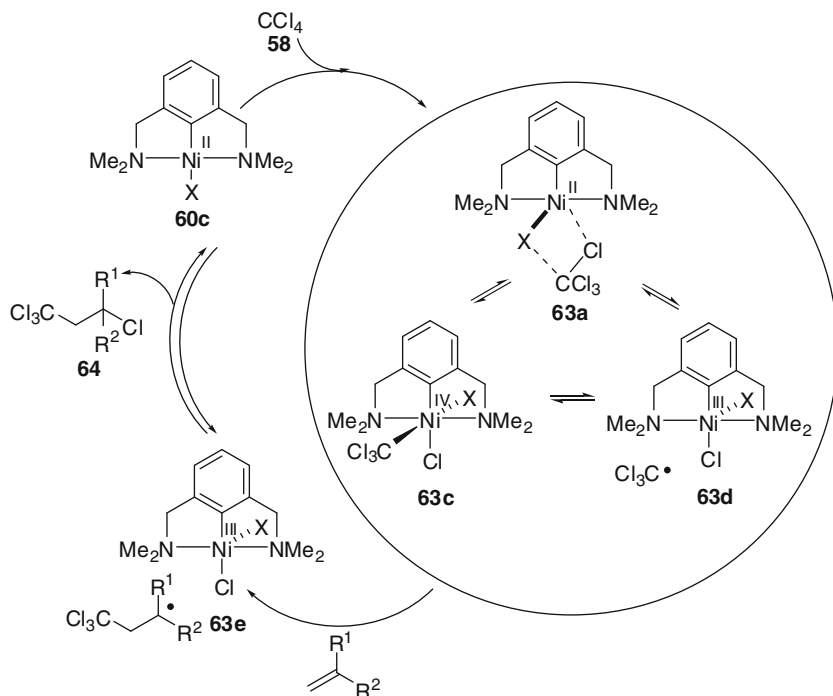


Scheme 32 Example for dendrimer supported nickel pincer complex catalyst [105]

The Suzuki coupling is a related and equally important palladium-catalyzed process for coupling of aryl halides (**65**) with aryl- (**68**) and vinyl boronic acids to obtain aryl–aryl (**69**) and aryl–aryl cross-coupling products (Scheme 35) [2, 41, 92, 112].

7.1 Application of Palladium Pincer-Complex Catalysts for Heck and Suzuki Couplings

Because of the extremely high importance of the Heck and Suzuki coupling reactions in both industrial and laboratory scale synthetic organic chemistry considerable efforts have been invested to obtain new efficient catalysts. In this work one of the most important factors is the development of new durable catalysts with high turnover number (mol product/mol catalyst, TON). Thus, a huge number of

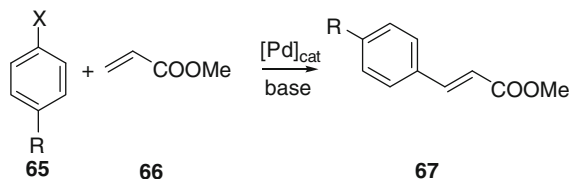


Scheme 33 Catalytic cycle for the pincer complex catalyzed Kharasch addition of carbon tetrachloride to terminal alkenes [106]

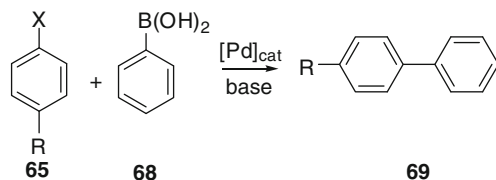
pincer complexes were prepared and applied as catalysts in Heck and Suzuki coupling reactions. Some of these catalysts are characterized with very high TONs (up to [113] 9×10^6). The most important basic skeletons of pincer-complex catalysts employed in these reactions are given in Scheme 36.

Milstein and coworkers [7, 113] reported the first pincer-complex catalyzed Heck reaction of various aryl iodides and bromides (**65**) with various acrylate esters (such as **66**) to obtain styrene derivatives (cf. Scheme 34). In these reactions PCP complex **70** and its analogs were employed as efficient catalysts. The yields of the products were often quantitative and TONs up to a 5×10^5 could be achieved.

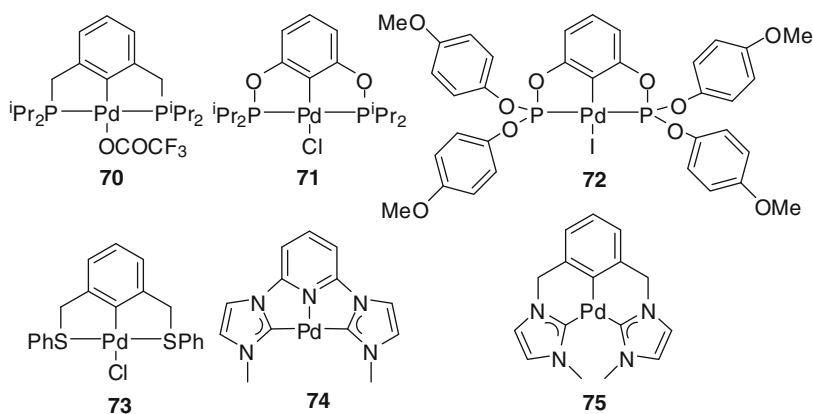
Jensen and Morales and coworkers [114, 115] employed phosphinito PCP complex **71** for Heck coupling reactions. It was shown that the phosphinito PCP complexes (such as **71**) are more active catalysts in Heck coupling than the phosphino analogs (such as **70**). For example, the phosphinito complex **71** is able to couple aryl chlorides (**65**, X = Cl) [115], while the synthetic scope of phosphino complexes (such as **70**) is limited to aryl iodides and bromides. Interestingly, aryl bromobenzene (**76**) undergoes (Scheme 37) a double Heck coupling with styrene (**77**) and other terminal olefins to give trisubstituted olefins (**78**) [114]. Shibasaki and coworkers [116] succeeded to increase the catalytic activity of complex **71** by replacement of the isopropyl groups with methyl hydroquinone substituents to obtain catalyst **72**. Although this catalyst required relatively high reaction



Scheme 34 Example for palladium-catalyzed Heck coupling reaction



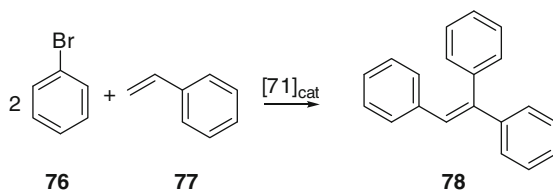
Scheme 35 Example for palladium-catalyzed Suzuki coupling



Scheme 36 Pincer complex architectures active catalysts in Heck and Suzuki coupling reactions

temperatures (140–180 °C) for Heck coupling, impressive TONs up to 9×10^6 could be achieved [116].

Bergbreiter and coworkers [117, 118] employed SCS complex (such as **73**) based catalysts for various Heck coupling reactions. Although the SCS catalysts proved to be somewhat less reactive than the PCP analogs (**70–72**) in homogenous Heck coupling reactions, these catalysts could be attached to poly(ethylene glycol) (PEG) support via ether and amide linkages [117]. The PEG supported SCS catalysts could be recycled up to three times without losing the catalytic activity. In subsequent studies Bergbreiter and coworkers [118] concluded that there is a substantial leaching of palladium from the homogenous and PEG bound SCS



Scheme 37 Disubstitution of styrene using phosphonito PCP complex **71** [114]

complexes, and therefore the applied pincer complexes are probably just precursors of highly reactive palladium catalysts (see Sect. 6.2) of the Heck coupling.

Crabtree and coworkers [119, 120] reported the synthesis of several carbene ligand-based CNC (**74**) and CCC (**75**) pincer complexes. In these complexes the metal atom is even more tightly bound to the ligand than in traditional pincer complexes with heteroatoms in the side arms, which lends a particularly high stability and durability for these complexes. Because of the high stability, these complexes could be employed for Heck coupling without employing an inert atmosphere. Complex **74** performed [120] much better in Heck couplings than its CCC analog **75**.

Dupont and coworkers [8, 121] employed mixed PCN and SCN pincer complexes as catalysts in Heck coupling reactions. These complexes usually perform better than the other phosphine free pincer complexes with TONs (up to 10^6). Based on kinetic studies it was concluded that the mixed PCN and SCN pincer complexes are not the active catalysts of the Heck coupling reactions, but they serve as reservoirs for catalytically active Pd(0) species [121].

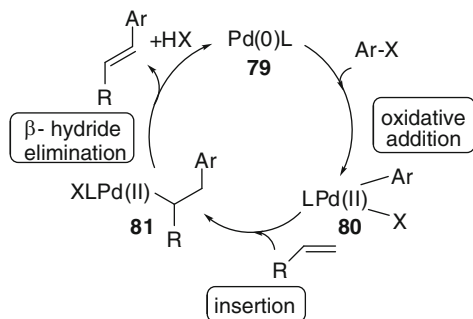
Bedford and coworkers [64] reported the synthesis of PCP complex **29** (Scheme 13) and its application in Suzuki coupling reactions (Scheme 35). In these reactions phenylboronic acid (**68**) could be efficiently coupled with bromoacetophenone (65, X = Br, R = COMe) and some other substrates. The reactions performed at relatively high temperature (130 °C) proceeded with excellent TONs and with usually high yields. Dupont and coworkers [122] studied the SCS pincer-complex catalyzed Suzuki reaction of bromotoluene (65, X = Br, R = Me) with phenylboronic acid (68). The catalyst performed well; however, the catalytic activity is lower than that for PCP complexes, such as **29**.

Frech and coworkers performed several successful applications for Heck, Suzuki, and Sonogashira coupling reactions using aminophosphine-based pincer complexes [123–126]. The same group has performed DFT modeling studied to gain mechanistic insights into the mechanism of the pincer-complex catalyzed C–C coupling reactions.

7.2 Mechanistic Aspects of the Pincer-Complex Catalyzed Coupling Reactions

Currently, the exact mechanism of the palladium-catalyzed coupling reactions is still a matter of debate. The main controversy arises from the fact that the palladium catalysts are known to undergo redox processes [2, 41, 111] in Heck reactions

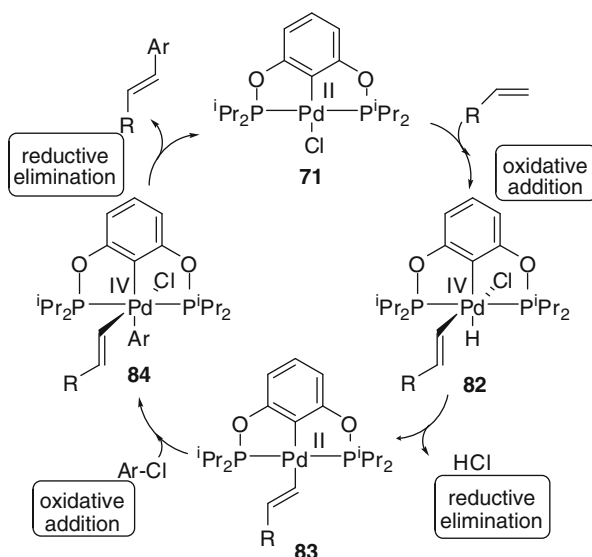
Scheme 38 The catalytic cycle of the classical Heck coupling reaction



(Scheme 34). However, in palladium pincer complexes (e.g., **70–75**) the palladium atom is in one of the most stable oxidation states +2. Reduction of the central atom for carbon–palladium bonded complexes (with exception of CNC carbon complex **74**) usually involves a complete decomposition of the complex under catalytic conditions. It should be however noted that Milstein and coworkers [123] have shown that in some cases the reduction of the palladium atom to Pd(0) can be reversible. On the other hand, oxidation of palladium(II) to palladium(IV) requires a high activation barrier, and therefore the +4 oxidation state is relatively unusual in palladium-catalyzed processes [2, 41, 111]. In this section, we focus on the mechanism of the Heck reaction; however, the same type of mechanistic problems arises in other coupling reactions involving aryl halides, such as in Suzuki coupling.

In the classical (i.e., not pincer-complex catalyzed) Heck coupling reaction (Scheme 38) the catalytic cycle is initialized by the oxidative addition of the palladium(0) catalyst (**79**) to the carbon–halogen bond of the aryl halide substrate. This process results in a palladium(II) aryl species (**80**), which undergoes insertion reaction with the activated alkene to give adduct **81**. The last step of the catalytic cycle is β-hydride elimination of **81** involving reduction of the palladium atom to recycle the catalyst (**79**) and to provide the coupling product. Thus, this catalytic cycle involves an oxidation step (**79** → **80**) and a reduction step (**81** → **79**). However, such a Pd(0) → Pd(II) → Pd(0) cycle is not possible for XCX (X = heteroatom) type of pincer complexes, which decomposes when the palladium atom enters to zero oxidation state [118, 127, 128].

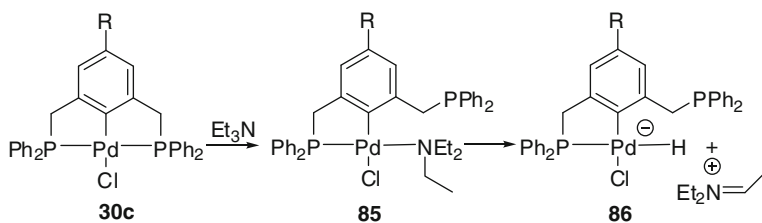
As an alternative to the traditional Pd(0) → Pd(II) → Pd(0) (Scheme 38) sequence a Pd(II) → Pd(IV) → Pd(II) cycle was suggested [113, 115] (Scheme 39), since palladium(IV) pincer complexes are supposed to be stable species. According to this mechanism (Scheme 39) the alkene substrate undergoes oxidative C–H activation with the employed pincer-complex catalyst (such as **71**) to give palladium(IV) species **82**, followed by reductive elimination of HCl affording vinyl palladium(II) complex **83**. The next step is a further oxidative addition of the aryl halogenide, such as chloride, to give complex **84**. Reductive elimination of the coupling product from **84** regenerates the catalyst (**71**), which may enter in the next catalytic cycle. Several experimental findings seem to support this Pd(II) → Pd(IV) → Pd(II) cycle such as the apparently high stability of palladium pincer complexes under the catalytic conditions, the dependence of the



Scheme 39 Proposed catalytic cycle for the Heck coupling involving Pd(IV) intermediates [115]

catalytic activity on the pincer-complex structure (Sect. 6.1), the high TON, as well as the surprisingly high reactivity of **71** for activation of aryl chlorides.

On the other hand, several recent studies pointed out that despite the high thermic and air stability of the pincer complexes partial or complete decomposition to palladium(0) species takes place under the reaction conditions of the Heck coupling [8, 11, 111, 118, 121, 127, 128]. These studies are based on kinetic studies, poisoning experiments, Hg(0) trapping of palladium(0), and NMR measurements. It was concluded that the decomposition of pincer complexes leads to the formation of highly active palladium(0) species. Accordingly, pincer complexes do not catalyze the Heck reactions themselves (such as in Scheme 39), but release active palladium(0) species, which catalyze the coupling reaction according to the classical catalytic cycle (Scheme 38). Jones and Weck and coworkers [127] studied the decomposition process of pincer complexes under the Heck conditions. These authors found (Scheme 40) that the employed base plays a very important role in degradation of the otherwise very stable PCP complexes (such as **30c**). It was suggested that triethyl amine or other bases employed in the catalytic process coordinate to palladium decoordinates one of the side arms of **30c** affording complex **85**. This complex is able to undergo irreversible β -elimination with one of the carbon–hydrogen bonds of the triethylamine ligand resulting in anionic complex **86**, which subsequently generate the active palladium(0) catalyst. Cámpora and coworkers [129] have shown that the Pd(II) atom of simple PCP complexes undergoes reduction to Pd(0) species in MeOH under mild conditions. These authors were able to isolate and characterize the resulting Pd(0) complexes.



Scheme 40 Proposed initial steps of the decomposition of PCP complexes under Heck conditions [127]

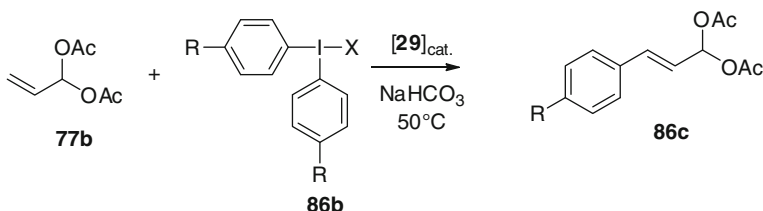


Fig. 5 Coupling of functionalized alkenes with hypervalent iodines

As mentioned above several findings supporting [113, 115, 126] that the Heck reaction of aryl halogenides with alkenes might proceed through Pd(IV) pincer species (Scheme 39). However, the scientific community tends to accept [8, 11, 111, 118, 121, 127, 128] that in most of these reactions pincer complexes serve as precatalysts for the Heck coupling reactions providing palladium(0) species, which are the active catalysts. Nevertheless, replacement of the aryl halides with strong oxidants, such as hypervalent iodines (Fig. 5), or application of chelating aryl-halogenides (Fig. 6) may open new synthetic routes for Heck couplings via Pd(IV) species rendering pincer complexes to the direct catalysts of these reactions.

For example the Szabó group [130] has developed a Heck coupling reaction of alkenes with hypervalent iodine **86b** (Fig. 5). Several findings supported the lack of Pd(0) intermediates in this process. Thus, the integrity of the pincer-complex catalyst completely retained under the reaction and mercury poisoning of the catalyst was not observed. The process was exploited to Heck coupling of allyl acetates (such as **77b**). These allylic species are known to undergo oxidative addition with Pd(0), which was not observed in this process. DFT modeling studies also supported the assumption of the oxidative addition of hypervalent iodines (such as **86b**) to pincer complexes. In subsequent studies the Szabó group further developed this concept and presented several related studies for C–H acetoxylation [131] and borylation [132] by pincer complexes. Formation of Pd(IV) pincer complexes could be detected under the catalytic conditions, when NCN complex **38** was reacted with hypervalent iodonium salts, such as $\text{PhI}(\text{OAc})_2$ [131] and $\text{PhI}(\text{OCOCF}_3)_2$ [132].

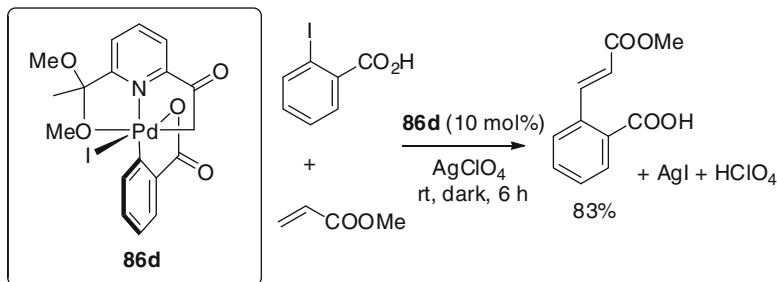


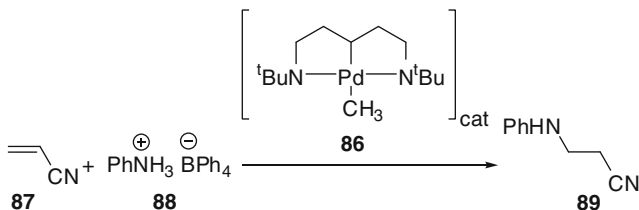
Fig. 6 Pd(IV) oxidation state is stabilized by a chelating aryl group [133, 134]

Vicente and coworkers [133, 134] have shown (Fig. 6) that in the presence of AgClO₄ *ortho*-iodobenzoic acid and methyl acrylate undergo Heck coupling via Pd (IV) intermediate **86d**. The chelating ligand arising from *ortho*-iodobenzoic acid stabilizes the Pd(IV) complex and AgClO₄ hinders the reductive elimination of the iodoaryl precursor. Species **86d** arises from the oxidative addition of the aryl iodide to the parent Pd(II) pincer-complex species.

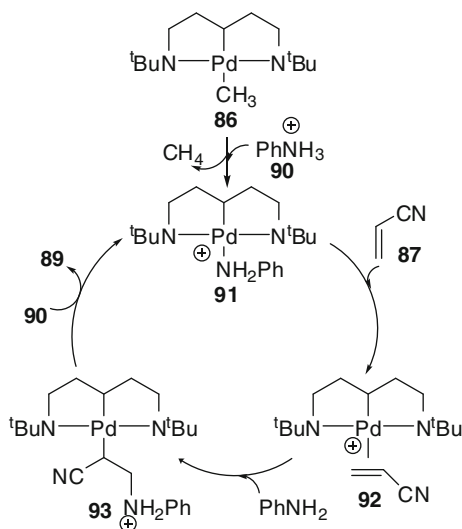
8 Hydroamination Reactions Catalyzed by Palladium Pincer-Complex Catalysts

Palladium-catalyzed hydroamination is an important and rapidly developing field in organic synthesis [40, 41]. The high synthetic value of this process involves formation of a new carbon–nitrogen bond via addition of amines to alkenes. Trogler and Seligson [135, 136] reported the synthesis of pincer complex **86** and its application for catalytic hydroamination reactions (Scheme 41). In this reaction acrylonitrile **87** was employed as activated terminal alkene and aniline salt **88** as the nitrogen source affording anilinopropionitrile **89** [135].

The mechanism of the reaction was studied by Milstein and coworkers [7, 137]. These authors proposed that the initial step of the catalytic cycle is protonolysis of **86** with ammonium salt **90** to give complex **91** and releasing methane. After ligand exchange with acrylonitrile (**87**) complex **92** undergoes nucleophilic addition with the palladium-activated olefin involving an $\eta^2 \rightarrow \eta^1$ slippage yielding complex **93** (Scheme 42). Subsequently, ligand exchange with **90** releases the product and regenerates the catalyst. Although there are relatively few examples for pincer-complex catalyzed hydroamination reactions, several new applications are expected based on C(sp³) type of catalysts, such as **86**. Michael and Cochran [138] published a new procedure (Scheme 43) for intramolecular hydroamination of unactivated alkenes (such as **94**) using PNP complex **95** as catalyst. These processes result in pyrrolidine derivatives (**96**) with excellent yields. Common palladium salts without terdentate pincer ligands were inefficient to produce the



Scheme 41 Hydroamination with C(sp³) pincer complex **86** [135]



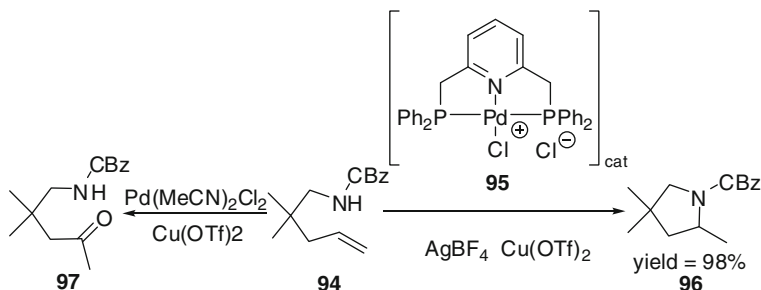
Scheme 42 Proposed catalytic cycle for pincer complex catalyzed hydroamination [7, 135]

cyclized products (such as **96**). For example, compound **94** underwent Wacker oxidation with catalytic amounts of Pd(MeCN)₂Cl₂ affording **97** (Scheme 43).

A possible explanation is that the terdentate pincer ligand inhibits the β-hydride elimination of the alkyl palladium intermediate of the reaction, and therefore the Wacker oxidation process (**97**) can be diverted favoring the hydroamination reaction (**96**).

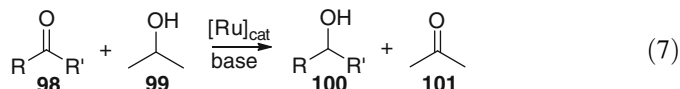
9 Ruthenium Pincer-Complex Catalyzed Transfer Hydrogenation Reactions

Hydrogenation of ketones (**98**) to alcohols (**100**) is a fundamental process in organic chemistry. This process can be carried out by catalytic transfer hydrogenation without employment of explosive hydrogen gas. In these reactions usually

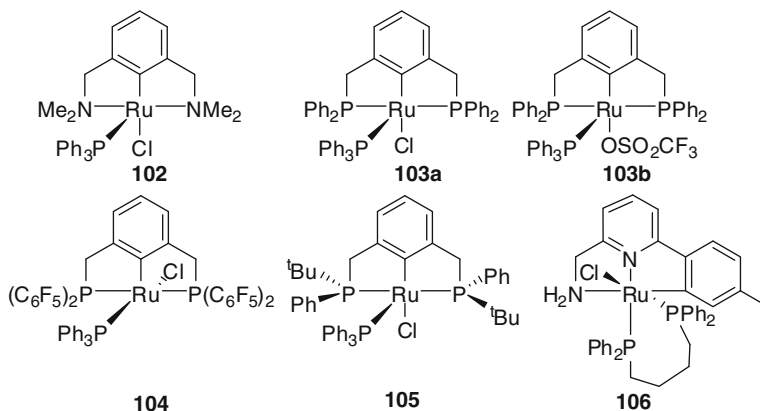


Scheme 43 Intramolecular hydroamination using a PNP pincer complex [138]

isopropanol (**99**) is used as a (safe) hydrogen source, which is oxidized to acetone **101** under the process (Eq. 7). The transfer hydrogenation reaction is readily catalyzed by ruthenium complexes in the presence of base (such as KOH or KO^tBu) [2, 139, 140].

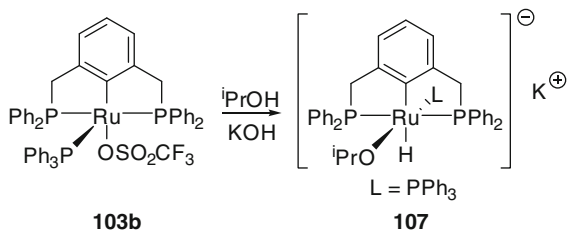


Van Koten and coworkers [141–143] developed a number of ruthenium pincer-complex catalysts (**102–105**, Scheme 44) for efficient transfer hydrogenation of ketones to secondary alcohols. As the structure of the pincer-complex catalysts is fully determined and characterized, an efficient tuning of the catalytic activity of these complexes could be achieved. It was shown [141] that PCP complexes **103a–b** catalyze the hydrogen transfer reactions with a higher turnover frequency (moles of ketone converted to alcohol per mol catalyst per hour, TOF) than NCN catalyst **102**. The best results, TOFs up to 27,000, could be achieved using triflate complex **103b** for reduction of cyclohexanone. This TOF value is superior to the performance of classical catalysts, such as $\text{RuCl}_2(\text{PPh}_3)_3$. Recently, synthesis of perfluoro analog of **103a** was reported (**104**) [142]. Catalyst **104** is more robust than its protio analog and also has a different configuration for the chloride ligand on ruthenium. Preliminary result shows that the catalytic activity of perfluoro complex **104** is somewhat lower than for **103a** [144]. In order to study the effects of alkylphosphino side arms on the reactivity of the catalytic process, Fogg and coworkers [145] synthesized cyclohexyl substituted complexes. However, replacement of the phenyl group of **103a** with cyclohexyl seems to decrease the TOF of the catalyst. Asymmetric catalysis was also attempted by synthesis of chiral pincer complex **105**. Complex **105** was applied for reduction of acetophenone, which so far gave relatively low ee (18 %). Bratta and Gladiali and coworkers [146] succeeded to improve the catalytic performance of pincer complexes in transfer hydrogenation by applying CNN complex **106**. Using catalytic amounts of complex **106** acetophenone and derivatives could be reduced with impressive TOFs (up to 2.5×10^6). It was suggested that the amino group in the side arm helps to orientate



Scheme 44 Ruthenium pincer complexes applied as catalysts for transfer hydrogenation reactions [141–143, 146]

Scheme 45 Formation of the active intermediate of the transfer hydrogenation reactions [141]



the ketone substrate prior to the hydrogen transfer, and therefore the catalytic activity is increased.

Van Koten and coworkers [141] studied the mechanistic aspects of the transfer hydrogenation reactions. It was found that when **103b** was heated in isopropanol in the presence of base (KOH) hydrido complex **107** was formed (Scheme 45), which was considered as the active intermediate of the reduction of ketones.

10 Conclusions and Outlook

Pincer-complex catalysts have found many applications in organic transition metal catalysis. The present review is focused on selective carbon–carbon, carbon–metal (C–B, C–Si, C–Sn), carbon–nitrogen formation reactions, and transfer hydrogenations. In these reactions, palladium, platinum, ruthenium, and rhodium pincer complexes have been applied as catalysts. Usually these catalysts perform better in terms of TON, TOF, and catalytic activity than the corresponding metal salt-based catalysts. In several cases (such as stannylation of propargyl substrates) the outcome of the pincer-complex catalyzed reactions is different from the

classical metal salt catalyzed transformations. The chemo-, regio-, and stereoselectivity of the pincer-complex catalysts could be effectively tuned by changing the heteroatoms in the side arms and substitution of the *para* position of the complexes.

Based on the large number of recently published pincer-complex catalyzed reactions it can be predicted that the number of new applications with pincer-complex catalysts will considerably increase in the next couple of years. The main targets are those carbon–carbon, carbon–nitrogen, and carbon–metal bond formation reactions, which are not amenable with traditional transition metal catalysis due to selectivity or reactivity issues. The design of new chiral pincer complexes for asymmetric catalysis is probably a very important area. The stable structure and well-defined stoichiometry of pincer complexes allow a rational design of effective chiral catalysts. Another important area is the immobilization of pincer complexes on solid support or dendrimers to obtain robust, recyclable catalysts. The strong metal bond interaction helps to create stable non-leaching catalysts, which can be employed several times in an economical way.

References

1. Crabtree RH (2005) The organometallic chemistry of the transition metals. Wiley, Hoboken
2. Tsuji J (2000) Transition metal reagents and catalysts. Innovation in organic synthesis. Chichester, Wiley
3. Hegedus LS (1999) Transition metals in the synthesis of complex organic molecules. University Science, Mill Valley, CA
4. Hartwig J (2010) Organotransition metal chemistry. University Science, Sausalito, CA
5. Albrecht M, van Koten G (2001) *Angew Chem Int Ed* 40:3750
6. Singleton JT (2003) *Tetrahedron* 59:1837
7. Van de Boom ME, Milstein D (2003) *Chem Rev* 103:1759
8. Dupont J, Consorti CS, Spencer J (2005) *Chem Rev* 105:2527
9. Szabó KJ (2006) *Synlett* 811
10. Bedford RB (2003) *Chem Commun* 1787
11. Beletskaya IP, Cheprakov AV (2004) *J Organomet Chem* 689:4055
12. Selander N, Szabó KJ (2009) *Dalton Trans* 32:6267
13. Selander N, Szabó KJ (2011) *Chem Rev* 111:2048
14. Morales-Morales D (2008) *Mini Rev Org Chem* 5:141
15. Serrano-Becerra JM, Morales-Morales D (2009) *Curr Org Synth* 6:169
16. van Koten G, Gebbink RJMK (2011) *Dalton Trans* 40:8731, Theme issue
17. Morales-Morales D, Jensen CM (2007) *The chemistry of pincer compounds*. Elsevier, Amsterdam
18. Choi J, MacArthur AHR, Brookhart M, Goldman AS (2011) *Chem Rev* 111:1761
19. Gunanathan C, Milstein D (2011) *Top Organomet Chem* 37:55
20. Ito Y, Sawamura M, Hayashi T (1986) *J Am Chem Soc* 108:6405
21. Gorla F, Togni A, Venanzi LM, Albinati A, Lianza F (1994) *Organometallics* 13:1607
22. Longmire JM, Zhang X, Shang M (1998) *Organometallics* 17:4374
23. Motoyama Y, Kawakami H, Shimozono K, Aoki K, Nishiyama H (2002) *Organometallics* 21:3408
24. Stark MA, Richards CJ (1997) *Tetrahedron Lett* 38:5881
25. Slagt MQ, Jastrzebski JTBH, Gebbink RJMK, Ramesdonk HJv, Verhoeven JW, Ellis DD, Spek AL, Koten Gv (2003) *Eur J Org Chem* 1692

26. Gosiewska S, Veld MHi, de Pater JJM, Bruijninx PCA, Lutz M, Spek AL, van Koten G, Gebbink RJMK (2006) *Tetrahedron Asymm* 17:674
27. Donkervoort JG, Vicario JL, Rijnberg E, Jastrzebski JTBH, Kooijman H, Spek AL, van Koten G (1998) *J Organomet Chem* 463:463
28. Giménez R, Swager TM (2001) *J Mol Catal A Chem* 166:265
29. Gosiewska S, Herreras SM, Lutz M, Spek AL, Havenith RWA, van Klink GPM, van Koten G, Gebbink RJMK (2008) *Organometallics* 27:2549
30. Aydin J, Kumar KS, Eriksson L, Szabó KJ (2007) *Adv Synth Catal* 349:2585
31. Aydin J, Rydén A, Szabó KJ (2008) *Tetrahedron: Asymmetry* 19:1867
32. Zografidis A, Polborn K, Beck W, Markies BA, van Koten G (1994) *Z Naturforsch B Chem Sci* 49:1494
33. Nishiyama H, Shiomi T, Tsuchiya Y, Matsuda I (2005) *J Am Chem Soc* 127:6972
34. Takenaka K, Minakawa M, Uozumi Y (2005) *J Am Chem Soc* 127:12273
35. Takenaka K, Uozumi Y (2004) *Org Lett* 6:1833
36. Stark MA, Jones G, Richards CJ (2000) *Organometallics* 19:1282
37. Fossey JS, Richards CJ (2004) *Organometallics* 23:367
38. Feng J-J, Chen X-F, Shi M, Duan W-L (2010) *J Am Chem Soc* 132:5562
39. Du D, Duan W-L (2011) *Chem Commun* 47:11101
40. Tsuji J (2004) *Palladium reagents and catalysts. New perspectives for the 21st century.* Wiley, Chichester
41. Negishi E, de Meijre A (2002) *Organopalladium chemistry for organic synthesis.* Wiley, New York
42. Szabó KJ (2004) *Chem Eur J* 10:5268
43. Motoyama Y, Narusawa H, Nishiyama N (1999) *Chem Commun* 131
44. Motoyama Y, Okano M, Narusawa H, Makihara N, Aoki K, Nishiyama H (2001) *Organometallics* 20:1580
45. Trost BM (1980) *Acc Chem Res* 13:385
46. Godleski SA (1991) In: Trost BM, Fleming I (eds) *Nucleophiles with allyl-metal complexes*, vol 4. Pergamon Press, New York, p Chap. 3.3
47. Trost BM, Vranken DLV (1996) *Chem Rev* 96:395
48. Szabó KJ (2001) *Chem Soc Rev* 30:136
49. Nakamura H, Iwama H, Yamamoto Y (1996) *J Am Chem Soc* 118:6641
50. Szabó KJ (2000) *Chem Eur J* 6:4413
51. Nakamura H, Shim J-G, Yamamoto Y (1997) *J Am Chem Soc* 119:8113
52. Nakamura H, Nakamura K, Yamamoto Y (1998) *J Am Chem Soc* 120:4242
53. Nakamura H, Aoyagi K, Shim J-G, Yamamoto Y (2001) *J Am Chem Soc* 123:372
54. Fernandes RA, Stimac A, Yamamoto Y (2003) *J Am Chem Soc* 125:14133
55. Solin N, Narayan S, Szabó KJ (2001) *J Org Chem* 66:1686
56. Solin N, Narayan S, Szabó KJ (2001) *Org Lett* 3:909
57. Goliaszewski A, Schwartz J (1985) *Tetrahedron* 41:5779
58. Nakamura H, Bao M, Yamamoto Y (2001) *Angew Chem Int Ed* 40:3208
59. Solin N, Kjellgren J, Szabó KJ (2003) *Angew Chem Int Ed* 42:3656
60. Solin N, Kjellgren J, Szabó KJ (2004) *J Am Chem Soc* 126:7026
61. Solin N, Wallner OA, Szabó KJ (2005) *Org Lett* 7:689
62. Wallner OA, Szabó KJ (2004) *Org Lett* 6:1829
63. Wallner OA, Olsson VJ, Eriksson L, Szabó KJ (2006) *Inorg Chim Acta* 359:1767
64. Bedford RB, Draper SM, Scully PN, Welch SL (2000) *New J Chem* 24:745
65. Rimml H, Venanzi LM (1983) *J Organomet Chem* 259:C6
66. Haenel MW, Oevers S, Bruckmann J, Kuhnigk J, Krüger C (1998) *Synlett* 3:301
67. Yao Q, Sheets M (2006) *J Org Chem* 71:5384
68. Johansson R, Wendt OF (2007) *Dalton Trans* 4:488
69. Johnson MT, Johansson R, Kondrashov MV, Steyl G, Ahlquist MSG, Roodt A, Wendt OF (2010) *Organometallics* 29:3521

70. Wallner OA, Szabó KJ (2006) *Chem Eur J* 12:6976
71. Aydin J, Kumar KS, Sayah MJ, Wallner OA, Szabó KJ (2007) *J Org Chem* 72:4689
72. Li J, Lutz M, Spek AL, van Klink GPM, van Koten G, Gebbink RJMK (2010) *Organometallics* 29:1379
73. Baber RA, Bedford RB, Betham M, Blake ME, Coles SJ, Haddow MF, Hurthouse MB, Orpen AG, Pilarski LT, Pringle PG, Wingad RL (2006) *Chem Commun* 37:3880
74. Beletskaya I, Moberg C (2006) *Chem Rev* 106:2320
75. Beletskaya I, Moberg C (1999) *Chem Rev* 99:3435
76. Marshall JA (2000) *Chem Rev* 100:3163
77. Horn KA (1995) *Chem Rev* 95:1317
78. Suginome M, Ito Y (2000) *Chem Rev* 100:3221
79. Ishiyama T, Ahiko T-A, Miyaura N (1996) *Tetrahedron Lett* 37:6889
80. Sebelius S, Olsson VJ, Szabó KJ (2005) *J Am Chem Soc* 127:10478
81. Sebelius S, Olsson VJ, Wallner OA, Szabó KJ (2006) *J Am Chem Soc* 128:8150
82. Olsson VJ, Sebelius S, Selander N, Szabó KJ (2006) *J Am Chem Soc* 128:4588
83. Selander N, Sebelius S, Estay C, Szabó KJ (2006) *Eur J Org Chem* 2006(18):4085
84. Selander N, Kipke A, Sebelius S, Szabó KJ (2007) *J Am Chem Soc* 129:13723
85. Selander N, Szabó KJ (2008) *Chem Commun* 29:3420
86. Selander N, Szabó KJ (2008) *Adv Synth Catal* 350:2045
87. Selander N, Szabó KJ (2009) *J Org Chem* 74:5695
88. Yao Q, Kinney EP, Zheng C (2004) *Org Lett* 6:2997
89. Baber RA, Norman NC, Orpen AG, Rossi J (2003) *New J Chem* 27:773
90. Batey RA, Quach TD (2001) *Tetrahedron Lett* 42:9099
91. Suzuki A (1999) *J Organomet Chem* 576:147
92. Miyaura N, Suzuki A (1995) *Chem Rev* 95:2457
93. Chemler SR, Trauner D, Danishefsky SJ (2001) *Angew Chem Int Ed* 40:4544
94. Petasis NA, Zavialov IA (1998) *J Am Chem Soc* 120:11798
95. Petasis NA, Zavialov IA (1997) *J Am Chem Soc* 119:445
96. McDonald AR, Dijkstra HP, Suijkerbuijk BMJM, van Klink GPM, van Koten G (2009) *Organometallics* 28:4689
97. Gagliardo M, Selander N, Mehendale NC, van Koten G, Klein-Gebbink RJM, Szabó KJ (2008) *Chem Eur J* 14:4800
98. Mitchell TN, Amamaria A, Killing H, Rutschow D (1986) *J Organomet Chem* 304:257
99. Tsuji Y, Nishiyama K, Hori S, Ebihara M, Kawamura T (1998) *Organometallics* 17:507
100. Kjellgren J, Sundén H, Szabó KJ (2004) *J Am Chem Soc* 126:474
101. Kjellgren J, Sundén H, Szabó KJ (2005) *J Am Chem Soc* 127:1787
102. Kharasch MS, Jensen EV, Urry WH (1945) *Science* 102:128
103. Kharasch MS, Urry WH, Jensen EV (1945) *J Am Chem Soc* 67:1626
104. Gossage RA, van de Kuil LA, van Koten G (1998) *Acc Chem Res* 31:423
105. Knapen JWJ, van de Made AW, de Wilde JC, van Leeuwen PWNM, Wijkens P, Grove DM, van Koten G (1994) *Nature* 372:659
106. Van de Kuil LA, Grove DM, Gossage RA, Zwikker JW, Jenneskens LW, Drenth W, van Koten G (1997) *Organometallics* 16:4985
107. Grove DM, van Koten G, Verschuuren AHM (1988) *J Mol Catal* 45:169
108. Grove DM, Verschuuren AHM, van Koten G (1989) *J Organomet Chem* 372:C1
109. Van de Kuil LA, Luitjes H, Grove DM, Zwikker JW, van de Linden JGM, Roelofsens AM, Jenneskens LW, Drenth W, van Koten G (1994) *Organometallics* 13:468
110. Gv K, Jastrzebski JTBH (1999) *J Mol Catal A Chem* 146:317
111. Phan NTS, van de Sluys M, Jones CW (2006) *Adv Synth Catal* 348:609
112. Hall DG (2005) *Boronic acids*. Wiley, Weinheim
113. Ohff M, Ohff A, van de Boom ME, Milstein D (1997) *J Am Chem Soc* 119:11687
114. Morales-Morales D, Grause C, Kasaoka K, Redón R, Cramer RE, Jensen CM (2000) *Inorg Chim Acta* 300:958

115. Morales-Morales D, Redón R, Yung C, Jensen CM (2000) *Chem Commun* 1619
116. Miyazaki F, Yamaguchi K, Shibasaki M (1999) *Tetrahedron Lett* 40:7379
117. Bergbreiter DE, Osburn PL, Liu Y-S (1999) *J Am Chem Soc* 121:9531
118. Bergbreiter DE, Osburn PL, Frels JD (2005) *Adv Synth Catal* 347:172
119. Gründemann S, Albrecht M, Loch JA, Faller JW, Crabtree RH (2001) *Organometallics* 20:5485
120. Peris E, Loch JA, Mata J, Crabtree RH (2001) *Chem Commun* 201
121. Consorti CS, Ebeling G, Flores FR, Rominger F, Dupont J (2004) *Adv Synth Catal* 346:617
122. Zim D, Gruber AS, Ebeling G, Dupont J, Monteiro AL (2000) *Org Lett* 2:2881
123. Frech CM, Shimon LJW, Milstein D (2005) *Angew Chem Int Ed* 44:1709
124. Bolliger JL, Blacque O, Frech CM (2008) *Chem Eur J* 14:7969
125. Bolliger JL, Frech CM (2009) *Adv Synth Catal* 351:891
126. Blacque O, Frech CM (2010) *Chem Eur J* 16:1521
127. Sommer WJ, Yu K, Sears JS, Ji Y, Zheng X, Davis RJ, Sherrill CD, Jones CW, Weck M (2005) *Organometallics* 24:4351
128. Eberhard MR (2004) *Org Lett* 6:2125
129. Melero C, Martínez-Prieto LM, Palma P, de Rio D, Álvarez E, Cámpora J (2010) *Chem Commun* 46(46):8851
130. Aydin J, Larsson JM, Selander N, Szabó KJ (2009) *Org Lett* 11:2852
131. Pilarski LT, Selander N, Böse D, Szabó KJ (2009) *Org Lett* 11:5518
132. Selander N, Willy B, Szabó KJ (2010) *Angew Chem Int Ed* 49:4051
133. Vicente J, Arcas A, Juliá-Hernández F, Bautista D (2010) *Chem Commun* 46:7253
134. Vicente J, Arcas A, Juliá-Hernández F, Bautista D (2011) *Angew Chem Int Ed* 50:6896
135. Seligson AL, Trogler WC (1993) *Organometallics* 12:744
136. Seligson AL, Trogler WC (1993) *Organometallics* 12:738
137. Kraatz H-B, Milstein D (1995) *J Organomet Chem* 488:223
138. Michael FE, Cochran BM (2006) *J Am Chem Soc* 128:4246
139. Zassinovich G, Mestroni G, Gladiali S (1992) *Chem Rev* 92:1051
140. Noyori R, Hashiguchi S (1997) *Acc Chem Res* 30:97
141. Dani P, Karlen T, Gossage RA, Gladiali S, van Koten G (2000) *Angew Chem Int Ed* 39:743
142. Gagliardo M, Chase PA, Lutz M, Spek AL, Hartl F, Havenith RWA, van Klink GPM, van Koten G (2005) *Organometallics* 24:4553
143. Medici S, Gagliardo M, Williams SB, Chase PA, Gladiali S, Lutz M, Spek AL, van Klink GPM, van Koten G (2005) *Helv Chim Acta* 88:694
144. Gagliardo M (2006) Ruthenium(II) complexes of anionic bisphosphinoaryl ligands as catalysts and building blocks for functional materials. Thesis, Utrecht University
145. Amoroso D, Jabri A, Yapp GPA, Gusev DG, de Santos EN, Fogg DE (2004) *Organometallics* 23:4047
146. Bratta W, Chelucci G, Gladiali S, Siega K, Toniutti M, Zanette M, Zangrando E, Rigo P (2005) *Angew Chem Int Ed* 44:6214

Optically Active Bis(oxazolinyl)phenyl Metal Complexes as Multipotent Catalysts

Jun-ichi Ito and Hisao Nishiyama

Abstract The bis(oxazolinyl)phenyl (abbreviated as phebox) ligand, which consists of two chiral oxazolines and a benzene backbone, is one of the most useful scaffolds for the construction of chiral NCN pincer complexes. The resulting phebox metal complexes can effectively deliver a C_2 -symmetric environment around the active metal center. Currently, various transition metals in the range of early to late metals have been introduced by cyclometalation and transmetalation reactions to construct phebox metal complexes. Among them, the phebox Rh and Ru complexes have been extensively investigated as molecular catalysts for asymmetric catalytic reactions. High efficiency and selectivity were obtained in functionalization reactions, such as hydrosilylation, conjugate reduction, and borylation, and carbon–carbon bond formation reactions, such as reductive aldol reaction and alkynylation. The phebox complex is a good representative multipotent catalyst.

Keywords Asymmetric catalysis · Chiral tridentate ligand · Oxazoline ligand · Rhodium catalyst · Ruthenium catalyst

Contents

1	Introduction	244
2	Preparation of Transition Metal Complexes with Phebox Ligands	246
2.1	Group 9 Metals (Rh, Ir)	246
2.2	Group 10 Metals (Ni, Pd, Pt)	247
2.3	Group 8 Metals (Fe, Ru)	249
2.4	Group 11 Metals (Au) and Early Transition Metals	251
2.5	Molecular Structures of Phebox Metal Complexes	251

J.-i. Ito · H. Nishiyama (✉)

Department of Applied Chemistry, Graduate School of Engineering, Nagoya University, Chikusa,
Nagoya 464-8603, Japan

e-mail: hnishi@apchem.nagoya-u.ac.jp

3	Organometallic Reactions of (Phebox)Rh Complexes	253
3.1	Reactions with Arenes	253
3.2	C–C Bond Formation Reactions	254
3.3	Molecular Recognition	256
4	Asymmetric Catalytic Reactions with (Phebox)Rh Complexes	257
4.1	Lewis Acid Catalysis	257
4.2	Hydrosilylation and Conjugate Reduction	258
4.3	Reductive Aldol Reactions	259
4.4	Direct Aldol Reactions	260
4.5	β -Borylation	263
4.6	Alkynylation	263
5	Asymmetric Reactions with (Phebox)Ru Complexes	264
5.1	Hydrogenation and Transfer Hydrogenation	264
5.2	Alkynylation	264
5.3	Cyclopropanation	265
6	Catalytic Reactions with Group 10 Metal Complexes	266
7	Conclusion	268
	References	268

1 Introduction

Anionic meridional ligands, such as PCP and NCN pincer ligands, can produce transition metal complexes that serve as highly reactive catalysts in homogeneous reactions [1–3]. Pincer transition metal complexes consist of a metal–carbon covalent bond and two metallacycles, which may stabilize the metal center and create unique electronic properties and steric environments. An additional advantage of the pincer ligand is the tunability of the molecular structure. This feature is useful for designing optically active catalysts. As shown in Fig. 1, chiral PCP and NCN ligands containing benzene backbones have been developed using several types of chiral sources to control the chiral reaction site. For example, Venanzi et al. introduced C-stereogenic centers at the benzyl positions to prepare the chiral Pt complex **A** [4]. Similar PCP and NCN ligands containing C-stereogenic centers were utilized in the Pd and Pt complexes **B–C** [5, 6]. Introduction of chiral centers at the coordinating position, such as P and N donors, expanded the diversity of the ligands. Chiral NCN ligands bearing hexahydro-1*H*-pyrrolo[1,2,*c*]imidazolone [7], tetrahydroquinoline [8], pyrrolidine [9], and imidazoline fragments [10] were applied to the preparation of the Pd(II) and Pt(II) complexes **D–G**. Phosphorus donors, namely phosphoramidite [11, 12] and phosphite fragments [13–15], were introduced into the PCP ligand framework to construct the Pd complexes **H–I**. In addition, PCP pincer ligands with P-stereogenic centers produced the Pd [16], Ir [17], and Ru complexes **J–K** [18]. The Pd and Pt complexes described earlier served as asymmetric catalysts in aldol reactions of aldehydes with isocyanoacetate [5, 8, 9], allylation of aldehydes or imines with allylic stannanes [11, 13, 14], Friedel–Crafts alkylation of indoles with nitrostyrene [10], Michael addition of α -cyanoesters to enones [7], Mannich reaction of imines with benzyl nitriles [15], and hydrophosphination of enones [19].

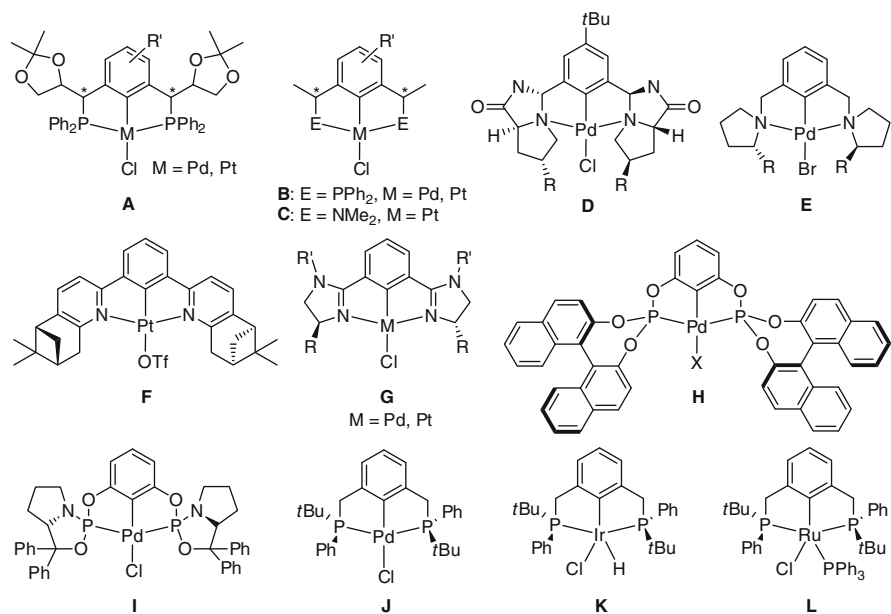


Fig. 1 Chiral pincer complexes

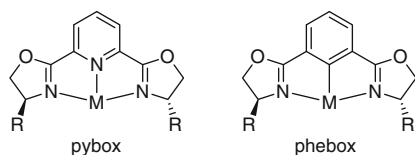
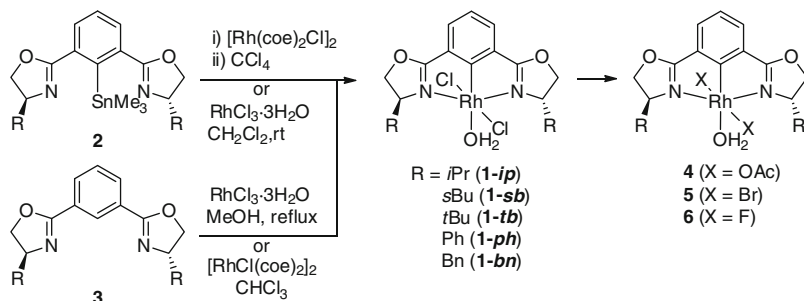


Fig. 2 Chiral pybox and phebox complexes

In 1997, the bis(oxazoliny)phenyl ligand (phebox) was developed as a chiral NCN pincer ligand by Nishiyama [20], Denmark [21], and Richards (Fig. 2) [22]. As bis(oxazoline)pyridine (pybox) ligands are a prominent class of chiral ligands for transition metal catalysts for asymmetric reactions [23], the structurally related phebox complex has the potential to be a chiral catalyst with high enantiomeric induction. Early studies focused on its function as a Lewis acid catalyst for allylation, hetero Diels–Alder, Michael addition, and aldol reactions using Rh, Pd, and Pt complexes. Recently, the (phebox)Rh complex was shown to be a highly effective catalyst for asymmetric hydrosilylation and conjugate reduction. Previous reviews covered those topics [24, 25]. In this chapter, we describe the preparation of metal complexes and involving group 4–11 metals. Asymmetric reactions and stoichiometric reactions mediated by the phebox metal complexes are also discussed.



Scheme 1 Synthesis of (phebox)Rh complexes

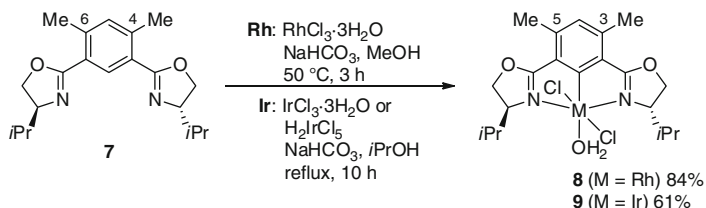
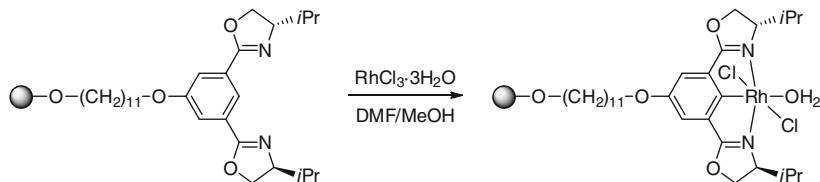
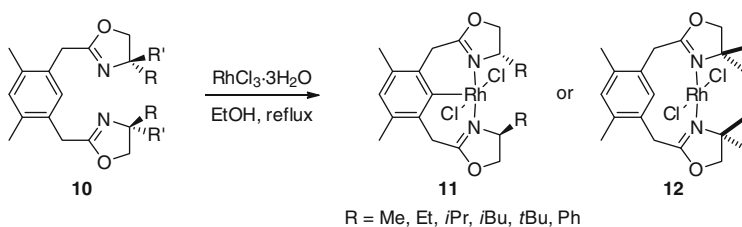
2 Preparation of Transition Metal Complexes with Phebox Ligands

2.1 Group 9 Metals (*Rh*, *Ir*)

The (phebox)Rh(III) complexes **1** were synthesized by transmetalation of (phebox)SnMe₃ **2** with $[\text{RhCl}(\text{coe})_2]_2$ (coe = cyclooctene) in CCl_4 or $\text{RhCl}_3 \cdot 3\text{H}_2\text{O}$ in CH_2Cl_2 (Scheme 1) [20, 26, 27]. Alternatively, the C–H bond activation of (phebox)H **3** with Rh(III) chloride in MeOH or $[\text{RhCl}(\text{coe})_2]_2$ in CHCl_3 was used for the preparation of **1** [28]. The resulting (phebox)Rh chloride complexes **1** readily gave the corresponding acetate complexes **4** by the ligand exchange reaction with AgOAc in CH_2Cl_2 . The bromide complex **5** was obtained by treatment of **1** with CBr_4 in MeOH, while the fluoride complex **6** was synthesized by the reaction of **1** with AgOAc, followed by addition of $n\text{Bu}_4\text{NF}$ and HBF_4 in CH_2Cl_2 [29]. Molecular structures of these (phebox)Rh complexes contain the meridionally coordinated phebox ligand. The Rh center adopts a distorted octahedral geometry, in which two halides or acetates are located in the *trans* positions and a H_2O ligand is coordinated in the phebox plane. Substituents on the oxazoline ring, such as isopropyl (*ip*), *sec*-butyl (*sb*), *tert*-butyl (*tb*), phenyl (*ph*), and benzyl (*bn*), were introduced by use of the proper β -aminoalcohols.

The phebox ligand **7** containing two methyl groups at the 4- and 6-positions on the benzene ring increased the yield of the corresponding (phebox)Rh complex **8** via the C–H bond activation method (Scheme 2) [30]. It was explained that blocking of cyclometalation at the 4- and 6-positions was important for selective cyclometalation at the 2-position. Furthermore, the phebox ligand **7** introduced a convenient method for the preparation of the (phebox)Ir complex **9**, which was obtained by the reaction of **7** with $\text{IrCl}_3 \cdot 3\text{H}_2\text{O}$ or $\text{IrH}_2\text{Cl}_4 \cdot \text{H}_2\text{O}$ in 2-propanol.

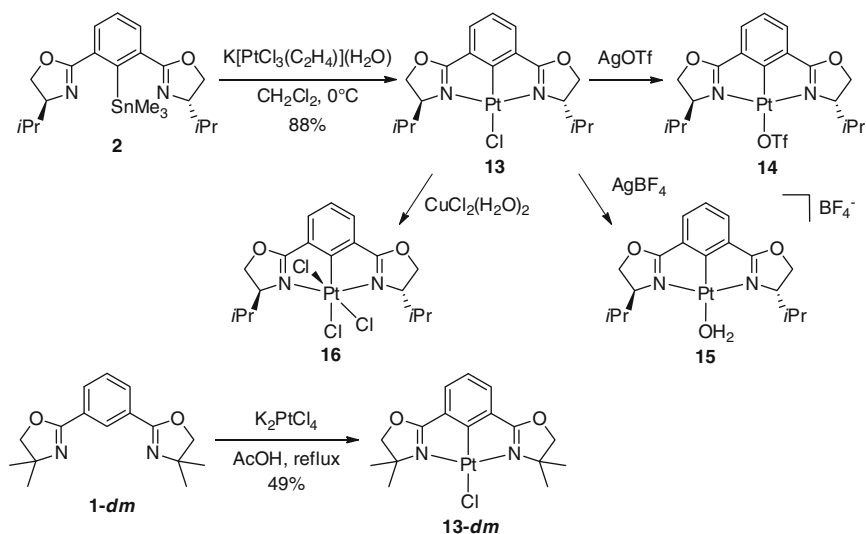
Portnoy reported the solid-phase synthesis of phebox ligands and Rh complexes [31] (Scheme 3). The phebox ligands were immobilized on Wang resin using a linear alkyl spacer. Introduction of the Rh atom into the ligand framework was successfully achieved by cyclometalation with $\text{RhCl}_3 \cdot 3\text{H}_2\text{O}$ in DMF/MeOH solution.

**Scheme 2** Synthesis of Rh and Ir complexes**Scheme 3** Solid-phase synthesis of (phebox)Rh complexes**Scheme 4** Synthesis of (benbox)Rh complexes

Bergman and Tilley designed a phebox analogue, the novel C₂-symmetric bis(oxazoline) pincer (benbox) ligand (**10**), in which a wider N-Me-N bite angle was expected [32]. Cyclometalation of the benbox ligand with RhCl₃·3H₂O resulted in the formation of the (benbox)RhCl₂ complexes **11** in 8–59 % yields (Scheme 4). Although the related (phebox)Rh complex was a coordinatively saturated 18-electron complex with coordination of a H₂O molecule, the (benbox)Rh complex **11** was found to be a coordinatively unsaturated complex with the Rh center adopting a square pyramidal geometry. Interestingly, in the case of bulky ligands, the unique (benbox)Rh(II) complex **12** was also produced. In complex **12**, the geometry of the Rh atom was determined to be square planar.

2.2 Group 10 Metals (Ni, Pd, Pt)

The (phebox)PtCl complex **13** was synthesized by transmetalation of (phebox)SnMe₃ **2** with the Zeise salt K[PtCl₃(C₂H₄)](H₂O) in CH₂Cl₂ at 0 °C (Scheme 5) [33]. Treatment of **13** with silver salts AgOTf or AgBF₄ gave the corresponding

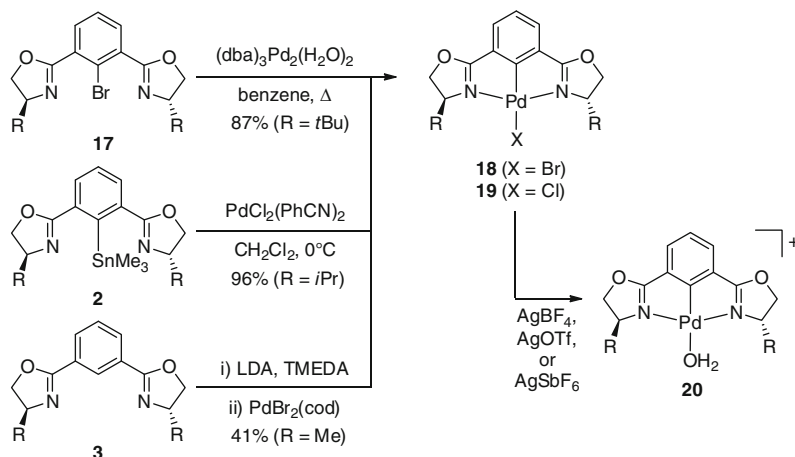


Scheme 5 Synthesis and reactions of Pt complexes

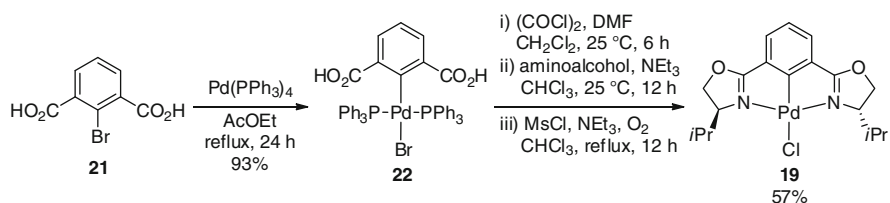
trifluoromethanesulfonate complex **14** or cationic aqua complex **15**, respectively. In addition, oxidation of **13** with $\text{CuCl}_2 \cdot 2\text{H}_2\text{O}$ in CH_2Cl_2 at 40°C afforded the (phebox)Pt(IV) complex **16**. Alternatively, the (phebox)PtCl complex **13-dm** was prepared by C–H bond activation of **1-dm** with K_2PtCl_4 in dry acetic acid at reflux temperature [34]. It was found that this synthetic method was dependent on the dryness of the acetic acid. Use of highly dried acetic acid increased the yield of **1-dm**.

There are several synthetic methods for the preparation of (phebox)Pd complexes (Scheme 6). Denmark reported the preparation of a (phebox)Pd bromide complex **18** via oxidative addition across the C–Br bond of (phebox)Br **17** with $(\text{dba})_3\text{Pd}_2(\text{H}_2\text{O})_2$ in benzene [21]. Independently, Richards reported that transmetalation of $\text{PdBr}_2(\text{cod})$ ($\text{cod} = 1,5\text{-cyclooctadiene}$) with a (phebox)Li compound, which was generated by *ortho*-lithiation of **3** with LDA, furnished the corresponding Pd complex **19** in 18–41 % yields [22]. The chloride complex **19** was also synthesized in 96 % yield by transmetalation of (phebox)SnMe₃ **2** with $\text{PdCl}_2(\text{PhCN})_2$ in CH_2Cl_2 at 0°C [35]. Addition of a silver salt to **18** or **19** afforded the corresponding cationic complex **20**.

Although phebox complexes are usually synthesized by the reaction of metal complexes or salts with phebox ligand precursors, such as **2** or **3**, the oxazoline ring can be introduced on a metal aryl complex. In this context, an aryl palladium complex **22** was proposed to prepare the (phebox)Pd complex **19** (Scheme 7) [36]. The aryl complex **22** was synthesized by oxidative addition of 2-bromoisophthalic acid (**21**) to $\text{Pd}(\text{PPh}_3)_4$. The reaction of **22** with oxalyl chloride, amidation with β -aminoalcohol, and subsequent cyclization with mesyl chloride in the presence of O_2 gave the desired (phebox)Pd complex **19** in 44–57 % yields accompanied by triphenylphosphine oxide. The bromide ligand of **22** was exchanged to the chloride ligand during the reaction.



Scheme 6 Synthesis of Pd complexes



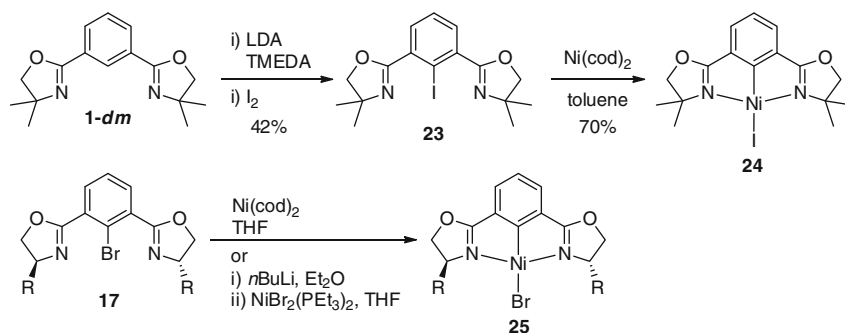
Scheme 7 Synthesis of Pd complex **19**

Richards reported the first preparation of a (phebox)Ni complex **24**, which was obtained by oxidative addition of (phebox)I **23** to $Ni(cod)_2$ in 70 % yield (Scheme 8) [37]. Similarly, the chiral (phebox)Br **17** was used to prepare the (phebox)NiBr complex **25** in high yield [38]. The Ni complex **25** was also synthesized by transmetalation of in situ generated (phebox)Li with $NiBr_2(P\dot{E}t_3)_2$. The latter reaction produced a side product, $NiBr(phebox)(P\dot{E}t_3)_2$, which contained a monodentate coordinated phebox ligand.

The properties of the phebox metal complexes could be controlled by substituents on the benzene backbone of the ligand. Connell et al. prepared a series of phebox ligands containing methoxy groups and their Ni and Pd complexes (Fig. 3) [39].

2.3 Group 8 Metals (*Fe*, *Ru*)

The (phebox)Ru complexes **26** were synthesized by C–H bond activation of the phebox ligand precursors by Ru chloride in the presence of zinc and cod (Scheme 9)



Scheme 8 Synthesis of Ni complexes

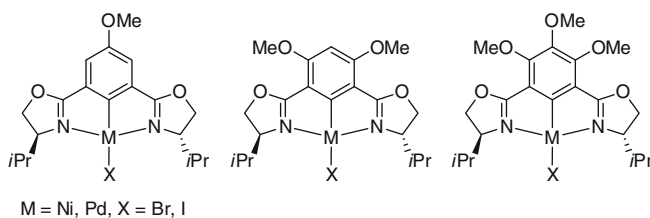
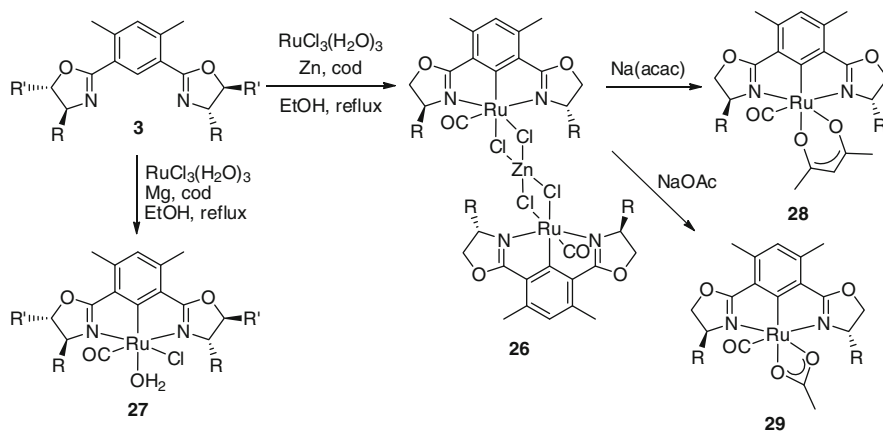
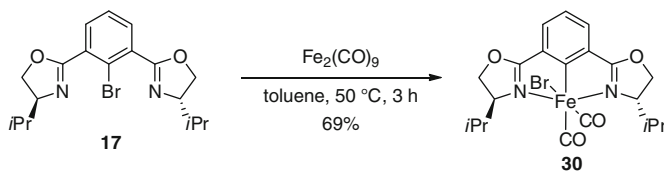


Fig. 3 Chiral (phebox)*M* (*M* = Ni, Pd) complexes



Scheme 9 Synthesis of Ru complexes

[40, 41]. The resulting (phebox)Ru complexes **26** consisted of a dimer structure, in which two (phebox)Ru moieties were connected by a Zn chloride bridge. In contrast, use of magnesium in place of Zn gave the mononuclear aqua complexes **27** [42]. The reaction of **26** with sodium acetylacetonate or sodium acetate gave the



Scheme 10 Synthesis of Fe complex

corresponding mononuclear acetylacetonate complex **28** or acetate complex **29**, respectively [40, 43].

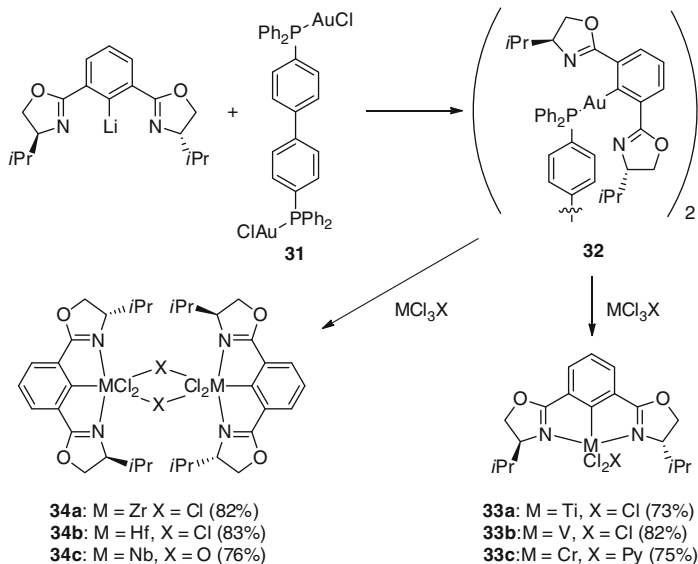
The (phebox)Fe complex **30** was prepared in 69 % yield by oxidative addition of the (phebox)Br **17** to $\text{Fe}_2(\text{CO})_9$ at 50 °C (Scheme 10) [44]. In contrast, reaction of other Fe carbonyl complexes, $\text{Fe}(\text{CO})_5$ and $\text{Fe}_3(\text{CO})_{12}$, with **17** failed. X-ray analysis of **30** revealed that the two CO ligands were oriented in the *cis* arrangement and the Br ligand was bound to the position vertical to the phebox plane.

2.4 Group 11 Metals (Au) and Early Transition Metals

Preparation of a gold complex containing the phebox ligand was achieved by van Koten [45, 46]. Transmetalation of (phebox)Li with $(\text{AuCl})_2(\text{dppbp})$ [**31**; dppdp = (diphenylphosphino)biphenyl] resulted in the formation of the corresponding (phebox)Au complexes (**32**) in high yields (Scheme 11). The Au complexes **32** were found to be good precursors for the preparation of other phebox metal complexes. In particular, phebox complexes containing early transition metals were obtained by transmetalation of **32** with metal salts in good yields. In this reaction, Ti, V, and Cr afforded mononuclear complexes **33**, while Zr, Hf, and Nb gave binuclear complexes **34**. These phebox complexes containing early transition metals served as catalysts for ethylene polymerization. The immobilized (phebox)V complex on MgCl_2 -based supports afforded polyethylene with a relatively narrow molecular weight distribution.

2.5 Molecular Structures of Phebox Metal Complexes

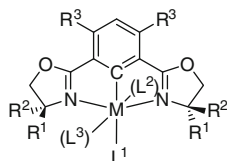
Molecular structures of the phebox metal complexes have been characterized by single X-ray diffraction studies. Selected bond distances and angles are listed in Table 1. The geometry of d_8 metal complexes [M = Ni(II), Pd(II), Pt(II)] is square planar, whereas that of d_6 metals [Rh(III), Ir(III), Fe(II), Ru(II), and Pt(IV)] is pseudo-octahedral (Fig. 4). Similarly, the geometry of early transition metal complexes is also described as the pseudo-octahedral coordination. In contrast, the Au complex contains a monodentate C-coordination of the phebox ligand.



Scheme 11 Synthesis of Au and early transition metal complexes

Table 1 Bond distances (Å) and angles

M	L ¹ , L ² , L ³	R ¹ , R ² , R ³	M-C	M-N (av.)	N-M-N	References
Ni	I	Me, Me, H	1.859(4)	1.975	161.04(13)	[37]
Ni	Br	<i>i</i> Pr, H, H	1.8491(19)	1.909	162.20(8)	[38]
Pd	Cl	<i>i</i> Pr, H, H	1.92(1)	2.053	159.6(5)	[35]
Pt	Cl	<i>i</i> Pr, H, H	1.928(10)	2.034	158.6(5)	[35]
Pt	Cl, Cl, Cl	<i>t</i> Bu, H, H	1.96(1)	2.065	159.3(3)	[35]
Rh	H ₂ O, Cl, Cl	Bn, H, H	1.921(7)	2.079	158.7(2)	[26]
Ir	H ₂ O, Cl, Cl	Me, Me, Me	1.930(3)	2.062	158.52(12)	[30]
Fe	CO, Br, CO	Me, Me, H	1.930(2)	2.009	157.42(7)	[44]
Ru	acac, CO	Ph, H, Me	1.9635(18)	2.095	156.37(6)	[40]
Au	PPh ₃	<i>i</i> Pr, H, H	2.060(2)	—	—	[46]
Ti	Cl, Cl, O <i>i</i> Pr	<i>i</i> Pr, H, H	2.141(3)	2.184	145.73(10)	[46]
V	Cl, Cl, Cl	<i>i</i> Pr, H, H	2.0906(17)	2.093	148.26(6)	[46]
Cr	py, Cl, Cl	<i>i</i> Pr, H, H	1.9973(19)	2.109	154.54(6)	[46]



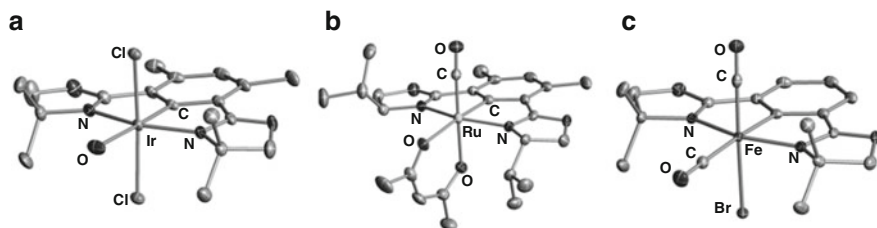


Fig. 4 Molecular structures of (phebox-*dm*)IrCl₂(H₂O) (a), (phebox-*ip*)Ru(acac)(CO) (b), and (phebox-*dm*)FeBr(CO)₂ (c)

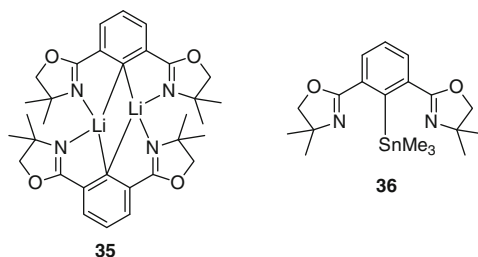


Fig. 5 (Phebox)Li and (phebox)SnMe₃

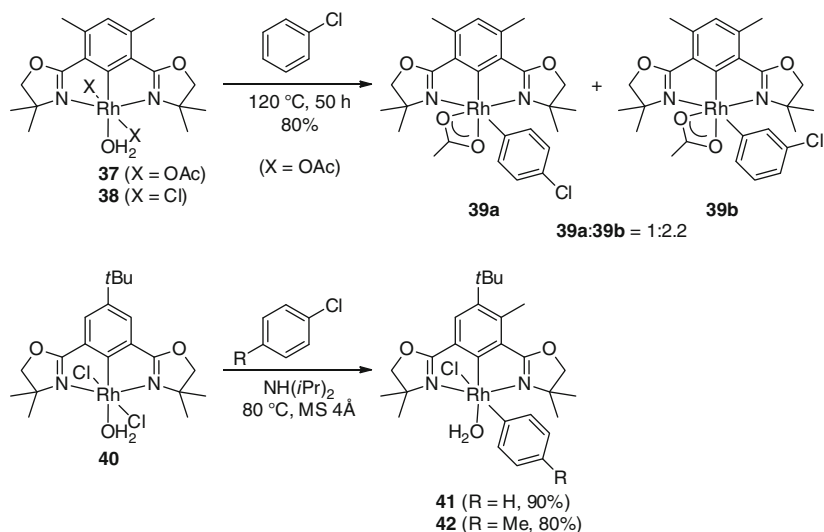
The M–C and M–N bond distances are 1.84–2.14 Å and 1.90–2.18 Å, respectively, and the N–M–N bond angles are 145.7–162.2° (Table 1). The Ni and Fe complexes have the tendency to have shorter M–C and M–N bond lengths. On the other hand, early transition metal complexes, such as Ti and V, exhibit longer M–C bond lengths.

The molecular structures of (phebox)Li **35** and (phebox)SnMe₃ **36** were also determined by X-ray analysis (Fig. 5) [47]. The (phebox)Li complex **35** has a dimer structure, with Li–C bond distances of 2.268(3)–2.299(3) Å. In the (phebox)Sn complex **36**, there is no interaction between the Sn atom and the N atoms. The Sn–C bond distance of 2.1810(18) Å is longer than those of other transition metal complexes.

3 Organometallic Reactions of (Phebox)Rh Complexes

3.1 Reactions with Arenes

The (phebox)Rh(III) complexes exhibited reactivity for the C–H and C–Cl bond cleavage of arenes. The reaction of the acetate complex **37** with aromatic compounds, such as benzene, toluene, chlorobenzene, acetophenone, and anisole,



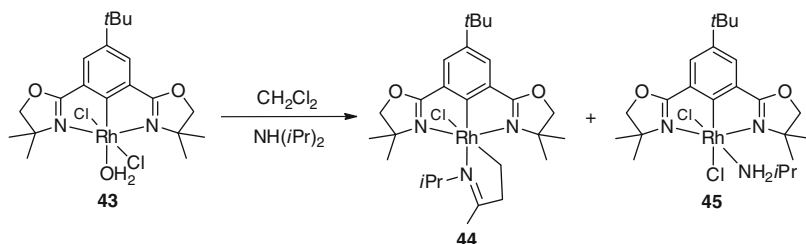
Scheme 12 C–H and C–Cl bond cleavage by (phebox)Rh complexes

afforded the corresponding aryl complexes via C–H bond cleavage (Scheme 12) [48]. For example, C–H bond activation of chlorobenzene resulted in the formation of the *p*- and *m*-substituted chlorophenyl complexes **39a** and **39b** in the ratio of 1:2.2. Although there are several mechanisms for C–H bond activation, the reaction with the Rh acetate complex **37** was proposed as a base promoted C–H bond activation. In contrast, the chloro analogue **38** did not react with chlorobenzene. This result supported the premise that the acetate ligand was required for C–H bond cleavage.

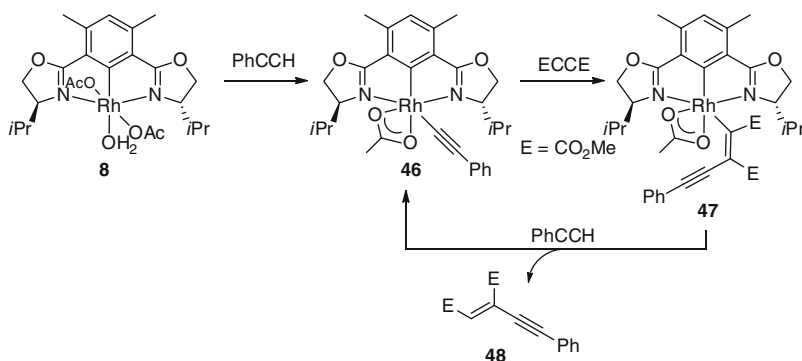
The (phebox)Rh complex was also found to undergo oxidative addition to the C–Cl bond. When the chloro complex **40** was treated with chlorobenzene in the presence of NH(*i*Pr)₂ at 80 °C, phenyl complex **41** was obtained in 90 % yield accompanied by N(=CMe₂)(*i*Pr) [49]. Generally, oxidative addition proceeds via a Rh(I) intermediate. The inactive (phebox)Rh(III) complex may be reduced by NH(*i*Pr)₂, which serves as a reductant. The preference between C–H and C–Cl bond cleavage of chlorobenzene can be tuned using different reaction conditions.

3.2 C–C Bond Formation Reactions

The (phebox)Rh complex can undergo a unique C–C bond formation reaction (Scheme 13) [50]. The reaction of **43** with dichloromethane and diisopropylamine at 50 °C resulted in formation of an azarhodacyclopentene complex **44**, accompanied by a small amount of the diisopropylamine Rh complex **45** in the ratio of 96:4. This reaction is formally described as a C–C bond formation via C–Cl bond cleavage of CH₂Cl₂ and C–H bond activation at the β-carbon of



Scheme 13 C–C bond formation on the (phebox)Rh complex

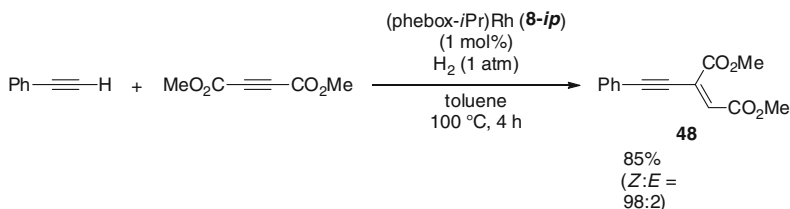


Scheme 14 Reaction of the (phebox)Rh complex with alkynes

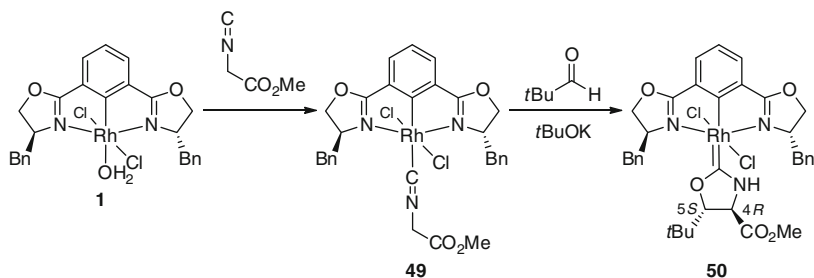
isopropylamine. The proposed reaction mechanism involves (1) reduction to a Rh(I) intermediate induced by oxidation of diisopropylamine to *N*-isopropylpropylideneamine, (2) oxidative addition of CH_2Cl_2 to the Rh(I) intermediate, (3) tautomerization to the enamine form, and (4) cyclization.

Activation of a terminal alkyne with a transition metal complex gives an acetylide complex, which serves as a key intermediate for alkynylation reactions such as dimerization. The acetate complex **8** reacted with phenylacetylene at 60°C to give the acetylide complex **46** (Scheme 14) [51]. The subsequent reaction of **46** with dimethyl acetylenedicarboxylate at room temperature readily afforded the corresponding vinyl complex **47** via insertion of the second alkyne into the Rh–acetylide bond. Finally, the reaction of **47** with phenylacetylene afforded the enyne **48** with regeneration of the acetylide complex **46**.

The formation of the enyne **48** suggests that the cross-coupling reaction of two different alkynes may be achieved. Such a catalytic cross-coupling reaction is a versatile method for the preparation of a variety of substituted enynes. Reaction of phenylacetylene with dimethyl acetylenedicarboxylate was catalyzed by 1 mol% of the acetate complex **8-*ip*** at 100°C to give the enyne **48** in 85 % yield with high *Z*-selectivity (Scheme 15). Interestingly, this catalytic transformation was accelerated under 1 atm of H_2 atmosphere.



Scheme 15 Cross-coupling of alkynes catalyzed by (phebox)Rh acetate complex

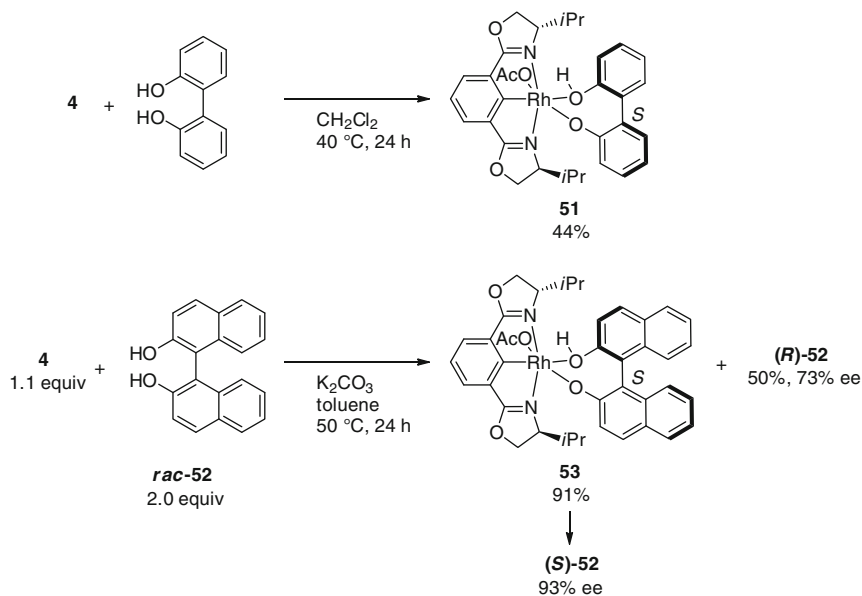


Scheme 16 Reaction of (phebox)Rh complex with isocyanoacetate and aldehydes

The (phebox)Rh complex reacted with isocyanoacetate to afford the isocyanide complex **49** in 99 % yield (Scheme 16) [52]. The complex **49** could then undergo an aldol type reaction with an aldehyde in the presence of a base to give the chiral Fisher carbene complex **50** with high dr and *trans*-selectivity. X-ray analysis of the major isomer revealed the (4*R*,5*S*) absolute configuration of the carbene fragment. The proposed mechanism of the aldol reaction involves an enolate intermediate, generated by deprotonation of **49**, which reacts with an aldehyde, followed by successive cyclization and protonation to form the carbene complex **50**. The *re*-face attack of the enolate constructs the observed (4*R*,5*S*) absolute configuration.

3.3 Molecular Recognition

The C_2 -symmetric cavity of the (phebox)Rh complex can provide a suitable environment for molecular recognition of organic substrates. The acetate ligand of the (phebox)Rh complex **4** underwent ligand-exchange reactions with 2,2'-biphenol and 1,1'-bi(2-naphthol) derivatives (Scheme 17) [53]. When 2,2'-biphenol was subjected to the ligand-exchange reaction, the corresponding biphenolate complex was formed. X-ray analysis showed that the absolute configuration was *S*. Furthermore, complex **4** could be used in the kinetic resolution of racemic 1,1'-bi(2-naphthol) (*rac*-**52**). Reaction of **4** (1.1 eq) with *rac*-**52** (2 eq) produced a binaphtholate complex **53** in 91 % yield along with (*R*)-**52** (73 % ee). Finally, the complex **53** afforded (*S*)-**52** with 93 % ee.

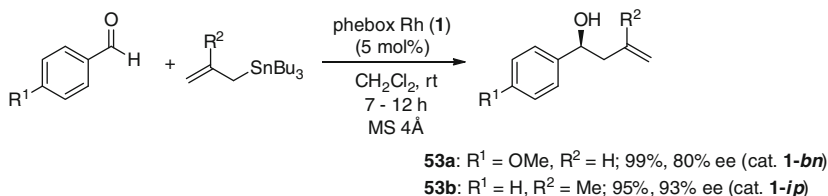


Scheme 17 Reactions with biphenol and binaphthol

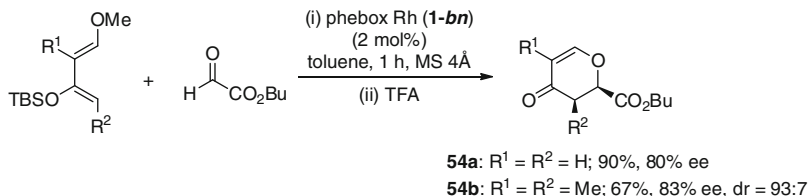
4 Asymmetric Catalytic Reactions with (Phebox)Rh Complexes

4.1 Lewis Acid Catalysis

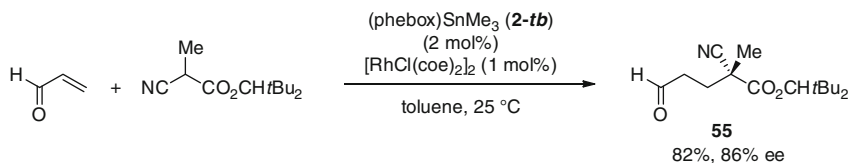
Dissociation of the H_2O ligand in the (phebox)Rh complex **1** generates a vacant site on the Rh center, which can accept a Lewis base such as pyridine or acetone. Complex **1** was used as a traditional Lewis acid catalyst in asymmetric C–C bond formation reactions. Complex **1** was found to be an efficient catalyst for allylation of aromatic aldehydes with allyltributyltin, giving the corresponding homoallylic alcohols in good yields with 61–80 % ee (Scheme 18) [26, 27]. The reaction with methallyltributyltin furnished the desired products with high enantiomeric excesses (up to 93 % ee) [54]. Complex **1** also serves as a mild Lewis acid catalyst for asymmetric hetero Diels–Alder reactions between Danishefsky’s dienes and glyoxylate derivatives (Scheme 19) [29]. In this reaction, high enantioselectivity and *cis*-(*endo*)-diastereoselectivity were observed. It was proposed that the catalytic reaction could proceed via a concerted [4 + 2] mechanism rather than the stepwise Mukaiyama-aldol mechanism. The (phebox)Rh system was also applied to the asymmetric Michael addition of α -cyanopropionates to acrolein (Scheme 20) [55]. The (phebox)Rh catalyst was prepared in situ by treatment of $[\text{RhCl}(\text{coe})_2]_2$ with (phebox)SnMe₃ (**2**). In this catalytic system, (phebox)RhCl(SnMe₃) was considered to be the active Lewis acid catalyst.



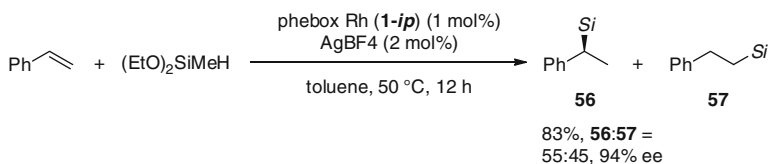
Scheme 18 Asymmetric allylation of aldehydes



Scheme 19 Asymmetric hetero Diels–Alder reaction of Danishefsky's diene



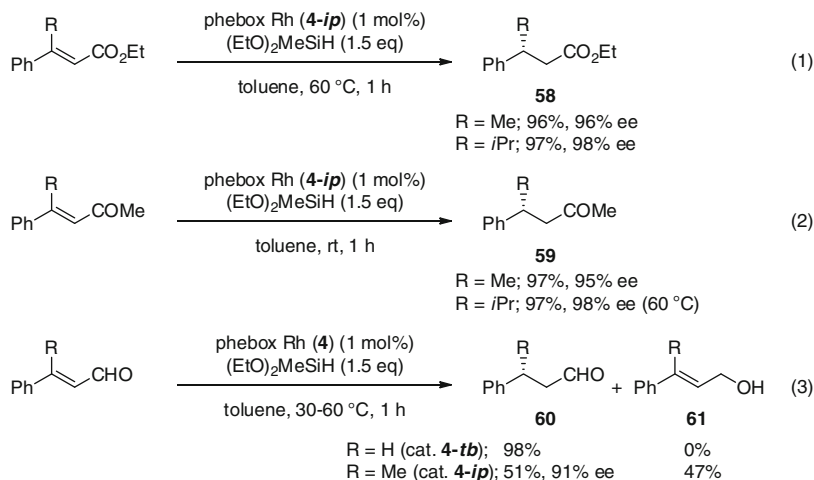
Scheme 20 Asymmetric Michael reaction



Scheme 21 Asymmetric hydrosilylation of alkenes

4.2 Hydrosilylation and Conjugate Reduction

The (phebox)Rh complex acts as an efficient catalyst for activation of hydrosilanes. Asymmetric hydrosilylation of aromatic alkenes proceeded in the presence of the (phebox)RhCl₂(H₂O) complex **1** (Scheme 21) [56]. Although diastereoselectivity between the α - and β -positions was moderate, high enantioselectivity of α -silylated compound **56** was obtained. The proposed mechanism was suggested to be the conventional Chalk–Harrod mechanism. This (phebox)Rh catalytic system can also be applied to the conjugate reduction of α,β -unsaturated carbonyl compounds



Scheme 22 Asymmetric conjugate reduction of α,β -unsaturated carbonyl compounds

(Scheme 22). In this reaction, the acetate complexes, (phebox)Rh(OAc)₂(H₂O) (**4**), were found to be efficient catalysts. The conjugate reduction of α,β -unsaturated esters in the presence of **4** and hydrosilane (EtO)₂MeSiH proceeded smoothly at 30–60 °C for 1 h to give dihydrocinnamate derivatives **58** in high yields with excellent enantiomeric excesses [Scheme 22 (1)] [28, 57]. β,β -Alkyl substituted α,β -unsaturated esters were also reduced by the (phebox)Rh complex **4** and hydrosilane in high yield with high ee. Similarly, complex **4** effectively catalyzed conjugate reduction of α,β -unsaturated ketones [Scheme 22 (2)]. Use of alkoxyhydrosilanes, such as (EtO)₂MeSiH, showed excellent 1,4-selectivity, while use of other hydrosilanes, such as Et₂MeSiH, Me₂PhSiH, and Ph₂SiH₂, caused side reactions such as the 1,2-reduction of the carbonyl group to give an allylic alcohol.

The conjugate reduction of α,β -unsaturated aldehydes has an inherent problem in selectivity between 1,2- and 1,4-reduction. When complex **4-*tb*** was subjected to the conjugate reduction of cinnamaldehyde, 1,4-reduction proceeded exclusively to afford dihydrocinnamaldehyde in 98 % yield [Scheme 22 (3)] [58]. The formation of cinnamyl alcohol arising from 1,2-reduction was not detected. In this reaction, selectivity between 1,2- and 1,4-reduction was significantly influenced by the substituents on the oxazoline rings and the hydrosilanes. Furthermore, asymmetric reaction was investigated. Complex **4-*ip*** was used in the asymmetric conjugate reduction of (*E*)- β -methylcinnamaldehyde to give the desired product with 91 % ee. However, there is still room for improvement of the selectivity in 1,4-reductions.

4.3 Reductive Aldol Reactions

As described earlier, the (phebox)Rh acetate complex **4** acts as a highly efficient catalyst for asymmetric conjugate reduction of β,β -disubstituted α,β -unsaturated

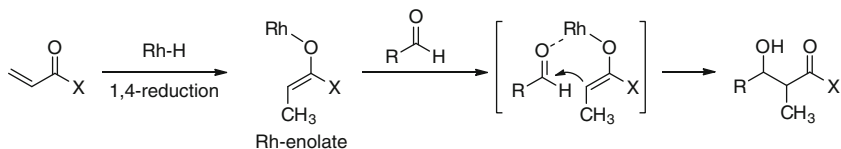
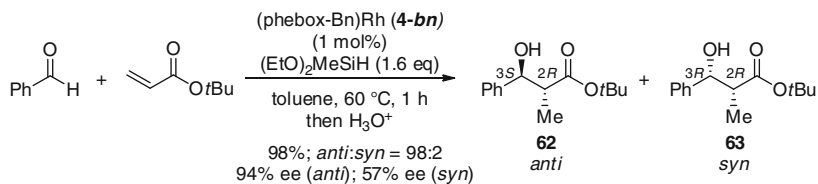
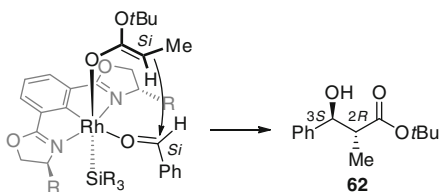
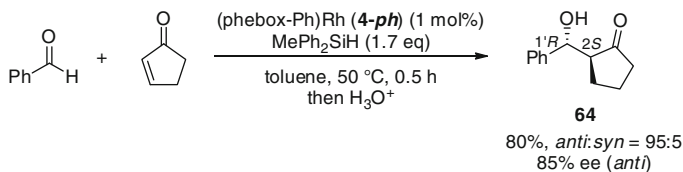
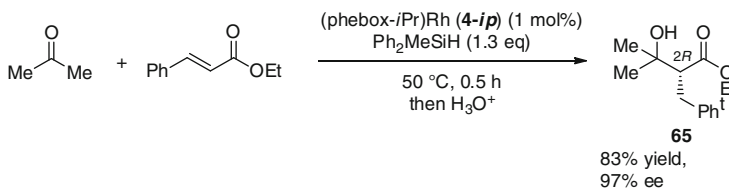
carbonyl compounds with hydrosilane as a reducing agent, giving a variety of optically active carbonyl compounds containing a chiral center at the β -position [28, 57, 58]. These results implied that the Rh enolate species formed via 1,4-reduction with a Rh-H species was a key intermediate (Scheme 23) [59]. Consequently, trapping the Rh-enolate by an electrophile, such as an aldehyde or ketone, could lead to a reductive aldol type coupling reaction.

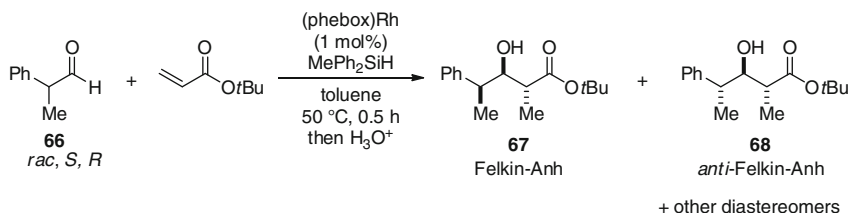
The catalytic reductive aldol coupling of benzaldehyde and *tert*-butyl acrylate with hydrosilane was successfully catalyzed by **4-bn** (1 mol%) to furnish the *anti*-coupling product **62** in high yield with high ee (Scheme 24) [60]. Both alkoxyhydrosilanes and alkylhydrosilanes appeared to be suitable hydride sources. Aromatic and aliphatic aldehydes could be used as electrophiles. Construction of the 2*R*,3*S*-absolute configuration of **62** was explained by the chair-like Zimmerman–Traxler-type transition state (Scheme 25). The attack of the *E*-enolate to the *si*-face of the coordinated aldehyde predominantly afforded the major product **62**. This proposed transition state was supported by density functional theory calculations (B3LPY) conducted by Wu and co-workers [61].

The complex **4-ph** also catalyzed the coupling reaction of cyclopent-2-enone and benzaldehyde with hydrosilane to give the corresponding *anti*- β -hydroxyketone **64** with high ee (Scheme 26) [62]. Reductive aldol reaction of α,β -unsaturated esters with ketones as acceptors gave ester derivatives bearing β -tertiary alcohols. Furthermore, complex **4-ip** was used in the coupling reaction of ethyl cinnamate and acetone with MePh₂SiH to yield the aldol product **65** in 83 % yield with 97 % ee (Scheme 27) [63]. Such reductive aldol reactions offer a convenient way to construct α,β,γ -stereotriads (Scheme 28) [64]. The coupling reactions of (*S*)-2-phenylpropanal (**S**-**66**) with *tert*-butyl acrylate in the presence of the achiral (phebox)Rh acetate complex **37** predominantly afforded the Felkin–Anh product **67** with (2*R*,3*R*,4*S*)-configuration accompanied by the *anti*-Felkin–Anh product **68** as a minor diastereomer. The use of the chiral (*S,S*)-(phebox-*i*Pr)Rh complex **4-ip** for the reaction with (*S*)-2-phenylpropanal (**S**-**66**) furnished the Felkin–Anh product **67** with high ee and dr, whereas the reaction of (*R*)-2-phenylpropanal (**R**-**66**) afforded the *anti*-Felkin–Anh product **68'** (enantiomer) as the major diastereomer with moderate enantioselectivity. These results indicated that a combination of (*S*)-2-phenylpropanal (**S**-**66**) with **4-ip** was a matched pair. α,β -Stereochemistry in the aldol product was constructed by the catalyst-controlled reaction via a transition state similar to that described in Scheme 25.

4.4 Direct Aldol Reactions

The (phebox)Rh complex serves as an acid–base bifunctional catalyst, in which the Rh center acts as a Lewis acid site and the acetate ligand acts as a Brønsted basic site. This synergistic interaction might promote a direct asymmetric aldol reaction [65]. Indeed, the acetate complex **4-ip** catalyzed the direct asymmetric aldol reaction of cyclic and acyclic ketones with benzaldehyde derivatives, giving *anti*- β -hydroxyketone derivatives **69–70** (Scheme 29) [66]. In this catalytic system,

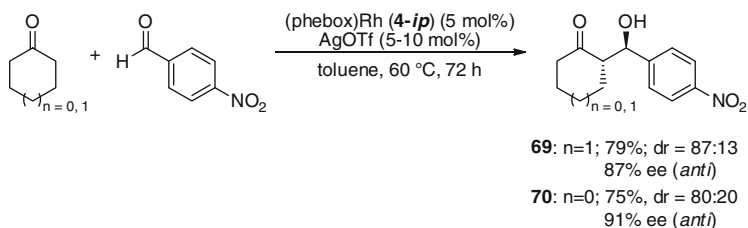
**Scheme 23** Reductive aldol reaction**Scheme 24** Asymmetric reductive aldol reaction of aldehydes**Scheme 25** Proposed mechanism**Scheme 26** Asymmetric reductive aldol reaction of aldehydes**Scheme 27** Asymmetric reductive aldol reaction of ketones



Cat.	Aldehyde (66)	Yield (%)	dr	ee (%)
achiral (37)	<i>S</i> (92% ee)	84	68 ^a :20 ^b :10:2	93 (2 <i>R</i> ,3 <i>R</i> ,4 <i>S</i>) ^a
<i>S,S</i> (4-<i>ip</i>)	<i>rac</i>	70	55 ^a :35 ^b : 8:2	76 (2 <i>R</i> ,3 <i>R</i> ,4 <i>S</i>) ^a
<i>S,S</i> (4-<i>ip</i>)	<i>S</i> (92% ee)	83	88 ^a : 4 ^b : 7:1	99 (2 <i>R</i> ,3 <i>R</i> ,4 <i>S</i>) ^a
<i>S,S</i> (4-<i>ip</i>)	<i>R</i> (95% ee)	75	20 ^a :65 ^b :14:1	71 (2 <i>R</i> ,3 <i>R</i> ,4 <i>R</i>) ^b

^a Felkin-Anh product **67**, ^b *anti*-Felkin-Anh product **68**

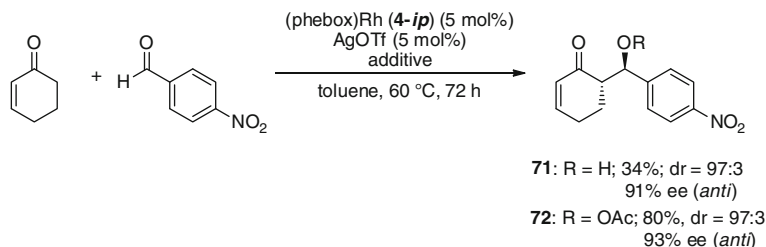
Scheme 28 Asymmetric reductive aldol reactions for construction of α,β,γ -stereotriads



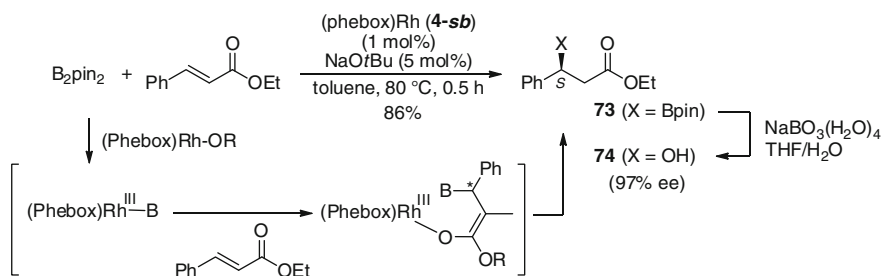
Scheme 29 Asymmetric direct aldol reaction of ketones

addition of AgOTf significantly improved both diastereoselectivity and enantioselectivity.

Direct aldol reactions with enone derivatives in place of ketones provide vinylogous unsaturated aldol products, which are useful components for organic synthesis. The acetate complex **4-*ip*** was used in the aldol reaction of 2-cyclohexenone with *p*-nitrobenzaldehyde, giving the coupling product **71** (Scheme 30) [67]. Addition of AgOTf was required for achievement of high diastereo- and enantioselectivity. However, the product yield was not sufficient, likely due to a competing retro-aldol reaction. To solve this problem, in situ trapping of the aldol product by addition of acetic anhydride was conducted. Gratifyingly, this reaction proceeded to furnish the acetylated product **72** in 80 % yield without loss of ee and dr. It is noted that the reaction of **71** with Ac₂O in the presence of **4-*ip*** and AgOTf gave only 10 % of the acetylated compound **72** and 90 % of recovered **71**. This control experiment indicated that most of the acetylation proceeded via the in situ formed Rh-aldolate species.



Scheme 30 Asymmetric direct aldol reaction of enones



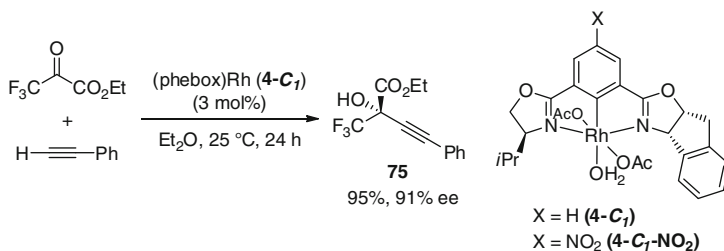
Scheme 31 Asymmetric β -borylation of cinnamate with diboron

4.5 β -Borylation

The (phebox)Rh complex **4-sb** appears to be an active catalyst for asymmetric β -borylation of cinnamate derivatives with bis(pinacolato)diboron (B_2pin_2) to give the β -borylated product **73** in 86 % yield (Scheme 31) [68]. The reaction of α,β -unsaturated ketone and amide derivatives also furnished the β -borylated ketones and amides in 70–84 % yields with 56–97 % ee. In the hypothetical catalytic cycle, a boryl-Rh(III) species, which was generated by σ -bond metathesis with a B–B bond, was proposed to be a key intermediate for the 1,4-addition of cinnamate.

4.6 Alkynylation

Asymmetric alkynylation of carbonyl compounds with terminal alkynes can provide chiral propargylic alcohols that are useful for materials science or pharmaceutical chemistry. Recently, Ohshima and Mashima developed C_1 -symmetric (phebox)Rh complexes **4-C₁** containing an indanyl substituent on the oxazoline ring. This complex served as a highly efficient catalyst for asymmetric direct alkynylation of a CF_3 -substituted α -ketoester with aromatic and aliphatic alkynes (Scheme 32) [69]. The catalytic reaction proceeded in the presence of 3 mol% of **4-C₁** at room temperature without any extra bases or additives. The desired propargylic alcohol **75** was obtained in high yield with high enantiomeric excess.



Scheme 32 Asymmetric alkylation of ketones

In this catalytic reaction, both aromatic and aliphatic alkynes could be used. In particular, the nitro-substituted C_1 -symmetric Rh complex **4-C₁-NO₂** showed high performance in the alkylation with aliphatic alkynes.

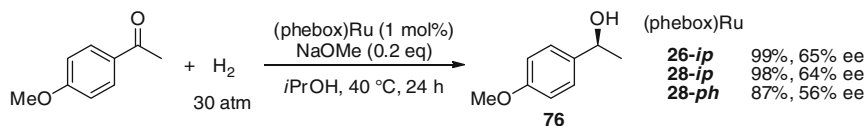
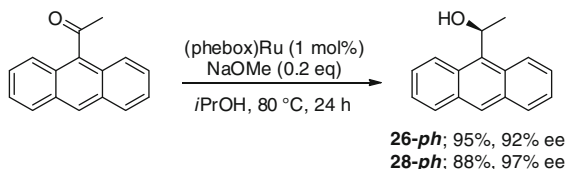
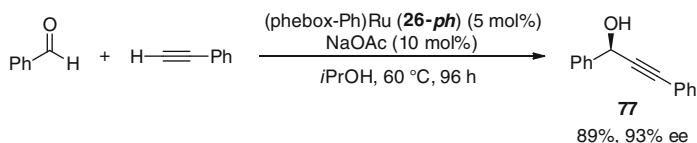
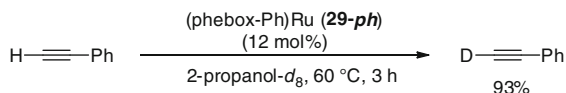
5 Asymmetric Reactions with (Phebox)Ru Complexes

5.1 Hydrogenation and Transfer Hydrogenation

The (phebox)Ru complexes **26** and **28** were found to exhibit catalytic activity in the asymmetric hydrogenation of simple aromatic ketones in the presence of bases such as NaOMe and KO^tBu (Scheme 33) [40, 41]. While hydrogenation of acetophenone derivatives showed moderate enantioselectivity (56–65 % ee), higher enantioselectivity was observed with bulky ketones, such as 2- and 9-anthracenylmethyl ketones (up to 98 % ee). Transfer hydrogenation of ketones was also catalyzed by the (phebox)Ru complexes **26** and **28** in the presence of NaOMe at 80 °C to give the *S*-alcohols (Scheme 34). High enantioselectivity was obtained with bulky ketones. The formation of the (*S*)-alcohol in both transfer hydrogenation and hydrogenation implied that these catalytic reactions involved a similar transition state with a prochiral face determination.

5.2 Alkynylation

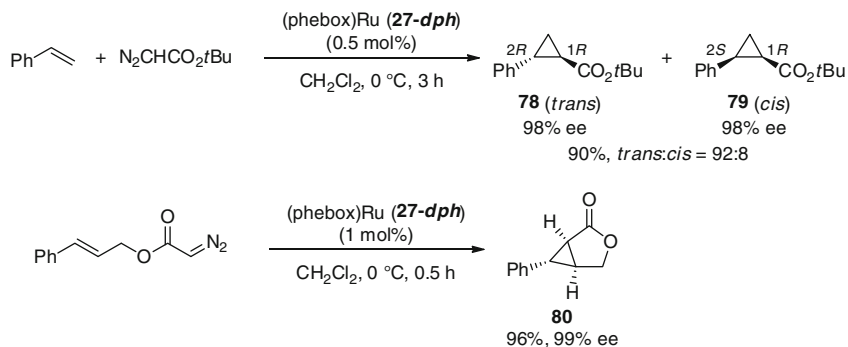
The (phebox)Ru complex functions as a catalyst for the direct alkynylation of aromatic and aliphatic aldehydes using terminal alkynes (Scheme 35) [43]. The catalytic reaction of benzaldehyde with phenylacetylene proceeded in the presence of **26-ph** and NaOAc to give the corresponding propargylic alcohol **77** with high enantiomeric excess. In addition, the acetate complex **29-ph** did not require any extra bases, such as NaOAc, giving **77** without loss of yield and enantioselectivity. It was found that **29-ph** catalyzed the H/D exchange reaction between the terminal acetylene proton and 2-propanol-*d*₈ to give the deuterated phenylacetylene in 93 %

**Scheme 33** Asymmetric hydrogenation of ketones**Scheme 34** Asymmetric transfer hydrogenation of ketones**Scheme 35** Asymmetric alkynylation of aldehydes with phenylacetylene**Scheme 36** H/D exchange reaction of phenylacetylene

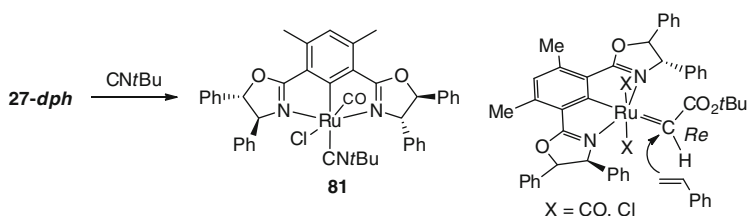
yield (Scheme 36). This result implied the formation of an acetylide intermediate by the reaction of **29-*ph*** with phenylacetylene.

5.3 Cyclopropanation

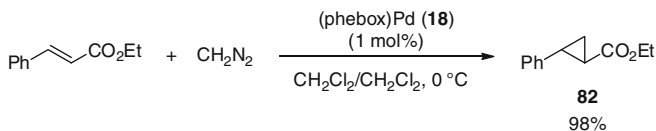
The (phebox)Ru complex effectively catalyzed asymmetric cyclopropanation (Scheme 37) [42]. In the presence of the [(4*S*,5*S*)-diphenyl-phebox]Ru aqua complex **27-*dph*** (0.5 mol%), cyclopropanation of styrene with *tert*-butyl diazoacetate gave the corresponding cyclopropane **78** in 90 % yield with 92 % *trans*-selectivity and 98 % ee. Intramolecular cyclopropanation also proceeded at 0 °C in the presence of **27-*dph*** (1 mol%) to furnish the bicyclic compound **80** in high yield with 99 % ee. The reaction of **27-*dph*** with *tert*-butylisocyanide afforded an isocyanide complex **81** via ligand exchange with H₂O (Scheme 38). This result implied that the *trans*-position of the phebox ligand was the reaction site that



Scheme 37 Asymmetric cyclopropanation with diazoesters



Scheme 38 Reaction of the (phebox)Ru complex with isocyanide and a proposed mechanism

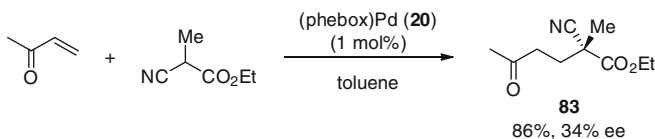
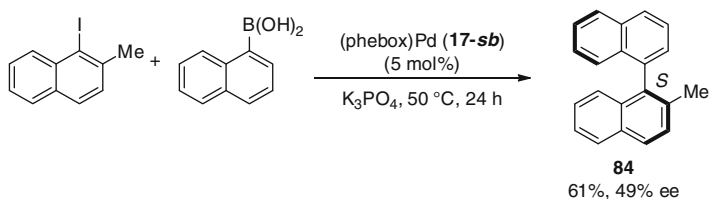
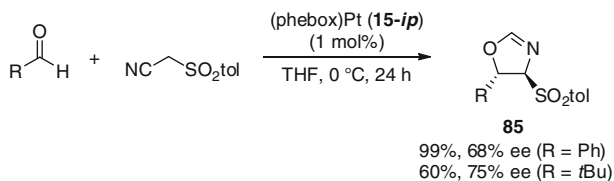


Scheme 39 Cyclopropanation

accepted the carbene ligand. Subsequent direct attack of the alkene to the carbene produced the cyclopropane with the observed absolute configuration.

6 Catalytic Reactions with Group 10 Metal Complexes

In 1997, Denmark reported cyclopropanation of ethyl cinnamate with diazomethane catalyzed by the (phebox)Pd complex **18** [21]. Although the catalytic cyclopropanation proceeded smoothly to give the corresponding cyclopropanone **82** in high yield, a racemic product was unfortunately obtained (Scheme 39). Around the same time, Richards reported that the cationic (phebox)Pd complex **20** acted as a Lewis acid catalyst for both the Diels–Alder reaction between cyclopentadiene and methacrolein and the aldol reaction between α -cyanoacetate and benzaldehyde [22]. Furthermore, complex **20** was used in the asymmetric

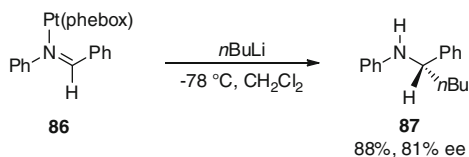
**Scheme 40** Asymmetric Michael reaction**Scheme 41** Asymmetric Suzuki–Miyaura cross-coupling**Scheme 42** Asymmetric aldol reaction

Michael addition of α -cyanopropionates to methylvinylketone to give **83** (Scheme 40) [70]. Iwasa reported that the (phebox)Pd complex **18** was an efficient catalyst for Suzuki–Miyaura cross-coupling between aryl boronic acids and aryl halides [71]. Asymmetric cross-coupling of 1-naphthoboronic acid and 2-alkyl or methoxy-1-iodonaphthalene also proceeded in the presence of (phebox)Pd (**18-sb**) to give the corresponding binaphthyl derivative **84** with moderate enantiomeric excess (Scheme 41).

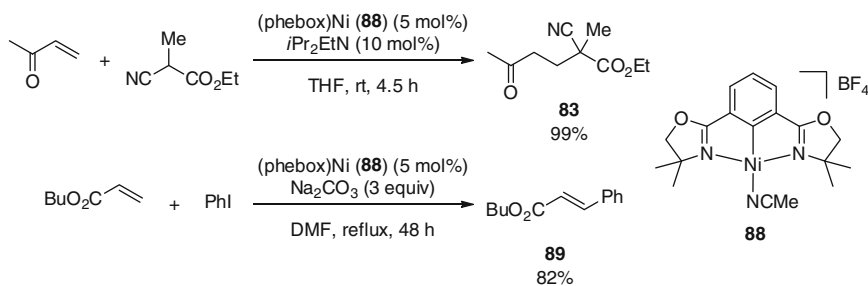
The cationic (phebox)Pt complex **15-ip** was used in the asymmetric aldol reaction of tosylmethyl isocyanide with aromatic and aliphatic aldehydes (Scheme 42) [35]. The catalytic reaction proceeded smoothly to give the corresponding oxazoline **85** in high yield with high *trans*-selectivity (99 %) and moderate ee (up to 75 % ee). This catalytic activity of **15** was in contrast with that of the (phebox)Rh complex, which produced the carbene complex.

The (phebox)Pt complex **15** also reacted with imines to give the imine complex **86** (Scheme 43) [33]. This imine complex **86** underwent stoichiometric alkylation by methyl and butyl lithium at -78°C to produce the corresponding amine **87** with 81 % ee.

Mitsudo and Tanaka synthesized a cationic [(phebox)Ni(NCMe)](BF₄) complex **88**, which was obtained by the reaction of the (phebox)Ni complex **24** with silver



Scheme 43 Asymmetric alkylation of imines



Scheme 44 Reactions with (phebox)Ni catalyst

salt in acetonitrile. The resulting Ni complex **88** catalyzed the Michael addition of α -cyanoacetate to methyl vinyl ketone in the presence of $i\text{Pr}_2\text{EtN}$ to give **83** in 99 % yield (Scheme 44) [72]. The complex **88** also catalyzed the Mizoroki–Heck reaction of acrylate with iodobenzene.

7 Conclusion

The phebox pincer skeleton can readily be introduced into a variety of metal atoms to form stable NCN-tridentate meridional frameworks having two chiral oxazoline rings, which confer desirable chiral environments around the metal centers. Chiral phebox Rh- and Ru-complexes exhibited high catalytic activity as multipotent catalysts to achieve high enantioselectivity for several types of asymmetric catalytic reactions. The phebox metal complex has the potential to advance the development of many organic transformations, such as C–C bond formation and functionalization reactions.

References

1. Albrecht M, van Koten G (2001) *Angew Chem Int Ed* 40:3750
2. van der Boom ME, Milstein D (2003) *Chem Rev* 103:1759
3. Morales-Morales D, Jensen CM (eds) (2007) *The chemistry of pincer compounds*. Elsevier, Oxford

4. Gorla F, Togni A, Venanzi LM (1994) *Organometallics* 13:1607
5. Longmire JM, Zhang X (1998) *Organometallics* 17:4374
6. Albrecht M, Kocks BM, Spek AL, van Koten G (2001) *J Organomet Chem* 624:271
7. Takenaka K, Miyakawa M, Uozumi Y (2005) *J Am Chem Soc* 127:12273
8. Yoon MS, Ramesh R, Kim J, Ryu D, Ahn KH (2006) *J Organomet Chem* 691:5927
9. Gosiewska S, Herreras SM, Lutz M, Spek AL, Havenith RWA, van Klink GPM, van Koten G, Gebbink RJMK (2008) *Organometallics* 27:2549
10. Wu L-Y, X-Q Ho, Xu Y-X, Jia M-Q, Wang Y-N, Gong J-F, Song M-P (2009) *Organometallics* 28:3369
11. Li J, Lutz M, Spek AL, van Klink GPM, van Koten G, Gebbink RJMK (2010) *Organometallics* 29:1379
12. Niu J-L, Chen Q-T, Hao X-Q, Zhao Q-X, Gong J-F, Song M-P (2010) *Organometallics* 29:2148
13. Baber RA, Bedford RB, Betham M, Blake ME, Coles SJ, Haddow MF, Hursthouse MB, Orpen AG, Pilarski LT, Pringle PG, Wingad RL (2006) *Chem Commun* 3880
14. Aydin J, Kumar KS, Sayah MJ, Wallner OA, Szabó KJ (2007) *J Org Chem* 72:4689
15. Aydin J, Conrad CS, Szabó KJ (2008) *Org Lett* 10:5175
16. Williams BS, Dani P, Lutz M, Spek AL, van Koten G (2001) *Helv Chim Acta* 84:3519
17. Morales-Morales D, Cramer RE, Jensen CM (2002) *J Organomet Chem* 654:44
18. Medici S, Gagliardo M, Williams SB, Chase PA, Gladiali S, Lutz M, Spek AL, van Klink GPM, van Koten G (2005) *Helv Chim Acta* 88:694
19. Feng J-J, Chen X-F, Shi M, Duan W-L (2010) *J Am Chem Soc* 132:5562
20. Motoyama Y, Makihara N, Mikami Y, Aoki K, Nishiyama H (1997) *Chem Lett* 951
21. Denmark SE, Stavenger RA, Faucher A-M, Edwards JP (1997) *J Org Chem* 62:3375
22. Stark MA, Richards CJ (1997) *Tetrahedron Lett* 38:5881
23. Desimoni G, Faita G, Quadrelli P (2003) *Chem Rev* 103:3119
24. Nishiyama H, Ito J (2010) *Chem Commun* 46:203
25. Nishiyama H (2007) *Chem Soc Rev* 36:1133
26. Motoyama Y, Okano M, Narusawa H, Makihara N, Aoki K, Nishiyama H (2001) *Organometallics* 20:1580
27. Motoyama Y, Narusawa H, Nishiyama H (1999) *Chem Commun* 131
28. Kanazawa Y, Tsuchiya Y, Kobayashi K, Shiomi T, Ito J, Kikuchi M, Yamamoto Y, Nishiyama H (2006) *Chem Eur J* 12:63
29. Motoyama Y, Koga Y, Nishiyama H (2001) *Tetrahedron* 57:853
30. Ito J, Shiomi T, Nishiyama H (2006) *Adv Synth Catal* 348:1235
31. Weissberg A, Portnoy M (2003) *Chem Commun* 1538
32. Gerisch M, Krumper JR, Bergman RG, Tilley TD (2003) *Organometallics* 22:47
33. Motoyama Y, Mikami Y, Kawakami H, Aoki K, Nishiyama H (1999) *Organometallics* 18:3584
34. Fossey JS, Richards CJ (2004) *Organometallics* 23:367
35. Motoyama Y, Kawakami H, Shimozono K, Aoki K, Nishiyama H (2002) *Organometallics* 21:3408
36. Kimura T, Uozumi Y (2008) *Organometallics* 27:5159
37. Fossey JS, Richards CJ (2004) *J Organomet Chem* 689:3056
38. Stol M, Snelders DJM, Godbole MD, Havenith RWA, Haddleton D, Clarkson G, Lutz M, Spek AL, van Klink GPM, van Koten G (2007) *Organometallics* 26:3985
39. Bugarin A, Connel BT (2008) *Organometallics* 27:4357
40. Ito J, Ujiie S, Nishiyama H (2009) *Organometallics* 28:630
41. Ito J, Ujiie S, Nishiyama H (2008) *Chem Commun* 1923
42. Ito J, Ujiie S, Nishiyama H (2010) *Chem Eur J* 16:4986
43. Ito J, Asai R, Nishiyama H (2010) *Org Lett* 12:3860
44. Hosokawa S, Ito J, Nishiyama H (2010) *Organometallics* 29:5773

45. Stol M, Snelders DJM, Kooijman H, Spek AL, van Klink GPM, van Koten G (2007) *Dalton Trans* 2589
46. Chuchuryukin AV, Huang R, Lutz M, Chadwick JC, Spek AL, van Koten G (2011) *Organometallics* 30:2819
47. Stol M, Snelders DJM, de Pater JJM, van Klink GPM, Kooijman H, Spek AL, van Koten G (2005) *Organometallics* 24:743
48. Ito J, Nishiyama H (2007) *Eur J Inorg Chem* 1114
49. Ito J, Miyakawa T, Nishiyama H (2008) *Organometallics* 27:3312
50. Ito J, Miyakawa T, Nishiyama H (2006) *Organometallics* 25:5216
51. Ito J, Kitase M, Nishiyama H (2007) *Organometallics* 26:6412
52. Motoyama Y, Shimozono K, Aoki K, Nishiyama H (2002) *Organometallics* 21:1684
53. Inoue H, Ito J, Kikuchi M, Nishiyama H (2008) *Chem Asian J* 3:1284
54. Motoyama Y, Nishiyama H (2003) *Synlett* 1883
55. Motoyama Y, Koga Y, Kobayashi K, Aoki K, Nishiyama H (2002) *Chem Eur J* 8:2968
56. Tsuchiya Y, Uchimura H, Kobayashi K, Nishiyama H (2004) *Synlett* 2099
57. Tsuchiya Y, Kanazawa Y, Shiomi T, Kobayashi K, Nishiyama H (2004) *Synlett* 2493
58. Kanazawa Y, Nishiyama H (2006) *Synlett* 3343
59. Nishiyama H, Shiomi T (2007) *Top Curr Chem* 279:105
60. Nishiyama H, Shiomi T, Tsuchiya Y, Matsuda I (2005) *J Am Chem Soc* 127:6972
61. Yang Y-F, Shi T, Zhang X-H, Tang Z-X, Wen Z-Y, Quan J-M, Wu Y-D (2011) *Org Biomol Chem* 9:5845
62. Shiomi T, Adachi T, Ito J, Nishiyama H (2009) *Org Lett* 11:1011
63. Shiomi T, Nishiyama H (2007) *Org Lett* 9:1651
64. Hashimoto T, Ito J, Nishiyama H (2008) *Tetrahedron* 64:9408
65. Trost BM, Brindle CS (2010) *Chem Soc Rev* 39:1600
66. Inoue H, Kikuchi M, Ito J, Nishiyama H (2008) *Tetrahedron* 64:493
67. Mizuno M, Inoue H, Naito T, Zhou L, Nishiyama H (2009) *Chem Eur J* 15:8985
68. Shiomi T, Adachi T, Toribatake K, Zhou L, Nishiyama H (2009) *Chem Commun* 5987
69. Ohshima T, Kawabata T, Takeuchi Y, Kakinuma T, Iwasaki T, Yonezawa T, Murakami H, Nishiyama H, Mashima K (2011) *Angew Chem Int Ed* 50:6296
70. Stark MA, Jones G, Richards CJ (2000) *Organometallics* 19:1282
71. Takemoto T, Iwasa S, Hamada H, Shibatomi K, Kameyama M, Motoyama Y, Nishiyama H (2007) *Tetrahedron Lett* 48:3397
72. Mitsudo K, Imura T, Yamaguchi T, Tanaka H (2008) *Tetrahedron Lett* 49:7287

Pincer Complexes as Catalysts for Amine Borane Dehydrogenation

Anthony St. John, Karen I. Goldberg, and D. Michael Heinekey

Abstract Amine boranes have received attention as attractive materials for the chemical storage of hydrogen. Thermal dehydrogenation of these materials is possible, but catalyzed dehydrogenation would allow for greater control of the rate and extent of H₂ release. Recent work has shown that metal complexes bearing pincer ligands are competent catalysts for amine borane dehydrogenation.

Keywords Amine borane • Dehydrogenation • Hydrogen storage • Pincer complex

Contents

1	Introduction	272
2	Dehydrogenation Studies with (POCOP)Ir(H) ₂	274
2.1	Dehydrogenation of AB	274
2.2	Mechanistic Studies of the Dehydrogenation of AB with 1	276
2.3	Dehydrogenation of MeAB	276
3	Ammonia Borane Dehydrogenation Catalysts Bearing Bifunctional Ligands	278
3.1	Dehydrogenation Studies with (P-N) ₂ RuCl ₂	278
3.2	Mechanistic Studies	280
3.3	Dehydrogenation Studies with (PNP)Ru(H)(PMe ₃)	280
4	Nonplatinum Group Metal Catalysts	283
4.1	Cobalt Complexes Bearing Pincer Ligands	283
4.2	Nickel Carbene System	284
5	Conclusion and Future Outlook	285
	References	286

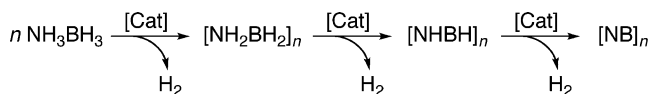
Abbreviations

$[\text{NH}_2\text{BH}_2]_5$	Pentamer
AB	Ammonia borane
BN	Boron–nitrogen
COD	Cyclooctadiene
DMAB	Dimethylamine borane
DOE	Department of Energy
ESI-MS	Electrospray ionization mass spectroscopy
GPC	Gel permeation chromatography
iPr PN	2-(diisopropylphosphino)ethylamine
IR	Infrared
KIE	Kinetic isotope effect
KO^tBu	Potassium <i>t</i> -butoxide
MAS	Magic angle spinning
MeAB	Methylamine borane
NH_2BH_2	Amino borane
NMR	Nuclear magnetic resonance
PGM	Platinum group metal
PNP^{H}	$\text{HN}(\text{CH}_2\text{CH}_2\text{P}^i\text{Pr}_2)_2$
POCOP	1,3-(OP^tBu_2) $_2\text{C}_6\text{H}_3$
PSiNSiP	$\text{N}(\text{SiMe}_2\text{CH}_2\text{PPh}_2)_2$
STP	Standard temperature and pressure
iBu PN	2-(ditertbutylphosphino)ethylamine
THF	Tetrahydrofuran
wt%	Weight percent
XRD	X-ray diffraction

1 Introduction

Renewable energy sources currently account for 18 % of global electricity production mainly from large hydroelectric installations [1]. The current energy climate has led to rapid growth in the other renewable sectors, mainly solar and wind. Available petroleum reserves are being rapidly consumed, which will require major changes to the current energy landscape during the next 50 years [2]. Due to global climate change concerns, development of a clean energy currency is an important goal.

Transmission of energy from new renewable sources has already proven to be a significant hurdle. Grid-connected wind farms and solar photovoltaic arrays generate electricity, but many such projects are currently on hold in places where the electrical grid cannot support the added input [3]. Storage of energy generated from renewable sources will help alleviate this problem. One promising energy carrier for these applications is hydrogen [4, 5]. Hydrogen has also been targeted by the



Scheme 1 Transition metal catalyzed dehydrogenation of AB

US Department of Energy (DOE) as a potential replacement for petroleum fuels in transportation [6].

Hydrogen has a high energy content per mass (120 MJ kg^{-1}), which is roughly three times that of petroleum. Unfortunately, at standard temperature and pressure (STP) the energy content per volume is very low (0.01 kJ L^{-1}). This means that alternative storage technologies are required for reasonable capacities to be reached.

For transportation applications, a variety of methods for on-board storage/release of hydrogen fuel have been investigated [7]. As of 2010, state-of-the-art fuel cell powered cars use high-pressure tanks to store hydrogen [8]. These cars emit only water, can be refueled in minutes, and have a viable range (*ca.* 500 km). Nevertheless, the space and weight requirements for the H_2 storage tank are considered to be excessive [6].

An alternative approach used in an early prototype vehicle was based on hydrolysis of NaBH_4 in alkaline aqueous solution [9]. The product from hydrolysis of NaBH_4 is NaBO_2 which must be regenerated off-board the vehicle in an energy-intensive process. Due to this and other drawbacks, development of this system for vehicles was discontinued. Another early prototype utilized a methanol fuel processor [10]. Methanol reformation has some advantages over hydrocarbon reformation; most notably significantly lower temperatures can be used. However, the challenge of meeting size and weight restrictions and long start-up times make these technologies impractical for use on-board vehicles [4]. To date, no satisfactory technology for hydrogen storage in large-scale mobile applications has been developed.

The concept of chemical hydrogen storage, wherein hydrogen is “stored” within other compounds and then released upon demand, is a particularly attractive strategy to meet the size and weight requirements for vehicular storage. Recent years have seen significant progress in this area with a number of potential systems investigated. Ammonia borane (AB) is the simplest and most studied boron and nitrogen (BN) containing chemical hydrogen storage material [11, 12]. AB contains a high weight percentage (wt%) of available hydrogen that could potentially be released as H_2 (19.6 %). Research over the past several years has shown that numerous late transition metal pincer complexes have remarkably high activity in catalyzing the dehydrogenation of AB to produce hydrogen and a variety of BN-containing products. Dehydrogenation of AB leads to products of the general form $[\text{NH}_2\text{BH}_2]_n$, $[\text{NHBH}]_n$, and $[\text{NB}]_n$ (Scheme 1).

Thermal decomposition of AB to release hydrogen was first reported in 1978 [13], and the first report of well-defined metal-catalyzed dehydrogenation appeared in 2001 [14]. In 2006 we reported the first efficient and well-characterized AB

dehydrogenation catalyst [15]. This system utilized the Ir pincer complex (POCOP) Ir(H)₂ (POCOP = [*κ*³-1,3-(OP^tBu)₂]₂C₆H₃) originally introduced by Brookhart for dehydrogenation of alkanes [16]. Since then there have been additional reports describing extremely rapid dehydrogenation of AB by Fagnou [17] and Schneider [18]. Notably, several of these catalysts employ platinum group metals (PGMs) bearing pincer ligands.

In recent years, significant attention has turned to the development of non-PGM catalysts for AB dehydrogenation [19]. For large-scale applications a hydrogen storage system must employ cheap, widely available materials. Therefore, a practical catalyst cannot be based on a PGM. To this end we have investigated pincer complexes of cobalt for application in amine borane dehydrogenation [20].

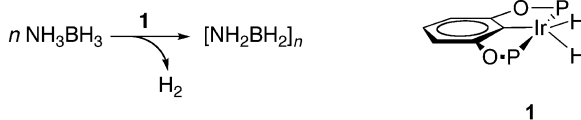
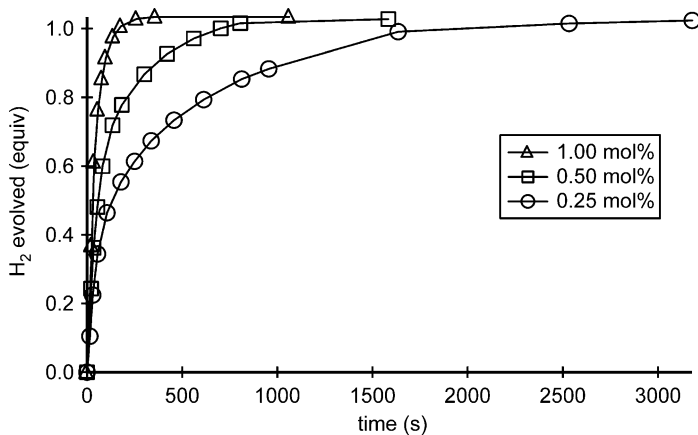
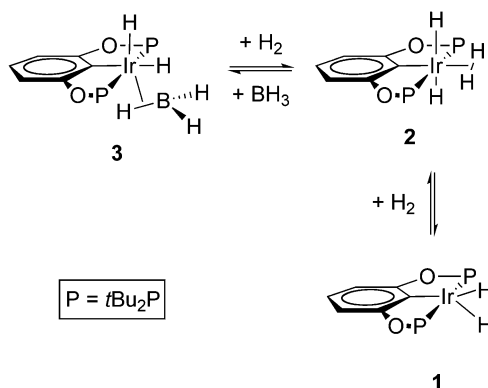
This chapter describes the current state of AB dehydrogenation catalyzed by various homogenous metal pincer complexes. Mechanistic studies of the dehydrogenation reactions and the resulting implications are discussed. Recently, two reviews summarizing the use of amine boranes [19], and more specifically of AB [21], for hydrogen storage have appeared.

2 Dehydrogenation Studies with (POCOP)Ir(H)₂

2.1 Dehydrogenation of AB

In 2003, the Manners group reported a rhodium-based catalyst for AB dehydrogenation [22, 23]. This system utilized a [Rh(1,5-cod)(μ-Cl)]₂ (cod = cyclooctadiene) precatalyst and effected the release of two equivalents of hydrogen from AB over 2–4 days at 45 °C (*ca.* 1 mol% catalyst loading). This was the most active known system until 2006 when the pincer-ligated iridium complex (POCOP)Ir(H)₂ (**1**, Scheme 2) was found to be a highly effective catalyst for AB dehydrogenation, promoting a rapid reaction at room temperature [15]. Using **1** as a catalyst (1.0 mol%), one equivalent of H₂ was released from AB in <5 min at room temperature (Fig. 1).

The BN-containing product of this reaction was insoluble in all common solvents and was characterized by infrared spectroscopy (IR) and X-ray powder diffraction (XRD). The data was consistent with formulation of this product as the same material previously reported and characterized by Shore and coworkers as the cyclic pentamer [NH₂BH₂]₅ [24]. The rate of the reaction was measured as a function of catalyst loading and a first-order dependence on [**1**] was observed. Monitoring the reaction by ¹H NMR spectroscopy revealed that the predominant iridium species in solution was the tetrahydride complex (**2**), later shown to be a dihydrogen/dihydride species [25]. Over long reaction times a catalytically inactive iridium species was formed. This species can be independently prepared from (POCOP)Ir(H)₂ by reaction with BH₃ and was later identified as a σ-borane complex (**3**) of iridium [26]. This dormant form of the catalyst can be pressurized with hydrogen to form the dihydrogen/dihydride complex **2**, which loses H₂ under vacuum to reform the active catalyst **1** (Scheme 3).

**Scheme 2** (POCOP)Ir(H)₂ catalyzed dehydrogenation of AB**Fig. 1** Dehydrogenation of AB with **1** (triangle = 1 mol% catalyst loading, square = 0.5 mol%, circle = 0.25 mol%)**Scheme 3** σ -borane complex **3** and regeneration pathway to active catalyst **1**

Alkane dehydrogenation reactions catalyzed by (POCOP)Ir(H)₂ are proposed to proceed via the 14 electron 3-coordinate species (POCOP)Ir [27]. This unsaturated intermediate is generated following hydrogenation of an alkene substrate (transfer dehydrogenation) or by reductive elimination of H₂ at high temperatures (thermal

dehydrogenation). Notably, in AB dehydrogenation there is neither an adequate hydrogen acceptor present nor sufficient thermal energy to generate the 3-coordinate species implicated in alkane dehydrogenation. Thus the mechanism by which (POCOP)Ir(H)₂ catalyzes the dehydrogenation of AB is necessarily different from that followed by the alkane dehydrogenation reactions.

2.2 Mechanistic Studies of the Dehydrogenation of AB with **1**

The mechanism of catalytic dehydrogenation of AB by **1** was studied computationally by Paul and Musgrave [28]. Two potential dehydrogenation pathways were analyzed. The first calculated mechanism used the 3-coordinate (POCOP^{Me})Ir as a model starting complex. Experimental results indicate that there is no viable route to the formation of this species from **1** under the reaction conditions: unfortunately this was not addressed by this computational study. The second proposed mechanism starts from the (POCOP^{Me})Ir(H)₂ complex and is highlighted by the concerted breaking of B–H and N–H bonds (Fig. 2).

In this mechanism one of the hydride ligands acts as a proton acceptor and the dehydrogenated product, NH₂BH₂, is released from the metal center. However, experimental observations are not consistent with this calculated mechanism. In a study by Pons *et al.*, trapping experiments with cyclohexene were performed using several known AB dehydrogenation catalysts including **1** [29]. Some important differences were noted among the catalysts studied. It was observed that catalysts that effected release of greater than one equivalent H₂ also released NH₂BH₂ into the bulk solution. This fragment could be trapped out by cyclohexene to form (C₁₂H₂₀BNH₂) (Scheme 4). In contrast, when catalysts were used that released only one equivalent of H₂ and formed the insoluble [NH₂BH₂]₅ species characterized as pentamer, no trapping of NH₂BH₂ by cyclohexene was observed. This suggests that NH₂BH₂ monomer is not released from the catalyst and that oligomerization to the pentamer form occurs in the coordination sphere of the metal. A viable mechanism consistent with experimental observations for the dehydrogenation of AB by **1** is still lacking.

2.3 Dehydrogenation of MeAB

Methylamine borane (CH₃NH₂BH₃, MeAB) is another BN-containing material that has received attention as a viable hydrogen-storage candidate [19]. MeAB has the potential to release two equivalents of hydrogen to yield up to 9.0 wt% H₂. When the (POCOP)Ir(H)₂ catalyst was applied to MeAB dehydrogenation, the reaction profile and extent of H₂ release (1 equiv.) was very similar to that observed for AB dehydrogenation [30]. In contrast to the AB reaction, the BN-containing products of MeAB dehydrogenation were soluble in tetrahydrofuran (THF). Despite the fact that the BN product of this dehydrogenation remained in solution, it was noted that

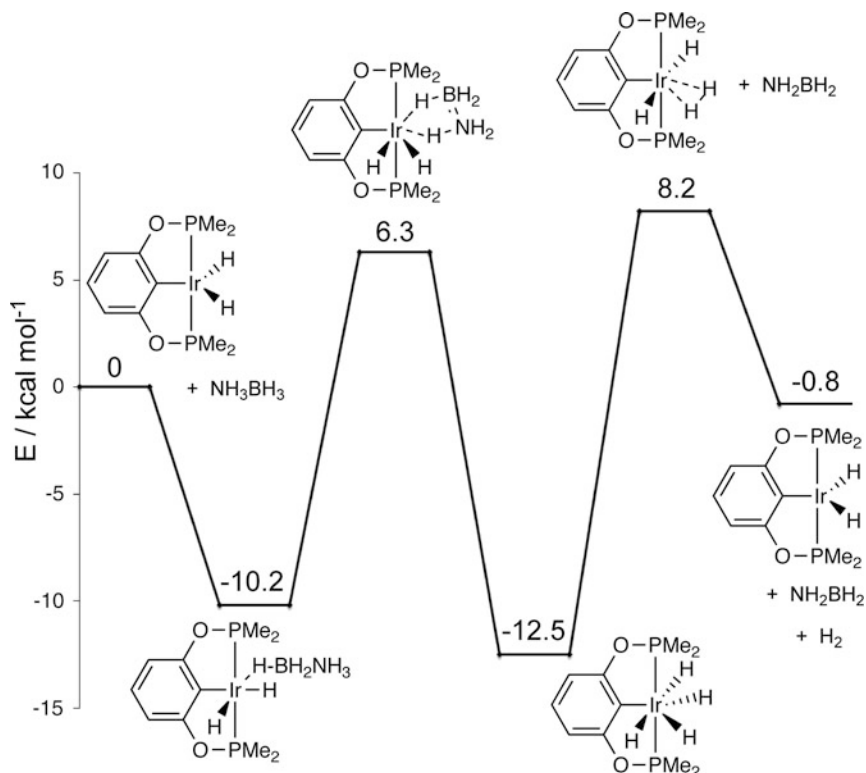
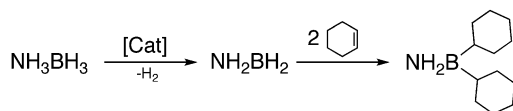


Fig. 2 Calculated energy diagram for dehydrogenation of AB from $(^{\text{Me}}\text{PCOP})\text{Ir}(\text{H})_2$



Scheme 4 Trapping of NH_2BH_2 with cyclohexene

extended reaction times and/or application of higher temperatures did not lead to further dehydrogenation activity. The BN products of this MeAB dehydrogenation reaction were analyzed using Electrospray Ionization Mass Spectrometry (ESI-MS) and found to be a mixture of cyclic and acyclic oligomers of the form $[\text{MeNHBH}_2]_n$ ($n = 2\text{--}20$ cyclic) and $[\text{MeNH}_2\text{BH}_2][\text{MeNHBH}_2]_n[\text{MeNH}_2]$ ($n = 4\text{--}48$ acyclic). Concurrent to this report, Manners and coworkers reported dehydrogenation of MeAB using the $(\text{POCOP})\text{Ir}(\text{H})_2$ catalyst, but with much higher concentrations of substrate [31]. Under these conditions it was found that polymers were formed (molecular weight of *ca.* 160,000 as determined by Gel Permeation Chromatography (GPC)). In a more recent report, Manners and coworkers extensively studied the products formed from dehydrogenation reactions of AB with **1** [32].

Dehydrogenation of both AB and MeAB with complex **1** as a catalyst was found to proceed at similar rates. This behavior was documented in individual experiments using either AB or MeAB as a substrate. Dehydrogenation of AB/MeAB mixtures with catalyst **1** was also studied [30]. Mixtures of AB/MeAB are intriguing because AB has a higher wt% hydrogen and the products of MeAB dehydrogenation are soluble. Reaction of a 1:1 mixture of AB/MeAB in THF with **1** resulted in the release of one equivalent of H₂ per BN bond. The THF soluble products of this reaction were formulated as co-oligomers of AB and MeAB. No solids or precipitates were observed. Other ratios of AB/MeAB were also studied, since higher loadings of AB would result in a higher wt% of hydrogen in the resulting system. As the AB:MeAB ratio was increased, however, insoluble products were observed. The increase in the solid products correlated with the increased proportion of AB. The IR spectrum of the insoluble product was consistent with the reported spectrum for pentamer formed from dehydrogenation of AB [24]. Integration of the ¹H NMR resonances of the reaction solution indicated that the soluble products were incorporating the BN fragments from AB and MeAB in approximately a 1:1 ratio despite the greater ratio of AB to MeAB in the initial solution.

Efficient catalysis of AB dehydrogenation allowed for the direct measurement of the enthalpy of the reaction. The reaction enthalpy (ΔH) for the dehydrogenation of AB was measured by differential scanning calorimetry and found to be -6.7 ± 0.6 kcal mol⁻¹. Similar ΔH values were found for dehydrogenation of MeAB and 1:1 AB/MeAB mixtures (-6.8 ± 0.6 and -6.7 ± 0.1 kcal mol⁻¹) [30]. These results indicate that direct regeneration of AB and MeAB dehydrogenation products with H₂ will not be feasible. When the negative entropic contribution to ΔG from release of H₂ is considered, it is clear that alternative methods of regenerating spent AB fuel will be needed if AB is to be used as a hydrogen storage material. Recently, a promising regeneration pathway was demonstrated wherein polyborazylene is converted back to AB in near quantitative yield [33].

3 Ammonia Borane Dehydrogenation Catalysts Bearing Bifunctional Ligands

3.1 Dehydrogenation Studies with (P-N)₂RuCl₂

Both the Fagnou and Schneider groups noted that AB is highly polarized and is more comparable to polar substrates such as alcohols than alkanes [17, 18]. In this respect, catalysts for the ionic hydrogenation/dehydrogenation of polar bonds (e.g. C=O and C–O) may be expected to be more effective for AB dehydrogenation than those used for olefin hydrogenation/alkane dehydrogenation. Noyori and others have developed highly effective ruthenium catalysts for the hydrogenation of polar double bonds [34, 35]. These bifunctional catalysts utilize a nitrogen site in the ligand backbone to transfer a proton to the ketone or aldehyde oxygen in the

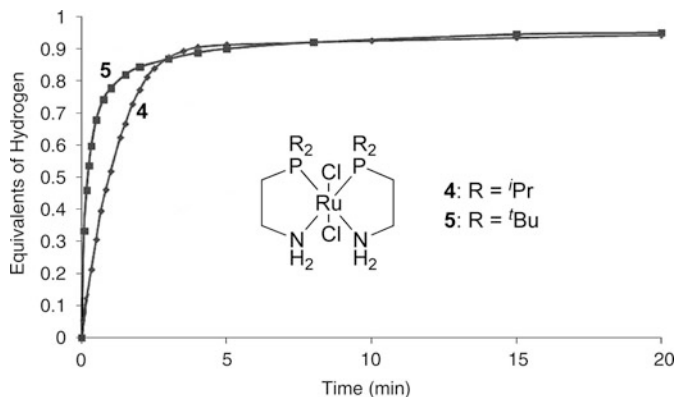


Fig. 3 Catalysts **4** and **5** and AB dehydrogenation with pre-catalysts **4** and **5** after activation with KO^{*t*}Bu

substrate [36]. A similar ionic pathway where the proton is removed from the nitrogen and a hydride is formally removed from boron was proposed to be potentially accessible for the dehydrogenation of AB based on the principle of microscopic reversibility [18].

A survey of known alcohol oxidation/reduction catalysts resulted in the discovery of several precatalysts [17]. The precatalysts were first activated by addition of KO^{*t*}Bu (3 mol% vs. 0.1 mol% precatalyst) in THF. Subsequent addition of AB to the activated catalysts resulted in the release of up to one equivalent of H₂ at an enhanced rate as compared to dehydrogenation with **1**. The best performing catalysts (**4** and **5**) effected the release of a full equivalent of H₂ within 5 min at only 0.1 mol% catalyst loading and at 25 °C (Fig. 3). The insoluble product of this reaction was identified by IR spectroscopy as the same material that was formed when **1** was used as the catalyst [15]. The catalyst lifetimes were not discussed.

Catalyst **4** was also applied to MeAB dehydrogenation reactions. Using a similar catalyst activation method as with AB dehydrogenation (KO^{*t*}Bu treatment), these reactions led to the immediate release of one equivalent of H₂. Release of the second equivalent of H₂ occurred at a much slower rate and gave a complex mixture of soluble products. It is notable that the rate of reaction of MeAB versus AB was dramatically different for these catalysts, with the first equivalent of hydrogen being released from MeAB significantly faster. This is in contrast to the observed rates for the (POCOP)Ir(H)₂ system [30], where the dehydrogenation of both AB and MeAB proceed at a similar rate.

As had been previously explored in the (POCOP)Ir(H)₂ system with the goal of increasing the gravimetric H₂ density of the system, mixed AB/MeAB systems were also examined with precatalyst **4**. Addition of 0.1 mol% catalyst **4** to a 1:1 mixture of AB/MeAB resulted in release of roughly 0.8 equivalents of hydrogen. Surprisingly, the rate of H₂ release is decreased compared to reactions with either AB or MeAB individually. The authors describe these results as preliminary and

suggest that the product is comprised of polymeric mixtures containing both dehydrogenated AB and MeAB fragments [17].

3.2 Mechanistic Studies

Although this ruthenium catalyst is not based on a pincer complex, important mechanistic information was obtained from these studies that is useful to understand metal-catalyzed AB dehydrogenation in general. The mechanism of AB dehydrogenation catalyzed by **4** was examined by DFT calculations using a model Ru complex (Fig. 4) [37]. It was found that binding of AB to the Ru-H species is energetically favorable by 9.5 kcal mol⁻¹. During this initial activation step the ligand acts as a proton acceptor. Notably, as shown in Fig. 5, this reaction mechanism suggests that NH₂BH₂ monomer is released from the metal center. No cyclohexene trapping experiments have been performed with this catalyst system, so experimental evidence of the release of free NH₂BH₂ is not available. Consistent with observations in previously studied systems, the formation of pentamer and the release of only one equivalent of H₂ suggest that NH₂BH₂ may not be released from the coordination sphere of the metal. A better understanding of the metal-ligand cooperativity in this nonpincer system can allow for further development of pincer systems capable of acting in a similar fashion.

3.3 Dehydrogenation Studies with (PNP)Ru(H)(PMe₃)

Concurrent to the report from Fagnou, Schneider and coworkers reported a similar bifunctional catalyst system [18]. They postulated that the Noyori-style catalysts utilized for hydrogenation of polar double bonds could be competent for AB dehydrogenation. Treatment of *trans*-[RuCl₂(PMe₃)(PNP^H)] (PNP^H = HN(CH₂CH₂PⁱPr₂)₂) (**6**) with excess KO^tBu affords complex **7**. Under pressure of H₂, **7** converts to the dihydride complex **8** which cannot be isolated in pure form due to facile loss of H₂ to form the hydride complex **9**, which can be isolated in 85 % overall yield (Scheme 5).

At 0.1 mol% catalyst loading and 25 °C, **9** effected the release of one equivalent of H₂ from a THF solution of AB within 4 min. The product was analyzed by powder diffraction, MAS-¹¹B NMR, and IR spectroscopy. The data suggested the formation of a polymeric product with general formula [NH₂BH₂]_n [18]. The IR and powder diffraction spectra of the insoluble BN product do not match that reported for pentamer [15]. Small amounts of borazine were also detected when monitoring the reaction via ¹¹B NMR. Borazine production accounts for the slight excess of H₂ over one equivalent observed at higher catalyst loadings.

Measurement of the kinetic isotope effects (KIE) using deuterated AB provided some insight into the mechanism of these reactions with catalyst **9**. Using 0.1 mol%

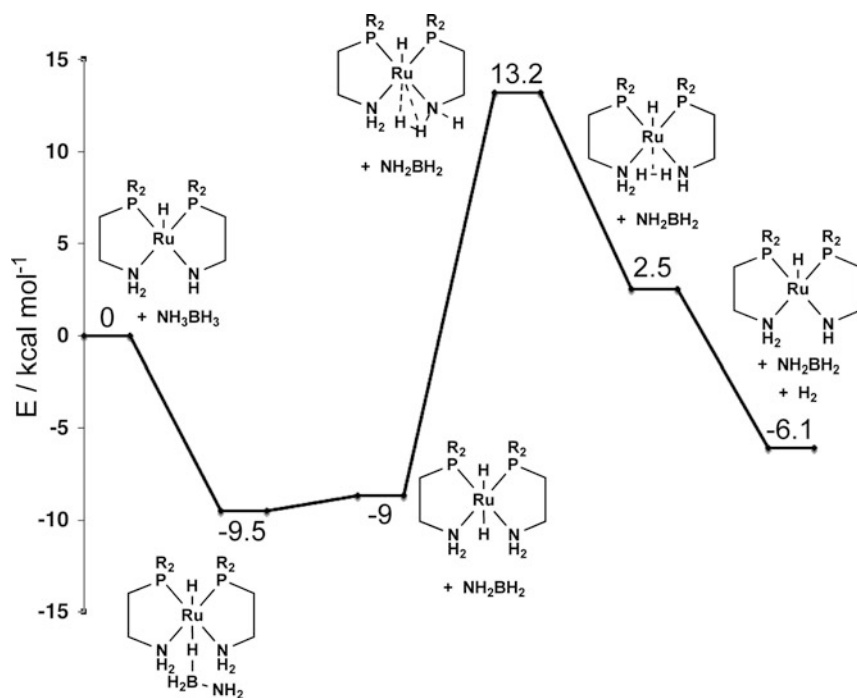


Fig. 4 Calculated reaction pathway for AB dehydrogenation from a model based on complex 4. Reported values are in kcal mol⁻¹

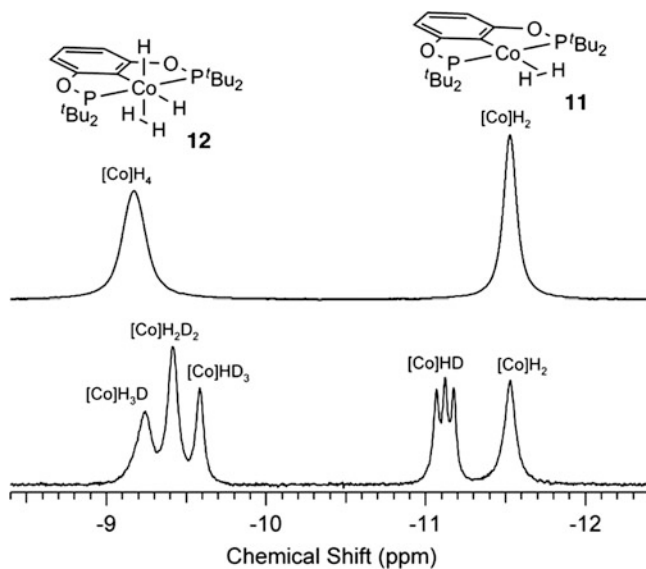
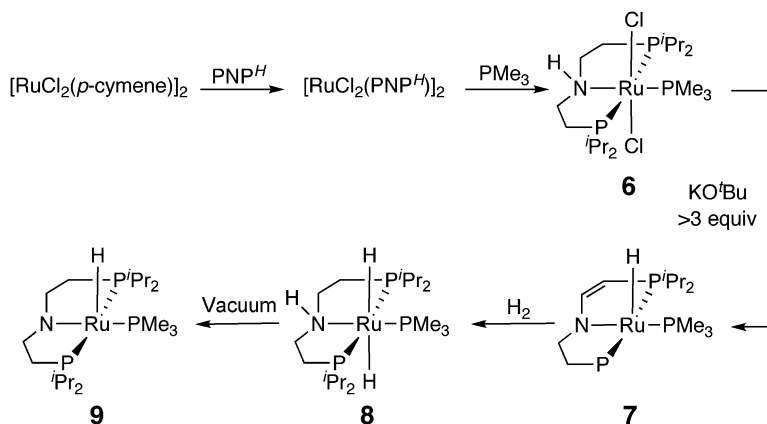


Fig. 5 Partial ¹H NMR spectrum depicting (POCOP)Co(H)_n complexes 11 and 12, n = 2, 4



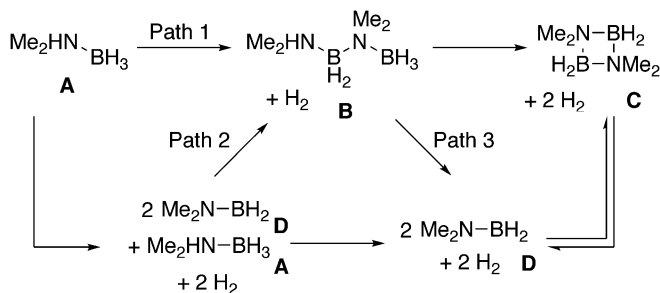
Scheme 5 Synthesis of amido complex **9** ($PNP^H = HN(CH_2CH_2P^iPr_2)_2$)

catalyst loadings, KIE values of 2.1 (D_3B-NH_3), 5.2 (H_3B-ND_3), and 8.1 (D_3B-ND_3) were found. These values are larger than other KIEs reported for AB dehydrogenation [38]. The KIE data are consistent with a concerted mechanism where both B–H and N–H bond cleavage occurs in the rate-determining step. Monitoring the reaction by ^{31}P NMR spectroscopy revealed that amino complex **8** is the predominant Ru-containing species in solution. However, loss of H_2 from complex **8** was observed to be too slow to be a kinetically competent intermediate in the catalytic cycle.

A later report by Schneider examined the dehydrocoupling of dimethylamine borane (Me_2NHBH_3 , DMAB) catalyzed by complex **9** [39]. Addition of **9** to a solution of DMAB results in rapid H_2 evolution. Monitoring the volume of evolved gas revealed two distinct catalytic regimes. At 2 mol% catalyst loading, **9** quickly dehydrogenates 70 % of the DMAB substrate before slowing, compared to complete conversion of AB at 0.1 mol% catalyst loading. Longer reaction times eventually lead to quantitative release of one equivalent H_2 .

Monitoring the dehydrogenation reaction of DMAB by ^{11}B NMR revealed nearly quantitative conversion to the cyclic dehydrogenation product **C** (Scheme 6). An intermediate BN coupled product with linear structure **B** was also observed. **B** was proposed to form via metal-mediated BN coupling (Path 1, Scheme 6). This is significant because one of the major unanswered mechanistic questions in AB dehydrogenation concerns BN coupling of dehydrogenated products.

These results show that for DMAB there is evidence for BN coupling occurring in the coordination sphere of the metal. This BN coupling is in competition with release of free **D** which then cyclizes to form **C**. The authors suggest that the observed linear BN coupling provides a mechanistic rationale for the formation of other linear amino borane oligomers [30, 40].



Scheme 6 Proposed mechanistic pathways for dehydrogenation of DMAB

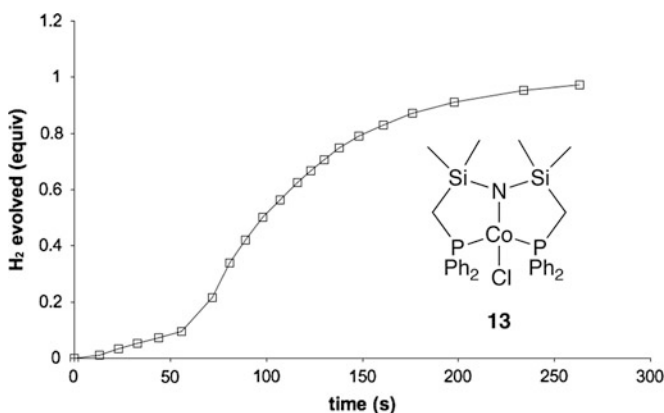


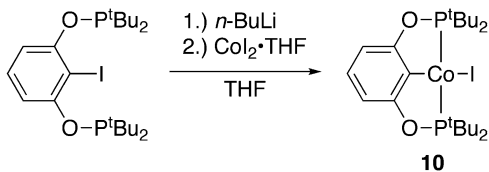
Fig. 6 Dehydrogenation of AB with (PSiNSiP)CoCl (2.0 mol%, 30 °C)

4 Nonplatinum Group Metal Catalysts

4.1 Cobalt Complexes Bearing Pincer Ligands

While the previously discussed catalysts display impressive AB dehydrogenation capabilities, the use of PGMs limits the practicality of wide-scale application in hydrogen storage systems. Moving forward from the success of the (POCOP)Ir(H)₂ system, an extension of the POCOP ligand motif to non-PGMs was attempted. In 2011, the synthesis and characterization of the first cobalt dihydrogen complex, (POCOP)Co(H)₂, was reported [20]. Synthesis of this complex was accomplished by first isolating the cobalt halide species (POCOP)CoI (**10**) via reaction between an iodinated POCOP proligand and CoI₂·THF (Scheme 7).

In order to generate the cobalt analog to the iridium system, the cobalt–halide complex was reduced with sodium amalgam. This reaction generated a highly reactive Hg-bridged species [20]. Reaction of this species with H₂ at low

Scheme 7 Synthesis of (POCOP)CoI (**10**)

temperatures resulted in formation of the desired cobalt dihydrogen complex (**11**). At increased pressures of H₂ a complex with four H atoms in the coordination sphere was formed, formulated as the dihydrogen/dihydride complex (**12**). Introduction of HD gas instead of H₂ resulted in the observation of new resonances attributed to isotopomers of **11** and **12** (Fig. 5).

Due to the instability of **11** at ambient temperatures, AB dehydrogenation reactions were not examined. However, a variety of (POCOP)CoX (X = Cl, I, N₂, H) complexes were studied as potential precatalysts. However, the activity of these complexes was limited and they were not pursued as AB dehydrogenation catalysts.

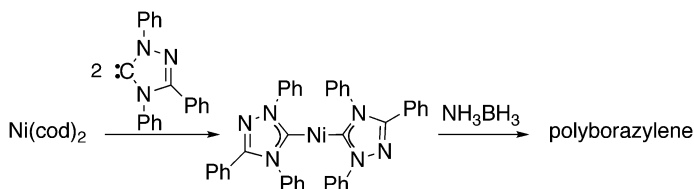
Cobalt complexes bearing PSiNSiP-type pincer ligands were also studied as precatalysts for AB dehydrogenation. The most promising complex was (PSiNSiP)CoCl (PSiNSiP = [N(SiMe₂CH₂PPh₂)₂] (**13**) [41]. Addition of a green THF solution of **13** (2.0 mol%, 30 °C) to a THF solution of AB resulted in a short induction period followed by a dramatic color change to brown and a second dehydrogenation regime during which one equivalent of H₂ is generated within 5 min (Fig. 6).

The length of the induction period was irreproducible and varied in time from ca. 45 to 120 s. An insoluble BN product resulted from this reaction and it was characterized by IR spectroscopy as the same [NH₂BH₂]₅ product [24] found in the dehydrogenation reactions with (POCOP)Ir(H)₂ and the Ru systems reported by Fagnou [15, 17]. The active catalyst was short-lived; addition of more AB to a spent reaction mixture resulted in continued activity but at a significantly decreased rate. Attempts to generate the active catalyst in situ by reduction with Mg⁰ resulted in formation of a new species; however, this material was not active for AB dehydrogenation. Monitoring the reaction by ¹H NMR spectroscopy revealed the formation of multiple metal and organic products.

The observed dehydrogenation activity with (PSiNSiP)CoCl is a promising lead for non-PGM catalyzed dehydrogenations of AB; however, additional studies are necessary to address the significant catalyst deactivation that was observed.

4.2 Nickel Carbene System

While the most active metal catalysts for AB dehydrogenation are pincer complexes, other reported complexes display promising reactivity. A nickel carbene-based system reported by Baker yields polyborazylene (Scheme 8) [38]. The extent of H₂ release in this system is the highest reported to date (>2.5 equiv.), although the rate of reaction is slow, requiring a reaction time of 150 min at 60 °C. The initial product of the reaction is borazine which is then cross-linked to form



Scheme 8 Dehydrogenation of AB catalyzed by a nickel carbene complex

polyborazylene. Mercury poisoning experiments did not affect the rate or extent of catalytic activity. The KIE data suggests a concerted mechanism for B–H and N–H bond cleavage in the rate-limiting step.

Discussion of the calculated reaction mechanism is outside of the scope of this chapter [42, 43]; however, a competition between release of free NH_2BH_2 and metal centered BN coupling is suggested. This same competition was implicated in the DMAB dehydrogenation observed by Schneider [39]. It is interesting to note that release of NH_2BH_2 has been suggested as evidence that the catalyst system may be capable of releasing more than one equivalent of H_2 [29]. A recent report by Conley and Williams employs Shvo's ruthenium catalyst to rapidly dehydrogenate AB to borazine [44].

5 Conclusion and Future Outlook

Driven by the need for sustainability, the world energy infrastructure will undergo significant changes in the coming decades. One key component to the development of a sustainable energy economy will be finding a suitable energy carrier. Presently, electrical storage in batteries and high-pressure hydrogen storage are the leading technologies for “green” vehicles. However, more research is necessary to meet performance standards expected by consumers have grown to expect.

AB is currently considered a strong contender as a potential material for chemical hydrogen storage. In recent years, several pincer complexes have been developed that rapidly dehydrogenate AB to release H_2 . Further research is needed to fully understand the mechanism through which H_2 is released, but trends are beginning to emerge already in terms of extent of hydrogen release and the mechanism of oligomerization of dehydrogenated BN material. Trapping experiments with cyclohexene have shown that release of NH_2BH_2 is potentially an important step in the generation of multiple equivalents of H_2 from AB. Experimental and theoretical studies have determined that complexes bearing bifunctional pincer ligands are especially competent catalysts and this looks to be a promising strategy for the development of AB dehydrogenation catalysts in the future.

Finally, calorimetric studies have shown that direct regeneration of spent fuel is not feasible and other indirect methods must be explored. Recently, the regeneration of polyborazylene to AB was reported [33]. Future work will be needed to continue to develop regeneration pathways.

References

1. REN21 (2010) Renewables 2010 global status report. REN21 Secretariat, Paris
2. Kerr RA (2007) *Science* 316:351
3. AWEA, "American Wind Energy Association (AWEA) Notes Wind Industry Highlights of 2009," press release. Washington, DC, 22 Dec 2009
4. Satayapal S, Petrovic J, Read C, Thomas G, Ordaz G (2007) *Catal Today* 120:246
5. Service RF (2009) *Science* 324:1257
6. Program's Multi-Year Research, Development, and Demonstration Plan (2009). http://www1.eere.energy.gov/hydrogenandfuelcells/storage/storage_challenges.html
7. Eberle U, Felderhoff M, Schüth F (2009) *Angew Chem Int Ed* 48:6608
8. <http://www.bloomberg.com/apps/news?pid=newsarchive&sid=a693eL42oJHo>
9. US Patent 6,534,033, 18 Mar 2003, assigned to Millenium Cell
10. Megede DZur (2002) *J Power Sources* 106:35
11. Stephens FH, Pons V, Baker RT (2007) *Dalton Trans* 2613
12. Marder TB (2007) *Angew Chem Int Ed* 46:8116
13. Hu MG, Geanangel RA, Wendlandt WW (1978) *Thermochim Acta* 23:249
14. Jaska CA, Temple K, Lough AJ, Manners I (2001) *Chem Commun* 11:962
15. Denney MC, Pons V, Hebden TJ, Heinekey DM, Goldberg KI (2006) *J Am Chem Soc* 128:12048
16. Göttker-Schnetmann I, White P, Brookhart M (2004) *J Am Chem Soc* 126:1804
17. Blaquiere N, Diallo-Garcia S, Gorelsky SI, Black DA, Fagnou K (2008) *J Am Chem Soc* 130:14034
18. Käß M, Friedrich A, Drees M, Scheinder S (2009) *Angew Chem Int Ed* 48:905
19. Hamilton CW, Baker RT, Staubitz A, Manners I (2008) *Chem Soc Rev* 38:279
20. Hebden TJ, St. John AJ, Gusev DG, Kaminsky W, Goldberg KI, Heinekey DM (2011) *Angew Chem Int Ed* 50:1873
21. Smythe NC, Gordon JC (2010) *Eur J Inorg Chem* 509
22. Jaska CA, Temple K, Lough AJ, Manners I (2003) *J Am Chem Soc* 125:9424
23. Jaska CA, Manners I (2004) *J Am Chem Soc* 126:9776
24. Böddeker KW, Shore SG, Bunting RK (1966) *J Am Chem Soc* 126:1804
25. Hebden TJ, Goldberg KI, Heinekey DM, Zhang X, Emge TJ, Goldman AS, Krogh-Jespersen K (2010) *Inorg Chem* 49:1733
26. Hebden TJ, Denney MC, Pons V, Piccoli PMB, Koetzle TF, Schultz AJ, Kaminsky W, Goldberg KI, Heinekey DM (2008) *J Am Chem Soc* 130:10812
27. Zhu K, Achord PD, Zhang X, Krogh-Jespersen K, Goldman AS (2004) *J Am Chem Soc* 126:10797
28. Paul A, Musgrave CB (2007) *Angew Chem Int Ed* 46:8153
29. Pons V, Baker RT, Szymczak NK, Heldebrant DJ, Linehan JC, Matus MH, Grant DJ, Dixon DA (2008) *Chem Commun* 48:6597–6599
30. Dietrich BL, Goldberg KI, Heinekey DM, Autrey T, Linehan JC (2008) *Inorg Chem* 47:8583
31. Staubitz A, Soto AP, Manners I (2008) *Angew Chem Int Ed* 47:6212
32. Staubitz A, Sloan ME, Robertson APM, Friedrich A, Schneider S, Gates PJ, auf der Günne JS, Manners I (2010) *J Am Chem Soc* 132:13332
33. Sutton AD, Burrell AK, Dixon DA, Garner EB III, Gordon JC, Nakagawa T, Ott KC, Robinson JP, Vasiliu M (2011) *Science* 331:1426
34. Noyori R, Hashiguchi S (1997) *Acc Chem Res* 30:97
35. Clapham SE, Hadzovic A, Morris RH (2004) *Coord Chem Rev* 248:2201
36. Noyori R, Okhuma T (2001) *Angew Chem Int Ed* 40:40
37. Ikariya T, Blacker AJ (2007) *Acc Chem Res* 40:1300

38. Keaton RJ, Blacquiere JM, Baker RT (2007) *J Am Chem Soc* 129:1844
39. Friedrich A, Drees M, Schneider S (2009) *Chem Eur J* 15:10339
40. Jaska CA, Temple K, Lough AJ, Manners I (2001) *Chem Commun* 962
41. Fryzuk MD, Leznoff DB, Thompson RC, Rettig SJ (1998) *J Am Chem Soc* 120:10126
42. Yang X, Hall MB (2008) *J Am Chem Soc* 130:1798
43. Yang X, Hall MB (2009) *J Organomet Chem* 694:2831
44. Conley BL, Williams TJ (2010) *Chem Commun* 46:4815

PC(sp³)P Transition Metal Pincer Complexes: Properties and Catalytic Applications

Dmitri Gelman and Ronit Romm

Abstract Carbometalated pincer complexes represent a family of powerful compounds having tremendous number of manifold applications in organometallic chemistry, synthesis, catalysis, material science, and bioinorganic chemistry. This chapter reviews the recent developments in the chemistry and catalytic applications of PC(sp³)P transition metal pincer complexes stressing their singular reactivity that stem from the unique electronic properties and topology.

Keywords catalysis · pincer · sp³-carbometalated

Contents

1	Introduction	289
2	C(sp ³)-Based Pincer Complexes	291
2.1	C(sp ³)-Metalated Pincer Complexes Based on All-Aliphatic Scaffolds	291
2.2	C(sp ³)-Metalated Pincer Complexes Based on Non-aliphatic Scaffolds	301
3	Conclusion	315
	References	315

1 Introduction

Carbometalated pincer-type complexes belong to a family of organometallic compounds in which the generally labile carbon–metal bond is reinforced by at least two neighboring donor groups (D is a neutral two-electron donor, see Fig. 1). This DCD η³-mer coordination mode gives rise to the formation of the

D. Gelman (✉) · R. Romm

Institute of Chemistry, The Hebrew University, Edmund Safra Campus, 91904 Jerusalem, Israel
e-mail: dgelman@chem.ch.huji.ac.il

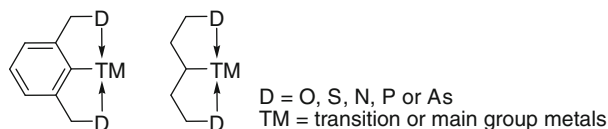


Fig. 1 Schematic Representation of the pincer complexes

thermodynamically favored C–M bond-sharing bicyclic structures [1, 2] that are usually translated into robust materials featuring exceptional thermal stability [3]. On the other hand, the ligand scaffold and the coordinating groups can be tailored to control reactivity of the carbon–metal bond by controlling steric environment as well as electronic properties of the metal center [4–6]. The combination of these factors makes pincer complexes very popular in many areas of chemical sciences like basic organometallic chemistry [7–9], catalysis [10–14], design of high-performance materials [15–17], bioinorganic [18, 19] and supramolecular chemistry [20–23].

Since their first appearance in the literature [24–26], differently crafted pincer ligands have been developed and placed at the disposal of chemists to address various applications. However, by far the most popular scaffold used to design DCD pincer ligands relies on an aromatic moiety (Fig. 1, left). This is not surprising because the carbon–metal bond in such complexes is essentially coplanar to the [2,6-(DCH₂)₂C₆H₃] system which, of course, greatly improves communication between the metal-centered d_{xz} orbitals and the π orbitals of the aromatic backbone [27–29]. This, together with high sensitivity of the arene rings toward electronic nature of the substituents in *para* position, and availability of the synthetic methods for their facile installation, marks the C(sp^2)-metalated pincer complexes as ideal candidates for systematic studies of structure/reactivity relationships.

On the contrary, reports on the chemistry and practical applications of the aliphatic C(sp^3)-metalated pincer complexes (Fig. 1, right) are far less common. Among the “weak points” of the all-aliphatic design is an excessive flexibility of the frame along with the presence of easily abstractable α - and β -hydrogens that significantly reduce their stability [30–32]. Furthermore, structural modification of the all-aliphatic skeleton is not a trivial task which makes fine-tuning of their properties practically impossible. Likewise, essentially “insulating” all-C(sp^3) scaffold almost disqualifies this class of compounds for material applications.

Nevertheless, some singular properties ascribed to C(sp^3)-metalated pincer complexes keep them at the focus of contemporary studies. For example, it is widely accepted that a better σ -donation exerted by the anionic sp^3 -hybridized pincer ligand increases electron density at the metal center which might significantly alter their reactivity compared to the aromatic counterparts. Another aspect advantageously distinguishing C(sp^3)-metalated compounds is their three-dimensionality. For example, with some exceptions of C₂-symmetrically twisted molecules [33–41], *ipso*-C–M bond-sharing five-membered rings characteristic of aromatic pincer complexes are averagely planar (Fig. 2). Arguably, this structural simplicity is reflected in a relatively limited number of aromatic pincer complexes successfully applied as stereoselective catalysts [14, 42]. Unlike those, more complex and three-dimensional environment around the metal center provided by the

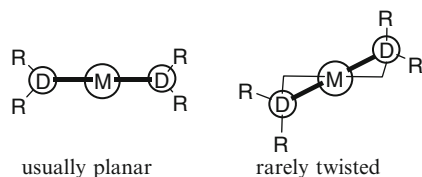


Fig. 2 Dimensionality of the aromatic pincer complexes

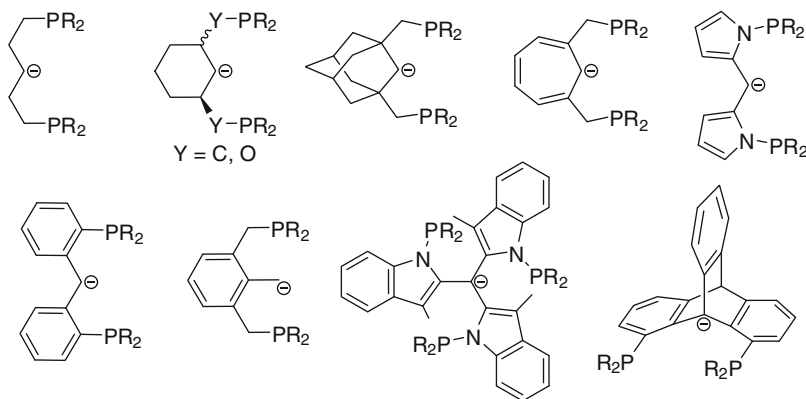


Fig. 3 C(sp^3)-based pincer preligands

C(sp^3)-based pincer ligands may open new venues in catalysis as well as in many other research areas where pincer complexes are in use.

Since fundamental and practical aspects of chemistry of the aromatic C(sp^2)-based pincer complexes are well reviewed, in this overview, we wish to concentrate on the recent developments in the chemistry of PC(sp^3)P-metalated pincer compounds.

2 C(sp^3)-Based Pincer Complexes

Although aliphatic pincer complexes have been long overshadowed by the more robust aromatic ones, several eye-catching C(sp^3)-based (almost exclusively, PCP-type) preligands may be named. For example, alkyl chain [24], cyclohexane [43], adamantane [44], cycloheptatriene [45], arylmethane [46], diarylmethane [47, 48], triarylmethane [49], ferrocene [50], and dibenzobarrelene [51] derivatives have been employed as platforms for the construction of the desired compounds (Fig. 3).

2.1 C(sp^3)-Metalated Pincer Complexes Based on All-Aliphatic Scaffolds

2.1.1 α,ω -Diphosphinoalkanes

It has been long recognized that structurally simple long-chain α,ω -diphosphinoalkanes react with transition metals yielding cyclometalated species (Eq. 1).

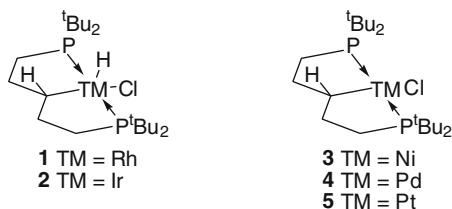
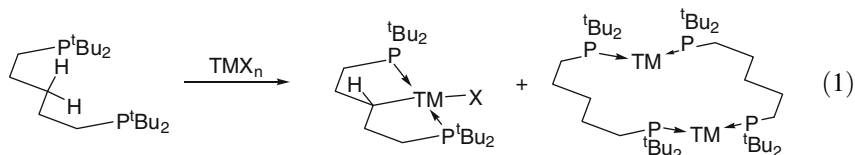


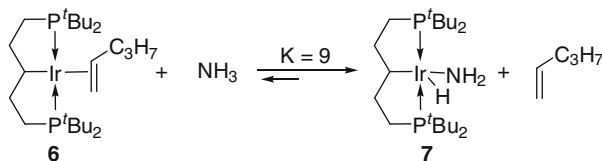
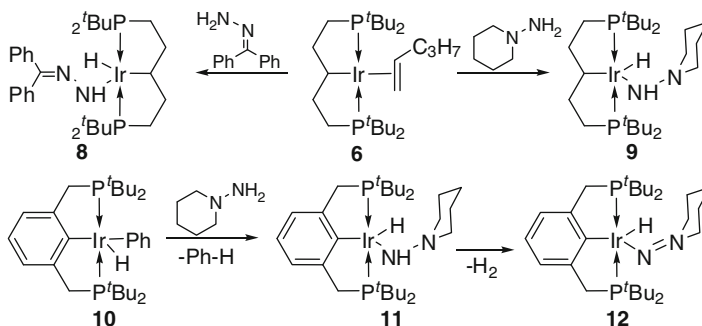
Fig. 4 Prototypical aliphatic pincer complexes

For example, iridium [52], rhodium [53], osmium [54], ruthenium [54, 55], platinum [56], palladium [56], and nickel [57] prototypes were synthesized employing 1,5-bis(di-*t*-butylphosphino)pentane and appropriate metal precursors (Fig. 4). Formation of the C(*sp*³)-metal bond may proceed either via electrophilic activation or via oxidative addition of low-valent metals across the C-H bond. However, in both of the cases, yield of the metalated compounds is poor to moderate (depending on the bulk of the phosphine donors) on account of the formation of large-ring chelates or linear oligomeric by-products.



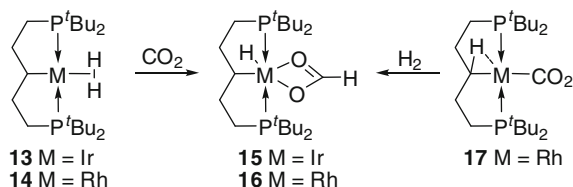
Initial comparative IR studies confirmed the expected *trans* influence of the *sp*³-metalated carbon. For example, $\nu(\text{M}-\text{Cl})$ vibrations in **2–5** were found 10–30 cm^{-1} lower than in the analogous aromatic *sp*²-metalated compounds, suggesting a more electron-rich character of the metal centers and, consequently, a more reactive carbon-metal bond [24].

Indeed, its high reactivity has been demonstrated by Zhao, Goldman, and Hartwig by an unprecedented oxidative addition/reductive elimination equilibrium displayed in Scheme 1, where the *sp*³-based Ir(I) complex **6** oxidatively adds across the N-H bond of ammonia to form the corresponding Ir(III) amido hydride **7** at room temperature and excellent yield [58]. Remarkably, analogous aromatic pincer complexes fail to establish the equilibrium favoring the oxidized product. This clear ligand effect may be attributed to a stronger donating ability of the aliphatic backbone that enhances electron density at the metal center needed to achieve activation of otherwise inert ammonia. On the other hand, according to the X-ray data interpretation, the lone pair of the amido nitrogen is oriented to allow π -donation into the empty *d*-orbital that lies in the plane of the iridium(III) centers containing the *ipso* carbon. This stabilization is, apparently, less pronounced in the presence of the conjugated π system of the aromatic PCP ligand, which may explain the favorable thermodynamics of the reaction. Computational studies have given support to these findings [59].

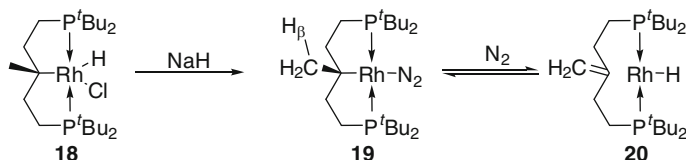
**Scheme 1** N–H activation in ammonia**Scheme 2** N–H activation in hydrazines and hydrozones

Very recent studies by the same group demonstrated similar N–H activation in hydrazines and hydrozones by **6** (Scheme 2) [60]. In this work, however, the transformation was not limited to the aliphatic pincer complexes and both **6** and its aromatic analog **10** were shown to react in a similar fashion, although resulted in the formation of products of different stability. For example, while **9** is stable at room temperature, **11** undergoes the second N–H activation at room temperature over several days to form aminonitrene complex **12** and one equivalent of molecular hydrogen. Here again, structural characterization of the aliphatic complexes **8** and **9** clearly pointed out on the presence of nitrogen-metal π -stabilizing interaction which can rationalize relative stability of the sp^3 -metalated complexes over the sp^2 -based ones.

Carbon dioxide reduction by rhodium [61] and iridium [62] complexes has an utmost catalytic potential. As was demonstrated, nonclassical dihydrogen complexes **13** and **14** form corresponding formate compounds in the presence of gaseous CO₂ (Scheme 3, left). The following sequence of the mechanistic events has been suggested (1) carbon dioxide coordination to the η^2 -H₂ binding PCP–Rh center gives rise to the formation of the dihydrogen complex with a weakly bound η^1 -CO₂ complex. This type of η^1 interaction can be viewed as the donation of the HOMO of the Rh–H₂ complex, a d_z^2 orbital, to the π^* orbital of the CO₂ molecule; (2) the dihydride species can undergo the hydride transfer from the Rh center to the C center of CO₂; (3) after the hydride insertion event, the kinetic products formed are hydridorhodium η^1 -formate complexes, which should transform into the most stable η^2 -formate coordination compounds [63].



Scheme 3 Hydrogenation of CO₂



Scheme 4 Coordination flexibility in all aliphatic rhodium pincer complexes

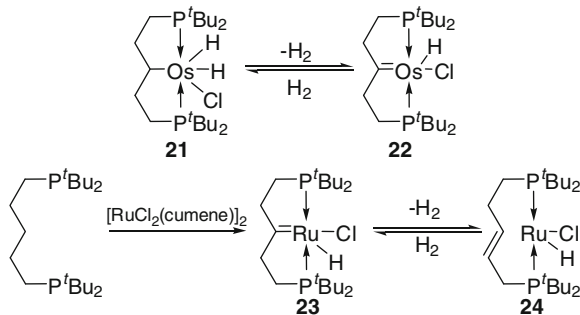
Interestingly, the rhodium formate complex **16** can be also prepared by the reaction of fully characterized **17** with molecular hydrogen (Scheme 3, right). The transformation, apparently, proceeds via predissociation of CO₂, as a small amount of **14** is co-produced. However, preparation of **17** is interesting by itself because carbon dioxide rarely coordinates transition metals and agostic stabilization was suggested to explain the stability of **17**.

Remarkably also, the stability of the formate complex **16** is significantly higher in comparison to the analogous compounds bearing *sp*²-based PCP ligand.

Tendency of transition metal complexes bearing all-aliphatic ligands to reversibly α - and β -hydride elimination to form isomeric carbene [52] or olefin chelate [55, 64] complexes is another evidence for high reactivity of the C(*sp*³)-metal bond. Thus, Vignalok et al. reported that reduction of the Rh(III) PC(*sp*³)P complex **18** leads to the formation of the dinitrogen Rh(I) complex **19** and the β -H eliminated **20**. It was found that under nitrogen atmosphere these complexes exist in the temperature-dependent equilibrium (Scheme 4) [64]. Remarkably, unlike classical migratory insertion process requiring *cisoid* coordination of the participating ligands, this reaction proceeds via direct *trans* insertion. Similar transformation has been reported for ruthenium complexes [55].

Gusev et al. performed an interesting study on the osmium and ruthenium PC(*sp*³)P complexes possessing both α - and β -hydrogens [54]. As shown, osmium carbometalated compound **21** demonstrates a clear agostic interaction between the osmium center and the central methine hydrogen that facilitates the extrusion hydrogen to form the thermodynamically stable carbene complex **22**. In contrast, the assumed Ru-based PC(*sp*³)P pincer compound disproportionates via competitive α - and β -hydride elimination pathways to form the 1.5:98.5 mixture of the carbene (**23**) and olefin (**24**) isomers (Scheme 5).

Zhou and Hartwig utilized this coordination flexibility for the design of very efficient catalyst for H/D exchange at vinyl groups that operates under very mild



Scheme 5 Coordination flexibility in all aliphatic ruthenium and osmium complexes

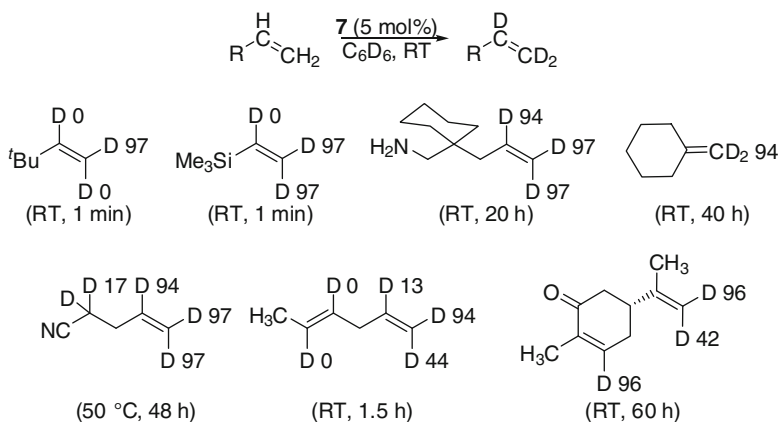


Fig. 5 H/D exchange catalyzed by **7**

conditions and without isomerization of the double bonds [65]. As was demonstrated, Ir(III) amido hydride complex **7** induces very fast (minutes to hours) room temperature deuteration of internal and terminal double bonds with absolute regioselectivity (Fig. 5).

In addition to absolute regioselectivity, the method is highlighted by excellent functional group compatibility. For example, nitriles, primary amines, alcohols, esters, and ketones can be present, although acidic α -hydrogens to the electron-withdrawing groups may suffer from partial exchange. Aliphatic hydrogens do not react under the developed reaction conditions. This regio- and chemoselectivity allowed efficient isotopic labeling of some biologically active molecules and natural products (Fig. 6).

Aromatic pincer complexes were found practically inactive under the described conditions and, therefore, it is suggested the reaction is operated by a mechanism in which the methine position of the backbone acts as a shuttle. If so, the following mechanistic scheme may be suggested: after dissociation of olefin, the iridium(I)

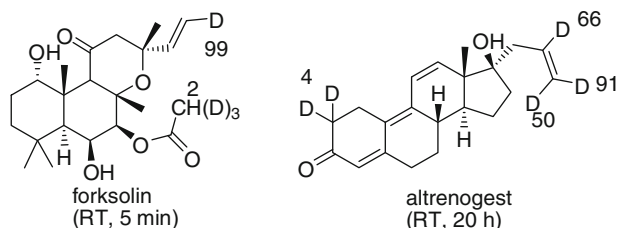
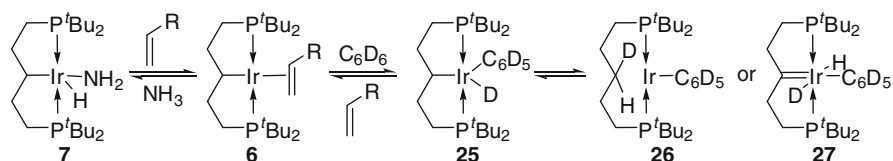
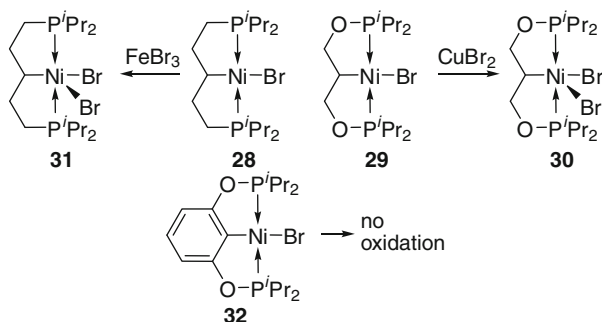


Fig. 6 Labeling of the functionalized targets



Scheme 6 Proposed mechanism for the Ir-catalyzed H/D exchange



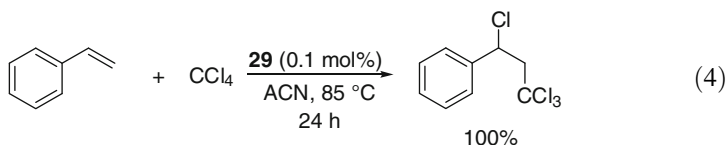
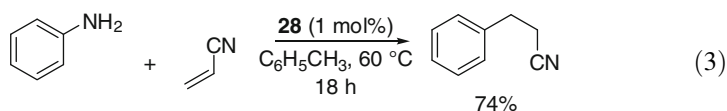
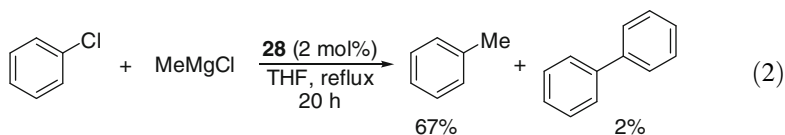
Scheme 7 Formation of the paramagnetic 17 electron Nickel pincer complexes

fragment (**6**) (generated by reductive elimination of NH_3 from **7**) undergoes oxidative addition of the aryl deuterium bond to form **25**. Subsequent reversible C–D reductive elimination involving the methine carbon center on the ligand could generate aryl iridium(I) complex **26**. Alternatively, the complex resulting from the oxidative addition of the arene (**25**) could undergo reversible α -hydrogen elimination from the ligand backbone to give iridium(III) carbene species **27** (Scheme 6). A parallel process with the vinylic C–H bonds would lead to incorporation of deuterium into the olefinic substrates.

$\text{C}(\text{sp}^3)$ -based group 10 transition metal complexes have been also reported as catalytically relevant. For example, Zargarian and coworkers synthesized a series of unprecedented Ni compounds bearing 1,5-diphosphinopentane [57] or 1,3-diphosphinitopropane (Scheme 7) [66]. The diamagnetic $\text{PC}(\text{sp}^3)\text{P}$ **28** and POC

(*sp*³)OP **29** are electrochemically active and undergo facile one electron oxidation to Ni(III) species. Indeed, chemical oxidation led to the formation of the paramagnetic 17-electron complexes **30** and **31** (Scheme 7) [67, 68]. Interestingly, attempts to oxidize the aromatic POC(*sp*²)OP **32** failed despite that cyclic voltammetry shows quasi-reversible single-electron oxidation wave ($E_{1/2} = 1.17$) [66].

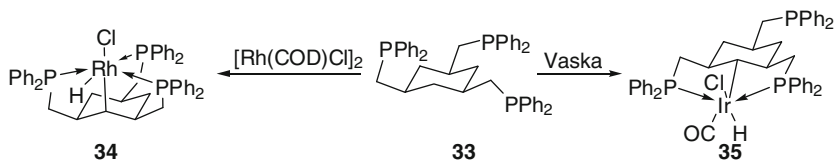
Ni(II) PC(*sp*³)P **28** (0.5–2 mol%) was found active in catalyzing Kumada coupling of chlorobenzene with MeMgCl and BuMgCl demonstrating maximal TON of 84 (Eq. 2) [68]. The same complex serves as a nucleophilic catalyst in regioselective hydroamination of acrylonitrile with aniline (Eq. 3) [69].



The same group demonstrated the use of Ni(III) POC(*sp*³)OP **29** as a promoter in Kharasch addition of CCl₄ to olefins (Eq. 4). The reaction gives the 1:1 anti-Markovnikov addition product exclusively. The catalyst shows up to 100 turnovers and works equally well with styrene and 4-methylstyrene, while somewhat less efficiently with acrolein, methyl acrylate, and acrylonitrile, and not at all with α -methylstyrene, 1-hexyne, and 3-hexyne.

2.1.2 Diphosphinocycloalkanes

The first C(*sp*³)-metalated compound bearing cyclohexyl-based pincer ligand was synthesized by Mayer and coworkers who studied coordination chemistry of a potentially tripodal *cis,cis*-1,3,5-tris[(diphenylphosphino)methyl]cyclohexane (**33**). They found that treatment of **33** with [Rh(COD)Cl]₂ [70] or Vaska complex [43] in hot toluene gives carbometalated **34** and **35** almost quantitatively (Scheme 8). In spite of the high flexibility of **33**, the third phosphine group is either non-coordinated (e.g., **35**) or loosely bound (e.g., **34**) and may be easily displaced in solution. Therefore, **34** exists in solution as oligomeric species.



Scheme 8 Prototypical cyclohexane-based pincer complexes

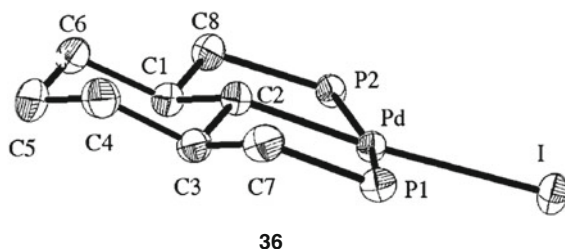
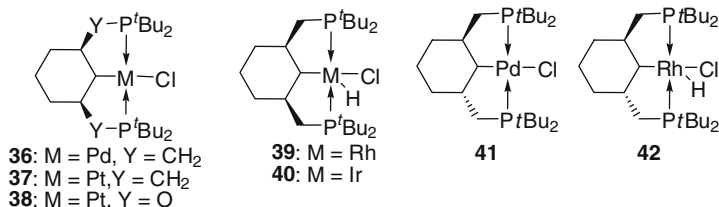
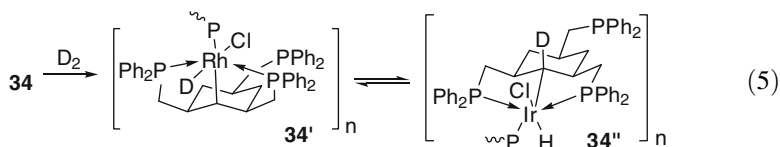


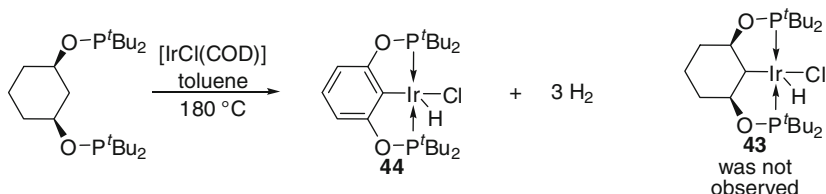
Fig. 7 Recently synthesized cyclohexane-based pincer complexes

Treatment of **34** with D_2 shows H/D exchange at both the hydride ligand and the methine hydrogen which suggests the lability of the metal–carbon bond (Eq. 5) [61].



More recently, Wendt [71] and Gusev [72] independently reported on the employment of *cis*- and *trans*-1,3-bis(di-*t*-butylphosphinomethyl)cyclohexane, as well as *cis*-1,3-bis(di-*t*-butylphosphinito) cyclohexane, as platforms for the construction of palladium, rhodium, platinum, and iridium pincer complexes (Fig. 7).

The chelate systems bearing *cis*-substituted cyclohexane derivatives adopt a double-bent conformation with a bisecting perpendicular pseudo-mirror plane (Fig. 7). For example, five of the atoms in **36** (P1, P2, C2, C7, and C8) are almost situated in the plane of the complex with the displaced methine groups C1 and C3 pointing away in the same direction. This arrangement results in magnetically



Scheme 9 Acceptorless dehydrogenation of the ligand scaffold

different environments above and below the square plane, which is also manifested in solution with dual resonances in the ¹³C NMR spectrum of **36** for the *tert*-butyl substituents on the phosphorus atoms.

The cyclohexane ring adopts the chair conformation and is aligned with the plane of the complex, with the equatorial C2–H bond being activated. There is almost no built-in strain in the cyclohexane ring, which is reflected by its endocyclic bond angles that do not deviate substantially from free cyclohexane [40, 73, 74].

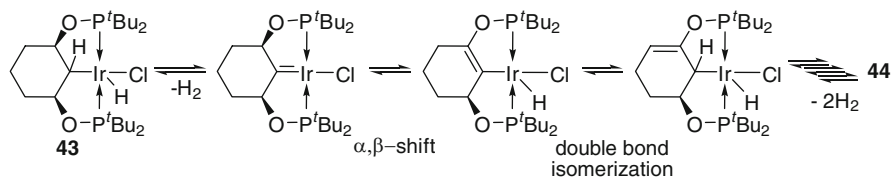
Despite that DFT calculations predicted more strain built in complexes bearing *trans*-substituted cyclohexane-based ligands (by 9–11 kcal/mol), comparison between the structural data of **39** and **42** revealed that cyclohexane rings are practically identical and both adopt almost ideal chair conformation [72].

In contrast to α,ω -diphosphinoalkane-based pincer complexes that often experience temperature induced α - and β -hydride elimination to form isomeric carbene or olefin-type complexes, cyclohexyl-based PC(*sp*³)P complexes are thermally stable. For example, according to TGA, **40** displays a first insignificant weight loss at 220 °C in both air and nitrogen, while substantial thermal decomposition starts only at 250 °C in air and 300 °C in nitrogen [74]. The thermal stability can be rationalized by a lesser flexibility of the cyclic ligand frame.

However, interesting aromatization of the *cis*-1,3-bis(di-*t*-butylphosphinito) cyclohexane ligand accompanied by extrusion of three equivalents of dihydrogen was discovered upon attempted synthesis of the corresponding Ir PC(*sp*³)P complex **43** (Scheme 9) [74].

Arguably, this unusual transformation may proceed either via iridium-catalyzed acceptorless dehydrogenation of cyclohexane ligand into the known aromatic POCOP followed by its facile metalation, or, alternatively, via the formation of the hypothetical POC(*sp*³)OP Ir(III) hydride species (**43**) that undergoes α -elimination of hydrogen, followed by α,β -hydride shift and double bond isomerization (Scheme 10). Thus, existence of α - and β -hydride elimination processes cannot be completely ruled out in the less flexible cyclohexyl-based systems.

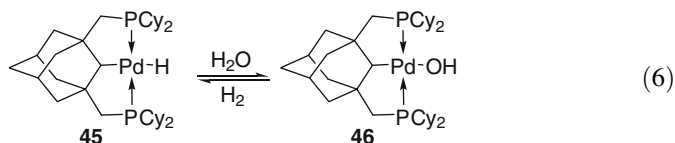
Complex **36** was employed as a catalytic promoter in the Suzuki–Miyaura cross-coupling [75] and Mizoroki–Heck olefination of aryl halides [38, 71]. Although both these reactions have been shown to proceed under very harsh conditions (140–160 °C), TONs achieved in, e.g., Heck reaction of aryl iodides with activated substrates were impressive (up to 5.34×10^5).



Scheme 10 Proposed mechanism for the acceptorless dehydrogenation of the ligand scaffold

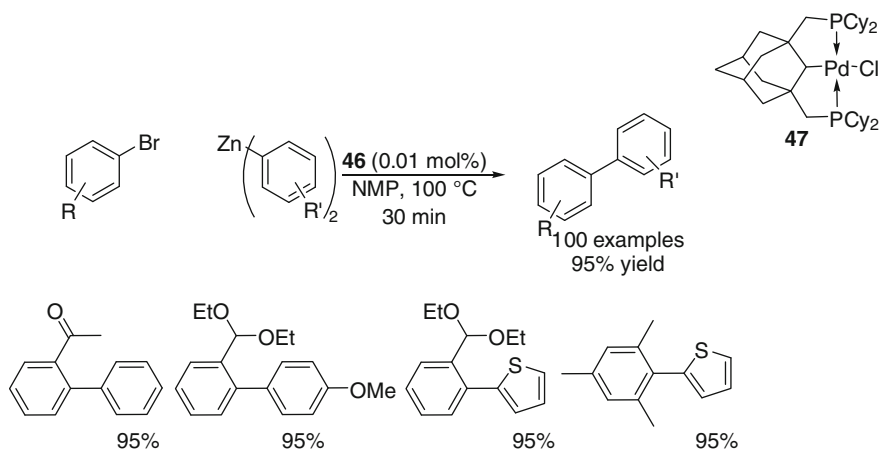
Frech and coworkers reported on the employment of the adamantanyl scaffold for the design of $\text{PC}(sp^3)\text{P}$ pincer ligands [44]. Unlike other all-aliphatic scaffolds mentioned in this section, the suggested ligand is very rigid and lacking labile β -hydrogens which ensures thermal stability of the resulting transition metal complexes.

Studying reactivity of the palladium hydride **45** revealed that in contrast to the aromatic pincer complexes [24], it reacts reversibly with water resulting in the formation of the palladium hydroxide **46** and molecular hydrogen (Eq. 6). This difference in reactivity was attributed to a greater “hydridic character” of the hydride ligand due to a stronger *trans*-effect exerted by the $\text{C}(sp^3)$ center.

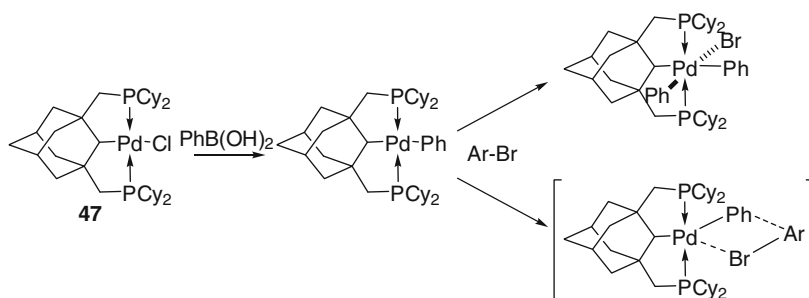


Yet, catalytic tests proved that palladium chloride bearing the new $\text{PC}(sp^3)\text{P}$ (**47**) is a robust catalyst for Suzuki–Miyaura [76] coupling of aryl bromides. This catalyst operates under much milder reaction conditions and enables quantitative coupling of a wide variety of electronically activated, deactivated, and/or sterically hindered, highly functionalized aryl bromides with phenylboronic acid in pure water with NaOH as base within very short reaction times under low catalyst loading and without the need for exclusion of air. Hydrophobic substrates, which lead to inefficient conversions in aqueous medium, were efficiently and quantitatively coupled in toluene with K_3PO_4 as base. Similar reactivity was exhibited by the same catalyst in Negishi cross-coupling (Scheme 11) [77].

Very often, activity of pincer complexes in cross-coupling chemistry is contested due to the fact that these compounds cannot participate in the widely accepted $\text{Pd}(0)/\text{Pd}(\text{II})$ catalytic cycle and they are only regarded as a source for palladium nanoparticles that virtually catalyze the reactions [78]. However, based on the results of the mercury test performed independently by the groups of Frech [76] and Wendt [75] for the reactions catalyzed by **36** and **47**, it was concluded that the reactions operate either via $\text{Pd}(\text{II})/\text{Pd}(\text{IV})$ catalytic cycle or via σ -bond metathesis (Scheme 12).



Scheme 11 Negishi cross coupling reaction catalyzed by **47**



Scheme 12 Proposed mechanism for the Suzuki cross coupling of aryl bromides catalyzed by **47**

2.2 *C(sp*³*)-Metalated Pincer Complexes Based on Non-aliphatic Scaffolds*

2.2.1 Cycloheptatriene-Based Scaffold

A seminal design of the PC(*sp*³)P pincer ligands taking advantage of cycloheptatriene platform was introduced by Kaska, Mayer, and coworkers [45]. Significance of the tropylium resonance form leading to the lability the α -methine hydrogen is the most striking difference between the all-aliphatic and the cycloheptatriene-based *sp*³-metalated pincer ligands because the corresponding transition metal pincer complexes, if prepared, must be regarded as organometallic species of a reversed polarity (Fig. 8).

The synthesis of the first representative of this family of compounds (**48**) was realized via the reaction of the corresponding ligand with tricarbonyl iridium chloride (Scheme 13). Complex **48** is a highly stable, coordinatively as well as

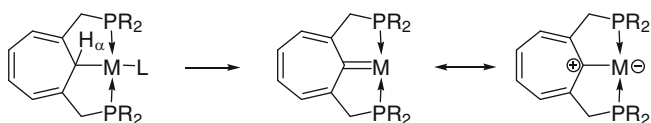
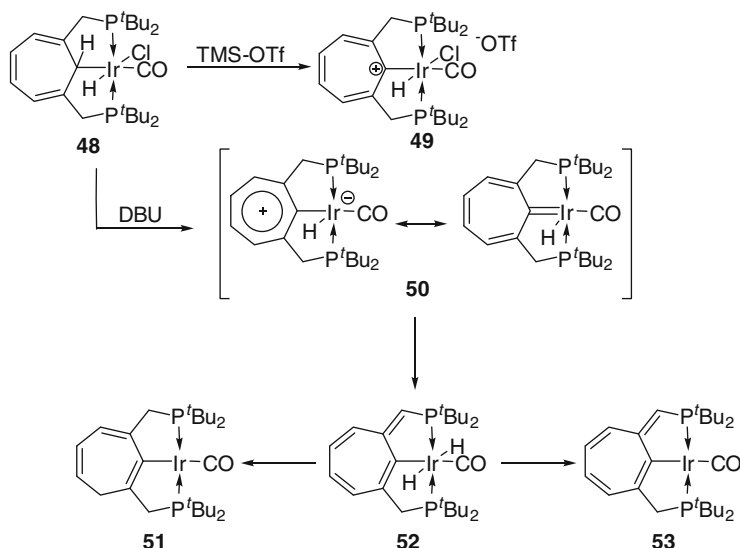


Fig. 8 Proposed reversed polarity in the cycloheptatriene based pincer complexes



Scheme 13 Attempted synthesis of 50

electronically saturated compound. As the carbonyl in it is located *trans* to the metalated carbon atom, the hydride and the chloride ligands are forced into a mutual *trans* orientation. The C–H group in the free backbone is strongly bent out of the plane which encompasses the three double bonds. Consequently, the residual hydrogen atom at the metal-bound C(sp^3) and the chloride ligand are *syn*-periplanar at the iridium center.

Indeed, treatment of **48** with one equivalent of TMS-OTf leads to the formation of a stable tropylium derivative **49** (Scheme 13) that is expectedly characterized by a longer ν (Ir–CO) vibration (2,030 cm^{-1} in **49** vs. 2,000 cm^{-1} in **48**) [79].

However, attempted treatment of **48** with DBU to form carbene-tropylium product **50** led to the formation of the sp^2 -carbometalated **51–53** [80]. As was suggested, HCl is removed from the cycloheptatrienyl PCP pincer **48** across the C(sp^3)–Ir bond forming a carbene structure as outlined in Scheme 13. The proposed carbene, however, was not observed due to the fast rearrangement affording **52**, which, in due turn, may rearrange into **51** or to expel H_2 to form **53**. Indeed, DFT calculations predict the **50** as the least stable species being destabilized by 10.7 kcal/mol in comparison to **52** and by 26.6 kcal/mol to **53**. Considerably higher stability of the C(sp^2)–Ir bond is, apparently, a driving force for the isomerization processes.

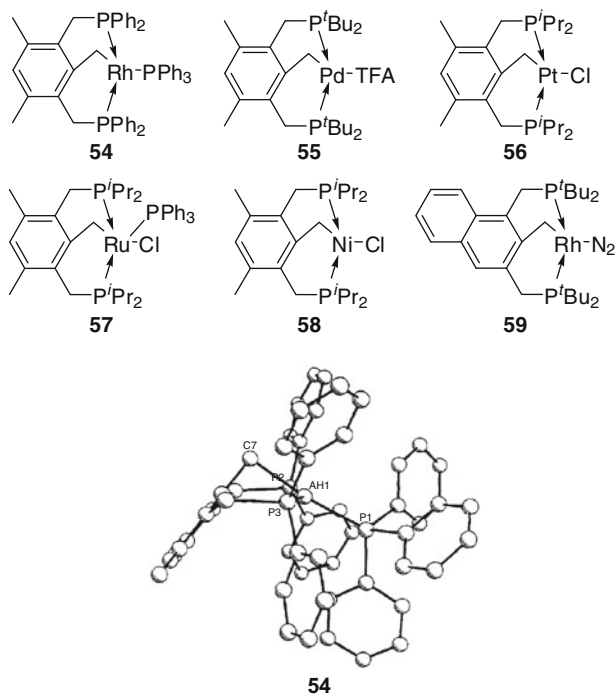


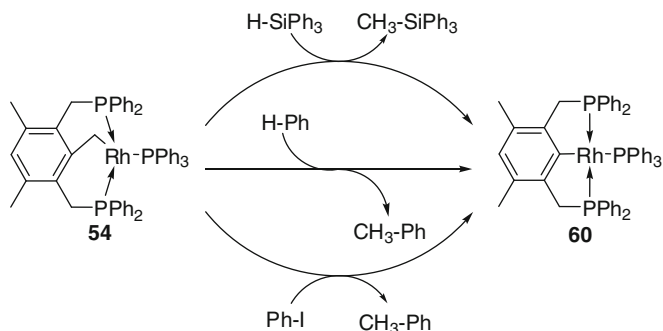
Fig. 9 C(sp^3)-metalated arylmethyl-based pincer complexes

No catalytic activity of such cycloheptatriene-based pincer complexes has been described so far.

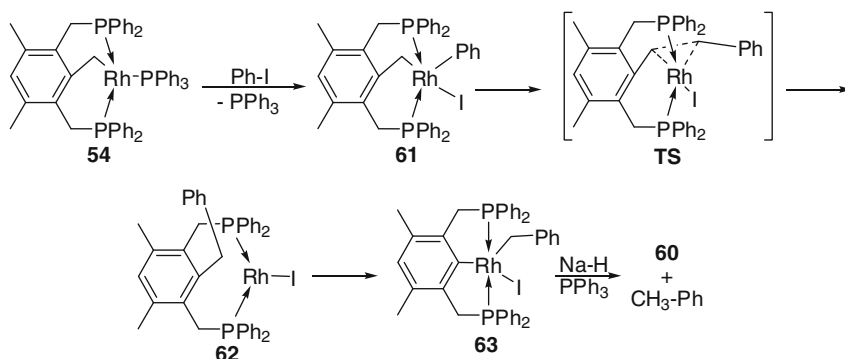
2.2.2 C(sp^3)-Metalated Arylmethyl-Based Scaffolds

In late 1990s, Milstein and co-workers developed a series of complexes bearing PC(sp^3)P ligands metalated at the benzylic position such as shown in Fig. 9. The complexes are synthesized via direct C(sp^3)–H bond activation at the benzylic position of the corresponding ligand by rhodium [46], iridium [81], ruthenium [82], platinum [82], nickel [83], or palladium [84]. Despite the visual strain in the six-membered C–M bond-sharing ring systems these complexes are relatively stable because there is no distortion of the metalated carbon from the plane of the aromatic ring and the favorable square planar geometry around the metal center is retained (e.g., ORTEP of **54** is given in the Fig. 9).

On the other hand, it was discovered that most of these complexes are capable of the non-catalytic room temperature cleavage of the C(sp^2)–C(sp^3) bond. For example, mild heating of **54** in the hydrogen atmosphere led to the extrusion of methane molecule to form the aromatic **60**. Moreover, as was demonstrated, the methylene



Scheme 14 Intermolecular methylene transfer from the arylmethyl-based pincer complexes

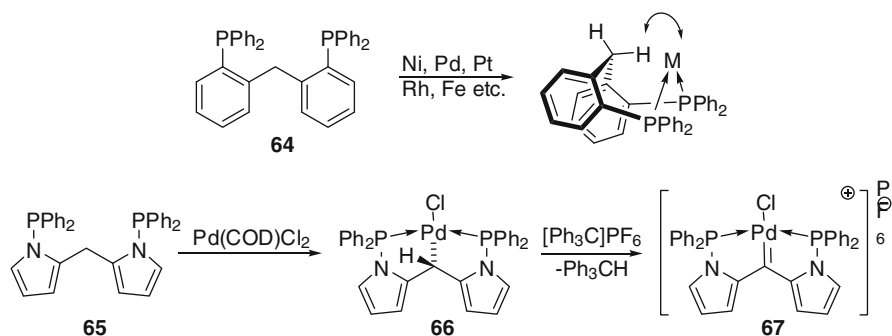


Scheme 15 Proposed mechanistic scheme for the methylene-transfer reactions

fragment maybe intermolecularly transferred to form new $C(sp^3)$ -element bonds [85] (Scheme 14).

The following sequence of mechanistic steps was suggested to explain the reactions. The first step is oxidative addition of C–I, C–H, and Si–H bonds to the low-valent rhodium center that has many literature precedents. Although the oxidative addition products were not directly observed in all cases, it was unequivocally proved in the transformation of iodobenzene to **61** (Scheme 15) [86]. The methylene transfer proceeds, apparently, in a two-step process via C–C bond-forming intramolecular reductive elimination to give non-metallated species **62** that are reorganized to **63** via oxidative addition of Rh(I) across the new C–C bond.

The initial preferential formation of the $PC(sp^3)P$ complexes metallated at the benzylic position is kinetic and may be explained by agostic interactions originating from charge donation from the C–H σ bond to the proximate metal atom accompanied by back-donation into the antibonding σ^* orbital, leading to the weakening of the C–H bond. Theoretical studies predict significantly lower C–H activation barrier in contrast to the competing C–C activation step that is predicted to be thermodynamically favored [87–89].



Scheme 16 Synthesis of diarylmethyl-based pincer complexes

Studies on this family of compounds mainly concerned their fundamental properties, although **55** was found to serve as a very efficient catalyst for the Heck olefination of nonactivated aryl bromides demonstrating exceptional TONs up to 5.3×10^5 [84].

2.2.3 C(sp^3)-Metalated Diarylmethyl-Based Scaffolds

Investigation of the coordination preferences of bis(2-(diphenylphosphino)phenyl)methane (**64**) [90] and dipyromethane diphosphine (**65**) ligands [47] led to conclusion that eight-membered metallacycles formed upon their coordination to transition metals adopt a rigid boat-like conformation, where the *endo* C(sp^3)-bound hydrogen approaches the metal center and, therefore, create ideal situation for the metalation of the methylene bridge (Scheme 16). The representative complex **66**, synthesized in excellent yield from the reaction of **65** with Pd(COD)Cl₂, is a stable compound featuring natural geometry around the metal center.

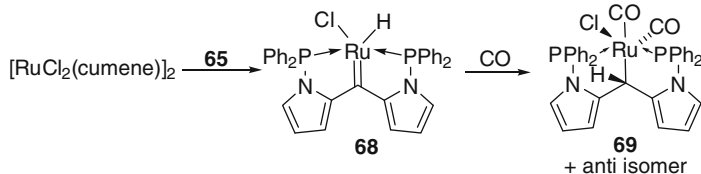
Despite initial expectations, α -proton abstraction leading to the formation of carbene complex was not facile in this particular case. However, abstraction of the formal hydride by the reaction of **66** with [Ph₃C]PF₆ afforded the cationic Pd(II) carbene/phosphine pincer complex **67** bearing the corresponding counterion.

Interestingly, the stability of the PC(sp^3)P pincer complexes of this type is metal dependent. For example, the reaction of **65** with [RuCl₂(cumene)]₂ proceeds directly and quantitatively to the formation of the carbene complex **68**, although exposure of the carbene product to CO regenerates C(sp^3)-metalated pincer demonstrating the reversibility of the 1,2-H shift (Scheme 17).

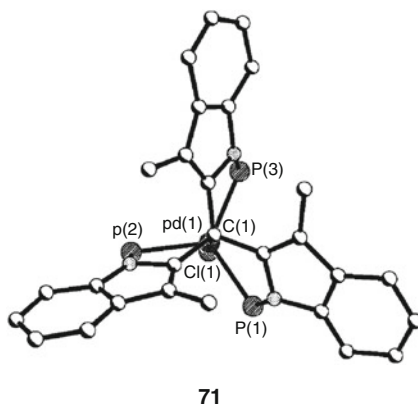
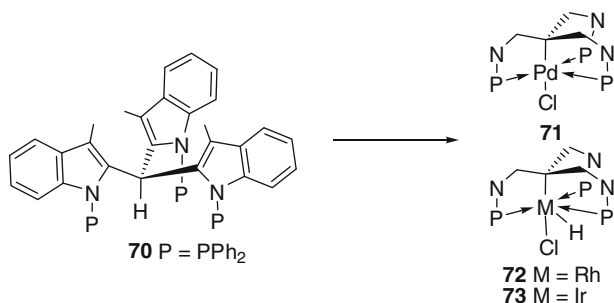
No catalytic activity was described for **66** and **69**.

2.2.4 C(sp^3)-Metalated Triarylmethyl-Based Scaffolds

Although it does not fit entirely the definition of pincer complexes, a very elegant C₃-symmetric C(sp^3)-metalated ligand developed by Lahuerta, Perez-Prieto, and



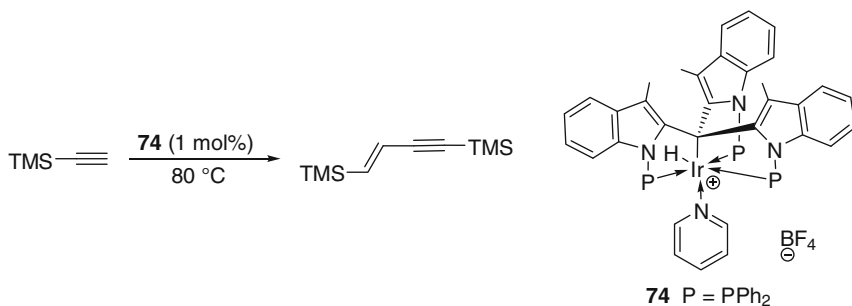
Scheme 17 Synthesis and chemical behavior of 68



Scheme 18 Synthesis of the $\text{C}(\text{sp}^3)$ metalated triarylmethyl-based pincer complexes

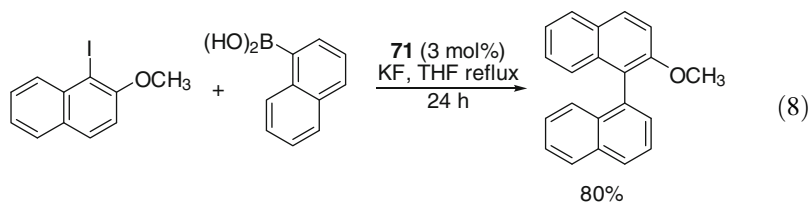
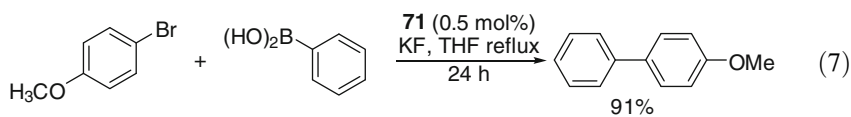
coworkers must be mentioned. They found that tris[1-(diphenylphosphino)-3-methyl-1H-indol-2-yl]methane **70** may be successfully metalated by $\text{PdCl}_2/\text{AgBF}_4$ [49], $[\text{IrCl}(\text{COE})]_2$ [91], or $\text{Rh}(\text{acac})(\text{CO})_2$ [92] resulting in the formation of the metalated species in very good yield (Scheme 18).

The view along the threefold molecular axis of, for example, the palladium complex **71** reveals the C_3 chirality of the system in the solid state. However, complexation to a chiral phosphine after successful conversion of **71** into the corresponding cationic species leads to the formation of a diastereomeric pair, which confirms that chirality retains in solution. Furthermore, separation of the

**Scheme 19** Dimerization of terminal alkynes catalyzed by **74**

enantiomers using chiral HPLC was possible. Neither of them was found to racemize after prolonged heating under reflux in THF solution.

Remarkably, the palladium complex **71** showed very nice activity in Suzuki coupling of aryl iodides and bromides demonstrating high yields of the cross-coupled products even with sterically demanding pairs of starting materials (Eqs. 7 and 8) [49].



Mechanism of the reaction has not been discussed in detail. However, active participation of nanoparticles was ruled out based on the results of the mercury test. In addition, according to the NMR and FAB GC–MS analysis, that showed presence of the single palladium organometallic species originating from chloride exchange in **71** by iodide or bromide (in accord with the halide present in the starting material), and taking into account the unusually crowded arrangement around the metal center, as well as its 18-electron configuration, σ -bond metathesis rather than Pd(II)/Pd(IV) pathway (Scheme 12) may be hypothesized.

More recently, the same group communicated on application of the square pyramidal iridium hydride complex **74** (derived from **73**/AgBF₄) as a catalyst for stereoselective dimerization of terminal alkynes (Scheme 19) [91].

Dibenzobarrelene-based PC(*sp*³)P pincer complexes were described by Gelman and coworkers (Fig. 10, left) [51]. Modularity, rigidity, and three-dimensionality were the three rationales behind employment of this particular structural motif for designing pincer compounds. First, unlike many known classes of PC(*sp*³)P pincer

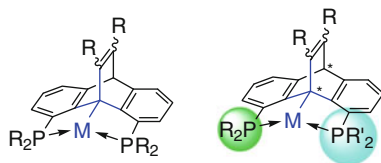
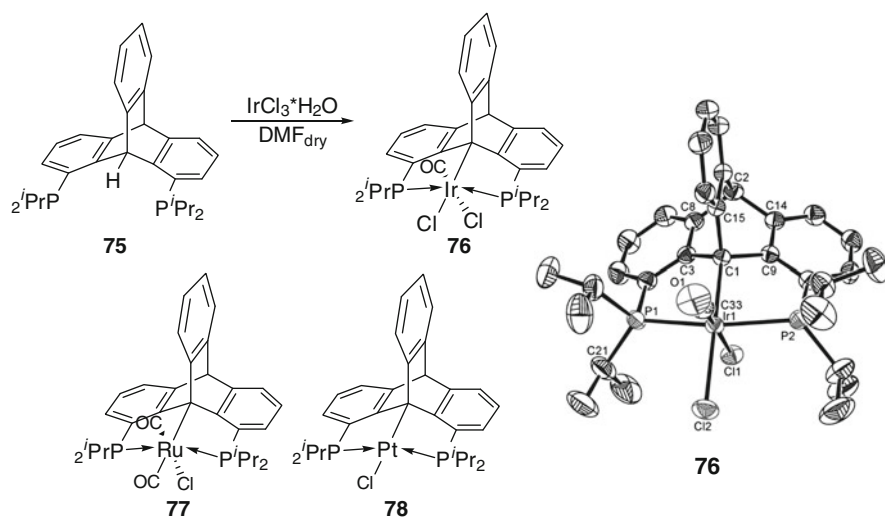


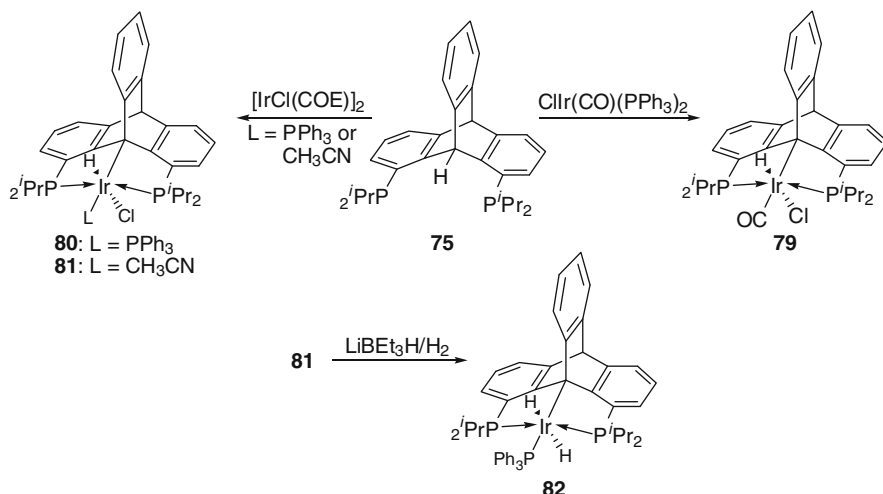
Fig. 10 Dimensionality of the dibenzobazzenelene-based pincer complexes



Scheme 20 Synthesis of the triptycene-based pincer complexes via C–H activation strategy

ligands, synthesis of dibenzobarrelene derivatives is very modular as accomplished through the use of reliable Diels–Alder cycloaddition methodology. In due course, facile access to readily modifiable platform will allow tailoring their steric and electronic properties. Second, rigidity of the almost all-aromatic frame and lack of labile α - and β -hydrogens will be translated into robustness and conformational stability, alongside with exceptional σ -donation of the metalated bridgehead sp^3 -hybridized carbon. (pK_a of the methine hydrogen in triptycene is ca. 44 vs. 33 of triphenylmethane, e.g., see [93].) Finally, unique topology of dibenzobarrelene molecules may, hopefully, be utilized to design chiral-at-frame pincer ligands providing more efficient chiral pocket compared to more conventional systems (Fig. 10, right).

The first representatives of the dibenzobarrelene-based $PC(sp^3)P$ pincer complexes were synthesized via traditional C–H activation strategy starting from 1,8-diphosphenotriptycene **75** [94–96] (Scheme 20) [51, 97]. For example, treatment of **75** with $IrCl_3 \cdot H_2O$ leads to the selective formation of **76** in high yield. According to X-ray analysis data, the iridium center in **76** adopts a slightly distorted octahedral coordination environment, with two nonequivalent chlorine atoms located in *trans* and *cis* positions with respect to the metalated carbon and to the



Scheme 21 Synthesis of the triptycene-based pincer complexed via oxidative addition

carbon monoxide ligand. Comparison of the iridium–chlorine bond lengths, *cis* and *trans* to $\text{C}(sp^3)\text{--M}$ bond, confirmed a strong *trans*-influence exerted by the sp^3 -carbon, indicating a possible lability of the *trans* chlorine. However, the most interesting structural feature of the new compound is an abnormal distortion of the metalated carbon C1 from its natural tetrahedral geometry. For example, the $\text{C}15\text{--C}1\text{--Ir}$ angle was found to be 127° (compared to 109° , as is normal for sp^3 -hybridized carbon). Remarkably, both octahedral ruthenium (**77**) and square planar platinum (**78**) complexes, synthesized via the same $\text{C}\text{--H}$ activation approach, feature similar structural properties. The complexes demonstrate excellent thermal stability decomposing at temperatures above 260°C and showing no structural mutations after prolonged heating in DMSO near to its boiling point.

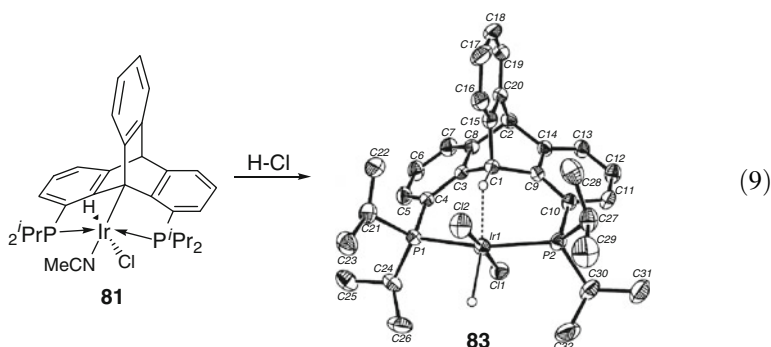
Iridium hydride complexes may be prepared via oxidative addition of low-valent iridium precursors such as $[\text{Ir}(\text{COE})\text{Cl}]_2$ or Vaska compound across the methine $\text{C}\text{--H}$ bond of **75** giving rise to the formation of **79–81**. The 18-electron complex **79** is quite inert due to the presence of the strongly bound CO ligand *trans* to the metalated $\text{C}(sp^3)$ donor [97], while **80** and **81** bearing more labile ligands can be converted into dihydride species **82** after treatment with superhydride (Scheme 21) [98].

As mentioned, these strikingly stable organometallic complexes possess a common structural feature—a strong deviation of the metal– $\text{C}(sp^3)$ bond from the geometry characteristic of sp^3 -hybridized atoms. For example, in the vast majority of the structurally defined complexes the $\text{C}\text{--C}(sp^3)\text{--M}$ bond ranges between 116° and 129° instead of the expected 109° . It has been suggested that this strong deformation may be reflected in a lability of the carbon–metal bond in the new three-dimensional $\text{PC}(sp^3)\text{Ps}$ despite the stabilizing “pincer effect.”

To check this hypothesis, possible heterolytic addition of HCl across the metal– $\text{C}(sp^3)$ bond in iridium (**81**) and platinum (**78**) complexes has been examined. Theoretical DFT calculations predicted that protonation of **81** by HCl is nearly

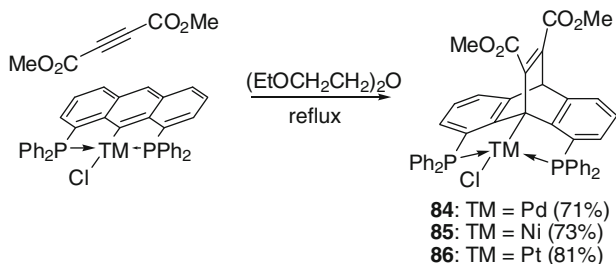
thermoneutral, while protonation of **78** is moderately exergonic ($DG_{rx} = 0.5$ kcal/mol for Ir, -4.3 kcal/mol for Pt) [99].

Indeed, it was found that treatment of **81** with gaseous HCl in $CDCl_3$ over 18 h at room temperature results in a gradual transformation of the starting material into the chelate complex **83** in which the metal center is surrounded with mutually *trans* coordinated phosphine and chloride ligands, while the *transoid* hydride and the methine proton complete the almost perfect pseudooctahedral geometry. The last proton was found in the difference Fourier map and refined. Although the location determined by X-ray analysis is not particularly accurate, the $H1 \cdots Ir$ and $Ir \cdots C1$ contacts are very short (1.89 and 2.696 Å, respectively), and, therefore, are definitely defined as agostic (Eq. 9). Similar transformation, albeit in a less selective fashion, was observed for **78**, proving that activation of small molecules may be achieved via 1,2-cleavage of the carbon–metal bond in PCP complexes possessing an appropriate topology. The reversed process of the regeneration of the carbon–metal bond via elimination of H–Cl is not surprising and is routinely used for the preparation of pincer complexes. Moreover, if these processes occur reversibly on a reasonable timescale they may have practical applications in catalysis.



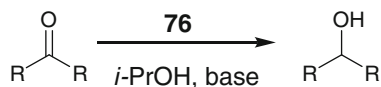
More diversity-oriented approach to the synthesis of the dibenzobarrelene-based $PC(sp^3)P$ pincer complexes was developed by the same group [100]. It was found that the desired structures may be accessed in one-step transformation of readily available and structurally simple anthracene-based 9- $C(sp^2)$ -metalated complexes [101] by means of Diels–Alder cycloaddition as depicted in Scheme 22. For example, **84** was synthesized in 71 % yield from the reaction of the known palladacycle and dimethyl acetylenedicarboxylate as a dienophile. Analogous transformations were performed using the Ni and Pt $C(sp^2)$ -cyclometalated precursors. The expected products **85** and **86** were isolated in 73 % and 81 % yield, respectively.

Thermogravimetric tests showed that the thermal stability of the new compounds is exceptional and in some cases exceeds the stability of $C(sp^2)$ -metalacycles. For example, the first weight loss detected for **84** takes place at 370 °C and this is 120 °C higher than for the parent compound. **85** and **86** also demonstrated decomposition points far over 280 °C.



Scheme 22 Synthesis of the dibenzobarcelene-based pincer complexes via cycloaddition approach

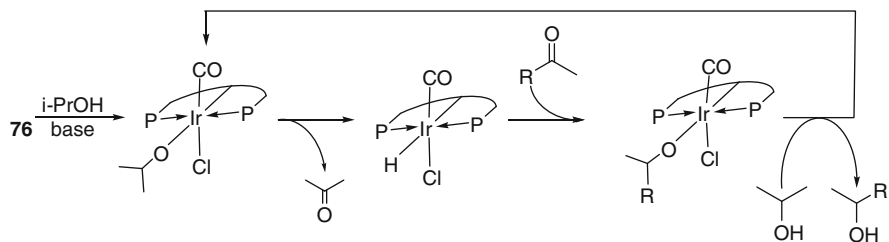
Table 1 Representative results in transfer hydrogenation of ketones by **76**



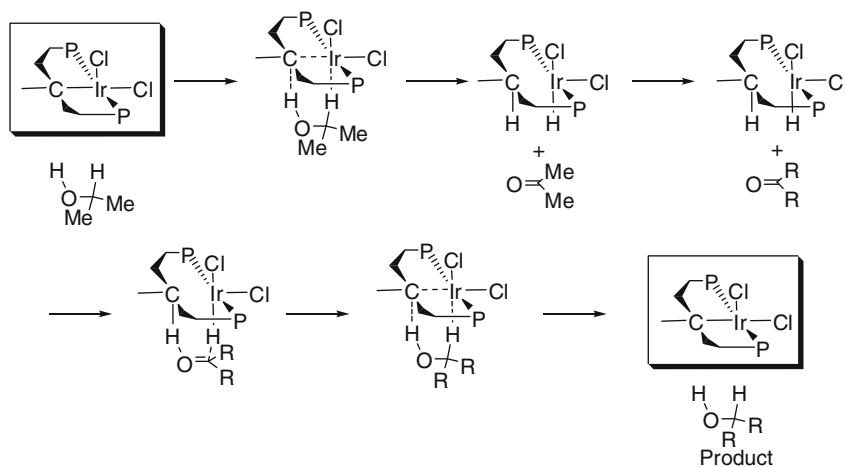
Run	Ketone	S/C	Time	TOF	Conv. %, (yield, %)
1	2'-chloroacetophenone	2,000/1	5 s	3.6×10^6	99 (98)
2	4'-bromoacetophenone	2,000/1	5 s	3.6×10^6	96 (95)
3	3'-bromoacetophenone	2,000/1	30 min	1.2×10^4	99 (98)
4	Acetophenone	2,000/1	30 min	1.2×10^4	94 (93)
5	2-acetonaphthone	2,000/1	30 min	1.2×10^4	95 (94)
6	Acetophenone	10,000/1	12 h	N/D	96 (95)
7	Acetophenone	100,000/1	48 h	N/D	94 (93)

Palladium-based PC(*sp*³)P **84** was found catalytically active. For example, Heck reaction between iodobenzene and *t*-butyl acrylate was driven to completion by only 0.001 mol% of **83** in 12 h which corresponds to at least 10^5 TON.

Other catalytic tests included transfer and acceptorless (de)hydrogenation chemistry. Thus, it was shown that iridium complexes **76** [51] and **79** [97] can efficiently catalyze transfer hydrogenation of ketones in isopropanol. The best results were achieved using 0.05 mol% of **76** under reflux conditions (Table 1). For example, injection of 2'-chloroacetophenone into a preheated solution of **76** (0.05 mol%) and NaOtBu (5 mol%) in isopropanol results in its rapid (<30 s) and essentially quantitative (>99 %) conversion into the corresponding alcohol under air. The turnover frequency (TOF) calculated for this run at 50 % conversion corresponds to $3.6 \times 10^6 \text{ h}^{-1}$ and is among the highest such values reported. The catalyst was also active at lower catalyst/substrate (C/S) ratios. For example, with the reduction in the concentration of **76** to 0.01 mol%, complete conversion was detected after 5 min with halogenated acetophenone substrates. However, the reduction of simple acetophenone proceeded rather slowly and complete conversion was achieved after 12 h. On the other hand, despite a lower TOF, the catalyst remains active



Scheme 23 Suggested mechanism for the transfer hydrogenation of ketones catalyzed by 76



Scheme 24 Alternative mechanism for the transfer hydrogenation of ketones catalyzed by 76

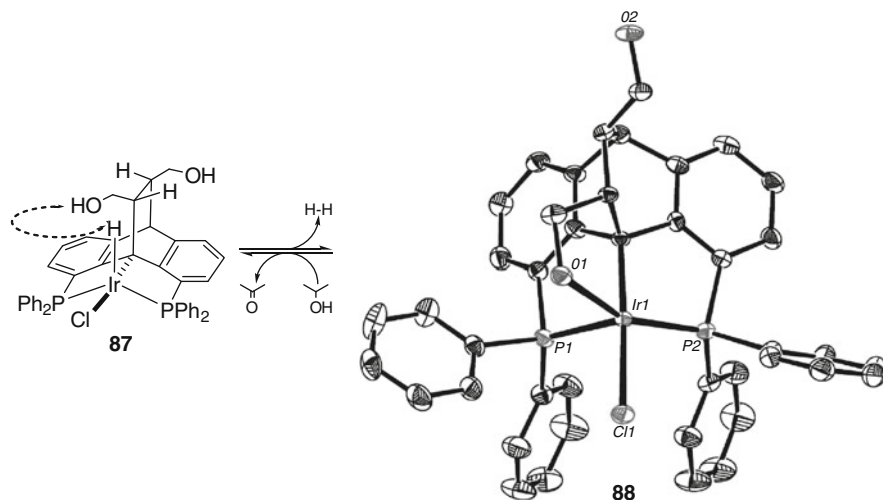
and the reaction goes to completion even under low catalyst loading conditions at 15 g scale ($C/S = 1:100,000$).

Based on isotopic labeling tests, it was suggested that the reaction is operated by the widely accepted monohydride mechanism, although steps such as ketone insertion into Ir–H bond and displacement of the product from Ir by the isopropoxide ligand might be greatly facilitated by a strong *trans*-influence imposed by the $C(sp^3)$ ligand (Scheme 23).

However, another interesting mechanism cannot be completely ruled out, particularly, on the background of the previously described activation of small molecules via 1,2-cleavage of the carbon–metal bond in these $PC(sp^3)P$ (e.g., Eq. 9). Based on this transformation, an alternative mechanistic scheme involving $C(sp^3)$ –metal bond cleavage/regeneration maybe suggested (Scheme 24).

Transfer dehydrogenation of alcohols to form ketones using the same catalytic system was also demonstrated [102].

Another study performed in the group aimed to demonstrate the advantage of three-dimensionality and molecular complexity for the design of multifunctional



Scheme 25 Metal-Ligand cooperation in **87**

catalytic systems [103]. To explore this possibility, iridium hydride pincer complex **87** possessing an acidic sidearm, which is capable of interacting with the catalytic site, was synthesized (Scheme 25).

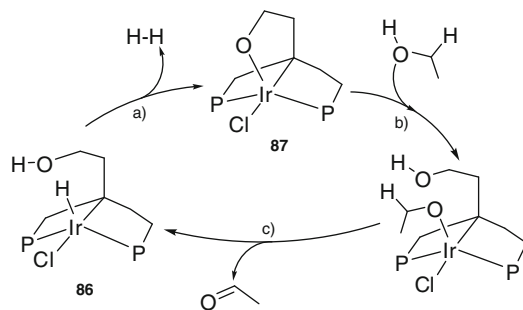
The complex **87** was prepared in three stages (1) the quantitative Diels–Alder cycloaddition of the known 1,8-bis-(diphenylphosphino)anthracene and dimethyl fumarate; (2) the reduction of the diester adduct; and (3) an essentially quantitative reaction of the resulting phosphine with [IrCl(COD)]₂.

Initial investigation of its properties revealed that **87** is moderately stable in solution and gradually, but selectively, transforms into a new compound upon extrusion of molecular hydrogen. Organometallic product of the transformation was identified as the arm-closed species **88**, which features strongly distorted trigonal bipyramidal geometry around the iridium center (Scheme 25). More interestingly, addition of isopropyl alcohol to the resulting solution of **88** recovers the parent **87**.

Remarkably, this simple stoichiometric experiment points to a hypothetical catalytic cycle through which the acceptorless dehydrogenation of alcohols may proceed (Scheme 26) (a) H₂-forming step, leading to the formation of the arm-closed iridium species **88**; (b) ligand exchange step, leading to the arm-open iridium alkoxide species; and (c) regeneration of the Ir–H catalyst **87** by β -hydride elimination with subsequent formation of the oxidized product.

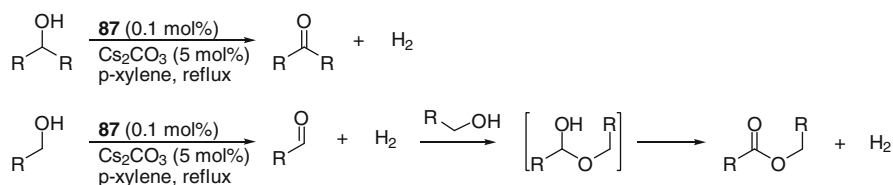
Indeed, this transformation was realized under catalytic conditions: 0.1 mol% of **87** in the presence of 5 mol% of Cs₂CO₃ dehydrogenate secondary alcohols into ketones in boiling *p*-xylene over 6 h.

The acceptorless dehydrogenation of primary alcohols and diols could also be catalyzed using **87**, but led to the formation of the corresponding esters and lactones. Mechanistically, formation of these Tischenko products can be rationalized,



Scheme 26 Proposed catalytic cycle for the acceptorless dehydrogenation of alcohols catalyzed by **87**

Table 2 Representative results in acceptorless dehydrogenation of alcohols by **87**



Run	Alcohol	Time	Product	Yield
1	1-phenylethanol	6	Acetophenone	94
2	Diphenylmethanol	12	Benzophenone	93
3	Octan-2-ol	6	Octan-2-one	92
4	L-carveol	12	Dihydrocarvones (1:1:1 mixture)	84
5	1,2-phenylenedimethanol	12	Benzofuran-2(3H)-one	99
6	Butane-1,4-diol	12	γ -butyrolactone	96
7	Diethylene glycol	12	1,4-dioxan-2-one	96
8	Benzyl alcohol	18	Benzyl benzoate	96
9	4-chlorobenzyl alcohol	36	4-chlorobenzyl 4'-chlorobenzoate	92
10	2-chlorobenzyl alcohol	36	2-chlorobenzyl 2'-chlorobenzoate	88
11	4-methylbenzyl alcohol	36	4-methylbenzyl 4'-methylbenzoate	94
			4-methylbenzaldehyde (4:1)	

as in previously published works [104] by tandem dehydrogenation/hemiacetalization/dehydrogenation reactions (Table 2).

3 Conclusion

In this chapter, recent developments in the chemistry of PC(*sp*³)P pincer complexes are described. Several principally different classes of ligands, alkyl chain-, cycloalkane-, cycloheptatriene-, arylmethanes-, and dibenzobarrelene-based platforms serve as suitable preligands for the construction of the desired compounds.

It is evident that structural uniqueness of the C(*sp*³)-based ligands is reflected in singular electronic/steric properties and reactivity of their complexes. Therefore, in the near future we expect the emergence of new PC(*sp*³)P pincers tailored to address manifold practical applications in different areas of chemistry.

References

1. Shaw BL (1975) *J Am Chem Soc* 97:3856
2. Dehand J, Pfeffer M (1976) *Coord Chem Rev* 18:327
3. Newkome GR, Puckett WE, Gupta VK, Kiefer GE (1986) *Chem Rev* 86:451
4. Moreno I, SanMartin R, Ines B, Churruca F, Dominguez E (2010) *Inorg Chim Acta* 363:1903
5. van Koten G (1989) *Pure Appl Chem* 61:1681
6. Benito-Garagorri D, Kirchner K (2008) *Acc Chem Res* 41:201
7. Mayer HA, Kaska WC (1994) *Chem Rev* 94:1239
8. Morales-Morales D (2008) Reactivity of pincer complexes toward carbon monoxide Wiley-VCH Verlag GmbH & Co. KGaA p 27
9. Limberg C (2009) *Angew Chem Int Ed* 48:2270
10. Jensen CM (1999) *Chem Commun* 2443
11. van der Boom ME, Milstein D (2003) *Chem Rev* 103:1759
12. Choi J, MacArthur AHR, Brookhart M, Goldman AS (2011) *Chem Rev* 111:1761
13. Gunanathan C, Milstein D (2011) *Acc Chem Res* 44:588
14. Selander N, Szabo KJ (2011) *Chem Rev* 111:2048
15. Albrecht M, van Koten G (2001) *Angew Chem Int Ed* 40:3750
16. Slagt MQ, van Zwieten DAP, Moerkerk AJCM, Klein Gebbink RJM, van Koten G (2004) *Coord Chem Rev* 248:2275
17. Lang H, Packheiser R, Walfort B (2006) *Organometallics* 25:1836
18. Wieczorek B, Dijkstra HP, Egmond MR, Klein Gebbink RJM, van Koten G (2009) *J Organomet Chem* 694:812
19. Guillena G, Kruihof CA, Casado MA, Egmond MR, van Koten G (2003) *J Organomet Chem* 668:3
20. Stiriba S-E, Slagt MQ, Kautz H, Klein Gebbink RJM, Thomann R, Frey H, van Koten G (2004) *Chem Eur J* 10:1267
21. Gerhardt WW, Zuccherro AJ, Wilson JN, South CR, Bunz UHF, Weck M (2006) *Chem Commun* 20:2141
22. Chen Y, Li K, Lu W, Chui SS-Y, Ma C-W, Che C-M (2009) *Angew Chem Int Ed* 48:9909
23. Suijkerbuijk BMJM, Schamhart DJ, Kooijman H, Spek AL, van Koten G, Klein Gebbink RJM (2010) *Dalton Trans* 39:6198
24. Moulton CJ, Shaw BL (1976) *J Chem Soc Dalton Trans* 1020
25. Creaser CS, Kaska WC (1978) *Inorg Chim Acta* 30:L325
26. van Koten G, Timmer K, Noltes JG, Spek AL (1978) *J Chem Soc Chem Commun* 250
27. van de Kuil LA, Luitjes H, Grove DM, Zwikker JW, van der Linden JGM, Roelofsens AM, Jenneskens LW, Drenth W, van Koten G (1994) *Organometallics* 13:468

28. Mohammad HAY, Grimm JC, Eichele K, Mack H-G, Speiser B, Novak F, Quintanilla MG, Kaska WC, Mayer HA (2002) *Organometallics* 21:5775
29. Riehl JF, Jean Y, Eisenstein O, Pelissier M (1992) *Organometallics* 11:729
30. Crocker C, Empsall HD, Errington RJ, Hyde EM, McDonald WS, Markham R, Norton MC, Shaw BL, Weeks B (1982) *J Chem Soc Dalton Trans* 1217
31. Errington RJ, McDonald WS, Shaw BL (1982) *J Chem Soc Dalton Trans* 1829
32. Vigalok A, Milstein D (2000) *Organometallics* 19:2061
33. Tulloch AAD, Danopoulos AA, Tizzard GJ, Coles SJ, Hursthouse MB, Hay-Motherwell RS, Motherwell WB (2001) *Chem Commun* 1270
34. Nielsen DJ, Cavell KJ, Skelton BW, White AH (2002) *Inorg Chim Acta* 327:116
35. Danopoulos AA, Tulloch AAD, Winston S, Eastham G, Hursthouse MB (2003) *Dalton Trans* 1009
36. Diez-Barra E, Guerra J, Lopez-Solera I, Merino S, Rodriguez-Lopez J, Sanchez-Verdu P, Tejada J (2003) *Organometallics* 22:541
37. Lee HM, Zeng JY, Hu C-H, Lee M-T (2004) *Inorg Chem* 43:6822
38. Nilsson P, Wendt OF (2005) *J Organomet Chem* 690:4197
39. Ma L, Woloszynek RA, Chen W, Ren T, Protasiewicz JD (2006) *Organometallics* 25:3301
40. Olsson D, Arunachalampillai A, Wendt OF (2007) *Dalton Trans* 5427
41. Morgan BP, Galdamez GA, Gilliard RJ Jr, Smith RC (2009) *Dalton Trans* 2020
42. Niu J-L, Hao X-Q, Gong J-F, Song M-P (2011) *Dalton Trans* 40:5135
43. Mayer HA, Fawzi R, Steimann M (1993) *Chem Ber* 126:1341
44. Gerber R, Fox T, Frech C (2010) *Chem Eur J* 16:6771
45. Nemeš S, Flesher RJ, Gierling K, Maichle-Moessmer C, Mayer HA, Kaska WC (1998) *Organometallics* 17:2003
46. Gozin M, Weisman A, Ben-David Y, Milstein D (1993) *Nature* 364:699
47. Weng W, Parkin S, Ozerov OV (2006) *Organometallics* 25:5345
48. Hoskins SV, Rickard CEF, Roper WR (1984) *J. Chem Soc, Chem Commun* 1000
49. Ciclosi M, Lloret J, Estevan F, Lahuerta P, Sanau M, Perez-Prieto J (2006) *Angew Chem Int Ed* 45:6741
50. Koridze AA, Polezhaev AV, Safronov SV, Sheloumov AM, Dolgushin FM, Ezernitskaya MG, Lokshin BV, Petrovskii PV, Peregudov AS (2010) *Organometallics* 29:4360
51. Azerraf C, Gelman D (2008) *Chem Eur J* 14:10364
52. Empsall HD, Hyde EM, Markham R, McDonald WS, Norton MC, Shaw BL, Weeks B (1977) *J Chem Soc Chem Commun* 589
53. Crocker C, Errington RJ, McDonald WS, Odell KJ, Shaw BL, Goodfellow RJ (1979) *J Chem Soc Chem Commun* 498
54. Gusev DG, Lough AJ (2002) *Organometallics* 21:2601
55. Gusev DG, Lough AJ (2002) *Organometallics* 21:5091
56. Al-Salem NA, Empsall HD, Markham R, Shaw BL, Weeks B (1979) *J Chem Soc Dalton Trans* 1972
57. Castonguay A, Sui-Seng C, Zargarian D, Beauchamp AL (2006) *Organometallics* 25:602
58. Zhao J, Goldman AS, Hartwig JF (2005) *Science* 307:1080
59. Bursten BE, Chen S, Chisholm MH (2008) *J Organomet Chem* 693:1547
60. Huang Z, Zhou J, Hartwig JF (2010) *J Am Chem Soc* 132:11458
61. Vigalok A, Ben-David Y, Milstein D (1996) *Organometallics* 15:1839
62. McLoughlin MA, Keder NL, Harrison WTA, Flesher RJ, Mayer HA, Kaska WC (1999) *Inorg Chem* 38:3223
63. Huang K-W, Han JH, Musgrave CB, Fujita E (2007) *Organometallics* 26:508
64. Vigalok A, Kraatz H-B, Konstantinovskiy L, Milstein D (1997) *Chem Eur J* 3:253
65. Zhou J, Hartwig JF (2008) *Angew Chem Int Ed* 47:5783
66. Pandarus V, Zargarian D (2007) *Chem Commun* 978
67. Pandarus V, Zargarian D (2007) *Organometallics* 26:4321
68. Castonguay A, Beauchamp AL, Zargarian D (2008) *Organometallics* 27:5723

69. Castonguay A, Spasyuk DM, Madern N, Beauchamp AL, Zargarian D (2009) *Organometallics* 28:2134
70. Mayer HA, Kaska WC (1990) *Chem Ber* 123:1827
71. Sjoevall S, Wendt OF, Andersson C (2002) *J Chem Soc Dalton Trans* 1396
72. Kuznetsov VF, Lough AJ, Gusev DG (2006) *Inorg Chim Acta* 359:2806
73. Olsson D, Janse VRJM, Wendt OF (2007) *Acta Crystallogr Sect E Struct Rep Online* E63:m1969
74. Arunachalampillai A, Olsson D, Wendt OF (2009) *Dalton Trans* 8626
75. Olsson D, Wendt OF (2009) *J Organomet Chem* 694:3112
76. Gerber R, Blacque O, Frech C (2009) *ChemCatChem* 1:393
77. Gerber R, Blacque O, Frech CM (2011) *Dalton Trans* 40(35):8996
78. Djakovitch L, Koehler K, de VJG (2008) *The role of palladium nanoparticles as catalysts for carbon-carbon reactions*. Wiley-VCH Verlag GmbH & Co. KGaA p 303
79. Winter AM, Eichele K, Mack H-G, Kaska WC, Mayer HA (2005) *Organometallics* 24:1837
80. Winter AM, Eichele K, Mack H-G, Kaska WC, Mayer HA (2008) *Dalton Trans* 527
81. Rybtchinski B, Vigalok A, Ben-David Y, Milstein D (1996) *J Am Chem Soc* 118:12406
82. van der Boom ME, Kraatz H-B, Hassner L, Ben-David Y, Milstein D (1999) *Organometallics* 18:3873
83. van der Boom ME, Liou S-Y, Shimon LJW, Ben-David Y, Milstein D (2004) *Inorg Chim Acta* 357:4015
84. Ohff M, Ohff A, van der Boom ME, Milstein D (1997) *J Am Chem Soc* 119:11687
85. Gozin M, Alzenberg M, Liou S-Y, Weisman A, Ben-David Y, Milstein D (1994) *Nature* 370:42
86. Cohen R, van der Boom ME, Shimon LJW, Rozenberg H, Milstein D (2000) *J Am Chem Soc* 122:7723
87. Sundermann A, Uzan O, Milstein D, Martin JML (2000) *J Am Chem Soc* 122:7095
88. Cohen R, Milstein D, Martin JML (2004) *Organometallics* 23:2336
89. Cao Z, Hall MB (2000) *Organometallics* 19:3338
90. Lesueur W, Solari E, Floriani C, Chiesi-Villa A, Rizzoli C (1997) *Inorg Chem* 36:3354
91. Ciclosi M, Estevan F, Lahuerta P, Passarelli V, Perez-Prieto J, Sanau M (2008) *Adv Synth Catal* 350:234
92. Ciclosi M, Estevan F, Lahuerta P, Passarelli V, Perez-Prieto J, Sanau M (2009) *Dalton Trans* 2290
93. Schwartz LH (1968) *J Org Chem* 33:3977
94. Grossman O, Azerraf C, Gelman D (2006) *Organometallics* 25:375
95. Ahlers W, Roeper M, Hofmann P, Warth DCM, Paciello R (2001) BASF A.-G., Germany p 51
96. Schnetz T, Roeder M, Rominger F, Hofmann P (2008) *Dalton Trans* 2238
97. Azerraf C, Gelman D (2009) *Organometallics* 28:6578
98. Azerraf C (2010) PhD thesis, The Hebrew University
99. Musa S, Romm R, Azerraf C, Kozuch S, Gelman D (2011) *Dalton Trans* 40(35):8760
100. Azerraf C, Shpruhman A, Gelman D (2009) *Chem Commun* 466
101. Haenel MW, Jakubik D, Krueger C, Betz P (1991) *Chem Ber* 124:333
102. Levy R, Azerraf C, Gelman D, Rueck-Braun K, Kapoor PN (2009) *Catal Commun* 11:298
103. Musa S, Shaposhnikov I, Cohen S, Gelman D (2011) *Angew Chem Int Ed* 50:3533
104. Zhang J, Leitus G, Ben-David Y, Milstein D (2005) *J Am Chem Soc* 127:10840

Physical and Materials Applications of Pincer Complexes

Jennifer L. Hawk and Stephen L. Craig

Abstract Pincer complexes have been shown to be widely useful and versatile in organic synthesis and catalysis, but they have also been employed in a wide range of intriguing physical and materials applications. The capacity for selective and directional metal–ligand coordination offers a tool for construction and function. Pincer complexes have been successfully used as a means for templating macrocycles, assembling metallodendrimers, functionalizing surfaces, and functionalizing polymer chains. Furthermore, pincer complexes have proven to be useful mechanistic probes of polymer physical processes, linear polymers, networks, cross-linked brushes, films, and gels. Recently, the activity of pincer complexes has extended into the realm of mechanochemistry, with applications in fundamental mechanistic studies as well as mechanocatalysis. This chapter explores the use of pincer metal–ligand coordination events in these various physical and materials contexts.

Keywords Mechanochemistry · Metallodendrimers · Physical applications · Pincer kinetics

Contents

1	Pincer–Ligand Coordination as a Materials Construction Tool	321
1.1	Building Metallodendrimers	321
1.2	Building Films and Surface Patterns with Pincer Complexes	325
1.3	Functionalizing Existing Polymer Chains	327
1.4	Metallodendrimers as Templates	331

2	Probing the Kinetic Influence of Pincer Coordination	333
2.1	Supramolecular Polymer Chains	334
2.2	Reversible Networks	336
2.3	Hybrid Gels: Combination of Covalent and Reversible Cross-Linkers	342
2.4	Mechanochemical Applications of Pincer Complexes	343
3	General Conclusions	348
	References	348

The broad utility of pincer complexes in various synthetic applications is complemented by their potential for use in a wide variety of physical applications. These applications derive from the ability of pincer complexes to participate in metal–ligand coordination events that offer both selectivity and strength. Pincer complexes that contain either Pd^{II} or Pt^{II} metal centers are often used because of their particular affinities for pyridines, nitriles, and phosphines [1]. As described below, the accessibility and diversity afforded by these metal–ligand coordination events provide opportunities for applications in polymer science, nanoscience, and materials science.

The utility of pincer complexes can broadly be divided into two categories: one in which they provide a purely (or largely) structural component, and a second in which they contribute a specific behavior of function that translates into material properties. Many applications obviously fall into both categories, but we employ this categorization in the organization of this chapter. At the level of structural manipulation, the metal–ligand coordination of the pincer complexes can be used as the primary mechanism to bring together small individual units to build a larger structure. Examples include the construction of various nanostructures such as metallo-dendrimers [2] and complex rosette architectures [3]. These specific interactions have also been used to functionalize existing polymer chains with specifically designed pendant ligand groups [4]. Placement of the pincer complexes along the polymer chains allows for easy side chain modifications.

On the functional end of the spectrum, pincer complexes can be used as a probe for understanding the kinetic influences of physical (i.e., supramolecular) associations on polymer properties [5]. Systems to which the probes have been applied include linear polymers [5], networks [6], cross-linked brushes [7], films [8], and gels [9]. By making small changes in the chemical structure of the pincer complexes, the kinetics of the interaction can be varied [10]. Studying the resulting changes in physical properties offers insight into the role of the kinetics of these metal–ligand associations, bearing direct relevance for future material design. The complexes have also found use in polymer mechanochemistry, further highlighting their versatility. This chapter will explore the utility of the pincer complexes: in creating complex structures through metal–ligand coordination, applications in molecular and material design, and investigation of the dependence of physical properties on molecular kinetics.

1 Pincer–Ligand Coordination as a Materials Construction Tool

A principle physical and materials application of pincer complexes is to employ their ligand coordination behavior as a construction tool. Pincer complexes have been successfully used to create a number of desired structures. These structures range in complexity from simple supramolecular chains [5] to complex nanostructures [11], surface patterns [12], and even thin films [13]. In addition to building new structures, pincer complexes can be employed to modify existing structures such as polymer backbones [1]. In these pursuits, pincer coordination offers some advantages over other traditional synthetic methods, and those advantages will be discussed in the context of specific examples, where appropriate.

1.1 Building Metallodendrimers

Current fabrication technologies often strive to create ever smaller structures. Often, methods for fabricating nanomaterials rely on a top-down approach that can be complemented by using chemistry to build up from the atomic level. In bottom-up materials design, specific and directional supramolecular interactions are often utilized as the glue through which to achieve the desired geometries of the nanostructures [14]. Self-assembly of this type is a popular and effective method for bottom-up synthesis, and pincer complexes have proven to be useful in this regard, by relying on the physical interactions of the metal–ligand coordination to drive assembly. Dendrimers are one example of nanostructures “with highly branched architecture leading to spherical shapes combined with high molecular weights” [15] that have been built successfully using branched pincer complexes.

There are two main methods for constructing metallodendrimers. One is a purely divergent technique. A divergent synthesis requires starting from the center of the structure and building out layer by layer [16], and it is by far the most common assembly technique. Divergent methods have been used in other construction motifs outside of self-assembly. Utilizing pincer complexes in divergent synthesis is a simple, yet elegant way to build different types of metallodendrimers. Additional complexity can be incorporated into the metallodendrimers by utilizing a convergent assembly method [16]. Convergent assembly brings previously established structures together. A beautiful example of convergent construction is demonstrated when metallodendrimer wedges are brought together using additional hydrogen bonds [16]. There are many other examples of convergent assembly methods that rely on covalently cross-linked wedges or other coordination techniques.

Whether utilizing a purely divergent or a combination of divergent and convergent techniques, pincer-based self-assembly of metallodendrimers is a prime example of the pincer’s usefulness as a construction tool. Pincer complexes offer a consistent and reliable platform for building intricate supramolecular structures.

Fig. 1 Chemical structure of the three-pronged repeating unit used to form metallo dendrimers. Two prongs contain pincer complexes, and the third contains a ligand for coordination to other units

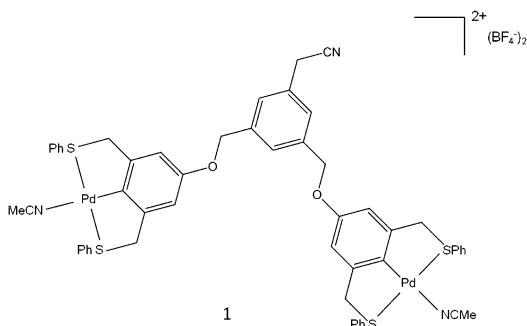
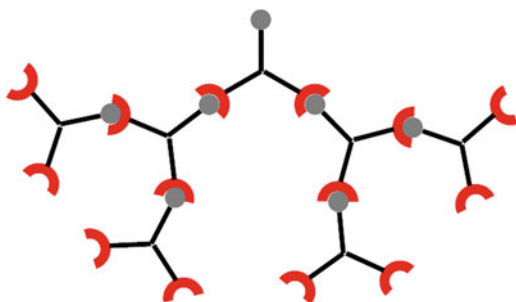


Fig. 2 Cartoon representation of a self-assembled metallo dendrimer built out to the second level. Curved wedges and balls represent pincer complexes and coordinating ligands, respectively



In this section, we explore some of the physical implications and considerations of using pincer complexes to build metallo dendrimers.

1.1.1 Branched Structures Using Pincer Complexes

The first example of pincer complexes being used to build dendritic nanospheres with well-controlled size distribution was demonstrated in 1995 by Huck et al. [14]. The core structure was a traditional tridentate pincer complex coordinated to the nitrile of an organic ligand. The coordination geometry of nitriles and similar ligands to the pincer Pd^{II} center is that of a square planar complex. The smallest unit (monomer) of a repeating dendritic structure was constructed by including three coordinations-ready prongs: two pincer complexes and one cyanomethyl group (Fig. 1).

When a solution of the repeat unit **1**, Fig. 1, is heated in nitromethane, the coordinating solvent molecules (acetonitrile) evaporate and the cyanomethyl group from a separate unit is replaced as the fourth coordinating ligand around one of the Pd^{II} centers. This coordination of the nitrile from one monomeric unit to the pincer motif of another results in a continuous branching pattern, shown out to the second level in Fig. 2.

The coordination can be followed using FT-IR spectroscopy to monitor the shift in the characteristic peak of the C≡N bond; the uncoordinated nitrile stretch at

$2,250\text{ cm}^{-1}$ shifts to a value of $2,290\text{ cm}^{-1}$ upon coordination [14]. The addition of small amounts of acetonitrile breaks the dendrimers apart and regenerates the original monomer. This result highlights how the spheres retain the reversibility of the pincer complex, in contrast to the irreversible nature of covalent bonds. As with other supramolecular interactions, reversibility of this sort is one of the main advantages achieved when using pincer complexes as a construction tool. Reversibility provides both advantages in synthesis (error correction) and performance (e.g., stimulus response) that might be useful for certain applications.

Further characterization allowed the size and shape of the presumed dendritic assemblies to be determined. Quasi-elastic light scattering (QELS) indicated that the hydrodynamic diameter of the assemblies in solution is 200 nm [14]. In addition, the assemblies were deposited onto surfaces and characterized by atomic force microscopy (AFM) in the solid state; the diameter of the spheres measured by AFM on the surfaces was on average 205 nm, in excellent agreement with the solution measurements. Both gold and glass surfaces were employed in the AFM experiments to show that the material of the surface did not dictate the size or shape of the assemblies. Lastly, transmission electron microscopy (TEM) was used to determine the size of the globular structures that resulted after the evaporation of the solution on a carbon-coated copper grid. The TEM results gave diameters in the range of 150–200 nm, a value that is consistent with both the QELS and AFM data. Branching was shown to be essential to the building of these spheres; when nonbranched complexes of similar composition were exposed to the same assembly conditions, no globular structures were observed by TEM [14].

The initial work described above demonstrated that pincer complexes are useful building blocks for the divergent construction of dendritic nanospheres, proving a new construction motif and concept for the synthesis of dendritic architectures. The relative ease of construction and multiple handles for structural variation on the molecular level suggested that pincer complexes might be used to produce more complicated and intricately designed structures. Further studies, described below, determined what factors influenced this method of construction and what limitations are inherent to the methodology.

1.1.2 Controlling the Size of Metallodendrimers

In later work, Huck et al. [2, 3] showed that they could extend the concepts developed in the first metallodendrimer system to build larger systems with the same repeating unit. They were also able to investigate what variables dictated the size of these branching structures. A modified approach was taken, built upon a similar but slightly modified repeat unit. Unlike the first system, composed of only the repeating unit, the metallodendrimer synthesis was initiated from a core unit that remains at the center of the dendrimer throughout its synthesis.

This core unit is similar in structure to the repeat unit **1** utilized above, but it has three pincer Pd^{II} complexes instead of two. The pincer complexes are initially protected with a chloride ligand, as chloride is not displaced by nitrile and it therefore prevents coordination by cyano groups from the other monomers.

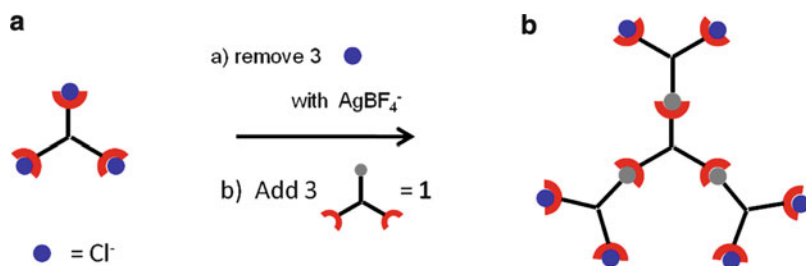


Fig. 3 Representation of the core unit (a) and the first layer of the divergent dendrimer (b) built with a branched pincer structure. The chloride ions act as a protecting group that inhibits undesired coordination. *Curved wedges* represent the pincer moieties

Growth is then activated with the addition of a silver salt of a weakly coordinating anion, e.g., AgBF_4 . The precipitation of AgCl leaves behind the non-coordinating BF_4^- , which allows a cyano-substituted, *bis*-PdCl pincer complex to add to the three sites of the core (Fig. 3). The deprotection/coordination cycle can be repeated to add additional generations or layers [2], and the methodology provides a very controlled process for iterative, divergent metallodendrimer synthesis. Although not discussed further here, the larger blocks constructed using this approach can be further combined using hydrogen bonds to build rosette structures [3]. The ability to simultaneously exploit hydrogen bonding and pincer–ligand coordination as orthogonal assembly motifs has also been advantageous in polymer modification, as discussed in later sections.

The counter ion that is introduced during the deprotection step influences the limiting sphere size that can be obtained with this methodology [11]. When larger polyatomic ions (ClO_4^- , PF_4^- , CF_3SO_3^- , *p*- $\text{MeC}_6\text{H}_4\text{SO}_3^-$, and BPh_4^-) were introduced as their corresponding silver salts, the bulkier counterions tended to be limited to smaller assemblies, as characterized by QELS, AFM, and TEM. The authors speculate that the correlation is a result of the overall charge distribution of the assembly, presumably as a consequence of the larger ions eventually becoming unable to fit inside the highly charged dendrimer or because the larger anions are less effective at shielding a growing number of cation–cation repulsions.

1.1.3 Physical Parameters to Consider When Building Metallodendrimers

Several common characteristics are seen in the dendritic systems, including that they meet the obvious requirement that each individual building block or repeating unit must contain all of the necessary information for complete self-assembly (i.e., both the pincer and the ligand) [17]. The orientation and components of these units can be varied, but they must be able to form the branched structures without additional materials or outside intervention. By building the individual units to contain all the necessary information, the ultimate assembly process is simplified and allows for structures to form quickly and easily.

Whereas the core pincer metal–ligand construction motif is held constant, different specific pincer complexes can be used to make similar metallodendrimers of varying structures. The SCS-pincer structure has traditionally been used for self-assembly applications, but the pincers can be converted to PCP structures in order to incorporate different transition metals. In addition to Pd^{II}, Ni^{II} and Pt^{II} have been effectively used to build other dendritic structures. These metals all have similar behavior, due to a shared square planar coordination geometry [15].

Overall, a wide variety of structures can be built with various pincer complexes, which have shown themselves to be highly useful for the construction of metallodendrimers. By harnessing the metal–ligand coordination event, they provide a simple and specific interaction that is robust under many conditions. Although the focus of this chapter is on applications at the interface of polymers and materials, we note that a range of other self-assembled structures have been formed using pincer coordination [18–21].

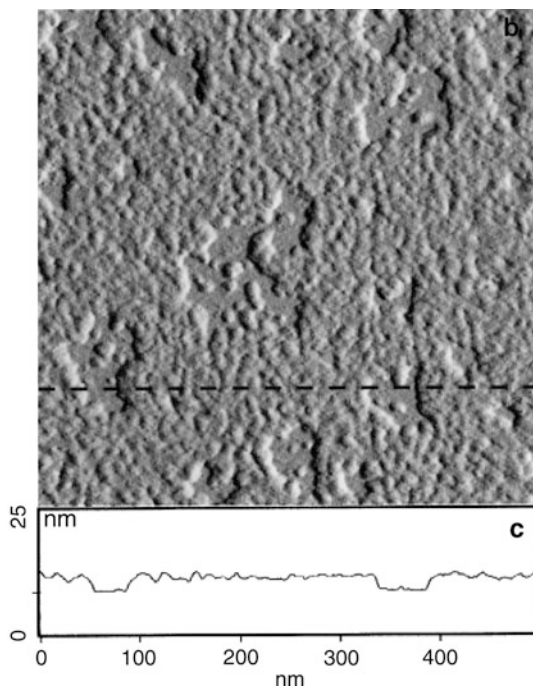
1.2 Building Films and Surface Patterns with Pincer Complexes

Because pincer coordination complexes can be quite strong, easy to work with, and maintain the reversible nature desired for construction, they offer an intriguing combination of potential uses within the materials arena. They offer a useful method for the physical construction of systems that have mechanical integrity, so that ultimately they might be developed into useful materials. The structural integrity of pincer-based metallodendrimers, for example, allows them to be spin-cast from solution to form molecularly thin films, which offer a wide variety of potential applications in material science [13]. Metallodendrimers of the fifth generation (Fig. 3) generated films of ~4 nm thickness as characterized by AFM and TEM (Fig. 4).

Another application of pincer-based assembly is found in surface patterning, for which existing techniques are often time consuming and costly. Developing a fast and simple method for functional surface patterning is an ongoing goal in the field of nanoscience. Metallodendrimers were linked to a surface by modifying them with long sulfide chains for attachment to gold surfaces [12]. These dendrimer tethers can then be inserted into a self-assembled monolayer on a gold surface at defect sites (essentially holes in the monolayer) that form during monolayer self-assembly. The dendrimer attachment pattern can be characterized using AFM [12]. The overall density and positions of the dendrimers are controlled using different techniques for the monolayer. Direct positioning of pendant groups using pincer complex affinity was posited to be useful for future surface patterning techniques [12].

In addition to serving as a critical structural unit in metallodendrimers for film and surface pattern fabrication, pincer complexes have also been employed as the primary structural “glue” for multilayer film deposition. The so-called Coordination Polymer Multilayer (CoPM) technique features polymer chains with pincer units incorporated along the backbone [22]. The CoPM strategy is shown in Fig. 5.

Fig. 4 Tapping scanning force micrographs of a non-closed molecular film of fifth generation metalodendrimer that was prepared by spin-casting a dilute solution of dendrimers in nitromethane onto a freshly cleaved surface. Reproduced from [13] with permission from Copyright © 1998 John Wiley and Sons



The pincer complex is linked via a tether to the backbone of a polymer synthesized by ring-opening metathesis polymerization (ROMP). The coordinating pyridine ligand is displayed as a side chain functionality on the second polymeric component, poly(vinyl pyridine) (PVP). CoPMs are synthesized by the alternating deposition of these two complementary polymeric components, in a process inspired by electrostatic layer-by-layer deposition. The ability to construct the CoPMs arises directly from the Pd^{II} pincer's responsiveness, inertness towards unwanted functionalities, and specific strength of coordination towards pyridine, in addition to its chemical compatibility with the ROMP conditions. The CoPMs are comparable in strength, durability, and stability to their covalent multilayer counterparts. Interestingly however, the CoPMs exhibit many responsive behaviors that are similar to polyelectrolyte multilayers, whose durability is not as great [22].

In contrast to building multilayers from polymer chains with the pincer monomers in the backbone, small molecule pincer complexes have also been used to cross-link layers of PVP chains [8]. The combination of PVP and pincer cross-linkers produces uniform films in nonaqueous environments. The structure and properties of these films can easily be modified by changing the solution concentrations and molecular weight of the PVP chains, adding competing ligands, or changing the pH. Figure 6 shows how different layers of polymers can be brought together by the coordination of the free small molecule, *bis*-pincer complex. Both types of multilayers offer interesting potential for building films of different desired properties [8].

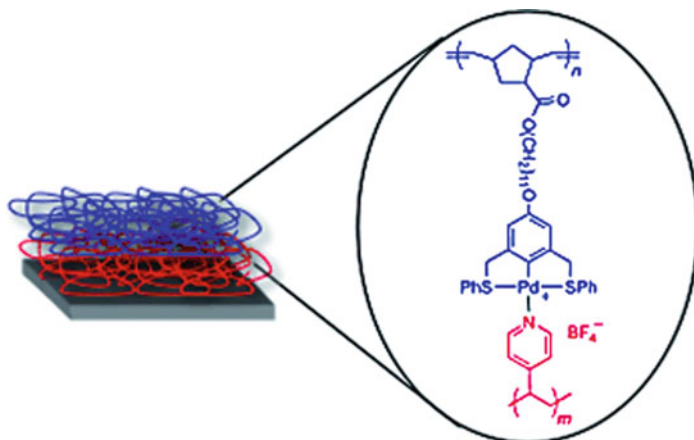


Fig. 5 Representation of coordination polymer multilayer (CoPM) buildup on gold, showing the pincer–ligand coordination responsible for building the layers. Reproduced from [22] with permission from Copyright © 2008 John Wiley and Sons

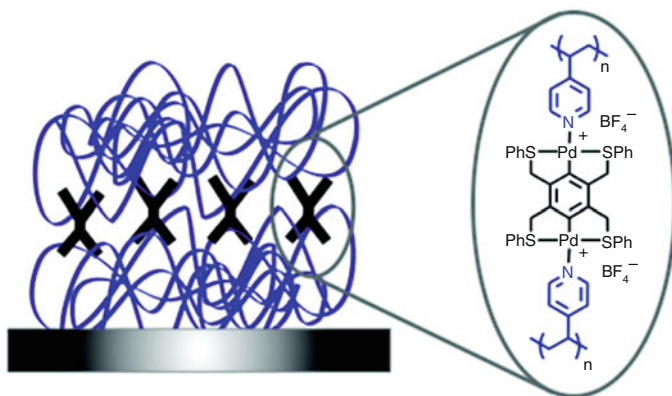


Fig. 6 Representation of separate PVP layers being brought together with the small molecule *bis*-pincer complexes. Reproduced from [8] with permission from Copyright © 2008 American Chemical Society

1.3 Functionalizing Existing Polymer Chains

There is a growing desire within the field of polymer chemistry for fast synthesis and easy post-synthetic polymer modification. Often, traditional methods of synthesis and additional side chain modifications rely on covalent chemistry. These reactions often require extensive steps and subsequent purification. If the reactions are not quantitative, unwanted side reactions and other modifications can take place along the polymer chain. The use of non-covalent chemistry has recently gained popularity for its ability to offer selectivity in associations as well as simplicity as a

side chain modification technique [1]. These associations can be useful in constructing novel molecular architectures. By incorporating specific pincer complexes as functional side chains along a polymer backbone, secondary functionalization can be obtained through metal–ligand coordination. The use of pincer coordination complexes offers faster and more selective functionalization of polymer backbones than traditional covalent reaction pathways, and the inherent robustness of the pincer complexes is passed on to the parent polymers [1]. Other variations on this theme have also been reported, including the simultaneous use of pincer coordination and pseudorotaxane formation as a tool for block copolymer modification [23].

1.3.1 Functionalizing Random Copolymers

The first use of pincer complexes as a tool for post-synthetic polymer modification was reported by Pollino et al. [1]. In order to take advantage of pincer coordination in this context, it is important to identify with what specificity the coordination events take place and what types of modifications can be made. Initially, Pollino et al. constructed random copolymers within which to demonstrate the viability of the approach and to characterize this method of functionalization [1]. Random copolymers were built with two different side chain functionalities: Pd^{II} pincer units and units capable of hydrogen bonding. The complementary partners for the pincer complexes were a range of pyridine ligands, while the hydrogen bonding units on the polymer had a separate partner motif with which to associate. The orthogonality of the pincer–pyridine coordination and the hydrogen bonding offered the chance for rapid and specific multifunctionalization. As noted in previous sections, pincer–Pd^{II}–pyridine coordination is characteristically reversible, spontaneous, simple and self-repairing (in that an undesired association tends to reverse quickly and give way to a desirable association event) in nature, and the system's potential to self-correct in this way was important in the context of the desired application, which involved two distinct but simultaneous non-covalent functionalization events. To better determine if the pyridine–pincer interactions were truly orthogonal to the hydrogen bonding interactions, a set of three different methodologies was employed [1].

This first methodology successfully showed that the pincer metal–ligand interaction is both selective and spontaneous. The pyridine ligand was added to the copolymer solution, and the pyridine ligand could only be observed to associate with the desired pincer complex, and not the hydrogen bonding unit. The second methodology revealed that a stepwise multifunctionalization was possible. The pyridine and hydrogen bonding ligands were added sequentially. The same final functionalized state was achieved regardless of the order of addition, and the extent of pyridine coordination matched that obtained in the absence of the hydrogen bonding unit. Finally, the authors reported that the same final state was obtained again if both types of ligands were added at the same time. Not only was the final state the same, but the rate of formation did not change as a function of order of addition. This combination of studies, shown schematically in Fig. 7, demonstrated

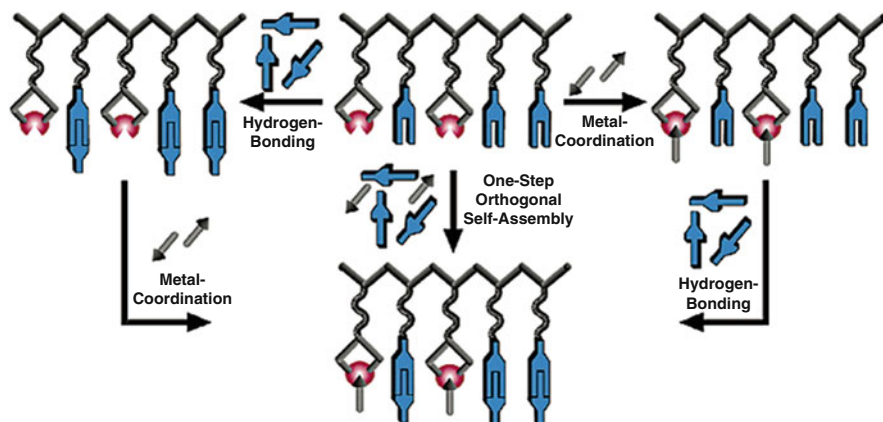


Fig. 7 Cartoon representation of the orthogonal self-assembly of both metal–ligand associations and hydrogen bonding associations in a random copolymer. Reproduced from [1] with permission from Copyright © 2004 American Chemical Society

the concept of non-covalent polymer multifunctionalization and showed that the orthogonal binding properties of pincer coordination and hydrogen bonding units, exploited in dendritic assembly as discussed in earlier examples in this chapter, provide a useful tool also for the post-synthetic modification of linear polymers.

1.3.2 Functionalizing Block Copolymers

It is well established that modifying the blocks in a copolymer can directly influence the physical properties of that polymer. However, as discussed above, traditional methods of post-synthetic modification can be costly, time consuming, and random in modification, sometimes destroying previously established “blockiness.” As a result, it was potentially useful to know if the approach used to modify random copolymers could be directly extended to block copolymers without undesired side effects. By using non-covalent coordination with the pincer complexes, block copolymers can be orthogonally modified to produce specific changes in physical properties without compromising the original block structure of the polymer chain [4].

Similar to the random copolymers of the Sect. 1.3.1, Nair et al. designed a polymer backbone with two types of blocks. One contained the pincer complex (for metal–ligand coordination) and the other contained a unit capable of hydrogen bonding. The pincer coordination event was broadened, however, and in addition to pyridine, a nitrile group was also shown to successfully bind to the pincer complex, either in the presence or absence of the potentially competing hydrogen bonding ligand. Figure 8 shows the three-point hydrogen bonding pair **2**, as well as the two different pincer complexes (with pyridine **3** and nitrile **4**) whose effectiveness was demonstrated in the block copolymer systems. This was the first example of a fast and easy non-covalent functionalization of block copolymers with defined

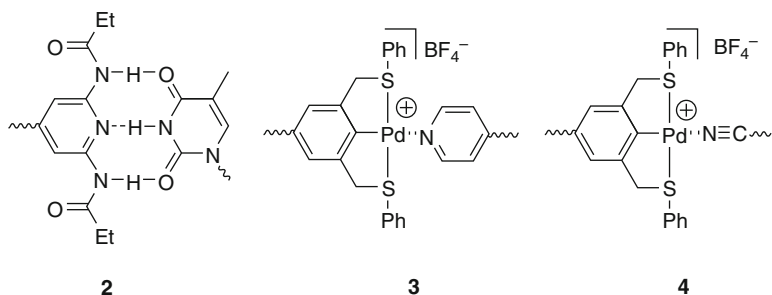


Fig. 8 The three different self-assembly motifs used in the study of post-synthetic polymerization multifunctionalization: (2) three-point hydrogen bonds, (3) pincer complex coordinated to pyridine, and (4) pincer complex coordinated to nitrile. Reproduced from [4] with permission from Copyright © 2006 American Chemical Society

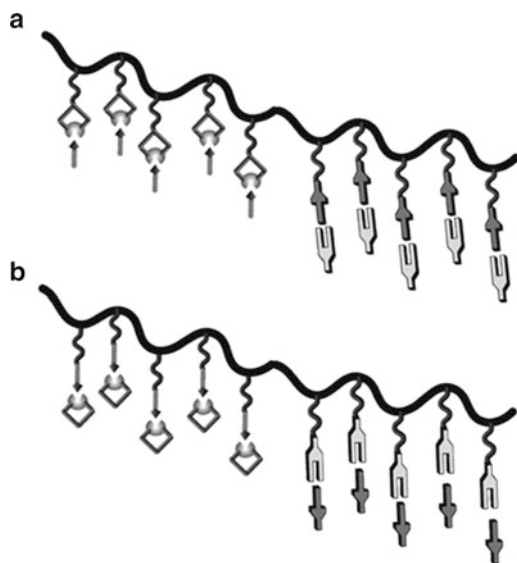


Fig. 9 A representation of the two different combinations of recognition units: (a) a block copolymer backbone containing the pincer units as the recognition units and (b) a block copolymer backbone containing the ligands as the recognition units. Reproduced from [4] with permission from Copyright © 2006 American Chemical Society

architectures of two blocks. Overall, the order and compositions of the blocks do not influence the coordination events between the pincer complexes and their complementary ligands [4].

The initial state (bound to polymer vs. free in solution) of the ligand and metal did not influence the self-assembly (Fig. 9), and orthogonality vs. hydrogen bonding was preserved in the reversed coordination cases.

Of course, the ultimate goal in functionalizing either block or random copolymers is to modify the properties. There were two observed changes in the thermal

properties of these polymers. First, metal coordination leads to a decrease in the glass transition temperature of the polymer, an observation the investigators attributed to the disruption in the original intermolecular forces between polymer chains. Second, the thermal stability drops when the polymers are coordinated to the ligands. Further work is necessary to accurately relate these changes in properties to the various structural changes that accompany functionalization, a general concern for polymer property prediction as increasingly complex functional groups are used more and more frequently in polymer science [4].

1.3.3 Functionalizing More Complex Terpolymers

More complex polymer structures were built using two different hydrogen bonding motifs in addition to the pincer complex [24]. Similar to the early systems, the functionalization behavior of these polymers was once again studied. As before, the presence of additional functional groups caused no observed change in the association constants of any of the individual coordination sites. The pincer groups were shown to coordinate rapidly and reversibly to the ligands, and functionalization was achieved without the need for subsequent purification. The multiple coordination events occurred independently of each other, and the order in which they were added did not influence their properties; pincer–ligand coordination was not disrupted by the hydrogen bonding groups, nor did it disrupt the association of those motifs [24].

To probe the physical properties of these modified terpolymers, a solvent study was carried out [25]. It was observed that by changing the solvent, one coordinating group could be selectively removed from the chain, with the addition of another coordinating ligand. These induced disassembly events can ultimately lead to tunable control over the polymer's properties. All previous studies carried out in halogenated solvents showed that the three coordination events were orthogonal, but when the solvent is changed to a chloroform/dioxane mixture, the hydrogen bonding is disrupted by the addition of the ligand that can coordinate with the pincer complexes. It was determined that the dioxane competes with and ultimately decreases the strength of the hydrogen bonding events. The pincer–ligand interaction, however, is robust in all solvents and is not susceptible to solvent disruptions. It was further determined that the presence of free silver ions from the pyridine–pincer–ligand exchange disrupts the hydrogen bonding. This disruption is not dependent on the anion of the silver salt or the solvent that the silver salt is added with. This same disassembly can also be triggered by changing the polarity of the solvent [25]. The pincer complexes offer a robust method of modifying polymer chains and ultimately changing the physical properties of these systems.

1.4 Metallodendrimers as Templates

Although the focus of this chapter is on the use of pincer complexes in materials-related physical applications, we point out that pincer coordination can also provide

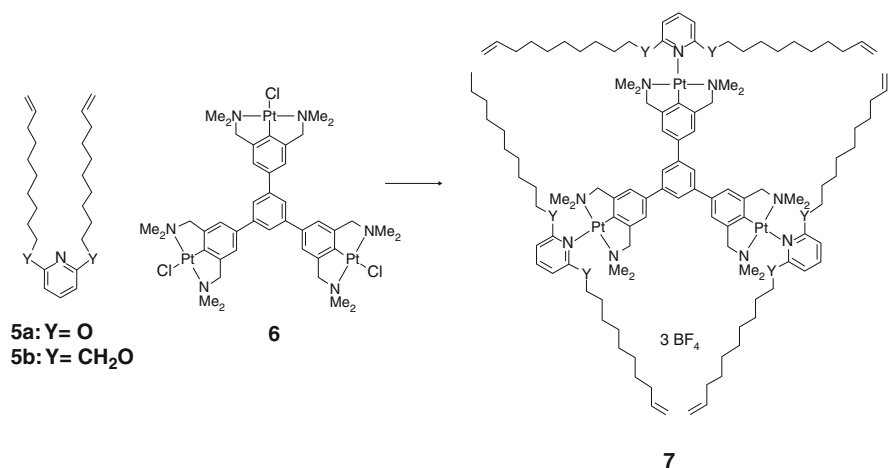


Fig. 10 Structures used in template directed synthesis: (5) pyridines bearing long alkyl chains with terminal olefins, (6) core template that is shape persistent and contains multiple pincer complexes available for coordination to the pyridine, and (7) coordinated template to olefin containing chains, ready for ring formation. Reproduced from [28] with permission from Copyright © 2003 John Wiley and Sons

a valuable tool for templated synthesis. The selectivity, orthogonality, and directionality of pincer coordination work to great advantage in this context, because reactants can be preorganized through coordination around a template and subsequently reacted to give a final molecular structure that is otherwise difficult to obtain. An elegant and useful example of the templating approach is found in the synthesis of macrocycles.

The core templates in this approach, developed by van Koten and coworkers [26–28], are shape persistent metallic units containing multiple of pincer complexes (Fig. 10). Pyridines bearing long alkyl chains with terminal olefins (5a and 5b) coordinated to the displayed pincer complexes (6), with the idea that the olefins could be joined through metathesis to form large macrocycles. It was observed that the template unit did coordinate to the pyridine containing chain quantitatively (7), setting the stage for subsequent ring formation.

Olefin-substituted chains of different lengths were studied to see if there was a specific length needed to enable full macrocyclization [26]. Depending on the olefin chain used, the isolated yield of the desired macrocycle ranged from 0 to 70 %. A minimum chain length of 11 atoms in each of the two branches on each of the three pyridine ligands was required for macrocyclization, leading to monodisperse macrocycles of over 60 bonds along their perimeters. Once the macrocycles were formed, the template could be removed easily with the addition of aqueous sodium chloride. These pyridine-functionalized macrocycles could then be further modified and used as components in reversible host/guest systems. Because a variety of shape-persistent templates can be prepared, including a hexametallc species [29], the strategy is potential suitable for a range of targets.

2 Probing the Kinetic Influence of Pincer Coordination

As described in Sect. 1, pincer coordination is useful and versatile motif through which a wide variety of polymeric structures and materials can be constructed, but pincer complexes have also proven to be useful probes of fundamental physical behaviors of polymeric materials. The context of the studies is the increasing use of self-assembly as a route to complex, supramolecular structures and materials [30]. As the number of accessible supramolecular structures grows, relating the properties of an assembly to those of the supramolecular constituents that define the assembly becomes increasingly important. As reviewed by Raymond [31], the dynamics of supramolecular assemblies are a particularly rich means by which chemists might engineer properties such as: catalysis [32–35], templation effects [36, 37], interconversion of assemblies [38], and kinetic compartmentalization [39].

In the context of polymer science, the use of supramolecular bonds as defining components of a material is distinguished from the use of covalent bonds by the reversibility of the former. In other words, it is the dynamic properties, rather than the equilibrium structure, of the supramolecular interactions that often contribute to new polymer properties. In order to probe mechanism at the molecular level, however, the effects of dynamics must be differentiated from the effects of equilibrium thermodynamics. This differentiation is a challenge with most reversibly assembled systems, for example those based on hydrogen bonding, because association typically occurs at or near the diffusion rate, and the equilibrium association constant and rate constant for dissociation are therefore strongly anti-correlated. In polymer science, the inverse correlation of these two descriptors subtly but intrinsically frustrates efforts to determine their relative importance. High association constants lead to larger structures and slower dynamics of the intact equilibrium structure, while slower dissociation rates lead to slower reversible dynamics within the material. Dynamic properties, whether controlled by equilibrium structure or main-chain reversibility, are slowed by both mechanisms. A method for decoupling the two therefore offers the potential for a rich investigation into the fundamental importance of the reversible interaction.

It is in this context that pincer coordination has proven to be extremely useful. NCN-Pincer compound **8** (Fig. 11) and analogs have been synthesized and studied extensively by van Koten [18]. With other organometal motifs [40, 41], they have found use in supramolecular chemistry by Reinhoudt, van Koten, and others [16, 42, 43]. The reversibility takes place through ligand exchange, which in square planar Pd^{II} and Pt^{II} occurs through a sterically congested associative mechanism. Bulk in the *N*-alkyl substituents **R** should therefore slow the exchange, but have only a minimal impact on the ligand association thermodynamics. The expected decoupling of kinetics and thermodynamics was confirmed in room temperature NMR spectra of the **R** = Me and Et complexes. At identical concentrations (DMSO-*d*₆; 1 mM in **8a/b**, 3 mM in **9**), effectively identical ratios of free and bound **9** are observed; the measured association constants are 1.6 and $1.3 \times 10^3 \text{ M}^{-1}$, respectively, for **8a** and **8b**. While the spectrum of **8b**•**9** is sharp,

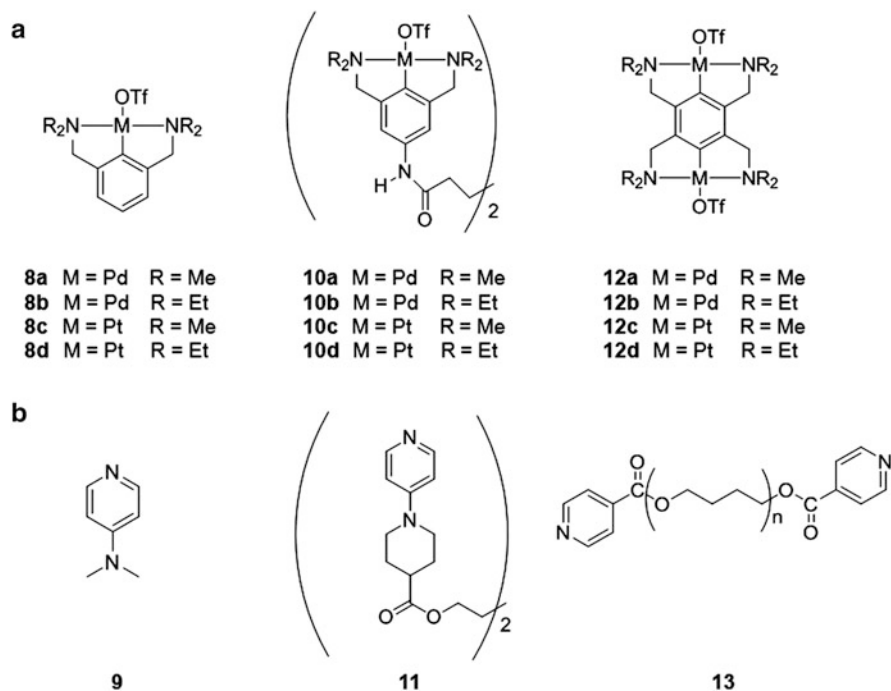


Fig. 11 (a) Several different pincer complexes used in kinetic studies with different metals and R groups and (b) various pyridine derived ligands which can coordinate to the different pincer complexes

however, that of **8a**•**9** shows broad peaks that are indicative of exchange near the NMR timescale. Heating the NMR sample to only 30 °C leads to coalescence of the peaks and corresponds to an exchange rate of 100 s⁻¹ at that temperature. In contrast, the same peaks in **8b**•**9** remain separated until 90 °C, above which the reduced concentration of bound ligand makes coalescence impossible to identify clearly. The orthogonal control of dissociation dynamics relative to complexation thermodynamics can be viewed as a “macromolecular analog of the kinetic isotope effect,” and its use in a variety of mechanistic physical studies is the focus of this section [5].

2.1 Supramolecular Polymer Chains

We have previously discussed how covalent polymer chains can be modified non-covalently by using side chain pincer coordination, but similar pincer associations are also useful for building the main chain structure by attaching the pincer complexes and ligands to the ends of difunctional polymers and small molecules [5]. The metal–ligand associations between chain ends lead to longer, reversible polymer chains. A specific example is shown in Fig. 12. Mixing a solution of *bis*-

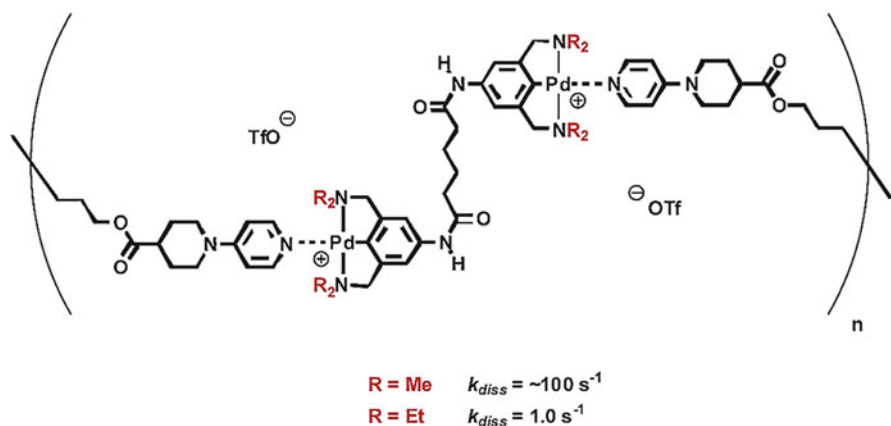


Fig. 12 Example of pincer coordinations to form supramolecular polymer chains with **10a** or **10b**. Reproduced from [5] with permission from Copyright © 2003 American Chemical Society

pincer complex **10** with another containing stoichiometric *bis*-pyridine capped chains led to an increase in the viscosity of the system, indicating that the longer chains (Fig. 12) had formed [5]. Similar effects were observed when analogous ditelechelic polymers are mixed. As described above, the main chain dissociation kinetics can be varied through the *N*-alkyl substituent on the NCN pincer complex. Changing the ligand exchange rate by approximately two orders of magnitude has no effect on the viscosities of the polymer solutions across a range of concentrations and molecular weights, demonstrating that the viscosity is determined by the equilibrium structure, and not the main chain dynamics, of the linear polymers.

Supramolecular polymers often have impressive solid-state mechanical properties [44–48], and identifying the extent to which the reversibility of the supramolecular interaction contributes, and the mechanism by which it does, to those properties, is of great interest. In some cases, direct rheological characterization [48–50] offers some insight. In case of the pincer-based linear polymers, reasonably strong and quite tough fibers of **12a/b•13** (Fig. 11) have been hand-drawn from solution. A rudimentary study of the fiber mechanical properties of one specific pincer-based polymer reveals tensile strengths of ~ 100 MPa and strains at break of roughly 70 %. Importantly, the tensile strengths of **12a•13** fibers are identical, within experimental error, to those of the **12b•13** fibers, providing compelling evidence that the nucleophilic displacement mechanism that governs failure under load in solution (as measured by single-molecule force spectroscopy [51]) is not operative in the solid state [52]. The absence of the typical associative ligand displacement pathway in the fibers is likely tied to their significant tensile strength, since the likely alternative failure mechanisms (chain disentanglement and/or purely dissociative scission of the coordination bond) would be comparable to those in conventional, covalent polymers [52].

2.2 Reversible Networks

Not only can pincer complexes be incorporated into polymer backbones to induce physical changes, but the *bis*-pincer small molecules can be used to cross-link polymer chains to form reversible networks [6]. When the *bis*-pincer complexes are added to solutions of PVP, the multiple pincer–pyridine coordination events act as cross-linkers, leading to the formation of reversible networks (Fig. 13) [6]. These systems provide excellent model systems for exploring the fundamental behavior of supramolecular polymer networks in general.

2.2.1 Pincer Kinetics and Network Properties

The network physical properties were monitored as the small molecule pincer cross-linkers were added to the PVP solutions [10]. As the concentration of cross-linkers went up, there was a concomitant increase in the sample viscosity, indicating the formation of reversible networks. The viscosity increase is reversed upon the addition of dimethylaminopyridine (DMAP), which outcompetes the pyridine side chains for the pincer complexes and disrupts the cross-linking. Furthermore, the addition of a mono-functional, rather than a *bis*-functional pincer complex to solutions of PVP leads to no observed increase in viscosity. Clearly, the *bis*-functionality of the pincer complexes, and the associated cross-linking, is responsible for the changes in the physical properties. Figure 14 shows the relationship between viscosity and the cross-linkers added (**10a** and **10b**).

While the pincer complexes are useful for forming the reversible networks, it is important to study the influence of the kinetics and thermodynamics of the system as well. As demonstrated with the main chain studies, k_{diss} is important in defining many of the physical properties. When pincer complexes of slightly different chemical structures were compared, a drastic difference in properties was observed. The resulting viscosities of the different networks scale with the k_{diss} of the specific pincer complex used. When comparing two systems with nearly identical values of K_{eq} but significantly different values for k_{diss} , the viscosities are still drastically different. This indicates that it is the lifetime of the cross-links that ultimately dictate the viscosity of the solution and not the strength of the interaction.

Changing the steric bulk of the pincer complex influences the kinetics of the interaction, but the thermodynamics of the interaction can be controlled with the metal in the complex. By changing the Pd^{II} to Pt^{II} the thermodynamic strength of the interaction increases even. When different pincer complexes with different K_{eq} values were used, however, the mechanical response still scaled with the k_{diss} . When the entire family of cross-linkers was compared (k_{diss} ranging from 0.0006 s⁻¹ to 1,450 s⁻¹) all relative viscosities scaled with the k_{diss} and not K_{eq} . Clearly, the chemical structure of these pincer complexes dictates the properties and physical functions of these reversible networks [10].

Within this family of pincer-based networks, the role of reversible molecular dynamics on material response was explored through the steric effects in the pincer

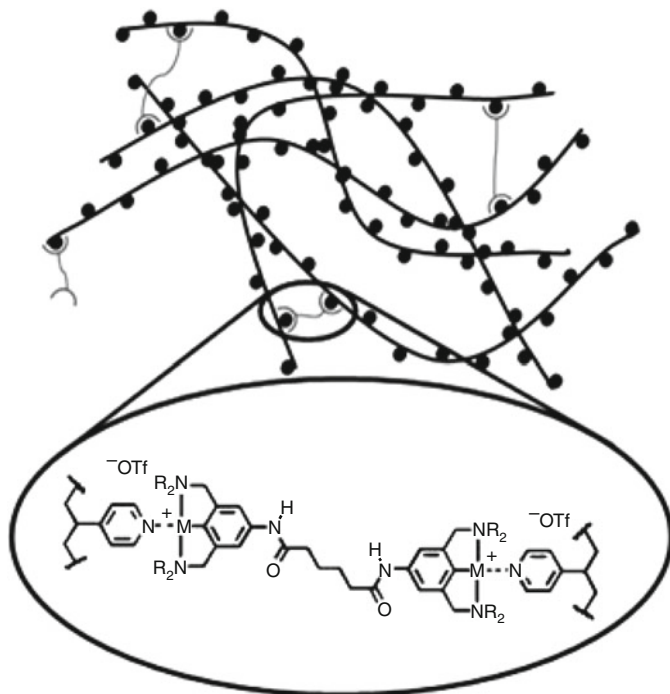


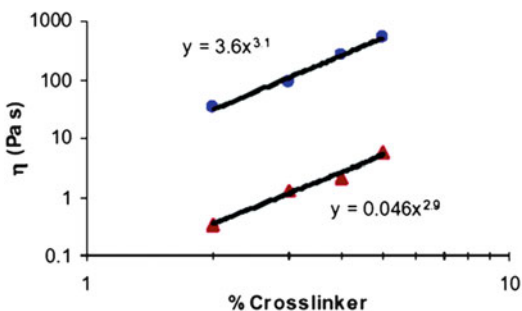
Fig. 13 Representation of reversible cross-links between *bis*-pyridine ligand **10** in PVP chains through coordination with the *bis*-pincer complexes. Reproduced from [6] with permission from Copyright © 2005 John Wiley and Sons

alkylamino ligands, both within the Pd complexes **10a–b** and the slower, more strongly coordinating Pt complexes **10c–d**. As with the linear polymers, the independent control of kinetics is effective and particularly useful; cross-linkers **10a** and **10b** are structurally identical components within the network, and so their similar thermodynamics ($K_{\text{eq}} = \sim 30 \text{ M}^{-1}$ for **8a•9** and **8b•9**) ensure that the extent and nature of cross-linking are essentially the same in the two samples (or between Pt (II) pincer molecules **10c–d**; where $K_{\text{eq}} = 8 \times 10^3 \text{ M}^{-1}$ for **8c•9** and $4 \times 10^3 \text{ M}^{-1}$ for **8d•9**).

Above a critical concentration of cross-linkers, the absolute and relative behaviors of the various networks are quite different, both qualitatively and quantitatively. As seen in Fig. 14, the viscosity increases by up to several orders of magnitude over a relatively narrow range of cross-linking content, and past this transition the materials behave like weak gels. This change in properties is attributed to a sol-to-gel transition, and once the macroscopic network is formed, the macroscopic mechanical response of the gel requires that the cross-links dissociate.

The central role of cross-link dissociation is seen in the relative viscosities at cross-linker concentrations beyond the sol–gel transition. In this regime, the

Fig. 14 Steady shear viscosity as a function of cross-linker **10a** (blue filled circle) and **10b** (red filled triangle) in 100 mg mL⁻¹ of **10•PVP** in DMSO. Reproduced from [10] with permission from Copyright © 2005 American Chemical Society



relative viscosities of the samples are proportional to the lifetime ($\tau = 1/k_d$) of the coordinative metal–pyridine bonds that define the cross-links [10, 53]; for example, the zero shear viscosity of 100 mg mL⁻¹ **10a•PVP** is a factor of 80 less than that of the isostructural network **10b•PVP** (Fig. 13). The difference of a factor of ~80 in the network viscosities is within experimental error of the difference in the ligand exchange rates, and a full spectrum of dynamic mechanical behavior is similarly well correlated. The frequency-dependent storage and loss moduli, G' and G'' , for networks of either **10a•PVP** or the related **10b•PVP**, are reduced to a single master plot when scaled by the corresponding ligand exchange rates, measured on model systems [10]. In other words, the full range of physical mechanical behavior of the networks can be tied back to a single-molecular event, the dissociation of a pyridine ligand from a pincer complex. The same relationship is valid for both the Pd (e.g., **10a/b**) and Pt (**10c/d**) cross-linkers, even though the equilibrium association constants for the Pt complexes are roughly a factor of 10^2 higher than those of the corresponding Pd complexes.

2.2.2 Complex Rheological Properties of Reversible Networks

Polymer networks formed via weak associations often have quite rich behavior under shear. Depending on the specific system and its environment, networks might grow less viscous once forced to flow (shear thinning, the most common example of which is found in striking a bottle of ketchup to get its contents to flow more easily), or they might become more viscous under induced flow (shear thickening, observed in quicksand and in concentrated cornstarch–water suspensions). Such responses are classified as “nonlinear rheology,” and the important point for purposes of this chapter is that the molecular mechanisms that dictate the various responses are often unclear. The kinetic control afforded by the pincer complexes has proven to be quite useful in establishing the details of these processes, and in fact have uncovered hidden and unanticipated polymer physics.

The nonlinear rheological properties of the pincer–PVP networks depend on the concentration of the PVP. When the networks are formed from less concentrated solutions of PVP (specifically, at concentrations in which the polymer chains are not entangled with each other), the application of shear above a critical shear rate



Fig. 15 Representation of the mechanism of shear thickening in pincer cross-linked PVP networks. Reproduced from [54] with permission from Copyright © 2010 American Chemical Society

leads to shear thickening [54]. As with the linear rheology, a change in cross-link dissociation rate provides immediate insight into the phenomenon, because the shear rate at which the shear thickening begins is proportional to the stress-free lifetime of the pincer–pyridine bond. The onset and magnitude of the shear thickening depend on the amount of cross-linkers added, and further experimental work has identified the primary mechanism of shear thickening to be the shear-induced transformation of intramolecular cross-linking to intermolecular cross-linking, as shown in Fig. 15.

The story changes somewhat when the concentration of the PVP is higher, so that the PVP polymer chains are wrapped around each other in addition to being bound to each through the pincer complexes. The kinetic control of pincer–pyridine dissociation becomes especially useful in this complex environment. Under steady shear, however, the scaling relationships in the semidilute unentangled regime break down dramatically. This breakdown is not only in the quantitative scaling behavior, but even in the qualitative shear response of different systems: shear thinning is generally observed for samples with cross-linkers that have a faster dissociation rate (e.g., **12a**), while shear thickening is still observed for cross-linkers that have a slower dissociation rate (e.g., **12b**). Clearly, the picture is much more complicated than that of the systems with lower concentrations of PVP. In addition, the change in fundamental mechanism was not predicted by any existing theories of shear thinning and shear thickening, and it is difficult to imagine how the effect of cross-linker dynamics might have been observed without the ability to vary the kinetics in otherwise identical systems that is afforded through the pincer complexes [55]. Further mechanistic work suggested that two critical processes compete in the time after a cross-linker dissociates: the cross-linker tries to re-associate, and at the same time the now freed polymer chain segment tries to orient in a way that would permit additional intermolecular cross-linkers to form. When cross-linker re-association is rapid, the polymer does not have time to orient for new cross-link formation under the shear flow and shear thinning, rather than shear thickening, results [56].

2.2.3 Multiple Component Reversible Networks

The pincer complexes have also been used to shed light on how more complex material mechanical properties might be programmed via a combination of multiple supramolecular interactions. Pincer–PVP networks were formed similarly to the

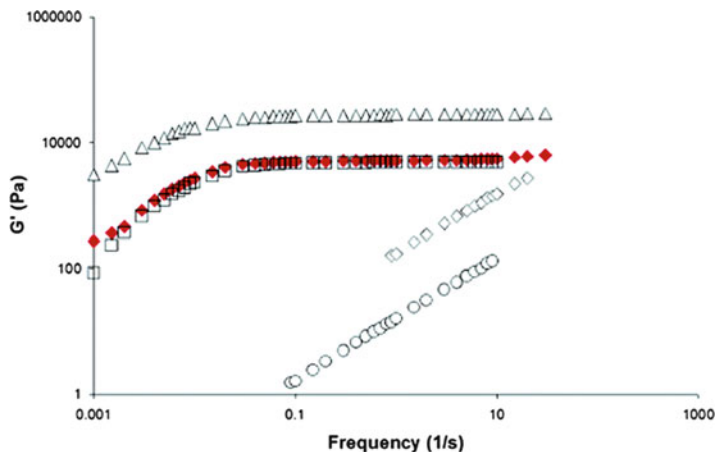


Fig. 16 Storage modulus, G' , vs. frequency for (red filled diamond) 2.5 % + 2.5 % (**12b** + **12c**) •PVP, (open square) 2.5 % **12c**•PVP, (open triangle) 5 % **12c**•PVP, (open circle) 2.5 % **12b**•PVP, and (open diamond) 5 % **12b**•PVP. All networks 10 % by total weight in DMSO, 20 °C. Reproduced from [57] with permission from Copyright © 2005 American Chemical Society

systems discussed in previous sections, but with the incorporation of combinations of multiple types of cross-linkers. The mechanical properties of mixtures of cross-linkers look not like the average of the multiple species, but instead a combination of both, showing that the response to an applied stress occurs through sequential, individual dissociation and re-association events [57]. Representative characterization is shown in Fig. 16, and similar effects are observed for different pair wise mixtures of cross-linkers as well as a network with three different cross-linkers. In all cases, the frequency onsets and magnitudes of the transitions are anticipated by the behavior of networks with a single cross-linker, and therefore on the intrinsic properties of the individual supramolecular interactions themselves.

The programmability demonstrated by the pincer complexes is less important in terms of applications of these specific materials than in its general point for supramolecular materials science that an understanding of isolated molecular behavior is often directly relevant to materials in which there is an interplay of multiple interactions and timescales. In this case, the behavior is that of transient networks, in which the independent relaxations of stress-bearing entanglements determine the dynamic mechanical response of a network [58–60]. The independence of the cross-links has significant consequences for the rational, molecular engineering of viscoelastic properties. When cross-linking is created through very specific interactions, the chemical control of properties follows. As long as the strength of the association is great enough to make the cross-linkers active, the dynamics of cross-link dissociation, rather than further details of its thermodynamics, are the key design criterion. As a result, quite complex materials mechanical response can be programmed if one has suitable knowledge of the small molecular behavior.

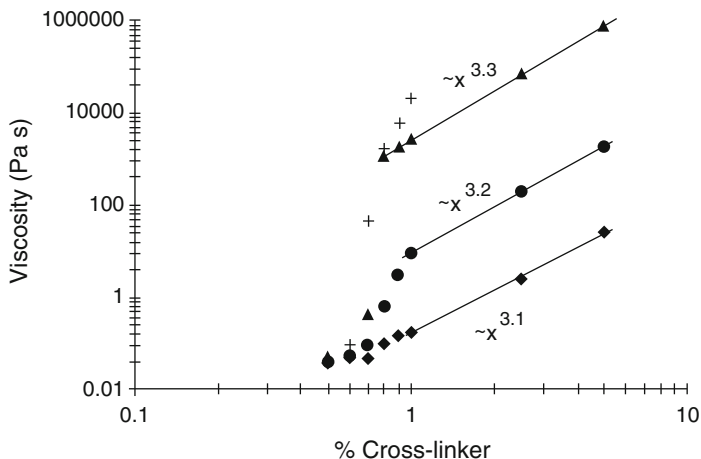


Fig. 17 The effect of cross-linking percentage on viscosity of transient networks formed from PVP with pincer complexes: **12a**●PVP (filled diamond), **12b**●PVP (filled circle), and **12c**●PVP (filled triangle). Reproduced from [53] with permission from Copyright © 2007 Royal Society of Chemistry

2.2.4 Stimuli-Responsive Networks

As previously discussed, the pincer-based reversible networks offer many advantages when it comes to designing networks. The networks were further used to demonstrate and characterize sensitive stimulus response, by taking advantage of the dramatic change in properties that accompanies the sol-to-gel transition (Fig. 17) [53]. For a fixed PVP concentration, the sol-gel transition occurs at the same concentration across the family of different pincer structures (**12a-c**) in a solution of PVP. The important point, the one mentioned above, is that the viscosity changes by several orders of magnitude over a modest change in active cross-linker concentration, suggesting that networks at or near the transition concentration should be very sensitive to external stimuli that influence the extent of active cross-linking [53].

This expectation was confirmed by monitoring the sample viscosity as a function of different added agents to the solution. For example, one specific pincer network had an initial zero-shear viscosity of $\sim 1,000$ Pa s. The viscosity drops by up to several orders of magnitude, however, in response to relatively small quantities of acids, basis, or other ligands that inhibit the pincer-pyridine coordination (Fig. 18). In some cases, the decrease in viscosity can be reversed by removing the competing ligand or treating the system with an additional stimulus. The work indicates the potential to engineer at the molecular level supramolecular and pincer-based networks for use as chemoresponsive systems [53].

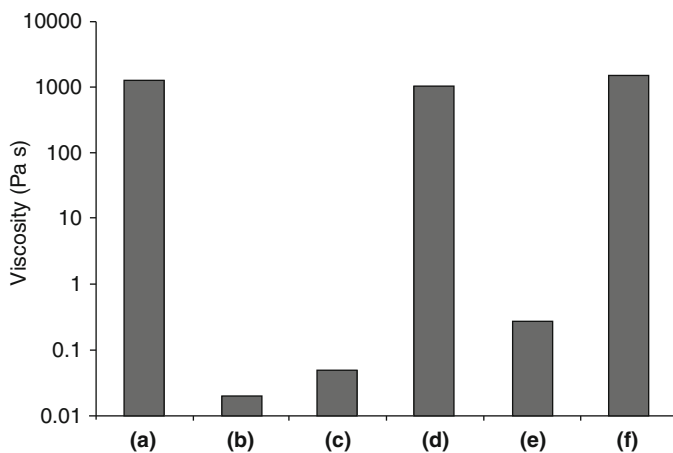


Fig. 18 A chart demonstrating the chemoresponsive nature of a network formed by cross-linking PVP with pincer complex **12c**. (a) Initial viscosity, (b) a + NaCl, (c) a + sulfuric acid, (d) c + NaHCO₃, (e) a + triflic acid, and (f) e + NaHCO₃. Reproduced from [53] with permission from Copyright © 2007 Royal Society of Chemistry

2.3 Hybrid Gels: Combination of Covalent and Reversible Cross-Linkers

The previous examples of pincer-based networks feature pincer–pyridine coordination as the only active cross-linking interaction. One of the advantages of the reversibility of the coordination is that the networks formed are “self-healing,” in the sense that if the networks are fractured or cut, they will reorganize and regain their initial structure. This “healing” behavior is enabled by the same dissociation/re-association processes that allow the networks to flow over extended periods of time (and in many cases the repair and the flow are really the same process). It is therefore interesting to consider the physics enabled by incorporating reversible interactions in combination with permanent covalent bonding, where the former might provide reversibility, repair, and added toughness, while the latter provides a permanent structure that will not flow over long time scales.

With that motivation, the same pincer motifs discussed in the previous sections were incorporated into a family of hybrid polymer gels in which covalent cross-links create a permanent, stiff scaffold onto which the reversible metal–ligand coordinative cross-links are added [9]. The hybrid gels exhibit frequency-dependent mechanical properties that are different from those of the parent, covalent-only gel (Fig. 19). On long timescales, the pincer complexes are dynamic and do not contribute to the storage modulus of the gels, but on shorter timescales they remain intact and the storage modulus increases measurably as a result. The underlying relaxation can be directly attributed to the dissociation and re-association of the supramolecular pincer cross-linker by employing the same kinetic variation strategy used to good effect in the reversible-only networks. The

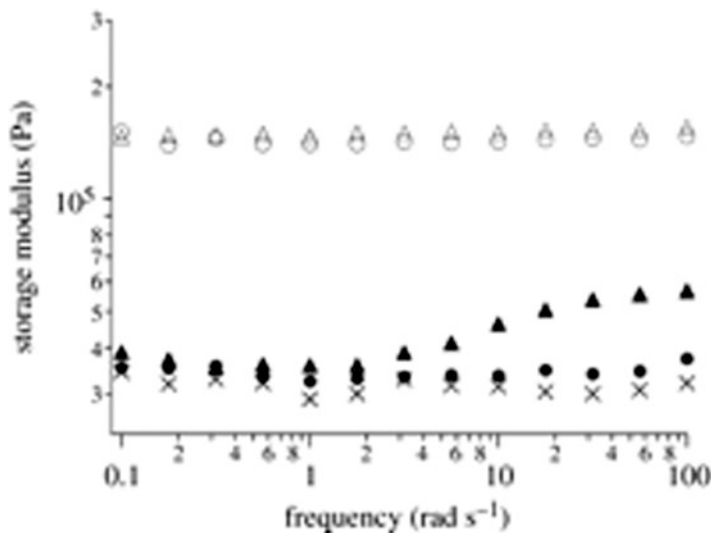


Fig. 19 Storage modulus as measured by the oscillatory rheology of covalent and hybrid DMSO gels: “pure” covalent gel (multiplication symbol); gel-12a (filled circle); gel-12b (filled triangle); gel-12c (open triangle); and gel-12d (open circle). Reproduced from [9] with permission from Copyright © 2006 The Royal Society

structural similarity of the related pincer complexes and their comparable pyridine coordination thermodynamics ensures that the equilibrium structures of the two gels are effectively identical. The timescales at which the various cross-linkers begin to contribute to material mechanical properties, however, are not identical, but instead reflect the intrinsic dissociation rates of the various pincer complexes. In the hybrid systems, as in the mixed reversible-only systems, the individual supra-molecular cross-links bear stress and act as largely independent contributors to the dynamic mechanical properties.

Looking ahead, these and related hybrid networks offer the opportunity for future mechanistic studies of important, but complex, processes whose mechanistic origins are still poorly understood, including: gel fracture [61], self-repair [62], and energy dissipation [63]. Studies in these areas would follow cleanly from the structure—activity studies described above, and should benefit from the groundwork laid by the prior efforts. The shear thinning and shear thickening behavior described in earlier sections shows how pincer complexes can be used as effective probes of highly complex responses for which conclusive molecular interpretations are often not available.

2.4 Mechanochemical Applications of Pincer Complexes

The field of polymer mechanochemistry, in which applied mechanical forces are coupled to bond making/breaking processes, has undergone a recent resurgence,

and pincer complexes have played a central role in at least two important advances within the field. They have been used (1) to demonstrate fundamental principles of mechanochemical activation and (2) as an early example for the mechano-responsive catalysts.

2.4.1 Pincer Complexes as Mechanochemical Probes

Given the central role of the pincers in storing and responding to an applied mechanical stress in the networks, it is reasonable to speculate on the effect of that stored mechanical stress on the cross-linker dissociation. This question of how a force of tension within a polymer affects the rates of bond dissociation processes, although considered in various contexts over the years [64], had not been quantified experimentally for systems other than homolytic bond scission until 2006, when it was approached in the specific context of pincer–pyridine complexes. The force-induced displacement of pyridine by dimethylsulfoxide (DMSO) was examined experimentally using single-molecule force spectroscopy by Kersey et al. [51]. Briefly, the tip of an atomic force microscope was used to pull one end of a polymer away from a surface to which the other end of the polymer was attached. A pair of pincer–pyridine coordinative bonds in the center of the polymer provided a spot for dissociation that could be characterized as a function of force. The AFM experiment is a kinetic measurement; the experiment probes the probability that the bond breaks as opposed to remaining intact under an applied load across a given time interval. A load is applied, and the mechanical energy is stored in the intact, elongated polymer until the metal–ligand bond breaks, at which point the energy is dissipated. The energy is stored in the elastic deformation of the polymer coupled to the deflected AFM tip, and so the release of the tip signals the breaking of the metal–ligand bond.

Several insights were established from investigations of the mechanics of ligand exchange in pincer complexes. A first general conclusion from the AFM studies is that, as might be expected, the rate of ligand dissociation increases as the force applied to the ligand increases. Second, as shown in Fig. 20, the probability of complex survival depends on the rate at which the force is loaded into the bond normalized by the stress-free lifetime of the bonds—scaling behavior that is strongly reminiscent of the mechanical behavior of the macroscopic networks. From a materials perspective, then, any contributions from force-induced rupture to the network mechanical response are likely to fall neatly within the same scaling behaviors reported earlier. Third, the nature of the force–rate relationship strongly suggests that the mechanism of ligand displacement under mechanical load is not greatly distorted from that of the force-free reaction. These general insights helped to validate qualitative notions of force–reactivity relationships that previously had been supported purely by theoretical arguments.

In addition to pulling on pincer complexes embedded in single, extended polymer chains, the effect of mechanical action on response was examined in the context of surface-tethered polymer brushes cross-linked by the pincer complexes **10** [7].

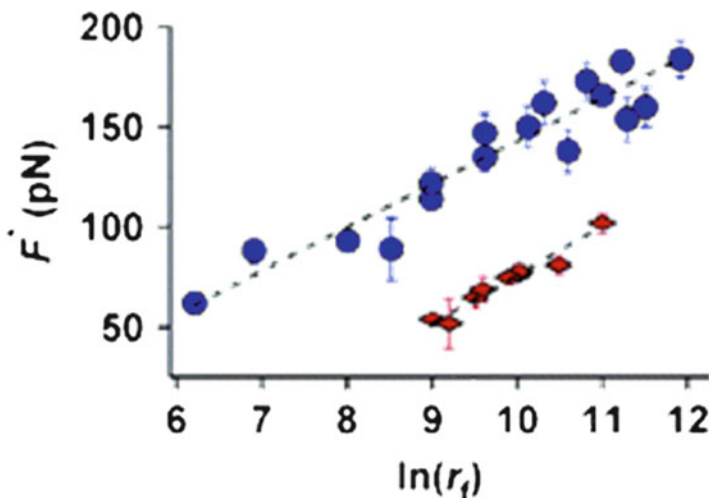


Fig. 20 Results of AFM experiments to determine most probable force vs. loading rate of mixtures of **10b** and two different teathered polymers capped with pyridine units. Reproduced from [51] with permission from Copyright © 2006 American Chemical Society

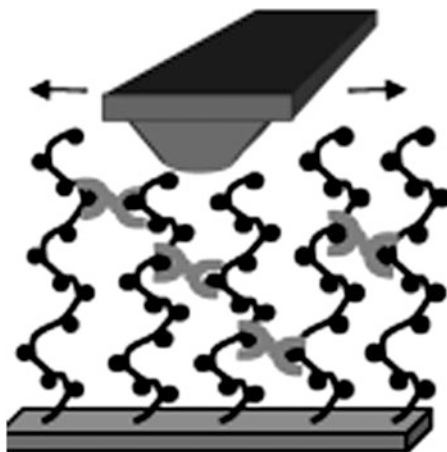
The mechanics of these brushes was examined using an AFM, but this time by dragging the AFM as a lateral probe of physical properties (friction) or by pulling the tip from the surface to characterize adhesion. Figure 21 shows a diagram of the cross-linked brush and the AFM tip dragging across the surface.

Rather remarkably, whether the friction increased or decreased was observed to depend on the *N*-alkyl substituent; adding a pincer-Pd^{II} cross-linker with the “faster” methyl substituents caused the friction to go down, while adding a cross-linker with the “slower” ethyl substituents caused the friction to increase. The unexpected and divergent response is reminiscent of that observed in the shear thickening vs. shear thinning behavior of the macroscopic networks, and while uncovered by the ability afforded by the pincer complexes to probe structure–activity relationships of this nature, a complete physical picture for the behavior has not yet been established. From a materials engineering point of view, however, we note that the pincer complexes are able to induce dramatic changes in fundamental surface properties, and that these changes are reversible, as demonstrated by the addition of a competing DMAP ligand to bring the thin film friction properties back to their original values [7].

2.4.2 Mechanically Activated Catalysts

In addition to being used as kinetic probes, Bielawski et al. have developed a mechanoresponsive catalyst that is based on a palladium pincer complex [65]. Mechanoresponsive materials need both a mechanophore [66] (a unit that experiences a structural or electronic change when a force is applied) and an

Fig. 21 Representation of grafted polymer brushes cross-linked by pincer complex **10**. The tribological properties of the brush can be probed by an atomic force microscope. Reproduced from [7] with permission from Copyright © 2006 John Wiley and Sons



actuator [67] (a unit that translates the applied force to the mechanophore). Bielawski et al. were able to meet these criteria when developing their mechanor-responsive catalyst. The *bis*-functional SCS-pincer complex is embedded in the center of a polymer via coordination to two pyridine capped polymer chains, in a manner reminiscent of Kersey et al.'s AFM studies (Fig. 22). Instead of applying force via an atomic force microscope, however, the mechanical force is generated by subjecting a solution to pulsed sonication, which generates transient elongational flow fields that rapidly stretch the polymer. The applied forces break the chain at the mechanophore [the pincer–pyridine ligand interaction (Fig. 22)]. As established by a variety of control experiments and characterizations, these transformations are mechanically, rather than thermally, induced.

Once pincer–pyridine dissociation was induced mechanically, the free palladium was shown to be catalytically active in palladium-catalyzed carbon–carbon bond formation. When the pincer infused polymers (**14**) were sonicated in the presence of 2-fluorobenzyl cyanide (**17**), and *N*-tosylbenzylimine (**18a**) for 2 h, a 93 % conversion to the coupled product **19** was observed (Fig. 23). Structure–activity relationships found in the conventional catalyst were also observed in the mechanically activated catalyst: increasing the electron density in the imine led to a decrease in catalytic efficiency [68]. Another set control experiments confirmed the necessity of mechanical activation from the precursor under the conditions of the experiment.

Additional catalytic activity was observed with the freed pyridine moieties (**16**). Previously, Willson et al. had shown that pyridine can be used to initiate anionic polymerization of α -trifluoromethyl-2,2,2-trifluoroethyl acrylate (**20**) [69]. Drawing inspiration from this earlier work, Bielawski et al. sonicated a solution containing the pincer bearing polymer, **14** and the substrate **20** for 2 h. Sonication removed the pincer “protecting group” from the pyridine and induced the expected polymerization, with product **P(20)** ultimately being obtained in 42% yield (Fig. 24). Consistent with the palladium-catalyzed systems, no polymerization

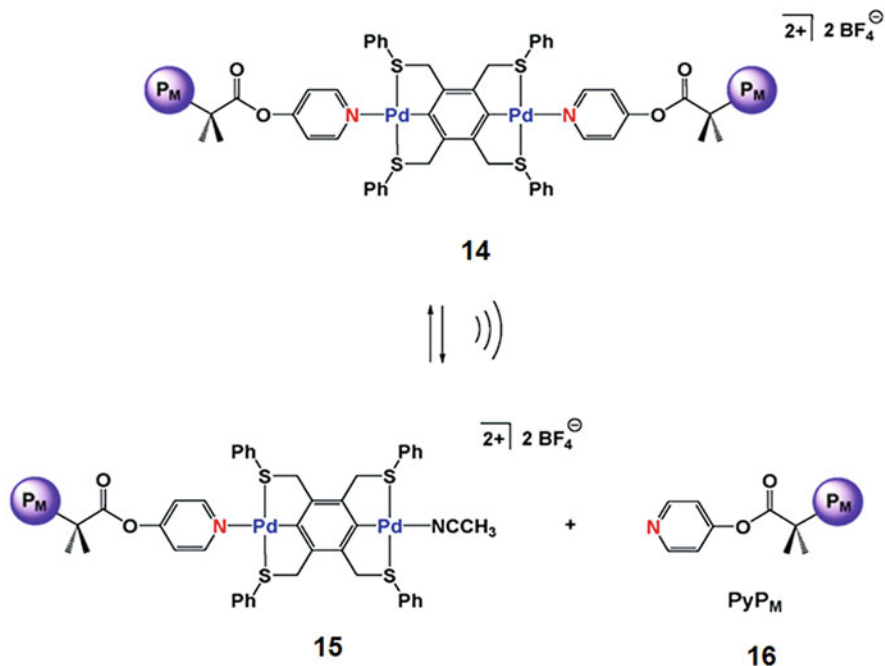


Fig. 22 When a polymer chain that contains the pincer complex (**14**) is subjected to sonication, the pyridine–metal bond is broken, resulting in the pincer complex capped chain (**15**), and the pyridine capped chain (**16**). Reproduced from [65] with permission from Copyright © 2010 American Chemical Society

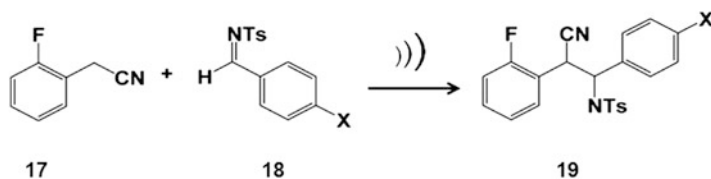


Fig. 23 Palladium-catalyzed carbon–carbon bond formation in the presence of mechanically activated polymers (**15** and **16**). Reproduced from [65] with permission from Copyright © 2010 American Chemical Society

was observed in the absence of sonication, and a variety of control experiments again confirmed the mechanical nature of the activation.

The mechanical activity of the pincer complexes not only demonstrates important new principles in chemical reactivity and strategies for responsive catalysis, it ties nicely to other examples in this chapter and elsewhere in this volume. The force-accelerated ligand exchange must occur, for example, in the fracture of pincer cross-linked networks. And the mechanical liberation of latent pincer complexes

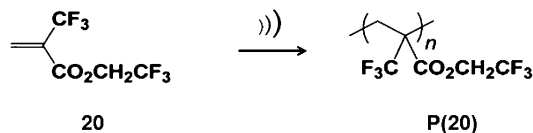


Fig. 24 Pyridine-catalyzed anionic polymerization in the presence of a latent pincer mechanocatalysts **15** and **16**. Reproduced from [65] with permission from Copyright © 2010 American Chemical Society

might potentially be coupled to many of the catalytic transformations discussed in other chapters.

3 General Conclusions

As testified by the bulk of this volume, pincer complexes have gained popularity largely through their ability to effect chemical transformations. Nonetheless, the ease of synthesis and handling, stability in a wide range of chemical environments, and the availability of handles for structural manipulation has provided a wealth of opportunities to use pincer complexes in a range of physical applications. They have been used to build complicated nanostructures and metallodendrimers by both convergent and divergent techniques. They have provided a mechanism for rapid and selective post-synthetic modification of random and block copolymers, and as the glue for new classes of multilayer thin films with impressive stability. They have served as probes of fundamental polymer physical behavior, and played a key role in seminal discoveries and demonstrations in the burgeoning field of polymer mechanochemistry. Looking ahead, it seems likely that pincer complexes will provide additional benefits to research in materials science, and for the same reasons that they have been so useful to date: they are compact, functional, and dependable, with metallosupramolecular coordination behavior that functions reliably even in complex environments. Their past utility in the context of materials is therefore not surprising, nor is likely to be their future use in a growing range of physical applications.

References

1. Pollino JM, Stubbs LP, Weck M (2004) One-step multifunctionalization of random copolymers via self-assembly. *J Am Chem Soc* 126:563–567
2. Huck WTS, van Veggel FCJM, Reinhoudt DN (1996) Controlled assembly of nanosized metallodendrimers. *Angew Chem Int Ed Engl* 35:1213–1215
3. Huck WTS, Hulst R, Timmerman P, van Veggel FCJM, Reinhoudt DN (1997) Noncovalent synthesis of nanostructures: combining coordination chemistry and hydrogen bonding. *Angew Chem Int Ed Engl* 36:1006–1008
4. Nair KP, Pollino JM, Weck M (2006) Noncovalently functionalized block copolymers possessing both hydrogen bonding and metal coordination centers. *Macromolecules* 39:931–940

5. Yount WC, Juwarker H, Craig SL (2003) Orthogonal control of dissociation dynamics relative to thermodynamics in a main-chain reversible polymer. *J Am Chem Soc* 125(50):15302–15303
6. Yount WC, Loveless DM, Craig SL (2005) Strong means slow: dynamic contributions to the bulk mechanical properties of supramolecular networks. *Angew Chem Int Ed* 44:2746–2748
7. Loveless DM, Abu-Lail NI, Kaholek M, Zauscher S, Craig SL (2006) Reversibly cross-linked surface-grafted polymer brushes. *Angew Chem Int Ed* 45:7812–7814
8. South CR, Weck M (2008) Bridged coordination polymer multilayers with tunable properties. *Langmuir* 24:7506–7511
9. Kersey FR, Loveless DM, Craig SL (2007) A hybrid polymer gel with controlled rates of cross-link rupture and self-repair. *J R Soc Interface* 4:373–380
10. Yount WC, Loveless DM, Craig SL (2005) Small-molecule dynamics and mechanisms underlying the macroscopic mechanical properties of coordinatively cross-linked polymer networks. *J Am Chem Soc* 127:14488–14496
11. Huck WTS, Snellink-Ruel BHM, Lichtenbelt JWT, van Veggel FCJM, Reinhoudt DN (1997) Self-assembly of hyperbranched spheres; correlation between monomeric synthon and sphere size. *Chem Commun* 9–10
12. Huisman BH, Schonherr H, Huck WTS, Friggeri A, van Manen HJ, Menozzi E, Vancso GJ, van Veggel FCJM, Reinhoudt DN (1999) Surface-confined metallodendrimers: isolated nanosize molecules. *Angew Chem Int Ed* 38:2248–2251
13. Huck WTS, van Veggel FCJM, Sheiko SS, Moller M, Reinhoudt DN (1998) Molecularly thin films of metallodendrimers. *J Phys Org Chem* 11:540–545
14. Huck WTS, van Veggel FCJM, Kropman BL, Blank DHA, Keim EG, Smithers MMA, Reinhoudt DN (1995) Large self-assembled organopalladium spheres. *J Am Chem Soc* 117(31):8293–8294
15. Huck WTS, Snellink-Ruel B, van Veggel FCJM, Reinhoudt DN (1997) New building blocks for noncovalent assembly of *homo*- and *hetero*-multinuclear metallodendrimers. *Organometallics* 16:4287–4291
16. Huck WTS, Prins LJ, Fokkens RH, Nibbering NMM, van Veggel FCJM, Reinhoudt DN (1998) Convergent and divergent noncovalent synthesis of metallodendrimers. *J Am Chem Soc* 120(25):6240–6246
17. Huck WTS, van Veggel FCJM, Reinhoudt DN (1997) Self-assembly of hyperbranched spheres. *J Mater Chem* 7:1213–1219
18. Albrecht M, van Koten G (2001) Platinum group organometallics based on “pincer” complexes: sensors, switches, and catalysts. *Angew Chem Int Ed* 40(20):3750–3781
19. Wieczorek B, Dijkstra HP, Egmond MR, Klein Gebbink RJM, van Koten G (2009) Incorporating ece-pincer metal complexes as functional building blocks in semisynthetic metalloenzymes, supramolecular polypeptide hybrids, tamoxifen derivatives, biomarkers and sensors. *J Organomet Chem* 694(6):812–822
20. Stiriba S-E, Slagt MQ, Kautz H, Klein Gebbink RJM, Thomann R, Frey H, van Koten G (2004) Synthesis and supramolecular association of immobilized ncn-pincer platinum(ii) complexes on hyperbranched polyglycerol supports. *Chem Eur J* 10(5):1267–1273
21. van de Coevering R, Alfery AP, Meeldijk JD, Martínez-Viviente E, Pregosin PS, Klein Gebbink RJM, van Koten G (2006) Ionic core–shell dendrimers with an octacationic core as noncovalent supports for homogeneous catalysts. *J Am Chem Soc* 128(39):12700–12713
22. South CR, Pinon V III, Weck M (2008) Erasable coordination polymer multilayers on gold. *Angew Chem Int Ed* 47:1425–1428
23. South CR, Higley MN, Leung KCF, Lanari D, Nelson A, Grubbs RH, Stoddart JF, Weck M (2006) Self-assembly with block copolymers through metal coordination of scs–pdii pincer complexes and pseudorotaxane formation. *Chem Eur J* 12(14):3789–3797
24. South CR, Leung KCF, Lanari D, Stoddart JF, Weck M (2006) Noncovalent side-chain functionalization of terpolymers. *Macromolecules* 39(11):3738–3744
25. Burd C, Weck M (2008) Solvent influence on the orthogonality of noncovalently functionalized terpolymers. *J Polym Sci A Polym Chem* 46:1936–1944

26. Chuchuryukin AV, Chase PA, Dijkstra HP, Suijkerbuijk BMJM, Mills AM, Spek AL, van Klink GPM, van Koten G (2005) General approach for template-directed synthesis of macroheterocycles by ring-closing metathesis (rcm). *Adv Synth Catal* 347(2–3):447–462
27. Chuchuryukin AV, Dijkstra HP, Suijkerbuijk BMJM, Klein Gebbink RJM, van Klink GPM, Mills AM, Spek AL, van Koten G (2003) Template-directed synthesis of macroheterocycles by ring-closing metathesis of olefin-substituted pyridines in the coordination sphere of a triplatinum complex. *Russ J Org Chem* 39(3):422–429
28. Chuchuryukin AV, Dijkstra HP, Suijkerbuijk BMJM, Klein Gebbink RJM, van Klink GPM, Mills AM, Spek AL, van Koten G (2003) Macrocyclization by olefin metathesis on a nanosized, shape-persistent tricationic platinum template. *Angew Chem Int Ed* 42(2):228–230
29. Dijkstra HP, Meijer MD, Patel J, Kreiter R, van Klink GPM, Lutz M, Spek AL, Canty AJ, van Koten G (2001) Design and performance of rigid nanosize multimetallic cartwheel pincer compounds as Lewis-acid catalysts. *Organometallics* 20(14):3159–3168
30. Whitesides GM, Mathias JP, Seto CT (1991) Molecular self-assembly and nanochemistry: a chemical strategy for the synthesis of nanostructures. *Science* 254:1312–1319
31. Davis AV, Yeh RM, Raymond KN (2002) Supramolecular assembly dynamics. *Proc Natl Acad Sci USA* 99:4793–4796
32. Ziegler M, Brumaghim JL, Raymond KN (2000) Stabilization of a reactive cationic species by supramolecular encapsulation. *Angew Chem Int Ed* 39:4119–4121
33. Kang J, Rebek J Jr (1997) Acceleration of a Diels-Alder reaction by a self-assembled molecular capsule. *Nature* 385:50–52
34. Kang J, Hilmersson G, Santamaria J, Rebek J Jr (1998) Diels-Alder reactions through reversible encapsulation. *J Am Chem Soc* 120:3650–3656
35. Yoshizawa M, Kusukawa T, Fujita M, Sakamoto S, Yamaguchi K (2001) Cavity-directed synthesis of labile silanol oligomers within self-assembled coordination cages. *J Am Chem Soc* 123:10454–10459
36. Scherer M, Caulder DL, Johnson DW, Raymond KN (1999) Triple helicate-tetrahedral cluster interconversion controlled by host-guest interactions. *Angew Chem Int Ed* 38:1588–1592
37. Rivera JM, Craig SL, Martin T, Rebek J Jr (2000) Chiral guests and their ghosts in reversibly assembled hosts. *Angew Chem Int Ed* 39:2130–2132
38. Kersting B, Meyer M, Powers RE, Raymond KN (1996) Dinuclear catecholate helicenes: their inversion mechanism. *J Am Chem Soc* 118:7221–7222
39. Chen J, Korner S, Craig SL, Rudkevich DM, Rebek J Jr (2002) Amplification by compartmentalization. *Nature* 415:385–386
40. Fujita M, Umemoto K, Yoshizawa M, Fujita N, Kusukawa T, Biradha K (2001) Molecular paneling *via* coordination. *Chem Commun* 509–518
41. Seidel SR, Stang PJ (2002) Higher-symmetry coordination cages *via* self-assembly. *Acc Chem Res* 35:972–983
42. Rodriguez G, Albrecht M, Schoenmaker J, Ford A, Lutz M, Spek AL, van Koten G (2002) Bifunctional pincer-type organometallics as substrates for organic transformations and as novel building blocks for polymetallic materials. *J Am Chem Soc* 124:5127–5138
43. Dijkstra HP, Chuchuryukin A, Suijkerbuijk BMJM, van Klink GPM, Mills AM, Spek AL, van Koten G (2002) Metathesis of olefin-substituted pyridines: the metalated ncn-pincer complex in a dual role as protecting group and scaffold. *Adv Synth Catal* 344:771–780
44. Sijbesma RP, Beijer FH, Brunsveld L, Folmer BJB, Ky Hirschberg JHK, Lange RFM, Lowe JKL, Meijer EW (1997) Reversible polymers formed from self-complementary monomers using quadruple hydrogen bonding. *Science* 278:1601–1604
45. Castellano RK, Clark R, Craig SL, Nuckolls C, Rebek J Jr (2000) Emergent mechanical properties of self-assembled polymeric capsules. *Proc Natl Acad Sci USA* 97(23):12418–12421
46. Burnworth M, Knapton D, Rowan SJ, Weder C (2007) Metallo-supramolecular polymerization: a route to easy-to-process organic/inorganic hybrid materials. *J Inorg Organomet Polym Mater* 17(1):91–103

47. Burke KA, Sivakova S, McKenzie BM, Mather PT, Rowan SJ (2006) Effect of stoichiometry on liquid crystalline supramolecular polymers formed with complementary nucleobase pair interactions. *J Polym Sci A Polym Chem* 44:5049–5059
48. Botterhuis NE, van Beek DJM, van Gemert GML, Bosman AW, Sijbesma RP (2008) Self-assembly and morphology of polydimethylsiloxane supramolecular thermoplastic elastomers. *J Polym Sci A Polym Chem* 46(12):3877–3885
49. Burattini S, Greenland BW, Merino DH, Weng W, Seppala J, Colquhoun HM, Hayes W, Mackay ME, Hamley IW, Rowan SJ (2010) A healable supramolecular polymer blend based on aromatic π - π stacking and hydrogen-bonding interactions. *J Am Chem Soc* 132(34):12051–12058
50. Fox J, Wie JJ, Greenland BW, Burattini S, Hayes W, Colquhoun HM, Mackay ME, Rowan SJ (2012) High-strength, healable, supramolecular polymer nanocomposites. *J Am Chem Soc* 134(11):5362–5368
51. Kersey FR, Yount WC, Craig SL (2006) Single-molecule force spectroscopy of bimolecular reactions: system homology in the mechanical activation of ligand substitution reactions. *J Am Chem Soc* 128:3886–3887
52. Jeon SL, Loveless DM, Craig SL (2010) Main-chain dynamics in metallo-supramolecular polymers: from solution to elastomeric fibres. *Supramol Chem* 22:698–703
53. Loveless DM, Jeon SL, Craig SL (2007) Chemoresponsive viscosity switching of a metallo-supramolecular polymer network near the percolation threshold. *J Mater Chem* 17:56–61
54. Xu D, Hawk JL, Loveless DM, Jeon SL, Craig SL (2010) Mechanism of shear thickening in reversibly cross-linked supramolecular polymer networks. *Macromolecules* 43(7):3556–3565
55. Xu D, Craig SL (2010) Multiple dynamic processes contribute to the complex steady shear behavior of cross-linked supramolecular networks of semidilute entangled polymer solutions. *J Phys Chem Lett* 1:1683–1686
56. Xu D, Liu C-Y, Craig SL (2011) Divergent shear thinning and shear thickening behavior of supramolecular polymer networks in semidilute entangled polymer solutions. *Macromolecules* 44(7):2343–2353
57. Loveless DM, Jeon SL, Craig SL (2005) Rational control of viscoelastic properties in multi-component associative polymer networks. *Macromolecules* 38:10171–10177
58. Lodge AS (1956) A network theory of flow birefringence and stress in concentrated polymer solutions. *Trans Faraday Soc* 52:120–130
59. Tanaka F, Edwards SF (1992) Viscoelastic properties of physically crosslinked networks. 1. Transient network theory. *Macromolecules* 25(5):1516–1523
60. Jongschaap RJJ, Wientjes RHW, Duits MHG, Mellema J (2001) A generalized transient network model for associative polymer networks. *Macromolecules* 34(4):1031–1038
61. Furukawa H, Kuwabara R, Tanaka Y, Kurokawa T, Na Y-H, Osada Y, Gong JP (2008) Tear velocity dependence of high-strength double network gels in comparison with fast and slow relaxation modes observed by scanning microscopic light scattering. *Macromolecules* 41(19):7173–7178
62. Cordier P, Tournilhac F, Soulie-Ziakovic C, Leibler L (2008) Self-healing and thermoreversible rubber from supramolecular assembly. *Nature* 451(7181):977–980
63. Kong HJ, Wong E, Mooney DJ (2003) Independent control of rigidity and toughness of polymeric hydrogels. *Macromolecules* 36:4582–4588
64. Vaccaro A, Marrucci G (2000) A model for the nonlinear rheology of associating polymers. *J Non-Newton Fluid Mech* 92(2–3):261–273
65. Tennyson AG, Wiggins KM, Bielawski CW (2010) Mechanical activation of catalysts for c-c bond forming and anionic polymerization reactions from a single macromolecular reagent. *J Am Chem Soc* 132:16631–16636
66. Caruso MM, Davis DA, Shen Q, Odom SA, Sottos NR, White SR, Moore JS (2009) Mechanically-induced chemical changes in polymeric materials. *Chem Rev* 109:5755–5798
67. Luche JL, Einhorn C, Einhorn J, Sinisterra-Gago JV (1990) Organic sonochemistry: a new interpretation and its consequences. *Tetrahedron Lett* 31:4125–4128

68. Aydin J, Conrad CS, Szabo KJ (2008) Stereoselective pincer-complex catalyzed c-h functionalization of benzyl nitriles under mild conditions. An efficient route to β -aminonitriles. *Org Lett* 10:5175–5178
69. Strahan JR, Adams JR, Jen W, Vanleenhove A, Neikirk CC, Rochelle T, Gronheid R, Willson CG (2009) Fluorinated polymethacrylates as highly sensitive nonchemically amplified e-beam resists. *J Micro/Nanolith MEMS MOEMS* 8:043011

Index

A

Acrolein, α -cyanopropionates, 257
Agostic pincer complexes, 21, 30
Aldehydes, asymmetric reductive aldol reaction, 261
Aldol coupling, reductive, 209
Aldol reactions, 203, 205
 reductive, 259
Alkenes, asymmetric hydrosilylation, 258
Alkyl hydride anionic complex, 43
Alkynes, cross-coupling, 256
Alkynylation, 263, 264
Allenyl silanes, 223
Allyl–allyl coupling, 213, 218
Allylation, 203, 211
Allylboronic acids, 218
Allyl stannanes, 220
Allyltributyltin, 257
Amine borane, dehydrogenation, 271
Ammonia borane, 273
Ammonia, N–H activation, 293
Antimony, 189
 fluorides, 190
 phosphates, 191
Arenes, 253
Arsenic, 189
Aryl–aryl cross-coupling, 227
Arylmethyl-based scaffolds, C(*sp*³)-metalated, 303
Asymmetric catalysis, 243
Atom transfer radical addition (ATRA), 225

B

Bathophenanthroline, 94
Binaphthol, 257
Bioimaging, 123
Biosensors, 123
2-(4-Biphenyl)-5-(4-*tert*-butylphenyl)-1,3,4-oxa-diazole, 94
Bisallylpalladium, 213
Bisamino-pincers, 3
Bis(azolylmethyl)phenyl, (NCN)NiBr, 154
2,6-Bis(2-benzimidazolyl)pyridine, 114
Biscycloplatination, 8
1,8-Bis(diphenylphosphino)anthracene (DPA), 97, 313
Bismuth, 189
 fluorides, 189
 phosphates, 191
1,3-Bis(*N*-methyl-benzimidazol-2-yl)benzene, 112
Bis(oxazoline)pyridine (pybox), 245
Bis(oxazoliny)phenyl (phebox), 152, 243
Bisphosphine-pincer ligand, 3
1,3-Bis(1-pyrazolyl)benzene, 121
1,3-Bis(2-pyridyl)-4,6-dimethylbenzene, 112
1,3-Bis(pyrrolidinothiocarbonyl)benzene, 93
1,3-Bis(8-quinolyl)benzene, 121
 β -Borylation, 263
2-Bromoisophthalic acid, 248

C

Carbometalated pincer complexes, 289
Carbon dioxide reduction, Rh/Ir, 293

C–C bond formation, 254
Chiral tridentate ligands, 243
Cobalt, 283
Collapse, 36
Coordination geometries, 49
Coordination properties/modes, 1, 3
C₂ pincer twist, 58, 68–69, 71
Cross-coupling–bromination–
cross-coupling, 117
5-Cyano-5-ethoxycarbonyl-2,
8-nonadione, 152
Cycloheptatriene-based scaffold, 301
2-Cyclohexenone, 262
Cyclometallated complex, 89
Cyclometallation, 7, 109
Cyclopropanation, 265

D
Danishefsky's diene, 258
Decomposition pathways, 1
Dehydrogenation, 14, 50, 80, 205,
271, 314
Dendrimers, 8, 101, 151, 227
Dialkyl anionic complex, 41
Diarylmethyl-based scaffolds
C(sp³)-metalated, 305
Dibenzobazzenelene-based pincers, 308
Dibenzylaminothiocarbonyl complex, 95
Dihydride anionic complex, 41
Diisopropylamine, 255
Dimethyl acetylenedicarboxylate, 255
Diphenyl anionic complex, 41
Diphenyl phosphine, 211
2,6-Diphenylpyridine, 113
(*S*)-Diphenyl(pyrrolidin-2-yl)-methanol, 166
Diphosphinoalkanes, 291
Diphosphinocycloalkanes, 297
1,3-Di(2-pyridyl)benzene, 107, 112
Distannyne, 182

E
(ECE)Ni, 131
ECE-pincer ligand, monoanionic, 1
Electroluminescence, 89
Electronic effects, 49
Enones, hydrophosphination, 244
Excimers, 122
Excited states, 89

G
Gallium, 177
Germanium, 179
Germylenes, 179
Germyne, 180
Gold, 251
Gold(I) phosphine, 8

H
H/D exchange, Ir-catalyzed, 296
Heck reaction, 226
Hexaalkylditin, 220
Hexahydro-1*H*-pyrrolo[1,2,*c*]imidazolone, 244
Hybrid gels, 342
Hydrazines/hydrozones, N–H activation, 293
Hydroamination, Pa-catalyzed, 234
Hydrogenation, 203
Ru pincer-complex catalyzed, 235
Hydrogen storage, 271, 273
Hydrosilylation, 258

I
Imaging, 89
Imines, 208, 211, 215, 244, 268
allylation, 211
Mannich reaction, 244
Indium, 177
Intersystem crossing (ISC), 90
Iridium, 89, 111, 246, 293
phenoxonium, 26
Iron, 249
Isocyanides, 205
Isocynoacetate, 256
N-Isopropylpropylideneamine, 255

K
Ketones, asymmetric alkynylation, 264
asymmetric reductive aldol reaction, 261
Kharasch addition, 225

L
Late transition metals, 21, 187, 273
Lead, 188
Lewis acid catalysts, 212, 257
Ligand conformation, 49
Ligand-to-ligand charge-transfer (LLCT), 115

Lithium, 2, 5, 177, 189

Luminescence, 89

M

Main group metals, 175

Mechanochemistry, 319

Metallo dendrimers, 319, 321

(NCN^{M_c})NiCl, 151

Methoxy-1-iodonaphthalene, 267

Methylamine borane, 276

Methylene arenium complexes, 21

Methylvinylketone, 267

Michael addition, 151, 203, 209, 257, 267

Molecular recognition, 256

N

1-Naphthboronic acid, 267

Naphthyl radical anion, 29

NCN, 1ff

gallium(III), 178

germylenes, 180

ligands, (non)aromatic amines, 100, 107

nickellation, 145

Nickel, 131, 247

carbene, 284

pincers, redox potentials, 80

p-Nitrobenzaldehyde, 262

O

Organic light-emitting devices (OLEDs), 89, 90, 116, 123

Organoantimony(III), 188

Organoarsenic(III), 188

Organobismuth, 189

Organocopper, 15

Organolithium, 10, 29, 41, 148, 183, 189

Organostannylenes, 182

Organotin(II), 181

Organotin(IV), 176

Organimony, 189

Osmium, 24, 108, 292, 294

Oxazolidines, 205

Oxazoline ligands, 243

Oxidation states, 15

Oxygen sensors, luminescent, 125

P

Palladium, 203, 212, 247

Pb, 178

PCCCP, 59

PCNCP, 64

PCN ligand, 39

PCP, 1ff

benzylic, 51

ligands, 97

metallation, 53

(PCP^{Ph})Ni(II)(*o*-semiquinones), 136

PC_{sp³}P, 141

transition metal pincer, 289

PENEP, 56

Perfluoroalkylphosphine PCP ligand, 52

Phenoxonium, 21

cations, 25

2-Phenylpyridine, 89

Phosphine ligands, 49

Phosphine pincers, electronic effects, 76

Phosphine sulphide, 92

Phosphonito PCP, 230

Phosphoramidite, 244

Phosphorescence, 89

Photochemistry, 89

Pincer-metal complexes, preparation, 6

Pincers, carbonyl complexes, 77

5-coordinate, 70

C₂ twist, 68

kinetics, 319

ligands, 1, 21, 49

nickel, 131

Platinum, 38, 89, 117, 247

Plumbylenes, 189

PMP, 49

angles, 69

PNCN, 131, 163

PNCNP, 55, 65, 131, 155

PNC_{sp³}NP, 162

PNNNP, 57, 66

(PNP)Ru(H)(PMe₃), 280

(P-N)₂RuCl₂, 278

POCN, 131, 163

POCOP, 61, 131, 155

nickel, 155

resorcinol-based, 53

(POCOP)Ir(H)₂, 274

(POC_{sp³}OP)Ni, 161

Polyborazylene, 284

Polydentate ligands, 49

Poly[3,4-(ethylenedioxy)thiophene]-poly(styrenesulfonic acid)

(PEDOT-PSS), 94

Poly(9-vinylcarbazole), 94

PONOP, 66

Precatalysts, 279

Propargyl chlorides, stannylation, 223
Propargyl epoxides, 223
Pt(dpyb–Br)Cl, 123
Pt(dpyb)Cl, 117
Pt(NCN)Cl, 120
Pyrazole, 120

Q

Quinone methides, 21, 23, 43

R

Reactive intermediates, 21, 23
Reversible networks, 339
Rhodium, 203, 246, 293
 catalysts, 243
 quinone methide, 23
Ruthenium, 89, 108, 203, 249
 catalysts, 243
 pincers, redox potentials, 79

S

Sb, 188
SCS ligands, 92, 131
Sensing, 89
Single electron transfer (SET), 226
Sn, 178, 180
Solar cells, dye-sensitised (DSSCs), 89, 110
Spin-orbit coupling (SOC), 90
Stannylation, 221
Stannylenes, 181
Steric effects, 49

Stilbenequinones, 27
Stimuli-responsive networks, 341
Sulfonimines, 216, 222
Suzuki coupling, 227
Suzuki–Miyaura cross-coupling,
 asymmetric, 267

T

Terdentate ligands, 49
Thallium, 178
Thioquinone methide complexes, 21
Tin, 178, 180
Transfer hydrogenation, 235
Triarylmethyl-based scaffolds,
 C(*sp*³)-metalated, 305
Triazine pincers, 57
Tributyl allyl stannane, 212
 α -Trifluoromethyl-trifluoroethyl
 acrylate, 346
Tris(2-pyridyl)benzene, 112

V

Vinyl aziridines, 218
Vinyl cyclopropanes, 218

W

White-light-emitting devices (WOLEDs), 124

X

Xylylene complexes, 21